Investigating the Roles of FOXO3 and FOXO4 in CLL Proliferation and Survival

Jamie Lees

MSc (R), BSc (Hons)

Submitted in fulfilment of the requirements for the Degree of *Doctor of Philosophy*

School of Cancer Sciences

College of Medical, Veterinary and Life Sciences

University of Glasgow

May 2025

Abstract

Chronic lymphocytic leukaemia is a B-cell malignancy emanating from the aberrant growth and accumulation of monoclonal lymphocytes whose origins can be traced to naïve or mature B-cell clones. A groundbreaking study revealed a heavy reliance of CLL cells on interactions with accessory cells within a 'tumour microenvironment' niche that drive proliferation, survival and drug resistance. As such, a core theme in the development of novel therapies has been perturbing the activity of intrinsic signalling components that are pivotal in driving these events, such as BCR and CD40 signal inhibition with the advent of BTK inhibitors (e.g. ibrutinib). Current small molecule inhibitor therapy has revolutionised CLL treatment. Even still, patient responses and suitability for treatments are highly variable, reinforcing an unmet clinical need for tailored therapeutics to treat CLL on a patient-specific basis.

Malignant cells often exploit proliferative and survival signalling components to aid their rapid, uncontrollable growth. A prime example is the PI3K-AKT-mTOR signalling axis, which is hyperactivated in most cancer contexts. This signalling axis can orchestrate proliferative and pro-survival events *via* downstream mTORC1/2 and AKT activity. mTOR components can promote cell growth and proliferation *via* a multitude of events including mTORC1-mediated translation initiation, as well as enhancing AKT activity. AKT itself can regulate the activity of several downstream substrates *via* phosphorylation, including FOXO transcription factors. Canonically, FOXO transcription factors mediate the expression of tumour-suppressive genes, and are negatively regulated by AKT-mediated phosphorylation and subsequent cytoplasmic sequestration. However, ever-emerging evidence (in B-cell malignancies and in the wider cancer context) suggests a bimodality to FOXO function, where they promote and/or suppress tumour progression in a context-dependent manner. Indeed, FOXO1's tumour suppressive roles in CLL have been characterised as part of previous investigations within the group. In this work, we aimed to characterise the behaviours of the FOXO3 and FOXO4 isoforms to determine the suitability of targeting FOXO activity as a potential novel therapeutic approach in CLL.

Initially, prominent FOXO3/4 expression was demonstrated in *ex vivo* patient samples and in MEC1 and HG3 CLL cell lines. Further investigation revealed that,

while FOXO3/4 protein and gene expression were negatively regulated by TME-associated signals (BCR ligation or CD40 activation), FOXO3/4 expression persisted in CLL cell nuclear fractions, indicative of a reliance of CLL cells on constitutive FOXO3/4 activity. Furthermore, global transcriptomic analyses of primary patient samples revealed that FOXO4 is heavily regulated by mTORC1/2-mediated signals downstream of CD40 activation, demonstrating a notable association between FOXO4 and mTOR activity in CLL. This was evidenced by tight regulation of FOXO3/4 localisation by BTK and mTOR, as well as the expression of discrete FOXO target genes downstream of CD40 activation. These findings demonstrate the complexity of FOXO biology in proliferating CLL cell populations.

To further characterise FOXO3/4 behaviour in CLL, we conducted shRNA-mediated knockdown of *FOXO3* or *FOXO4* in CLL cell lines (and primary patient samples: *FOXO4*). Here, we demonstrated an isoform-specific reliance of CLL cells on *FOXO3/4*; in both cases, viability and proliferative capacity were adversely affected. Cells lacking *FOXO3* exhibited a loss of drug-mediated cell kill, while extensive investigation revealed that *FOXO4* depletion sensitised CLL cells to multiple targeted agents including AZD8055, ibrutinib and venetoclax. Further investigation identified that *FOXO4* depletion increased CLL cell susceptibility to DNA damage, coincident with the aberrant expression of *GADD45A* and BCL2 family members, as well as a dysregulation of mTORC1/2 signalling components; the latter perhaps due to a lack of FOXO4-mediated *SESN3 expression*.

Together, these findings improve our understanding of the characteristics of FOXO transcription factors in CLL, demonstrating their ability to exhibit discrete behaviours and orchestrate distinct cellular functions. We argue that, while they are inextricably regulated by TME-associated signals and may facilitate tumour-suppressive effects, FOXO transcription factors are also required to promote CLL cell proliferation, survival and drug resistance in a context- and isoform-dependent manner. These data have the capacity to contribute to future pre-clinical investigation as well as the consideration of novel therapeutic strategies in CLL and in the wider context of malignancy.

Table of contents

List of tables

List of figures

Additional publications

Lees, J., et al. (2023). "The discrete roles of individual FOXO transcription factor family members in B-cell malignancies." Front Immunol **14**: 1179101.

Malik, N., et al. (2023). "mTORC1-selective activation of translation elongation promotes disease progression in chronic lymphocytic leukemia." Leukemia **37**(12): 2414-2425.

Hay, J., et al. (2022). "PKCbeta Facilitates Leukemogenesis in Chronic Lymphocytic Leukaemia by Promoting Constitutive BCR-Mediated Signalling." Cancers (Basel) **14**(23): 6006.

Acknowledgements

This PhD has been an absolute whirlwind.

My initial thanks go to my primary supervisor Professor Alison Michie. Without your unwavering support and enthusiasm, I would not be where I am today. Your guidance has truly shaped my scientific understanding, and for that, I am eternally grateful. Thank you for all you do for your group, the POG and the wider blood cancer community.

I would also like to thank my secondary supervisor Dr Karen Keeshan. While our contact was limited, you were always very kind and willing to give advice should I need it. Thank you.

To the students and staff at the POG-LRC and the wider SCS, it was a pleasure to do my PhD in such a nurturing, supportive and friendly environment. I will miss working with you all. Naturally, countless thanks go to the Michie group: Jodie, Jen, Hassan and Jiatian. Your friendship, advice and partnership mean the world to me and I wish you all the best in everything that you do. Thank you as well to all the students that I supervised; I hope I was able to share at least a modicum of support to aid you in your studies.

To my family, I cannot thank you enough. Your enthusiasm and encouragement for my studies were so valued. I always appreciated our chats about my work and I am so lucky to have you all routing for me. To my darling Mum, Moira, thank you for being my biggest fan. I miss you more than you will ever know.

Special thanks go to the Snodgrass family. Without their kind philanthropic donations to leukaemia research, this studentship would not have been possible. I would also like to thank all the patients who kindly donated samples to support CLL research at the POG-LRC.

Lastly, I would like to thank my amazing partner, Molly. Your love, support and encouragement have been invaluable. Thank you for putting up with living with a student for years; you can finally relax!

Author’s declaration

I declare that this thesis is a product of my own work and has not been submitted for any other degree at the University of Glasgow or any other institution.

Abbreviations

µM	Micromolar
1L	First-line
4E-BP1	Eukaryotic translation initiation factor 4E-binding protein 1
7-AAD	7-Aminoactinomycin D
Ab	Antibody
ABC-DLBCL	Activated B-cell-like subtype Diffuse large B-cell lymphoma
AID	Activation-induced cytidine deaminase
AKT	Protein kinase B
AML	Acute myeloid leukaemia
AMPK	AMP-activated protein kinase
APRIL	A proliferation-inducing kinase
ATCC	American Type Culture Collection
ATCC	American Type Culture Collection
ATM	Ataxia-telangiesctasia mutated
B2M	ß2-microglobulin
BAFF	B-cell activating factor
BAK	BCL2-antagonist/killer
BAX	BCL2-associated protein X
BBC3	BCL2 binding component 3
BCA	Bichinchoninic acid
BCAP	B-cell adapter for phosphoinositide 3-kinase
BCL2	B-cell lymhoma 2
BCL2L1	B-cell lymphoma extra large (gene)
BCL2L11	BCL2-like protein 11
BCL6	B-cell lymphoma 6
BCP-ALL	B-cell precursor acute lymphoblastic leukaemia
BCR	B-cell receptor
BH3	BCL2 homology 3
BIM	BCL2-like protein 11
BL	Burkitt's lymphoma
BM	Bone marrow
BMSC	Bone marrow stromal cell
BSA	Bovine serum albumin
BTK	Bruton's tyrosine kinase
CCL	C-C motif chemokine ligand
CCND1	Cyclin D1
CCND2	Cyclin D2
CCNG2	Cyclin G2
CD40L	CD40 ligand
CDK2	Cyclin-dependent kinase 2
CDKN1A	Cyclin-dependent kinase inhibitor 1A
CDKN1B	Cyclin-dependent kinase inhibitor 1B
cDNA	Complementary DNA
cHL	Classical hodgkin lymphoma
CIT	Chemoimmunotherapy

CK	Complex karyotype
Clb	Chlorambucil
CLL	Chronic lymphocytic leukaemia
CLL-IPI	the CLL international prognostic index
CLP	Common lymphoid progenitor
CML	Chronic myeloid leukaemia
CNS	Central nervous system
CO2	Carbon dioxide
COMBO	Combination
CR	Complete response
CRM1	Chromosomal region maintenance 1
CSR	Class switch recombination
CTLA-4	Cytotoxic T-lymphocyte-associated protein 4
CTV	CellTrace Violet
CXCL	C-X-C motif chemokine
CXCR4	C-X-C chemokine receptor type 4
CXCR5	C-X-C chemokine receptor type 5
DAG	Diacylglycerol
DAPI	4',6-diamidino-2-phenylindole
DBD	DNA binding domain
DEG	Differential gene expression
DLBCL	Diffuse large B-cell lymphoma
DMEM	Dulbecco's modified eagle medium
DMSO	Dimethyl sulfoxide
DNA	Deoxyribonucleic acid
DSMZ	Deutsche Sammlung von Mikrooganismen und Zellkulturen
DZ	Dark zone
EDTA	Ethylenediaminetetraacetic acid
ERIC	European research initiative on CLL
ERK	Extracellular signal-regulated kinase
ESSCA	European society for clinical cell analysis
F(ab')	Fragment antibody binding
FBS	Foetal bovine serum
Fc	Fragment crystallisable
FCR	Fludarabine-cyclophosphamide-rituximab
FDA	US food and drug administration
FHRE	Forkhead reponse element
FL	Follicular lymphoma
FOX	Forkhead box
FOXO	Forkhead box class O
FOXO1	Forkhead box class O isotype 1
FOXO3	Forkhead box class O isotype 3
FOXO4	Forkhead box class O isotype 4
FOXO6	Forkhead box class O isotype 6
G0	Resting phase/quiescence
G1	Gap 1 phase
G2	Gap 2 phase
GAB1	GRB2 associated binding protein 1
GADD45	Growth arrest and dna damage inducible
GADD45A	Growth arrest and dna damage inducible alpha

GAP	GTPase activting protein
GC	Germinal centre
GCB-DLBCL	Germinal centre B-cell subtype diffuse large B-cell lymphoma
GCLLSG	German CLL study group
GF	Growth factor
GO	gene ontology
GSEA	Gene set enrichment analysis
GSK	Glycogen synthase kinase
H	Heavy
H2AX	H2A. X variant histone
HCC	Hepatocellular carcinoma
HCDR3	Heavy complementary determining region 3
HEK293T	Human embryonic kidney 293 cells (SV40 T-antigen)
HSC	Haematopoietic stem cells
Ig	Immunoglobulin
IgD	Immunoglobulin D
IGF1R	Insulin-like growth factor 1 receptor
IgM	Immunoglobulin M
IGVH	Immunoglobulin heavy-chain variable region
IGVL	Immunoglobulin light-chain variable region
IL-21	Interleukin 21
IL-4	Interleukin 4
IP3	Inositol-1,2,5-triphosphate
ITAMs	Immunoreceptor tyrosine-based activation motifs
ITIMs	Immunoreceptor tyrosine-based inhibition motifs
iwCLL	International workshop on CLL
JNK	c-Jun N-terminal kinase
KEGG	Kyoto encyclopedia of genes and genomes
L	Light
LMPP	Lympho-myeloid primed progenitor cells
LN	Lymph node
LYN	Tyrosine-protein kinase Lyn
LZ	Light zone
M	Mitosis
M	Molar
mAbs	Monoclonal antibody
MAPK	Mitogen-activated protein kinase
MCL-1	Induced myeloid leukaemia cell differentiation protein 1
M-CLL	Mutated CLL
MDM2	Mouse double minute 2 homolog
MEK	Mitogen-activated protein kinase
miRNA	MicroRNA
miRNA	Micro RNA
mM	Millimolar
MM	Multiple myeloma
mRNA	Messenger RNA
MSC	Mesenchymal stem cell
mTOR	Mehcanistic target of rapamycin
mTORC1	Mehcanistic target of rapamycin complex 1
mTORC2	Mehcanistic target of rapamycin complex 2

MYC	Myelocytomatosis oncogene
MZL	Marginal zone lymphoma
NCK	non-catalytic region of tyrosine kinase adaptor protein
NES	Nuclear export sequence
NFAT	Nuclear factor of activated T-cells
NF-κB	Nuclear factor kappa-light-chain enhancer of activated B-cells
NLC	Nurse-like cell
NLS	Nuclear localisation sequence
nM	Nanomolar
NOTCH1	Neurogenic locus notch homolog protein 1
NT-L	Mouse fibroblast L cells
OR	Overall response
OS	Overall survival
PARP	Poly (ADP-ribose) polymerase
PB	Peripheral blood
PBMC	Peripheral blood mononuclear cells
PBS	Phospho-buffered saline
PCA	principal component analysis
PCR	Polymerase chain reaction
PD-1	Programmed cell death protein 1
PDCD4	Programmed cell death protein 4
PDK1	Phosphoinositide-dependent kinase 1
PFS	Progression-free survival
PH	Pleckstrin homology
PI	Propidium iodide
PI3K	Phosphoinositide 3-kinase
PI3Kγ	PI3k isoform γ
PI3Kδ	PI3k isoform δ
PIK3CA	Phosphatidylinositol-4,5-Bisphosphate 3-Kinase catalytic subunit alpha
PIKK	PI3K-related protein kinases
PIP2	Phosphatidylinositol(4,5)P2
PIP3	Phosphatidylinositol(3,4,5)P3
PKA	Protein kinase A
PKC	Protein kinase C
PLCγ2	Phospholipase C gamma 2
pre-B	Precursor B cells
pro-B	Progenitor B cells
PS	Phosphatidylserine
PSMD	Proteasome 26S subunit, non ATP-ase
PTEN	Phosphatase and tensin homolog
PVDF	Polyvinylidene Fluoride
R/R	Relapsed/Refractory
RANK	Receptor activator for NF-kB ligand
RAPTOR	Regulatory protein associated with mTOR
RICTOR	Rapamycin insensitive companion of mTOR
RNA	Ribonucleic acid
RNA-Seq	RNA Sequencing
RPMI	Roswell Park Memorial Institute
RT	Room temperature

RTK	Receptor tyrosine kinase
RT-qPCR	Real time quantitative reverse transcription PCR
S	Synthesis phase
S6	Ribosomal protein S6
S6K1	p70-S6 kinase
SCR	Scrambled
SDF-1	Stromal cell-derived factor 1
SESN3	Sestrin 3
SESN3	Sestrin 3
SH2	Src homology 2
SHIP1	SH2-domain-containing inositol 5'-phosphatase 1
SHM	Somatic hypermutation
SHP-1	SH2 domain-containing tyrosine phosphatase 1
shRNA	Short hairpin RNA
sIg	Surface immunoglobulin
SIN1	MAPK associated protein 1
SINE	Selective inhibitors of nuclear export
SLOs	Secondary lymhpoid organs
SMAD	Mothers against decapentaplegic homolog
SYK	Spleen associated tyrosine kinase
TB	Terrific broth
TGF-ß	Transforming growth factor beta
TKI	Tyrosine kinase inhibitor
TME	Tumour microenvironment
TNF	Tumour necrosis factor
TP53	Cellular tumour antigen p53
TSC1/2	Tuberous sclerosis 1/2
U-CLL	Unmutated CLL
UK	United Kingdom
USP	Ubiquitin-specfic processing protease
V(D)J	Variable (Diversity) Joining
WES	Whole exome sequencing
WGS	Whole genome sequencing
WT	Wild type
XPO1	Exportin 1
ZAP-70	ζ chain associated kinase 70

Introduction

1. Chronic lymphocytic leukaemia

Chronic lymphocytic leukaemia (CLL) is a malignancy that is characterised by an accumulation of mature B-lymphocytes in the blood, bone marrow (BM) and secondary lymphoid organs (SLOs) [1]. CLL cells are small and monoclonal, where the disease's origin can be traced back to a single $CD5^+$ B-lymphocyte [2]. CLL cell populations are distinct from healthy B-cell populations in their cell surface marker expression where, unlike healthy B-cells, they co-express CD5, CD23, CD19, CD20, CD79b and surface membrane immunoglobulin (smIg) [2, 3]. CLL patients will exhibit an expansion of these monoclonal B-lymphocytes, and have highly variable prognoses; some patients will exhibit a aggressive disease requiring immediate treatment, whereas others will not require treatment but will be burdened with the disease for decades [2, 4]. The emergence and subsequent clinical behaviour of the disease can be associated with specific intracellular alterations, both genetic and epigenetic. Examples include: somatic mutation(s) [5]; mutational status of the Ig heavy-chain variable region (*IGHV*) of the B-cell receptor (BCR) [6, 7]; and aberrant expression of distinct signalling molecules [8, 9]. These events can all give rise to changes in disease biology and prognosis, and some are used as markers for prognostic stratification.

Although CLL is typically diagnosed in the peripheral blood (PB) [10], it is in a tumour microenvironment (TME) within lymph nodes and lymphatic organs that CLL cells are stimulated to proliferate and survive *via* interactions with particular accessory cells, thereby acting as a major contributor in the pathogenesis of CLL (discussed in section 1.4) [11]. An improved understanding of the interactions between these cells has led standardised patient treatment that deviates from broad-spectrum chemoimmunotherapy (CIT) to more 'targeted' therapies, involving the inhibition of pathways known to be crucial for promoting CLL proliferation and survival that are activated *via* TME-mediated signals [12]. Examples include Bruton's tyrosine kinase (BTK) inhibitors and BCL-2 Homology 3 (BH3) mimetics (e.g. ibrutinib and venetoclax, respectively) [12];

these novel treatments have been revolutionarily effective in treating CLL patients. However, with CLL being a disease primarily affecting the elderly population, both the prevalence of drug-related side effects and an increasing incidence of drug resistance [12, 13] drive a need for the development of novel treatment strategies that are tailored in a patient-specific manner, to improve survival rates for those with currently unmet clinical needs.

1.1. CLL Epidemiology

Epidemiological data from Cancer Research UK and the Haematological Malignancy Research Network (HMRN UK) set the incidence rate for CLL in the UK at 7.2/100,000 persons each year, totalling ~3800 cases each year (2016-2018) [14, 15]. This accounts for ~1% of all annual cancer diagnoses, with the highest incidence rate being in elderly patients, where 41% of those diagnosed are over the age of 75 [14]. Clinical data demonstrates a gender-specific difference in prognosis, where males are more likely to develop CLL (63% of cases are male (7.9/100,000 vs 3.9/100,000), while females are more likely to respond better to treatment, exhibit better prognostics and ultimately have better overall survival than men [16]. In the context of mortality, CLL deaths account for <1% of all cancer-related mortality (mortality rate: 1/100,000 persons, totalling 947 deaths in 2017) [14]. Furthermore, CLL has been shown to exhibit 'familial' characteristics, an association higher than that of any other leukaemia, where close relatives of those with diagnosed CLL are themselves 8.5 times more susceptible to developing the disease (or other lymphoma subtypes) [17], suggesting a potential inheritance of leukaemic risk factors. Genetic risk also manifests between races, where those of Asian lineage are much less likely (5-10 times) to develop CLL than those of European/American background [18], substantiating the need for a genetic signature to monitor CLL development. Of note, CLL incidence in the Asian populace of 'higher-risk' countries is no different from that of those who have not emigrated [18], suggesting the factors affecting CLL development between races are more genetic than they are environmental. Nine genetic loci have been identified as a result of genome-wide association studies (GWAS) that contain genes that are transcriptionally active in CLL and are involved in the control of immune function or B-cell

development [19]. Additional investigation by Went *et al*. revealed shared risk loci between GWAS of CLL and myeloma patients that are affected by changes to B-cell regulatory components that themselves regulate genes involving B-cell development [20]. These studies encapsulate how CLL aetiology can emerge from the dysregulation of genes involved in healthy B-cell development. Additionally, susceptibility to herpes zoster, respiratory tract infection or cellulitis correlates with an increased risk of CLL development [21-23], perhaps due to preceding immune defects. Further, hypogammaglobulinaemia is prevalent in many CLL patients and is sometimes diagnosed prior to CLL as the primary disease [24, 25].

Environmental risk has also been associated with CLL development, including exposure to pesticides (deltamethrin) [26] and herbicides. Agent Orange, a herbicide mixture used as part of the herbicidal warfare program of the Vietnam War, has been extensively studied due to its implications on the development of leukaemias and lymphomas [27]. It has been reported that Radon exposure leads to similar complications [28]. There are mixed views on the implications of exposure to ionising radiation on CLL development; studies of Japanese survivors of atomic bomb blasts did not reveal any changes in CLL incidence [29]; however, people exposed to radiation as a result of the Chernobyl power plant meltdown harboured an increased incidence of CLL development [30-32], suggesting a potential link between ionising radiation and CLL incidence, though this needs further consideration.

1.2. CLL diagnosis, staging and prognostic stratification

This section will discuss the diagnostic guidelines set out by the International Workshop on CLL (iwCLL), outlining the appropriate clinical diagnosis, staging and prognostic stratification of CLL [10, 12].

1.2.1. Diagnosis

In most Western countries, CLL is diagnosed *via* blood testing and subsequent immunophenotyping. During a routine medical check, if a patient is found to have elevated lymphocyte levels in a complete blood count (≥5 x10^9/L lymphocytes in the PB, sustained for ≥3 months) [2, 12], flow cytometry will be conducted to assess lymphocyte clonality, typically involving Ig light chain restriction - CLL cells identified through this method will have large nuclear and small cytoplasmic components [12]. Patients will be typically asymptomatic at the time of diagnosis. However, during disease progression, symptoms such as weight loss, lethargy, night sweats and reports of swollen glands are common [2]. Immunophenotyping to detect CLL cells *vs.* 'healthy' B-cells and B-cell malignancies was first established in 1994, utilising CD5 and CD23 markers as well as surface Ig and CD22 expression. This has now been updated by collaborations between the European Research Initiative on CLL (ERIC) and the European Society for Clinical Cell Analysis (ESCCA) - establishing CD19, CD5, CD20, CD23, κ and λ Ig light (L) chains as "required" for CLL diagnosis. Other markers such as CD79b, CD81 and ROR1 have been designated "recommended" for diagnosis of those with 'borderline' CLL [12, 33].

1.2.2. Staging

Classical methods for stratifying CLL patients involve the use of two staging principles: the Binet and Rai systems, to subcategorise CLL patients according to disease 'risk' [34, 35]. The simplicity of staging allows for an inexpensive method to determine patient treatment strategies (or lack thereof) by utilising standard laboratory testing. Both staging systems outline three major prognostic cohorts that determine clinical outcomes for patients.

Rai staging classifies patients according to the prevalence of CLL-associated symptoms; patients deemed 'low-risk' are those with lymphocytosis concurrent with the presence of leukaemic cells (>30% lymphoid cells, termed Rai stage 0);

‘intermediate-risk’ patients exhibit lymphocytosis as well as enlarged lymph nodes (LN), splenomegaly and/or hepatomegaly (termed Rai stage I-II); ‘high-risk’ patients will manifest these disorders as well as thrombocytopaenia (platelet count: $<100x10^9$/L) and disease-related anaemia (haemoglobin levels: <11 g/dL, termed Rai stage III-IV) [36, 37]. Binet staging, however, bases its approach on a combination of the number of ‘affected areas’ and the prevalence of anaemia/thrombocytopaenia; ‘affected areas’ considered are enlarged LNs with a diameter of >1 cm or the presence of organomegaly; Binet staging considers particular areas of LNs as well as enlargement of the spleen and/or liver. CLL patients will be assigned to one of three stages: A, B, or C depending on the symptoms described above [36]. Although Rai staging is commonly used in the United States, Binet staging is preferred clinically within Europe [38].

1.2.3. Prognostic stratification

Historically, Rai and Binet staging methods grouped CLL patients to quickly and simply determine treatment approaches. However, due to the subjective nature of the staging systems and the difference in disease characteristics on a patient-patient level, they were considered insufficient to classify distinct CLL prognostic subgroups [39]. As such, a scoring system based on prognostic markers was developed: the CLL International Prognostic Index (CLL-IPI) [40]. The CLL-IPI aims to provide an accurate, comprehensive picture of disease ‘risk’ according to a combination of clinical, biological and genetic information [39, 41-43]. Namely, the CLL-IPI scores patients on a ‘weighted’ scoring system using five prognostic factors: patient age; clinical stage (Rai/Binet); serum $ß_2$-microglobulin levels; *IGHV* mutational status; and *TP53* mutation and/or deletion (Table 1.1). Of note, only those classified as ‘high-risk’ or ‘very high-risk’ as part of this scoring system would be subject to treatment, as treatment of early-stage CLL has been shown to have no therapeutic benefit [44-46]. The CLL-IPI (described in Table 1.1) has been validated in various studies, demonstrating its effectiveness at stratifying CLL patients in different contexts [47, 48].

Prognostic factor	Indicator of risk	Scoring
Age	>65 years	1
Clinical stage	Rai I-IV / Binet B/C	1
B2M levels	>3.5 mg/L	2
IGHV mutational status	Unmutated	2
TP53 status	Deleted (del(17p13)) and/or mutated	4
	Total risk score:	0-10
	Low	0-1
	Intermediate	2-3
	High	4-6
	Very High	7-10

Table 1.1: The CLL-IPI [40, 49].

1.3. CLL prognostic/predictive factors

1.3.1. Prognostic factors

As mentioned above, several prognostic factors can be associated with CLL disease characteristics, and subsequently patient 'risk' and treatment requirements. Prognostic factors have evolved over the years to include, not only generic Rai/Binet staging and patient age, but also genetic and chromosomal alterations that reflect the variability of disease biology seen between patients. These determinants can be used as a way of assessing disease prognosis in the absence of treatment. Of note, prognostic biomarkers can also be classed as 'predictive', whereby the presence of said biomarker has implications on the effectiveness of treatment. An example of a predictive biomarker is the presence of *BCR/ABL1* transcript (due to the typical translocation event) and the subsequent use of tyrosine kinase inhibitors in Chronic Myeloid Leukaemia [50].

1.3.2. *IGHV* mutational status

During maturation in germinal centres (GCs), B-cells are induced to generate high-affinity antibodies *via* somatic hypermutation (SHM) of their BCR to produce a mature, specific, functional BCR. This is achieved through high-frequency point mutations at hypervariable sites within *IGHV* and *IGLV* genes, producing a variety of amino acid conformations within the BCR variable regions [51]. Further, variability in the mutational status of *IGHV* is a known and prominent prognostic and predictive CLL biomarker, whereby *IGHV* mutational status can be associated with disease progression and response to treatment. Of note, 'mutated' *IGHV* genes are described as those with <98% identity compared to that of germline *IGHV* nucleotide sequences [50]. In 1999, Hamblin *et al*. reported that - after sequencing *IGHV* within 84 CLL patients – 45.2% of patients showed *IGHV* sequence homology reflecting that of the nearest germline gene, while 54.8% of patients showed somatic *IGHV* gene mutation. Within this study, those in the unmutated *IGHV* (U-CLL) gene cohort displayed reduced survival, advanced staging and disease progression compared with those in the mutated *IGHV* (M-CLL) cohort. Interestingly, these clinical outcomes persisted irrespective of prior Binet staging [7]. These outcomes have been validated in other studies [6, 52], as well as in systematic review and meta-analysis [53]. As well as wider mutational status, the activity of particular *IGHV* genes has also been linked to CLL prognosis: *IGHV3-21* activity is demonstrated to affect disease progression, while *IGHV4-39* activity is suggested to be involved in Richter's transformation [54-56], further indicating the importance of *IGHV* status and expression in CLL progression. Of note, Richter's is the transformation of CLL into a more aggressive lymphoma, affecting 2-10% of CLL patients and has dismal outcomes (described in [57]).

Those with U-CLL have a phenotype resembling a pre-germinal, $CD5^+$ centre B-cell [58], including higher sIgM levels [52], higher ZAP70 levels [59] and a more poly-reactive BCR [60], demonstrating an increased predisposition for BCR signalling in leukaemic cell populations. In contrast, M-CLL patients exhibit a phenotype mimicking B-cells following prolonged antigen exposure within the

germinal centre (GC) [58], including lower signalling affinity. As such, M-CLL cells exhibit more favourable prognostics [61].

“Stereotyped” BCRs are also common in CLL patients, with 30% of patients displaying homogenous BCR expression [62]; this is primarily due to the retention of a variable heavy complementarity determining region 3 (VH-CDR3) between CLL patients [62] - a trait shown to occur in 30-35% of CLL patients, the majority of which are found within U-CLL patients [62]. An in-depth analysis by Agathangelidis *et al*. determined that 23 subsets of *IGHV* sequence stereotypy were shared between 12% of unrelated, geographically independent patients from a series of 21,123 *IGHV* sequences [62], indicating that the origins of CLL stereotypy are not random and instead emanate from a common determinant [61]. Between subsets, patients exhibit variable prognoses associated with *IGHV*, apparent genetic lesions and BCR function. Subset #1, for example, reports patients exhibiting a poor prognostic type U-CLL, while those in subset #4 are shown to exhibit an indolent M-CLL. Subset #1 is reported to display increased IgM-crosslinking-mediated CLL cell proliferation compared to that of other U-CLL subsets, perhaps due to the presence of homogenous VH-CDR3s where other subsets express VH-CDR3 heterogeneity [63]. These studies further support the importance of *IGHV* status and composition in disease progression and subsequent prognosis.

1.3.3. Somatic mutations and genetic lesions

Although apparent, somatic mutations within CLL are not stochastic and rather affect pathways such as those involved in B-cell proliferation and survival. Advancements in whole exome sequencing (WES) have revealed previously unrecognised driver genes which are mutated in CLL [64-69], increasing our understanding of the relationship between the CLL genetic environment and its impact on clinical outcomes. Some novel driver genes revealed from WES are described below (Table 1.2).

Signalling Pathway	Recurrent gene mutations
Microenvironment-dependent signalling	*NOTCH1, FBXW7*
Inflammatory response	*MYD88*
MAPK signalling	*BRAF, KRAS, NRAS, MAP2K1*
NF-κB signalling	*BIRC3, TRAF3, NFKBIE*
DNA damage	*ATM*
Cell cycle	*ATM, TP53, SAMHD1, POT1*
Chromatin modification	*HIST1H1E, CHD2, ZMYM3*
Transcription	*EGR2, IRF2, BCOR, MED12*
Ribosomal processing	*XPO1, SF3B1, RPS15*

Table 1.2: Recurrent somatic mutations within CLL cells [50, 65, 66].

Somatic mutation of distinct genes has now been established as prognostic markers and, in some cases, predictive markers of CLL prognosis [50]. This includes mutations to *TP53, NOTCH1* and *SF3B1* genes. *TP53* abnormalities exhibit highly detrimental clinical outcomes: throughout CLL progression, *TP53* abnormalities (mutation, deletion or a combination of both) will rise from 4%-8% at the time of diagnosis up to 30-40% in relapsed/refractory (R/R) CLL, and even 50-60% in Richter's syndrome, as *TP53* abnormalities can be acquired over the disease course [50]. Patients with *TP53* abnormalities have a median overall survival (OS) of 3-5 years [70], are much more likely to fail CIT and have an increased probability of Richter's transformation [71]. This has been validated *via* systematic review and meta-analysis [53]. Of interest, therapies targeting BTK (ibrutinib and ibrutinib analogues)-, BCL2 (venetoclax)- and PI3K (idelalisib)-mediated signalling are shown to successfully treat those CLL patients with *TP53*

abnormalities, primarily in R/R disease, thereby demonstrating the effectiveness of targeted therapy over standard CIT [72-74].

NOTCH1 and *SF3B1* mutations are apparent in 10-15% of newly diagnosed CLL, which increases to ~20% in progressive/relapsed CLL [65]. These mutations are found in intermediate-risk patient subsets, with survival rates 50% less than that of the general population [70]. Patients with these mutations have shorter time to progression, and faster relapse rates if the preceding treatment involves CIT [50]. Further, patients with *NOTCH1* mutations also have increased risk of Richter's transformation [56, 71, 75]. Clinically, *NOTCH1* mutation has been identified as an independent risk factor for shorter progression free survival (PFS) as part of the UK LRF CLL4 trial which compared different chemotherapies [76], although subsequent CLL8 and CLL11 chemotherapy trials have not been able to produce the same results [77, 78]. Further clinical trial involving anti-CD20 monoclonal antibody (mAb) treatment combined with chemotherapy has identified further links between *NOTCH1* mutation and inferior PFS [78, 79]. Therefore, it was concluded that *NOTCH1* mutation could be used as a predictive marker to determine responsiveness to CIT [50]. Indeed, the prevalence of 'driver' aberrations (*TP53* mut/del, del(17p), *IKZF3*) reflect the leukaemic 'clonal evolution' of CLL cells, whereby CLL can adapt to specific selection pressures to maintain or enhance disease progression.

Treatment-induced mutation is also apparent in patients treated with targeted therapies, leading to reduced patient responsiveness to treatment which was initially highly effective. A leading example is the emergence of *BTK* (C481S) and *PLCG2* (R665W) mutation following ibrutinib treatment [80]; these mutations are apparent in ~85% of CLL patients with acquired ibrutinib resistance, and affect the binding affinity of ibrutinib to BTK or allow for activation of *PLCG2* irrespective of BTK activity, respectively; as such, they can be detected up to 15 months before relapse and are strongly associated with ibrutinib efficacy, perhaps due to the emergence of ibrutinib-resistant leukaemic populations from small CLL subclones that have acquired *BTK*/*PLCG2* mutation [80]. More investigation is needed into the repercussions of developing such mutations.

However, the emergence of next generation BTK inhibitors has shown promise in treating ibrutinib-resistant CLL, perhaps due to changes in specificity to BTK and binding properties (i.e. covalent vs non-covalent (reviewed extensively in [81]). Nevertheless, these mutations demonstrate the divergent and adaptable nature of CLL genetics in response to pressures such as drug-mediated cell kill.

1.3.4. Cytogenetic alterations

Several cytogenetic aberrations are present in CLL and confer disease characteristics due to alterations in the activity of genes pivotal to cell function. So, as well as the somatic mutations described above (section 1.3.3), CLL cells can hijack the genetic environment by possessing chromosomal alterations affecting the expression of distinct genes. Consequently, these aberrations are strongly linked to disease prognosis.

A hallmark paper initially describing these alterations revealed chromosomal aberrations in 82% of patients. The major aberrations revealed by this study were three forms of chromosomal deletion and trisomy 12: del(13q) (55% of total aberrations), del(11q) (18% of total aberrations), del(17p) (7% of total aberrations), and 12q trisomy (16% of total) [5]. Here, patients were grouped according to major chromosomal aberrations and disease prognosis was monitored. Del(13q), the most common aberration, conferred an indolent CLL (median survival: 133 months) [5]. Patients with a single chromosomal lesion of del(13q) typically had great clinical outcomes, reflected by a progression rate of <1%/year, longer PFS and a low risk of transformation [5]. The targeted region of 13q (13q14) harbours microRNA (miRNA) sequences *miR15A* and *miR16A* [82], which regulate major components of apoptosis and the cell cycle [83]. It has been reported that deletion of these miRNAs alleviates miRNA-mediated B cell lymphoma 2 (*BCL2*) gene expression, leading to its subsequent upregulation [84]. Supporting this, Klein *et al*. demonstrated that miR15A and *miR16A* deletion promote CLL development and tumour cycling in CLL mouse models [83]. BCL2, a protein with antiapoptotic characteristics, is overexpressed and contributes

heavily to CLL pathogenesis; effective CLL treatment *via* selective inhibition of BCL2 via BH3 mimetics (venetoclax) [85] demonstrates the importance of BCL2 in CLL survival. On the other hand, del(13q) can also be associated with inferior outcomes as this genomic region also incorporates other crucial genes including *RNASEH2B* – whose codeletion with miR15A & miR16 promotes resistance to therapies targeting DNA damage components [86], highlighting the bimodality of chromosomal deletions and their influence on prognosis. Del(11q) is found in patients with a more aggressive CLL (median survival: 79 months) [5]; Del(11q) results in Ataxia-telangiectasia mutated (*ATM*) gene deletion (del(11q22-23)) and is found in <10% of diagnosed CLL, rising to 30% during disease relapse [50, 70]. Patients with del(17p) exhibit the worst prognoses, with disease characteristics such as rapid disease progression and a lack of responsiveness to chemotherapy-containing treatments due to them functioning through genotoxic means and requiring *TP53* activity [87]. It is because of this that del(17p) is considered a prognostic and predictive biomarker, while the other major chromosomal aberrations (11q, 13q and T12) are only considered prognostic markers [50]. The combined emergence of gene mutation and/or deletion [36] (e.g. *ATM, TP53*) *via* chromosomal lesion highlights the dynamic nature of CLL and its ability to override and overcome mechanisms that would typically block cancer development. Finally, patients with trisomy 12 experience an indolent CLL (median survival: 114 months) [5], though these patients experience an increased frequency of *NOTCH1* mutations – a characteristic also present in 1/3 of Richter's cases [88].

1.3.4.1. 'Complex karyotype' CLL

A number of patients exhibit complexities with regard to cytogenetic abnormality: CLL patients with three or more structural/numerical abnormalities within the same clone are defined as exhibiting complex karyotype (CK) CLL - a classification present in other haematological malignancies [89]. CK was first associated with disease prognosis by Juliusson *et al.*, where CLL patients with multiple chromosomal aberrations displayed poor clinical outcomes *vs.* patients with normal karyotypes [90]. Further study within CLL patient cohorts has

revealed CK prevalence in ~15% of patients, and is associated with U-CLL, 17p/11q deletions and subsequent abysmal clinical outcomes [91]. Baliakas *et al*. described multiple levels of CK complexity. Within a large retrospective study within an intra-continental patient cohort of >5,000, patients could be grouped according to the number of aberrations possessed (e.g. low-CK: 3 aberrations, high-CK: ≥5 aberrations); patients with high-CK CLL displayed much poorer clinical outcomes than those in other subgroups [92], further demonstrating the association between CK and disease prognosis. This highlights the variability of CLL disease biology between patients. The importance of CK in treatment responsiveness has also been addressed: patients with CK are less responsive to ibrutinib monotherapy and have reduced PFS and OS compared to patients with ≤2 chromosomal aberrations [93]. Investigation into therapies involving a combination of either Idelalisib or Venetoclax with Rituximab (IR/VenR) have revealed poorer treatment responses in those with CK [94, 95]; reduced efficacy of targeted therapies in patients exhibiting CK CLL may perhaps be due to patient CLL harbouring multiple high-risk features that combined drive drug resistance, such as a combination of unmutated *IGHV* and *TP53* deletion *via* del(17p) [93].

1.3.5. Consideration of other prognostic biomarkers

Other prognostic markers are prevalent in CLL and should be considered to further understand the heterogeneity of CLL disease biology. For example, the surface expression of CD38 is found to be elevated within U-CLL patients [6]. As such, CD38 expression is associated with shorter PFS, shorter time to first treatment and reduced OS [6]. One model proposes that CLL cells with increased CD38 expression are more sensitive to CXCL12, thereby promoting CLL-lymphoid tissue migration to enhance CLL-TME interactions [96]. Another established prognostic marker is that of 70-kDa zeta-associated protein (ZAP70) expression. ZAP70 is not expressed in normal mature B-lymphocytes [97], and its expression is highly associated with U-CLL [98]. As such, it is strongly considered as a surrogate marker for *IGHV* mutational status, and is readily detected via flow cytometry or immunohistochemistry versus the more technical profiling of *IGHV*

status. As a member of the Syk-ZAP70 protein tyrosine kinase family, it is a vital component of CLL-T/NK-cell interactions [99] and is therefore associated with increased BCR-mediated signalling in CLL cells [100]. Study by Schroers *et al*. demonstrated ZAP70 could be profiled in conjunction with CD38 expression as prognostic markers, where increased expression of both markers is associated with poorer clinical outcomes [101].

1.4. The CLL tumour microenvironment

CLL cells are found in circulating PB and BM compartments. However, *in vivo* studies have revealed that it is within SLOs that CLL cells are provided with signals from accessory cells to induce proliferation and survival [102, 103]. This has been demonstrated *in vitro* through rapid and profound apoptosis of *ex vivo* CLL cells unless co-cultured with either BM stromal cells (BMSCs) [104] or monocyte-derived nurse-like cells (NLCs) [105]. This is known as the CLL tumour microenvironment (CLL-TME), in which a small population of a patient's monoclonal cells will reside and undergo massive proliferation. The rest of the CLL cell population will be found in a 'resting' state, awaiting entry to, and proliferation within, SLOs [106]. Befitting survival and proliferation, CLL cells within SLO compartments have morphological, immunophenotypic and expression uniqueness to PB- and BM-resident CLL cells [107]. Within SLOs, CLL cells accumulate into "pseudofollicles" or "proliferation centres" (PC) - a characteristic histopathological observation in CLL patient SLOs [107]. Here, CLL cells replicate in the range of 0.1-1% of the entire clone in a 24-hour cycle [108]. PB- and BM-resident CLL fated for SLO PCs migrate by the activity of distinct chemokine receptors (e.g. CXCR4/CXCR5) and adhesion molecules (e.g. VLA-4) [105, 109]. The abrogation of CLL-SLO migration *via* ibrutinib's influence on CXCR4/5 activity (through VLA-4 inhibition [110]) highlights the importance of migratory signalling in CLL pathogenesis. Indeed, the importance of wider TME signalling in CLL pathogenesis is of clinical interest, as novel therapeutics targeting CLL-TME crosstalk could impede such communication and therefore

improve CLL treatment. The following sections will describe CLL-TME interactions enabling effective CLL proliferation and survival in different tissue compartments, as well as the ways by which CLL cells manipulate their surrounding cellular environment to promote these interactions and to evade immune suppression.

1.4.2. Supportive cell differentiation and inflammatory/soluble factor signalling

A number of cell types are characterised as CLL accessory cells, including mesenchymal stem/stromal cells (MSCs); NLCs; T-cells, natural killer (NK) cells; endothelial cells (EC) and follicular dendritic cells (FDC). CLL-mediated polarisation of the TME niche gives rise to functions characteristic of CLL pathogenesis such as: (1) inflammatory signalling (NK cell/MSCs); (2) immune evasion (NK cell/T-cell); (3) survival/proliferation (T-cell/NLCs); and (4) CLL migration to SLOs (NCLs/MSCs) (Figure 1.1; reviewed in [111]). CLL cells promote MSC activation by platelet-derived growth factor (PDGF) secretion, subsequently inducing PI3K signalling and an upregulation of vascular endothelial growth factor (VEGF) secretion [112]. CLL-MSC interactions have also been shown to induce MSC protein-kinase-C beta (PKCβ)/NOTCH2 cascades, amplifying MSC NF-κB signalling and thereby enhancing CLL cell survival [113, 114]. Additionally, Vom Stein *et al*. demonstrated that CLL cell survival in *in situ* LNs requires stromal overexpression of LYN kinase – a characteristic that polarises MSCs *via* inflammatory signalling [115]. As such, MSCs promote the CLL-TME by an enhancement of pro-inflammatory cytokine secretion, as well as gene signatures involved in the production of the extracellular matrix and/or wound healing [116]. This creates a positive feedback loop, driving CLL cells to further produce inflammatory cytokines themselves [116]. These findings demonstrate the importance of MSCs in providing positive signalling feedback to induce CLL proliferation and survival within the microenvironmental niche.

CLL cells have also been shown to affect PB-circulating monocyte populations, actively transforming them into supportive NLCs – a finding first described in *in vitro* study by Burger *et al*. [105]. Here, due to NLC differentiation, CLL cells were protected from spontaneous apoptosis *via* binding of stromal cell-derived factor-1 (SDF-1) to CLL-CXCR4 receptors [105]. NLC differentiation has been further characterised in *in vivo* study, akin to that of tissue-resident macrophage populations [117]. Further, NLC differentiation has been shown to be induced *via* CLL-derived IL-10 release [118], as well as interactions with CLL death markers (HMGB1) [119], highlighting the diverse range of ways through which accessory cells are attuned to support CLL proliferation and survival. NLCs can also secrete pro-inflammatory CXCL12, a cytokine recognised by membrane-bound CXCR4 on CLL cells [111]. CXCR4 is overexpressed in CLL [120], and its activation is crucial for inducing BCR-mediated signalling cascades to promote proliferation and survival [121]. Of note, CXCR4 can be used as a marker (in conjunction with CD5) to discern PB- to LN-resident CLL cells [122]. NLCs also secrete CXCL13, which has binding affinity for CLL-CXCR5, producing effects akin to that of CXCR4 activation [109]. Moreover, NLCs, in conjunction with MSCs, ECs, T-cells and NK cells, secrete B-cell activating factor (BAFF) ligand and a proliferation-inducing ligand (APRIL) [123, 124], both of which bind to CLL cells *via* TNF receptors (BAFF-BAFFR, APRIL-BCMA/TACI) and induce downstream NFκB and BCR crosstalk [125, 126]. Indeed, other soluble co-factors can induce CLL cell proliferation and survival. For example, CpG binding to toll-like receptors (TLRs) can facilitate BCR activation [127]; this can be enhanced in the presence of IL15 cytokine [128]. Additionally, CLL and TME-resident accessory cells can relay information *via* extracellular vesicles (ESVs), allowing for the crosstalk of cellular material. The use of ESVs as novel prognostic markers due to their roles as mediators of CLL-TME communications is currently in discussion [129]. CLL cells can further shape the leukaemic TME by recruiting T-cell populations: CCL3 and CCL4 cytokines are secreted by CLL cells to recruit $CCR5^{+}$ regulatory T-cells (T_{reg}), while CCL17 and CCL22 can recruit other T-cell populations [130].

ECs are also utilised by CLL cells; CLL-EC adhesion promotes CLL cell activation, drug resistance and survival, concurrent with an increase in secretion of endothelium-enhancing neuroendocrine polypeptide (e.g. CgA) [131], which enhances both CLL and supportive cell populations. EC migration, proliferation

and subsequent angiogenesis are further enhanced by CLL-EC-mediated activation of MAPK/AKT/NFκB signalling [132]; an early *in vitro* study by Panayiotidis *et al*. revealed a reliance of CLL cells on FDC populations, whereby CLL cells are induced to survive *via* FDC-mediated CD44 ligation and subsequent MCL1 upregulation [133].

1.4.3. Direct cell-cell TME interactions

Inflammatory signalling drives CLL cells towards SLOs, in which they interact with supportive cells to induce rapid proliferation - a process not seen in other tissue subpopulations [102, 103]. Within SLOs, CLL cells are exposed to heightened BCR, NF-κB, NOTCH and MYC signalling, as well as an enhancement of JAK/STAT, MAPK/AKT and TLR signalling [102, 134-136]. These pathways work in partnership to induce potent proliferative and survival signals critical to CLL pathogenesis. For example, VLA4 ligand binding to VCAM-1 on MSCs can stimulate NF-κB signalling in CLL cells; Park *et al*. demonstrated that VCAM-1-mediated VLA4 ligation reduces CLL chemosensitivity *via* upregulation of BCL-XL [137]. Transmembrane NOTCH receptors expressed by CLL cells can bind to their respective NOTCH ligands expressed by supportive cells, initiating the CLL-intrinsic release of transcription-regulating NOTCH proteins [138]. NOTCH protein and gene signatures are overexpressed and frequently mutated in LN CLL populations – characteristics established as prominent drivers of CLL pathogenesis (see **section 1.3.3** [65, 136, 139, 140]). As mentioned in section **1.3.5**, overexpression of CD38 in LN-CLL subpopulations is associated with poor clinical outcomes [6]. CD38 can induce CLL proliferation and survival *via* interactions with CD31 on NLC, EC and T-cell populations. These interactions induce CLL cells to express CD100 - a ligand with binding affinity for FDCs, MSCs and $CD4^+$ T-helper cells, orchestrating a complex, multi-cellular interaction event to enhance CLL proliferation and survival [141]. Further, CLL cells possess a TNF receptor involved in cell-cell interactions: receptor activator for NF-κB ligand (RANK) - a TNF receptor with binding affinity for RANK ligands (RANKL) on the MSC cell surface [111]. Alankus *et al*. demonstrated elevated RANK expression in CLL cells *in vivo*, where hyperactive RANK signalling induced a CLL-

like disease and RANK inhibition prohibited disease progression *in vivo* and *in vitro* [142], highlighting its potential importance. Examples of CLL-TME interactions are illustrated below (Figure 1.1).

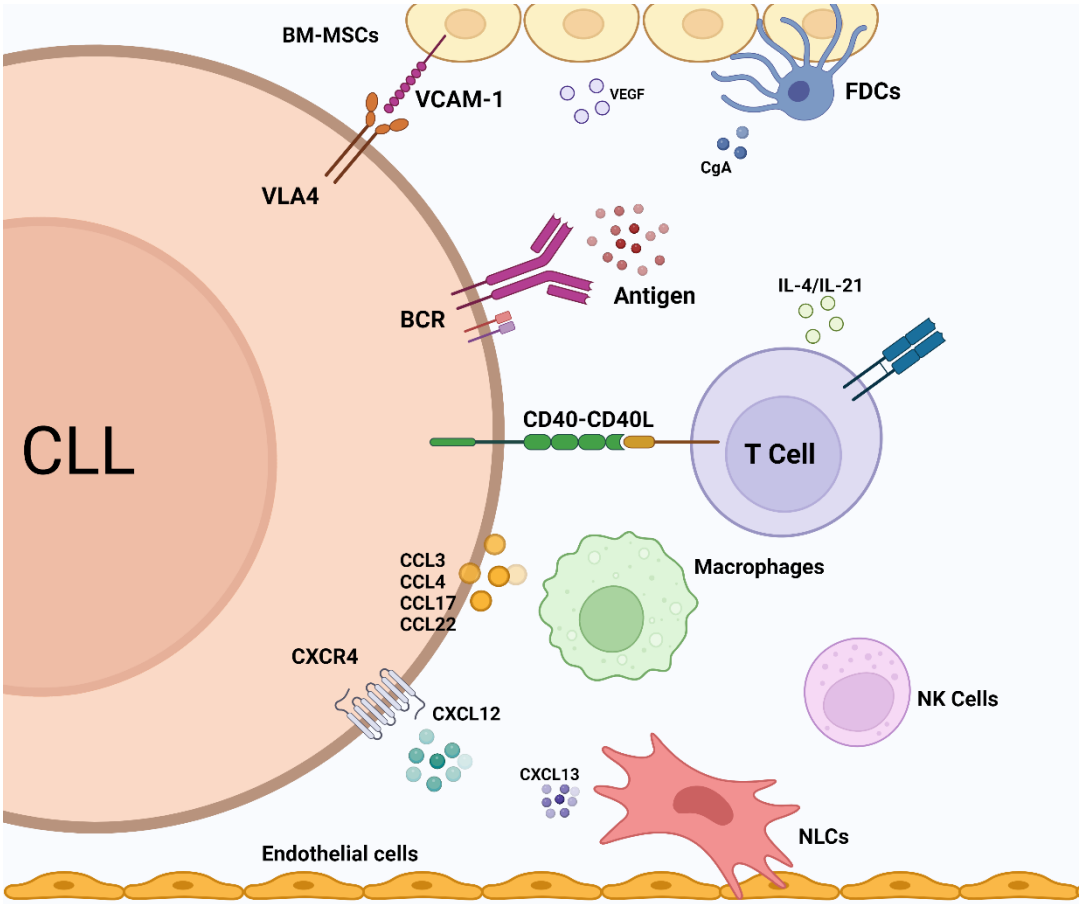

Figure 1.1: The CLL tumour microenvironment. CLL cell interactions with accessory cells are vital to promote proliferation and survival (Modified from [143]).

1.5. BCR-mediated signalling

BCR-mediated signalling is a primary driver of rapid and diffuse proliferation in SLO-resident B lymphocytes [102, 103]. CLL proliferation is considered to emanate primarily from BCR-mediated signalling (much like healthy B-cells) in lymphoid tissue compartments. Here, CLL cells generate a pseudofollicular niche akin to that of mature B-lymphocytes [144] where they engage with follicular T-helper (Tfh) cells [145]. Deuterium labelling revealed that proliferation occurs only in SLO-occupying CLL cells [103] - an observation validated by gene expression studies, revealing massive upregulation of BCR and NF-κB pathway gene signatures [102]. Furthermore, deuterium labelling of CLL cells revealed an

abrogation of CLL cell proliferation following ibrutinib treatment [146]. Of note, it is BCR signalling that is the predominant signalling pathway activated in the LN-CLL pseudofollicle architecture [107]. Indeed, the association of CLL prognosis with *IGHV* mutational status further implies BCR signalling dependency in CLL cells [107]. Here, we will discuss BCR-mediated signalling in the context of B-cell development, maturation, and how this vital signalling axis is exploited by CLL cells to elicit strong tumourigenic effects (reviewed in [61]).

1.5.1. BCR maturation

B-cell development emanates from BM-residing HSCs. Upon exposure to particular selection pressures, HSCs differentiate into common lymphoid progenitor (CLP) cells, which are driven to commit to the B-cell lineage via the expression of particular gene signatures (described further in **1.10.3)** [51]**.** CLP cells committed to the B-cell lineage (progenitor (pro)-B-cells - the first B-cell progeny to express CD19 [147]), undergo maturation processes to then develop into pre-B cells expressing a pre-BCR.

1.5.1.1. VDJ recombination

Pre-B-cell development relies on rearrangement of IgH segments (VDJ recombination), followed by the rearrangement of V and J regions on BCR light chains (IgL) [148]. It is in part due to the high number of BCR V, D and J regions that B-cells exhibit BCR hypervariability – a characteristic essential for the development of effective mature B-cell's in the adaptive immune response (variety of BCRs generated: $\leq 3x10^{11}$ [149]). The IgH incorporates coding regions for 123-129V, 27D and 9J genes [150], giving rise to variable, distinct BCR architecture with high affinity for antigen. Pre-B-cells first undergo D-J rearrangement, then subsequent V-DJ rearrangement, which leads to pre-BCR

expression – an immature BCR precursor with a "surrogate" light chain (consisting of VpreB (CD179a) and λ5 (CD179b) proteins) [61, 151]. Differentiation of pre-B-cells to immature B-cells relies on further BCR differentiation; at this step, pre-B-cells undergo IgL V-J recombination, replacing the surrogate light chain to produce a mature BCR in an M-isotype formation (IgM). Mature BCRs then recruit membrane-resident Igα/Igβ subunits (CD79a/CD79b) - an association crucial for transducing BCR-mediated downstream signals [152]. At this stage, any immature B-cells with autoreactive BCRs are isolated and destroyed *via* apoptosis [61]. If the immature B-cells in question express non-autoreactive BCRs, they are allowed to further mature and eventually express a combination of mature BCRs with Ig heavy chains in both M- and D-isotypes (IgM^+ IgD^+) [149].

Following antigen binding, mature IgM^+IgD^+ B-cells then migrate to GCs and undergo SHM events to positively select B-cells with enhanced antigen-binding affinity [61, 149]. Class-switch recombination (CSR) can also occur in GCs, further diversifying BCR architecture; CSR results in the formation of IgG, IgE and IgA heavy chain isotypes, all of which are vital in responding to invading pathogens. This is achieved by the substitution of IgM (μ) and/or IgD (δ) constant regions by γ, ε, or α, respectively [61]. Indeed, BCR signalling in GCs is crucial for B-cell differentiation to produce either memory or plasma B-cells following interactions with distinct cellular or molecular components within the GC [149]. Interestingly, while it is well established that CLL originates from mature B-lymphocytes, an existence of 'stem-like' cells that premeditate CLL development has been purported [153]; one such argument for the existence of 'stem-like' CLL cell populations in PB and SLO compartments is due to the discovery of pre-CSR B-cell populations in IgG-expressing CLL patients that express CLL-specific *IGHV/D/J* mRNA transcripts [154]. Furthermore, differentiation of CLL cells into Ig-secreting plasma cells has been reported [155]. These findings allude to the presence of distinct 'stem-like' malignant B-cell clones, though more work would be needed to pinpoint potential alternative origins for CLL.

1.5.2. Structure of the BCR

The major structural components of the BCR are the membrane-bound Ig (mIg), associated non-covalently with a disulfide-linked Igα/Igß (CD79a/b) heterodimer, which expresses cytoplasm-facing immunoreceptor tyrosine-based activation motifs (ITAMs) [156, 157]. The mIg itself works on a basis of 1:1 stoichiometry [158], consisting of two mIg chains in a Y-formation [157]. The mIg can be further subdivided into two domains: (1) a flexible fragment antigen-binding (Fab) region – the site of antigen binding, and (2) the fragment crystallisable (Fc) region – the tail-end of the mIg that is associated with the cell membrane [157]. The Fab domains contain the variable regions of the mIg (V_H/L_H) and is bound to the Fc region, which is the site determining the mIg isoform [61]; for BCR-IgD, the Fc region consists of four constant Ig heavy chain domains (C_H), while the BCR-IgM incorporates five constant domains [159]. These constant domains are linked by recurring lysine-valine-lysine (KVK) amino acid sequences [159]. The mIg itself does not have signalling capacity, however, its association with Igα/Igß triggers downstream signal activation [157]. This is achieved *via* ITAM motifs incorporated into the cytoplasmic region of Igα/Igß. ITAM motifs consist of a conserved sequence of four amino acids, beginning with a tyrosine residue and ending in either a leucine or isoleucine (YxxL/I). This sequence is typically repeated twice, separated by 7-12 amino acids ($YxxL/I_{7\text{-}12}YXXL/I$) [160].

The basic structure of the BCR is well established, however the complex 3D mIg-Igα-Igß structure remains difficult to pinpoint, thus the mechanisms by which the BCR complex transduces downstream signals remain elusive [161, 162]. A recent study involving single-particle cryo-EM unveiled novel insights into mIg- Igα-Igß architecture, revealing that assembly of the signalling complex occurs *via* interactions between mIg and Igα/Igß extracellular domains (ECDs), transmembrane (TM) helices and membrane-proximal connecting-peptide regions [163-166]. mIg is also reported to hold the complex in place *via* interactions with Igα/Igß ECDs [166], while Igα/Igß TM helices tightly group together *via* strong polar and hydrophobic interactions [158]. Interestingly, the relative position of mIg to Igα/Igß is reported to be isoform-dependent [166], revealing further

complexity in BCR architecture. Differences in isoform structure allow for BCRs to exhibit distinct roles; IgD isotype BCRs differ from IgM isotype BCRs in mature B-cells in their architecture by the inclusion of a polypeptide “hinge” region located between the Fab and Fc motifs, promoting increased flexibility of the Fab region to allow for polyvalent antigen binding [167], whereas IgM-BCRs display affinity for solely monovalent antigen [61, 149].

1.5.3. BCR signal transduction

As stated, mIg cannot induce signal transduction alone, and so mIg actively recruits Igα/ß (CD79a/CD79b) to enable this [156, 157]. Here, the CD79 heterodimer ITAM motifs are bound to by the LYN, FYN and B-lymphoid tyrosine kinase (BLK) SRC kinases. mIg-antigen binding and subsequent BCR activation mediates the phosphorylation of ITAMs by these SRC kinases [168, 169]. SRC-ITAM phosphorylation promotes the recruitment and phosphorylation of the non-SRC tyrosine kinase: spleen tyrosine kinase (SYK), a major constituent of a signalosome complex to which other signalling proteins are recruited; namely, SYK phosphorylation and activation by CD79-bound ITAMs aggregates B-cell linker protein (BLNK) formation and phosphorylation, which in turn phosphorylates and activates BTK, phospholipase Cγ2 (PLCγ2), VAV and growth factor receptor-bound protein 2 (GRB2) [169, 170]. Mutations in SRC and non-SRC kinases (namely LYN, SYK and BTK) are shown to be detrimental to B-cell development, signalling and overall function [171-173]. Following LYN- or SYK-mediated phosphorylation of BTK (BTK^{Y551}), BTK autophosphorylation facilitates the activation of PLCγ2 (*via* phosphorylation at distinct tyrosine residues such as $PLC\gamma2^{Y753}$) and subsequent signal transduction to the secondary messengers inositol-1,2,5-triphosphate (IP_3) and diacylglycerol (DAG) [174]. IP_3 facilitates Ca^{2+} ion release and NFAT-mediated gene regulation, whereas DAG levels regulate the activity of various signalling pathways: NF-κB, p38, jun N-terminal kinase (JNK) and mitogen-activated protein kinase (MAPK) signalling (i.e. activation of ERK1/2). Of note, DAG and Ca^{2+} achieve this *via* activation of protein kinase Cß (PKCß) [175] (Figure 1.2).

BCR-mediated signalling can also recruit other proximal signalling axes. One such signalling component is the CD19 co-receptor, a B-cell-specific membrane receptor expressing nine conserved tyrosine residue motifs on its cytoplasmic tail [176, 177]. BCR stimulation facilitates the phosphorylation of these tyrosine residues and provides a docking site for the p85α subunit of PI3K (*via* its SH2 domain) [176]. Although critical for PI3K activation, Aiba *et al*. revealed that only a double deletion of CD19 and B cell adaptor for PI3K (BCAP) abrogated activation of PI3K, demonstrating a requirement for BCAP in tandem with CD19 for PI3K activation [178]. Downstream, PI3K activation facilitates the phosphorylation and conversion of phosphatidylinositol-4,5-biphosphate (PIP_2) to an active secondary messenger - phosphatidylinositol-3,4,5-triphosphate (PIP_3). Accumulation of PIP_3 actively recruits phosphoinositide-dependent protein kinase 1 (PDK1) and AKT to the signalling complex, where PDK1 and mammalian target of rapamycin (mTOR) complex 2 (mTORC2) facilitate AKT activation *via* phosphorylation of distinct threonine/serine residues [179]. AKT activation is responsible for a breadth of B-cell functionality *via* direct protein (in)activation, including, but not limited to, cell growth, proliferation and survival. The PI3K-AKT-mTOR axis is described more in detail in sections 1.7 & 1.8. CD19 recruitment can retroactively promote BCR component aggregation [180] and BTK activation [181], highlighting the importance of CD19 recruitment in facilitating BCR signalling.

BCR signalling is tightly controlled by both positive and negative feedback loops to limit its activation and to reduce the incidence of B-cell self-reactivity. An example of this is the regulation of LYN; LYN, albeit a positive effector of BCR signalling, can negatively regulate BCR signalling by favouring immunoreceptor tyrosine-based inhibitory motifs (ITIM) phosphorylation over ITAM phosphorylation [182]. ITIMs are tyrosine motifs resident on the inhibitory co-receptors FcγRIIB and CD22, where ITIM phosphorylation leads to the recruitment of tyrosine phosphatases such as SRC homology region 2 domain-containing phosphatase-1 (SHP-1) – an enzyme involved in tightly regulating BCR

signalling capacity [183]. Signal transduction downstream of BCR activation is outlined below (Figure 1.2).

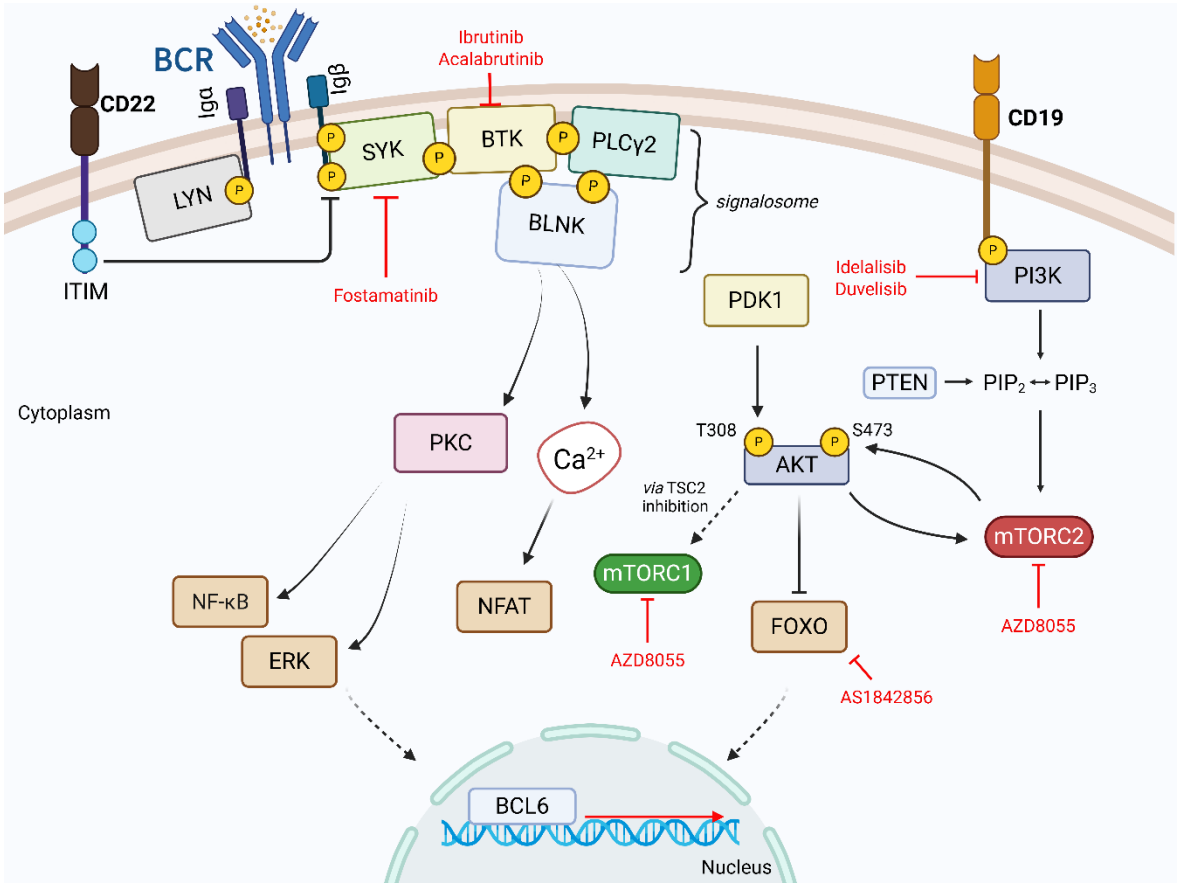

Figure 1.2: The BCR signalling pathway. BCR signalling promotes the proliferation and survival of both healthy B- and CLL cell populations. Highlighted in red are pharmacological inhibitors of distinct BCR signalling components.

1.5.4. BCR signalling in CLL cells

CLL cells are known to exploit BCR signalling to promote proliferation and survival [102]. The existence of 'tonic' BCR signalling in SLO-residing proliferative pseudofollicles [107], and the effectiveness of targeted BTK inhibition to induce CLL cell death and lymphocytosis [146, 184] highlight the dependency of CLL on BCR signalling. Nevertheless, such dependency on BCR-mediated signalling does not infer a diminishment of signalling capacity when compared to LN-resident B-cells. Instead, CLL cells incorporate additional dysfunctionality to their BCR signalling axes to further enhance the already

highly pro-proliferative and survival-promoting effects of typical BCR signalling seen in healthy B-cells. Work by Damle *et al*. demonstrated that CLL cells express a BCR-associated cell surface marker phenotype reflecting that of BCR-activated B-cells [185]. This is supported in work by Muzio *et al*., revealing that major members of BCR-associated signalling pathways (ERK1/2, MEK1/2, NFAT) are constitutively active in CLL patient samples [186]. Other BCR signalling components (PI3K, BTK, PKC) also exhibit increased basal activity [186]. Indeed, LYN and SYK also showed increased expression and activity in CLL [187, 188]. Our group has recently highlighted the importance of PKCβ in modulating key BCR signalling components [189], further addressing the importance of PKC activity in promoting BCR activation and constitutive signalling.

A recent study by Arbel *et al*. revealed that aggressive subtype CLL exhibits 'clustering' of surface BCR components, concurrent with an increase in intrinsic BCR signalling activity [190], demonstrating further complexity of BCR dysfunction associated with disease biology. Additionally, CLL cell BCRs exhibit autonomous BCR signalling in systems devoid of antigen expression. Specifically, the heavy-chain complementarity determining region 3 (HCDR3) was shown to facilitate this, as installation of this sequence into other surface receptors allowed the receptor to exhibit the same autonomous signalling capacity [191]. Interestingly, the downstream effects of autonomous BCR signalling differ in a mIg-isoform-dependent manner [192]. The current paradigm argues that antigen-induced BCR ligation is responsible for massive CLL cell replication in SLO proliferation centres, while autonomous BCR signalling (e.g. from IgM-BCRs) is responsible for mediating CLL cell survival in circulating CLL cells lacking supportive signalling from a tumour microenvironmental niche [193], although this remains to be fully elucidated [107]. Nevertheless, autonomous BCR signalling provides a means for CLL cells to exploit intrinsic BCR effectors to promote CLL proliferation and survival irrespective of antigen presentation.

The mutational status of *IGHV* genes determines the physical functionality of BCR signalling in CLL. As described in section 1.3.2, patients with U-CLL exhibit a much more aggressive CLL subtype associated with an *IGHV* sequence with very

little deviation from B-cell germline sequences [50]. In this subtype, CLL cells exhibit heightened BCR responsiveness due to more permissive antigen recognition, whereas patients with mutated *IGHV* sequences are more selective to antigen, eliciting higher antigen specificity within a smaller pool of recognisable antigen [194]. CLL subtypes exhibit multiple differences associated with signalling responsiveness. For example, M-CLL cells exhibit depleted surface IgM concurrent with constitutive ERK phosphorylation and activated Ca^{2+} signalling, reflecting characteristics seen in 'anergised' B-cells with extended antigen exposure. U-CLL cells, however, express increased BCR-IgM levels concomitantly with increased ZAP-70 [59]. Unlike BCR-IgM, M- and U-CLL cells express similar IgD isotype BCR activity [194, 195]; the fact that BCR-IgD stimulation lacks the same survival and proliferative effects compared to BCR-IgM stimulation [196], and that BCR-IgD is rapidly internalised following its activation [197], suggests an exclusivity of BCR-IgM signalling to promote CLL proliferation and survival in SLOs and in circulation [193]. The permissive nature of U-CLL BCRs allow for stimulation by several self-antigens ('autoantigens') such as vimentin and calreticulin cytoskeletal proteins on NLC and MSC cells [198], as well as binding to apoptotic markers such as non-muscle myosin heavy chain IIA [199] or oxidised LDL [200]. This autoreactivity is associated with BCR pathogenicity and is described in an Eμ-TCL CLL mouse model, where a combination of CLL light chains with virus-specific heavy chains elicited the same permissive BCR autoreactivity seen in U-CLL patients [201], supporting this association between BCR responsiveness and CLL pathogenesis. M-CLL cells are much less autoreactive and have an affinity for specific antigen [61], reflected by their affinity for pathogenic antigen, such as fungal- [60], bacterial- [200] and viral-associated antigens [202].

1.5.4.1. Modulating BCR activity *in vitro*

Experimentally, to gain insights into the mechanisms of BCR ligation and subsequent downstream signalling *in vitro*, CLL cells can be cultured using conditions that successfully mimic different contexts of BCR stimulation seen *in situ*. Early *in vitro* study tried to mimic BCR ligation by the addition of anti-Ig

antibodies and bacterial fragments, such as those from the *S. aureus* Cowan strain [203]. In 2001, Bernal *et al*. demonstrated that BCR stimulation could be effectively triggered by using anti-human IgM $F(ab')_2$, where the addition of $F(ab')_2$ led to massive upregulation of anti-apoptotic protein signatures (e.g. MCL1), as well as an increase in NF-κB and PI3K activity [204]. A follow-up study by Nédellec *et al*. supported these data, revealing that $F(ab')_2$-stimulated CLL cells had increased levels of cell survival concomitant with increased ERK1/2-MAPK activity [205]. Indeed, the *in vitro* responsiveness of CLL cells to $F(ab')_2$ differs according to *IGHV* mutational status [206]. Nevertheless, $F(ab')_2$'s ability to recreate gene expression profiles only seen within LN-resident CLL cells highlights the clinical and experimental relevance of using anti-IgM stimulation to provide novel mechanistic insight into BCR-mediated signals *in vitro* [102]. Since then, other BCR stimulatory models have since been established such as the use of immobilised IgM [207] and co-cultures with either NLCs [208] or vimentin-expressing stroma [198] to induce BCR activation.

1.6. CD40 signalling

Intrinsic CD40 signalling is necessary for facilitating adaptive immunity as a secondary signal component following primary signalling within both T- and B-cells (T- and B-cell receptor (TCR/BCR) activation, respectively). Following activation, T-cells interact with B-cells leading and upregulate B-cell intrinsic, CD40-associated signalling components – a requirement for the activation of the B-cell-mediated inflammatory response [209]. Abrogating CD40 signalling in B-cells is known to produce several immunophysiological defects [210], highlighting the importance of CD40 signalling in normal B-cell function, differentiation and adaptive immunity. Moreover, CD40 signalling is strongly established in CLL pathogenesis: CLL cells promote follicular T-helper (T_{fh}) activation to enhance CLL proliferation and survival in LN PCs [211]. This section will discuss T-cell-mediated CD40 signalling in healthy B- and CLL cells, addressing the typical effects of CD40 signalling; how this signalling pathway is harnessed by CLL cells to enhance pathogenesis; as well as how CD40 can be engaged in *in vitro* models to further mimic the CLL-TME.

The CD40 receptor (TNFRSF5, illustrated in Figure 1.3) is a 48 kDa, type I transmembrane protein found on the B-cell surface. It is a member of the TNFR superfamily - a costimulatory receptor superfamily, consisting of an intracellular domain (90 amino acids); a transmembrane domain (22 amino acids); a 21 amino acid leader sequence and an extracellular domain (193 amino acids) [212]. The CD40 receptor contains 22 evolutionary-conserved cysteine residues throughout its structure - a cysteine-rich profile conserved between TNFR family members [212]. The costimulatory CD40 receptor was first described in B-cells, however, it is known to be expressed in other haemopoietic cells including DCs, macrophages, monocytes and platelets [213]. The ligand for CD40 (CD154 or CD40L) is a 32-39 kDa type II transmembrane protein part of the TNF superfamily, defined by a conserved extracellular architecture consisting of a ß-sheet, then an α-helix loop, followed by another ß-sheet [214]. CD40L's specific structure allows for ligand trimerisation, a typical feature of TNF family members [214]. In the context of B-cell activation, CD40L is expressed by T-cells activated by DCs. Activated T-cells then engage with B-cells [215], where CD40-CD40L ligation coincides with BCR ligation and cytokine recognition to promote GC formation, subsequently facilitating CSR and SHM processes to induce B-cell maturation and differentiation into memory and long-lived plasma cells [216]. BCR activation by itself is not enough to induce CSR, even in the presence of cytokine; it is CD40 stimulation that facilitates this, providing a signalling pathway that regulates the activity of distinct checkpoint molecules independent of, but working in tandem with, BCR signalling [217].

CD40-CD40L engagement promotes CD40 'clustering' and promotes the docking of CD40-associated adaptor proteins known as TNFR-associated factors (TRAF1-7) to the CD40 intracellular cytoplasmic region [218] - a process also seen following RANK-RANKL ligation [219]. Further, CD40 signalling is widely understood to initiate canonical and non-canonical NF-κB signalling (reviewed in [220]), with different TRAF family members being involved in these different methods of NF-κB signalling (TRAF1, 2, 3, 6: canonical, TRAF2, 3, 5: non-canonical) [221]. In canonical NF-κB signalling, IκB proteins are degraded by IκB kinases (IKKa/b), freeing the NF-κB heterodimers NF-κB1 (p50) and NF-κB2 (p65) to regulate the transcriptional activity of NF-κB target genes [222]. In the non-canonical pathway, IKKα is activated, resulting in the degradation of REL-B-bound p100 to

produce gene-activating REL-B-p52 heterodimers (NF-κB2) [222]. Ultimately, NF-κB signalling tightly regulates B-cell proliferation, differentiation, development and survival [220]. CD40-CD40L ligation also activates other signalling mechanisms, including ERK-MAPK, PLCγ and PI3K signalling [218], providing an alternative mechanism - other than BCR signalling - through which these pathways are activated. Moreover, CD40 signalling promotes the activation of JAK/STAT proteins [220], which subsequently promote TRAF-independent B-cell proliferation and survival. Indeed, JAK/STAT activation is also required for CD40-mediated CLL cell proliferation [223], highlighting the necessity of CD40-CD40L interactions in both normal and pathophysiological scenarios.

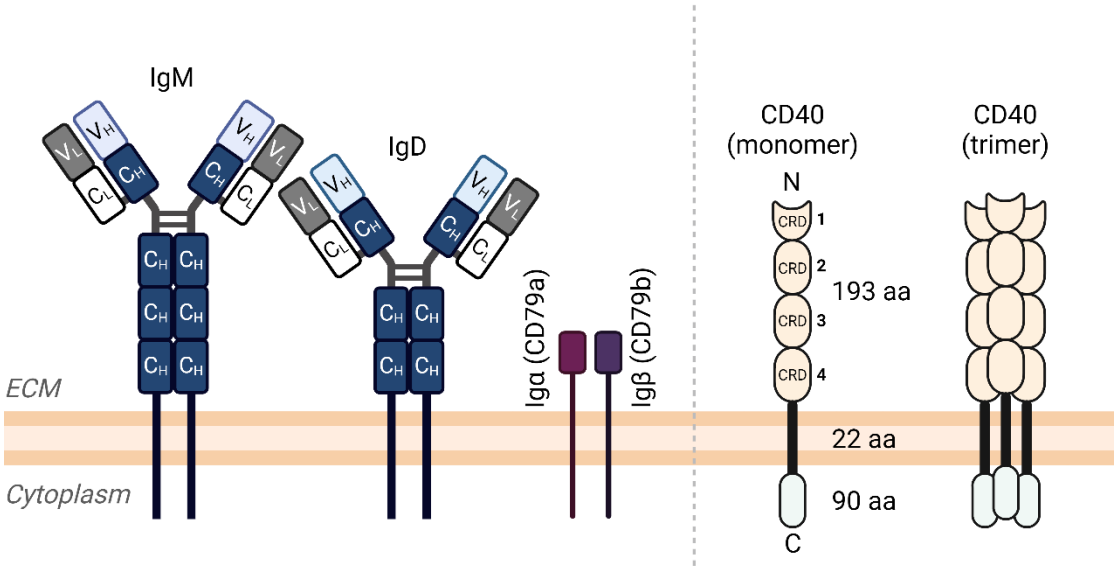

Figure 1.3: The structure of B-cell and CD40 receptors. Illustrated are IgM and IgD BCR structures, Igα (CD79a)/Igβ (CD79β) subunits, alongside monomeric and trimeric CD40 receptor conformations. 'aa' denotes amino acid length of specific CD40 receptor domains.

1.6.1. T-cell and CD40L interactions in CLL

Mimicking a phenotype of GC-resident B-cells, CLL cells are known to express high levels of CXCR5, allowing for effective homing of CLL cells to lymphoid tissues [109]. To accommodate CLL proliferation, CLL patient LNs exhibit heightened T helper cell infiltration [224], coincident with increased $CD4^+$ T-cell presence in PB compartments [225]. SLO-resident T_{fh} cells engage in direct contact with CLL cells with high CD40L expression [130]. These T-cell populations

are characteristically immunocompromised by their interactions with CLL cell populations [226]. Further, interactions with cell death protein-1 (PD-1) and cytotoxic T-lymphocyte-associated protein 4 (CTLA-4) on SLO-resident T-cells *via* CLL cell surface receptors elicits an exhaustive phenotype in CLL-associated T-cells. These findings demonstrate how CLL cells exploit pro-proliferative interactions with T-cells (e.g. *via* CD40-CD40L) while providing a direct mechanism of immune evasion [227]. Further, CLL-BCR engagement and NLC interactions produce a T-cell-recruiting positive feedback loop, whereby CCL3/4 are generated and provide a chemokine gradient to stimulate T-cell homing to CLL-resident lymphoid tissues [208]. Once in lymphoid tissues, T-cells can be engaged by CLL cells actively mimicking the surface marker phenotype of an antigen-presenting cell (APC) [228], thereby influencing $CD4^+$ T-cell expansion and facilitating further CLL-T-cell interactions [107]. Following CLL-T-cell interaction, T-cells express reduced CD40L [229] in a phenotype that promotes CLL cell proliferation. Work by Furman *et al*. revealed CLL cells exhibit heightened NF-κB signalling compared to normal B-cells collectively with *NFKB1* gene mutations [230]. *NOTCH1* mutation, an established driver of CLL pathogenesis, causes increased NF-κB signalling [231]. Interestingly, CLL-BCR engagement leads to an increase in CD40 receptor expression [232], and *vice versa* [233], highlighting crosstalk between these two critical components of CLL cell proliferation and survival in lymphoid tissues. Of note, CD40L is also expressed by small cohorts of B- and CLL cells [234], highlighting another avenue through which CLL cells may elicit autoreactive characteristics.

CLL interactions with T-cell-resident CD40L are shown to also promote resistance to chemotherapy and targeted therapies (e.g. the BH3 mimetic venetoclax [235]) - a mechanism that is enhanced in the presence of IL-21 cytokine [236]. Burley *et al*. demonstrated that inhibition of NF-κB-associated kinase (NIK), a kinase involved in activation of downstream non-canonical CD40 signalling, overcomes CD40-CD40L mediated drug resistance and induces CLL cell death [237]. Therapeutic targeting of CD40 signalling has also been considered in CLL and other CD40-associated B-cell malignancies, leading to the development of aCD40 mAbs with affinity for the CD40 receptor (CLL: Selicrelumab [238], diffuse large B-cell lymphoma (DLBCL) & multiple myeloma: Dacetuzumab [239]).

Dacetuzumab treatment has undergone phase 1 and phase 2 clinical trial [240], highlighting the clinical relevance of targeting CD40 signalling in CLL treatment.

1.6.2. Modulating TME signalling *in vitro*

Engagement of the CD40 receptor in *in vitro* study allows for mechanistic insight into the role of CD40-CD40L interactions in CLL cell proliferation, survival and drug resistance. Seminal study by Planken *et al*. demonstrated employment of CD40 signalling *via* combined anti-CD40 mAb FcγRII exposure induced – in both normal and malignant contexts – B-cell proliferation [241]. This work confirmed that CD40-CD40L interactions can be achieved *in vitro*, providing a model system for recapitulating CLL-TME interactions [242]. Since then, multiple groups have established CLL-supportive models to facilitate CLL-CD40 engagement *in vitro*, particularly using CD40L-expressing fibroblasts to mimic T-CLL cell interactions [243]. In combination with exogenous cytokine (as it is required to fully induce proliferation), this is considered an effective model for recapitulating CLL-TME interactions. Although IL-4 is the most widely used CD40L co-culture-associated soluble factor, other soluble factors (IL-2, IL-6, IL-10, IL-13, IL-21, IFN-γ, CPG-oligonucleotides) can be implemented [244]. Adaptations of the *in vitro* CLL co-culture model have since been developed. For example, CD31-expressing fibroblasts and HMEC-1 cells (a vascular endothelial cell line) can be co-cultured with primary CLL cells to mimic CLL interaction with NLCs and ECs, respectively [245].

1.7. The PI3K-AKT-mTOR signalling axis

Downstream of BCR [246], CD40 [247] and CXCR4 [120] engagement, PI3K-AKT-mTOR signalling is pivotal for coordinating cellular functions such as proliferation, survival, growth, metabolism and migration [248]. Due to the ability of this axis to induce these effects, malignant cell growth is often linked with PI3K-AKT overexpression and hyperactivity [248]. Indeed, this is the case in

the context of B-cell malignancy, where pharmacological targeting of this axis has strong clinical relevance (e.g. idelalisib [74]). This section will describe the structure and functions of the distinct members of this PI3K-AKT-mTOR axis, highlighting the importance of PI3K-AKT-mTOR signalling in normal B-cell function, as well as how these functions are exploited by CLL cells to favour disease progression.

Multiple forms of PI3K exist, however, only the class I PI3K can induce downstream phosphorylation in response to receptor ligation [249]. Class I PI3Ks can be split further into four distinct isoforms: p110α (PI3Kα), p100ß (PI3Kß), p100δ (PI3Kδ) or p100γ (PI3Kγ). PI3Kα and PI3Kß isoforms are ubiquitously expressed, while PI3Kδ and PI3Kγ isoforms are constrained to leukocyte populations [250]. Class I PI3Ks are composed of a heterodimer of two distinct subunits: (1) a regulatory subunit (p85) and (2) a catalytic subunit (p110) [251]; it is *via* PI3K's p85 subunit that PI3K has binding affinity to phosphorylated tyrosine residues located on the cytoplasmic domain of CD19, while p110 is recruited to p85 and completes the full enzyme structure [252]. PI3K plays crucial roles in both B-cell development and the homeostatic regulation of both normal and malignant B-cells; PI3Kα and δ isoforms are needed by pre-B cells to transduce signals critical for the transition of pre-B cells to the pro-B cell stage [253], whereas PI3Kδ is the predominant PI3K isoform in mature and malignant B-cells. More specifically, PI3K activity has been associated with the expression of Pax5 - a transcription factor heavily involved in B-cell differentiation and lineage commitment [254]. Depletion of PI3K in developing B-cells reduces lineage 'plasticity' (committing CLPs to B-lineage), coinciding with decreases in Pax5 expression [255]. Although multiple pathways exist within B-cells that possess PI3K-activating capability, BCR-mediated CD19 co-receptor recruitment is considered the best-characterised means of inducing downstream PI3K activity [256]. Srinivasan *et al*. demonstrated alleviation of BCR dysfunction by exclusively activating PI3K signalling [257], illustrating the breadth to which the PI3K-AKT-mTOR axis facilitates BCR signalling.

Following LYN-mediated CD19 phosphorylation, PI3K binds to CD19 tyrosine residues *via* its p85 subunit. Simultaneously, BCAP is recruited to CD19 following NCK1/2 binding to CD79α (Y^{204}); BCAP recruitment to the site of CD19

phosphorylation is critical for activating PI3K [258]. The activity of a small GTPase, TC21, is also necessary for PI3K activity [259]. Once activated, PI3K phosphorylates PIP_2 to the secondary messenger PIP_3 (achieved *via* binding of PIP_2 to PI3K's pleckstrin homology (PH) domain), eliciting the recruitment of AKT and PDK1 to the signalosome [179]. Once docked at the plasma membrane, PDK1 phosphorylates AKT at a specific threonine residue (T^{308}), allowing for complete activation of AKT *via* mTORC2-mediated phosphorylation of a hydrophobic-region-residing serine residue (S^{473}) [179]. This is thought to occur *via* subsequent phosphorylation of mammalian stress-activated MAP kinase-interacting protein-1 (mSIN1) found within the mTORC2 complex ($mSIN1^{T86}$) following AKT^{T308} phosphorylation. AKT-mediated mSIN1 phosphorylation creates a positive feedback loop, allowing 'active' mTORC2 to phosphorylate and 'fully' activate AKT (S^{473}) [260]. AKT activity determines a wide range of cellular fates, including growth, metabolism, proliferation and survival [261]. In the context of the 'hallmarks of cancer' [262], almost every cancer neoplasm exhibits elevated AKT signalling (examples described in [248]), highlighting the importance of AKT activity in positively regulating cellular function in both normal and malignant contexts. Indeed, a canonical method through which AKT promotes cell proliferation and survival is by the negative regulation of FOXOs – whose transcriptional activity is involved in mediating a plethora of downstream effects [263].

PI3K activity can exhibit intrinsic negative regulation by proteins including phosphatase and tensin homolog (PTEN) and the inositol polyphosphate 5-phosphatase-1 (SHIP-1). PTEN reverses PI3K activity by hydrolysing the secondary messenger PIP_3, reverting it to inactive PIP_2 [264]. Suzuki *et al*. demonstrated that B-cell-specific, *PTEN*-deficient mice had enhanced autoantibody-producing capabilities, perhaps due to an impairment of B-cell apoptosis due to BCR-AKT hyperactivation [265]. Further, SHIP1 has been demonstrated to be crucial for negative regulating PI3K signalling: Helgason *et al*. demonstrated in an *in vivo* knockout (KO) of SHIP1 B-cells exhibited enhanced activation and proliferation following BCR and CD40 stimulation [266]. These findings were corroborated in a deletion study by Maxwell *et al*. within a B-cell specific context for SLE-like autoimmune disease [267].

1.7.1. The PI3K-AKT axis in CLL

Several B-cell malignancies possess dysfunctional PI3K-AKT-mTOR signalling, including, but not limited to, DLBCL, marginal zone lymphoma (MZL), follicular lymphoma (FL) and CLL [268]. As will be discussed in section 1.9, understanding of the critical involvement of dysfunctional PI3K-AKT-mTOR signalling in B-cell-specific lymphogenesis, as well as the importance of PI3K signalling in facilitating BCR-mediated signals, has led to the development of therapeutics targeting PI3Kδ activity [269], highlighting strong clinical relevance in developing novel therapeutics targeting this signalling arm. In the context of CLL, PI3K has both intrinsic and extrinsic importance:

Intrinsically, dysfunctional PI3K activity is critical for CLL cell homeostasis in multiple compartments. For example, constitutive PI3K activity is needed to maintain CLL cell survival in circulating PB populations, where abrogation of constitutively active PI3K in patient samples (using LY294002) has been shown to initiate CLL cell apoptosis [270]. In SLO-resident CLL cell populations, BCR signals are carried en mass *via* PI3K-AKT-mTOR signalling to drive CLL proliferation and survival [186]. Further, U-CLL patients exhibit much greater PI3K expression than M-CLL patients [271], reflecting the hyperreactivity of germline BCRs particularly within the U-CLL disease subtype. As well as AKT, PI3K can influence other downstream components to promote CLL proliferation and survival, such as IKK (NF-κB), B-cell lymphoma 2 (BCL2) associated agonist of cell death (BAD), as well as inhibiting lysosomal Notch1 degradation [272, 273], a key oncogenic driver of CLL. Of note, AKT-mediated Notch1 overactivity can also promote Richter's transformation [274]. Increased activity of PI3K-AKT has also been associated with acquired resistance to current targeted therapies [275], demonstrating how PI3K overactivity can outcompete inhibition of other PH-domain-containing kinases.

Extrinsically, PI3K activity impacts CLL homing and migration, as evidenced by its activation downstream of CXCR4 [276]. An *in vitro* study demonstrated that antigen, cytokine and chemokine receptors, as well as costimulatory molecules, can influence intracellular PIP_3 levels. Further, pharmacological inhibition of

PI3Kγ (CZC24832) demonstrates a requirement for PI3Kγ activity in CLL migration, highlighting the need for other PI3K isoforms [277]. Additionally, PI3Kδ activity is important for maintaining regulatory T-cell populations [278], highlighting the importance of PI3K signalling in other cell populations within the CLL-TME. Within these confines, $CD4^+$ T-cells and macrophages require PI3Kγ to facilitate differentiation and/or migration [279, 280]. Interestingly, in CLL, PI3Kγ expression increases following CD40 stimulation [277], alluding to a context-dependent expression of discrete PI3K isoforms. Unexpectedly, Ecker *et al*. revealed that further genetic activation of PI3K-AKT lead to cell death *via* excessive oxidative phosphorylation and the subsequent generation of reactive oxygen species (ROS, *via* SHIP phosphatase inhibition) [281]. These data support how CLL cells effectively enhance the tumour-promoting capabilities of inherent B-cell signals while mitigating detrimental outcomes associated with further activation (e.g. ROS accumulation).

The downstream activation of AKT promotes CLL cell survival and proliferation in part by inducing the expression of pro-survival BCL2 family members (e.g. BCL-XL and MCL1) [282]. siRNA-mediated ablation of MCL1 induces CLL cell death [282], demonstrating the importance of MCL1 expression in CLL cell survival. Indeed, direct pharmacological inhibition of AKT (*via* AKTi1/2/A443654 treatment) elicits a similar effect *in vitro* [283]. Investigations of the presence of AKT^{S473} phosphorylation in different CLL compartments are somewhat conflicting; study of *ex vivo* patient samples within our group [284] and other groups [283, 285] has revealed differential AKT phosphorylation, perhaps due to differences in the cycling of CLL cells between PB and SLO compartments.

1.8. mTOR signalling

A member of the PI3K-like protein kinase (PIKK) family, the serine/threonine mTOR components are multi-domain proteins with incorporated protein kinase activity [286]. Due to mTOR complexes incorporating various regulatory components, the homeostatic regulation of B-cell functions by mTOR complexes is multi-faceted and orchestrates a plethora of physiological functions [287]. As a

result, mTOR activity can be influenced by multiple upstream factors including, but not limited to, insulin and insulin growth factors [287, 288], the availability of ATP [287, 289] as well as other environmental stressors. mTOR is comprised of two distinct multi-domain complexes: mTOR complex 1 (mTORC1) and mTOR complex 2 (mTORC2). mTORC1 is comprised of six major components: mTOR (the central evolutionarily conserved catalytic subunit), regulatory-associated protein of mTOR (Raptor), DEP domain-containing mTOR-interacting protein (Deptor), mammalian lethal with SEC13 protein 8 (mLST8), raptor binding protein PRAS40 and FK506-binding protein 38 (FKBP38). mTORC2, however, is comprised of mTOR, rapamycin-insensitive companion of mTOR (Rictor), mLST8, mSIN1, a protein observed with Rictor (PROTOR1/2) and Deptor [290]. The distinct protein compositions of these complexes facilitate different structural and functional outcomes, reflected by their differences in rapamycin sensitivity [291]. Nevertheless, mTORC1/2 activities are critical for regulation of biological processes in both healthy and malignant contexts [290].

1.8.1. mTORC1

mTORC1 is activated downstream of the aggregation of intracellular stressors (e.g. ROS, DNA damage, ATP abundance) and availability of nutrients. Though critical for B-cell homeostasis, these functions are beyond the scope of this thesis. Mechanistically, mTORC1 is indirectly activated by AKT through its regulation of tumour sclerosis complex 2 (TSC2) as part of a wider TSC nexus (comprised of TSC1, TSC2 and TBC1D7) [292]. In the absence of active AKT, the TSC complex exhibits GTPase activating protein (GAP) characteristics, negatively regulating an mTORC1-activating GTPase called Rheb. Following AKT-mediated TSC2 inactivation, Rheb is rapidly converted from Rheb-GDP to Rheb-GTP, which binds to and activates mTORC1 [287]. Further mTORC1 activity is dictated by its subunit PRAS40; AKT-mediated PRAS40 phosphorylation ($PRAS40^{T246}$) facilitates dissociation of Raptor from mTORC1, enabling further signal transduction from mTORC1 to its substrates [293]. mTORC1 activation is also achieved by MAPK/ERK-mediated inactivation of TSC2 (mediated by $p90^{RSK}$) [179].

mTORC1 activity can be independent to that of mTORC2, as the complexes interact with distinct proteins responsible for eliciting different cellular effects [294]. mTORC1 coordinates responses to proliferation, growth and survival, primarily by orchestrating translation initiation [295]. mTORC1-bound Raptor influences mTORC1 localisation by binding to the mTORC1 substrates p70 S6 kinase (S6K) and eIF4E-binding proteins (4E-BPs such as 4E-BP1) *via* TOR signalling motifs [296]. mTORC1 phosphorylation of S6K ($S6K^{T389}$) primes S6K, PDK1-mediated phosphorylation of S6K at S229 ($S6K^{S229}$) activates S6K [297], subsequently facilitating S6K-mediated phosphorylation of ribosomal protein S6 (part of the ribosomal 40S subunit; $S6^{S235/236}$) [287]. Though initially defined as the upstream kinase of S6, S6K regulates other translation-initiation-associated proteins including eIF4B [298], PDCD4 [299] and eEF2K [300]. At rest, 4E-BP1 is bound to eukaryotic translation initiation factor 4E (eIF4E) on the 5'-cap site of mRNA, preventing the formation of a 'pre-initiation' complex. Activation of mTORC1 from upstream stimuli induces a Raptor-mediated release of 4E-BP1 (*via* phosphorylation of T37/46 & S65/T70) from eIF4E, allowing eIF4G to assemble with eIF4E on the 5' mRNA cap, together with eIF4A (eIF4F complex). S6K's phosphorylation of eIF4B [298] induces the recruitment and binding of eIF4A to eIF4B, further enhancing eIF4A helicase capacity. Concurrently, S6K phosphorylates PDCD4 (an inhibitor of eIF4A), marking it for proteosomal degradation [299]. Together, the activation of translation initiation factors and prevention of 4E-BP1 and PDCD4 activity allow for the binding of the 40S ribosome and its associated ternary complex, thus facilitating the formation of the pre-initiation complex and driving cap-dependent translation [301].

mTORC1 activity is also pivotal for other processes, such as providing downstream effects to mitigate autophagy [302]. Interestingly, B-cell development is reported to be dependent on mTORC1 activity; specifically, the expression and activity of mTORC1-Raptor has been associated with the development of functional IgH, pre-B-cell survival and homeostasis, as well as antibody production in mature B-cells [303]. Further, mTORC1-Raptor activity is crucial to provide differentiation-inducing signals to developing B-cells [303]; ablation of Raptor activity in osteoblasts restricts IL-7 secretion and therefore abrogates IL-7R signalling - a vital signalling axis for B-cell progeny progressing from pro- to pre-B cell developmental stages. The role of Raptor in B-cell

development is extensively reviewed in [304]. Our group has underlined further the importance of mTORC1 in B-cell development: using Mx1-cre and Vav-cre *in vivo* mouse models, we have shown that, in the absence of Raptor, foetal mice lack red blood cells, and CLPs are blocked from B-cell lineage commitment [305], highlighting the necessity of mTORC1-Raptor signalling in B-cell development.

It is worth noting that S6K is also important in regulating the activity of mTORC2 as it generates a negative feedback loop in which mTORC2 is negatively regulated by mTORC1. Here, S6K1 can directly phosphorylate mTORC2 (*via* Rictor) at T1135 [306]. Not only this, but S6K1 can directly phosphorylate other mTORC2 components such as mSIN1 (T86/T389). As well as direct inhibition, S6K can prohibit mTORC2 activity by phosphorylating, inhibiting and downregulating IRS1 – an adaptor protein involved in insulin growth factor signalling; attenuation of subsequent intrinsic insulin signalling can lead to a dampening of mTORC2 activity [307, 308]. Interestingly, mTORC1 can also negate insulin signalling *via* growth factor bound-receptor protein 10 (Grb10) activity [309]. mTORC1's phosphorylation of Grb10 at multiple phosphorylation sites stabilises Grb10, while destabilising and preventing the activity of components of the insulin signalling pathway (e.g. IRS1 and the insulin receptor (insR)) [310]. B-cells express InsR on their cell surface [311] and, although its distinct role in B-cell biology has yet to be elucidated, it is considered to function downstream of PI3K-AKT-mTOR signalling as it does in other leukocytes (reviewed in [312]).

1.8.2. mTORC2

In the absence of upstream stimulation, the mTORC2 subunit mSIN1 holds mTORC2 in an inhibitory state. Once activated, PI3K drives the migration of the mTORC2 complex to the plasma membrane where, upon interaction of PIP_3 with the PH domain of mSIN1, mTORC2 is released from its inhibitory state and is deemed active [313]. Following this, association of mTORC2 with AKT^{T308} and AKT phosphorylation of $mSIN1^{T86}$ drive phosphorylation of AKT at S473, promoting 'full' activation of AKT *via* a phosphorylation-mediated shift in kinase

conformation [260]. Following activation, Rictor transfers the signal to targets downstream of mTORC2, akin to the role of Raptor in mTORC1. mTORC2's targeting and phosphorylation of AKT creates a positive feedback loop that drives mTORC1 activity by directly phosphorylating and inhibiting TSCs (S939/T1462), and phosphorylating PRAS40 (S246) [293, 314]. Downstream, AKT modulates the activity of effectors such as glycogen synthase kinase-3 (GSK3) [315] and FOXO transcription factors [263] to coordinate cell growth, proliferation and survival. The mTORC2 complex also has the capacity to phosphorylate PKC family members, and therefore controls outcomes such as chemotaxis, migration as well as reshaping of the actin cytoskeleton [292]. An *in vivo* study has revealed a potential role for mTORC2 in B-cell development; *RICTOR* KO mouse models reveal that early B-cell lineage commitment (CLP – pro-B cell stages) is independent of *RICTOR* expression. However, a reduced population of mature B-cells [316] and increased aggregation of pro-, pre- and immature IgM$^+$ B-cells (consistent with increased FOXO1 and RAG1 expression) [317] suggests a role for mTORC2 in the later stages of B-cell development. An illustration of the signalling components of the mTOR pathway in B-cells is highlighted below (Figure 1.4).

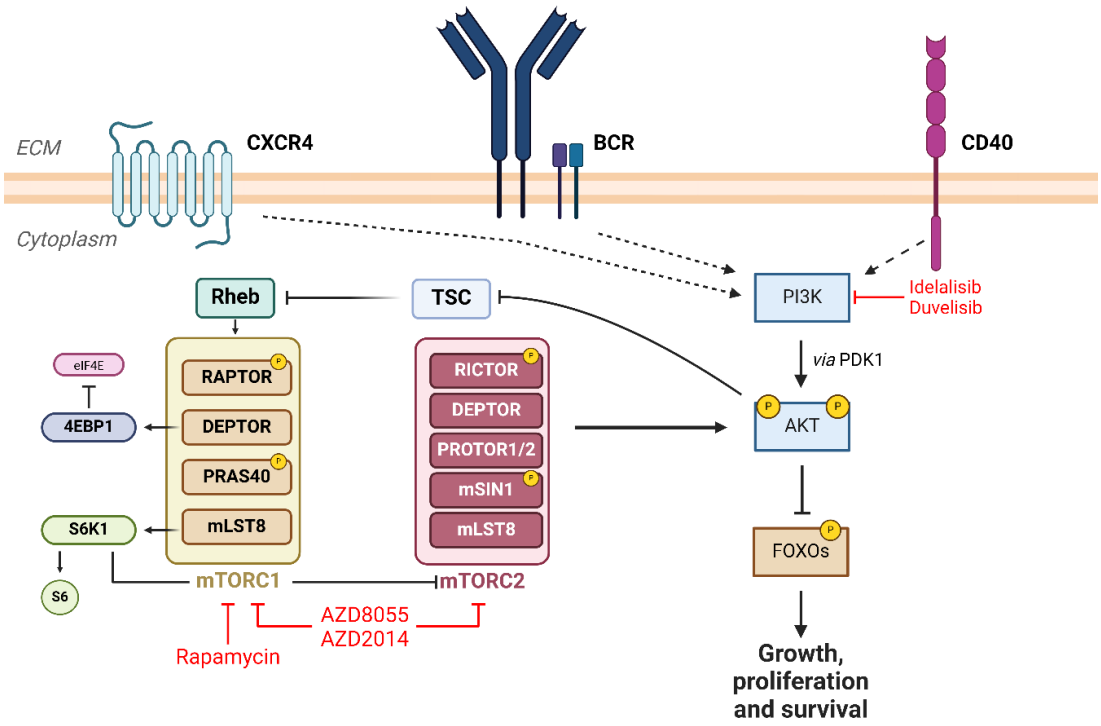

Figure 1.4: The mTOR signalling pathway. Highlighted in red are pharmacological inhibitors of distinct mTOR components. Of note, AZD2014 is the clinical analogue of AZD8055 and, as such, exhibits similar affinity for mTORC1/2 inhibition as AZD8055.

1.9. CLL treatment

1.9.1. Historic approaches to CLL therapy

1.9.1.1. Chemotherapy

Broad-spectrum chemotherapy was the go-to method for treating CLL for several years. Alkylating agents were the first established within clinical practice for first-line (1L) CLL treatment, including chlorambucil and cyclophosphamide [318, 319]. These were later replaced by nucleoside analogues (namely the purine analogue fludarabine) [320], as they were shown to be a more effective treatment option; in a comparative study, patients treated with fludarabine were shown to have increased complete response (CR) rates than that of patients on chlorambucil monotherapy (20% vs 4%) [321], demonstrating its effectiveness. Follow-up studies revealed that a combination of fludarabine and cyclophosphamide (FC) had enhanced cytotoxicity compared to that of fludarabine monotherapy, reflected by an increase in OS rates in phase II clinical trial patients treated with FC [322-324].

1.9.1.2. Chemoimmunotherapy

In conjunction with chemotherapeutic strategies, targeting of the transmembrane CD20 protein has been proven to be an effective method of treatment in other B-cell malignancies [325]. Of note, patients would receive chemotherapeutic regimens depending on age, fitness and the prevalence of existing conditions; younger, fitter patients would receive combined FC therapy; however, due to the toxic nature of FC treatment, elderly patients would receive either bedamustine or chlorambucil therapy, while unfit patients would be treated with chlorambucil [12].

Anti-CD20 mAb therapy first emerged with the use of rituximab in addition to either FC or bendamustine therapies (FCR, BR) [326, 327]. A clinical trial conducted by Keating *et al*. revealed a CR rate of 70% in 224 patients with progressive/advanced CLL following FCR treatment [327], demonstrating the effectiveness of combined FCR as a treatment. Further studies have shown that FCR treatment improved OS of patients (PFS: 56.8 months) [328, 329]. Additionally, patient remission is associated with CLL disease prognostics; the CLL8 clinical trial revealed that 'high-risk' patients typically have the shortest time to remission, represented by the shortest PFS. Specifically, the shortest PFS rates recorded at 5 years were exhibited by those with either del(17p) (15.3%), del(11q) (31.4%) or U-CLL (33.1%) [328]. Those with favourable aberrations (e.g. del(13q)) had improved clinical outcomes versus high-risk patients [328]. Additional study comparing FC treatment either with or without rituximab in untreated M-CLL patients revealed similar results (PFS: 53.9% at 12.8 years) [330].

Rituximab was also typically used in conjunction with bendamustine (BR). BR treatment was shown to be effective in patients with previously untreated and R/R CLL, thus demonstrating therapeutic effectiveness. The CLL10 phase III clinical trial conducted by the German CLL Study Group (GCLLSG) determined that FCR treatment led to prolonged PFS versus patients on BR treatment (55.2 months vs 41.7 months respectively) [326], demonstrating an increased effectiveness of FCR therapy compared to that of BR treatment. However, FCR treatment was also shown to be much more intensive compared to BR, notably due to patients exhibiting increased myelosuppression on the FCR regimen [326]. As such, FCR was used as a treatment option for younger CLL patients, while 'low-intensity' BR treatment was used more for fit, elderly patients with no prior complications [12].

The mAb Obinutuzumab (GA101) is another fully humanized CD20 antibody considered for CLL treatment. In *in vitro* pre-clinical study, obinutuzumab induced increased B-cell apoptosis compared to cells treated with rituximab [331]. Following pre-clinical success, phase I/II clinical trial testing of

obinutuzumab (GAUGUIN trial) revealed activity in CLL (OS rates: 62% in phase I, 30% in phase II) [332]. Obinutuzumab treatment was then characterised in conjunction with chemotherapy; In a phase III trial by GCLLSG (CLL11 trial), patients treated with combined Obinutuzumab-chlorambucil (G-Clb) displayed increased PFS compared to patients treated with combined rituximab-chlorambucil (R-Clb) or chlorambucil monotherapy (26.7, 16.3 and 11.3 months respectively). Patients treated with G-Clb also showed increased CR rates compared to those treated with R-Clb (20.7% versus 7% respectively) [333].

The emergence of now widely available novel agents has removed the need for CIT in most Western countries. Now, BTK inhibitors or BH3 mimetics (in conjunction with obinutuzumab) are considered for global CLL treatment in patients with no prior treatment, in part due to the prevalence of haematologic toxicity and the development of secondary myeloid neoplasms associated with CIT [328, 334]. Indeed, CIT can still be considered in areas where targeted therapies are inaccessible [335].

1.9.2. Small molecule signalling inhibitors

1.9.2.1. Kinase inhibitors

Kinase inhibitors such as ibrutinib and idelalisib have revolutionised the treatment of CLL. The clinical effectiveness of these novel agents has been demonstrated through their ability to overcome and treat patients with poorer prognostics. In a 5-year follow-up study of CLL patients, long-term ibrutinib treatment was associated with high overall survival, irrespective of patient subtype (U/M-CLL) [336]. Kinase inhibitors typically function by abrogating CLL-TME signalling, overriding BCR-mediated signalling and subsequent TME-resident CLL cell proliferation [146]. Additionally, BCR signal inhibitors demonstrate further clinical effectiveness by triggering the migration of CLL cells into the PB

(termed “redistribution/transient lymphocytosis”) [184], thereby reducing the incidence of lymphadenopathy.

Ibrutinib is a first-generation BTK inhibitor. It is a compound with covalent binding affinity to BTK *via* an active-site-resident cysteine residue (C481) [337]. More detail on BCR signalling and the importance of BTK is described in section 1.5.3. BTK’s signal transmission *via* chemokine receptors and adhesion molecules allows for CLL homing to LNs and SLOs [338]; it is the inhibition of BTK and subsequent inhibition of these particular homing factors that induce CLL redistribution lymphocytosis [110, 339], thereby increasing patient lymphocyte counts during the early stages of ibrutinib therapy. It is estimated that ~1/4 of CLL tissue is redistributed to the PB during BTKi treatment [184]. Interestingly, deuterium labelling of CLL cells revealed that SLO-resident CLL cells also exhibit major proliferative block and enhanced cell death are shown in patients who have initiated ibrutinib therapy, revealing ibrutinib efficacy in multiple tissue compartments [146].

Ibrutinib initially showed promise in *in vitro* study, where it was shown to abrogate oligonucleotide-based, CpG-mediated proliferation, TME-mediated signalling and stromal-cell-mediated survival signalling [340]. This was validated *in vivo*, where ibrutinib treatment was shown to antagonise BCR and subsequent NF-κB signalling, thereby abrogating the proliferation of CLL cells in both LN and BM compartments [341]. Supportive studies demonstrated that ibrutinib treatment abrogated BCR-mediated efflux of CCL3/CCL4, thereby blocking CLL-CXCL12/CXCL13 migration [339], and that ibrutinib treatment is antagonistic to BCR/chemokine-induced CLL cell adhesion/chemotaxis [110].

Ibrutinib treatment in patients with R/R CLL (Phase Ib/II studies PCYC-1102/1103) revealed increased responsiveness and longer remission periods in patients with no prior treatment (83% vs 34% PFS, follow up: 7 years) [342]. Common side effects with ibrutinib treatment were bleeding, bruising, diarrhoea and myalgia [342]; bleeding and bruising are associated with the inhibition of BTK-mediated platelet adhesion [343]. Further complications, such as infections, were known to be prevalent during the initiation of ibrutinib therapy, but did not warrant a discontinuation of treatment [342].

The improved clinical effectiveness of ibrutinib was demonstrated in a pioneering study (RESONATE clinical trial) [344], comparing ibrutinib to αCD20 mAb treatment (ofatumumab). Ibrutinib was shown to elicit more favourable clinical outcomes, including much better responsiveness than ofutumumab (42.6% vs 4.1%, respectively) as well as improved overall survival (90% vs 81% respectively) [344]. Indeed, the behaviour of ibrutinib treatment was consistent regardless of patient cytogenetics and resistance to chemotherapy [344], demonstrating ibrutinib's efficacy irrespective of patient heterogeneity to effectively treat the wider populace. A follow-up trial validated ibrutinib as a suitable 1L therapy for CLL (RESONATE-2) [72, 336], where survival rates were compared between ibrutinib and chlorambucil-treated patients. The study found better PFS [72] and OS rates [336] in ibrutinib-treated patients. Further studies investigated ibrutinib-rituximab combination therapy (compared to BR) [345]; ibrutinib combined with obinutuzumab (compared to G-Clb) [346]; and ibrutinib-rituximab to FCR [347], all of which demonstrated improved survival rates in ibrutinib-treated patient cohorts.

Next-generation BTK inhibitors have since been developed following the clinical effectiveness of ibrutinib treatment, seeking to enhance the BTK selectivity to reduce the prevalence of drug-associated side effects. Acalabrutinib, a covalent BTK inhibitor, was the first successor of ibrutinib being clinically approved for 1L and R/R CLL treatment, whereby patients treated with acalabrutinib (+/- Obinutuzumab) displayed improved PFS than patients on G-Clb treatment (ELEVATE-TN) [348]. A parallel randomised study (ASCEND) demonstrated that acalabrutinib was superior to idelalisib (+/- rituximab) and BR treatments, as evidenced by superior PFS [349]. Throughout the trial, acalabrutinib was shown to be more tolerable in patients than ibrutinib, reflected by a reduction in adverse effects [349]. Another covalent BTK inhibitor, zanubrutinib, has since been developed. Zanubrutinib treatment has shown promising results within R/R CLL patients, with PFS being 88% in patients with no prior ibrutinib treatment [350]. Cross-comparison to trials with ibrutinib treatment revealed decreased toxicity, with only 3% of patients terminating treatment due to adverse side effects [350]. Further study in R/R CLL patients (phase III ALPINE trial) confirmed these findings, where patients in zanubrutinib-treated cohorts exhibited a decreased prevalence of adverse events. In addition, overall responsiveness rate

(ORR) (78% vs 63% respectively) and 12-month PFS (95% vs 84% respectively) were also increased [351]. Final analysis revealed Zanubrutinib as being superior to ibrutinib with respect to PFS (24 months: 78.4% vs 65.9% respectively), with PFS being superior across every major prognostic subgroup, partnered with a lower prevalence of adverse events [352].

With the arrival of next-generation BTK inhibitors, patients now have the freedom to explore novel compounds to alleviate drug tolerance associated with ibrutinib treatment. As stated before, one way through which ibrutinib tolerance is achieved is by the development of treatment-associated C481S mutation in the BTK-ibrutinib binding site (found within 80% of ibrutinib-intolerant patients [353]), or *via* PLCγ2 gain-of-function mutation (R665W). Non-covalent BTK inhibitors have been developed to combat resistance to covalent BTK inhibitors, such as pirtobrutinib, and successfully demonstrate clinical activity in ibrutinib-resistant patients [354] following success *in vivo* [355]. Of note, pirtobrutinib resistance has also emerged in patients with progressive CLL [356]. Interestingly, CLL patients resistant to BTK inhibition share a characteristic kinase-domain-resident L528W mutation associated with global resistance to both covalent and non-covalent BTK inhibitors [357]. Specifically, analysis of mutations of the BTK kinase domain by Wang *et al*. unearthed that, while ibrutinib-resistant C481S mutations are sensitive to non-covalent BTK inhibitors, non-C481S BTK mutations are particularly insensitive to both covalent and non-covalent BTK inhibitors [357], thus rendering them insensitive to global BTK inhibitor therapy. Indeed, the persistence of treatment-induced resistance drives the need for the discovery of novel treatments/treatment combinations to better treat CLL.

Phosphatidylinositol-3 kinase (PI3K) inhibition is an alternative method for targeting BCR-mediated signalling in CLL, further highlighting the clinical relevance in targeting different components of survival/proliferative pathways in CLL treatment. Clinical examples of PI3K inhibitors include idelalisib and duvelisib. Idelalisib, an orally active PI3Kδ inhibitor, induces transient lymphocytosis, akin to ibrutinib treatment [358]. This was first suggested in pre-clinical study, whereby idelalisib treatment abrogated CXCL12/CXCL13-mediated migration, as well as survival and downstream ERK/AKT activities in *in vitro* patient samples [359]. Moreover, PI3K inhibition can improve upon αCD20 monotherapy; a randomised phase III trial revealed improved PFS (93% at 24

weeks, 20.3-month median survival) and OS rates compared to patients on rituximab alone [94], demonstrating the clinical effectiveness of PI3K inhibition. However, Idelalisib treatment is less efficacious than BTK inhibition and, with an increased prevalence of adverse events compared to BTK inhibitors [349], idelalisib is not the preferred choice for CLL treatment. Still, the availability of idelalisib allows for an alternative method of treatment for patients who suffer from side effects associated with other methods of treatment [360]. Duvelisib is another example of a clinically approved PI3K inhibitor that targets both PI3Kδ and PI3Kγ isoforms [361]. Compared with ofatumumab mAb treatment, duvelisib treatment resulted in increased PFS (13.3 vs 9.9 months respectively) and higher ORR [362].

1.9.2.2. BH3 mimetics

B-cell lymphoma-2 (BCL2) is a protein that positively regulates B- and CLL cell survival. Resident in the outer mitochondrial membrane (OMM), BCL2 actively inhibits the activity of proapoptotic factors, thus promoting survival [361]. BCL2 is part of a wider family of BCL2-like proteins, all of which share sequence homology within their BCL2 homology (BH) domains. BCL2-like proteins are subcategorised as pro-apoptotic multidomain (BAX and BAK), pro-apoptotic BH3-only (BIM, NOXA, PUMA) or anti-apoptotic (BCL2, BCL-XL, MCL1) [363]. The intracellular expression of these proteins dictates cellular apoptosis, leading to a fine balance of BCL2 family proteins to facilitate cell survival [363]. BH3 mimetics function by reducing an influx of pro-apoptotic BH3-only proteins to the OMM, where they then prevent the anti-apoptotic activity of BCL2 proteins *via* binding to a hydrophobic cleft [363]. BH3 mimetic treatment was first considered in CLL due to BCL2 being overexpressed in CLL cell populations [364]. Of note, BCL2 overexpression in CLL is associated with ablation of miRNA miR-15 and miR-16, both of which are tumour-suppressive and function by negatively regulating *BCL2* expression. It is found that miR-15/16 expression is downregulated in ~70% of CLL patients [82, 365], due to aberrations such as del(13q) but can also be mediated by other epigenetic factors [365, 366].

The effectiveness of anti-apoptotic BCL2 protein inhibitors was first described with the development of ABT-737 [367], a compound with BH3 homology to that of BAD. Further development produced a clinical analogue, navitoclax [368], which showed promise in phase I non-small lung cell carcinoma trials [369]. However, due to navitoclax's affinity for BCL-xL [370], patients suffered from dose-dependent thrombocytopaenia [369], preventing the clinical use of navitoclax monotherapy within cancer treatment [371]. Nevertheless, the potent killing potential of BCL2 inhibitors justified the development of novel counterparts. Soon after, obatoclax (GX15-070) emerged as a potential inhibitor, which possesses affinity for all anti-apoptotic BCL2 family members and showed effectiveness in pre-clinical studies [372]. However, later clinical trials involving CLL patients reported limited obatoclax activity and severe toxicity [373], halting its clinical use. The characteristics of obatoclax treatment are suggested to be due to obatoclax's affinity for MCL-1 and BCL-xL, both of which play critical roles in haemopoietic stem cells (HSCs) and megakaryotes respectively [374, 375].

Subsequently, a more selective BCL2 inhibitor has been developed. ABT-199, more commonly known as venetoclax, was the first selective BCL2-only protein inhibitor [376]. It is a BH3 mimetic, and as such has a high binding affinity to BCL2 *via* its BH3 binding motif [371]. Functional redundancy exists between BCL2 family members [371], whereby one can rescue the function of another, however, venetoclax treatment has been shown to overcome said redundancy, due to the dependency of cancer survival on the overexpression particularly of BCL2 [364, 377]. The selective nature of venetoclax has much improved the incidence of thrombocytopaenia in patients (compared with navitoclax and obatoclax) [376], leading to further study in CLL patients. In a phase I trial [85], 79% of patients displayed responsiveness to venetoclax, with a further 69% of patients exhibiting PFS at 15 months, 20% of which achieved CR. *in vitro,* Anderson *et al*. supported these findings by demonstrating rapid apoptosis in primary patient samples following exposure to venetoclax [87]. In a multicentre, international phase II trial [378], CLL patients with poor prognostic (del(17p)) R/R CLL were treated with increasing doses of venetoclax for 4-5 weeks. Results from this study revealed impressive venetoclax activity, with an ORR of 79.4% [378]. It is an accumulation of these findings that has led to venetoclax being

approved by both the US Food and Drug Administration (FDA) and the European Medicines Agency (EMA) for the treatment of patients with poor prognostic subtype (del(17p)), R/R CLL [379]. Observations of venetoclax effectiveness, such as low remission rates, signify an innate resistance to venetoclax monotherapy in wider CLL. As such, it was proposed that a combination of venetoclax with other targeted agents could elicit better responsiveness within CLL patients. Typically, venetoclax treatment has been considered in conjunction with anti-CD20 monoclonal antibodies: a phase Ib trial in R/R CLL patients presented 50% achieving complete response within an arm of treatment combining venetoclax with rituximab [380]; a phase III trial (MURANO) in R/R CLL patients corroborated these findings, where venetoclax-rituximab-treated patients exhibited prolonged PFS compared to patients treated with BR therapy [381]. Of note, venetoclax-rituximab therapy provided excellent treatment of R/R patients irrespective of disease prognostics [381]. Venetoclax has also seen success with other mAb combinations – venetoclax-obintutuzumab treatment was shown to elicit prolonged PFS in elderly, previously untreated patients compared to once-typical G-Clb treatment (CLL14 trial) [382]. As such, venetoclax-mAb combinations are now well established as 1L CLL treatments [383], particularly as a treatment alternative for patients with limited responsiveness or unacceptable side effects following treatment with BTK inhibitors [361].

Ongoing studies are investigating the therapeutic potential of synergistic BTKi-venetoclax treatment. A phase II clinical trial (NCT02756897) in >80 patients showed a CR rate of 88%, where 61% of patients had undetectable minimal residual disease (MRD) [384]. Ongoing trials, such as the GCLLSG's CLL17 trial (NCT04608318), will hopefully highlight the potential of long-term venetoclax-ibrutinib therapy (in comparison to venetoclax-obinutuzumab). Ibrutinib-venetoclax combinations are proposed as a method of facilitating remission in ibrutinib-treated patients, as BTK inhibitor treatment elicits strong clinical outcomes, albeit in the absence of remission, leading to somewhat unfavourable long-term treatment strategies. Of note, long-term treatment is undesirable due to the prevalence of adverse side effects [385]. All things considered, venetoclax treatment is currently administered in conjunction with α-CD20 mAbs as an alternative 1L therapy (Figure 1.5) [335].

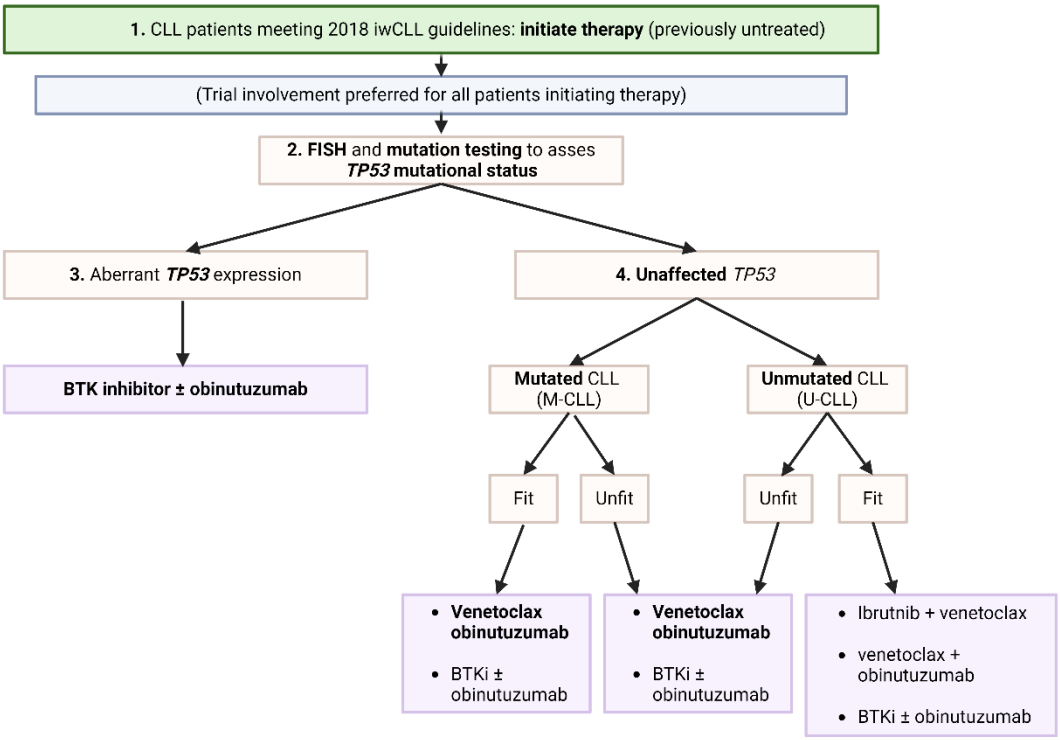

Figure 1.5: Current approaches to CLL treatment according to iwCLL2018 guidelines. Of note, it is preferred that either acalabrutinib or Zanubrutinib be used for current BTK inhibitor therapy. Highlighted treatment strategies are preferred treatments for different prognostic CLL subsets (Modified from [335]).

Unfortunately, acquired resistance can also emerge following venetoclax treatment and diminishes treatment effectiveness. This can occur through mutation of the BCL2 protein (G101V) that hinders venetoclax-BCL2 associations [386]. Additionally, B-cell translocation (*BTG1*) gene mutation, aberrant *CDKN2A/B* expression and overexpression of BCL-xL and MCL-1 all lead to a complex karyotype associated with increased venetoclax resistance [387]. These findings drive further the need for novel CLL therapeutics to effectively treat patients harbouring resistant disease subclones.

1.9.3. mTOR as a therapeutic target

The mTOR complexes were discovered following breakthrough studies in the 1990s involving rapamycin (sirolimus), an antibiotic derived from *Streptomyces hydroscopicus* [388] that showed promising anti-cancer characteristics. Investigation of rapamycin's mechanistic effect led to the discovery of mTORC1 and mTORC2 [389-391], with mTORC1 activity being the direct target of rapamycin. Specifically, rapamycin associated with a protein called FK506-binding protein. FKBP-rapamycin can then bind to the FRB domain near the catalytic cleft of mTOR, rendering substrate binding ineffective [392]. The insensitivity of mTORC2 to rapamycin is due to Rictor's ability to overhang the catalytic site of mTOR, in conjunction with mSIN1, thereby masking the site from potential FKBP-rapamycin binding [393]. Although long-term rapamycin treatment exerts an indirect inhibition of mTORC2 (*via* binding of free mTOR proteins prior to mTORC2 complex formation [394]) rapamycin treatment is dependent solely on the sensitivity of mTORC1. In the context of cancer therapy, rapamycin treatment would be considered due to mTOR hyperactivity being a prolific occurrence in multiple cancers, particularly mTORC1, where mTOR signalling promotes enhanced cell growth and survival (i.e. immortality) as per the 'hallmarks of cancer' [262]. Indeed, rapamycin treatment has shown success in pre-clinical *in vivo* studies, increasing the lifespan of mice in various tumour models (discussed in [395]). This led to the development of 'rapalogs', analogues of rapamycin with improved clinical properties, though their clinical effectiveness is weak at best [292]. This is partly because by inhibiting mTORC1, mTORC2 is hyperactivated, as attenuating mTORC1-mediated signals removes an mTORC1-mediated negative regulation of mTORC2 (i.e. through S6K activity), subsequently enhancing pro-survival signalling through downstream AKT^{S473} [396]. Additionally, rapalogs do not fully abrogate 4E-BP1 phosphorylation, suggesting a partial ineffectiveness of mTORC1 inhibitor treatment [397]. Therefore, ATP-competitive dual mTOR kinase inhibitors have been developed, possessing affinity for both mTOR complexes. Two such examples are AZD8055 and its clinical analogue AZD2014 (vistusertib), both of which have demonstrated effective abrogation of mTORC1 ($S6K1^{T389}$ and $4E\text{-}BP1^{T37/T46}$) and mTORC2

(AKT^{S473}) signalling [398]. Notably, AZD8055 treatment also reduces phosphorylation of downstream proteins (S6$^{S235/236}$ and FOXO1^{T24}) [398]. The tumour suppressive effect of AZD8055 treatment has been described in various cancer models [399-403], with its optimised clinical analogue currently under review in phase II clinical trials [404], highlighting the clinical relevance in blocking mTOR-mediated orchestration of pro-tumourigenic events. Gupta *et al*. demonstrated that activity of another dual mTOR inhibitor, OSI-027, attenuated AKT^{S473} phosphorylation, thereby inducing apoptosis in B-cell precursor acute lymphoblastic leukaemia (BCP-ALL), mantle cell lymphoma (MCL) and MZL [405], reinforcing mTORC1/2 inhibition as a potential therapeutic approach for the treatment of B-cell malignancies. Limitations to dual mTORC1/2 inhibition have been reported; receptor tyrosine kinase (RTK) overexpression has been associated with prolonged mTORC1/2 inhibition, thereby promoting overactivation of AKT^{T308} and inducing further pro-survival signalling [406]. To combat these compensation mechanisms, inhibitors targeting both PI3K and mTOR activity have been developed (e.g. PQR309, BEZ-235, DS7423), showing success in recent clinical trials (described in [248]), although no dual PI3K/mTOR inhibitors have currently been FDA approved for clinical use [248].

1.9.4. Targeting mTOR signalling in CLL

Typically, the mTOR signalling capacity seen in cancers is elicited through the hyperactivity of upstream signal components (PI3K-AKT, MAPK/ERK) [407]. However, aberrant mTOR activity can also arise from mutations of genes encoding PI3K-AKT signalling components (PI3K, AKT, PTEN) [408], promoting tumourigenesis through the aberrant expression and activity of PI3K-AKT-mTOR components. Despite there being much attention focused on the targeting of PI3K in CLL, and other haematological malignancies (idelalisib) [94], little is known with regards to targeting of mTOR components in CLL, even though mTOR is hyperactivated [409]. Our group has demonstrated a crucial role for mTORC1 in CLL disease initiation and preservation; generation of an *in vivo* CLL mouse model with a *Raptor* deficiency attenuated disease burden, concomitant with significant increases in mouse survival. Furthermore, mice with a more

aggressive-like CLL were more sensitive to rapamycin than AZD2014 treatment, supporting CLL maintenance being tied to mTORC1-Raptor signalling [409].

A study in CLL by Decker *et al*. demonstrated a therapeutic application of rapamycin in CLL, where treatment induced cell cycle arrest *in vitro*, consistent with a depletion of cyclins D3, E and A [410]. This was supported in work by Åleskog *et al*., where *in vitro* primary cells displayed rapamycin sensitivity, regardless of patient prognostics [411]. In the clinical setting, a phase II study using the rapalog everolimus led to partial remission in 18% of patients, generating a CLL lymphocytosis in the PB [412]. This study suggests that everolimus could be used as an alternative to BTK inhibitors to induce lymphocytosis, allowing for combined treatments with therapies exerting CLL cytotoxicity [412]. Another rapalog, temsirolimus, has been investigated in the context of CLL therapy following success and FDA approval for the treatment of renal cancer [413]. In the context of B-cell malignancy, temsirolimus treatment is also being investigated in conjunction with rituximab (NCT01653067) as a potential treatment for DLBCL [414], with preceding study showing promising activity and response rates in a phase II trial [415]. Current phase I study have proposed that everolimus could be used in conjunction with novel BTK inhibitors, highlighting a potential synergy between mTOR and BTK inhibition [416]. While promising, the abrogation of the mTORC1-mTORC2 negative feedback loop following mTORC1 inhibition would lead to enhanced PI3K/AKT activity [417], driving the need for further investigation of dual mTORC inhibitors as potential therapeutic agents.

Our group has extensively investigated AZD8055 as a potentially novel agent for the treatment of CLL, demonstrating its application abrogating CD40L-induced proliferation, inhibiting protein synthesis and synergistically reducing primary CLL cell viability in combination with ibrutinib [409]. In addition, we have demonstrated AZD8055 activity in BCR-stimulated CLL cells: primary cells stimulated with soluble $F(ab')_2$ antigen underwent increased levels of apoptosis in AZD8055-pretreated samples, coincident with depleted $FOXO1^{T24}$ and increased FOXO1 nuclear activity [284]. Extensive work was conducted by a former PhD Michael Moles, who elucidated that prevalent mTOR signalling downstream of BCR crosslinking was effectively ablated following combined

AZD8055-ibrutinib therapy. Further, downstream of mTORC2-AKT inhibition, nuclear FOXO1 activity induced an increase in FOXO family gene regulation and subsequent tumour suppressive effects (cell death and cell cycle arrest) [49]. These data provide strong insight into a potential clinical effectiveness of targeted mTOR inhibition in CLL therapy, specifically with the use of AZD8055 and AZD2014. Mechanistically, however, the use of AZD8055 warrants further investigation, as the wider implications of mTOR inhibition in CLL have yet to be fully elucidated.

1.10. FOXO transcription factors

FOXO transcription factors are a family of proteins belonging to a larger superfamily that contains an evolutionarily conserved forkhead domain ordered alphabetically from FOXA to FOXR (the FOX transcription factor superfamily; reviewed in [418]). The FOXO family comprise four highly related members: FOXO1 (FKHR), FOXO3 (FKHRL1), FOXO4 (AFX) and FOXO6 in mammals, which are orthologs of DAF-16 in *Caenorhabditis elegans* and dFOXO in *Drosophila melanogaster*. Mammalian FOXO family members were initially reported as part of pro-oncogenic fusion proteins of paired box protein 3/7 (PAX)-FOXO1 in alveolar rhabdomyosarcoma, whereby FOXO1 trans-activation and the FOXO-dependent TGF-β response was inhibited, thus promoting tumorigenesis [419, 420]. Similarly, FOXO3 and FOXO4 form mixed lineage leukaemia (MLL) fusion partners, and aggressive paediatric acute leukaemia, from translocation of t(6;11)(q21;q23) and t(X;11)(q13.1;q23) respectively [421-423].

FOXO family members regulate gene expression through activation or repression. As such, FOXOs are vital for the regulation of a plethora of cellular processes, from cell cycle arrest and apoptosis to metabolism and oxidative damage modulation [424]. Structurally, FOXOs differ from the rest of the FOX superfamily, containing a specific amino acid sequence flanking the DNA-binding domain (DBD) (Gly-Asp-Ser-Asn-Ser) enabling interaction with the FHRE (forkhead response element; 5’-(G/C)(T/A)AA(C/T)AA-3’) [425]. Within the family, FOXOs have shared DBD homology, however the structure of their transactivation

domains (TAD) differ; it is this difference in TAD structure that determines the nature of FOXO interactors to define role specificity [426]. Partnered with differences in TAD structure are the tissue-specific expression patterns of FOXO isoforms, suggesting FOXOs have cell-specific roles [425]. While FOXO1, FOXO3 and FOXO4 family members are ubiquitously expressed, FOXO6 has a more restricted expression pattern. Interestingly, FOXO1-deficient mice are embryonic lethal, dying at day 10.5 of gestation, due to a block in vascular development, while FOXO3- and FOXO4-deficient mice are viable and largely indistinguishable from wildtype control mice [427]. Therefore, functional redundancy exists between FOXO family members [428], with studies suggesting that FOXOs can be overexpressed to fulfil the roles of other family members should they become dysfunctional [429]. In addition to TAD sequences, FOXO proteins also contain NLS (nuclear localisation signal), NES (nuclear export signal) (Figure 1.6), all of which are regulated by post-translational modification [421, 430]. Naturally, as FOXOs require nuclear DNA binding to produce cellular effects, FOXO activity is partnered with subcellular localisation.

1.10.1. AKT-mediated FOXO regulation

AKT regulates a wide array of cell functions via phosphorylation of target proteins including the FOXO family. Multiple serine/threonine RxRxxS/T regions within the N-terminus, NLS and NES of FOXOs are present, which are conserved from the *C. elegans* protein DAF-16 (FOXO1 - T24, S256, S319; FOXO3 - T32, S253, S315; FOXO4 - T28, S193, S258; FOXO6 - T26, S184. FOXO6 lacks a C-terminal phosphorylation site; [424, 429, 431]). AKT-mediated phosphorylation leads to FOXO inactivation by enabling docking of 14-3-3 proteins *via* RSxpS/TxP and RxxxpSxP motifs [263, 432]. 14-3-3 proteins can also affect the binding affinity of DNA for FOXOs by interrupting the DNA binding process at the DBD [433]. This leads to a conformational change that exposes more of the NES than the NLS, thus preventing FOXO from returning to the nucleus post-translocation [434, 435]. Downstream of AKT, mTORC1 also has a pivotal role in inducing positive cellular effects such as protein translation, cell growth and proliferation [436]. FOXOs hinder mTORC1 function by inducing *RICTOR* expression, thus

reducing RAPTOR-mTOR association, in turn mTORC1 function and preventing cell proliferation [437]. FOXOs also downregulate mTORC1 via *SESN3* (sestrin3) upregulation, which in turn activates tuberous sclerosis 1 and 2 (TSC1 & TSC2) via AMPK [438]. Interestingly, TSC1 and TSC2 can also amplify mTORC1 activity if activated by other proteins [437], demonstrating the effectiveness of FOXOs in overriding proliferative signals. Interestingly, FOXOs can also regulate responses to DNA damage *via* regulation of the expression of GADD45 proteins, particularly GADD45A, which has the capacity to induce growth arrest at the G2-M checkpoint to promote DNA damage repair following S-phase-mediated DNA replication [439]. An illustration of AKT-mediated FOXO nuclear export is found below (Figure 1.6).

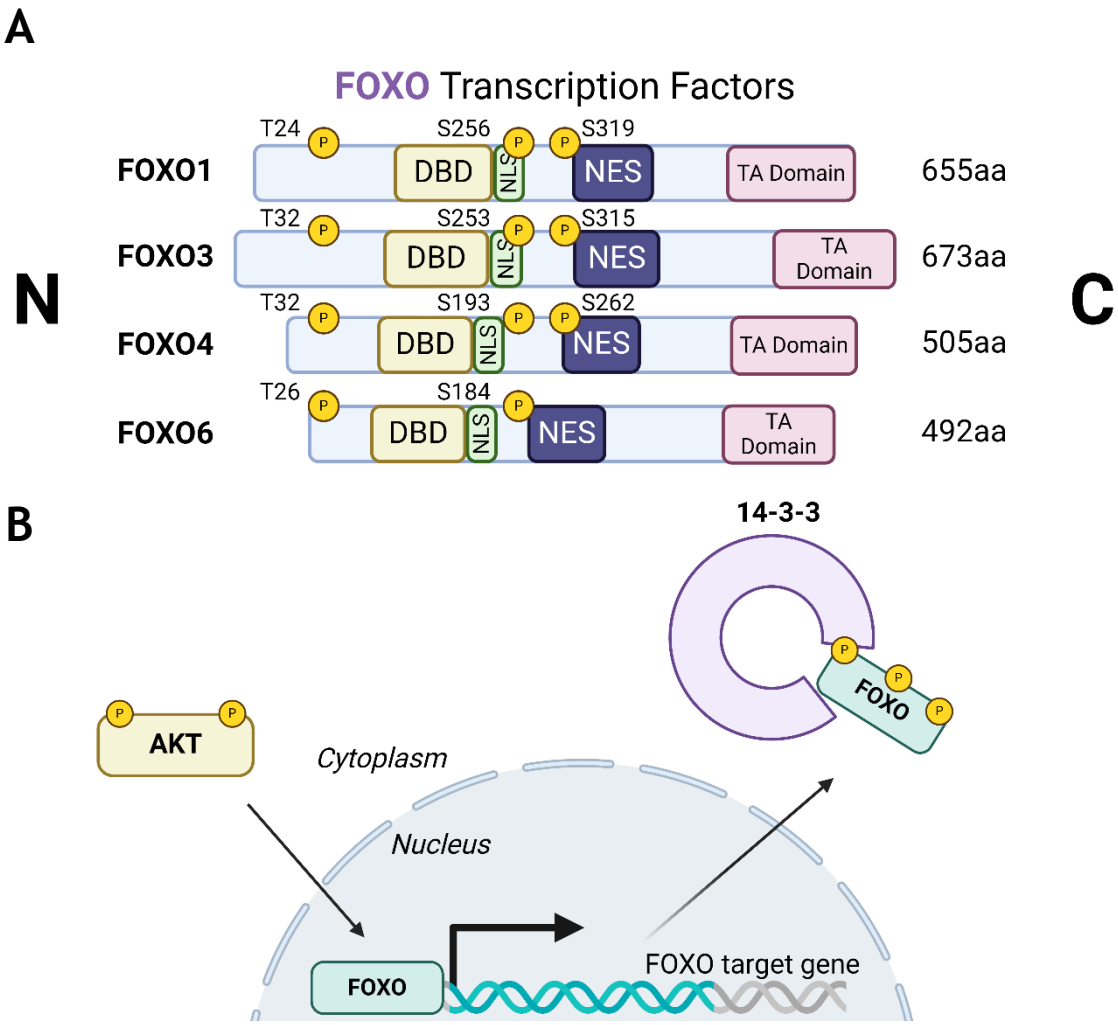

Figure 1.6: AKT-mediated FOXO nuclear export. (A) Simplified structure of the FOXO transcription factor family. FOXOs harbour four conserved regions: the DNA-binding domain (DBD), a nuclear localisation sequence (NLS), a nuclear export sequence (NES) and a transactivation (TA) domain. FOXOs have their own specific residues that are phosphorylated by AKT (denoted by a yellow 'p'). (B) The mechanism of AKT-mediated FOXO nuclear export: phosphorylation of FOXOs facilitates 14-3-3 binding and cytoplasmic shuttling.

1.10.2. Additional mechanisms of FOXO regulation

Although AKT-mediated FOXO phosphorylation is the most understood post-translational modification of FOXO activity, there are other pathways through which FOXO activity is modulated leading to a broad range of biological effects. FOXO localisation (and subsequent transcriptional activity) is also negatively regulated by MAPK/ERK, CDK2 and casein kinase 1-mediated phosphorylation [440-444]. Conversely, FOXO activity is upregulated by JNK-mediated phosphorylation in response to oxidative stress or AMPK-mediated phosphorylation in response to reduced intracellular ATP, leading to enhanced nuclear localisation and subsequent transcriptional activity, for example through phosphorylation of FOXO1 at Ser^{383} and Thr^{649} [445, 446]. In these cases, FOXOs respond to intracellular stress stimuli by upregulating genes that maintain homeostasis, such as *GPX1* (oxidative damage) and *PGC1a* (metabolism) [429]. FOXOs are also susceptible to post-translational modification via acetylation, methylation and ubiquitination [447, 448]. Several acetyltranferases, deacetylases, ubiquitin ligases and methyltransferases can either activate or repress FOXO activity through lysine modification, resulting in subsequent changes in DNA binding efficacy, protein interaction effectiveness and overall stability [449-452], while mono- and poly-ubiquitination of FOXO transcription factors impact on protein stability and subcellular localisation [440, 453]. miRNAs also regulate the FOXO family post-transcriptionally, such as miR-27a, miR-96 and miR-182 reducing *FOXO1* expression in MCF7 cells by targeting the 3’ untranslated region of *FOXO1* [454].

1.10.3. The discrete roles of FOXOs in B-cell development

1.10.3.1. Early B-cell development

Selective FOXO family members play important roles at distinct stages during B-cell lineage commitment and development (described in Figure 1.7). During the initial stages of B cell lineage commitment, *FOXO1* enables the differentiation of common lymphoid progenitor (CLP) cells towards the pro-B cell stage. This is initiated by E2A and HeLa E-box binding (HEB) proteins, with the ablation of these proteins diminishing *FOXO1* expression and inducing a block at the CLP stage [455]. The transition from the pro-B to pre-B cell stage is dependent on the generation of a functionally rearranged Ig heavy chain, surrogate light chains (VPREB and IGLL1) and the signalling components CD79A and CD79B, to form the pre-BCR [456].

FOXO1 plays a critical role during these stages of development through transcriptional activation of the recombination-activating gene (RAG) proteins RAG1 and RAG2, which are responsible for initiating Ig gene rearrangement [51, 457, 458]. In addition, positive regulators of early lymphopoiesis (IL7R, SYK, *PIK3CA* and VPREB1/3) are regulated by and can regulate FOXO1 activity [458]. During the pre-B cell stage, SYK inactivates or activates FOXO1 via downstream activation of PI3K or BLNK, respectively [456]. An absence of *FOXO1* during this stage prevents somatic recombination in pro-B cells and reduces Ig light chain rearrangement in pre-B cells, while an absence of *FOXO3* has no effect [458]. Interestingly, a loss of FOXO1 in pro-B cells also provokes increased levels of apoptosis linked to an increase in the expression of *BCL2L11* (BIM) and lowered *BCL2L1* (BCL-XL) expression [458]. These studies highlight a key role for FOXO1 in driving early B cell differentiation and supporting pro-B cell survival.

FOXO1 can mediate both positive and negative impacts on pre-B cell proliferation through upregulation of *CCND3* or *BCL6* respectively. *CCND3*

(encoding Cyclin D3) is a FOXO target and crucial for pre-B cell proliferation [459]. BCL6 is a repressor of DNA recombination-induced cell death (induced by p53 downregulation) but also prevents proliferation via MYC/CCND2 repression [460]. This temporal regulation can lead to cell cycle arrest of pre-B cells (54). These observations demonstrate the significant role of FOXO1 in B-cell development and how crucial it is to the overall process of B-cell maintenance and regulation. However *FOXO3* and *FOXO4* are also expressed during development [460]. Although the role of *FOXO4* expression in B-cell development is unclear, evidence is emerging for the significance of *FOXO3*, as FOXO3$^{-/-}$ mice exhibit a loss of abundance of pre-B cell population, and a reduction of B cells in the BM and PB [461]. Although the loss of FOXO1 impaired B cell lineage commitment, studies using a FOXO3 conditional deletion model demonstrated that *FOXO3* deletion affected the production of lympho-myeloid primed progenitor cells (LMPPs), CLPs and B-cell precursors [462]. Furthermore, deletion of both FOXO1 and FOXO3 results in a complete block of CLP commitment towards the B-cell lineage [462]. These data shed light on the importance of FOXO3, in addition to FOXO1, in normal B-cell development and indicate a predominant switch of *FOXO3* to *FOXO1* expression is pivotal for B-cell lymphopoiesis.

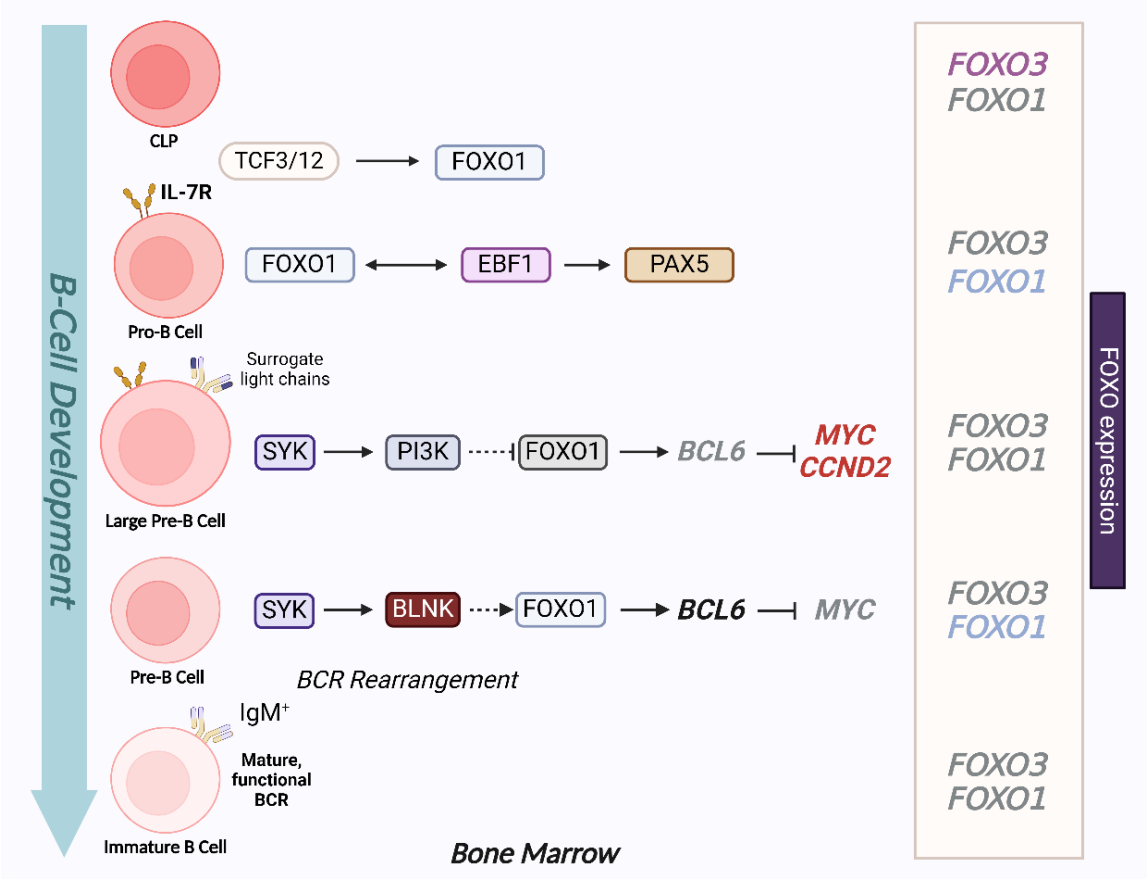

Figure 1.7: The role of FOXO in B-cell lymphopoiesis (Modified from [463]). FOXO expression is critical for early B-cell development. B-cells undergo a specific set of developmental stages in the bone marrow (BM), which are tightly controlled by the expression of particular FOXO transcription factors, enabling differentiation and proliferation at distinct stages of lymphopoiesis. *FOXO3* regulates commitment of CLP cells to the B-cell lineage, whereupon *FOXO1* expression enables pro-B cell differentiation via E2A and HEB activity. FOXO1, in conjunction with EBF1, promotes B-cell lineage commitment via activation of PAX5, alongside positive regulators such as IL-7R. Cells advancing to the pre-B cell stage are coordinated by SYK activity, which promotes proliferation or differentiation via activation of PI3K or BLNK respectively. PI3K signalling inactivates FOXO1, leading to an upregulation of *MYC* and *CCND2* expression driving pre-B cell proliferation, while BLNK induces cell cycle arrest via FOXO1 and *BCL6* upregulation. *FOXO1* expression is ablated to allow for differentiation of small pre-B cells into immature B-cells primed to leave the BM to further mature and differentiate in GC reactions.

1.10.3.2. B-cell maturation

Mature B-cells express both FOXO1 and FOXO3. Upon BCR crosslinking and downstream PI3K-AKT activation, FOXO1 is downregulated and inactivated [464, 465]. There is conflicting evidence regarding the function of FOXO1 in mature B cells. Srinivasan *et al.*, demonstrated that FOXO1 induces apoptosis in response to a lack of BCR signalling, partnered with elevated *BCL2L11* and *CDKN1B* FOXO

target expression [466]. This was supported by studies in which constitutively active FOXO1 (FOXO1-A3) promoted apoptosis and cell cycle arrest in B-cells [465]. However, *FOXO1* expression also supports B-cell populations: conditional deletion of *FOXO1* (*CD21-Cre*$^{+}$) reduced B-cell LN populations, presenting FOXO1 expression as being crucial for correct B cell migration [458]. *FOXO1* deletion resulted in a reduced capacity for B cells to induce BCR signalling and effectively proliferate [458, 465]. The role of FOXO3 in mature B cell maintenance and regulation is also conflicting; constitutively active FOXO3 increased levels of cell cycle arrest and apoptosis in B-cells [465], suggesting a pro-apoptotic function for FOXO3 in mature B-cells. On the other hand, *FOXO3*$^{-/-}$ Em-myc transgenic mice were shown to have accelerated levels of B-cell lymphomagenesis [467], suggesting that FOXO3 is required for normal B-cell maintenance and regulation. These data demonstrate the context-specific bimodality of FOXO function, with FOXO activity either hindering or promoting cell growth and proliferation.

GCs are specialised structures within SLO in which B-cells undergo clonal expansion and SHM, leading to the generation of antibodies that possess a higher affinity for antigen (affinity maturation) and the export of long-lived plasma cells (PC) and memory B cells [468]. Upon initial recognition of antigen, B cells (pre-GC B cells) congregate at the border between the follicle and the T cell zone and undergo proliferation, which leads to the development of the GC structure. GCs comprise a proliferation-rich dark zone (DZ), in which B-cells undergo SHM and clonal expansion, and a light zone (LZ), in which B-cells (centrocytes) undergo selection processes: the new antibody is tested for interaction with follicular DC bound antigen and receive help from T_{fh} cells [469]. Following positive selection of B cells expressing higher affinity antibodies, the B-cells re-enter the DZ and proliferate further, driven by cyclin D3 [470]. Activation-induced cytidine deaminase (AID) is an essential component of affinity maturation due to its ability to initiate SHM [471, 472]. While introducing nucleotide changes in the variable regions of *Igh*, processing of these mutations can induce DNA double stranded breaks which leads to CSR resulting in the generation of IgG, IgA and IgE antibodies. However, evidence indicates that CSR mainly occurs earlier in pre-GC cells (66). Bcl-6 also plays a vital role within the GC B cell program, modulating *Myc* and *Prdm1* (encoding Blimp1) expression which, together with FOXO1 activity assist in normal GC function [473-475].

Indeed, FOXO1 is a critical component in the DZ phenotype, as indicated by the finding that deletion of FOXO1 in GC B cells results in a loss of the anatomical structure of the DZ [473, 476]. This happens in part because of the absence of CXCR4 assisted B cell migration: FOXO1-mediated *CXCR4* expression ensures the retention of B-cells in the DZ [473]. While *FOXO1* knockdown in GC-B cells prevents DZ formation and inhibits CSR, SHM and clonal expansion are unaffected suggesting that FOXO1 may act to delay the LZ transcription program [458, 473, 476]. Supporting these findings, an enhancement in CSR was noted in B cells with nuclear sequestered $FOXO1^{T24A}$ via subsequent *AICDA* (AID) upregulation, while inactivation of FOXO1 through AKT-mediated signals led to IRF4-driven PC differentiation [477]. In addition to FOXO1 function being required for DZ B-cell populations and GC anatomical formation, FOXO1-mediated induction of *BATF* is required for effective LZ B-cell proliferation [478], demonstrating a need for *FOXO1* expression in both GC compartments. Of note, FOXO1 plays a key role in positive GC B-cell selection, as BCR signalling is programmed to signal via FOXO1 activity, while CD40 ligation induces NF-κB activity: both CD40- and BCR-mediated signals are required to induce c-Myc upregulation thus promote B-cell survival [479]. Further, FOXO1 induces upregulation of *CCND3* in the GC DZ B cells, enabling GC B cell expansion [480]. Collectively, these findings demonstrate that FOXO1 plays a central role in regulating GC processes.

FOXO3 is also important in B-cell maturation through T_{fh} cell function, an essential cellular component of GC formation [481, 482]. *FOXO3*-deficient mice exhibit lower levels of IL-21, anti-ovalbumin antibodies when challenged with ovalbumin, and decreased T_{fh} and B-cell populations. Additionally, there is a marked reduction in the occurrence of T cell co-stimulator (ICOS)-induced Tfh differentiation [482]. *FOXO3* is strongly expressed in B cells committed to PC differentiation [481]. Thus, FOXO1 and FOXO3 play inverse roles, both being critical in facilitating mature B-cell differentiation as part of the adaptive immune response. A schematic of FOXO activity in B-cell maturation is found below (Figure 1.8).

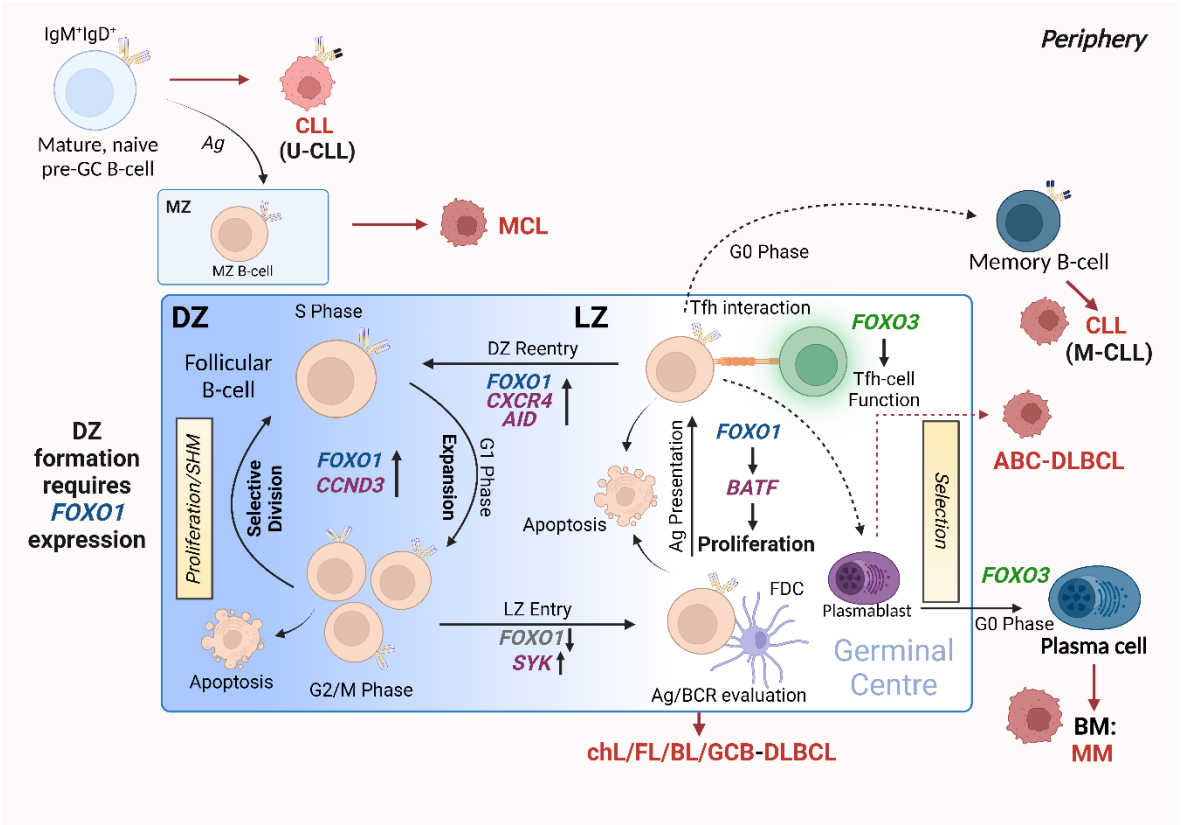

Figure 1.8: FOXO expression is essential in GC B-cell maturation [463]. FOXO expression assists in germinal centre (GC) B-cell differentiation. The formation of the GC is crucial for the generation of B-cells that produce high affinity antibodies towards specific antigens and differentiate into plasma cells (PCs) and memory B-cells. This occurs through GC-centralised processes: SHM, affinity maturation and clonal expansion. GCs consist of two distinct compartments: the DZ, in which B-cells cycle between proliferation and SHM, and the LZ, in which cells undergo evaluation and selection processes. *FOXO1* expression is critical for forming and retaining cells in the DZ. Cells then enter the LZ, where the modified/mutated antibody is tested for high-affinity towards antigen: this process requires *FOXO1* downregulation via SYK. Here, B-cells interact with FDCs to evaluate antigen affinity and BCR function, while Tfh-cell interactions aid in B-cell differentiation and proliferation by providing the appropriate signals. Of note, the LZ requires specific regulation of *FOXO1* expression to allow for correct LZ proliferation via *BATF* induction. B-cells from the LZ gain re-entry into the DZ to undergo clonal expansion regulated by *FOXO1* and *CCND3*. All the while, *FOXO3* expression maintains GC Th-cell populations and allows for the differentiation of PCs. Red arrows and malignant-like cells indicate stages in GC B-cell differentiation where B-cell malignancy can originate.

1.10.4. The differential roles of FOXOs in B-cell malignancies

FOXOs are traditionally regarded as tumour suppressors due to their canonical activity being associated with detrimental cellular fate (e.g. cell cycle arrest and apoptosis; [429]). Indeed, early studies demonstrated that the conditional triple *FOXO1/3/4* deletion in adult mice resulted in the development of thymic lymphomas and hemagiomas [483]. However, in line with FOXO family members playing an important physiological role in maintaining self-renewal in stem cell compartments [484], more recent studies revealed that FOXO family members can maintain leukaemia-initiating cells in myeloid leukaemias (AML and CML), and promote breast tumour invasion, suggesting that in certain cellular contexts FOXOs play a tumour-promoting role [485-487]. The paradox of FOXO proteins driving the inhibition or promotion of cancer development in specific contexts, and the complex regulatory mechanisms that subvert FOXO function in malignant cells identifies the need for a deeper understanding of the cellular and molecular function of these proteins in discrete cancer neoplasms.

FOXO signalling is often compromised and exploited during B-cell development and maturation to promote proliferative and anti-apoptotic signals, providing malignant cells with the means to bypass checkpoints preventing classical cancer hallmarks. Typically, this occurs in a disease-specific context, where FOXOs can exhibit bipartite behaviours, either aiding or preventing tumourigenesis. Of note, somatic point mutations of FOXO1 occur more frequently across B cell malignancies than other cancers, and within B cell malignancies occur predominantly in Burkitt's lymphoma (BL), FL and DLBCL, with a frequency of ~11%, 6% and ~5% respectively [65, 488-490]. Within these diseases, five point mutations have been identified as driver mutations of oncogenesis, where drivers are defined as mutations, fusions and copy number alterations in OncoKB [491] or CancerHotspots [492], with mutations occurring mostly in the N-terminus or forkhead DBD within exon 1. All five driver mutations are considered to be oncogenic through either: gain of function, as demonstrated in *in vitro*

studies, which showed escape from PI3K/AKT regulation through loss of AKT phosphorylation; increased nuclear sequestration and increased DNA binding compared to wildtype [493], or; loss-of function, identified through preserved AKT phosphorylation, cytoplasmic retention and decreased transcriptional activity compared to wildtype [494, 495]. Mutations of the other FOXO family members are less frequent within B cell malignancies. Further reviewed in [491]. It should be noted that the 6q21 region encoding *FOXO3* is frequently deleted in DLBCL (with deletions of 6q21-q22 occurring in 40% of ABC-DLBCL cases and 22% of GCB-DLBCL cases) [496] and is associated with adverse prognosis [497]. Deletions of 6q21 also occur in MCL, FL, ALL and CLL [496, 498].

1.10.4.1. The role of FOXOs in CLL

FOXO family members play a vital role in CLL biology, with regulation of individual family members impacting on CLL survival. FOXO family mutations occur infrequently in CLL patients, with analysis of the ICGC database (containing data from 551 CLL patients) showing that single base substitutions within *FOXO* family genes occurred in 4% (22/551) of CLL patients, of which 2% (11/551) occurred in *FOXO1*, with a functionally “high impact” missense mutation of *FOXO1* encoded in just one patient [499]. Therefore, the CLL-TME has a more significant impact on the activity of FOXO family members in CLL. FOXO3 is inactivated by chemokine expression (CCL19, CLL21, CXCL12, CXCL13) leading to subsequent BIM downregulation and increased cell survival. Expression of constitutively active FOXO3 increased levels of cell death whereas a reduction in FOXO3 expression increased cell survival, providing evidence for FOXO3 playing a tumour suppressor role in CLL cells [285]. Palacios *et al*. showed that CLL cells required elevated levels of miR-22 expression for effective proliferation, with miR-22 leading to decreased PTEN and increased PI3K-AKT signalling, particularly in poor prognostic patient cohorts. Subsequent FOXO1 inhibition coincided with reduced levels of *CDKN1B* [500]. We have demonstrated that while FOXO1 expression was upregulated in CLL cells compared with B cells from healthy donors, it appeared to be inactive, perhaps due to tonic CLL-BCR signalling. However, pharmacological inhibition of PI3K-mTOR/AKT signalling

reduced FOXO1 phosphorylation, increased FOXO1 nuclear localisation and resulted in an upregulation of FOXO1-mediated genes, ultimately inducing CLL cell death [284]. These studies indicate that FOXO1 is being prevented from performing a tumour suppressor role due to TME factors supporting the CLL cells, similar to that noted for FOXO3 [285]. In contrast, in an aggressive CLL mouse model, FOXO1 was shown to be a driver of disease through induction of *IGF1R* in PI3K-inhibitor-resistant SLO tumours: this was attenuated by pharmacological FOXO1 inhibition (AS1842856) [501]. Interestingly, FOXO1 has also been reported to induce *GAB1* which aids in maintenance of CLL cell survival through sustained basal AKT phosphorylation [502]. These studies suggests that a low level of FOXO1 activity, possibly promoted through tonic BCR signalling, sustains CLL cell survival, while higher FOXO1 activity induced by inhibition of upstream PI3K/AKT signals through drug treatment triggers CLL cell death [284, 502]. A recent study demonstrated that hyperactivation of PI3K/AKT activity mediated by SHIP1 inhibition, can induce CLL cell death [281]. While this study did not directly address the involvement of the FOXO family in the induction of cell death, it suggests that the strength of signal upstream of FOXO may regulated the threshold of FOXO activity induced, which in turn impacts on cell fate decisions within CLL. Of note, discrete TMEs are also likely to play a major role in modulating FOXO activity.

1.11. Project aims

Previous work has significantly improved our understanding of the mechanisms surrounding FOXO1 activity and its subsequent downstream effects in CLL. However, roles for FOXO3 and FOXO4 have yet to be fully elucidated. This thesis aims to investigate further the intricate roles and regulation of FOXO1, while exploring potential novel roles for FOXO3 and FOXO4. We will look to understand how FOXOs are differentially expressed and regulated within the context of CLL disease biology, utilising BTK and dual mTOR inhibition as pharmacological tools to understand distinct FOXO family regulation in different CLL disease contexts. Downstream of mTOR-AKT pathways, we will look to understand the specific effects modulated by distinct FOXO activity. Fundamentally, this thesis aims to provide information regarding whether harnessing FOXO activity *via* the inhibition of upstream FOXO negative regulators is a potentially effective, novel therapeutic approach for the treatment of CLL. As such, we hypothesise that activation of FOXO family members elicits tumour suppressive effects in CLL. The three major aims of this project are as follows:

i. Understand the expression and regulation of distinct FOXOs in different *in vitro* CLL models.

ii. Use pharmacological signal inhibition as a tool to elucidate the mechanisms by which FOXO and FOXO targets are regulated

iii. Assess the implications of reducing FOXO expression on cell fate decisions including CLL proliferation and survival.

These aims will address the overarching hypothesis by determining the expression, regulation and activity of FOXO isoforms and their transcript targets, as well as providing information on discrete functions of FOXO isoforms in CLL.

2. Materials & methods

2.1. Materials

2.1.1. Companies/suppliers

Company	Address
Abcam plc	Discovery Drive Cambridge Biomedical Campus, Cambridge CB2 0AX, UK
Active Motif	Office Park Nysdam, Avenue Reine Astrid 92, B1310 La Hulpe, BE
Agilent Technologies LDA UK Ltd (DAKO)	Cheadle Royal Business Park, Stockport, Cheshire SK8 3GR, UK
Applied Biosystems (ThermoFisher Scientific)	Unit 3, Fountain Dr, Inchinnan, Renfrew PA4 9RF, UK
AstraZeneca PLC	1 Francis Crick Avenue, Cambridge Biomedical Campus, Cambridge CB2 0AA, UK
BD Biosciences	Binningerstrasse 94, 4123 Allschwil, CH
Biolegend UK Ltd	4B, Highgate Business Centre, 33 Greenwood Pl, Kentish Town, London NW5 1LB, UK
Cell Signalling Technology Europe BV (CST)	Dellaertweg 9b, 2316 WZ Leiden, NL
Fisher Scientific (ThermoFisher Scientific)	Unit 3, Fountain Dr, Inchinnan, Renfrew PA4 9RF, UK
Griener Bio-One Ltd.	Unit 5 Brunel Way, Stonehouse GL10 3SX, UK
Invitrogen (Thermo Fisher Scientific)	Unit 3, Fountain Dr, Inchinnan, Renfrew PA4 9RF, UK
LI-COR Biosciences	Siemensstraße 25, 61352 Bad Homburg vor der Höhe, DE
Merck Millipore	Merck KGaA, Frankfurter Strasse 250, Darmstadt, 64293, DE
Miltenyi Biotech	Friedrich-Ebert-Straße 68, 51429 Bergisch Gladbach, DE
New England Biolabs	75-77 Knowl Piece, Hitchin SG4 0TY, UK
Novogene	25 Science Park,Milton, Cambridge CB4 0FW, UK

PeproTech EC Ltd.	29 Margravine Rd, Hammersmith, London W6 8LL, UK
QIAGEN Ltd	Skelton House, Lloyd Street North, Manchester M15 6SH, UK
Santa Cruz Biotechnology	Bergheimer Str. 89-2, 69115 Heidelberg, DE
Sartorius GmbH	Otto-Brenner-Str. 20, 37079 Götingen, DE
Scientific Lab Supplies (SLS) Ltd.	204 Main St, Coatbridge, ML5 3RB, UK
Sigma-Aldrich Co Ltd.	Second Ave, Heatherhouse Industrial Estate, Irvine KA12 8NB, UK
STEMCELL Technologies	Cambridge Research Park, 8100 Beach Dr, Waterbeach, Cambridge CB25 9TL, UK
Stratech Scientific Ltd.	Cambridge House, St Thomas' Pl, Ely CB7 4EX, UK
Thermo Fisher Scientific	Unit 3, Fountain Dr, Inchinnan, Renfrew PA4 9RF, UK

Table 2.1: Companies/Suppliers

2.1.2. Flow cytometry

2.1.2.1. Antibodies/dyes

Antibodies/Stains/Reagents	Cat.	Supplier
7-AAD	559925	BD Biosciences
Alexa Fluor® 647 Mouse anti-H2AX (pS139)	560447	BD Biosciences
Alexa Fluor® 647 Mouse IgG1, κ Isotype Control	566011	BD Biosciences
Annexin V (FITC)	556419	BD Biosciences
APC-Cy7 Mouse Anti-Human CD19	557791	BD Biosciences
APC-Cy7 Mouse Anti-Human CD45	557833	BD Biosciences
CellTrace™ Violet	C34557	ThermoFisher Scientific
CountBright™ Absolute Counting Beads	C36950	ThermoFisher Scientific
DAPI	564907	BD Biosciences

PI/Rnase Staining Buffer	550825	BD Biosciences

Table 2.2: Flow cytometry antibodies/dyes

2.1.3. Western blotting

2.1.3.1. Antibodies

Antibody	Dilution	Diluent	Cat.	Supplier
4E-BP1 (53H11) Rabbit mAb	1 in 1000	5 % BSA/TBST	9644S	CST
AKT (pan) (C67E7) Rabbit mAb	1 in 1000	5 % BSA/TBST	4691S	CST
AKT Thr308 (D25E6) XP Rabbit mAb	1 in 1000	5 % BSA/TBST	13038S	CST
BCL2 (124) Mouse mAb	1 in 1000	5 % BSA/TBST	15071S	CST
BCL-XL Rabbit Ab	1 in 1000	5 % BSA/TBST	2762S	CST
BIM (C34C5) Rabbit mAb	1 in 1000	5 % BSA/TBST	2933S	CST
Cyclin D2 (D52F9) Rabbit mAb	1 in 1000	5 % BSA/TBST	3741	CST
eEF2 Rabbit Ab	1 in 1000	5 % BSA/TBST	2332	CST
eEF2 Thr56 Rabbit Ab	1 in 1000	5 % BSA/TBST	2331	CST
eIF4E Rabbit Ab	1 in 1000	5 % BSA/TBST	9472	CST
FOXO1 (C29H4) Rabbit mAb	1 in 1000	5 % BSA/TBST	2880S	CST
FOXO3 (D19A7) Rabbit mAb	1 in 1000	5 % BSA/TBST	12829	CST
FOXO4 Rabbit Ab	1 in 1000	5 % BSA/TBST	9472	CST
GADD45A (D17E8) Rabbit mAb	1 in 1000	5 % BSA/TBST	4632	CST
GAPDH (D16H11) XP Rabbit mAb	1 in 2000	5 % BSA/TBST	5174S	CST
IRDye 680RD Goat anti-Rabbit IgG	1 in 5000	TBST	92668071	LI-COR

IRDye 800CW Goat anti-Mouse IgG	1 in 5000	TBST	82708364	LI-COR
Lamin A/C Rabbit Ab	1 in 1000	5 % BSA/TBST	2032S	CST
MCL1 Rabbit Ab	1 in 1000	5 % BSA/TBST	4572S	CST
p21 waf1/cip1 (12D1)	1 in 1000	5 % BSA/TBST	2947S	CST
p27 kip1 (D69C12) XP Rabbit mAb	1 in 1000	5 % BSA/TBST	3686	CST
p4E-BP1 Thr37/46 Rabbit Ab	1 in 1000	5 % BSA/TBST	9459S	CST
p70 S6 Kinase (49D7) Rabbit mAb	1 in 1000	5 % BSA/TBST	2708	CST
pAKT Ser243 (D9E) XP Rabbit mAb	1 in 1000	5 % BSA/TBST	4060S	CST
PARP (46D11) Rabbit mAb	1 in 1000	5 % BSA/TBST	9532S	CST
PDCD4 (D29C6) XP Rabbit mAb	1 in 1000	5 % BSA/TBST	9535	CST
pFOXO1 Thr24/pFOXO3 T32 Rabbit Ab	1 in 1000	5 % BSA/TBST	9464S	CST
pFOXO3 Ser253 Rabbit mAb	1 in 1000	5 % BSA/TBST	9466	CST
pFOXO4 Ser193 Rabbit mAb	1 in 1000	5 % BSA/TBST	9471	CST
phospho-p70 S6 Kinase Thr389 (108D2) Rabbit mAb	1 in 1000	5 % BSA/TBST	9234	CST
pPRAS40 Thr246 (C77D7) Rabbit mAb	1 in 1000	5 % BSA/TBST	2997	CST
PRAS40 (D23C7) XP Rabbit mAb	1 in 1000	5 % BSA/TBST	2691S	CST
pRictor Thr1135 (D30A3) Rabbit mAb	1 in 1000	5 % BSA/TBST	3806	CST
pS6 Ribosomal Protein Ser235/236 (D57.2.2E) XP Rabbit mAb	1 in 1000	5 % BSA/TBST	4858S	CST
Rictor (D16H9) Rabbit mAb	1 in 1000	5 % BSA/TBST	9476	CST
S6 Ribosomal Protein (54D2) Mouse mAb	1 in 1000	5 % BSA/TBST	2317S	CST
β-actin (8H10D10) Mouse mAb	1 in 2000	5 % BSA/TBST	3700	CST
β-tubulin Rabbit Ab	1 in 2000	5 % BSA/TBST	2146S	CST
γ-H2AX Ser139	1 in 1000	5 % BSA/TBST	2577	CST

Table 2.3: Antibodies used for Western blotting

2.1.4. RT-qPCR

2.1.4.1. TaqMan assays

Target	Assay ID	Supplier
18S	Hs03003631_g1	ThermoFisher Scientific
B2M	Hs00187842_m1	ThermoFisher Scientific
BBC3	Hs00248075_m1	ThermoFisher Scientific
BCL2L1	Hs00236329_m1	ThermoFisher Scientific
BCL2L11	Hs00197982_m1	ThermoFisher Scientific
CCND1	Hs00765553_m1	ThermoFisher Scientific
CCND2	Hs00153380_m1	ThermoFisher Scientific
CCNG2	Hs00171119_m1	ThermoFisher Scientific
CDKN1A	Hs00355782_m1	ThermoFisher Scientific
CDKN1B	Hs01597588_m1	ThermoFisher Scientific
FOXO1	Hs01054576_m1	ThermoFisher Scientific
FOXO3	Hs00818121_m1	ThermoFisher Scientific
FOXO4	Hs00172973_m1	ThermoFisher Scientific
FOXO6	Hs01010449_s1	ThermoFisher Scientific
GADD45A	Hs00169255_m1	ThermoFisher Scientific
IGF1R	Hs00609566_m1	ThermoFisher Scientific
MCL1	Hs01050896_m1	ThermoFisher Scientific
MTOR	Hs00234508_m1	ThermoFisher Scientific
RAPTOR	Hs00375332_m1	ThermoFisher Scientific

RICTOR	Hs00380903_m1	ThermoFisher Scientific
SESN3	Hs00914870_m1	ThermoFisher Scientific
TP53	Hs01034249_m1	ThermoFisher Scientific

Table 2.4: TaqMan primers used for RT-qPCR

2.2. Methods

2.2.1. General tissue culture

All procedures involving cell culture were conducted within a laminar flow hood using sterile technique. The cell cultures themselves were incubated at 37°C in 5% carbon dioxide (CO_2) in a humidified atmosphere.

2.2.1.1. Cell culture media

Specific cells/cell lines require specific supplements and nutrients to support the growth and maintenance of the cells. Within this work, 'complete' DMEM was used to culture MEC-1 cells, where 'complete' denotes the addition of 10% FBS, 50 U/mL penicillin, 50 mg/mL streptomycin (1% Pen Strep) and 2 mM L-glutamine (1% L-glutamine [ThermoFisher Scientific]) to DMEM media. 'Complete' RPMI was used for culturing primary CLL cells and HG3 cells (RPMI-1640 media containing 10% FBS, 50 U/mL penicillin, 50 mg/mL streptomycin [1% Pen Strep] and 2 mM L-glutamine [1% L-glutamine] [ThermoFisher Scientific]). Both types of media were used in the culture of HEK293T cells, depending on the subsequent cell line targeted for shRNA mediated knockdowns. Of note, when not being used for shRNA applications, HEK293T cells would be cultured in 'complete' DMEM media.

2.2.1.2. Primary CLL cells

For patient samples, ethical approval was attained from the West of Scotland Ethics Committee, NHS Greater Glasgow and Clyde, UK. CLL cells were isolated from CLL patient PB samples following informed consent [503]. Peripheral blood mononuclear cells (PBMCs) were isolated from total PB *via* density centrifugation with Histopaque-1077 Hybri-Max Histopaque (Sigma) according to manufacturer's instructions: CLL PB was washed 1:1 with RT CLL wash buffer (PBS containing 0.5 % FBS, 2 mM EDTA) and layered on top of either 10 mL (for 30 mL of PB) or 4 mL (for 10 mL of sample) Histopaque in a 50 mL or 15 mL reaction tube, respectively. Samples were then centrifuged at 400 *g* for 30 min at RT. Of note, the centrifuge brake was disabled to prevent any undue disruption of the Histopaque:PBMC layer. Following centrifugation, the white 'buffy' layer of white blood cells located between the blood plasma and Histopaque fractions was collected into a new 50 mL reaction tube, where the fraction was then washed with CLL wash buffer at a ratio of 1:4 mononuclear cells:wash buffer. Isolated mononuclear cells were then spun at 300 *g* for 10 min at RT. The supernatant was then removed and 10 mL CLL wash buffer was used to resuspend the cell pellet and centrifuged again at 300 *g* for 10 min at RT. The cells were resuspended in a volume of CLL wash buffer (<40 mL) and counted to determine absolute cell number. In cases where cell numbers were low, flow cytometry was used to determine the purity with regards to CLL cell populations, defined as >90% $CD19^+$ $CD5^+$. It is worth noting that healthy $CD19^+$ B-cell donor samples were isolated using human CD19 Microbeads using MACS separation according to manufacturer's instructions (Miltenyi). Of note, only protein lysates derived from healthy B-cell donor samples that were >90% pure (following enrichment, determined by flow cytometry) were used in this study (n=5), and B-cell donor samples were not age-matched to CLL patients.

In instances where leukocyte counts were low (classified as <40 x 10^9 leukocytes/L), RosetteSep human B-cell enrichment cocktail (STEMCELL Technologies) was used to enrich for B-cell populations (according to manufacturer's instructions). PB samples were incubated in a 50 mL reaction tube for 20 min at RT with 50 µL/mL PB blood of the RosetteSep reagent.

Samples were then diluted 1:1 with CLL wash buffer and were processed according to the Histopaque procedure described above. Populations enriched for CLL-B-cells were defined as >90 % $CD19^{+}CD5^{+}$ (*via* flow cytometry). CLL cell populations were either cultured at >5 x 10^{6} cells/mL in complete RPMI or cryopreserved. Information detailing primary samples used within this thesis are described below (Table 2.5), outlining the presence of prognostic markers including Binet stage, ZAP-70 status, *IGHV* mutational status, as well as prominent cytogenetic aberrations (Del(17p)/(11q) or T12). Of note, with regards to cytogenetic aberrations, typically only del(17p) and del(11q) are assessed in clinic, so patients lacking either of these aberrations could still possess other characteristic aberrations that have not yet been profiled.

Patient ID	**Tx (Y/N)**	**Sex (M/F)**	**Binet**	**ZAP-70**	***IGHV* mut**	**Cytogenetics**
8	N	F	A	neg	U-CLL	del(11q)
18	Y	F	B	pos	U-CLL	del(11q)
35	N	M	A	pos	U-CLL	del(11q)
46	N	F	A	pos	M-CLL	no del(11q) /del(17p)
97	Y	M	C	-	-	-
106	Y	M	B	pos	-	no del(11q) /del(17p)
116	N	M	A	pos	-	no del(11q) /del(17p)
119	N	F	B	-	-	del(17p)
125	N	M	C	pos	-	no del(11q) /del(17p)
132	N	F	B	pos	-	del(17p)
138	Y	F	A	pos	-	no del(11q) /del(17p)
142	Y	F	B	pos	-	no del(11q) /del(17p)
143	Y	F	C	pos	-	del(11q)
150	N	M	A	pos	-	no del(11q) /del(17p)
151	N	M	B	-	-	del(11q)
155	Y	M	B	-	-	del(11q)
162	-	M	-	-	-	-
165	N	M	C	-	-	del(11q)
166	Y	M	C	-	-	del(11q)/del(17p)
167	N	M	C	-	-	-
168	N	M	B	-	-	del(13q)/T12

169	N	F	C	-	-	no del(11q) /del(17p)
170	Y	F	-	-	-	-
171	N	M	C	-	-	no del(11q) /del(17p)
172	-	M	-	-	-	no del(11q) /del(17p)
173	Y	M	B	-	-	-
175	Y	M	C	-	-	-
176	N	M	A	-	-	no del(11q) /del(17p)
177	N	M	B	-	-	no del(11q) /del(17p)
179	Y	M	B	-	-	no del(11q) /del(17p)
180	Y	F	B	-	-	no del(11q) /del(17p)
185	-	M	C	-	-	-
186	N	M	C	-	-	-
187	N	M	B	-	-	-
189	Y	M	B	-	-	no del(11q) /del(17p)
190	N	M	C	-	-	no del(11q) /del(17p)
191	N	M	A	-	-	del(11q)/del(17p)
193	-	F	A	-	-	-
194	N	M	C	-	-	-
196	N	F	B	-	-	-
197	Y	M	C	-	-	del(17p)
198	Y	M	-	-	-	-
200	N	M	C	-	-	no del(11q) /del(17p)
201	-	M	B	-	-	-
203	N	M	C	-	-	no del(11q) /del(17p)
215	N	F	B	-	-	no del(11q) /del(17p)

Table 2.5: CLL patient information. Tx = prior therapy (Y/N), Gender (M/F), Binet stage (A, B, C); ZAP-70 status (positive/negative); *IGHV* mutational status (U- or M-CLL, limited information available); cytogenetics (as explained); hyphens indicate prognostic information that was not considered in clinic.

2.2.1.3. Cell lines

The general procedure for maintaining cell lines is performed in line with ATCC/DSMZ guidelines. Cell lines would be grown to the point of 20 passages before a new vial of cells would be thawed.

Cell line	Origin	Culture conditions	Details
MEC1	MEC-1 cells were initially extracted in 1993 from the peripheral blood of a 61-year-old Caucasian male suffering with CLL. MEC-1 cells are $CD5^+$ $CD19^+$ with a del(17p) deletion [504].	**DMEM (10% FBS; 1% P/S; 1% L-glutamine)**; Maintained around 0.5-2.0 x 10^6 cells/mL; subculture to be split in a dilution of 1:3 every 2-3 days. Cultured upright in $T75^2$ culture flasks (DSMZ, 2021)	The MEC-1 cell line was received as a gift from Dr Joseph Slupsky (University of Liverpool, UK).
HG3	HG3 cells were isolated from a 70-year-old male CLL patient. HG3 cells are $CD5^+CD19^+$ with a del(13q) deletion [505].	**RPMI (10% FBS; 1% P/S; 1% L-glutamine);** Maintained around 0.5-2.0 x 10^6 cells/mL; subculture to be split at a dilution of 1:3 every 2-3 days. Cultured upright in $T75^2$ culture flasks.	The HG3 cell line was received as a gift from Dr Mark Catherwood (Queen's University Belfast, UK).
NT-L	Mouse fibroblast L cells derived from subcutaneous connective tissue and are an effective 'empty vector' for potential subsequent transfection [506].	**RPMI (10% FBS; 1% P/S; 1% L-glutamine);** Adherent cells, passaged typically at 70-80% confluency, optimal split dilution of 1:4-1:10 every 2-3 days. Cultured in $T75^2$ culture	NT-L cells were gifted by Professor J. Gordon of the University of Birmingham.

		flasks (ATCC, 2021)	
CD40L	Mouse fibroblast L cells (**NT-L**) subsequently transfected with human CD154 (CD40L).	**RPMI (10% FBS; 1% P/S; 1% L-glutamine);** Same culture and splitting conditions as NT-L cells (see above [**NT-L**]).	The CD40L cell line was gifted by Professor J. Gordon of the University of Birmingham.
HEK293T	Specific Human Embryonic Kidney (HEK) cell variant, highly transfectable, contains the SV40 T-antigen [507].	**DMEM/RPMI (10% FBS; 1% P/S; 1% L-glutamine);** Seeded at ~2 x 10^6 cells and passaged at 70% confluency every 2-3 days at 1:9 ratio. Cultured in $T75^2$ culture flasks.	POG-LRC lab stocks

Table 2.6: Cell lines (origin, culture conditions and acquisition details)

2.2.1.4. Cryopreservation of cells

2.2.1.4.1. Primary cells

PB CLL cells not required for immediate use were stored in the POG-LRC CLL cell bank. Following initial counts of freshy isolated mononuclear cells, cells were resuspended at a concentration of 5 x10^7 – 1 x10^8 cells/mL in CLL 'freezing solution' (FBS supplemented with 10 % DMSO), aliquoted into cryovials (Greiner Bio-One) and transferred to a Mr. Frosty™ freezing container (ThermoFisher Scientific), which is filled appropriately with 100% isopropanol. The container was transferred to a -80°C freezer to allow for freezing at 1°C/min. Following prolonged exposure to -80°C temperature, cryovials were transferred to liquid nitrogen storage.

2.2.1.4.2. Cell lines

Suspension cell lines were cryopreserved using methods similar to that of primary CLL cells, albeit at lower concentrations of 6 – 8 x10^6 cells/mL. Of note, cell line stocks were initially created from 'master' stocks, where subsequent 'working' stocks were created to allow for a sufficient supply of cell line samples, where cell lines would be cryopreserved at passages lower than 10 to allow for maximal use from thaw; cells would be discarded after completion of experiments at later passages, where cells would not be used any later than passage 20. Adherent NTL, CD40L and HEK293T cells were cryopreserved from following expansion of master stocks after achieving <70% confluency. Following this, cells were washed gently with 10 mL PBS and detached using 3 mL Trypsin-EDTA (0.5 %; ThermoFisher Scientific) for 3 – 5 min. Cell flasks were then lightly tapped to ensure complete detachment of cells and viewed under a light microscope to confirm >90 % detachment. Once the cells were detached, 7 mL PBS was added to neutralise the effects of Trypsin-EDTA and to effectively aspirate the cells into a 15 mL reaction tube. A cell count was taken, and the cells were spun at 300 *g* for 5 min. The cell pellet was then resuspended in freezing solution at 6 – 8 x 10^6 cells/mL to be frozen as per the same procedure.

2.2.1.5. Cell thawing

2.2.1.5.1. Primary cells

Banked CLL samples were thawed in a 37 °C water bath and then transferred to 50 mL reaction tubes. The cells were diluted dropwise over 10 min using 'DAMP' solution (PBS containing 10 U/mL DNase I, 1% Human Serum Albumin (HSA), 2.5 mM $MgCl_2$, 8.2 mM Tri-Sodium Citrate [$Na_3C_6H_5O_7$]). Following this, the cells were spun at 300 *g* for 5 min then resuspended in 10 mL 'complete' RPMI. The centrifugation process was then repeated a second resuspension in 'complete' RPMI at a concentration of 1x10^7 cells/mL and were cultured overnight at 37°C

to aid with recovery. The cells were counted again following recovery to provide a viable cell count. While being a rare occurrence, samples that were not suitably viable upon thaw (typically >70%) upon thaw were discarded, made note of, and not used for further experimental work.

2.2.1.5.2. Cell lines

Cell lines were thawed in a 37°C water bath and transferred to a 15 mL reaction tube. Here, the cells were diluted (slowly) with 10mL 'complete' DMEM/RPMI warmed to 37°C. The cells were then centrifuged at 300 *g* for 5 min and resuspended in 10 mL 'complete' DMEM/RPMI and transferred to either a $T25^2$ or a $T75^2$ flask and were left to recover in a 37°C incubator. Experiments commenced after at least the first passage.

2.2.1.6. Drug treatments

AS1842856 (FOXO1 inhibitor), AZD5363 (pan AKT inhibitor), AZD8055 (mTORC1/2 inhibitor), ibrutinib (BTK inhibitor), rapamycin (mTORC1 inhibitor) and venetoclax (BH3 mimetic) were solubilised in DMSO to make 10 mM stock solutions. AZD5363 was solubilised in DMSO to make a 100 mM stock solution. Stock solutions were stored as 10 µL aliquots for up to 2 years at -80°C. Aliquots could be thawed and stored at 4°C for up to a week, however they were discarded after experimental use at RT. Standard working concentrations of these drugs are described below (Table 2.7):

Drug	Stock concentration (mM)	Working concentration (nM)
AS1842856	10	100
AZD5363	100	1000
AZD8055	10	100
Ibrutinib	10	1000
Rapamycin	10	10
Venetoclax	10	1 – 1000

Table 2.7: Drug stocks and working concentrations

Stock drug aliquots were diluted to working concentrations in cell culture media used to culture the cell type of choice. A DMSO 'vehicle' or 'no drug' control (NDC) was used as a negative control in experiments with drug treatments with drugs solubilised in DMSO. In experiments involving drug treatment, cells were exposed to drug for the entirety of the experiment. Of note, in experiments involving AS1842856 treatment in combination with other drugs, AS1842856 was added as a pre-treatment 30 min before the addition of other drugs (e.g. AZD8055 and ibrutinib). In addition, in experiments involving F(ab')$_2$ stimulation, drugs were added as a pre-treatment 30 min prior to the addition of F(ab')$_2$. In experiments involved the CD40L system, primary cells were co-cultured O/N with NTL/CD40L co-cultures before the addition with drug to allow for the cells to equilibrate in the system.

2.2.1.7. F(ab')$_2$ stimulation

F(ab')$_2$ fragments (Stratech Scientific) are IgM-specific antibodies that were generated by selective pepsin digestion of IgG antibodies. F(ab')$_2$ fragment stimulation is established as an effective method of inducing BCR signalling in CLL cells. F(ab')$_2$ fragments were solubilised at a concentration of 1.3 mg/mL and stored at 4 °C for up to a year. F(ab')$_2$ fragment stimulation was used to stimulate primary CLL cells for 1 hr on 'plastic' (i.e. no stromal co-culture) at a concentration of 13 µg/mL F(ab')$_2$ fragments in samples containing 5 – 10 x 10^6 cells/mL. Cells were subsequently collected after this time period and were processed to be used in subsequent studies.

2.2.1.8. NTL and CD40L (+IL-4/IL-21) co-culture systems

Co-culture of primary CLL cells with CD40L-expressing stroma is an established model designed to investigate CLL-TME interactions by mimicking CLL-T-cell interactions [243].

3 x10^5 cells/mL NT-L or CD40L were seeded into cell culture plates and left for >2 hr to adhere. Once adherence was confirmed, freshly isolated or thawed CLL cells were added to the NT-L monolayer at concentrations of 2-5 x10^6 cells/mL in complete RPMI and were supplemented with either 10 ng/mL IL-4 or 15 ng/mL IL-21 *via* direct dilution from 10 µg/mL stocks of recombinant human exogenous cytokine (PeproTech) that were previously reconstituted in ddH_2O. Of note, these stocks were prepared in 50 µL aliquots and were stored at -80°C. Following addition of cytokine, co-cultures were incubated O/N to allow for CLL cell equilibration to the co-culture system prior to the addition of drug treatments. The length of incubation described discounts the O/N equilibration period.

2.2.2. Flow cytometry

2.2.2.1. Apoptosis assays

Annexin V/7AAD or Annexin V/DAPI staining allows us to discern viable (Annexin^{neg}/7AAD^{neg}) cell populations from early (Annexin V^{pos}/7AAD^{neg}/DAPI^{neg}) and late (Annexin V^{pos}/7AAD^{pos}/DAPI^{pos}) apoptotic cell populations. Unless stated otherwise, Annexin V/7AAD was primary conducted in cell populations with prior CellTrace Violet staining (Figure 2.1), while Annexin V was partnered with DAPI staining in the absence of CTV.

Apoptotic staining was conducted following drug treatments of cells for specific time periods. Once the time periods had concluded, cells were collected and transferred to FACS tubes. Cells were washed with 1 mL HBSS (ThermoFisher

Scientific) and centrifuged at 500 *g* for 1 min using a SeroFuge (Clay Adams). HBSS was used as it contains calcium to allow binding of Annexin V to phosphatidylserine molecules. After a further wash step, the cells were resuspended in 100 µL HBSS and stained at a concentration of 1 x10^6 cells/100 µL HBSS with Annexin V/7AAD (Table 2.8). The cells were then incubated at RT for 15 min protected from light. Following 15 min incubation, the cells were 'quenched' with 300 µL HBSS and visualised *via* flow cytometry. For Annexin V/DAPI staining, cells were stained with Annexin V for 15 min followed by the addition of DAPI just prior to analysis. Table 2.8 outlines the volumes of dye used for Annexin V/7-AAD or Annexin V/DAPI staining:

Stain	Volume/sample (µL)
Annexin V (FITC)	3
7-AAD (PerCP-Cy5)	3
DAPI	1
in **HBSS**	Total volume: **100 µL**

Table 2.8: Stains/dyes used in FACS apoptosis assays for CLL cell lines

For primary CLL cells on NTL/CD40L co-culture, CLL cells were first stained with either anti-human CD45 or anti-human CD19 antibody for 30 min at 4°C prior to Annexin V/7AAD staining in 100 µL HBSS to discern CLL cell populations from NTL populations. Following this, cells were washed with 1 mL HBSS and centrifuged at 500 *g* for 1 min. The cells were then resuspended in 100 µL HBSS to be stained with Annexin V/7AAD. Table 2.9 outlines volumes for selecting and staining primary CLL cells with Annexin V/7AAD:

For primary CLL cells,	Volume/sample (µL)
Human anti-CD45 (APC-Cy7)	3
or Human anti-CD19 (APC-Cy7)	3
(30 min incubation at 4 ºC), wash	in **100 µL HBSS**
Annexin V (FITC)	3
7-AAD (PerCP-Cy5)	3
Final volume	**100 µL HBSS**

Table 2.9: Stains/dyes used for determining cell apoptosis in primary CLL cells

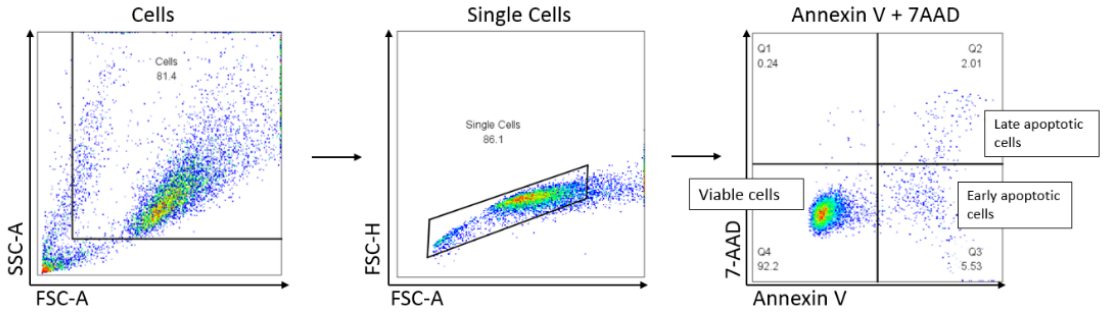

Figure 2.1: Gating strategy for Annexin/7AAD staining in CLL cells. Cells were gated by FSC/SSC, followed by gating of single cells on FSC-A/H. Cells could then be gated on a scatter plot for Annexin V (FITC)/7-AAD (PerCP-Cy5) to determine viable (Annexin V^{neg}/7-AAD^{neg}), early apoptotic (Annexin V^{pos}/7-AAD^{neg}) and late apoptotic (Annexin V^{pos}/7-AAD^{pos}) cell populations. Of note, the same gating strategy applies to cells stained with DAPI instead of 7-AAD (against Annexin V), although the 405 nm laser line is used (DAPI) instead of the 488 nm line (7-AAD).

2.2.2.2. PI staining

Cell cycle analysis allowed for the quantification of the DNA content in the cells in response to stimulatory or drug conditions. CLL cells were transferred to FACS tubes at the end of their culture/treatment period and were washed twice in 1 mL ice-cold PBS. Following this, the cells were 'fixed' using 1 mL ice-cold 80% ethanol (Sigma) which was added slowly dropwise to the cell pellet while gently vortexing. The cells were then incubated on ice for >30 min (or stored at -20˚C to be analysed within a <7 days). After fixation, the cells were washed in 1 mL ice-cold PBS and centrifuged using the Serofuge at 500 *g* for 1 min. To stain the cells, 400 µL PI/RNase staining buffer (BD Biosciences) was added and incubated

for 20 min, protected from light. Finally, the cells were analysed *via* flow cytometry at a 'low' flow rate to allow for suitable acquisition of cells in different cell cycle stages (Figure 2.2).

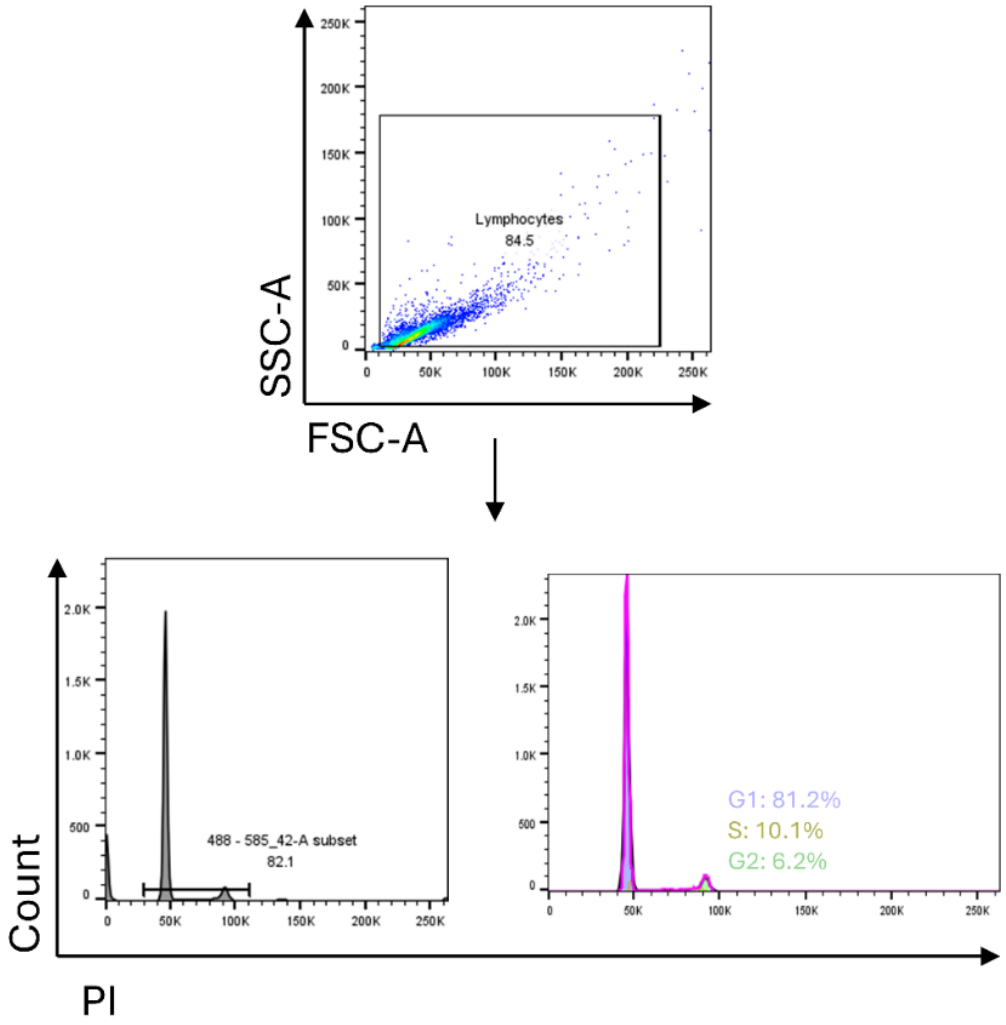

Figure 2.2: Gating strategy for PI staining. Cells were gated using SSC/FSC scatter plots, followed be acquisition of the PI stain using the 488 nm laser line to determine DNA content of cell lines/primary CLL cells. DNA content was determined using the histogram display with the Watson Pragmatic algorithm (shown bottom right). DNA content could be subsequently calculated for cell populations in G0/G1 (blue/purple), S (yellow) and G2 (green) cell cycle phases.

2.2.2.3. CellTrace™ Violet cell proliferation assay

CellTrace™ Violet measures the rate of cell division via dye dilution using flow cytometry, where the CTV dye is shared between daughter cells, thereby the rate of proliferation is associated with a reduction in mean fluorescence

intensity (MFI) [508]. CLL cell lines (MEC1 and HG3) and primary cells were first washed with 5 mL PBS, then counted and resuspended in PBS at a concentration of 2 x10^6 cells/mL. Here, the CTV dye was added at a 1:1000 dilution, and the cells were incubated at 37°C for 20 min, protected from light. The cells were then spun for 5 min at 300 *g* and resuspended in an appropriate volume of media (1.25 x10^6/mL for CLL cells). 1 mL CTV-labelled CLL cells was then added to stromal cell co-cultures in a 6-well plate. Co-cultures were then supplemented with 10 ng/mL IL-4 or 15 ng/mL IL-21 (Peptrotech) per well, followed by drug treatment after O/N equilibration. A 'no drug control' (NDC) well containing CD40L stromal cells was used as a negative control. The cells were then co-cultured for 3 days then analysed every 2 days via flow cytometry for a period of up to 14 days; every second analysis would involve removing the CLL cells and presenting them to a plate containing fresh NT-L/CD40L cells (including fresh IL-4/IL-21 and drugs). In the case of CLL cell lines, 2 mL cells (0.5 x10^6/mL) were added to each well of a 6-well plate followed by drug treatment.

To analyse *via* flow cytometry, cells were collected into FACS tubes, centrifuged at 500 *g* for 1 min (Serofuge), washed with 1 mL PBS (or 1X HBSS if staining further with Annexin V/7AAD) and resuspended for analysis in 0.5 mL PBS/HBSS accordingly. Gating strategies for CTV analysis are shown (Figure 2.3). Primary CLL cells on NTL/CD40L co-culture, cultures were stained with either anti-Human CD45 or CD19 antibody prior to sample acquisition to discern CLL cells from NTL stroma - this was conducted in 100 µL PBS prior to resuspension in 0.5 mL PBS. This was not conducted for MEC1 or HG3 cells as they are immortalised and do not require CLL-CD40L co-cultures to proliferate.

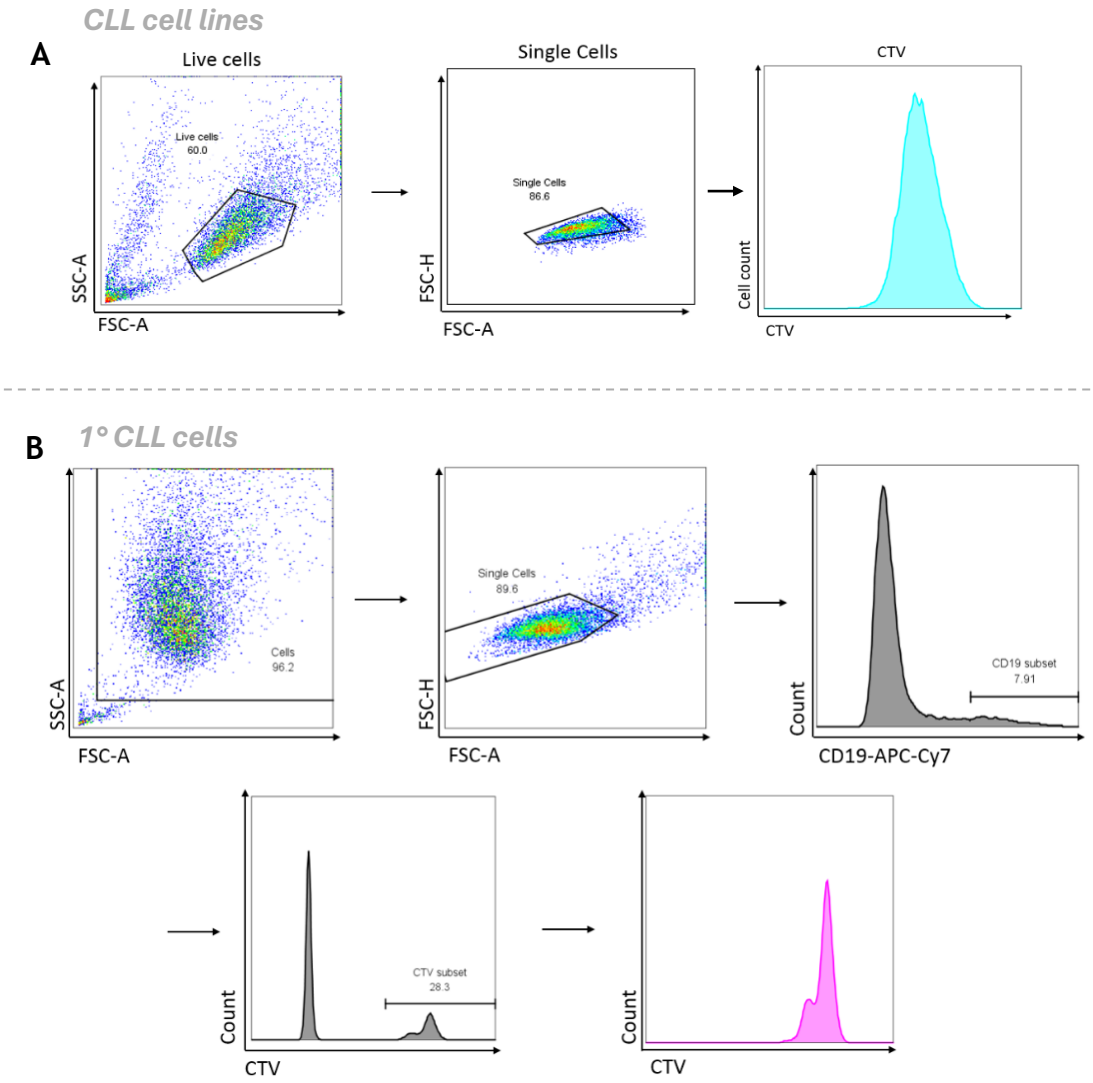

Figure 2.3: CTV gating strategy for CLL cell lines and primary CLL cells. (A) Gating strategy for CLL cell lines: acquisition of single cells followed by visualisation of CTV intensity. (B) Gating strategy for primary CLL cells: acquisition of single cells followed by positive selection of $CD19^{+}/CD45^{+}$, CTV^{+} cells. In both cases, CTV intensity was determined by geometric mean (450 nm channel).

2.2.2.4. Cell counting

Cell counts were retrieved using Countbright™ Absolute Counting Beads (Thermofisher Scientific) as per manufacturer's instructions. Prior to analysis, 50 µL Countbright™ beads were added to each cell sample and vortexed. Cells were monitored via FSC and SSC channels on the FACSCanto II analyser (BD Biosciences, Figure 2.4), where counting beads displayed with higher SSC to that

of the cell population, enabling gating. As such, samples with beads were recorded with a set number of beads (≥1000 bead events) for each sample: the same number of beads were counted for each sample.

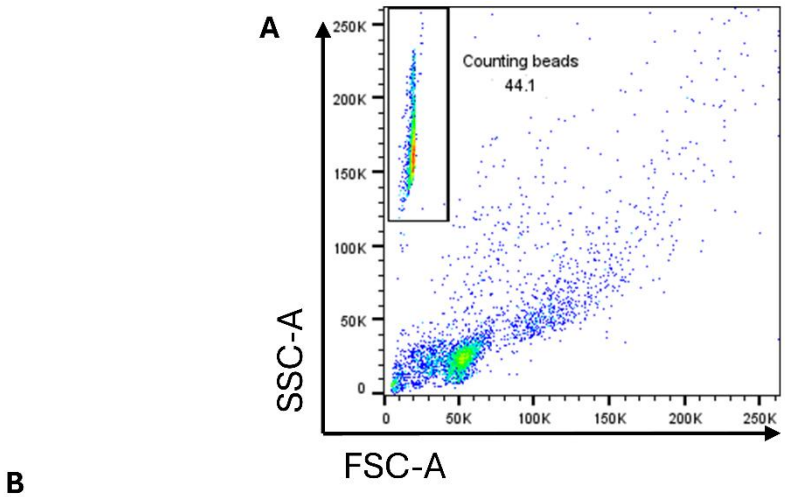

B

$$Absolute\ count\ \left(\frac{cells}{\mu L}\right) = \frac{(cell\ count\ \times counting\ beads\ volume)}{(counting\ beads\ count\ \times cell\ volume)} \times counting\ beads\ concentration\ (\frac{beads}{\mu L})$$

Figure 2.4: Counting bead acquisition and determination of cell count. (A) Counting beads were acquired by SSC/FSC scatter plotting, exhibiting much higher SSC and much lower FSC than that of viable cells. (B) Calculation used to determine absolute cell count (cells/μL) as per manufacturer's instructions.

2.2.2.5. Intracellular staining – γ-H2AX^{S139}

Following completion of their respective time periods, MEC1, HG3 and primary CLL cells were collected at 5 x10^5 cells and transferred into FACS tubes. These cells were then centrifuged at 300 *g* for 5 min followed by fixation/permeabilization using 250 μL cytofix/cytoperm solution (BD Biosciences) at 4°C for 20 min. The cells were then washed with 1 mL Perm/Wash buffer (BD Biosciences), spun down at 300 *g* for 5 min, followed by resuspension in 100 μL PBS where they were then stained with 5 μL anti- mouse pH2AX antibody (BD Pharmingen) or an isotype control (incubated for 30 min at RT). The cells were then washed once more with PBS and visualised via flow cytometry, where increases in mean fluorescence (Alexa Fluor 647, laser line: 633 nm) are associated with increases in abundance of γ-H2AX. The isotype control was used to gate against any potential background fluorescence due to

the staining process, where levels of fluorescence above those produced by the isotype control were considered positive for γ-H2AX accumulation. These data were analysed either as γ-H2AX percentage positive or as γ-H2AX mean fluorescence intensity (MFI).

2.2.3. Western blotting

Western blotting was used to assess protein expression and activity of distinct signalling pathways within cells following drug treatment and/or stimulation. These results allow us to determine the effects of various conditions on protein level expression within our cells of interest.

2.2.3.1. Lysate preparation

Lysate preparation was achieved with the reagents used being always on ice. Following cell culture and incubation, cells were taken and transferred to 15 mL reaction tubes. Here, the cells were washed with 1 mL ice-cold PBS and spun at 300 *g* for 5 min at 4°C. The cells were then washed again with 1 mL PBS and spun a second time under the same conditions. The cells were then resuspended a final time in 500 µL PBS and transferred to 1.5 mL Eppendorf tubes, where they were spun again at 300 *g* for 5 min at 4°C, to pellet the cells. The cell pellets were then resuspended in 35 µL protein lysis buffer (1X Tris-EDTA pH 8.0, 1% Triton X-100, 1mM DTT) with added 1X c0mplete mini, EDTA-free protease inhibitor cocktail (Sigma) and 1X PhosSTOP phosphatase inhibitor cocktail (Sigma). These suspensions were then placed on ice for 20 min. Following this incubation, the suspensions were spun at 15000 *g* for 20 min at 4°C, allowing for the separation of protein lysate from cellular debris. The subsequent supernatant was transferred to a fresh Eppendorf tube to be later quantified and used in Western blotting (stored at -80°C). Table 2.10 highlights lysis buffer volumes used for primary CLL cells and CLL cell lines:

Cells	Cell count (x10^6)	Volume of RIPA buffer (µL)
Primary CLL cells	~ 5 - 10	35
MEC1/HG3	~ 2	35

Table 2.10: Cell quantity used for CLL protein lysates

2.2.3.2. Subcellular fractionation

Subcellular fractionation was conducted to assess the expression and localisation of FOXO proteins between nuclear and cytoplasmic compartments in response to stimulation, drug treatment and modulating FOXO expression. In most cases, a whole-cell lysate (WCL) was included as a 'fractionation' control to confirm expression of protein in a cell lysate. Subcellular fractionations were conducted 1 hr post stimulation and/or drug treatment depending on the context.

The protocol to produce nuclear and cytoplasmic lysates was in accordance with the established method of fractionating CLL cells developed by the group [503]. It is worth noting that the largest ratios of detergent were added in the generation of cytoplasmic fractions (1:20, e.g. 2.5 µL detergent:50 µL hypotonic buffer) to ensure effective rupturing of the cell membrane prior to centrifugation. Nuclear and cytoplasmic lysates were stored at -80˚C for <4 months until required but were typically used immediately after generation due to potential degradation of sample. Lysates were made under the assumption that identical cell numbers were collected from each sample. As such, quantification was not conducted for samples derived from subcellular fractionation. Instead, 15 µL lysate sample were utilised as part of Western blot analysis.

2.2.3.3. Protein quantification

Concentration of protein in prepared lysates were quantified using the Bicinchoninic acid (BCA) assay (Thermofisher Scientific) according to 'Microplate Procedure' instructions. Protein lysate (5 µL) was added to a 96-well assay plate in duplicate, alongside 20 µL of each standard. Here, 200 µL of working reagent was added to each well. The wells were then mixed by pipetting, and the plate was covered and placed in an incubator at 37 °C for 30 min. The plate was subsequently cooled and the absorbance measured at 562nm on a SpectraMax M5 microplate reader (Molecular Devices).

2.2.3.4. Gel electrophoresis and membrane transfer

Gel electrophoresis and membrane transfer were conducted using the XCell SureLock Mini-Cell and XCell II Blot Module systems respectively (Thermofisher Scientific), according to manufacturer instructions. 10-20 µg of protein was transferred to a 1.5 mL Eppendorf tube containing 4X LDS Sample Buffer (Thermofisher Scientific), 10X Sample Reducing Agent (Thermofisher Scientific) and ddH_2O to create equal volumes between samples. Samples were mixed and 'boiled' at 70°C for 10 min. Samples were then loaded onto 10, 12 or 15-well NuPageTM 4-12% Bis-Tris Protein Gels (Thermofisher scientific). The gel tanks were filled with 1X MOPS Running Buffer (Thermofisher scientific), with the incorporation of a PageRuler Plus Prestained Protein Ladder (Thermofisher scientific) for the identification of target proteins following separation *via* electrophoresis. 'Mirror' blots (blots containing equal amounts of protein in duplicate) were ran – when necessary – to compare the differences in total and phosphorylated protein following stimulation and/or drug treatment. These gels were run at 120 V for 20 min, followed by 150 V until the 'dye front' had reached the bottom of the gel. Separated protein was transferred from gel to methanol-activated 0.45µm Polyvinylidene (PVDF) membrane using 1X Transfer

Buffer (Thermofisher) containing 10% methanol. Transfer was achieved at 20 V for 90 min.

2.2.3.5. Immunoblotting

To confirm successful transfer, the membranes were removed from the apparatus and stained with Ponceau solution (Sigma). The membranes were then washed with 5 mL TBST (1X TBS, 0.1% Tween 20) four times for 5 min to remove Ponceau staining. The membranes were then blocked with 10 mL 5% (w/v) Milk/TBST for 1 hr at RT. Blocked membranes were then washed 4 times for 5 min with 5 mL TBST, cut according to size, and transferred to 50 mL reaction tubes. Here the membranes were then incubated with 5 mL primary antibodies (Table 2.3) - in 5% (w/v) BSA/TBST or 5% (w/v) Milk/TBST – O/N at 4°C. The next day, the blots were washed in 5 mL TBST, 4 times for 5 mins. After washing, 5 mL HRP-linked (or – on occasion – 680RD goat anti-rabbit [TBST]) secondary antibody was added to the membrane at RT for 1 hr (in 5% (w/v) BSA/TBST). The washing step was repeated following this, where the blots were then visualised using the Odyssey Fc Imaging System (LI-COR) within the ImageStudio v5.2.5 software (LI-COR). Membranes probed with fluorescent secondary antibodies were detected using the 700nm channel, whereas membranes probed with HRP-linked secondary antibodies were detected through chemiluminescence following addition of Immobilon Forte Western HRP Substrate (Millipore). Blots were then rinsed in dH_2O and stored in 50 mL dH_2O for potential later re-probing. Membranes could also be dried at RT and stored at -20°C for long-term storage.

2.2.3.6. Membrane re-probing

Where appropriate, membranes were re-probed without the use of harsh ‘stripping’ methods to identify proteins that were of dissimilar molecular weight. This was conducted only on blots where non-specific staining was

absent. Here, probed membranes were washed 4 times for 5 min in TBST to remove excess ECL and bound antibody and were then probed O/N at 4 °C with the desired primary antibody. Following this, the blots were developed as part of the typical immunoblotting protocol.

2.2.3.7. Densitometry

Densitometry allows for quantitative analysis of protein expression following recording of western blot signal intensity. Images acquired from the Odyssey Fc Imaging System (LI-COR) were analysed using the Image StudioTM Lite (5.2.5) software (LI-COR), where protein expression was normalised against a reference protein loading control (e.g. ß-actin, GAPDH). This allowed for accurate quantification of band intensities relating to specific target protein expression.

2.2.4. RT-qPCR

The 'two-step' method of RT-qPCR was used to reverse-transcribe RNA to complementary DNA (cDNA). This synthesised DNA was then used as the template in qPCR reactions. All reagents and equipment were purchased from ThermoFisher Scientific, with TaqMan gene expression assays being used to monitor target gene expression.

2.2.4.1. RNA isolation

RNA was first isolated using the PureLink™ RNA Mini Kit (ThermoFisher) according to the manufacturer's instructions.

After stimulation and/or drug treatment, cells were collected and resuspended in either 350 µL (cell lines) or 600 µL (primary CLL cells) of RNA lysis buffer. The lysates were then briefly homogenised using a vortex for 30 s. Lysates could then

be used for immediate RNA extraction or stored at -80°C in lysis buffer for extraction at a later timepoint. Table 2.11 outlines RLT volumes for primary CLL and CLL cell line resuspension:

Cells	Cell count (x10^6)	Volume of RLT buffer (µL)
Primary CLL cells	~ 5 - 10	600
MEC1/HG3	~ 2	350

Table 2.11: Cell quantity used for RNA isolation

For *ex vivo* CLL samples (with large cell numbers, ~2 x 10^7 cells), pellets were thawed gently on ice then lysed in 600 µL of lysis buffer with 30 s of vortexing. The protocol was then followed as per manufacturer's instructions.

Concentration and purity of isolated RNA was determined using a NanoDrop spectrophotometer (ThermoFisher) according to manufacturer's instructions. Samples were considered at concentrations >50 ng/µL, alongside the consideration of A260/A280 and A260/A230 values. Of note, RNA was always kept on ice on clean worktops (using RNAZap™ (ThermoFisher) and 70% ethanol) and was stored long-term at -80°C.

2.2.4.2. First-strand cDNA synthesis and polymerase chain reaction (PCR)

cDNA was synthesised from RNA using SuperScript III Reverse Transcriptase according to the manufacturer-provided protocol, using 500 ng RNA per condition. This was achieved using the ProFlex PCR system (ThermoFisher) following thermal conditions provided by the manufacturer. Synthesised cDNA

was then diluted 1:5 with RT-PCR grade water (ThermoFisher) and either used immediately in the RT-qPCR assay or stored at -20˚C until required. Table 2.12 describes a single reaction of cDNA synthesis:

First-strand cDNA synthesis	
Component	**Volume (µL)**
Oligo(dT) 12-18 Primer	1
dNTP Mix PCR Grade (10 mM)	1
500 ng RNA	x
1. PCR-grade H_2O to 13 µL **2. Incubate at 65 °C for 5 min**	
5X First-Strand Buffer	4
0.1 M DTT	1
RNaseOUT Rnase Inhibitor	1
SuperScript III RT	1
3. Incubate for 60 min at 50 °C **4. Inactivation for 15 min at 70 °C**	

Table 2.12: Reagents for First-strand cDNA synthesis

2.2.4.3. RT-qPCR

Synthesised cDNA was then loaded into MicroAmp Optical 384-Well Reaction Plates (ThermoFisher) alongside qPCR reagents. RT-qPCR was subsequently performed using the QuantStudio™ 6 Pro system (ThermoFisher). Cycling conditions included: (1) 2 min @ 50˚C, (2) 2 min @ 95˚C, (3) 15 s @ 95˚C, (4) 1 min @ 60˚C (step 3 underwent 40 cycles). CT values were then generated using the supplied QuantStudio™ software. *B2M* and *18S* were used as internal reference genes. Of note, a reverse transcriptase negative (RT^{neg}) sample was included - where possible - to assess potential DNA contamination. Data was analysed and presented as 'fold change' using the $2^{-\Delta\Delta CT}$ method [509], where:

$$\Delta \boldsymbol{Ct} = Ct\,(target\ gene) - Ct\,(housekeeping\ gene),$$
$$\Delta\Delta \boldsymbol{Ct} = \Delta Ct\ value\ of\ condition - \Delta Ct\ value\ of\ control,$$
$$\boldsymbol{2^{-\Delta\Delta Ct}} = 'fold\ change'.$$

Table 2.13 outlines volumes of reagent used in a single RT-qPCR reaction:

RT-qPCR components	Volume (µL)
20X TaqMan Gene Expression Assay	0.5
4X TaqMan Universal Master Mix	2.5
cDNA	2
RT-qPCR grade H2O	5
Total	**10**

Table 2.13: Reagents for a single RT-qPCR reaction. Of note, technical triplicates were conducted (3 x 10 µL) per condition.

2.2.5. Generation and analysis of bulk RNA-sequencing data

CLL patient samples (n=5), selected according to their ability to effectively proliferate, were thawed using 'DAMP' solution and left overnight to equilibrate at 37°C, 5% CO_2. The following day, the cells were co-cultured on CD40L-expressing NTL cells and left to equilibrate O/N at 37°C 5% CO_2, including a $CD40L^{neg}$ NTL non-proliferative control. The next morning, the cells were treated as follows: 1. NTL no drug control (NDC, non-proliferative control); 2. NDC (on CD40L); 3. 100 nM AZD8055; 4. 1 µM Ibrutinib; 5. AZD8055 + Ibrutinib (COMBO). Of note, conditions 2-5 were cultured on NTL cells expressing CD40L and all conditions were cultured with 10 ng/mL exogenous IL-4. These cells were cultured at 37°C for 24 hr. The cells were then removed from the monolayer and introduced to fresh 6-well plates for 2 hr to ensure separation of suspended CLL cells from adherent NTL cells, followed by subsequent RNA extraction using the PureLink™ RNA Mini Kit (Invitrogen). Following successful extraction, the integrity of the RNA samples was analysed using the Agilent RNA 6000 Nano Kit (Agilent) with a 2100 Bioanalyzer (Agilent), testing the RNA purity and quality.

Here, samples were processed in the Bioanalyzer via electrophoretic separation to produce fluorescent bands that coincided with particular RNA species such as 28S and 18S ribosomal RNA (rRNA) species. The software then compared the ratio of intensity of these bands as well as other factors to determine an RNA integrity number (RIN) that determines overall RNA quality. Once confirmed for acceptable quality (RIN 7-10), the samples were sent to Novogene to conduct bulk RNA sequencing, and comparisons of global transcript data were generated between the conditions. In summary, cDNA libraries were prepared by Novogene using a Next® Ultra™ RNA Library Preparation Kit (NEB) and sequenced using a NovaSeq 6000 platform (Illumina). Reads were aligned to the hg38 human genome using their *STAR* alignment method, followed by quantification of gene expression using the *HTseq* package, which determined gene counts as FPKM. Differential gene expression was conducted using the *DeSeq2* package (R Studio) which collectively analysed differential gene expression within conditions between all patient samples. 'p' values were corrected (p-adj) using the DeSeq2 package *via* the Benjamani and Hochberg (BH) method. Subsequent analysis of differential expression data and generation of diagrams were primarily performed in R Studio, with the exception of KEGG analysis figures and Venn diagrams (see Figures 4.2-4.5), which were generated in prior data analyses by Novogene.

Volcano plots and global heatmaps were generated using GraphPad Prism. PCA, Pearson correlation and differential expression heatmaps were generated using RStudio. Of note, all analyses were conducted using differential gene counts generated by Novogene.

2.2.6. FOXO1 activity assay

A TransAM FKHR (FOXO1) activity kit (Active Motif) was used to observe FOXO1 DNA binding activity in CLL cell nuclear extracts. These were generated *via* the protocol described in 2.2.3.2. Of note, only the nuclear extract was used for this purpose, however both the nuclear and cytoplasmic fractions could subsequently be used to assess FOXO localisation *via* Western blotting.

FOXO1 DNA binding was assessed according to the manufacturer's instructions. Nuclear extracts were quantified as per the protocol in section **2.2.3.3**, so that equal protein loading was achieved between conditions (>4 µg). Positive (Raji) and negative (blank) controls were included. A 'binding' control was also implemented to determine the specificity of FOXO1 binding to either wild-type (WT) or mutated consensus oligonucleotides. It is important to note that the developing solution (step 4) was incubated for a minimum of 10 min before use. Subsequently, absorbance was read within 5 min at 450nm (reference wavelength 655nm) using a SpectraMax M5 microplate reader (Molecular Devices).

2.2.7. shRNA-mediated knockdown of *FOXO3* and *FOXO4*

shRNA-mediated knockdown of *FOXO3* was achieved in MEC1 cells. shRNA-mediated knockdown of *FOXO4* was achieved in MEC1, HG3 and primary CLL cells on CD40L (+IL-4) co-culture. shRNA can achieve gene knockdown *via* introduction of RNA interference (RNAi) in the target cell type. Described below are the collective methods of generating shRNA plasmids, lentiviral production and specific methods of cell transduction according to the targeted cell type.

2.2.7.1. shRNA construct glycerol stocks

Various shRNA constructs for *FOXO3* and *FOXO4* were considered. All constructs were incorporated into the pLKO_TRC005 or pLKO.1 TRC cloning vectors (Table 2.14):

Target	Clone Name	Clone ID	Vector	Target Sequence	Region
FOXO3	NM_001455.3-6977s21c1	TRCN0000235491	pLKO_TRC005	CTTGCTCATATCCCATATAAT	3' UTR
FOXO3	NM_001455.3-6977s21c1	TRCN0000235491	pLKO_TRC005	CTTGCTCATATCCCATATAAT	3' UTR
FOXO3	NM_001455.3-1573s21c1	TRCN0000235489	pLKO_TRC005	GAGCTCTAGCTTCCCGTATAC	CDS
FOXO3	NM_001455.3-2206s21c1	TRCN0000235487	pLKO_TRC005	ATGTGACATGGAGTCCATTAT	CDS
FOXO4	NM_005938.1-1733s1c1	TRCN0000039718	pLKO.1	GCGTGTTCATATCTACTCTTT	3' UTR
FOXO4	NM_005938.x-950s1c1	TRCN0000010290	pLKO.1	CAGTTCAAATGCCAGCAGTGT	CDS
FOXO4	NM_005938.x-1975s1c1	TRCN0000010291	pLKO.1	CACTTAGGCTTTGTAGCAAGA	3' UTR

Table 2.14: shRNA glycerol stocks for *FOXO3* and *FOXO4* utilised within this study

shRNA constructs were generated following culture of bacterial glycerol stocks cultured in Terrific Broth (TB - ThermoFisher Scientific, 100 µg/mL ampicillin, 15% glycerol) that were transformed with the appropriate pLKO vectors (Sigma (MISSION shRNA)). These stocks were kindly donated by Dr. Xu Huang's lab (University of Glasgow, Glasgow, UK). Of note, the pLKO vectors contain both bacterial and mammalian antibiotic resistance genes for generation of pLKO DNA from bacteria (ampicillin) and subsequent selection of transduced target cells (puromycin) (illustrated in Figure 2.5).

2.2.7.2. Isolation and inoculation of bacterial cultures

Terrific Broth (TB, ThermoFisher Scientific) agar plates containing 100 µg/mL ampicillin were prepared. Using a sterile plastic inoculating loop, a small amount of glycerol stock was scratched onto the loop and streaked onto a TB-amp plate. The plate was then incubated upside down O/N at 37°C. This protocol was repeated for every shRNA construct required in new TB-amp agar plates. A single TB-amp plate was also set at 37°C as a negative control to ensure bacterial growth emanated from glycerol stocks. Upon successful generation of bacterial colonies, a single colony was selected and transferred to 5 mL TB-amp (TB + 100 µg/mL ampicillin) in a sterile 13 mL inoculation tube (Fisher Scientific) using a sterile pipette tip. These cultures were then incubated O/N shaking at 37ºC to generate small-scale liquid bacterial cultures.

2.2.7.3. Miniprep

Plasmid miniprep allows for the extraction of small quantities of plasmid DNA from liquid bacterial cultures. Following O/N bacterial culture in 5 mL TB-amp, this was performed using 4 mL of culture using the QIAprep Spin Miniprep Kit (QIAGEN) according to manufacturer's instructions. The purpose of pLKO miniprep was to determine successful production of a pLKO vector containing the desired shRNA sequence. This was achieved using 4 mL of the 5 mL TB-amp liquid culture, while the remaining 1 mL was used either to create fresh glycerol stocks or for larger-scale bacterial culture to create large quantities of shRNA-containing pLKO plasmid for use in shRNA transfection. These large scale 'maxipreps' were only performed once the shRNA construct was determined *via* restriction digest. The concentration of the extracted DNA was determined using the NanoDrop spectrophotometer (ThermoFisher Scientific) used for quantifying isolated RNA, followed by storage of extracted DNA at -20ºC.

2.2.7.4. Maxiprep

As described above, upon determining the presence of the shRNA construct, the remaining 1 mL of bacterial liquid culture was added to conical flasks containing 100 mL TB-amp. These cultures were incubated O/N in a flask shaker at 37 ºC. The following day, the cultures would be used to perform a plasmid DNA maxiprep using the PureLink™ Fast Low-Endotoxin Maxi Plasmid Purification Kit (ThermoFisher Scientific) according to manufacturer's instructions, aside from the DNA elution step, which was conducted using 150 µL elution buffer rather than 400 µL total elution buffer as suggested. Once again, plasmid DNA concentration and purity was determined using the NanoDrop spectrophotometer. This DNA was then used for diagnostic digests to confirm successful large-scale cloning of shRNA-containing vector before being stored at -20 ºC.

2.2.7.5. Restriction digests

Restriction digests were performed to determine successful generation of pLKO vector DNA containing the desired shRNA insert. Here, 500 ng plasmid DNA was digested with Nco1_HF and EcoRI_HF (both New England Biolabs), generating insert and plasmid backbone fragments of sizes: ~1973 bp and ~5077 bp (pLKO.1) or ~2527 bp and 6808 bp (plKO_TRC005). This was achieved in a reaction mixture containing 1X CutSmart Buffer (New England Biolabs) for 1 h at 37ºC. Uncut plasmid vector and 'Single' cuts using either Nco1_HF or EcoRI_HF were included as negative controls.

2.2.7.6. DNA gel electrophoresis

DNA gel electrophoresis was conducted to separate DNA by size to visualise plasmid DNA following restriction digest as described above. Initially, a 1 %

agarose gel was created using 1 g agarose (Sigma) in 100 mL 1X TAE buffer (derived from a 50X stock solution: 40 mM Tris, 20 mM acetate, 1 mM EDTA, pH 8.2) in a glass conical flask. This mixture was then boiled using the microwave, gently to prevent overboiling. Once the agarose was successfully dissolved, SYBR Safe DNA Gel Stain Concentrate (ThermoFisher Scientific) was added at a dilution of 1:10000 (i.e. 10 µL in 100 mL TAE buffer) and mixed. Finally, before cooling and solidifying, the liquid agarose was poured into a gel mould and left to cool for ≥1 hr. Of note, a comb was in the gel in its liquid phase to create wells for loading DNA samples.

Samples were mixed with 6X TriTrack DNA Loading Dye (ThermoFisher Scientific) to ensure proper loading of samples into the wells. This was performed at a dilution of 1:5 loading dye:digested DNA (diluting the loading dye from 6X to 1X) at a suitable volume (>15 µL). Once solidified, the gel was placed into a tank and submerged in 1X TAE buffer. Digested samples or uncut controls were run alongside GeneRuler 1 kb DNA ladder (ThermoFisher Scientific). This gel would then be exposed to a current at 5 V/cm until the dye had travelled ~70% of the gel. The gel was subsequently removed from the buffer and visualised using the LiCOR Odyssey Fc Imaging System using the ImageStudio v5.2.5 software and the 600nm channel. An example of restriction digest of the shFOXO3 construct is outlined in Figure 2.5:

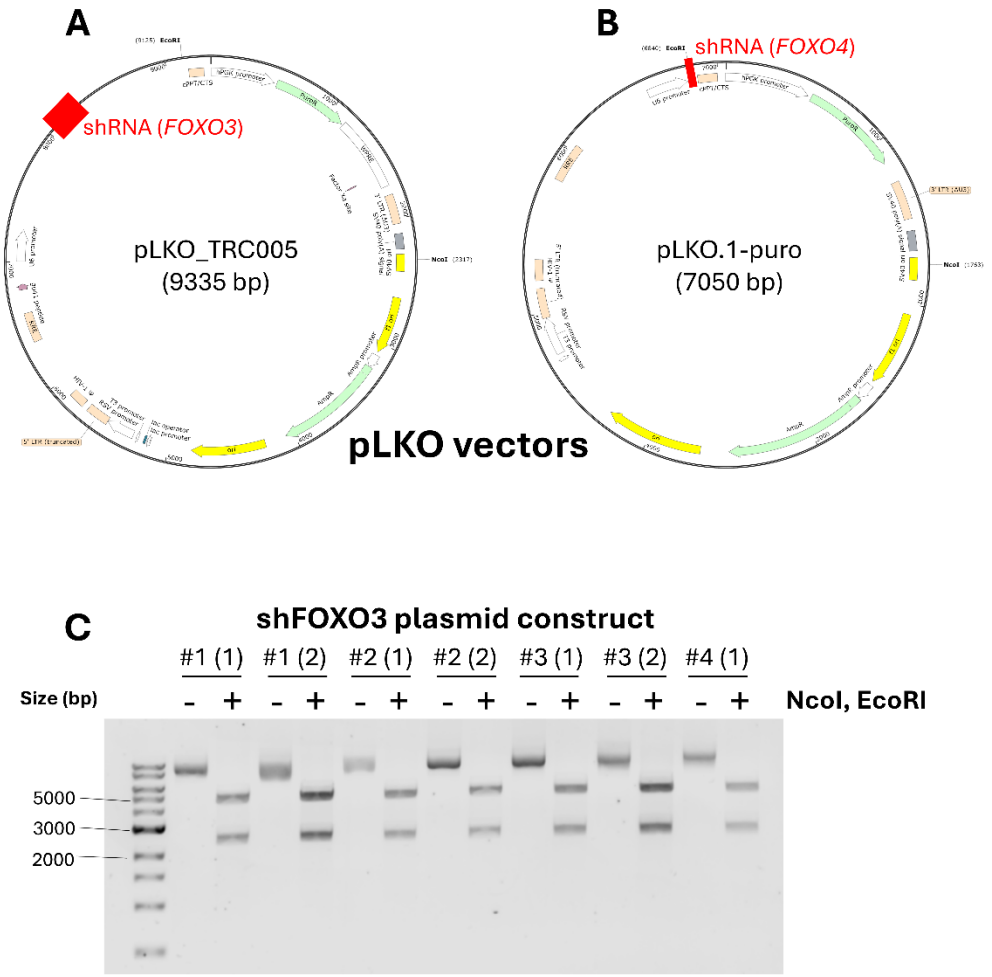

Figure 2.5: Diagnostic digests of shRNA-containing pLKO vectors. pLKO_TRC005 (A) and pLKO.1 (B) plasmid vectors containing shRNA constructs to deplete FOXO3 and FOXO4 expression, respectively, were cultured from bacterial glycerol stocks and purified for plasmid DNA to be used in subsequent lentiviral knockdown of FOXO3/4 in CLL cells. Plasmid vectors were mapped using Snapgene. Highlighted are restriction sites for EcoRI and NcoI as well as the site of the gene sequence encoding the shRNA construct (between U6 promoter and cPPT sequences, displayed in red). (C) Agarose gel electrophoresis of a restriction digest of pLKO_TRC005 plasmid vectors purified from plasmid minipreps of different shFOXO3 constructs (#1 - #4) using NcoI and EcoRI restriction enzymes. Uncut controls were included to confirm digest from NcoI and EcoRI. Aside from construct #4, plasmid minipreps were conducted in duplicate from two separate bacterial colonies (denoted as '(1)' and '(2)').

2.2.7.7. Transfection

Transfection of HEK293T cells was performed using the calcium phosphate method to produce lentiviral particles (containing shRNA constructs) in transfectable HEK293T cells to infect target cells [510].

For shRNA transfection, 3 x10^5 HEK293T cells were seeded into 6-well culture plates in either 'complete' 2 mL DMEM or RPMI, depending on the target cell type. For example, HEK293T cells were cultured in DMEM to generate virus for targeting MEC1 cells, while HEK293T cells were instead cultured in RPMI if targeting HG3 and primary CLL cells. These cells were then cultured at 37ºC, 5% CO_2 until ~60-70% confluent. Prior to the transfection process, the cells were introduced to fresh DMEM/RPMI. To begin the transfection procedure, two separate solutions were created: Solution A (5 µg HIV-1 packaging vector (psPAX2), 2.5 µg VSVG envelope vector, 50 µL 2.5 M $CaCl_2$ and 10 µg shRNA construct, made up to 150 µL with sterile ddH_2O) and solution B (150 µL 2X HEPES buffer saline (Sigma)) in two separate 1.5 mL Eppendorf tubes (Figure 2.6A). Solution A was then carefully added to solution B with a P1000 pipette, dropwise, followed by vigorous 'bubbling' of the mixture to mechanically stimulate virus formation. The resultant mixture was then vortexed briefly and incubated at RT for 30 min. Following incubation, the solution was added to the HEK293T cells dropwise, the wells were swirled, and the cells were incubated O/N at 37ºC, 5% CO_2. Following O/N incubation, the HEK293T cell media was discarded and replaced with fresh complete DMEM/RPMI, followed by a further 48 hr incubation step at 37ºC, 5% CO_2. Within this time, the cells generated large amounts of shRNA-containing lentivirus. Of note, 'scrambled' (SCR) and GFP control constructs were also included to provide comparison to the knockdown and confirmation of transduction, respectively (Figure 2.6B). A negative control well was also included with complete media lacking any transfection procedure.

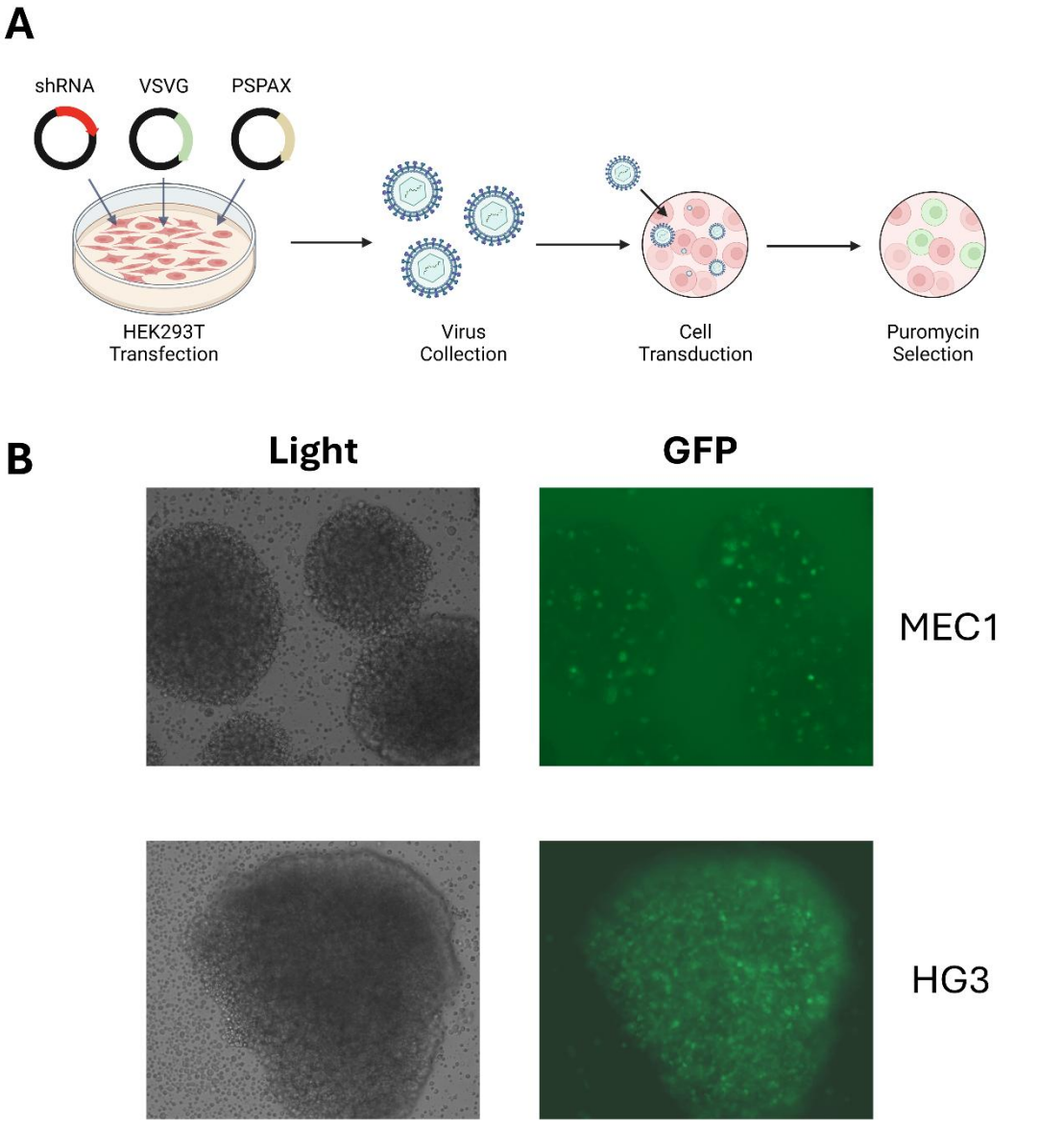

Figure 2.6: Transfection confirmation using the GFP control vector in MEC1 and HG3 cells. (A) Simplified schematic of shRNA-mediated knockdown in CLL cell lines, where shRNA-containing lentivirus was generated *via* transfection of HEK293T cells and was subsequently collected and used to transduce MEC1, HG3 (B) or primary CLL cells. (B) Following detection of GFP fluorescence in MEC1/HG3 cells transduced with a GFP-containing control vector, MEC1 and HG3 cells were positively selected using 2 µg/mL puromycin and left to grow in puromycin-containing media.

After 48 hr, the media was harvested from the HEK293T cells using a sterile 5 mL syringe and filtered into a 15 mL reaction tube using a 0.20µm filter (Sartorius) to remove any debris. This media contained large amount of shRNA-containing lentivirus. This 'viral supernatant' was then used immediately to induce the target cell type but could also be stored at 4 ºC for 2-3 days. Next, another 2 mL complete media was added to the HEK293T cells and incubated for another 24 hr at 37 ºC, 5% CO_2. This media was collected by the same method the following day and would be used to provide a second round of virus to the target cells. Of

note, plastics that had come into contact with viral supernatant at any stage would be submerged in Virkon solution for a minimum of 24 hr to ensure effective destruction of viral particles.

2.2.7.8. Lentiviral transduction

2.2.7.8.1. Stable knockdown in CLL cell lines

1 x10^6 MEC1 or HG3 cells were plated into 6-well plates the day before lentiviral transduction and incubated O/N at 37 ºC, 5% CO_2. The following day (preferably the same day as collection of the first batch of viral supernatant from HEK293T cells), the cells were resuspended in 1 mL fresh DMEM/RPMI, alongside 16 µg/mL polybrene (Sigma), to ensure efficient uptake of the pLKO-puro vector in the target cells. To this was added 1 mL viral supernatant, taken immediately from transfected HEK293T cells, to give a final working concentration of 8 µg/mL polybrene. The cells were then incubated for 24 hr at 37ºC, 5% CO_2. After incubation, the cells were centrifuged at 300 *g* for 5 min in a 15 mL tube and were then resuspended in fresh 1 mL complete DMEM/RPMI. Here, the cells were exposed to another 1 mL (total volume: 2 mL/condition) of viral supernatant with a final concentration of 8 µg/mL polybrene. The cells would then be incubated for another 24 hr at 37ºC, 5% CO_2 prior to puromycin selection.

Puromycin selection would be performed only once there was detection of GFP fluorescence in the GFP control either by fluorescent microscopy or by flow cytometry (using the FITC channel, laser line: 488 nm). Here, MEC1 and HG3 cells were centrifuged at 300 *g* for 5 min followed by resuspension of the cells in fresh complete DMEM/RPMI containing 2 µg/mL puromycin. The cells would then be incubated for 24 hr at 37ºC, 5% CO_2. The following day, the cells were spun at 300 *g* for 5 min, followed by resuspension in fresh DMEM/RPMI containing 2 µg/mL puromycin. The cells were then monitored for proliferation and clustering (as it typical of viable CLL cell lines). Once sufficient growth was determined

(typically ≥48 hr in culture + 2 µg/mL puromycin), a fraction of the cells population was taken to determine expression of FOXO3 or FOXO4 *via* RT-qPCR and Western blotting. The remaining cells would then be transferred to appropriate cell culture flasks to ensure further growth of the stable knockdown population. Specifically, the shRNA constructs inducing the most efficient stable knockdown were selected to be cultured in T25cm^2 or T75cm^2 flasks in media containing 1 µg/mL puromycin to maintain knockdown selection.

2.2.7.8.2. shRNA-mediated knockdown of *FOXO4* in primary CLL cells

Lentiviral transduction of primary CLL cells was conducted exclusively using shRNA construct #3 (shFOXO4-3) as it was shown to effectively deplete *FOXO4* expression in MEC1 and HG3 cells. The initial generation of lentivirus was identical to that of lentivirus used to target CLL cell lines using HEK293T cells (see **section 2.2.7.7**). Primary CLL cells were thawed as described in **section 2.2.1.5.1** and incubated O/N at 37ºC, 5% CO_2. The following day, 3 x10^5 NT-L cells (lacking CD40L expression) were seeded into 6-well culture plates and incubated for >1 hr at 37ºC, 5% CO_2 to ensure adherence to the plate. CLL cells were then co-cultured with the adhered NTL cells at a minimum of 7.5 x10^6 cells/mL in 2 mL complete RPMI. The cells were then incubated O/N at 37ºC, 5% CO_2 to equilibrate the primary CLL cells to the NTL co-culture. The following day, the cells were collected and centrifuged at 300 *g* for 5 min and then resuspended in 1 mL complete RPMI with 16 µg/mL polybrene. 1 mL viral supernatant was then added to the CLL cells to culture the cells in 2 mL RPMI with a final concentration of 8 µg/mL polybrene. The cells were then incubated for 24 hr at 37ºC, 5% CO_2. The following day, the cells were collected into 15 mL tubes, centrifuged at 300 *g* for 5 min and resuspended in 1 mL fresh complete RPMI and 1 mL filtered viral supernatant collected the same day from HEK293T cells (total volume: 2 mL with final concentration 8 µg/mL polybrene). The cells were then incubated for a further 72 hr at 37ºC, 5% CO_2 to ensure efficient transduction with the shRNA construct. ShRNA-transduced primary CLL cells, were not selected using puromycin, and were used in experiments immediately.

Therefore, following 72 hr in incubation with lentivirus, a small fraction of the cell population (~2 x10^6 cells) from both the SCR and knockdown conditions were used to extract RNA to determine efficient *FOXO4* knockdown *via* RT-qPCR. The remaining cells were centrifuged at 300 *g* for 5 min and introduced to a fresh 6-well plate containing fresh NTL or NTL-CD40L cells (5 x10^5 cells seeded the night before) in 2 mL complete RPMI (+10 ng/mL IL-4). The cells would then be incubated O/N at 37ºC, 5% CO_2, followed by drug treatment the following day, where appropriate. Of note, day 0 of shFOXO4 CLL co-culture was defined as the morning following O/N equilibration with CD40L-expressing NTL cells (+10 ng/mL IL-4). From this point, the cells were co-cultured for 24 hr at 37ºC, 5% CO_2 before being collected to isolate RNA for use in RT-qPCR reactions.

2.2.8. Statistics

Data were analysed using Prism 9/10 software (GraphPad). Graphical data are shown as mean values ± standard error of the mean (SEM). In all cases, *n* values depict biological replicates. *P* values were calculated using paired and unpaired two-tailed Student's *t* tests for analysis between two groups. One-way ANOVA was conducted for comparison between multiple conditions, while a two-way ANOVA was conducted for comparisons between multiple conditions within ≥2 groups. In all cases, *P* values ≤ 0.05 were deemed statistically significant. Significant results are depicted as asterisks as follows: $P \leq 0.05$ *, $P \leq 0.01$ **, $P \leq 0.001$ ***, $P \leq 0.0001$ ****. Values that are not significant are indicated as 'n.s'.

Results

3. Determining FOXO3/4 expression and regulation *in vitro*

3.1. Introduction

B-cell malignancies are known to promote lymphomagenesis by means of depleting intracellular *FOXO* expression [500, 511, 512] or through the activity of different signalling mechanisms resulting in the inactivation of FOXOs [284, 285, 513], the most studied of which being AKT-mediated FOXO phosphorylation [263, 432]. Although FOXOs have been extensively studied in the context of normal B-cell biology, and other B-cell malignancies, our understanding of FOXO biology in CLL is limited to FOXO1, with FOXO3's association with CLL survival being somewhat addressed [463]. As such, the mechanisms regulating intracellular FOXO activity and regulation in CLL remain obscure, with the understanding of these intracellular mechanisms being critical to identifying whether we should harness FOXO activity for therapeutic purposes.

Our group has established that BCR crosslinking tightly regulates FOXO1, by inducing FOXO1 phosphorylation, coinciding with increased AKT^{T308} and AKT^{S473} levels, *in vitro* [49, 284]. These insights demonstrate how the PI3K-AKT-mTOR axis regulates FOXO1, providing CLL cells with a means to inhibit FOXO1-mediated gene regulation to promote proliferation and survival. In contrast, our current understanding of the regulation and expression of other distinct FOXO family members in CLL is minimal; it may be that FOXO3, FOXO4 and FOXO6 are regulated and expressed differently to that of FOXO1 in CLL. This chapter will explore how the FOXO family is expressed and regulated in different *in vitro* CLL model systems, and different physiological contexts.

3.1.1. Aims

1. Assess the expression of FOXO3 and FOXO4 in CLL cell lines and primary CLL cells

2. Investigate FOXO regulation following CLL cell stimulation with $F(ab')_2$ or CLL-CD40L co-culture

3. Establish the implications of pharmacological AKT inhibition on FOXO expression and regulation

3.2. Results

3.2.1. FOXO3 and FOXO4 are expressed in a cell-type-specific manner in CLL

Although FOXO1 is abundantly expressed in CLL PB samples [49, 284], it does not discount expression of other FOXO family members in CLL. Here, FOXO3 and FOXO4 expression was determined first in MEC1 and HG3 cells – immortalised CLL cell lines associated with distinct CLL prognostics (poor and favourable, respectively), characterised by disparate cytogenetic profiles. Specifically, MEC1 cells are a U-CLL, del(17p) cell line with overactive BTK signalling, indicative of poor prognostic CLL, while HG3 cells are a U-CLL cell line containing del(13q), indicative of a more favourable prognosis through del(13q)'s contribution to an indolent CLL as well as endogenous *TP53* expression [514, 515]. For these reasons, CLL cell lines can be used to understand basic biological principles within CLL (e.g. links to prognostics), although the activity of mechanisms within CLL cell lines may not be truly indicative of how these mechanisms are regulated within primary CLL cells. FOXO3 expression was significantly higher in the MEC1 cell line than in HG3 cells (Figure 3.1A & B), while FOXO4 expression was significantly higher in HG3 cells (Figure 3.1A & C). Using ΔCt values derived from RT-qPCR of MEC1 and HG3 RNA samples, MEC1 cells exhibited significantly higher *FOXO3* ΔCt values than HG3 cells (Figure 3.1D), indicative of lower gene expression, while there was no difference between *FOXO4* ΔCt values in the two cell types (Figure 3.1E).

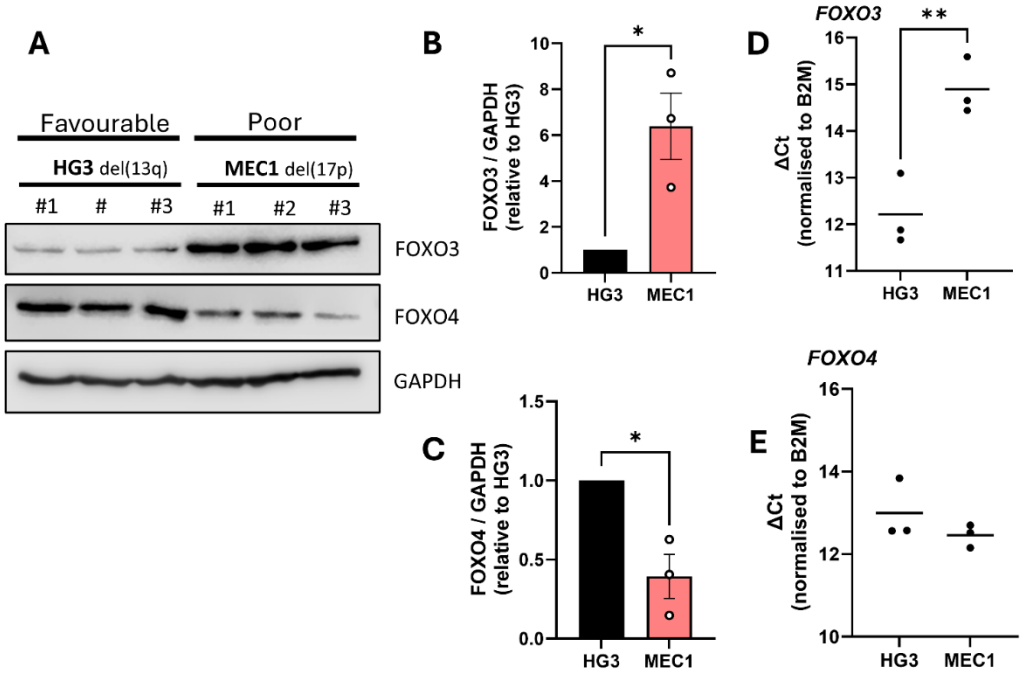

Figure 3.1: FOXO3 and FOXO4 expression in MEC1 and HG3 cell lines. (A) Western blot of lysates from either HG3 (left) or MEC1 (right) cells (n=3) followed by detection of FOXO3, FOXO4 and GAPDH. (B) Quantified expression values for FOXO3 normalised to HG3, where MEC1 FOXO3 intensity is relative to the mean HG3 intensity. (C) Quantified expression values for FOXO4 normalised to HG3, where MEC1 FOXO4 intensity values are relative to the mean intensity for HG3. (D & E) Raw ΔCt scores for HG3 and MEC1 cells derived from RT-qPCR probing for *FOXO3* and *FOXO4* expression, respectively (n=3 independent MEC1 & HG3 RNA samples). Data points are captured as either white (protein, B & C) or black (RT-qPCR, D & E) circles, and data is represented as the mean ±SEM. Statistics were conducted using an unpaired Student's t-test, where * $p \leq 0.05$, ** $p \leq 0.01$.

3.2.2. FOXO protein expression is elevated and distinct in different prognostic CLL subtypes

Differences in FOXO isoform gene expression in CLL cell lines indicates potential differences in FOXO family expression within CLL patients; expression of FOXOs in CLL may be associated with disease progression, much like in other cancers [516, 517]. As such, we looked at gene (Figure 3.2) and protein (Figure 3.3) expression of each member of the FOXO family in CLL *ex vivo* patient samples, comparing their expression values to that of healthy B-cell donors (BCs), with an emphasis on distinct patient prognostics (Figure 3.2B-E). Compared to BCs, *FOXO1* exhibited significantly lower overall ΔCt values - indicative of increased

expression (Figure 3.2A). Further, *FOXO4* exhibited lower ΔCt values, trending on significance (p = 0.09, Figure 3.2A), while there was no significant change in *FOXO3* ΔCt values. In the future, the significance of *FOXO4* expression, and indeed of the other family members, would be better considered by including more B-cell donor samples (n=5 was used due to a lack of availability). Interestingly, *FOXO6* ΔCt values in *ex vivo* samples were significantly increased compared to the BC cohort, indicating a significant reduction in expression. These data confirm a disparate regulation of FOXO expression in patient PB samples, where *FOXO4* expression experienced the lowest ΔCt scores (Figure 3.2A), suggesting the highest expression.

It is worth noting that, due to no noticeable differences being observed between CLL disease stages, comparisons were made between patients with no cytogenetic aberrations and those with a poor prognostic 11q deletion (Figure 3.2B-E). Between prognostic subgroups, *FOXO1* and *FOXO3* ΔCt values were lower in patients with 11q deletions (p = 0.045 & 0.070, respectively, Figure 3.2B & C), while *FOXO4* and *FOXO6* were unaffected by 11q deletion (Figure 3.2D & E).

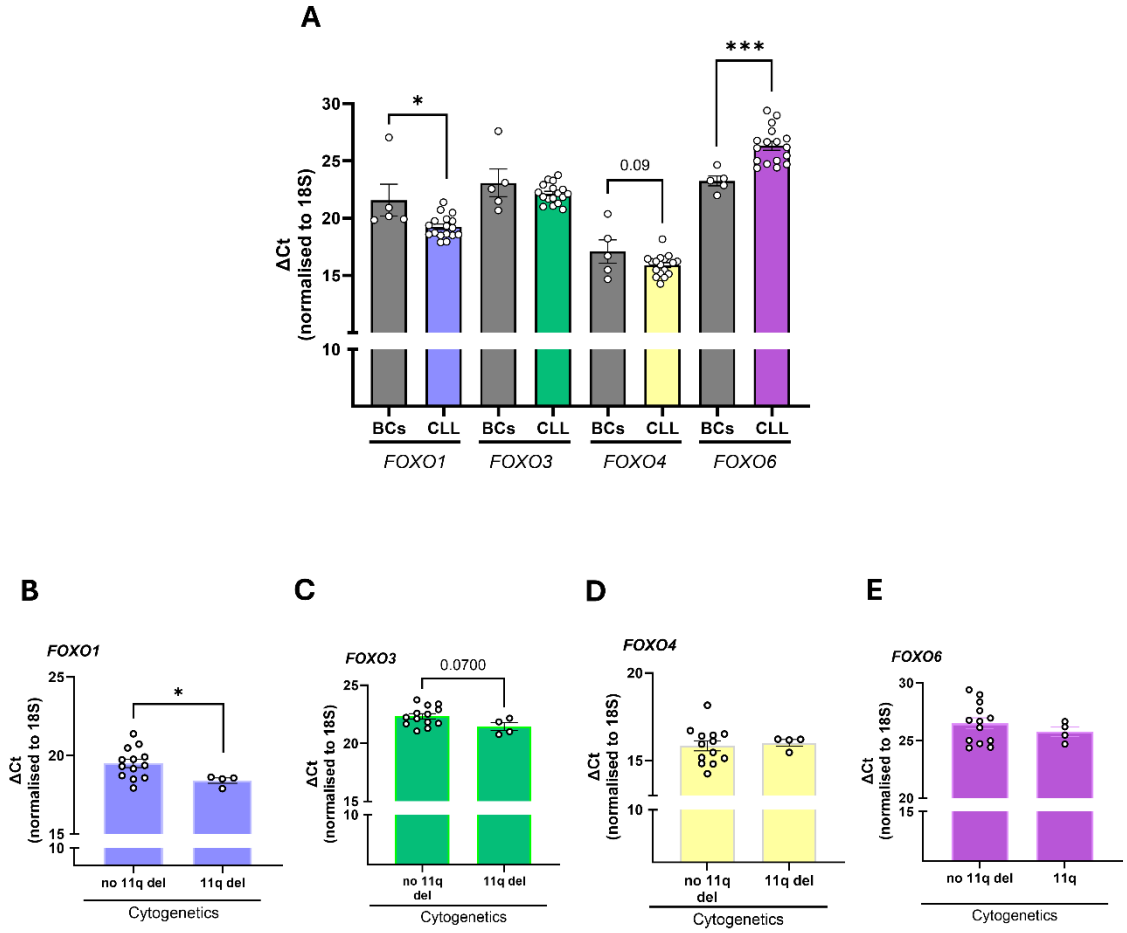

Figure 3.2: FOXO gene expression in ex vivo patient samples. (A) ΔCt values generated *via* RT-qPCR of *ex vivo* patient samples (CLL, n=17) and healthy, $CD19^+$ B-cell donor samples (BCs, n=5 independent replicates), assessing FOXO*1, FOXO3, FOXO4* and *FOXO6* transcript abundance. (B-E) *Ex vivo* samples (seen in A, n=17 independent patient samples) were subcategorised according to distinct prognostics (specifically del(11q)) to compare ΔCt values of each *FOXO* gene isoform between patients with or without 11q deletions. For the expression of each target gene, *18S* expression was used for normalisation purposes. Data points for individual patients are captured as white circles, represented as the mean ±SEM. (A) Statistics were conducted using an unpaired t-test, while B-E used one-way ANOVA, where * $p \leq 0.05$, *** $p \leq 0.001$.

Comparing FOXO1 expression in *ex vivo* CLL samples to healthy B-cell donors, FOXO1 was increased in CLL (Figure 3.3A & B), albeit not significantly, and there was no significant difference in FOXO1 expression within distinct Binet stage subgroups (Figure 3.3B). Interestingly, FOXO3 was significantly increased in patient samples compared with healthy B-cell donors (Figure 3.3C). Although expression was increased in each Binet stage subgroup (Figure 3.3C), Binet stage C CLL patients expressed significantly more FOXO3 than B-cell donors (Figure 3.3C), suggesting an association between FOXO3 expression and poor disease prognosis. In contrast, although western blots investigating FOXO4 expression in *ex vivo* samples indicated a rise in FOXO4 expression in CLL PB samples (Figure

3.3D & E, p = 0.16), FOXO4 expression was significantly increased in the Binet stage A CLL subgroup (figure 3.3E), implying a potentially disparate association between FOXO family member expression and disease prognosis. Although comparisons of relative expression can be made between healthy donor and CLL *ex vivo* samples, regardless of cytogenetics, FOXO1, FOXO3 and FOXO4 expression was highly heterogeneous in PB-derived CLL cells (Figure 3.3).

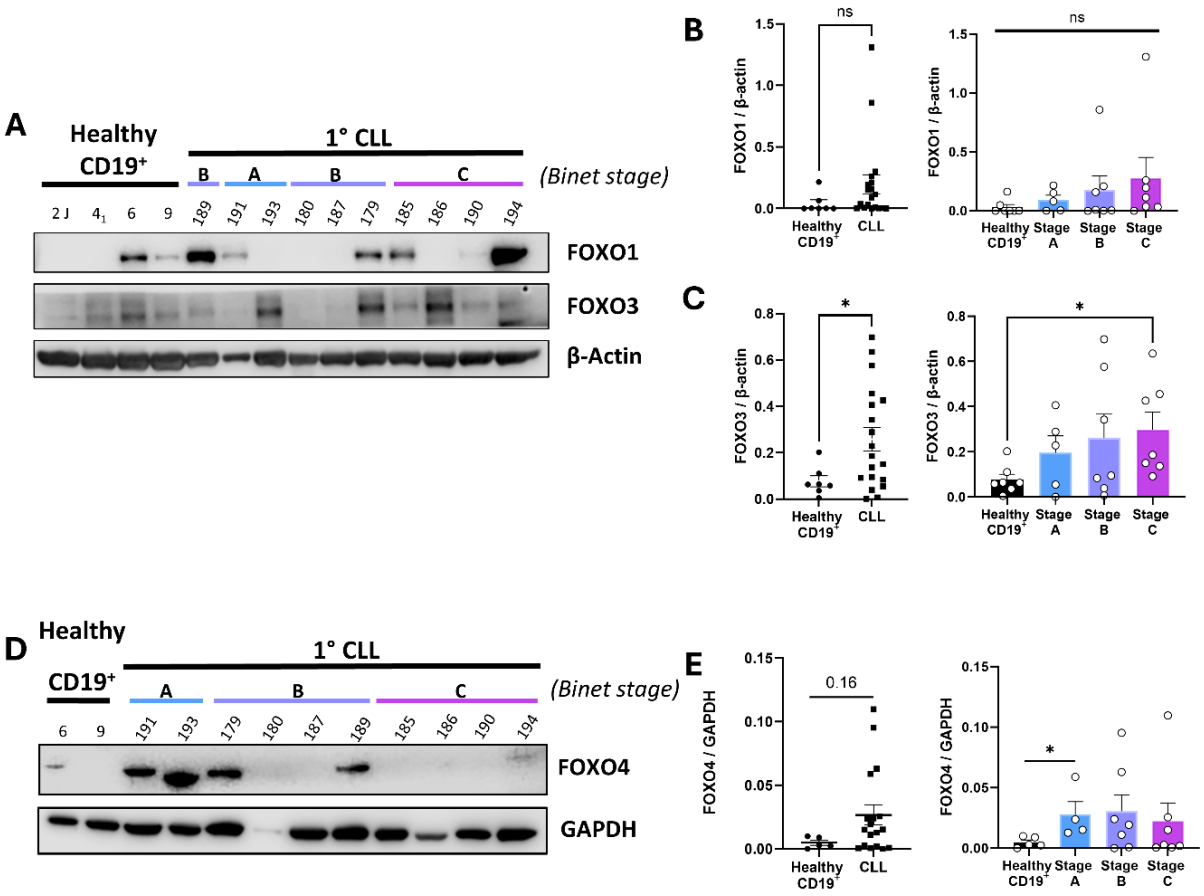

Figure 3.3: FOXO protein expression in ex vivo patient samples. *Ex vivo* samples were produced by taking CLL patient PB samples followed by isolation of the lymphocyte fraction. Protein lysates were generated and run alongside healthy *ex vivo* donor samples ('healthy CD19^{+}'), probing for either FOXO1, FOXO3 and β-actin (A), or FOXO4 and GAPDH (D). (B, left) The relative expression values from FOXO1 protein intensity scores in CD19 donor samples *versus* CLL patients, normalised to β-actin. (B, right) Relative expression values were subcategorised *via* Binet staging (stages A, B, C). (C, left) The relative expression values for FOXO3, normalised to β-actin. (C, right) Relative expression values subcategorised *via* Binet staging (n=7 independent healthy donor samples, n=16 independent CLL patient samples). (E, left) relative expression values for FOXO4, normalised to GAPDH. (E, right) Expression values subcategorised *via* Binet staging (n=7 independent healthy donor samples, n=15 independent patient CLL samples). Data points are captured as black circles (CD19 donors) and squares (CLL patients, in overall expression graphs, (B, C, E, left) while Binet stage graphs depict FOXO1/3/4 expression as white circles (B, C, E, right). Of note, Western blots A & D were conducted at different times, and the absence of GAPDH in CLL sample #180 caused it to be discounted from analysis. Data is represented as the mean ±SEM. Statistics were conducted using an unpaired Student's t-test, where * $p \leq 0.05$.

3.2.3. CD40 stimulation leads to phosphorylation and downregulation of FOXO transcription factors

Long-term IgM co-culture systems or CD40-CD40L systems can be used to facilitate CLL proliferation and provide survival signals to promote CLL proliferation and viability [207, 244]. Here, primary CLL cells were cultured with supportive, CD40L-expressing fibroblasts and either exogenous IL-4 (Figure 3.4A) or IL-21 (figure 3.4B). After 24 hr in the CD40L (+IL-4) system, we investigated FOXO3 expression, FOXO3^{S253} levels (Figure 3.4C), FOXO1 expression and FOXO1^{T24} (Figure 3.4D), as well as proteins associated with viability: the proapoptotic BCL2-like proteins MCL1 (Figure 3.4E) and BCL-XL (Figure 3.4F), and the proapoptotic BH3-only protein BIM (Figure 3.4G). FOXO3^{S253} levels were increased following CD40L-mediated stimulation (Figure 3.4A & B), albeit not significantly (Figure 3.4C, left), while FOXO3 expression was significantly downregulated following 24 hr on CD40L co-culture ($p = < 0.0001$, Figure 3.4C (right)). Additionally, FOXO1^{T24} levels were significantly increased following CD40 stimulation, and FOXO1 expression was significantly downregulated (Figure 3.4D). Further, MCL1 expression slightly increased with exposure to CD40L (Figure 3.4E), while BCL-XL expression significantly increased (Figure 3.4F, $p = 0.003$). Inversely, BIM was significantly downregulated following CD40 stimulation (Figure 3.4G, $p = 0.01$). Collectively, these data demonstrate an increase in survival signalling following combined exposure of primary CLL cells to CD40L and exogenous cytokine, coincident with FOXO inactivation and downregulation.

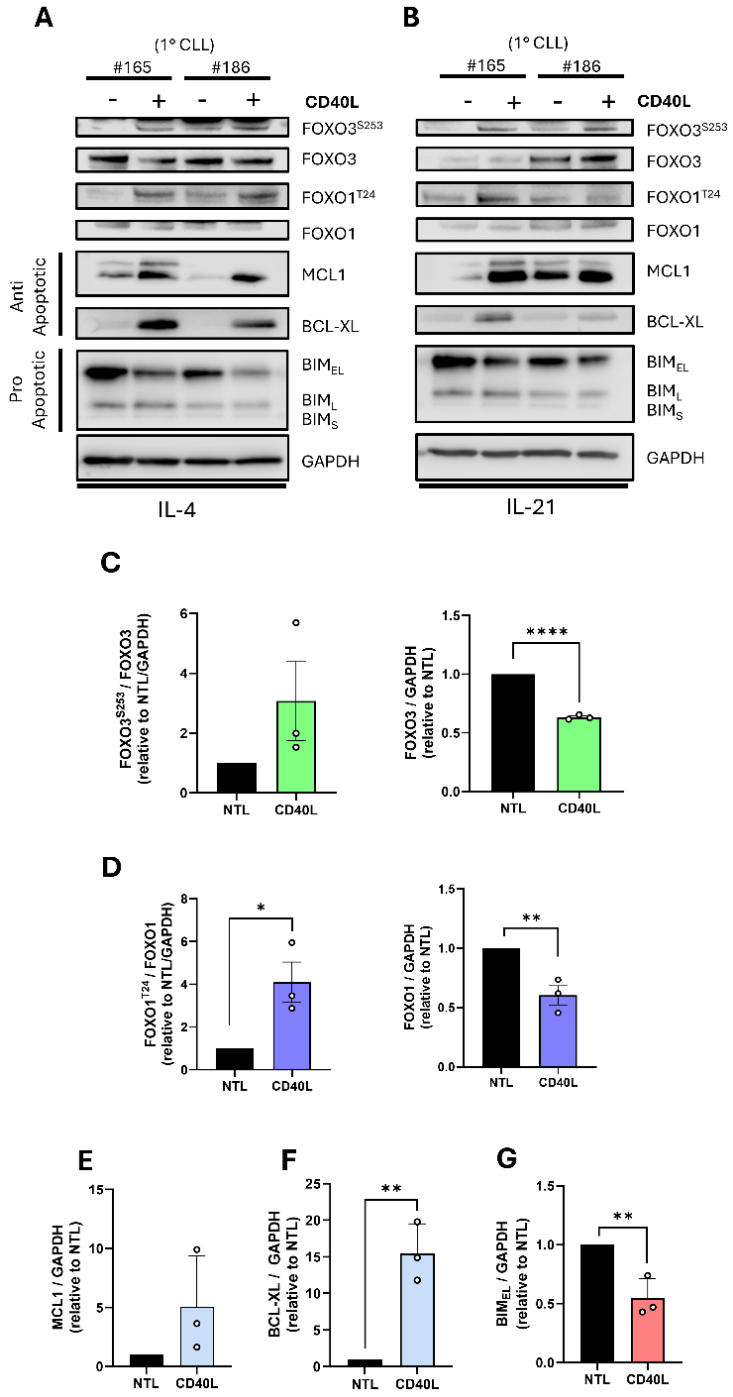

Figure 3.4: CD40-CD40L engagement promotes survival while inactivating FOXO3 and FOXO1. Primary patient samples were cultured for 24 hr in a mouse fibroblast co-culture either expressing (+CD40L) or not expressing ('NTL' – an unstimulated control) CD40L expression (+ 10 ng/mL IL-4 (A) or 15 ng/mL IL-21 (B)). CLL protein lysates were visualised *via* western blot (A & B) to investigate the phosphorylation status and expression of FOXO3, FOXO1, and the expression survival-associated proteins MCL1, BCL-XL and BIM. GAPDH was used as a loading control. Subsequent densitometry was conducted for results in the CD40L (+IL-4) system; (C, left) $FOXO3^{S253}$ levels were calculated as a proportion of total FOXO3 expression, normalised to GAPDH and relative to the unstimulated 'NTL' cohort. (C, right) Total FOXO3 protein quantified, normalised to GAPDH and relative to NTL. (D, left) $FOXO1^{T24}$ levels were calculated as a proportion of total FOXO1, normalised to GAPDH and relative to the unstimulated 'NTL' cohort. (D, right) Total quantified FOXO1 protein, normalised to GAPDH and relative to NTL. (E-G) The expression of MCL1, BCL-XL and BIM in CLL-CD40L co-cultures compared to the 'NTL' control, normalised to GAPDH and relative to the unstimulated 'NTL' cohort (n=3). Data points are captured as white circles in the CD40L condition. Matched samples were used for comparing ±CD40L. The data is represented as the mean ±SEM. All replicates are biological replicates from patient-derived CLL cells. Statistics were calculated using a paired t-test, where * $p \leq 0.05$, ** $p \leq 0.01$, **** $p \leq 0.0001$.

3.2.4. FOXO family gene expression is downregulated following CD40-CD40L interactions

The expression of distinct FOXOs has been associated with NF-κB signalling in the context of lymphocyte chemotaxis, a process driven by FOXO1-mediated CCL20 secretion [518] downstream of CD40 stimulation [519]. The requirement of *FOXO1/3* expression to form the GC architecture found within LN compartments, in which B-cells interact with CD40L-expressing T-cells [463], suggests an association between FOXO expression and CD40 activity in B-cell biology. In addition, FOXO target genes are differentially expressed following CD40 stimulation [520, 521], suggesting regulation of FOXO family genes. In Figure 3.5, we addressed the expression of genes encoding each FOXO isoform alongside survival-associated genes following 24 hr exposure to CD40L in the presence of either exogenous IL-4 or IL-21 (Figure 3.5A, C, D or B, E, F, respectively). In CLL samples stimulated with CD40L and IL-4, *FOXO1*, *FOXO3*, *FOXO4* and *FOXO6* were all significantly downregulated following CD40L stimulation (Figure 3.5A). In comparison, samples stimulated with exogenous IL-21 exhibited significantly diminished *FOXO1* and *FOXO3*, while *FOXO4* downregulation was not significant (Figure 3.5B). Further, *FOXO1* and *FOXO3* downregulation in IL-21-stimulated primary cells displayed reduced significance compared to their IL-4-stimulated counterparts (*FOXO1*: $p = 0.01$ *vs.* $p = <0.0001$, *FOXO3*: $p = 0.003$ *vs.* <0.0001). The impact of FOXO isoform depletion following CD40L-mediated stimulation is reflected by the expression of distinct survival-associated genes: in cells stimulated with IL-4, *MCL1* expression was reduced, trending on significance (Figure 3.5C, $p = 0.08$), while *BCL2L1* (BCL-XL) was significantly upregulated. Similarly, in cells cultured with IL-21, *MCL1* expression was significantly reduced, and *BCL2L1* upregulation had elevated significance (Figure 3.5E). However, the expression of *BCL2L11* (BIM) was significantly downregulated in CD40-stimulated cells +IL-4 (Figure 3.5D) - a depletion not seen in the IL-21 cohort (Figure 3.5F), demonstrating that cells cultured in the CD40L-IL-4 system elicit enhanced FOXO family gene downregulation, coincident with gene expression signatures indicating an enhancement of CLL cell survival.

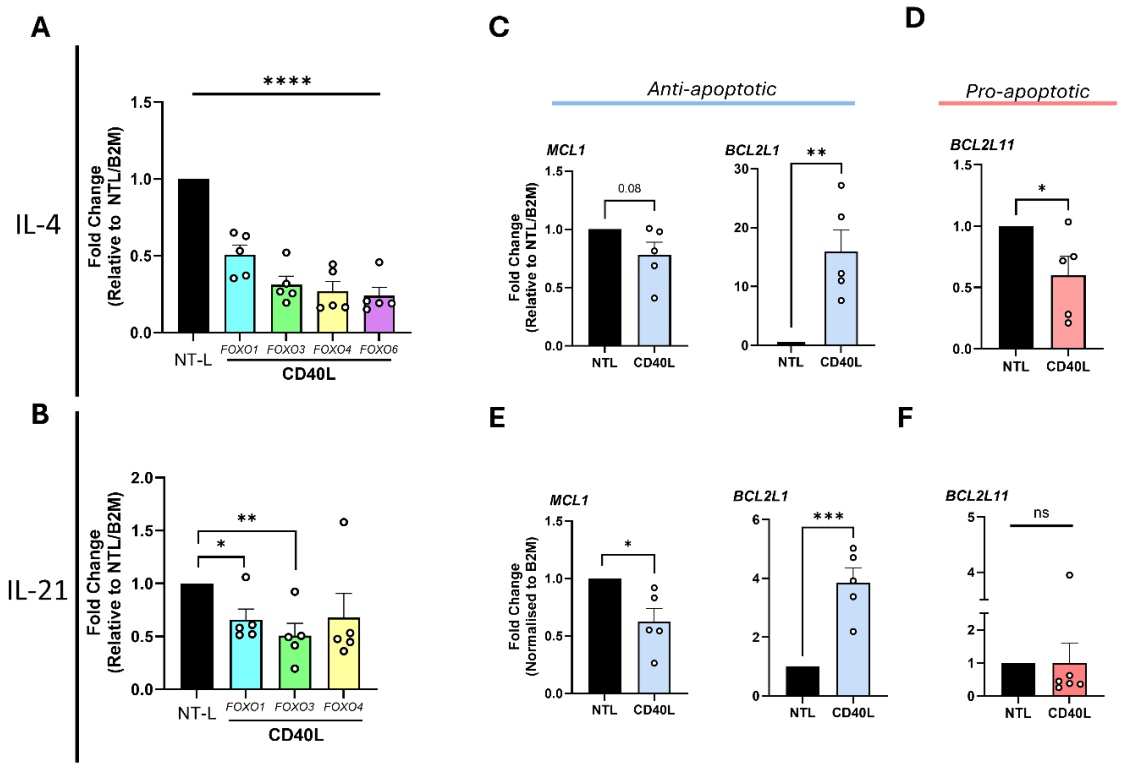

Figure 3.5: CD40-CD40L engagement promotes CLL cell survival and downregulates FOXO expression. Primary patient samples were cultured in a mouse fibroblast co-culture for 24 hr either expressing or not expressing ('NTL' unstimulated control) CD40L (+10 ng/mL IL-4 (A, C, D) or 15 ng/mL IL-21 (B, E, F)) and were subsequently analysed *via* RT-qPCR. (A) The gene expression of *FOXO1*, *FOXO3, FOXO4* and *FOXO6* in CD40L co-cultures relative to the unstimulated 'NTL' fraction. (C) The gene expression of *MCL1* and *BCL2L1*, relative to the 'NTL' control. (D) The gene expression of *BCL2L11* relative to the 'NTL' cohort. (B-F) follows the same order, albeit without the presence of *FOXO6* gene analysis. In all cases, *B2M* expression was used for normalisation purposes (n=5). Data points are captured as white circles, and the data is represented as the mean ±SEM. All replicates are biological replicates from patient-derived CLL cells. Statistics were calculated using a paired t-test, where * $p \leq 0.05$, ** $p \leq 0.01$, *** $p \leq 0.001$, **** $p \leq 0.0001$.

3.2.5. FOXO3 exhibits cytoplasmic shuttling following BCR stimulation

As transcription factors, FOXOs exhibit shuttling capacity, where their regulatory capabilities are determined by their abundance within either cytoplasmic or nuclear compartments [434]. As such, we employed subcellular fractionation techniques to understand how upstream stimulation regulates FOXO activity through cytoplasmic sequestration [503]. In Figure 3.6, we investigated whether BCR stimulation of CLL cells with soluble antigen has any impact on FOXO3 localisation to further validate whether FOXO3 is regulated downstream of BCR signalling. FOXO1 was used as a control, as it is proven to be sequestered in the cytoplasm following $F(ab')_2$ stimulation [284, 503]. As expected, FOXO1

expression was increased in cytoplasmic compartments following 1 hr of F(ab')$_2$ stimulation (Figure 3.6A & D), while nuclear compartments exhibited reduced FOXO1 expression (Figure 3.6A & E). While the data was limited (n=2), FOXO1 showed the same trend as with published data [284]. FOXO3 was highly abundant in the nucleus *in vitro*, regardless of BCR-crosslinking (Figure 3.6A). Following F(ab')$_2$ stimulation, FOXO3 expression in cytoplasmic fractions was significantly increased (Figure 3.6B), reflected by a depletion of FOXO3 in nuclear compartments (Figure 3.6C). These data demonstrate that F(ab')$_2$-mediated BCR stimulation affects the subcellular localisation of FOXO3 in primary CLL cells *in vitro*.

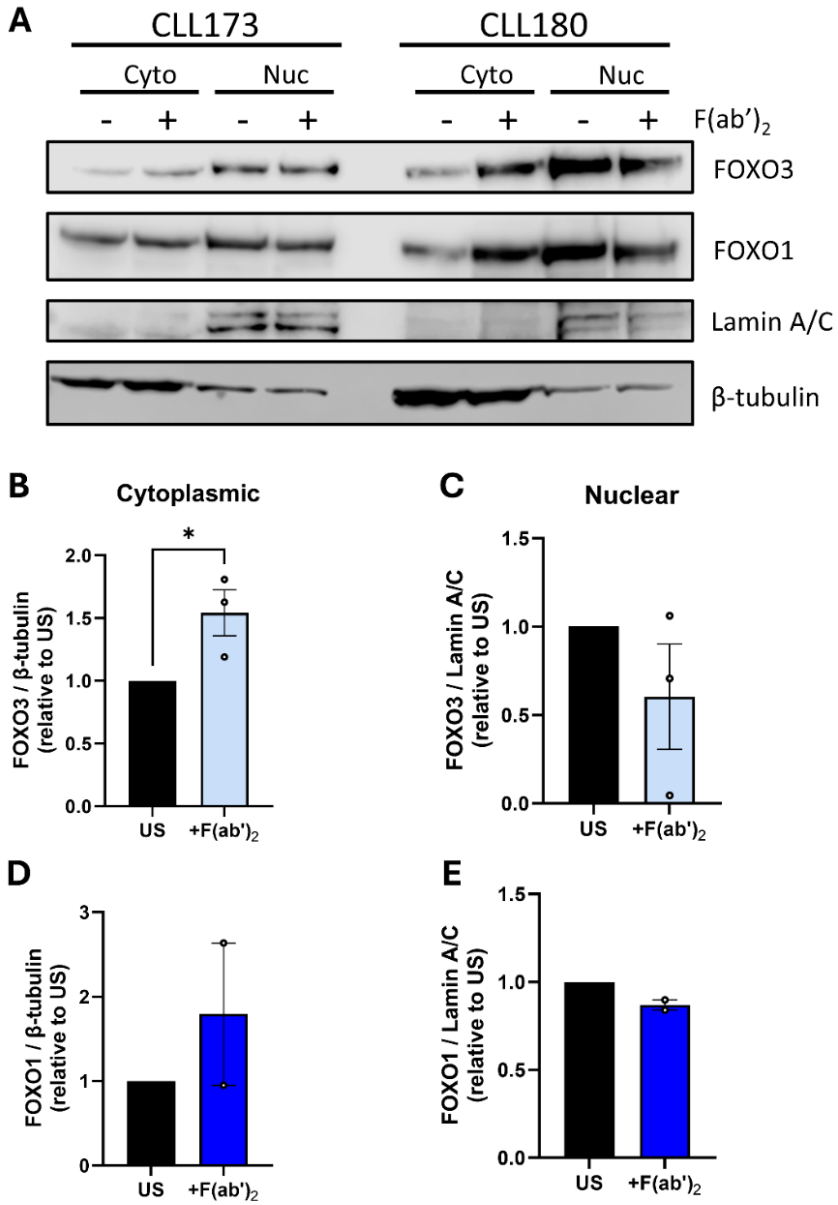

Figure 3.6: BCR activation facilitates cytoplasmic shuttling of FOXO3. (A) Western blot to investigate the localisation of FOXO3 and FOXO1 in cytoplasmic and nuclear compartments of primary CLL cells with and without 1 hr stimulation with 10 µg/mL F(ab')$_2$ antigen. Lamin A/C and β-tubulin were used as nuclear and cytoplasmic loading controls, respectively. (B & D) Quantification of the cytoplasmic expression of FOXO3 (B) and FOXO1 (D), relative to cells without F(ab')$_2$ stimulation, normalised to β-tubulin. (C & E) Quantification of the expression of FOXO3 (C) and FOXO1 (E) in nuclear lysates, relative to cells lacking F(ab')$_2$ stimulation and normalised to Lamin A/C (n=2 for FOXO1, n=3 for FOXO3). Data points are depicted as white circles, and data is represented as the mean ±SEM. Statistics were calculated using a paired t-test, where * $p \leq 0.05$. All replicates are biological replicates from patient-derived CLL cells.

3.2.6. AKT inhibition influences FOXO3 and FOXO4 phosphorylation

As AKT^{S473} phosphorylation is present in resting *in vitro* CLL samples [49], this suggests FOXO regulation occurs both in the presence and absence of $F(ab')_2$-mediated BCR activation. Using the pan-AKT inhibitor AZD5363 in combination with the BTK inhibitor ibrutinib, in primary CLL cells, we addressed whether inhibiting AKT activity affected the phosphorylation status of FOXO3 and FOXO4 (Figure 3.7). While ibrutinib treatment diminished both AKT^{T308} and AKT^{S473} levels, cells pre-treated with AZD5363 exhibited enhanced levels of AKT^{T308} and AKT^{S473} (Figure 3.7A) – an expression profile indicative of successful AKT inhibition [522]. Further, AZD5363 treatment induced a modest decrease in $FOXO3^{S253}$ (Figure 3.7B) and $FOXO4^{S193}$ (Figure 3.7C) levels, alone or in combination with ibrutinib, more notably in the absence of $F(ab')_2$ (Figure 3.7C). Subcellular fractionation of CLL sample #179 revealed an abundance of nuclear FOXO3 that was increased following AZD5363 treatment (Figure 3.7D). $F(ab')_2$ stimulation showed contrasting results for FOXO3 regulation in that $FOXO3^{S253}$ levels were decreased following $F(ab')^2$ stimulation compared to an increased $FOXO3^{S253}$ following $F(ab')_2$ stimulation in Figure 3.4. While more replicates are needed, these results suggest that the phosphorylation status of FOXO3 and FOXO4 are closely tied to AKT activity, in the context of BCR-mediated signalling.

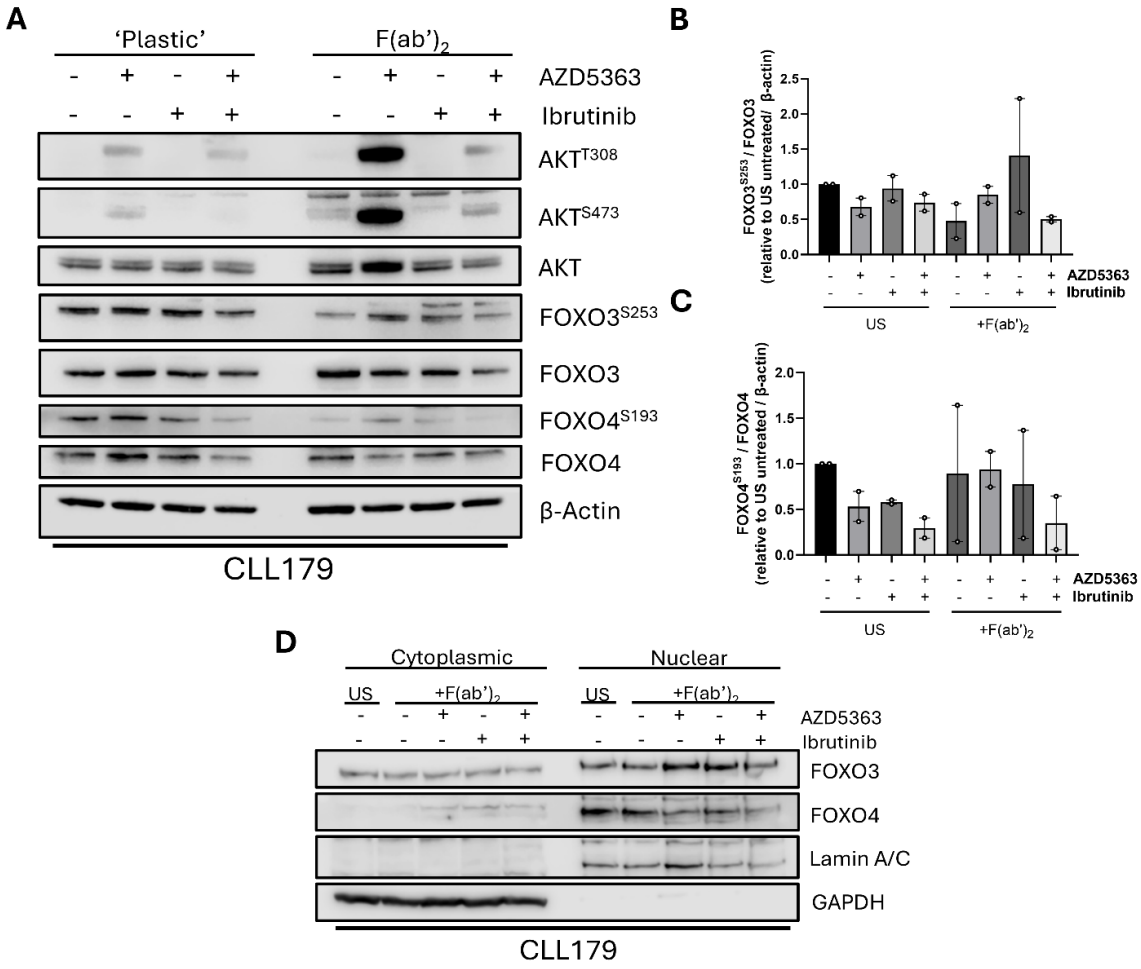

Figure 3.7: AKT inhibition reveals AKT-mediated FOXO3/4 regulation in BCR-activated CLL cells. (A) Western blot of primary CLL cells pre-treated for 30 min with 1 μM AZD5363 and/or 1 μM ibrutinib cultured for 1 hr with ($F(ab')_2$) or without ('plastic') 10 μg/mL $F(ab')_2$. Blots were developed to observe changes in AKT (T308/S473), FOXO3 (S253) and FOXO4 (S193) phosphorylation, with β-actin being used as a loading control. (B) Quantified phosphorylation of FOXO3 relative to total FOXO3 protein, normalised to β-actin and relative to the unstimulated, untreated control. (C) Quantified phosphorylation of FOXO4 relative to total FOXO4 protein, normalized to β-actin and relative to the unstimulated, untreated control (n=2). (D) Western blot of patient sample #179 following subcellular fractionation of cells stimulated with 10 μg/mL $F(ab')_2$ antigen for 1 hr, with or without single or combination 30 min pre-treatments with AZD5363 (1 μM) and ibrutinib (1 μM). GAPDH and Lamin A/C were used as cytoplasmic and nuclear loading controls, respectively. An unstimulated control (US) was included to observe changes in FOXO localisation following $F(ab')_2$ treatment (n=1). Quantified data points are depicted as white circles, and data is represented as the mean ±SEM. All replicates are biological replicates from patient-derived CLL cells.

3.2.7. AKT inhibition affects FOXO localisation in the CD40L (+IL-4) system

Due to AKT activation and FOXO inactivation downstream of CD40 signalling ([247] & Figure 3.4), it is important to address AKT inhibition in the context of CLL-CD40 signalling. This was assessed by equilibrating primary CLL cells on NTL-

CD40L (IL-4) overnight, followed by short-term AZD5363 and/or ibrutinib treatment. Here, AKT^{T308} and AKT^{S473} levels increased following AZD5363 treatment (Figure 3.8A), where an elevation in AKT^{T308} was potentiated by combined AZD5363-ibrutinib treatment (Figure 3.8A). Although AKT was inhibited, $FOXO3^{S253}$ levels were unchanged (Figure 3.8B). $FOXO3^{S253}$ was increased following CD40 stimulation and subsequently decreased with AZD5363-ibrutinib treatment (Figure 3.8B). Nevertheless, subcellular fractionation of AZD5363- and ibrutinib-treated cells in the CD40L (+IL-4) system (figure 3.8C-E) suggest that CD40L-mediated stimulation reduced FOXO3 and FOXO4 in CLL nuclear compartments. However, in this study, group size is limited, and variable FOXO3 expression in the nuclear compartment of the 'NTL' control suggests more replicates are required to determine CD40L-mediated FOXO3/4 nuclear translocation in this context. AKT inhibition, either alone or in combination with ibrutinib, increased the nuclear abundance of FOXO3 and FOXO4 (figure 3.8C-E). These data highlight that phosphorylated $FOXO3^{S253}$ can be detected in the NTL co-culture system, and it is difficult to detect changes in FOXO3 phosphorylation following the pharmacological inhibition of AKT and BTK. Of note, $FOXO4^{S193}$ levels were difficult to detect and were discounted from this experiment. These results allude to AKT downstream of CD40 influencing FOXO3/4 subcellular localisation, though these data are limited by the group size in the context of AKT inhibition.

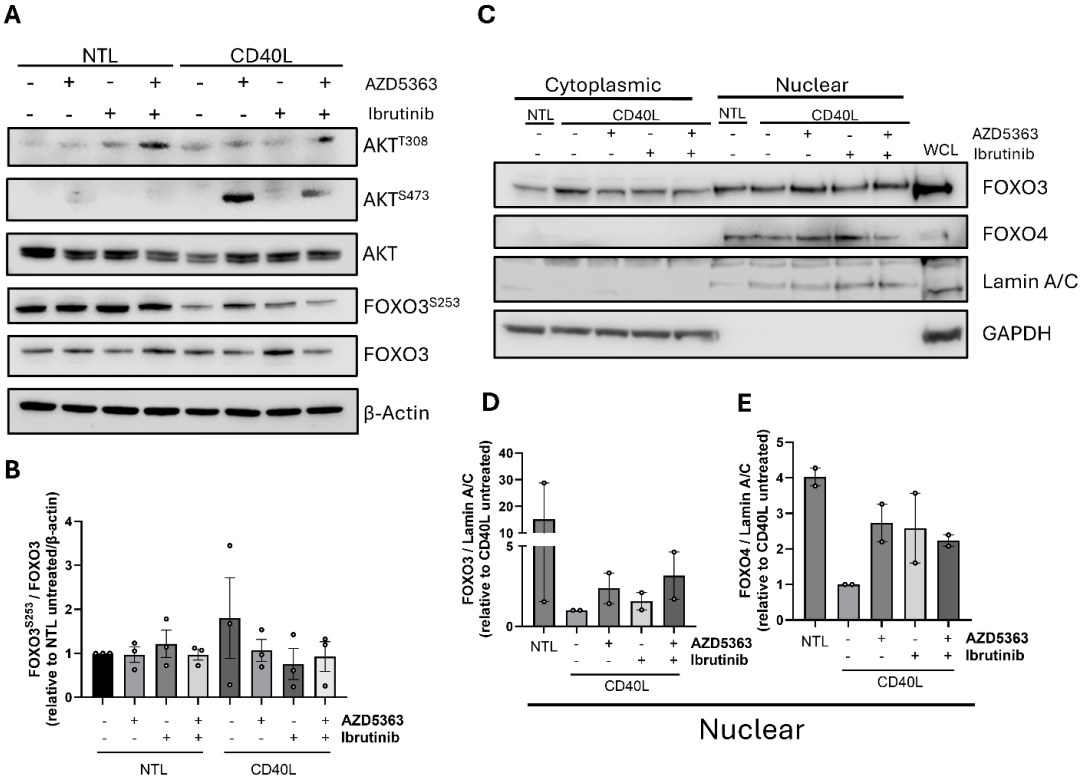

Figure 3.8: CD40 stimulation depletes FOXO nuclear abundance, mediated by AKT. (A) Western blot of CLL cells in overnight co-culture (+10 ng/mL IL-4) with 'NTL' or CD40L-expressing NTL cells (CD40L) followed by 1 hr treatments with AZD5363 (1 μM) and/or ibrutinib (1 μM). Blots were used to detect AKT phosphorylation (T308/S473), compared to total AKT, as well as AKT-mediated FOXO3 phosphorylation (S253) compared to FOXO3 total protein. β-actin was used as a loading control. (B) Quantified expression of FOXO3^{S253} levels compared to total FOXO3 protein, normalized to β-actin and made relative to the untreated, unstimulated condition (n=3). (C) Western blot of fractionated CLL cells that have been cultured overnight with NTL-CD40L cells (+10 ng/mL IL-4) with and without single or combination treatments of AZD5363 (1 μM) and ibrutinib (1 μM), observing relative expression of FOXO3 and FOXO4 in cytoplasmic and nuclear compartments. GAPDH and Lamin A/C were used as cytoplasmic and nuclear loading controls, respectively. A 'whole cell lysate' (WCL) sample was used as a positive control to confirm the presence of GAPDH and Lamin in CLL cell lysates. (D) Quantified expression of FOXO3 in nuclear compartments, normalized to Lamin A/C and relative to untreated cells on NTL-CD40L. (E) Quantified expression of FOXO4 in nuclear compartments, normalized to Lamin A/C and relative to untreated cells on NTL-CD40L (n=2). Data points are depicted as white circles, and the data is represented by the mean ±SEM. All replicates are biological replicates from patient-derived CLL cells.

3.2.8. Direct AKT inhibition affects FOXO4 phosphorylation in MEC1 cells

To explore FOXO regulation in other model systems, these experiments were repeated in the MEC1 cell line. Attention was focused on how pharmacological AKT and/or BTK inhibition affected FOXO4 phosphorylation (FOXO4^{S193}, Figure 3.9A & B) and subsequent localisation (Figure 3.9C & D). AZD5363 treatment induced AKT hyperphosphorylation, attenuated by combined treatment with ibrutinib (Figure 3.9A). MEC1 cells harboured limited but apparent FOXO4^{S193} (Figure 3.9A), which was significantly depleted following AZD5363 or AZD5363-ibrutinib therapy (Figure 3.9A & B). Further, subcellular localisation of MEC1 cells revealed FOXO4 abundance within nuclear compartments (Figure 3.9C), in conjunction with low endogenous FOXO4^{S193} (Figure 3.9A). Combined AZD5363 and ibrutinib treatments increased FOXO4 nuclear abundance (Figure 3.9D, $p = 0.17$). These data provide evidence that FOXO4 phosphorylation is mediated by AKT activity and that, although this affects subcellular localisation, both FOXO3 and FOXO4 are expressed within patient and MEC1 nuclear compartments (Figures 3.6-3.9).

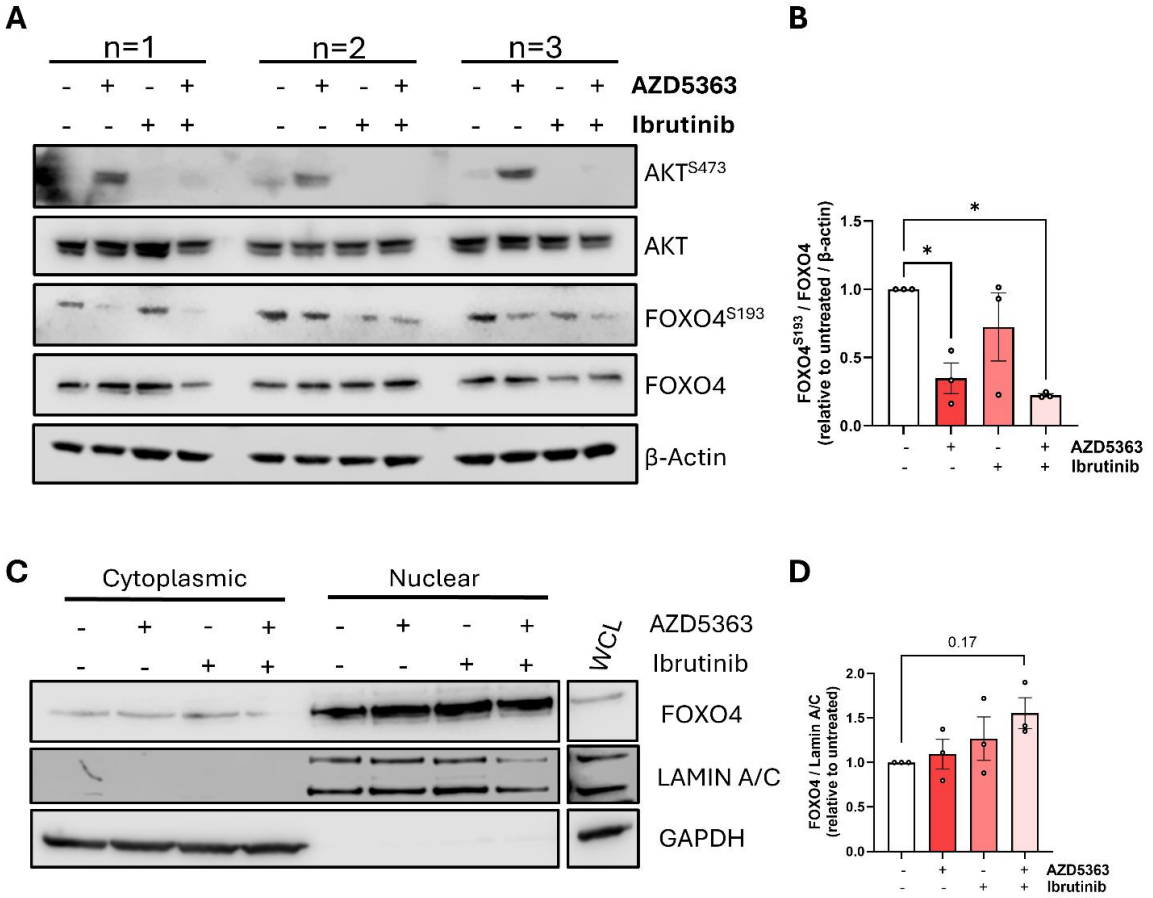

Figure 3.9: FOXO4 is actively regulated by AKT in MEC1 cells. (A) Western blot showing three replicates (n=1, n=2, n=3) of MEC1 cells following short-term, 1 hr single or combination treatments of AZD5363 (1 μM) and/or ibrutinib (1 μM), where phosphorylated (AKT^{S473}, $FOXO4^{S193}$) and total protein expression of AKT and FOXO4 were detected. β-actin was used as a loading control. (B) Quantified expression of $FOXO4^{S193}$ levels compared to total FOXO4 expression, normalised to β-actin and relative to untreated cells (n=3). (C) Subcellular fractionation of MEC1 cells following the same 1 hr treatments with AZD5363 and ibrutinib, where FOXO4 expression is detected in cytoplasmic and nuclear compartments. GAPDH and Lamin A/C were used as cytoplasmic and nuclear loading controls, respectively. A 'whole cell lysate' (WCL) sample was used as a positive control to confirm the presence of GAPDH and Lamin in CLL cell lysates. (D) Quantified expression of FOXO4 in MEC1 nuclear lysates, normalised to Lamin A/C and relative to the untreated control (n=3). Data points are depicted as white circles, and the data is represented as the mean ±SEM. Statistics were calculated using one-way ANOVA, where * $p \leq 0.05$.

3.2.9. FOXO expression is modulated over the course of CD40 stimulation

CD40-associated gene signatures are known to change in expression over time [523]. This, together with the necessity of distinct FOXO family gene expression in the context of GC formation [477] and the maintenance of GC-resident B- and

T-cell populations [482] - postulate that FOXO expression could be further modulated in the presence of chronic CD40 stimulation. To address this, primary CLL cells were co-cultured with NTL-CD40L cells over the course of 10 days. Subsequently, samples were taken to assess protein and transcript abundance of FOXO family members (Figure 3.10). Comparisons were made between lysates collected at 1 and 10 days, with the addition of an unstimulated control to assess the regulation of FOXO family genes (Figure 3.10D-G). FOXO3 expression increased significantly in 10-day cultures compared to its expression following culture for 24 hours (1 day) (Figure 3.10A & B). In contrast, FOXO1 expression showed no change between timepoints (Figure 3.10C). Further, *FOXO1* (Figure 3.10D) and *FOXO4* (Figure 3.10F) genes were significantly downregulated following CD40L stimulation, subsequently returning to basal levels following 10 days in culture. While *FOXO3* and *FOXO6* were also significantly downregulated at day 1 (Figure 3.10E & G), their expression failed to return to basal levels following 10 days in culture. These data demonstrate that, as well as FOXO regulation occurring following acute CD40 activation, long-term CD40L signals apply further regulatory pressure to the expression of FOXO isoforms at gene and protein level.

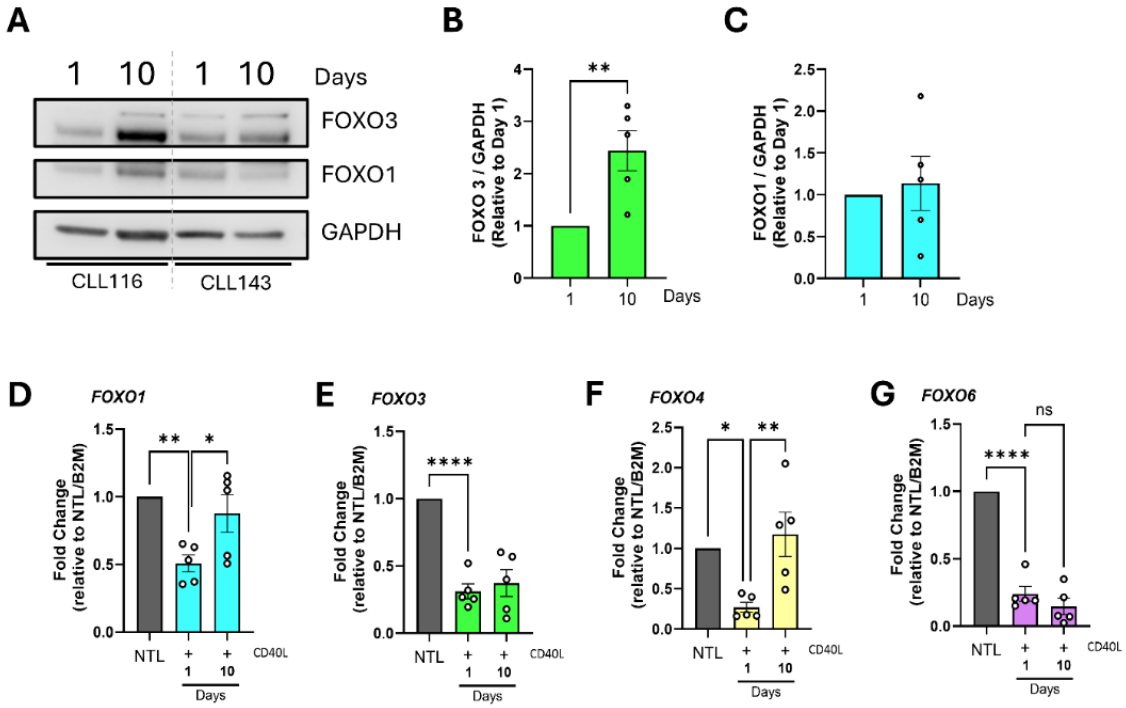

Figure 3.10: FOXOs are further regulated over time in CD40L co-cultures. (A) Western blot of primary CLL cells in CD40L co-culture for 1 and 10 days (Patients #116 and #143), detecting the expression of FOXO3 and FOXO1. GAPDH was used as a loading control. (B) Quantified expression of FOXO3 in samples co-cultured with CD40L-expressing NTL cells for 1 and 10 days, normalized to GAPDH and relative to 1-day cultures. (C) Quantified expression of FOXO1 in samples co-cultured with CD40L-expressing NTL cells for 1 and 10 days, normalized to GAPDH and relative to 1-day cultures (n=5). (D-G) RT-qPCR was conducted in samples generated from CLL cells following 1 or 10 days in

CD40L co-culture (+10 ng/mL IL-4) to detect *FOXO1, FOXO3, FOXO4* and *FOXO6* gene expression. Gene expression was normalized to *B2M* expression and was made relative to an unstimulated control (-CD40L) taken at the 1-day timepoint (depicted by the solid grey bar), where expression is presented as fold change (n=5). Of note, only FOXO3 and FOXO1 proteins were detected as this experiment was conducted before FOXO4 detection was established as part of the project Data points are depicted as either black squares or triangles, and the data is represented as the mean ±SEM. All replicates are biological replicates from patient-derived CLL cells. Statistics were calculated using a paired t-tests, where * $p \leq 0.05$, ** $p \leq 0.01$, **** $p \leq 0.0001$.

3.2.10. Long-term ibrutinib therapy alters the expression of FOXO transcription factors *ex vivo*

In the context of B-cell malignancy, studies have shown that downstream of BTK inhibition, constitutive FOXO activity enhances cell death [524]. In DLBCL, reduced ibrutinib efficacy is linked to both AKT activation and the downregulation of FOXO3 [524]. Further, in MCL, FOXO3 downregulation confers resistance to PI3K-AKT [525], inferring that FOXO expression is closely associated with clinical responsiveness to targeted inhibition of BCR signal effectors. To address this in the context of CLL, we assessed how FOXO family expression changes during the treatment course of ibrutinib therapy (Figure 3.11). Here, *ex vivo* patient samples were collected pre- and post-ibrutinib therapy (illustrated in Figure 3.11A) and subsequently profiled for FOXO3 and FOXO4 protein (Figure 3.11B-D) and gene (Figure 3.11E & F) expression. Though endogenous levels of FOXO3/4 varied between patients (Figure 3.11A), when comparing before and after the initiation of treatment, FOXO3 protein expression was significantly higher post-treatment (Figure 3.11C). FOXO4 protein expression was also increased, though the high variance between samples lacked any statistical significance (Figure 3.11D). These results were also reflected with respect to their genes: *FOXO3* expression was significantly upregulated in samples post-treatment (Figure 3.11E); *FOXO4* expression was also increased (Figure 3.11F), however the variance between patients resulted in no significance. These data would benefit from a larger pool of patient samples to better discern the impact of long-term ibrutinib therapy on FOXO3/4 expression. Even so, these data demonstrate an association between ibrutinib therapy and FOXO3/4 expression in circulating CLL cell populations.

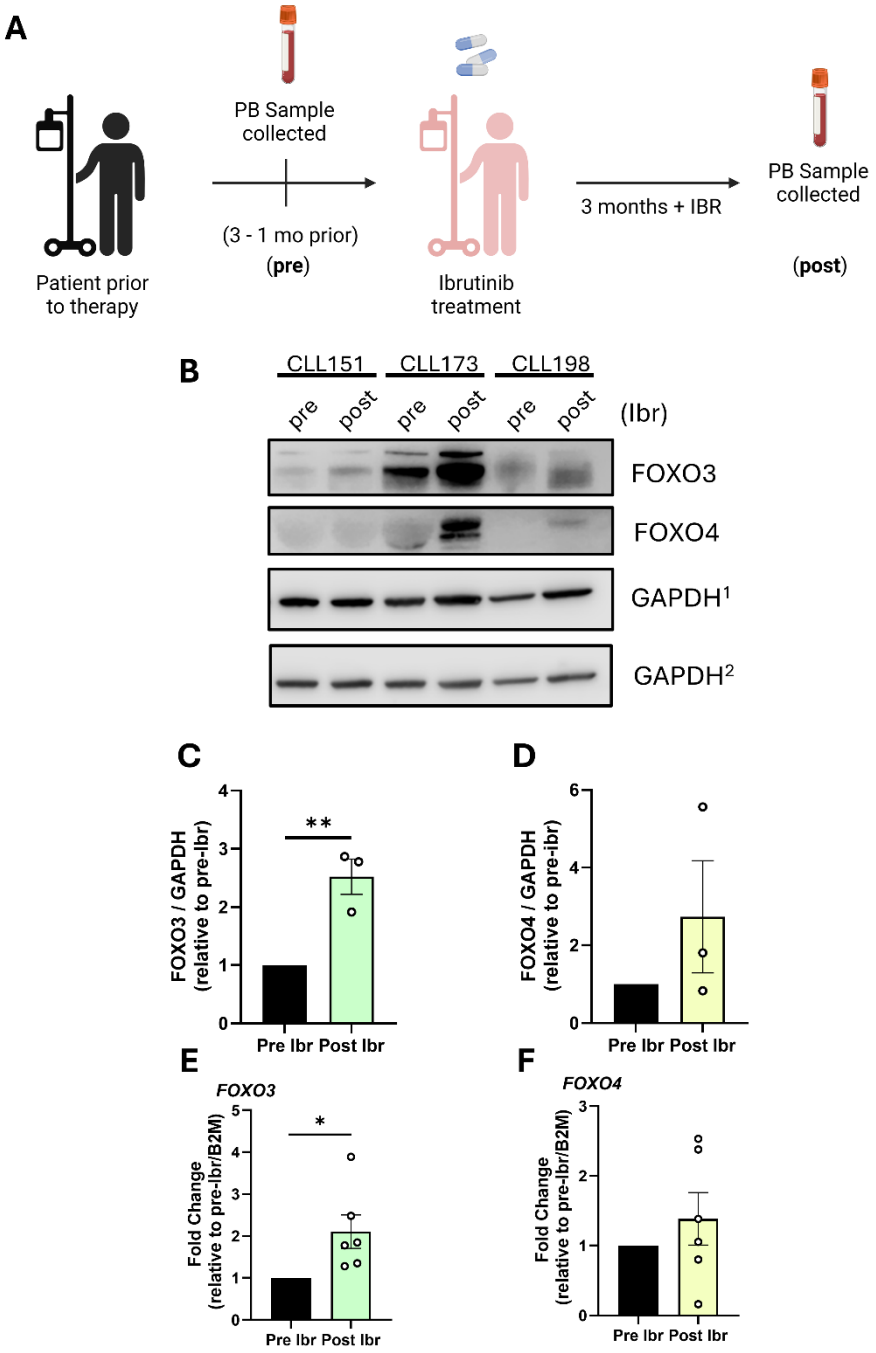

Figure 3.11: FOXO expression is increased in ex vivo samples of CLL patients undergoing ibrutinib therapy. (A) Illustration depicting how *ex vivo* patient samples were acquired either pre- before or 3 months post-ibrutinib treatment. (B) Western blot of *ex vivo* samples of patients either before (pre) or 3 months after (post) the initiation of ibrutinib therapy. Protein expression of FOXO3 and FOXO4 was detected, while GAPDH was used as a loading control (the small numbers following GAPDH describe GAPDH detection in multiple blots). (C) Quantified protein expression of FOXO3 in *ex vivo* samples, normalized to GAPDH and relative to expression pre-treatment. (D) Quantified protein expression of FOXO4 in *ex vivo* samples, normalized to GAPDH and relative to expression pre-treatment (n=3). (E-F) *FOXO3* and *FOXO4* gene expression obtained *via* RT-qPCR of *ex vivo* samples before and after ibrutinib treatments. *B2M* expression was used for normalisation purposes, and expression is presented as fold change, relative to samples pre-ibrutinib treatment (n=6). Data points are depicted as white circles, and the data is represented as the mean ±SEM. All replicates are matched replicates from CLL patients before and after Ibr therapy. Statistics were calculated using a paired t-test, where * $p \leq 0.05$, ** $p \leq 0.01$.

3.3. Discussion

Ex vivo patient sample analysis revealed differential FOXO expression in different CLL prognostic subtypes, reflected by disparate FOXO3 and FOXO4 expression MEC1 and HG3 cells. Furthermore, engagement of the major TME signalling components (BCR, CD40) actively induced FOXO downregulation, phosphorylation and cytoplasmic shuttling. Pharmacological abrogation of AKT activity using AZD5363 attenuated AKT-mediated FOXO phosphorylation and cytoplasmic sequestration, demonstrating that FOXO activity and expression is regulated downstream of AKT in proliferating CLL cells - supporting FOXO expression in patients undergoing long-term ibrutinib therapy. These data demonstrate a tight regulation of FOXO expression and activity in both circulating CLL cells and in response to TME-mediated signals. Regardless, nuclear FOXO expression suggests that, as well as harbouring tumour-suppressive behaviour, there is a requirement of FOXO expression and activity to promote context-dependent CLL proliferation and survival.

3.3.1. CLL cells exhibit elevated FOXO expression

FOXO expression is associated with disease progression in numerous cancer neoplasms and is prevalent within B-cell malignancies [463]. In CLL, Michael Moles also demonstrated elevated FOXO1 expression in MEC1 cells compared with HG3 cells [49], indicating a relationship between patient prognostics and FOXO expression. Supporting this, Cosimo *et al*. revealed an upregulation of *FOXO1* and *FOXO4* in *ex vivo* CLL cells compared to healthy $CD19^+$ cells, where immunohistochemical staining revealed a further increase in FOXO expression in patients with poor prognostics [284], demonstrating a potential link between FOXO1 expression and disease progression. These data indicate that *FOXO3* and *FOXO4* gene expression is increased in *ex vivo* CLL PB samples *vs*. healthy $CD19^+$ B-cell donor samples. In addition, differential expression of FOXO3 and FOXO4 proteins in different prognostic subsets supports a potential link between

prognosis and discrete FOXO expression and highlights potential differences in FOXO behaviour in different malignant contexts. In AML, FOXO3 expression is associated with reduced overall survival and recurrence-free survival [526], supporting increased *FOXO3* expression in patients harbouring del(11q) (Figure 3.2). Moreover, FOXO4 expression is associated with favourable prognosis in renal and head-and-neck cancers [527, 528] and is actively downregulated in these disease contexts [529, 530]. Study of FOXO expression between prognostic subtypes is limited, however, these data determine that FOXO3 and FOXO4 are expressed in circulating PB CLL cells, potentially indicating a relationship between distinct FOXO expression and disease prognosis. Interestingly, Jurcevic *et* al. found – in neuroblastoma cells - that miRNA-548l, located in the chromosomal 11q region, is reported to impede *FOXO1* and *FOXO3* gene expression [531], perhaps explaining how *FOXO1* and *FOXO3* are upregulated in del(11q) CLL patients. Investigation by miRPathDB revealed that miRNA-548l affects, amongst other targets, *FOXO1* and *FOXO3* gene isoforms [532], possibly explaining why *FOXO4* and *FOXO6* are unaffected by 11q deletion. Indeed, more work investigating the implications of 11q deletion on the expression of discrete FOXO isoforms would be instrumental in developing our understanding of how FOXO biology contributes to CLL pathophysiology. It is worth mentioning that lower FOXO expression in distinct prognostic subtypes does not preclude that particular FOXO family member from having a role in lymphomagenesis due to their ability to harbour specific characteristics [425], reflecting disparate FOXO expression in GC-resident B-cells [456, 463]. This could be the case for *FOXO6*, evidenced by its downregulation in *ex vivo* CLL cells compared with healthy $CD19^{+}$ B-cell donor cells. FOXO6 proved difficult to detect *via* Western blot and, due to the scarcity of literature investigating roles for FOXO6 in disease biology, the project focus was directed at investigating the roles of FOXO3 and FOXO4 in the context of CLL proliferation and survival. Due to FOXOs harbouring tissue specificity [533], the role of FOXO6 has been extensively studied in cells with high FOXO6 expression, including hepatic cells, where FOXO6 expression is important for regulating insulin signalling. Here, FOXO6 dysfunction is associated with inferior outcomes including obesity and type II diabetes [534]. FOXO6 being detected in B- and CLL cell populations suggests a role for FOXO6 in CLL disease biology that has yet to be elucidated. FOXO6 has only 30% sequence homology

with the rest of the FOXO family, suggesting that it may possess unique functions in FOXO6-expressing cell types [535].

3.3.2. CLL cells downregulate and inactivate FOXO transcription factors and promote survival following CD40 stimulation

Introducing primary CLL cells to CLL-CD40L co-culture elicited a marked downregulation of FOXO protein and gene expression following short-term co-culture, as well as an increase in FOXO3^{S253} and FOXO1^{T24} phosphorylation. Collectively, these findings reveal an association between CD40 stimulation and FOXO inactivation. Concurrently, CLL survival signalling was promoted through the upregulation of MCL1, BCL-XL, as well as downregulating BIM. This is known to be facilitated by non-canonical NF-κB signalling downstream of CD40 [235], facilitating CD40-mediated drug resistance. Thus, it is convincing that FOXO inactivation could also emanate from CD40-mediated signals that modulate PI3K-AKT activity [247]. However, these data are in contrast to published data, demonstrating a lack of FOXO1 phosphorylation in cells stimulated with anti-CD40 antibody [479]. Indeed, this study of FOXO1 phosphorylation downstream of CD40 activation was performed in naïve and GC-resident murine B-cell populations, where CD40-CD40L interactions may confer different mechanistic outcomes to that of CLL cells. Further, it could be that CLL-like splenocytes derived from an *in vivo* mouse model may elicit different responses to CD40 stimulation than that of circulating PB CLL cells [479]. Nevertheless, FOXO downregulation triggered by CD40 activation suggests an association between FOXO expression and engagement of CLL cells with supportive cells within the CLL-TME. Zhu *et al*. reported a downregulation of FOXO1 in mouse B-cells following stimulation with several factors including anti-CD40 antibodies [536] - an observation also seen in BCR-activated B-cells. In this context, the reduced expression of FOXO family genes is PI3K-dependent [464], supporting FOXO isoform downregulation as a necessary consequence of PI3K-AKT activation to faciliate proliferation downstream of either CD40 or BCR ligation. Further, these findings illustrate that FOXO expression is heightened in circulating CLL cells

than those engaged in CD40-CD40L interactions, suggesting a need for FOXO expression to mediate tissue-specific cell function - perhaps to facilitate cell quiescence; in endothelial cells, FOXO1 has been demonstrated as a critical driver of quiescence, in part by suppressing MYC signalling [537]. This is characteristically induced by FOXO1 in pre-B cells [538] but has also been reported in quiescent CML stem cells, where TKI-mediated FOXO activation in mature progenitor cells induced quiescence [539].

3.3.3. FOXO3 and FOXO4 are abundant in the CLL cell nucleus, irrespective of AKT activity

In this thesis, we initially studied whether AKT regulates FOXO3 and FOXO4 by utilising the AKT inhibitor AZD5363, which has been shown to abrogate FOXO1^{T24} levels in CLL [49]. Findings in primary CLL cells in F(ab')$_2$ and CD40L co-culture systems were limited yet inferred that FOXO3 and FOXO4 were regulated by AKT. As such, utilised the MEC1 cell line to investigate FOXO4 expression and AKT-mediated phosphorylation downstream of 'tonic' BCR signalling as a means of understanding the mechanisms underlying the PI3K-AKT-FOXO axis *in vitro*. A reduction in FOXO4^{S193} supports that FOXO4 is regulated by AKT activity in proliferating CLL cells. Irrespective of AKT activity, FOXO3/4 expression was primarily localised within the CLL nucleus suggesting that, while AKT regulates FOXO activity, an abundance of FOXO3/4 is necessary for CLL cells to coordinate gene expression to facilitate CLL homeostasis. These results are strongly consistent throughout multiple *in vitro* models, alluding to FOXO activity in proliferating CLL cells and PB CLL cells exposed to TME signals. Kapoor *et al.*, demonstrated that FOXO3 is prevalent in the nucleus irrespective of AKT activity [524]. This is a common occurrence in other B-cell malignancies, including BL and BCP-ALL [540, 541], both of which rely on FOXO nuclear activity to drive lymphomagenesis. Though not as prominently, FOXO1 has also been shown to harbour nuclear expression in BCR-ligated CLL cells, though FOXO1 is subject to strong nuclear shuttling following abrogation of BTK and mTOR activity [49, 284]. These findings highlight the mechanistic complexity of FOXO regulation downstream of signal transduction, where multiple factors could collectively

facilitate FOXO nuclear homing, counterbalancing the canonical understanding of AKT-mediated FOXO inactivation. Nevertheless, these data support the current dogma that AKT regulates FOXO activity in proliferating CLL cells [463]. Interestingly, AKT^{S473} levels were persistently increased in CLL cells treated with the AKT inhibitor AZD5363. In renal cell carcinoma cells, Lin *et al*. demonstrated that inhibition of PI3K-AKT signalling induced FOXO-mediated upregulation of *RICTOR*, revealing a FOXO-mediated regulatory feedback mechanism inducing Rictor-mediated AKT hyperactivation in response to PI3K-AKT signal abrogation [542]. These findings demonstrate that, while AKT negatively regulates FOXO activity, FOXO activity could maintain components of the PI3K-AKT-mTOR signalling axis to prevent cellular dysfunction. These findings are purported to exist in MEC1 and CLL patient cells [543], though roles for FOXOs in regulating mTORC1/2-mediated signals in the context of CLL has yet to be elucidated. These are discussed later in section 5.3.2.

3.3.4. FOXO expression is differentially regulated in long-term CD40L co-culture

Progenitor cells committed to the B-cell lineage display differential FOXO1/3 expression at different developmental stages [456]. Moreover, naïve B-cells localised in hyper-selective GC compartments express *FOXO1* and *FOXO3* to facilitate distinct maturation processes [284], highlighting the capability and importance of developing and mature B-cells to differentially express FOXO transcription factors to facilitate B-cell development. FOXO3 was significantly upregulated in primary CLL cells exposed to CD40L for 10 days as opposed to 1-day exposure. Furthermore, while FOXO expression was effectively downregulated in 1-day CD40L co-cultures, *FOXO1* and *FOXO4* were significantly higher in 10-day cultures compared with identical patient samples following 1-day culture, demonstrating that FOXOs are proactively regulated during CLL-TME interactions. It is interesting to hypothesise how this occurs; one possibility could be that, as FOXO3 is required as part of

plasma cell differentiation following CD40-CD40L engagement with GC-resident T_{fh}-cells [481], leukaemic B-cells may recreate this mechanism of FOXO3 expression following CD40L exposure *in vitro*. However, this process typically involves inducing *FOXO3* gene expression of which is prevalent in CLL cells irrespective of CD40 ligation and time in culture. Thompson *et al*. demonstrated in DCs that the FOXO3 protein was actively bound to NF-κB p65, thereby preventing NF-κB activity and prohibiting FOXO3 degradation [544] - this finding provides a more mechanistic explanation for an abundance of FOXO3 downstream of long-term CD40-mediated NF-κB activation. However, more work is needed to fully elucidate this. While there is minimal literature surrounding the role of FOXO4 in normal and malignant B-cell physiology, *FOXO4* is also known to be expressed during B-cell development [460], suggesting a requirement for FOXO4 that has yet to be elucidated. As well as abundant FOXO4 gene and protein expression in circulating CLL cells (Figures 3.2 & 3.3), increased *FOXO4* expression in long-term CLL co-cultures demonstrate dynamic FOXO4 expression and regulation in both quiescent and proliferative tissue compartments. This could be to promote cell 'stemness' and survival as seen in DLBCL cells. Ryu *et al*. examined multiple B-cell lymphoma cell lines and refractory patient-derived lymphoma cells and found that cell lines overexpressing *FOXO4* were resistant to doxorubicin/phenylbutyrate treatment. Further investigation found that *FOXO4* expression was associated with enhanced self-renewal, while depletion of *FOXO4* led to a loss of stem cell marker expression and the ability to form colonies [545], demonstrating FOXO4's capacity to facilitate disease maintenance and progression in mature B-cell neoplasms. Moreover, like FOXO3, FOXO4 has also been shown to regulate NF-κB activity [546], suggesting a potential mechanism of FOXO3- and/or FOXO4-mediated regulation of CD40 activity in CLL cells, akin to how FOXO activity provides regulatory feedback to reinforce AKT-mediated signalling *via* regulation of distinct target genes [547, 548].

3.3.5. FOXO expression is modulated with ibrutinib therapy

Elevated FOXO expression has been associated with the development of resistance to treatment with tyrosine kinase inhibitors (TKIs) in AML and CML model systems; in TKI-resistant AML cells, FOXO1 and FOXO3 induce the expression of FMS-like receptor tyrosine kinase (FLT3) - a poor prognostic marker indicative of relapse [549]; in CML cells, elevated FOXO1 is associated with BCL2 and phospho-ERK expression [550], demonstrating that FOXO1 can support the survival of leukaemic cell populations. Resistance to BTK inhibitors can also be acquired in CLL patients [80]. Kapoor *et al.* demonstrated that FOXO3 nuclear abundance is reduced, and that FOXO3 nuclear retention promotes ibrutinib-mediated apoptosis [524], demonstrating an inverse association between FOXO activity and drug resistance that opposes FOXO-mediated drug resistance as seen in myeloid malignancies. Here, we investigated the expression of FOXO3 and FOXO4 in *ex vivo* patient samples prior to - and after - 3 months of ibrutinib therapy, to assess the prevalence of disparate FOXO expression following long-term pharmacological BTK inhibition. The expression and activity of FOXO1 in this context has already been explored: long-term ibrutinib therapy did not allow for FOXO1 expression but did affect its phosphorylation *via* AKT (T24) downstream of $F(ab')_2$-mediated BCR ligation [49]. Marked increases in FOXO3 and FOXO4 expression in *ex vivo* samples following 3-month ibrutinib treatment indicate a mechanism of FOXO expression induced by prolonged BTK inhibition. FOXO1 and FOXO3 are known to be downregulated downstream of BCR activation [465], so it is understandable that long-term abrogation of BTK signals could rescue a BCR-mediated mechanistic dampening of FOXO expression, perhaps including FOXO4. Furthermore, fitting into the classical dogma of FOXO behaviour, we could argue that FOXO upregulation enhances FOXO-mediated tumour suppression, subsequently inducing ibrutinib-FOXO-mediated cell death. However, the prevalence of FOXO expression in the context of drug resistance in other leukaemic cell models [549, 550] suggests a role for FOXOs in enhancing cell survival to overcome cell death induced by targeted agents. As previously mentioned, FOXO4 is required for promoting drug resistance in

DLBCL [545], suggesting an association between FOXO expression and ibrutinib responsiveness. We previously mentioned a potential for FOXO-mediated quiescence in circulating CLL cells (section 3.3.2). This could indirectly explain an ibrutinib-mediated elevation in FOXO3/4 expression; FOXOs directly interact with the mediators of Transforming Growth Factor ß (TGFß) SMAD3 and SMAD4, subsequently promoting TGFß activity [551]. Interestingly, TGFß is known to facilitate chemoresistance and quiescence in squamous cell carcinoma [552], providing a mechanistic explanation for FOXO expression in this context. This is supported in work by Holmes *et al.*, demonstrating that *FOXO1* and *FOXO3* are protected from chromatin reorganisation following ibrutinib therapy, indicative of sustained gene activity downstream of SMAD [553]. FOXOs are known drivers of cell quiescence to defend against environmental stress [554], so another argument could be that FOXO expression is elevated to induce quiescence in circulation following ibrutinib-mediated lymphocytosis. Of course, this is speculative; more work would need to be conducted to determine the role of the FOXO-SMAD-TGFß axis in CLL cells. However, Naka *et al.* demonstrated that *FOXO3*$^{-/-}$ mice exhibit reduced disease burden associated with CML recurrence, where a FOXO-TGFß axis confers maintenance of leukaemia-initiating cells [485] - a mechanism that could perhaps exist in other leukaemic cell populations.

4. The expression and regulation of FOXO transcription factors downstream of BCR and CD40 signalling

4.1. Introduction

Targeted inhibition of proteins regulating cell survival and proliferation have been revolutionary in treating CLL. Venetoclax-mediated BCL2 inhibition has proven an effective CLL treatment [85], however, the development of multiple generations of inhibitors targeting downstream components of BCR-mediated signalling [72, 74, 93] reaffirms the importance of this signalling axis in promoting CLL proliferation and survival. AKT phosphorylates FOXO transcription factors downstream of BCR ligation, sequestering them in the cytoplasm and prohibiting their transcriptional activity [463]. Further, the subsequent activation of the PI3K-AKT axis *via* other signalling hubs (e.g. CD40 and CXCR4 [120, 247]) illustrate multiple avenues through which CLL cells facilitate the hyperactivation of downstream signals to promote proliferation and survival.

Targeted inhibition of BTK, PI3K and mTOR have all shown clinical effectiveness in different CLL pre-clinical contexts [284, 340, 359, 410], with BTK and PI3K inhibitors being approved for clinical use [335]. Interestingly, study in CLL and DLBCL cells demonstrated an association between pharmacological BTK and PI3K inhibition and discrete FOXO activity, achieved by abolishing AKT-mediated FOXO phosphorylation [524]. Around the same time, a published study from our group demonstrated that AZD8055, a potent dual mTORC1/2 inhibitor, diminishes both AKT and FOXO1 phosphorylation, coincident with increased apoptosis in BCR-activated CLL cells [284], reinforcing that FOXO1 inactivation is a necessary consequence downstream of BCR engagement. This work, as well as work by PhD student Michael Moles [49], highlighted that FOXO1 nuclear localisation is enhanced by combining AZD8055 with ibrutinib, resulting in enhanced FOXO isoform gene expression. These data highlight a potentially novel therapeutic approach to CLL treatment in combining BTK and mTOR inhibition to harness the ‘tumour-suppressive’ characteristics elicited by FOXOs.

As transcription factors, FOXOs are known to harbour distinct transcriptional targets, as well as overlapping gene targets to accommodate for redundancy in other FOXOs [428]. FOXOs also regulate the transcription of other FOXO isoforms [555]. Moreover, in the context of CLL, FOXOs are subject to further negative regulation [284], perhaps due to the prevalence of PI3K-AKT hyperactivity [268]. However, discrete FOXO isoforms can exhibit different characteristics in different malignant contexts [429], suggesting that CLL may exploit the expression and subsequent activity of discrete FOXO isoforms. Together, these factors highlight the complexity of FOXO activity in normal and pathophysiological contexts and stress the need to understand FOXO family regulation downstream of distinct FOXO regulators. In the previous chapter, we described the discrete expression of FOXOs in different CLL models, as well as how pharmacological AKT inhibition affects the activity of FOXO3 and FOXO4. However, while FOXO1 is potently activated following AZD8055-ibrutinib treatment, the effect of mTOR-BTK inhibition on the downstream regulation of FOXO3 and FOXO4 is not currently understood and may well differ from that of FOXO1.

4.2. Aims

1. Explore the impact of PI3K-AKT-mTOR signalling on the expression, regulation and subcellular localisation of FOXO3 and FOXO4

2. Assess the functional impact of pharmacological BTK and mTOR and FOXO1 inhibition in primary CLL cells and cell lines

3. Determine an association between CLL cell function and FOXO target gene activity in multiple *in vitro* contexts.

4.3. Results

4.3.1. RNA Seq analysis reveals the global genomic impact of AZD8055 and ibrutinib treatments in CD40-stimulated CLL cells

The importance of CLL-CD40L interactions in promoting CLL cell survival, in-part through PI3K-AKT-mTOR activation [247], suggests that AZD8055 treatment may influence FOXO activity in the context of CD40 stimulation. However, AZD8055 treatment could influence many intracellular mechanisms, as mTORC1/2 activity in CLL orchestrates a vast, pro-leukaemic regulatory network downstream of PI3K-AKT [268]. Therefore, we conducted bulk RNA-Seq in primary CLL cells to investigate (1) the regulation of global gene expression following CD40-CD40L engagement, and (2) how AZD8055 and/or ibrutinib treatments impact gene expression in proliferating CLL cells. As the scope of this thesis was to investigate FOXO regulation in CLL, the analysis focus was to investigate the expression of the FOXO signalling pathway.

Five different primary CLL samples (CLL125, 173, 175, 186, 203) were cultured for 24 hr in CD40L co-culture, with or without single or combination 100 nM AZD8055 1 μM ibrutinib treatment. An unstimulated NTL control was included to discern differential gene expression (DEG) following 24 hr exposure to CD40L. RNA samples were generated following this incubation period and were sent for bulk RNA-Seq analysis. Gene counts were generated from these samples, revealing marked changes in global gene expression in samples cultured with CD40L (Figure 4.1 A & B). Interestingly, AZD8055 treatment strongly impacted global gene expression, indicated by a reversal of gene regulation mediated by CD40L co-culture. These changes were also seen in combination with ibrutinib, though ibrutinib single treatments did not impact DEG to the same degree as AZD8055 treatment (Figure 4.1A & B). Gene expression changes in response to AZD8055 and ibrutinib treatment were sample-dependent: some CLL patient samples exhibited different responses to AZD8055- and ibrutinib-mediated gene

expression (Figure 4.1A). Nevertheless, changes in gene expression induced by CD40-CD40L engagement universally affected CLL cells (Figure 4.1B), demonstrating the overriding effects of CD40 stimulation in the context of transcriptional activation and/or repression. These effects were clear in the total number of differentially expressed genes (Figure 4.1C). Interestingly, stimulation *via* CD40L lead to more gene downregulation than upregulation (2076 genes *vs.* 1657, respectively). Inversely, AZD8055 treatment induced gene upregulation more than downregulation (1697 genes *vs.* 1220, respectively) which was enhanced in combination with ibrutinib (total number of differentially expressed genes: 2917 AZD8055 *vs.* 3439 COMBO, Figure 4.1C). Comparatively, ibrutinib treatment influenced the expression of only a small number of genes (total: 118, Figure 4.1C), further demonstrating that it was AZD8055 treatment which potentiates drug-induced gene alteration. We investigated the characteristics of DEG between primary CLL samples by means of employing a Pearson correlation (Figure 4.1D) and principal component analysis (PCA, Figure 4.1E). Comparing between conditions within a single patient sample, R^2 values were high, demonstrating that sample data was reliable between conditions (e.g. CLL173_1 *vs.* CLL173_2, Figure 4.1D). R^2 values decreased between samples, highlighting sample heterogeneity. Nevertheless, when comparing any condition between any sample, R^2 values did not drop below ~0.8, indicating strong correlations irrespective of heterogeneity (Figure 4.1D). PCA also highlighted differences in sample characteristics, as there were notable differences in DEG in samples on CD40L compared with the NTL control (Figure 4.1E). Sample-specific clustering was widely skewed over principal components 1 (PC1) and 2 (PC2), where AZD8055 and ibrutinib minimally affected sample variance (Figure 4.1E). Samples 125, 175 and 186 were similar in their variance, while 173 and 203 were skewed more in PC1 and PC2 variance, respectively (Figure 4,1E).

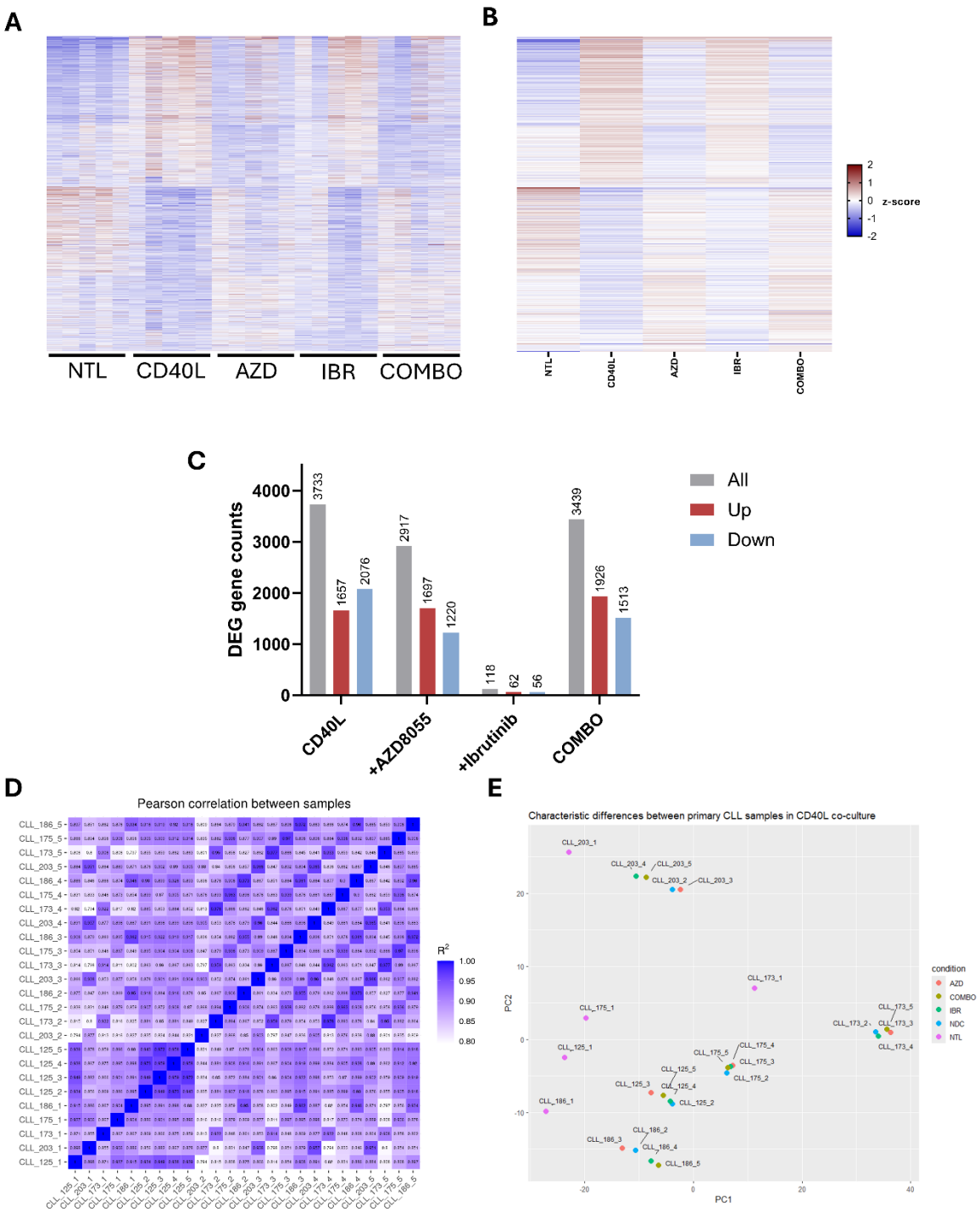

Figure 4.1: Bulk RNA-seq revealed differential gene expression following CD40 stimulation, AZD8055 and ibrutinib treatments. Bulk RNA-seq was conducted in 5 primary patient samples incubated in CD40L co-culture (+10 ng/mL IL-4) for 24 hr, ±100 nM AZD8055 and 1 μM ibrutinib, alone or in combination (COMBO) or vehicle control. (A & B) Global DEG heat maps were generated assessing sample-specific (A) and condition-specific (B) gene expression in the different conditions. Genes were plotted by z-score attained from normalised gene counts. Conditions were labelled by sample number (e.g. CLL125) followed by a number denoting the respective condition: 1 = NTL, 2 = CD40L, 3 = AZD8055, 4 = Ibrutinib, 5 = COMBO. (C) Normalised DEG counts that were significantly regulated in the different conditions (p = > 0.05). Total gene expression is denoted by the grey bar, while gene upregulation and downregulation are denoted by red and blue bars, respectively. (D) Pearson correlation plot generated assessing the R^2 value (Pearson *r* coefficient squared) between samples and conditions, where $R^2 = 1$ is the absolute value. (E) PCA of normalised counts between the 5 conditions in the 5 patient samples. Samples are labelled on the plot, while conditions are colour-coded. PC1 variance: 40%, PC2 variance: 20%.

4.3.1.1. Gene expression in CLL cells exposed to CD40L

Analysing gene expression following CD40L stimulation (Figure 4.2), 3733 genes were significantly regulated in cells stimulated with CD40L compared to the NTL control (Figure 4.2A). Of note, 11606 genes were co-expressed between NTL and CD40L samples, with the expression of 810 and 592 genes exclusive to NTL and CD40L conditions, respectively (Figure 4.2B). Volcano plots of DEG demonstrated strong global gene regulation in response to CD40 stimulation. Interestingly, *FOXO3* and *FOXO4* were significantly downregulated ($p = 0.0084$ and $1.03x10^{-8}$, respectively, Figure 4.2C). A heat map investigating the most significant genes that are subject to the largest regulation following CD40-CD40L engagement, included *BCL2L1* upregulation (supporting Figures 3.4 & 3.5) and the FOXO target genes *CCND2* and *CDKN1A* (Figure 4.2D). In addition, KEGG analysis revealed a link between distinct gene expression and functional information, where CD40 stimulation affected cell cycle signalling, proteasomal function, and the FOXO signalling pathway (Figure 4.2E).

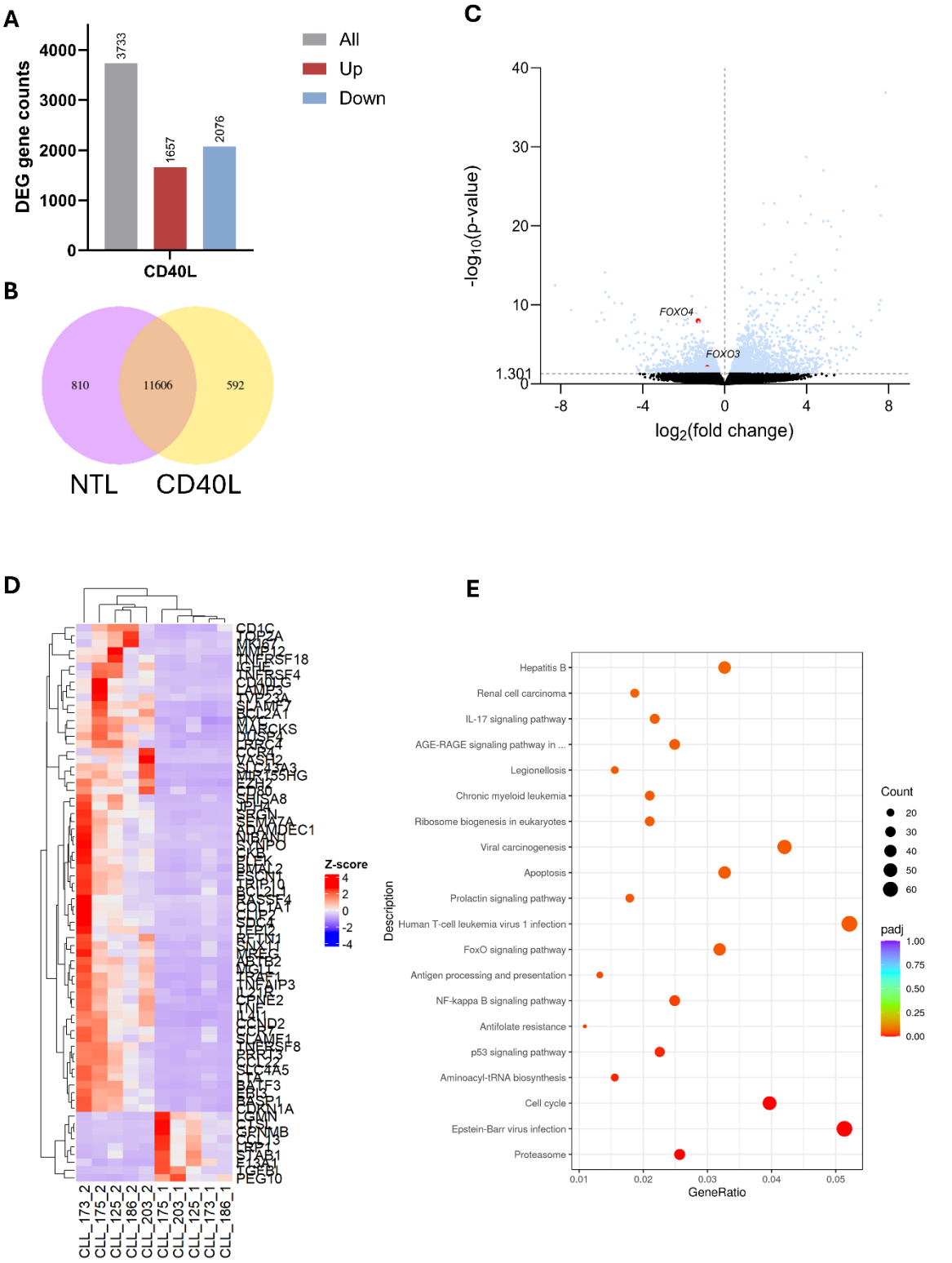

Figure 4.2: Assessment of differential gene expression following CD40 stimulation. Comparison of the expression of genes between 'NTL' unstimulated (1) and CD40L-stimulated (2) conditions in the RNA-Seq dataset. (A) Normalised DEG counts that were significantly regulated in the different conditions (p = > 0.05). Total gene expression is denoted by the grey bar, while gene upregulation and downregulation are denoted by red and blue bars, respectively. (B) Coexpression analysis was conducted by Novogene, determining which genes are coexpressed between conditions, as well as genes that are exclusive to certain conditions. (C) Volcano plot of DEGs in the CD40L condition compared to the NTL condition, plotted on $-\log_{10}$(p-value) over $\log_2$(fold change). Coloured dots are significantly expressed (p > 0.05). *FOXO3* and *FOXO4* values are highlighted in red. (D) Heatmap of z-scores attained from normalized gene count data, plotting genes that are most significantly regulated following CD40L exposure. Upregulated genes are indicated in red, while downregulated genes are

indicated in blue (padj > 0.05, $\log_2$(fold change) > 2.5). (E) KEGG enrichment analysis from gene expression data, where gene expression is categorised by gene function into the most significantly affected signalling pathways. The number of genes is depicted by the size of the circle, while the colour depicts padj value. GeneRatio (x-axis) is the percentage of significant genes over the total genes in the given pathway.

4.3.1.2. Gene expression following AZD8055 treatment

In CD40L co-cultures, 2917 genes were significantly regulated in response to AZD8055 treatment (Figure 4.3A). Co-expression analysis revealed that 11820 genes were co-expressed in the presence or absence of AZD8055 treatment (Figure 4.3B). Interestingly, the expression of 378 and 808 genes were exclusive to cells in the presence or absence of AZD8055 treatment, respectively (Figure 4.3B). Volcano plots highlighted the strong influence of AZD8055 on DEG in CD40-stimulated cells, indicated by marked significance in the regulation of multiple genes (Figure 4.3C). This included *FOXO3* and *FOXO4*, both of which were significantly upregulated in AZD8055-treated cells ($p = 0.016$ and $1.9x10^{-9}$, respectively, Figure 4.3C). Of note, *FOXO4* was the second-most significantly upregulated gene in response to AZD8055 treatment. *CTSF,* a gene encoding a cysteine protease involved in proteasome degradation, lipoprotein degradation and autophagy [556], was the most significantly upregulated gene ($p = 6.8x10^{-10}$). These results were demonstrated further *via* heatmap analysis of the most significantly regulated genes following AZD8055 treatment. This revealed upregulation of genes including – but not limited to - *CTSF, FOXO4,* and the FOXO target genes *BBC3* and *FBXO32*. Downregulated genes included those involved in redox pathways (*PRDX4, TXN*) and proteosome assembly (*PSMD1* and *PSMD14*) (Figure 4.3D). KEGG analysis revealed distinct regulation of genes involved in several pathways including protein export, cell cycle regulation and proteasomal function (Figure 4.3E). Further, KEGG enrichment analysis determined that genes associated with the FOXO signalling pathway were enriched in cells treated with AZD8055 compared to CD40L co-culture alone (Figure 4.3F).

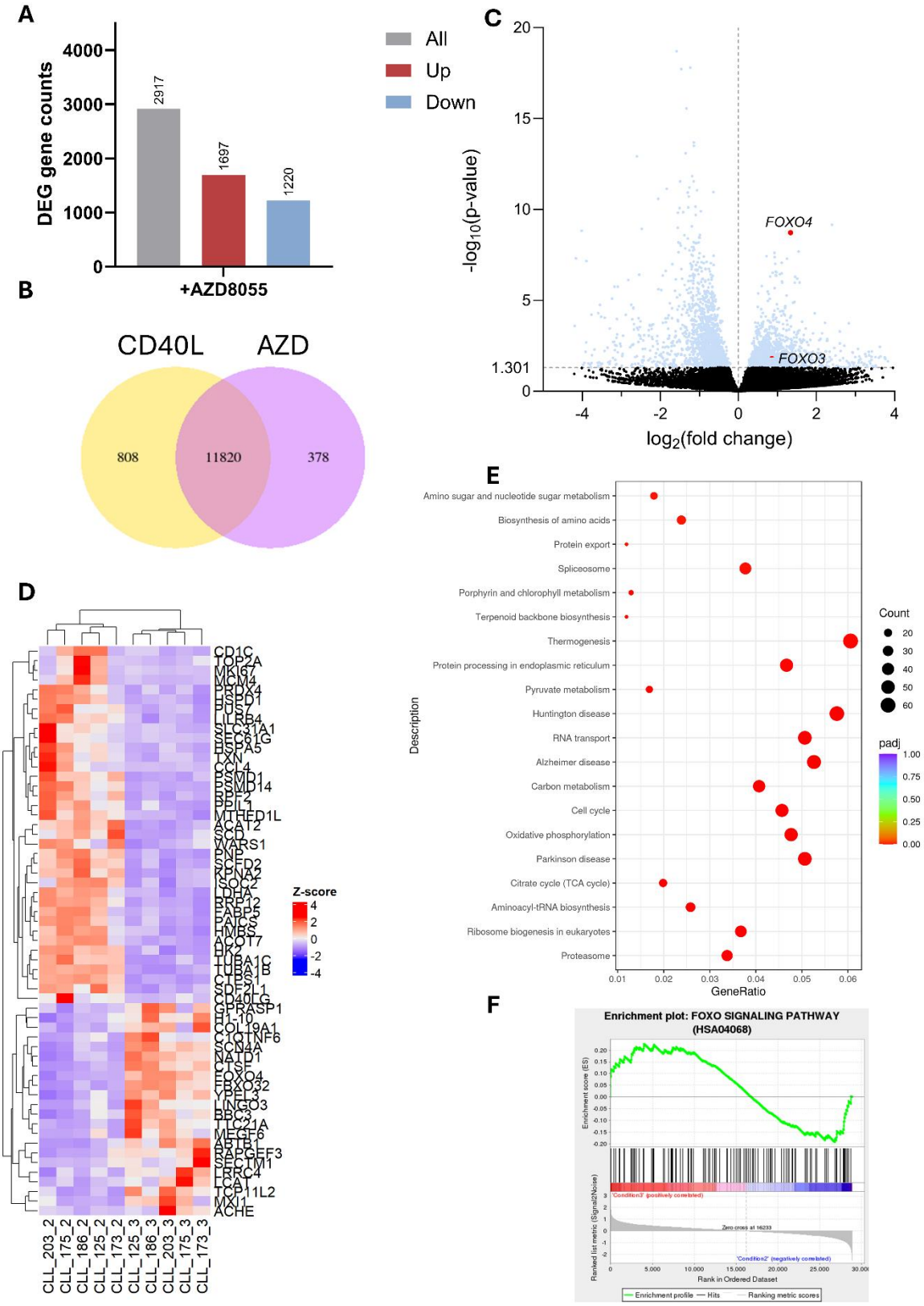

Figure 4.3: Assessment of differential gene expression following AZD8055 treatment Comparing the expression of genes between 'CD40L' untreated (2) and cells treated with 100 nM AZD8055 (3) in the RNA-Seq dataset. (A) Normalised DEG counts that were significantly regulated in the different conditions (p = > 0.05). Total gene expression is denoted by the grey bar, while gene upregulation and downregulation are denoted by red and blue bars, respectively. (B) Coexpression analysis was conducted by Novogene, determining which genes are coexpressed between conditions, as well as genes that are exclusive to certain conditions. (C) Volcano plot of DEGs following AZD8055 treatment, plotted on $-\log_{10}$(p-value) over $\log_2$(fold change). Coloured dots are significantly expressed (p > 0.05). *FOXO3* and *FOXO4* values are highlighted in red. (D) Heatmap of z-scores attained from normalized

gene count data, plotting genes that are most significantly regulated following AZD8055 treatment. Upregulated genes are indicated in red, while downregulated genes are indicated in blue (padj > 0.05, log_2(fold change) > 1.3). (E) KEGG enrichment analysis from gene expression data, where gene expression is categorised by gene function into the most significantly affected signalling pathways. The number of genes is depicted by the size of the circle, while the colour depicts padj value. 'GeneRatio' (x-axis) is the percentage of significant genes over the total genes in the given pathway. (F) KEGG enrichment plot for the FOXO signalling pathway with or without AZD8055 treatment. Enrichment scores (ES) determine the level of enrichment of genes in a particular signalling pathway. Positive correlation is depicted in red, while negative correlation is depicted in blue, where colour intensity increases with the abundance of genes in a location.

4.3.1.3. Gene expression following ibrutinib treatment

Minimal DEG occurred following ibrutinib treatment - only 118 genes were significantly regulated (Figure 4.4A). 11849 genes were co-expressed between ibrutinib-treated and untreated cells on CD40L, where 389 and 349 genes were expressed in untreated and ibrutinib-treated cells, respectively (Figure 4.4B). The reduced significance of gene regulation in ibrutinib-treated primary CLL cells was highlighted in a volcano plot (Figure 4.4C). However, as noted in AZD8055-treated cells, *FOXO4* was significantly upregulated in ibrutinib-treated cells (p = 0.02, Figure 4.4C). Heatmap generation revealed multiple genes that were regulated by ibrutinib treatment. For example, *SLC12A4* and *TRD-AS1* are downregulated, while *MANF, CALR* and *CRELD2* are upregulated (Figure 4.4D). Finally, KEGG analysis revealed that gene signatures of the FOXO signalling pathway were affected by ibrutinib treatment (Figure 4.4E), albeit not significantly.

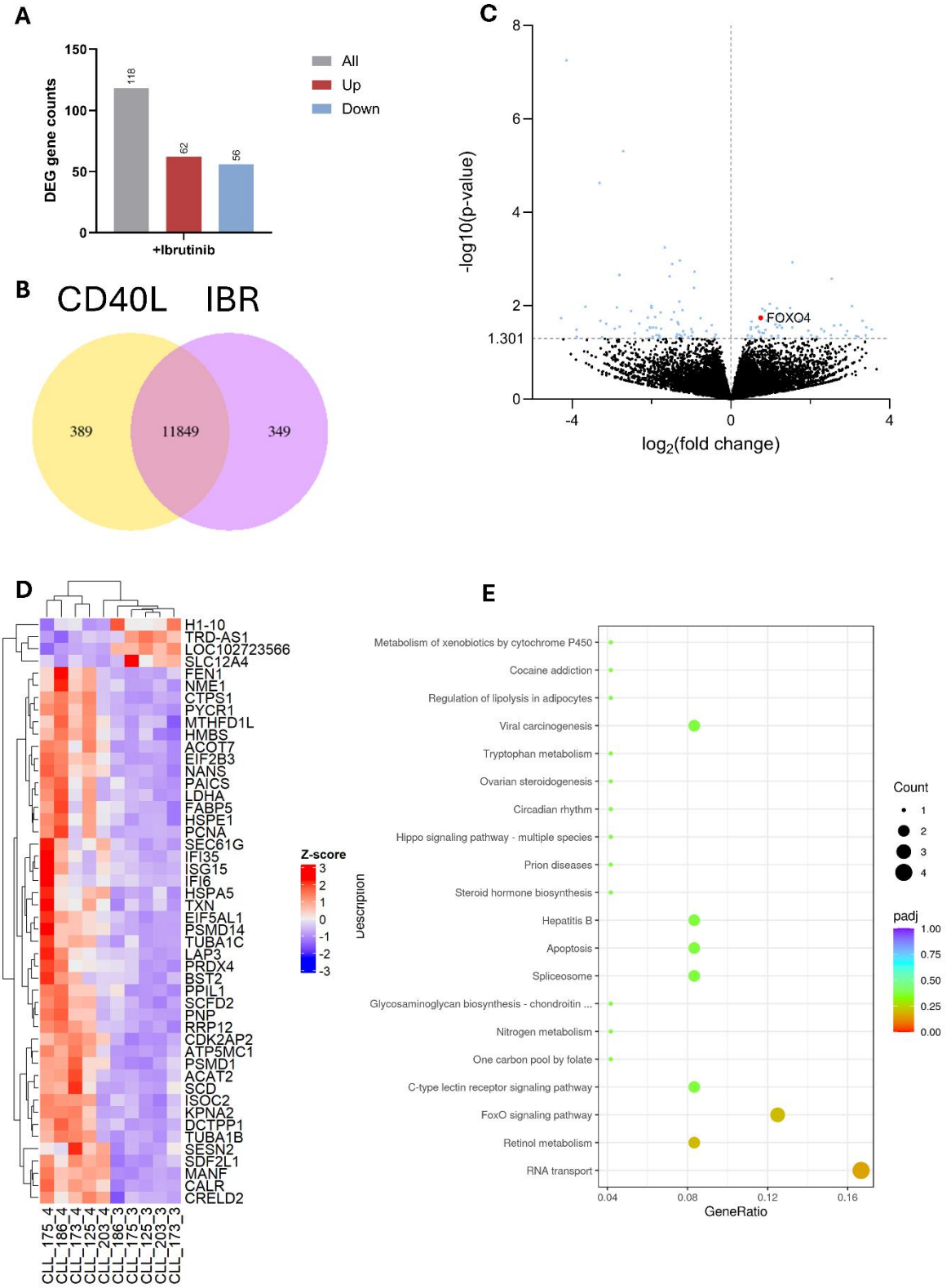

Figure 4.4: Assessment of differential gene expression following ibrutinib treatment. Comparing the expression of genes between 'CD40L' untreated (2) and cells treated with 1 μM ibrutinib (4) in the RNA-Seq dataset. (A) Normalised DEG counts that were significantly regulated in the different conditions (p = > 0.05). Total gene expression is denoted by the grey bar, while gene upregulation and downregulation are denoted by red and blue bars, respectively. (B) Coexpression analysis was conducted by Novogene, determining which genes are coexpressed between conditions, as well as genes that are exclusive to certain conditions. (C) Volcano plot of DEGs following ibrutinib treatment, plotted on $-\log_{10}$(p-value) over $\log_2$(fold change). Coloured dots are significantly expressed (p > 0.05). *FOXO4* values are highlighted in red. (D) Heatmap of z-scores attained from normalized gene count data, plotting genes that are most significantly regulated following ibrutinib treatment. Upregulated

genes are indicated in red, while downregulated genes are indicated in blue (padj > 0.05, log_2(fold change) > 1). (E) KEGG enrichment analysis from gene expression data, where gene expression is categorised by gene function into the most significantly affected signalling pathways. The number of genes is depicted by the size of the circle, while the colour depicts padj value. 'GeneRatio' (x-axis) is the percentage of significant genes over the total genes in the given pathway.

4.3.1.4. Gene expression following COMBO treatment

COMBO treatment (AZD8055 and ibrutinib) enhanced the regulatory effects of AZD8055 treatment, inducing the differential expression of 3439 significant genes (Figure 4.5A). A high degree of co-expression was seen between CD40L cells with or without COMBO treatment. 858 and 445 genes were expressed exclusively in untreated and COMBO-treated cells, respectively (Figure 4.5B). Further, *FOXO4* expression was significantly increased in COMBO-treated cells ($p = 5.5x10^{-9}$, figures 4.5C & D), as was the pro-apoptotic FOXO target gene *BBC3* (Figure 4.5D). Of note, similar gene regulation was evident in COMBO-treated cells as in AZD8055-treated cells (e.g. *FOXO4, CTSF,* and *GPRASP1* upregulation, *PUS7, PSMD14* and *ACOT7* downregulation), as well as similar gene signature enrichment (e.g. proteasomal degradation and oxidative phosphorylation, Figure 4.5E). Finally, KEGG enrichment analysis determined that genes associated with the FOXO signalling pathway were enriched in COMBO-treated cells (Figure 4.5F).

These data demonstrate an AZD8055-mediated regulation of DEG in CD40-stimulated primary CLL cells. Interestingly, this also included a reversal of *FOXO3/4* downregulation as seen in CLL-CD40L co-cultures (Figure 3.5). Ibrutinib single treatment also influenced the expression of *FOXO4*, albeit not to the same degree as AZD8055, or by combining ibrutinib with AZD8055 (Figures 4.3 & 4.5, respectively), revealing that *FOXO4* expression is tightly regulated by upstream mTOR activity.

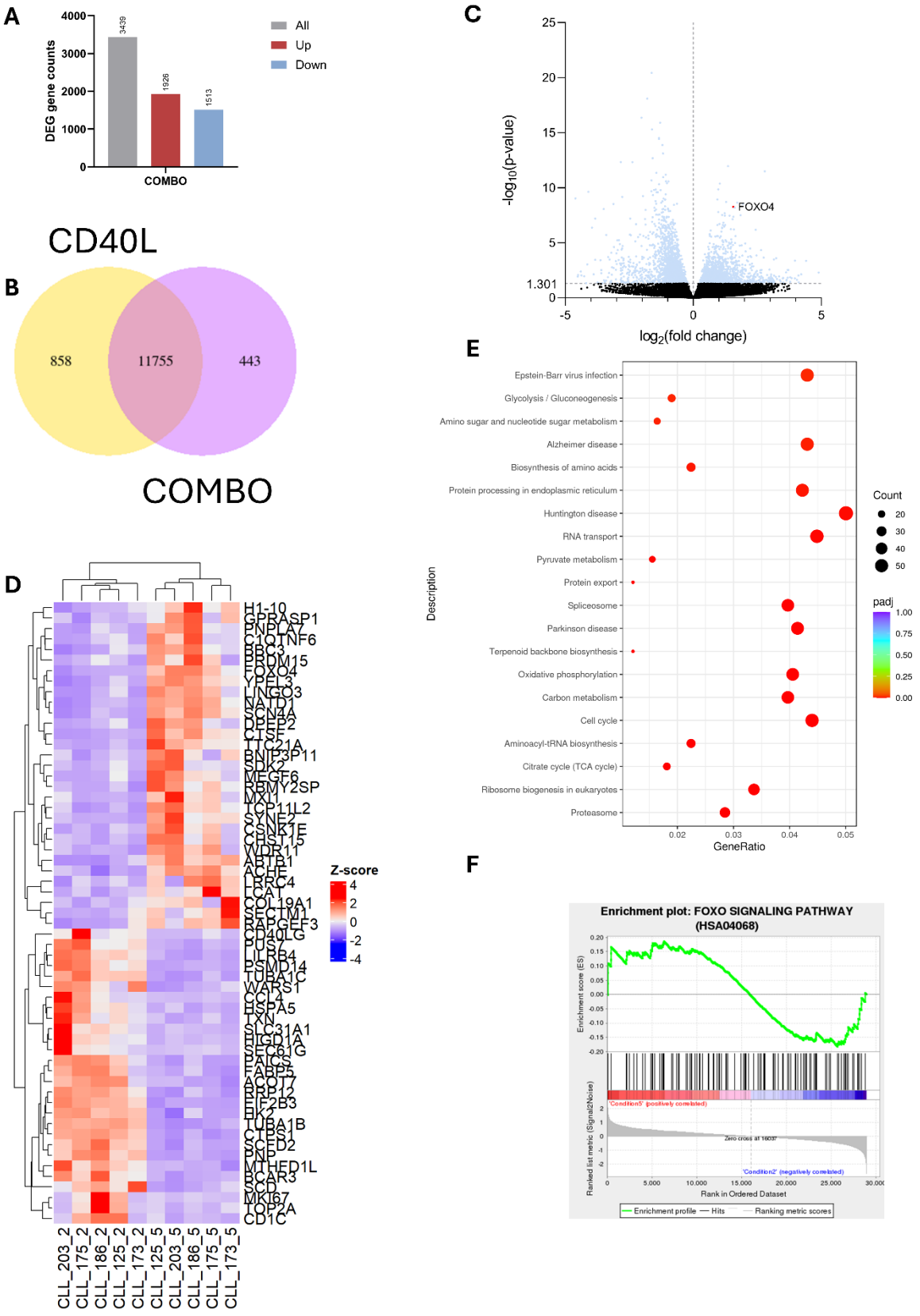

Figure 4.5: Assessment of differential gene expression following COMBO treatment. Comparing the expression of genes between 'CD40L' untreated (2) and cells treated with 100 nM AZD8055 and 1 μM ibrutinib (COMBO, 5) in the RNA-Seq dataset. (A) Normalised DEG counts that were significantly regulated in the different conditions (p = > 0.05). Total gene expression is denoted by the grey bar, while gene upregulation and downregulation are denoted by red and blue bars, respectively. (B) Coexpression analysis was conducted by Novogene, determining which genes are coexpressed between conditions, as well as genes that are exclusive to certain conditions. (C) Volcano plot of DEGs

following COMBO treatment, plotted on $-\log_{10}$(p-value) over $\log_2$(fold change). Coloured dots are significantly expressed (p > 0.05). *FOXO4* values are highlighted in red. (D) Heatmap of z-scores attained from normalized gene count data, plotting genes that are most significantly regulated following COMBO treatment. Upregulated genes are indicated in red, while downregulated genes are indicated in blue (padj > 0.05, $\log_2$(fold change) > 1.3). (E) KEGG enrichment analysis from gene expression data, where gene expression is categorised by gene function into the most significantly affected signalling pathways. The number of genes is depicted by the size of the circle, while the colour depicts padj value. 'GeneRatio' (x-axis) is the percentage of significant genes over the total genes in the given pathway. (F) KEGG enrichment plot for the FOXO signalling pathway with or without AZD8055 treatment. Enrichment scores (ES) determine the level of enrichment of genes in a particular signalling pathway. Positive correlation is depicted in red, while negative correlation is depicted in blue, where colour intensity increases with the abundance of genes in a location.

Figure 4.6 highlights the differential expression of *FOXO1, FOXO3 and FOXO4* attained from this RNA-Seq dataset in boxplots of normalised gene counts that were directly related to FOXO family gene expression. These data illustrate the downregulation of FOXO gene expression following CD40 stimulation (supporting Figure 3.5), and how AZD8055, alone or combined with ibrutinib, upregulated *FOXO1/3/4* expression. Of note, expression values for *FOXO1* regulation were not significant, and so were disregarded from other analyses.

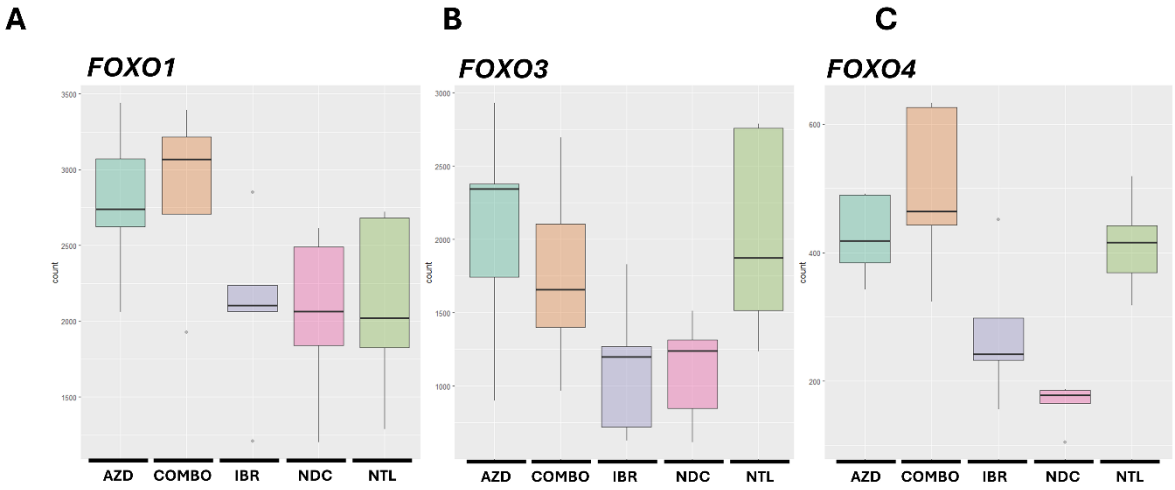

Figure 4.6: The expression of FOXO in CD40L co-cultures. (A-C) Boxplots of normalised gene counts of *FOXO1* (A), *FOXO3* (B) and *FOXO4* (C) attained from the RNA-Seq dataset *(via* DeSeq2 analysis). Gene counts are directly related to expression and plotted by condition, where sample counts are depicted by circles, minimal and maximum data values are depicted by straight lines, and boxes depict lower and upper quartiles, separated by the median value (the line intersecting the box) (n=5).

4.3.2. mTOR/BTK inhibition alters *FOXO3/4* expression, coinciding with modulation of FOXO target gene expression

Following the bulk RNA-Seq dataset of CD40-stimulated patient samples, we cultured CLL cell lines to further define the regulatory effects of mTOR and BTK inhibition on distinct components of the FOXO signalling pathway (Figure 4.7). Data from our group previously demonstrated that FOXO1 expression and activity is associated with changes in expression of distinct FOXO target genes involved in multiple cellular processes [284]. However, the expression of *FOXO3* and *FOXO4* have been scarcely addressed. Here, initial study characterising *FOXO3* and *FOXO4* expression following 100 nM AZD8055 single treatment in MEC1 cells revealed that *FOXO3* and *FOXO4* were both significantly upregulated in response to mTOR inhibition (Figure 4.7A), suggesting that mTOR-mediated FOXO3/4 regulation in MEC1 cells mimics that of primary cells.

Dual targeting of mTOR and BTK synergistically modulate FOXO1 expression and activity in CLL [49, 284]. Here, in MEC1 and HG3 cells, we investigated whether AZD8055 (100 nM), ibrutinib (1 μM) or combination treatments enhance the expression of *FOXO3, FOXO4* and FOXO target genes involved in distinct processes including cell survival (*BCL2L11* and *BCL2L1* (4.7C & D, respectively)), cell cycle (*CDKN1B* (4.7E)), AKT-mTOR signalling modulation (*SESN3* [438] (4.7F)) and DNA damage (*GADD45A* [439] (4.7G)). Both *FOXO3* (Figure 4.7B) and *FOXO4* (Figure 4.7C) were upregulated following combined BTK-mTOR inhibition. Reflecting the expression of *FOXO4* following BTK-mTOR inhibition in CD40L co-cultures (Figure 4.5), *FOXO4* (Figure 4.7C) – and not *FOXO3* – was significantly upregulated following combined AZD8055-ibrutinib treatment in MEC1 cells. HG3 cells also exhibited increased *FOXO4* expression, albeit not significantly. Increased *FOXO3* and *FOXO4* expression following AZD8055-ibrutinib treatment was reflected by distinct changes in the expression of FOXO target genes. *BCL2L11* (BIM) was significantly upregulated (Figure 4.7D), indicative of FOXO activity ([49, 284], Figure 4.7B-C). This also occurred in HG3 cells, albeit not significantly ($p = 0.18$). Inversely, MEC1 cells exhibited a significant depletion of

BCL2L1 (BCL-XL), while HG3 cells exhibited a nominal increase in *BCL2L1* expression, though the results for HG3 cells were variable between replicates (Figure 4.7E). Expression of *CDKN1B* ($p27^{kip1}$, Figure 4.7F) was conflicting between MEC1 and HG3 cells: AZD8055-treated MEC1 cells exhibited *CDKN1B* upregulation, while HG3 cells exhibited a downregulation of *CDKN1B* following AZD8055 and ibrutinib treatment (Figure 4.7F), albeit not significantly. In MEC1 cells, *SESN3* was upregulated in response to AZD8055 and ibrutinib treatment, albeit not significantly (Figure 4.7G), while *SESN3* was significantly downregulated in HG3 cells (Figure 4.7G). Finally, in MEC1 cells, *GADD45A* was significantly downregulated with AZD8055 (Figure 4.7H), while HG3 cells exhibited nominal change in *GADD45A* expression. These data reinforce that FOXO and FOXO-associated genes are regulated by dual mTOR inhibition, where ibrutinib can synergistically enhance *FOXO4* expression (Figure 4.7C), as well as FOXO-associated genes that induce cell death (e.g. *BCL2L11*, Figure 4.7D).

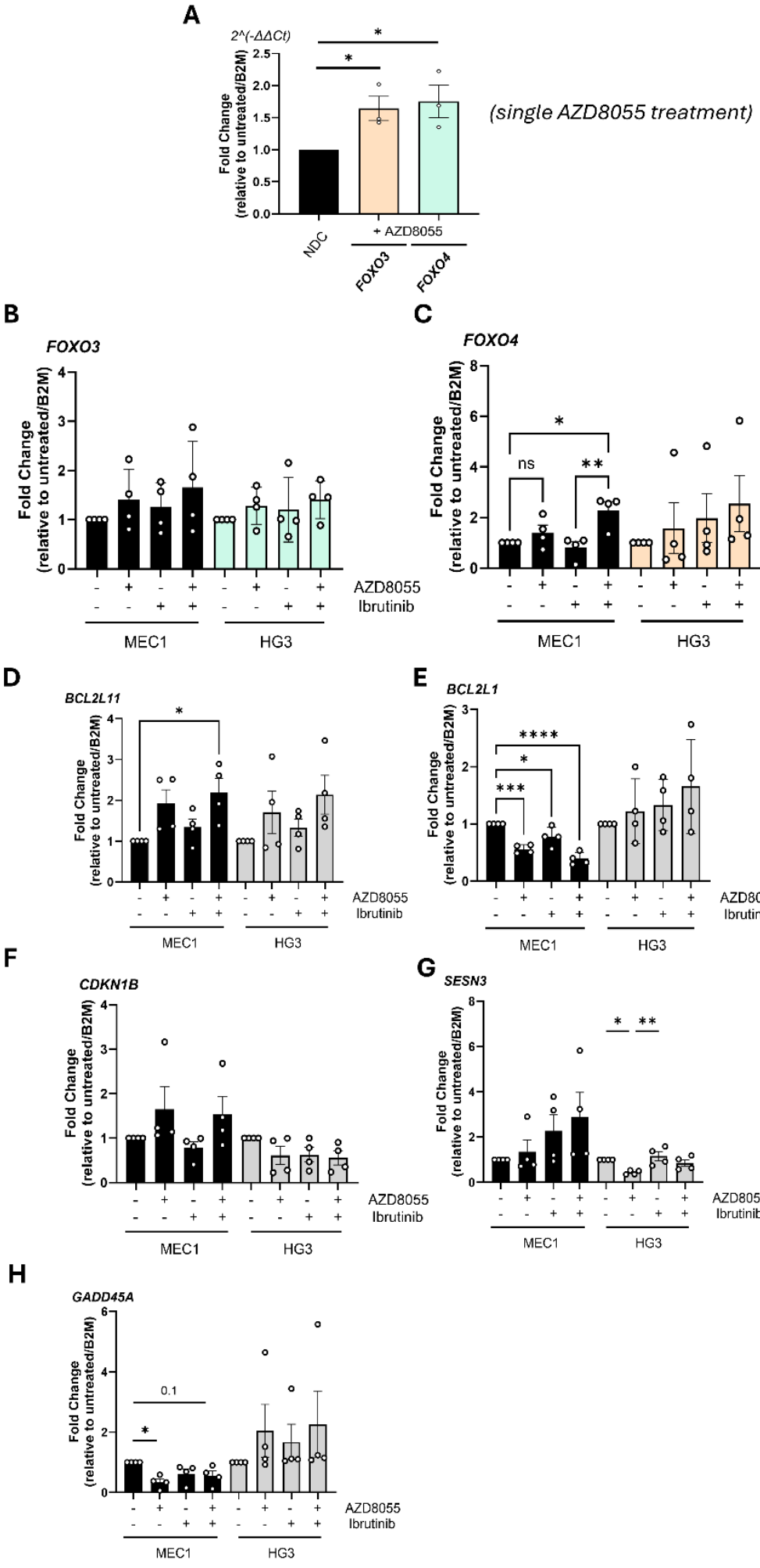
A
2^(-ΔΔCt)
Fold Change (relative to untreated/B2M)
NDC
+ AZD8055
FOXO3
FOXO4
(single AZD8055 treatment)
B
FOXO3
C
FOXO4
ns
AZD8055
Ibrutinib
MEC1
HG3
D
BCL2L11
E
BCL2L1
F
CDKN1B
G
SESN3
H
GADD45A
0.1

Figure 4.7: FOXO and FOXO-associated genes are regulated downstream of BTK/mTOR inhibition in MEC1 cells. Gene expression values were generated *via* RT-qPCR following 24 hr in culture with or without AZD8055 (100 nM) or ibrutinib (1 μM) single or combination treatments or vehicle control, with *B2M* expression being used to normalise generated ΔCt values. Changes in expression are presented as fold change relative to untreated samples. (A) *FOXO3* (orange) and *FOXO4* (green) expression in MEC1 cells treated for 24 hr with 100 nM AZD8055, relative to untreated MEC1 cells (n=3). (B-H) Fold change in gene expression of *FOXO3* (B), *FOXO4* (C), *BCL2L11* (BIM, D), *BCL2L1* (BCL-XL, E), *CDKN1B* ($p27^{kip1}$, F), *SESN3* (G) and *GADD45A* (H) after 24 hr treatments of MEC1 or HG3 cells with single/combination treatments with AZD8055 (100 nM) and ibrutinib (1 μM) compared to the vehicle control (n=4). Fold change was calculated relative to untreated samples. Data points are depicted as white circles, and the data is represented as the mean ±SEM. Statistics were calculated using a paired Student's t-test for two conditions (A), and one-way ANOVA for three or more conditions, where * $p \leq 0.05$, ** $p \leq 0.01$, *** $p \leq 0.001$, **** $p \leq 0.0001$.

4.3.3. Synergistic BTK and mTOR inhibition reduces MEC1 cell viability

Studies have revealed the cell killing capacity of AZD8055 in the context of cancer therapy [399-403]. Additionally, the synergistic killing of BCR-stimulated primary CLL cells by AZD8055 and ibrutinib [284] highlights clinical relevance in targeting BTK and mTOR in CLL. Indeed, a common strategy for novel treatments in leukaemia is considering their application in conjunction with effective TKI therapy [335]. Further, AZD8055 and ibrutinib induce apoptosis in MEC1 and HG3 cell lines [49]. Though established, a link between the regulation of other FOXO transcription factors and CLL cell death has yet to be elucidated. In this context, AZD8055 and ibrutinib may affect the distinct protein expression of FOXO transcription factors as they do for FOXO1 [49]. To assess this, MEC1 and HG3 cells were cultured for 48 hr in the presence of AZD8055 (100 nM) and ibrutinib (1 μM) to monitor changes in apoptosis (detected *via* flow cytometry, Figure 4.8A & B), with AKT phosphorylation status, BIM and FOXO4 expression being analysed by western blotting (Figure 4.8C). AKT^{S473} phosphorylation status was used as a control to confirm upstream inhibition following AZD8055-ibrutinib treatment (Figure 4.8C). Annexin and 7-AAD staining revealed increased MEC1 cell death following AZD8055 and ibrutinib treatment, where combined pharmacological inhibition lead to a significant increase in cells undergoing apoptosis (Figure 4.8A & B), confirming enhanced cell death with combined BTK-mTOR inhibition as seen in other CLL studies [49, 284]. We then addressed a potential association between MEC1 cell death and the expression of the apoptosis-associated protein BIM and FOXO4 protein expression following 48 hr culture (Figure 4.8C) of MEC1

and HG3 cell lines. AKT^{S473} phosphorylation levels were effectively depleted in both MEC1 and HG3 cells, indicating that AKT activity was diminished (Figure 4.8C). Interestingly, drug treatments downregulated total FOXO4 expression; MEC1 cells exhibited AZD8055-mediated FOXO4 downregulation, trending towards significance (Figure 4.8D, $p = 0.06$), achieving significance in combination with ibrutinib (Figure 4.8D, $p = 0.02$). HG3 cells exhibited a similar depletion of FOXO4 expression, albeit not significantly (Figure 4.8D). Further, in MEC1 and HG3 cells, combined AZD8055-ibrutinib treatment significantly upregulated BIM expression (Figure 4.8E). While AZD8055 treatment elicited more cell death than ibrutinib, upregulation of BIM expression was induced more by ibrutinib, as shown by HG3 cells exhibiting a significant increase in BIM when treated with ibrutinib alone (Figure 4.8E). These data allude to an association between pro-apoptotic AZD8055-ibrutinib treatment and a loss of FOXO4 protein expression in long-term culture.

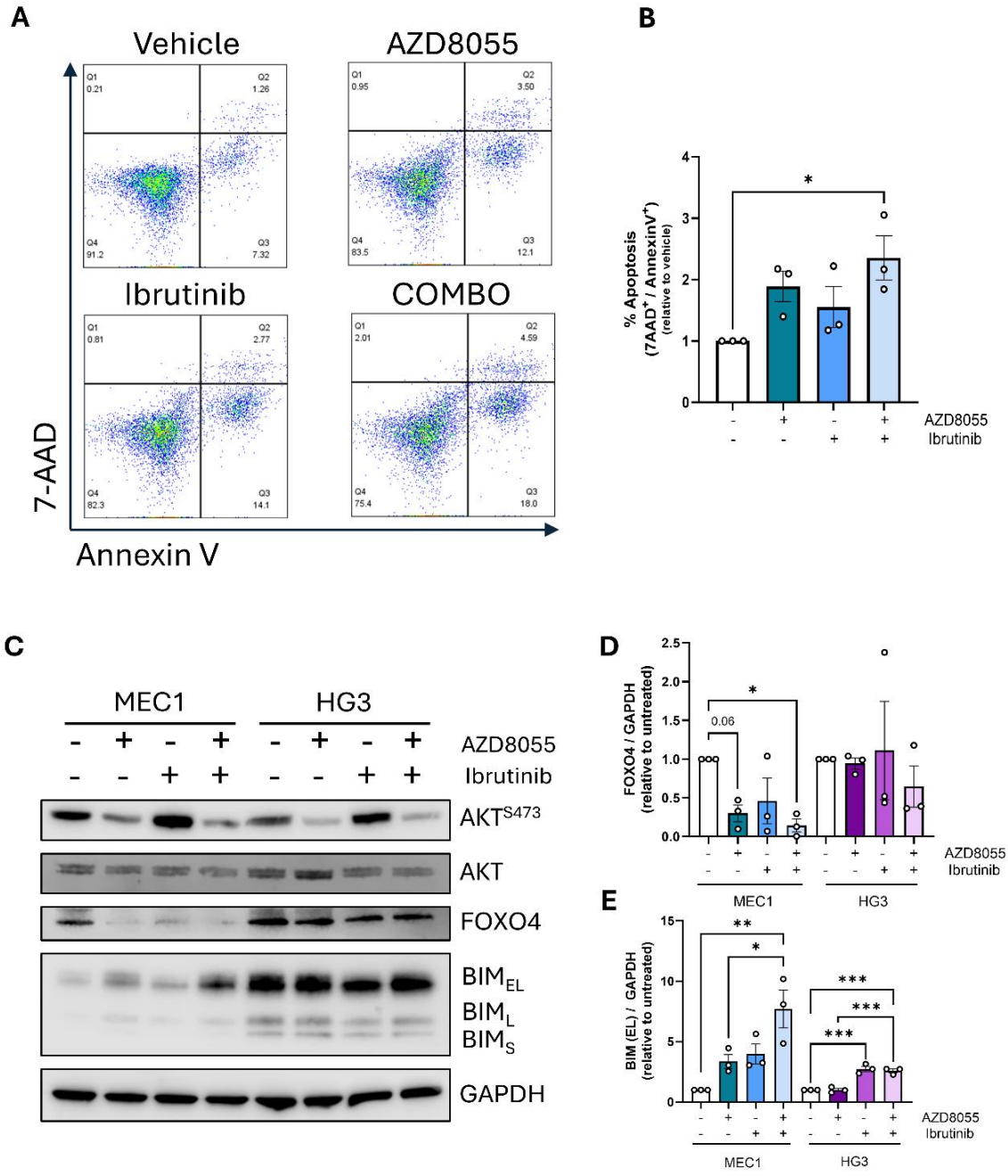

Figure 4.8: AZD8055 and ibrutinib synergistically induce apoptosis, coincident with BIM upregulation and FOXO4 depletion in MEC1 and HG3 cells. (A) FACS plot to observe changes in MEC1 apoptosis *via* flow cytometry using Annexin V/7-AAD staining methods following 48 hr in culture with 100 nM AZD8055 and/or 1 μM ibrutinib or vehicle control. (B) Percentages of cells from the total cell population depicted in (A) that were positive for Annexin V and/or 7-AAD staining, made relative to untreated samples (n=3). (C) Western blot of MEC1 and HG3 cells in long-term 48 hr cultures with AZD8055 (100 nM) and ibrutinib (1 μM) single/combination treatments compared to vehicle control, visualising the phosphorylation status of AKT (AKT^{S473}), as well as the expression of FOXO4 and the different isoforms of BIM (BIM_{EL}, BIM_L and BIM_S). GAPDH was used as a loading control (n=3). Data points are depicted as white circles, and the data is represented as the mean ±SEM. Statistics were calculated using one-way ANOVA, where * $p \leq 0.05$, ** $p \leq 0.01$, *** $p \leq 0.001$.

4.3.4. MEC1 proliferative capacity was lost following combined AZD8055-ibrutinib treatment

To validate the effectiveness of AZD8055-ibrutinib treatment on the proliferative capacity of MEC1 cells, CTV staining was used to visualise cell proliferation. MEC1 cells were cultured for 72 hr with or without AZD8055 and/or ibrutinib treatments, with their proliferation subsequently monitored *via* flow cytometry (Figure 4.9A). MEC1 cell proliferation was significantly reduced in cultures treated with AZD8055 (Figure 4.9B). While ibrutinib treatment reduced MEC1 cell proliferation, a significant difference to the 'vehicle' control was only seen when combined with AZD8055 (Figure 4.9B), determining that a block in MEC1 cell proliferation is predominantly AZD8055-mediated. Cell count data support a lack of proliferation, as cell numbers were significantly reduced in AZD8055-treated cultures (Figure 4.9C). Further, we investigated the expression of the cell-cycle-associated gene *CCND1* which is known to be regulated downstream of FOXO activity [557, 558]. Partnered with reduced proliferative capacity, MEC1 cells exhibited significant *CCND1* downregulation following AZD8055 treatment, potentiated further in combination with ibrutinib (Figure 4.9D). These data demonstrate the potency of AZD8055-ibrutinib treatment in inducing cell cycle arrest *via* downregulation of FOXO target genes required for cell cycle progression.

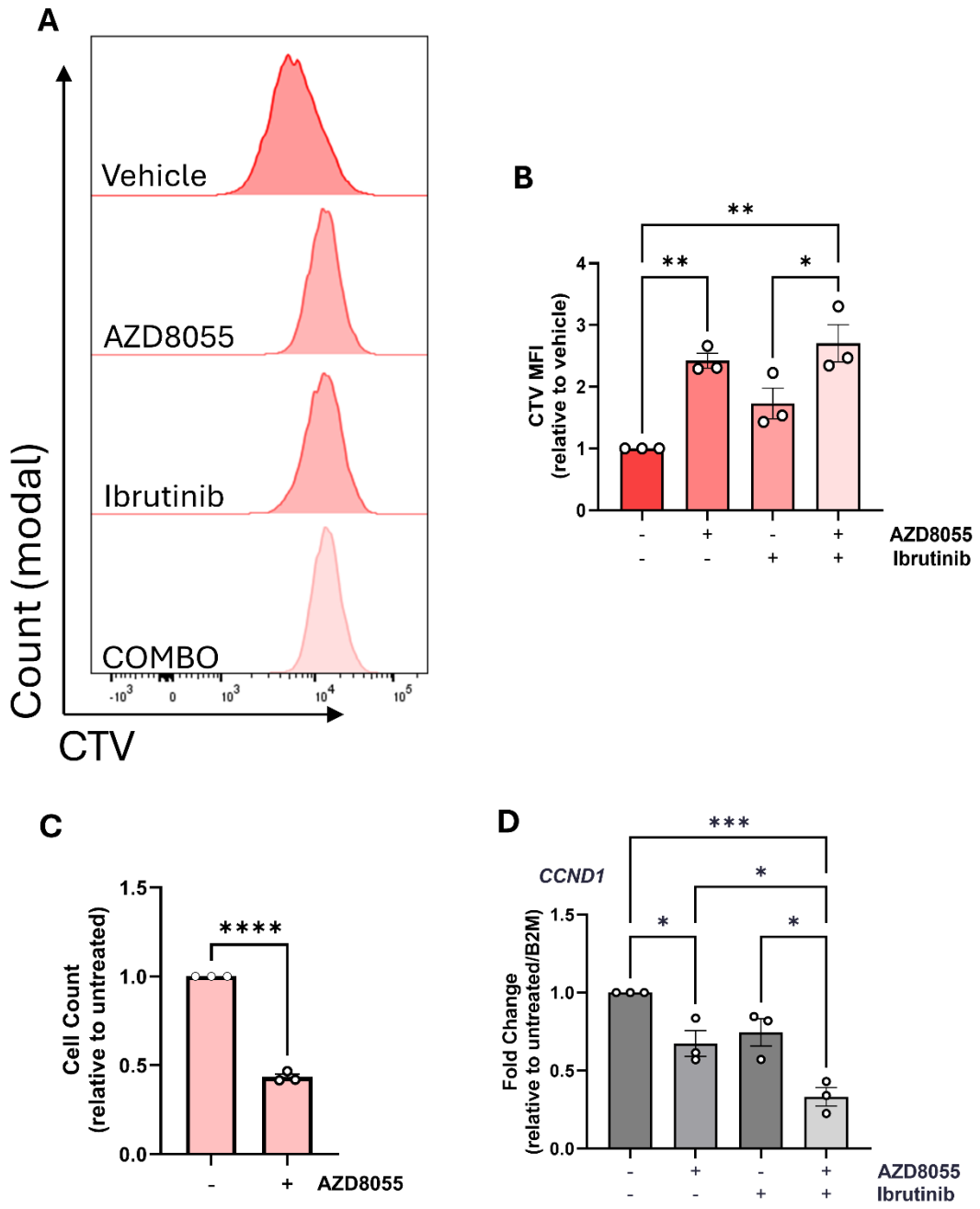

Figure 4.9: Pharmacological mTOR inhibition mediates a block in MEC1 cell proliferation. (A) Representative FACS histogram depicting MEC1 cells cultured for 72 hr in the presence of AZD8055 and/or ibrutinib treatments (or vehicle control) following CTV staining. Cells were gated using forward and side scatter (FSC-A & SSC-A, respectively). (B) CTV mean fluorescence intensities (MFI) generated *via* flow cytometry of proliferating MEC1 cells following 72 hr in culture with or without AZD8055/ibrutinib treatments, relative to the untreated 'vehicle' control (n=3). (C) Cell count data generated *via* flow cytometry of MEC1 cells following 72 hr of culture with or without (vehicle) 100 nM AZD8055 (n=3). (D) The expression of *CCND1* generated *via* RT-qPCR of MEC1 cells following 24 hr culture with AZD8055 and/or ibrutinib or vehicle control. *CCND1* expression was normalised to *B2M* expression is presented as fold change, relative to the 'vehicle' control (n=3). Data points are depicted as black circles, and the data is represented as the mean ±SEM. Statistics were calculated using a paired Student's t-test (C) and one-way ANOVA (B & D), where * $p \leq 0.05$, ** $p \leq 0.01$, *** $p \leq 0.001$, *** $p \leq 0.0001$.

4.3.5. Combined AZD8055-ibrutinib treatment ablates FOXO4^{S193} levels in MEC1 and HG3 cells and increases FOXO4 nuclear abundance

In Figure 4.10, we addressed how FOXO3 and FOXO4 phosphorylation, and FOXO4 subcellular localisation were affected by AZD8055-ibrutinib treatment in MEC1 and HG3 cells. As noted previously, AKT^{S473} phosphorylation was depleted following AZD8055 and ibrutinib treatment, indicative of effective mTOR/BTK inhibition (Figure 4.10A). Due to a lack of FOXO3 detection *via* western blot in HG3 cells, we did not carry out further experiments with FOXO3 in HG3 cells (Figure 4.10A). FOXO3 was modestly expressed in MEC1 cells (Figure 4.10A), where individual AZD8055 or ibrutinib treatments nominally enhanced FOXO3^{S253} phosphorylation (Figure 4.10B). However, as this lacked significance it suggested that MEC1 cell line was not the most appropriate model for studying FOXO3 regulation in the context of PI3K-AKT-mTOR signalling. In contrast, FOXO4 was readily detected in both MEC1 and HG3 cells, albeit at considerably lower levels than FOXO3 in MEC1 cells (Figure 4.10A). In addition, both MEC1 and HG3 exhibited nominal and variable changes in FOXO4^{S193} following AZD8055 and ibrutinib single treatments. However, AZD8055-ibrutinib combination treatments reduced FOXO4^{S193} levels (Figure 4.10C), albeit not significantly. Subcellular fractionation of HG3 cells revealed strong nuclear FOXO4 expression (Figure 4.10D, supporting that of figures 3.6 – 3.9) which was increased following short-term ibrutinib monotherapy (Figure 4.10E, $p = 0.09$) and significantly enhanced in combination with AZD8055 (Figure 4.10E, $p = 0.02$). These results indicate that MEC1 and HG3 cells can be utilised to gain basic mechanistic insight as to the post-translational regulation of FOXO4, while FOXO3 protein expression could perhaps be analysed more clearly in patient samples.

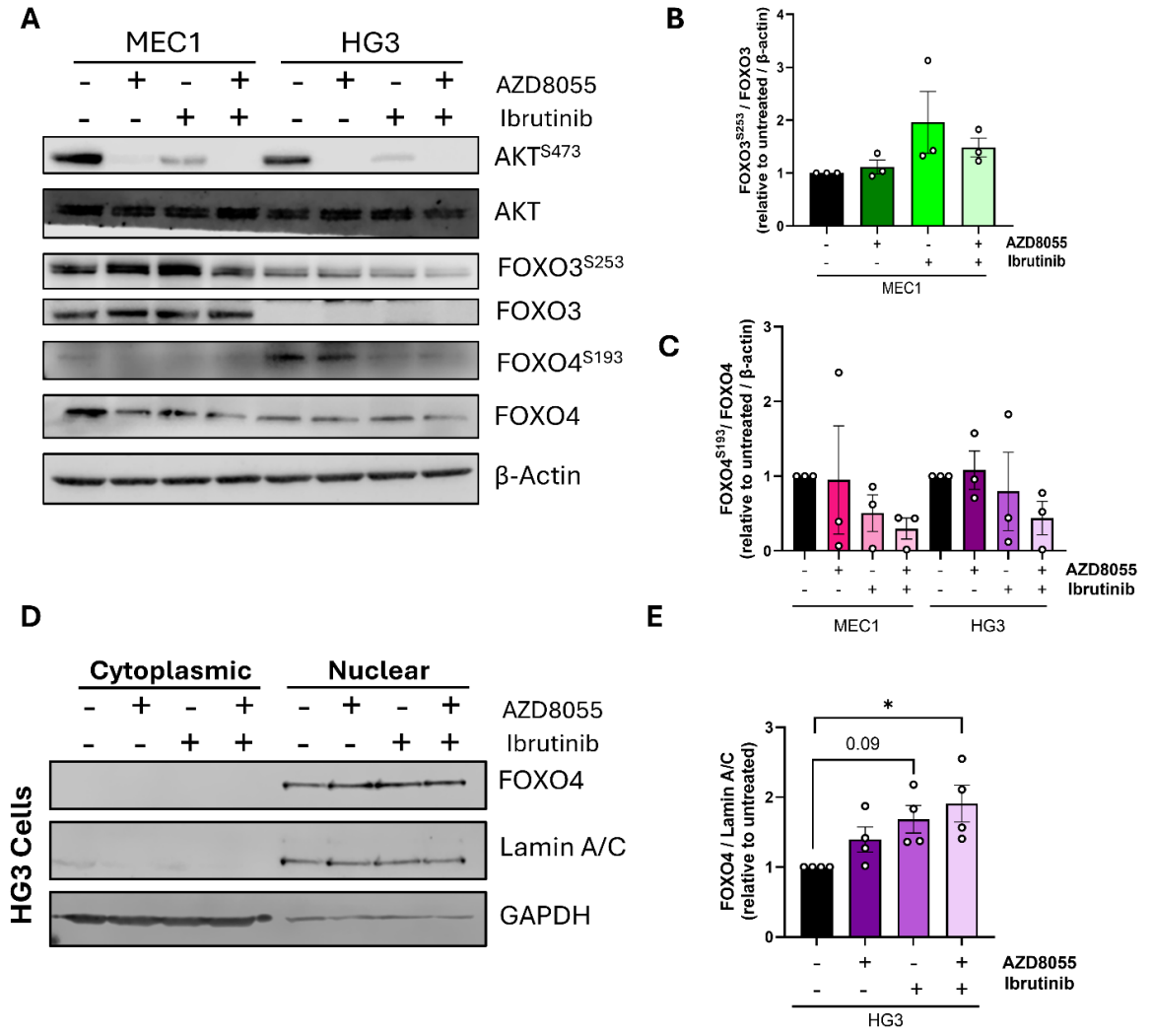

Figure 4.10: BTK-mTOR inhibition facilitates FOXO4 nuclear localisation in HG3 cells. (A) Representative Western blot of MEC1 and HG3 cells following short-term 1 hr single or combination treatments with 100 nM AZD8055 or 1 μM ibrutinib or vehicle control, observing changes in phosphorylation of AKT^{S473}, FOXO3^{S253} and FOXO4^{S193} (compared to total protein expression). β-actin was used as a loading control. (B) Quantified phosphorylation of FOXO3 (S253) in MEC1 cells, compared to total FOXO3 expression in MEC1 cells following AZD8055-ibrutinib treatments or vehicle control, normalised to β-actin and made relative to untreated MEC1 cells. (C) Quantified FOXO4^{S193} levels compared to FOXO4 protein in MEC1 and HG3 cells following AZD8055-ibrutinib treatments or vehicle control, normalised to β-actin and made relative to untreated MEC1 and HG3 cells (n=3). Of note, comparisons are made between cell line conditions and not between MEC1 and HG3 cells. (D) HG3 cells treated for 1 hr with 100 nM AZD8055 and/or 1 μM ibrutinib or vehicle control were separated into cytoplasmic and nuclear compartments *via* subcellular fractionation, where FOXO4 expression was detected *via* Western blotting. GAPDH and Lamin A/C were used as cytoplasmic and nuclear loading controls, respectively. (E) Quantified nuclear expression of FOXO4 in HG3 cells shown in (D), normalised to Lamin A/C and made relative to untreated HG3 cells. Data points are depicted as white circles, and the data is represented as the mean ±SEM. Statistics were calculated using one-way ANOVA (B & D), where * $p \leq 0.05$.

4.3.6. FOXO3 is regulated downstream of BCR-mediated signalling

Here, we addressed FOXO3 regulation in primary CLL cells downstream of F(ab')$_2$-mediated BCR activation (Figure 4.11). We also addressed whether inhibition of BCR signalling *via* AZD8055 (100 nM) or ibrutinib (1 μM) affected the discrete regulation (Figure 4.11A-C) and subsequent localisation (Figure 4.11D-F) of FOXO3 in this context. AKT^{S473} levels were significantly increased in F(ab')$_2$-treated cells (Figure 4.11B), indicative of active BCR signalling, and were significantly attenuated by AZD8055 and ibrutinib single and combination treatments (Figure 4.11B). Interestingly, regardless of exposure to F(ab')$_2$ antigen, minimal change in FOXO3^{S253} was observed (Figure 4.11C). Nevertheless, FOXO3^{S253} levels were reduced in AZD8055-ibrutinib treated cells, trending towards significance ($p = 0.08$, figure 4.11C). Further, there was a significant difference in FOXO3^{S253} between cells treated with AZD8055 alone or in combination with ibrutinib (Figure 4.11C). Although minimal differences in FOXO3^{S253} levels were seen following stimulation with F(ab')$_2$, subcellular fractionation of primary CLL cells revealed a depletion of nuclear FOXO3 following F(ab')$_2$ stimulation (Figure 4.11D & E), which was rescued by AZD8055-ibrutinib combination therapy ($p = 0.05$). Complimentary to these data, subcellular fractionation of primary cell lysates in Figure 4.11F illustrated the effective shuttling of FOXO3 and FOXO4 between nuclear and cytoplasmic compartments following F(ab')$_2$-mediated BCR activation, which is actively reversed in cells treated with AZD8055.

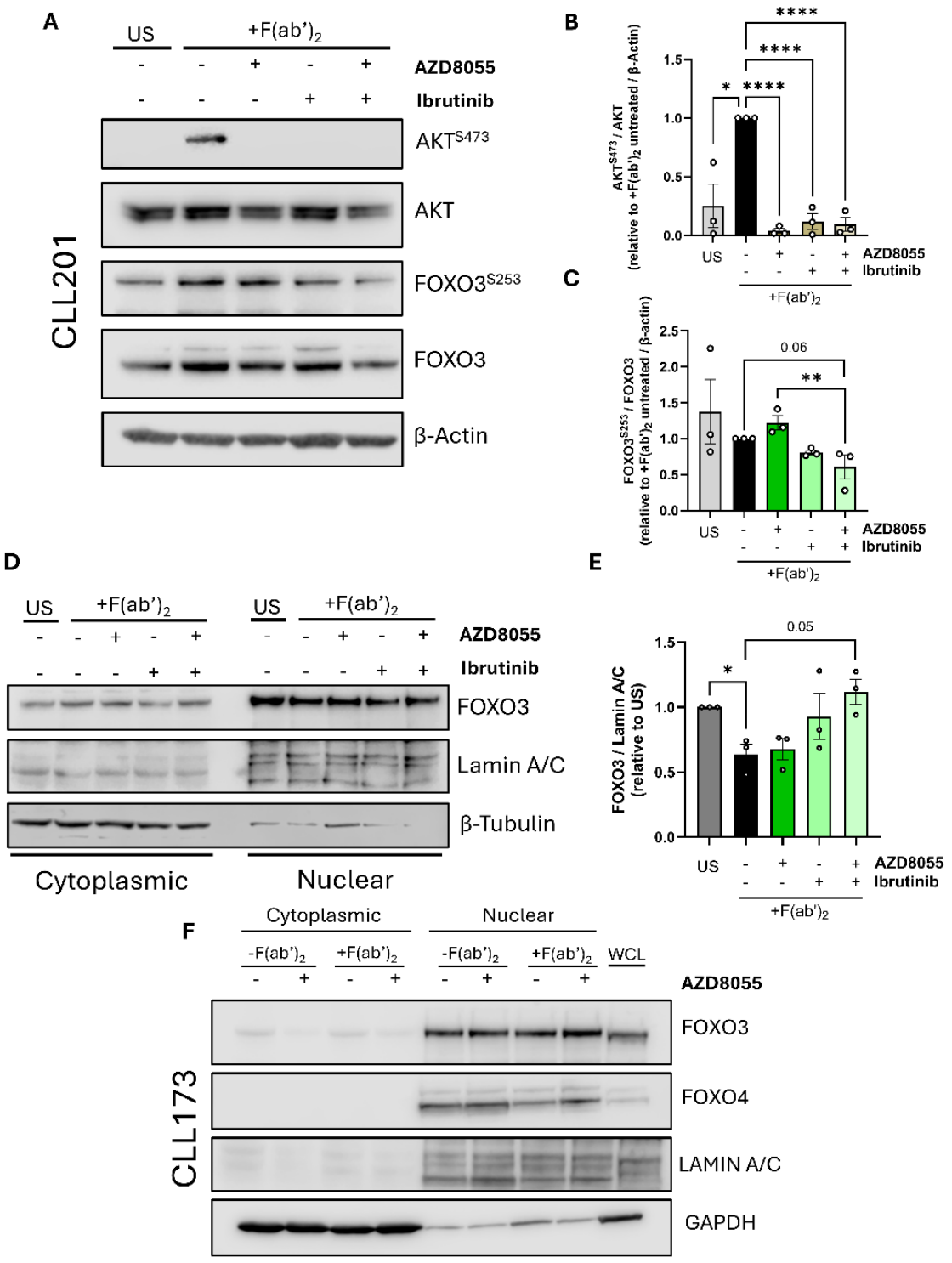

Figure 4.11: BTK-mTOR inhibition negates AKT-mediated FOXO3 phosphorylation. (A) Primary CLL cells treated with F(ab')$_2$ fragments were cultured in the presence or absence (vehicle) of AZD8055 (100 nM) and/or ibrutinib (1 μM) for 30 min prior to 1 hr F(ab')$_2$ stimulation. The subsequent lysates were used in Western blotting to detect changes in phosphorylation status of AKT (S473) and FOXO3 (S253). β-actin was used as a loading control. (B) AKT^{S473} levels were quantified compared with total AKT protein, normalised to β-actin and made relative to F(ab')$_2$-stimulated, untreated cells. (C) FOXO3^{S253} levels were quantified compared with total FOXO3 expression, normalised to β-actin and relative to F(ab')$_2$-stimulated, untreated cells (n=3). (D) Representative western blot of fractionated primary cells following 1 hr F(ab')$_2$ stimulation (10 μg/mL) ±30 min AZD8055 (100 nM)/ibrutinib (1 μM) pre-treatments. FOXO3 subcellular localisation was detected, and made relative to the compartment's respective loading control (cytoplasmic: β-tubulin, nuclear: Lamin A/C). (E) Quantification of relative

FOXO3 expression in F(ab')$_2$-stimulated nuclear lysates, normalised to Lamin A/C (nuclear loading control) and made relative to the unstimulated control (n=3). In the case of A-E, untreated cells showed basal phosphorylation of AKT and FOXO3 *in vitro*. (F) Western blot of patient sample #173 comparing the nuclear and cytoplasmic expression of FOXO3 and FOXO4 in response to 1 hr F(ab')$_2$ stimulation (10 µg/mL) ±30 min AZD8055 (100 nM) pre-treatment, achieved *via* subcellular fractionation (n=1). GAPDH and Lamin A/C were used as cytoplasmic and nuclear loading controls, respectively. Data points are depicted as white circles, and the data is represented as the mean ±SEM. All replicates are biological replicates from patient-derived CLL cells. Statistics were calculated using a paired Student's t-test for comparing samples ±F(ab')$_2$, while one-way ANOVA was used to calculate statistics within F(ab')$_2$-stimulated conditions, where * $p \leq 0.05$, ** $p \leq 0.01$, **** $p \leq 0.0001$.

4.3.7. FOXO4 is phosphorylated downstream of BCR activation

FOXO4 regulation in different CLL contexts has yet to be elucidated. Therefore, we investigated how F(ab')$_2$-mediated BCR activation affects FOXO4 phosphorylation and localisation by utilising upstream mTOR (AZD8055, 100 nM) and BTK (ibrutinib, 1 µM) inhibitors as tools to observe changes in discrete FOXO4 phosphorylation. In primary patient samples stimulated with F(ab')$_2$ antigen, there was a significant elevation in FOXO4^{S193} (Figure 4.12A & B), suggesting that BCR-mediated signals regulate distinct FOXO4 activity. Further, single pre-treatments with AZD8055 and ibrutinib decreased FOXO4^{S193} levels (Figure 4.12B). Subcellular fractionation of primary cells in the F(ab')$_2$ system revealed strong basal FOXO4 expression in unstimulated CLL cells (Figure 4.12C), which was reduced following F(ab')$_2$ treatment (Figure 4.12C & D), suggesting F(ab')$_2$-mediated shuttling of FOXO4 to cytoplasmic compartments. However, AZD8055 and/or ibrutinib single pre-treatment did not change FOXO4 localisation (Figure 4.12D). Therefore, while further studies are required to confirm the effect of AZD8055/ibrutinib pre-treatments and subsequent F(ab')$_2$ stimulation on the subcellular localisation of FOXO4, these data confirm that both FOXO3 and FOXO4 are actively phosphorylated downstream of BCR-PI3K-AKT activation in primary CLL cells (Figure 4.12E), though more work would be need to discern the phosphorylation status of FOXO4 following AZD8055-ibrutinib treatment in F(ab')$_2$-stimulated cells.

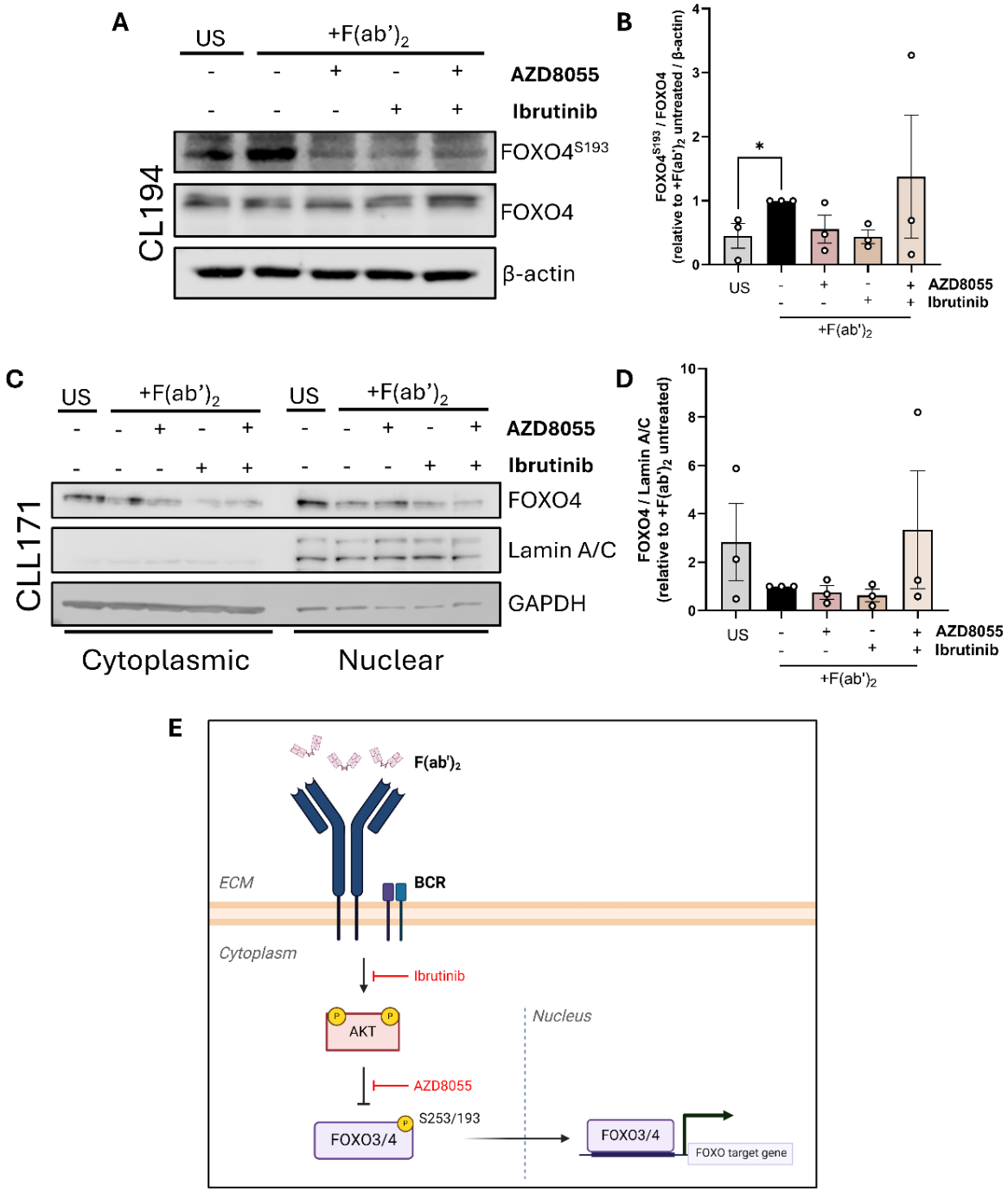

Figure 4.12: Short-term BCR activation induces AKT-mediated FOXO4 phosphorylation in vitro. (A) Representative Western blot of primary CLL cells stimulated with 10 µg/mL F(ab')$_2$ antigen for 1 hr with or without (vehicle) 100 nM AZD8055 and/or 1 µM ibrutinib 30 min pre-treatments, to detect levels of FOXO4^{S193}, total FOXO4 protein and β-actin. An unstimulated (US) vehicle control was also included. (B) Quantified expression of FOXO4^{S193} compared to total FOXO4 protein, normalised to β-actin and made relative to the F(ab')$_2$-stimulated control (n=3). (C) Subcellular fractionation of primary CLL cells treated under the same conditions as A & B, addressing the expression of FOXO4 in cytoplasmic and nuclear compartments. Lamin A/C and GAPDH were used as nuclear and cytoplasmic loading controls, respectively. (D) Quantified expression of FOXO4 in nuclear primary cell lysates, normalised to Lamin A/C and made relative to the F(ab')$_2$-stimulated control (n=3). (E) Illustration of F(ab')$_2$-mediated BCR activation and subsequent AKT-mediated regulation of FOXO activity *via* phosphorylation. Points at which ibrutinib and AZD8055 inhibit BCR signal transduction are shown, leading to FOXO nuclear localisation. Data points are depicted as white circles, and the data is represented as the mean ±SEM. All replicates are biological replicates from patient-derived CLL cells.

Statistics were calculated using a paired Student's t-test for comparing samples ±F(ab')$_2$, while one-way ANOVA was used to calculate statistics within F(ab')$_2$-stimulated conditions, where * p ≤ 0.05.

4.3.8. FOXO3 and FOXO4 phosphorylation is reduced following AZD8055-ibrutinib treatment in CD40-stimulated cells

Our RNA-seq data revealed marked increases in FOXO3/4 expression following mTOR-BTK inhibition (Figures 4.1-4.6). Furthermore, FOXO4 phosphorylation was significantly reduced in MEC1 cells following AZD5363-mediated AKT inhibition (Figure 3.9), suggesting that FOXO3 and FOXO4 are regulated downstream of AKT activation in CLL. In Figure 4.13, we investigated whether CD40L-(+IL-4)-mediated CD40 stimulation and short-term AZD8055 (100 nM) and/or ibrutinib (1 μM) treatments affect FOXO3/4 phosphorylation. AKT^{S473} levels were highly varied in NTL-cultured CLL samples although exhibited similar levels as cells exposed to CD40L (Figure 4.13B & E). Nevertheless, AKT^{S473} levels were significantly diminished following 1 hr treatment with AZD8055 and ibrutinib (Figure 4.13B & E), demonstrating that AKT inhibition can be achieved in the CD40L system using AZD8055 and ibrutinib. While AKT^{S473} levels were varied, FOXO3^{S253} levels were significantly increased in cells stimulated with CD40L compared to the unstimulated NTL control (Figure 4.13C). However, short-term drug treatments failed to inhibit AKT-mediated FOXO3 phosphorylation (Figure 4.13C).

Basal phosphorylation of FOXO4 in the absence of CD40L exposure (NTL) was varied between samples (Figure 4.13F). Interestingly, following CD40L stimulation, FOXO4^{S193} phosphorylation was decreased in AZD8055-treated cells (Figure 4.13F), enhanced in combination with ibrutinib (trending towards significance, p = 0.14, Figure 4.13F). While more replicates are required, these data allude to the differential regulation of FOXO3 and FOXO4 downstream of both BCR-PI3K-AKT- (Figures 4.11 & 4.12) and CD40-PI3K-AKT-mediated signals (Figure 4.13).

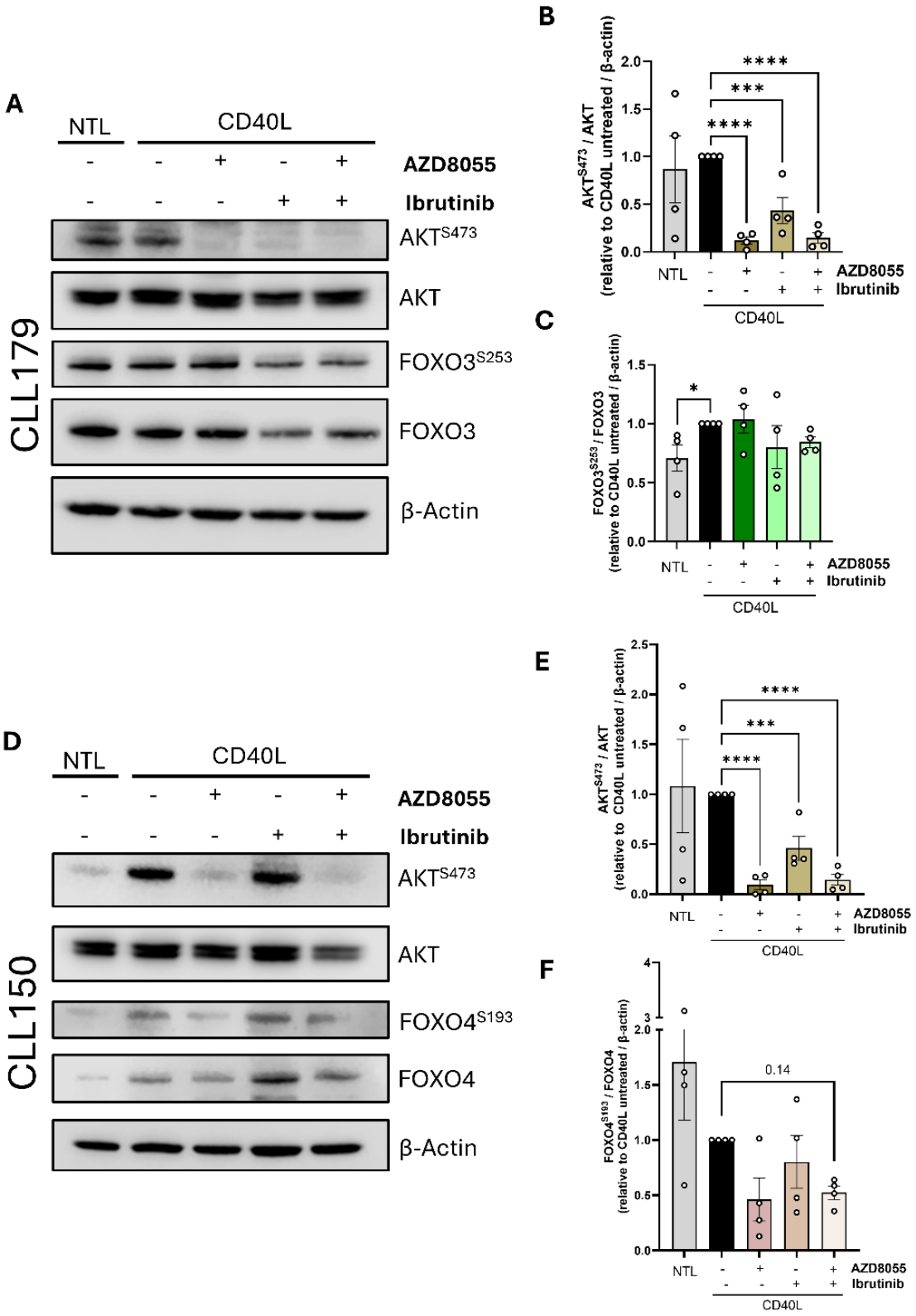

Figure 4.13: AZD8055-ibrutinib treatment reduces AKT^{S473} and subsequent FOXO3^{S253}/FOXO4^{S193} levels. (A) Primary CLL cells were cultured overnight on CD40L-expressing stroma (+10 ng/mL IL-4), followed by 1 hr treatment with AZD8055 (100 nM) and/or ibrutinib (1 μM) or vehicle control. Lysates were collected and visualised *via* Western blot to detect the expression of AKT^{S473}, AKT, FOXO3^{S253}, FOXO3 and β-actin. (B) Quantified expression of AKT^{S473} compared to total AKT protein, normalised to β-actin and made relative to the CD40L-stimulated control. (C) Quantified expression of FOXO3^{253} compared to total FOXO3 protein, normalised to β-actin and made relative to the CD40L-stimulated control (n=4). (D) Western blot addressing changes in AKT^{S473} and FOXO4^{S193} compared to total protein using identical conditions to those described in A. (E) Quantified expression of AKT^{S473} compared to total AKT protein, normalised to β-actin and made relative to the CD40L-stimulated control.-(F)

Quantified expression of FOXO4^{S193} compared to total FOXO4 protein, normalised to β-actin and made relative to the CD40L-stimulated control (n=4). An unstimulated 'NTL' control was included in both cases (A-C, D-F). Data points are depicted as white circles, and the data is represented as the mean ±SEM. All replicates are biological replicates from patient-derived CLL cells. Statistics were calculated using a paired Student's t-test for comparing samples ±CD40L, while one-way ANOVA was used to calculate statistics between CD40L-stimulated conditions, where * p ≤ 0.05, *** p ≤ 001, *** p ≤ 0.0001.

4.3.9. Primary CLL cells exhibit FOXO3 and FOXO4 nuclear abundance that is enhanced with mTOR-BTK inhibition

To determine whether CD40 activation and subsequent mTOR and BTK inhibition affect FOXO3/4 subcellular localisation, primary CLL cells were exposed to NTL (+10 ng/mL IL-4, ±CD40L) overnight, followed by short-term AZD8055 (100 nM), ibrutinib (1 μM) or AZD8055-ibrutinib combination treatment. Of note, FOXO3 and FOXO4 were detected independently, as the use of Lamin A/C as a nuclear loading control can mask FOXO signals. In addition, we determined FOXO localisation *via* quantification of the nuclear compartment (Figure 4.14B & D), as this compartment had the most consistent FOXO3 and FOXO4 expression in CLL cells. In figure 4.14A, FOXO3 expression was reduced in nuclear compartments in cells exposed to CD40L compared to the NTL control - a finding near significance (Figure 4.14B, p = 0.06). Furthermore, short-term AZD8055-ibrutinib combination treatment significantly rescued CD40L-mediated nuclear depletion (Figure 4.14B).

CD40L exposure, however, did not alter the nuclear abundance of FOXO4 (Figure 4.14C & D). Yet, short-term AZD8055 and ibrutinib treatments increased FOXO4 nuclear expression, where ibrutinib treatment induced a near-significant increase in nuclear FOXO4 (Figure 4.14D; p = 0.053). These data align with Figure 4.13, demonstrating a partnership between AZD8055-ibrutinib treatment, a depletion in FOXO3 and FOXO4 phosphorylation and enhanced FOXO3/4 nuclear expression.

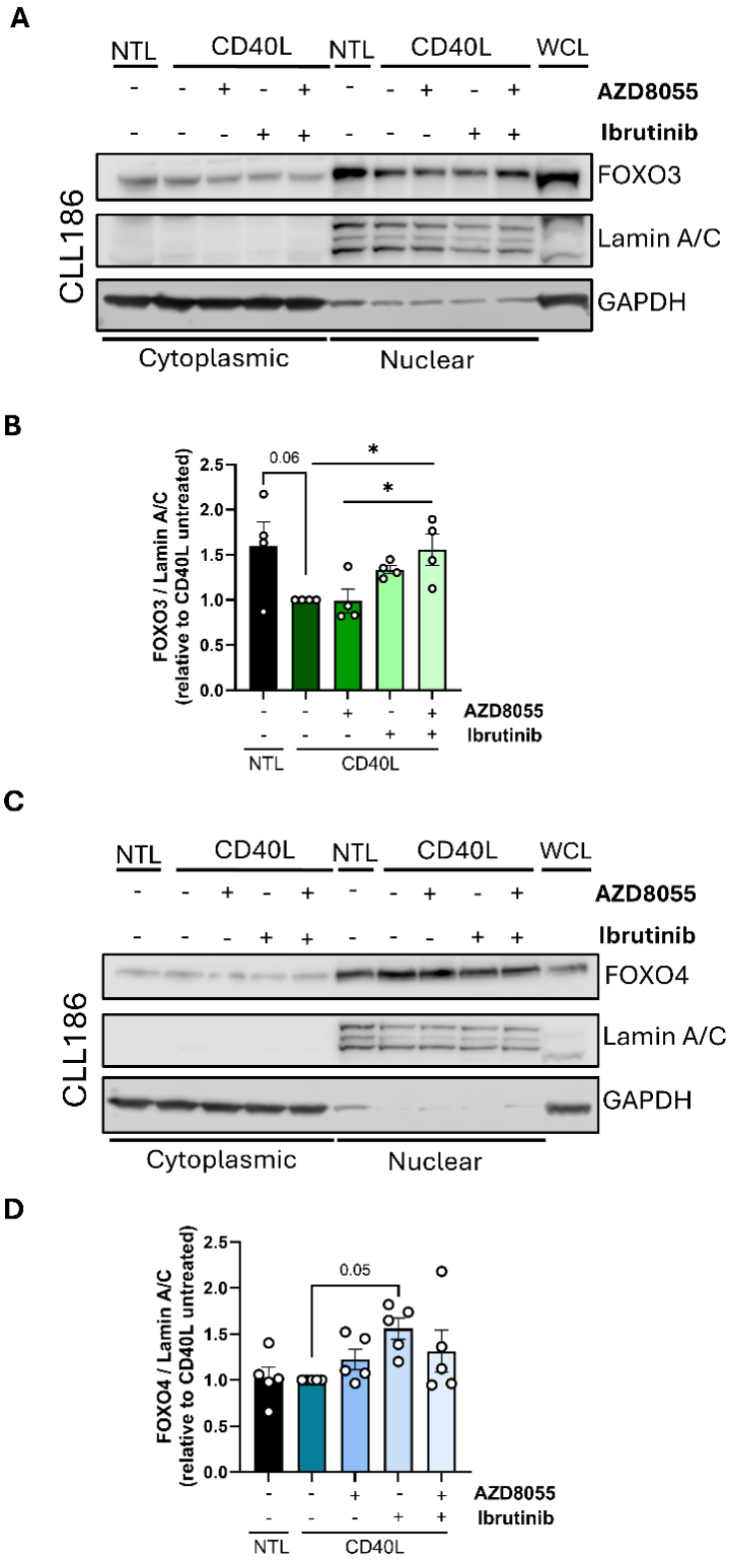

Figure 4.14: AZD8055 and ibrutinib promote the nuclear localisation of FOXO3 and FOXO4. (A & C) Western blots depicting subcellular fractionations of primary CLL cells following overnight CD40L (+10 ng/mL IL-4) co-culture and subsequent 1 hr AZD8055 (100 nM) and/or ibrutinib (1 μM) treatment or vehicle control. Western blot was conducted to address the expression of FOXO3 (A) and FOXO4 (B) in cytoplasmic and nuclear lysates. Lamin A/C and GAPDH were used as nuclear and cytoplasmic loading controls, respectively, with a WCL sample being included as a positive control. In both cases, an unstimulated 'NTL' sample was also included. (B) Quantified nuclear expression of FOXO3, normalised to Lamin A/C and made relative to CD40L-stimulation alone (n=4). (D) Quantified nuclear expression of FOXO4, normalised to Lamin A/C and made relative to CD40L-stimulation alone (n=5). Data points are depicted as white circles, and the data is represented as the mean ±SEM. All replicates are biological replicates from patient-derived CLL cells. Statistics were calculated using a paired Student's t-test for comparing samples ±CD40L, while one-way ANOVA was used to calculate statistics between CD40L-stimulated conditions, where * $p \leq 0.05$.

4.3.10. CD40-mediated FOXO regulation is sustained in long-term CD40L co-cultures

We have demonstrated that FOXO family gene and protein expression changes following prolonged CD40L exposure (Figure 3.10). Therefore, FOXO activity may be modulated following prolonged CD40L co-culture. A previous study determined that FOXO1 phosphorylation is reduced in long-term CD40L co-cultures in a CD40L system with exogenous IL-21 [49]. Here, we addressed the phosphorylation status of FOXO3 in proliferating, long-term CLL-CD40L co-cultures, and determined the expression of *FOXO1, FOXO3* and *FOXO4* in long-term cultures. Protein and RNA samples were generated from CLL cells following 8-day co-culture (+IL-4) with supportive cells (±CD40L) with or without the AZD8055 (100 nM) and ibrutinib (1 μM) single or combination treatment. AKT^{S473} levels were depleted in long-term CD40L co-cultures - a finding previously seen [49] that was distinct from CLL cells in short term co-culture (Figure 4.13). $FOXO3^{S253}$ phosphorylation was significantly higher in CLL cells with prolonged exposure to CD40L, which was significantly reduced with AZD8055 treatments. Accompanying this, FOXO3 expression was significantly decreased in CD40L co-cultured CLL cells compared to the 'NTL' control (Figure 4.15C), which was marginally attenuated by AZD8055 treatments (single or in combination). Expression profiling of *FOXO1, FOXO3* and *FOXO4* genes (Figure 4.15D-F) revealed that their expression was downregulated in long-term CD40L co-cultures, significantly for *FOXO3*, while *FOXO4* was trending towards significance ($p = 0.06$). Further, AZD8055 and ibrutinib treatments elicited nominal change in *FOXO1/3/4* expression (Figure 4.15D-F), suggesting distinct regulation of FOXO family genes in long-term *vs.* short-term cultures. These results indicate that FOXO protein and gene downregulation displayed in short-term CD40L co-cultures is sustained during prolonged CD40-CD40L engagement, and that AKT-mediated FOXO3 phosphorylation is more prominent during prolonged exposure to CD40L.

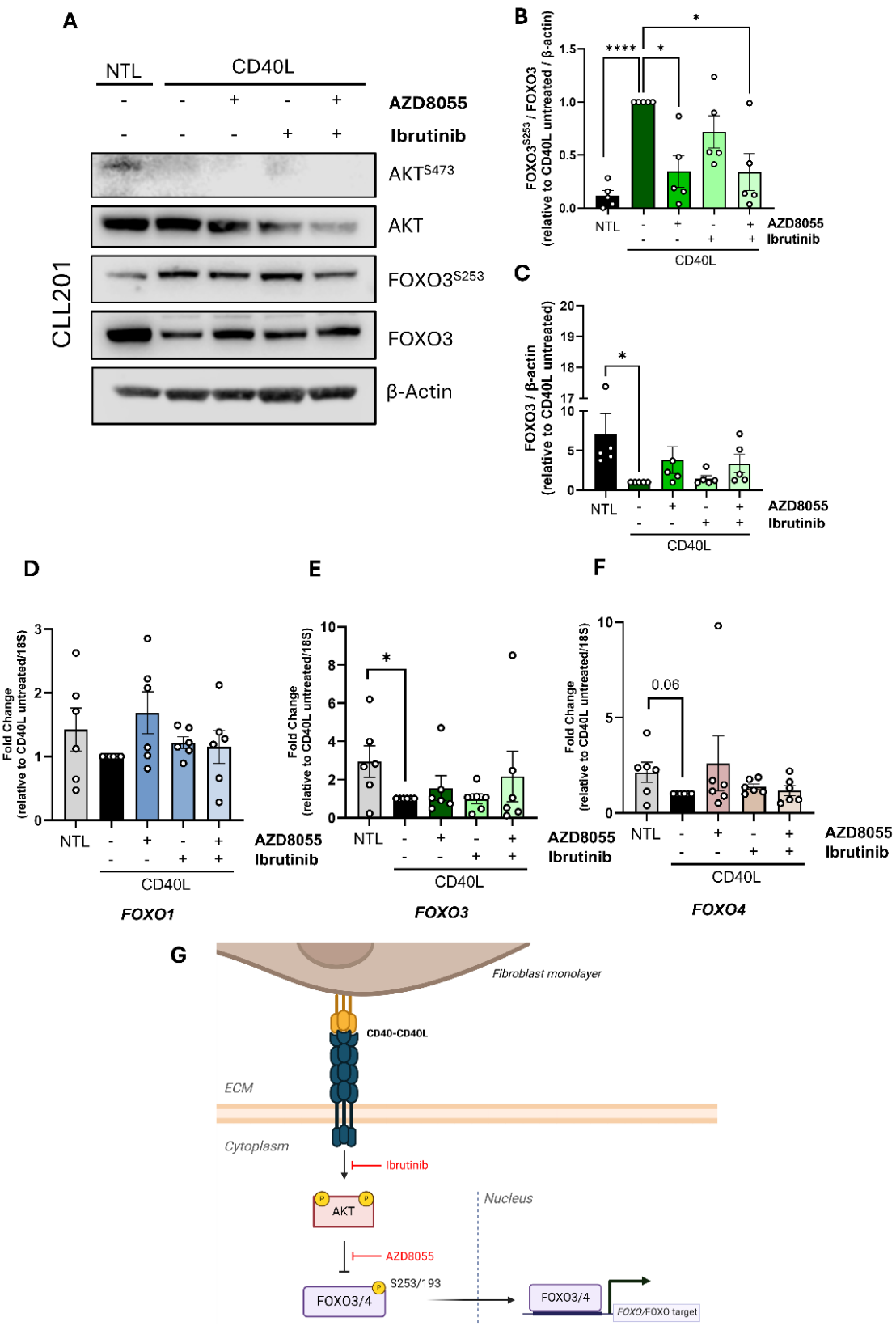

Figure 4.15: FOXO3 is phosphorylated and downregulated downstream of long-term CD40 stimulation. (A) Western blot of primary CLL cells cultured for 8 days in CD40L co-culture (+10 ng/mL IL-4) with or without (vehicle) AZD8055 (100 nM) and ibrutinib (1 μM) single or combination treatment, addressing expression of AKT^{S473}, AKT, FOXO3^{S253}, FOXO3 and β-actin. An unstimulated 'NTL' sample was also included. (B) Quantified expression of FOXO3^{S253} compared to total FOXO3 protein in 8-day cultures (n=5), normalised to β-actin and made relative to CD40L stimulation alone. (C) Quantified

expression of total FOXO3, normalised to β-actin and made relative to CD40L stimulation alone. (D-F) RT-qPCR was conducted to detect the expression of *FOXO1* (D), *FOXO3* (E) and *FOXO4* (F) in primary CLL cells following 8-day CD40L as described above, normalised to *18S* and presented as fold change relative to CD40L stimulation alone (n=6). (G) Illustration of the regulation of FOXO activity orchestrated by AKT downstream of CD40-CD40L engagement, where inhibition of CD40 signalling by ibrutinib and AZD8055 abrogates AKT-mediated FOXO phosphorylation, leading to FOXO nuclear localisation. Data points are depicted as white circles, and the data is represented as the mean ±SEM. All replicates are biological replicates from patient-derived CLL cells. Statistics were calculated using a paired Student's t-test for comparing samples ±CD40L, while one-way ANOVA was used to calculate statistics between CD40L-stimulated conditions, where * $p \leq 0.05$, *** $p \leq 0.001$.

4.3.11. mTOR activity is necessary for CLL cell proliferation in *in vitro* CD40L co-culture

To characterise proliferation in long-term CD40L co-cultures and how cell-cycle-associated FOXO targets are regulated in long-term CD40L co-cultures, two independent experiments were performed to characterise CLL cell proliferation in CD40L co-cultures in the presence of either exogenous IL-4 (10 ng/mL) or IL-21 (15 ng/mL). CLL cells exhibited significant levels of proliferation compared to their respective non-proliferative controls (Figure 4.16A-C). Of note, IL-21 cultures achieved significance in a shorter period than their IL-4 counterparts (5 days *vs* 7-14 days, respectively [49, 409]). In both instances, AZD8055 treatment significantly attenuated CD40L-mediated CLL cell proliferation (Figure 4.16B & C).

Protein and gene expression of the FOXO targets cyclin D2 (*CCND2*, Figure 4.16E), $p21^{cip1}$ (*CKDN1A*, Figure 4.16F) and $p27^{kip1}$ (*CDKN1B,* Figure 4.16G) were considered due to their distinct roles in permitting (cyclin D2) or inhibiting ($p21^{cip1}$ & $p27^{kip1}$) cell cycle progression [559, 560]. Following 8-days in culture, cyclin D2 expression was significantly decreased in CD40L co-cultures compared to the control (Figure 4.16E, left). In contrast, *CCND2* expression was significantly increased in expression in CLL cells exposed to CD40L (Figure 4.16E, right), indicative of cell cycle progression. AZD8055 and ibrutinib treatments elicited nominal change in cyclin D2/*CCND2* expression (Figure 4.16E). Interestingly, $p21^{CIP}$/*CDKN1A* levels were both significantly increased in cells stimulated with CD40L (Figure 4.16F). AZD8055 and ibrutinib treatments did not induce change in $p21^{cip1}$ expression, however, *CDKN1A* was depleted in AZD8055-ibrutinib-treated cells, albeit not significantly (Figure 4.16F). Although *CDKN1B*

expression was sustained throughout, NTL-cultured CLL cells exhibited high levels of endogenous p27^{kip1}, which was significantly absent in CD40L co-cultures (Figure 4.16G). Reflecting results seen for cyclin D2 and p21^{cip1}, AZD8055 and ibrutinib treatments did not affect the expression of p27^{kip1}/*CDKN1B* (Figure 4.16G).

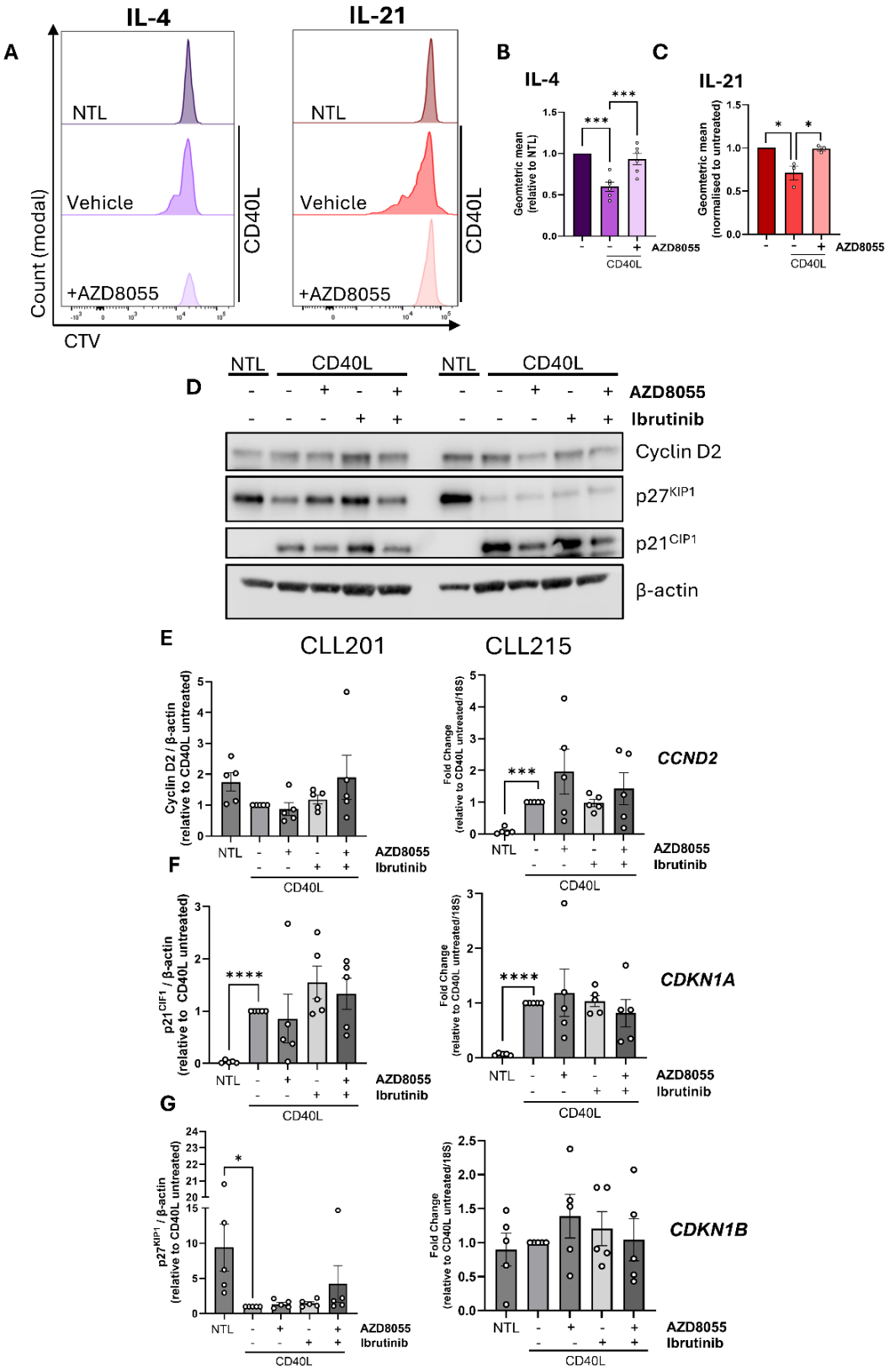

Figure 4.16: CD40L co-culture induces CLL cell proliferation and influences the expression of FOXO targets. (A) Representative FACS histograms of primary CLL cells stained with CTV and co-cultured with CD40L-expressing stroma (+10 ng/mL IL-4, left, +15 ng/mL IL-21, right). As the cells proliferate, CTV dye is shared between daughter cells, reducing CTV intensity (presented as mean fluorescence (MFI)). Samples were cultured with 'NTL' (unstimulated) cells or CD40L-expressing cells, with or without (vehicle) 100 nM AZD8055. (B) CTV mean fluorescence intensity (MFI) of primary CLL cells in CD40L (+IL-4) co-culture for 5-14 days ±AZD8055, relative to the 'NTL' control. (B) CTV mean fluorescence intensity (MFI) of primary CLL cells in 5-day CD40L (+IL-21) co-culture ±AZD8055, relative to the 'NTL' control. (D) Western blot of 8-day primary CLL CD40L co-cultures (+10 ng/mL IL-4) ± single or combination 100 nM AZD8055 and 1 μM ibrutinib treatments. Western blot was used to detect the expression of Cyclin D2, $p27^{kip1}$ $p21^{cip1}$ and β-actin. (E) Quantified expression of Cyclin D2 (left) and *CCND2* transcript abundance detected *via* RT-qPCR (right). (F) Quantified expression of $p21^{cip}$ (left) and *CDKN1A* (right). (G) Quantified expression of $p27^{kip1}$ (left) and *CDKN1B* transcript (right). In all cases, protein and gene expression were normalised to β-actin and *18S,* respectively, and were all made relative to CD40L stimulation alone (n=5). Data points are depicted as white circles, and the data is represented as the mean ±SEM. All replicates are biological replicates from patient-derived CLL cells. were calculated using a paired Student's t-test for comparing samples ±CD40L, while one-way ANOVA was used to calculate statistics between CD40L-stimulated conditions, where * $p \leq 0.05$, *** $p \leq 0.001$, **** $p \leq 0.0001$.

4.3.12. mTOR inhibition reduces S-phase progression in proliferating CLL cells

We recently demonstrated a block in CLL cell proliferation in MEC1 and CD40L co-culture systems following treatment with rapamycin, as well as the dual mTORC1/2 inhibitor AZD8055 [409]. However, the effects of rapamycin and AZD8055 treatments (alone or in combination with ibrutinib) on cell cycle progression within the CD40L (+IL-4) system have been scarcely addressed. Here, conducting PI staining *via* flow cytometry, it was revealed that long-term CD40 stimulation significantly decreased G0/G1 cell populations (Figure 4.17B), coincident with increased S- (Figure 4.17C) and G2-CLL populations (Figure 4.17D). AZD8055 treatment significantly depleted the S phase populace (Figure 4.17C), coincident with a median increase in cells in G0/G1 (Figure 4.17B). Ibrutinib did not affect cell cycle progression at any stage (Figure 4.17). Combination treatment significantly depleted CLL cell populations undergoing S-phase progression, mimicking results seen following single AZD8055 treatment (Figure 4.17C). Moreover, rapamycin treatment induced a significant depletion of cells S phase progression (Figure 4.17C), coincident with increased G0/G1 (Figure 4.17B). Notably, AZD8055, ibrutinib and rapamycin treatments did not affect the proportion of G2 populations (Figure 4.17D). These findings

demonstrate the importance of mTOR activity, perhaps specifically mTORC1, in facilitating CLL cell cycle progression.

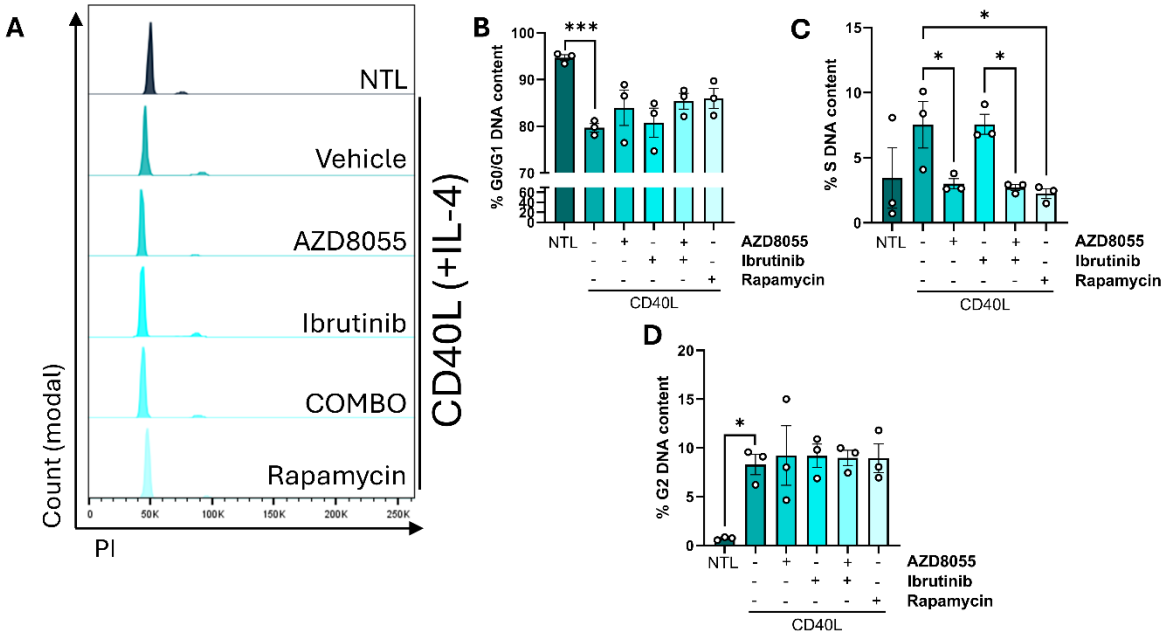

Figure 4.17: mTOR inhibition abrogates CLL cell cycle progression. Primary CLL cells were cultured for 8 days in CD40L co-culture (+10 ng/mL IL-4) with or without (vehicle ctl) treatment with 100 nM AZD8055, 1 μM ibrutinib, alone or in combination, or 10 nM rapamycin. CLL cells were then fixed, permeabilised and stained with PI stain. (A) Representative FACS histogram plot revealing the DNA content of 8-day CLL CD40L co-cultures following PI staining. (B-D) Percentage DNA content of CLL cells in CD40L co-culture reflecting DNA content found in G_0/G_1, S and G2 phases of the cell cycle, respectively (n=3). Data points are depicted as white circles, and the data is represented as the mean ±SEM. All replicates are biological replicates from patient-derived CLL cells. Statistics were calculated using a paired Student's t-test for comparing samples ±CD40L, while one-way ANOVA was used to calculate statistics between CD40L-stimulated conditions, where * $p \leq 0.05$, ** $p \leq 0.01$.

4.3.13. AZD8055-mediated BIM expression is sustained in long-term CLL-CD40L co-culture

To investigate whether AZD8055 treatment induces apoptosis in CLL-CD40L co-cultures, primary CLL cells were cultured for 3 days in the presence or absence of 100 nM AZD8055 and 1 μM ibrutinib single or combination treatment. CLL cell viability was significantly reduced in cells treated with AZD8055 (Figure 4.18A & B), corroborated by a significant reduction in CLL cell count (Figure 4.18C), supporting an AZD8055-mediated induction of apoptosis and/or cell cycle arrest (Figures 4.8, 4.16 & 4.17). Further, long-term CD40L exposure significantly enhanced BCL-XL protein and gene expression (Figure 4.18D & E), while long-

term CD40-CD40L interactions depleted intracellular BIM and *BCL2L11* expression (BIM expression trending towards significance - p = 0.06 and 0.01, respectively - Figure 4.18F). These data reveal sustained anti-apoptotic signalling generated by distinct BCL2 family members, corroborating findings observed in CLL cells engaged in short-term CD40-CD40L interactions (Figures 3.4 & 3.5). AZD8055 and ibrutinib single treatments did not affect BCL-XL protein expression, however, AZD8055 treatment induced a nominal increase in *BCL2L1*. Further, ibrutinib treatment did not affect BIM protein or gene expression (Figure 4.18F). However, AZD8055 treatment significantly enhanced *BCL2L11* expression (Figure 4.18F). Although this was absent in the combination, BIM protein expression was enhanced, trending towards significance (p = 0.13, Figure 4.18F). Unexpectedly, AZD8055 and ibrutinib combination treatment increased BCL-XL protein and gene expression, albeit not significantly (p = 0.12 and 0.16, respectively –Figure 4.18E).

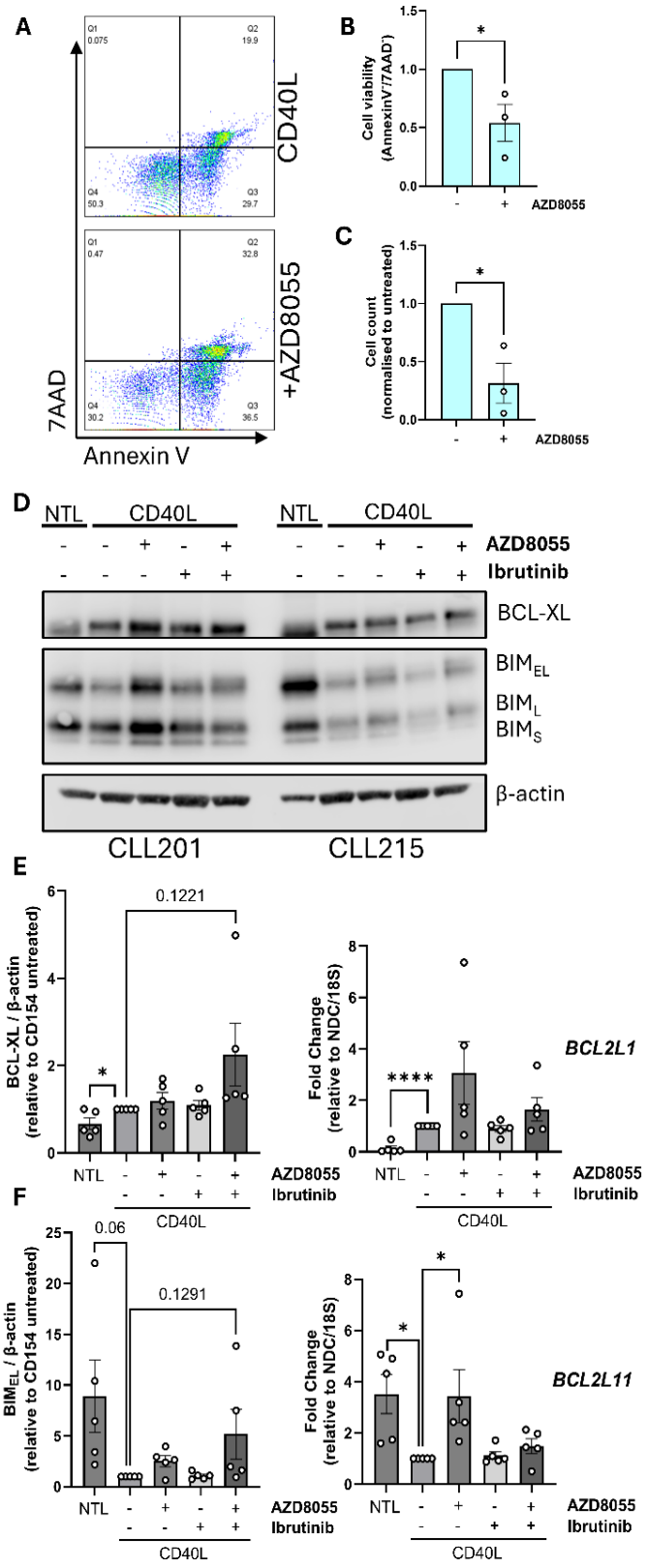

Figure 4.18: AZD8055 treatment overcomes CD40L-mediated CLL cell survival. (A) FACS plot of primary CLL cells following 72 hr in CD40L (+10 ng/mL IL-4) co-culture ±100 nM AZD8055 and staining with Annexin/7AAD. (B) Percentage of CLL cells in 72 hr CD40L culture that are considered 'viable' (Annexin^{neg}/7AAD^{neg}), relative to untreated cells. (C) Cell counts were conducted by including CountBright™ beads in FACS samples and were gated on forward (FSC-A) and side (SSC-A) scatter. Cell count is expressed relative to untreated cells (n=3). (D) Western blot of 8-day primary CLL cell CD40L co-cultures (+10 ng/mL IL-4) ± 100 nM AZD8055 and 1 μM ibrutinib single or combination treatments, detecting BCL-XL and BIM expression. β-actin was used as a loading control. An unstimulated 'NTL' condition was also included. (E) Quantified expression of BCL-XL (left) and *BCL2L1* (right) in 8-day CD40L co-cultures. (F) Quantified expression of BIM (left) and *BCL2L11* (right) in 8-day CD40L co-cultures. Protein and gene expression were normalised to β-actin and *18S*, respectively, and were made relative to CD40L-stimulated, untreated cells (presented as 'fold change' for gene expression) (n=5). Data points are depicted as white circles, and the data is represented as the mean ±SEM. All replicates are biological replicates from patient-derived CLL cells. Statistics were calculated using a Student's t-test for comparing between two conditions, while one-way ANOVA was used to calculate statistics between CD40L-stimulated conditions, where * $p \leq 0.05$, **** $p \leq 0.0001$.

4.3.14. PARP expression is increased following CD40-CD40L engagement

In other cancer models, the cleavage of PARP - a protein heavily involved in DNA damage repair - is associated with DNA-damage-induced apoptosis, whereby PARP cleavage inhibits PARP binding to DNA strand breaks [561, 562]. In the context of CLL, inhibition of PARP activity has been considered as a novel therapeutic target [563, 564]. In Figure 4.19, we investigated the implications of PARP expression in long-term CLL-CD40L co-cultures to further understand the apoptotic environment following CD40 stimulation in the presence or absence of AZD8055 (100 nM) and ibrutinib (1 μM) treatments, alone or in combination, as well as investigating the link between CD40 activation and expression of DNA damage repair components in CLL patient samples. Here, the expression of both total (Figure 4.19B) and cleaved (Figure 4.19C) forms of PARP were significantly increased in CD40-stimulated cells. Furthermore, AZD8055 treatment elicited a modest decrease in total PARP expression, which was enhanced in combination with ibrutinib (Figure 4.19B). Comparatively, single and combined AZD8055/ibrutinib treatments led to a higher average decrease in the expression of cleaved PARP. These data indicate that CD40 activation mediates PARP expression in CLL-CD40L co-cultures, perhaps as a cofactor to facilitate NF-κB signalling and promote survival (described in Figure 4.19D, [565]). Further investigation to determine PARP activity *via* synthesis of poly(ADP-ribose) would serve to further elucidate the role of PARP expression downstream of CD40 activation [566].

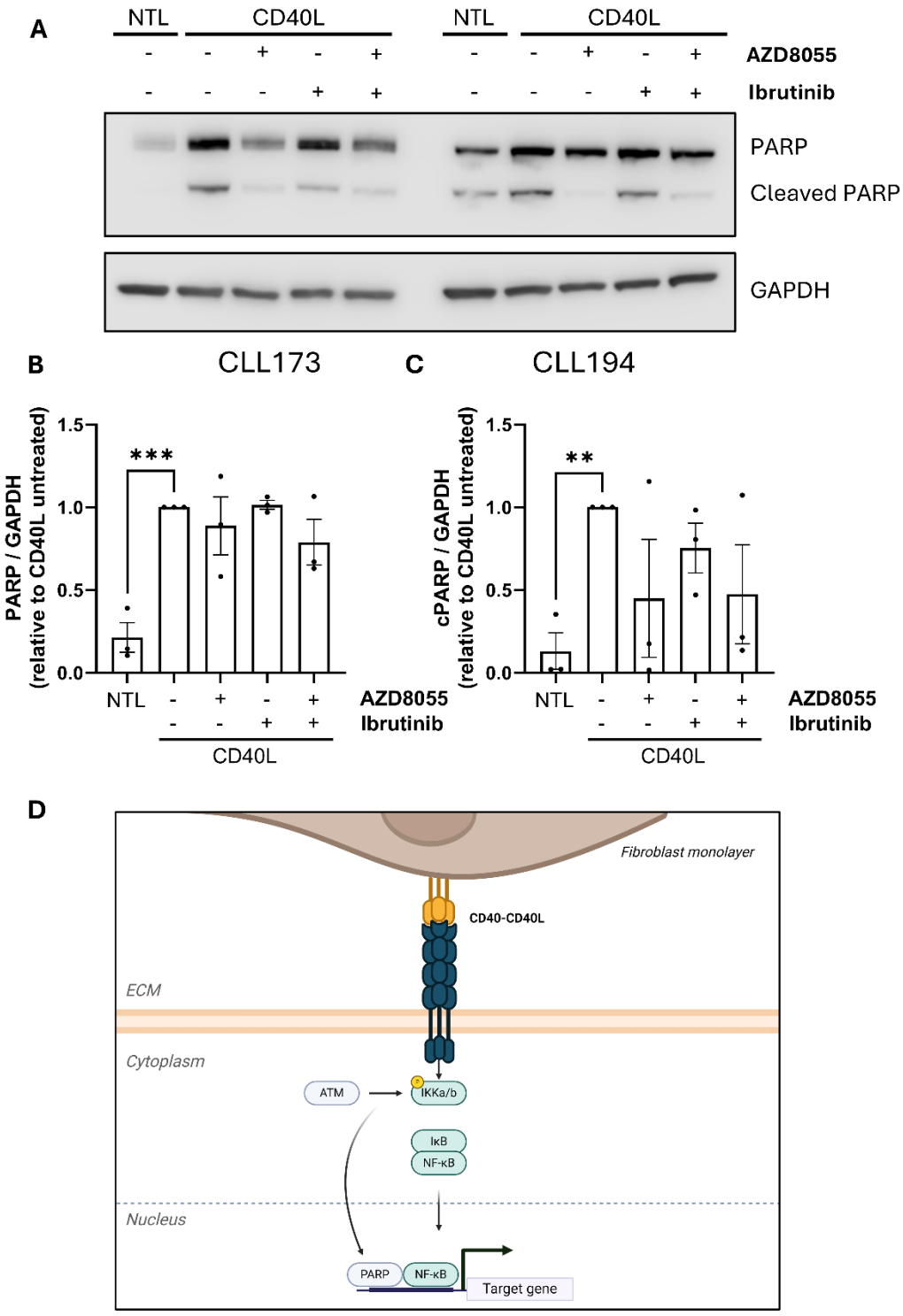

Figure 4.19: CD40L stimulation induces PARP expression. Primary CLL cells were cultured for 8 days in CD40L co-culture (+10 ng/mL IL-4) ±100 nM AZD8055 and 1 μM ibrutinib, alone or in combination. A vehicle control was used as a comparison. (A) Western blot depicting two primary CLL samples co-cultured for 8-days in CD40L co-culture ±AZD8055 and/or ibrutinib treatment, developed to detect the expression of PARP, cleaved PARP and GAPDH. An unstimulated 'NTL' condition was also included. (B) Quantified expression of total PARP protein, normalised to GAPDH and made relative to untreated cells on CD40L. (C) Quantified expression of cleaved PARP (cPARP), normalised to GAPDH and made relative to untreated cells on CD40L. (D) Illustration of the proposed mechanism PARP activity downstream of CD40-CD40L engagement, where PARP expression is required as part of a protein complex with NF-κB to promote NF-κB-mediated gene transcription [565]. Data points are depicted as black circles, and the data is represented as the mean ±SEM. All replicates are biological replicates from patient-derived CLL cells. Statistics were calculated using a paired Student's t-test for

comparing samples ±CD40L, while one-way ANOVA was used to calculate statistics between CD40L-stimulated conditions, where ** $p \leq 0.01$, *** $p \leq 0.001$.

4.3.15. mTOR inhibition abrogates the expression of DNA damage components in long-term CD40L co-cultures

Other markers are known to be induced in response to DNA damage, which can be actively monitored *in vitro* to provide insight into changes in intracellular stress. In Figure 4.20, we investigated the accumulation of two such established markers of DNA damage in long-term CLL-CD40L co-cultures in the presence or absence of 100 nM AZD8055 and/or 1 μM ibrutinib: (1) GADD45A - a member of the GADD45 family involved in regulating several processes of DNA damage repair (reviewed in [567]); and (2) γ-H2AX – a histone that, when phosphorylated at its serine residue (S139), is found as an octamer at sites of DNA double-strand breaks (reviewed in [568]). Of note, *GADD45A* is a downstream target of FOXO activity [439]. Here, γ-H2AX^{S139} accumulation was detected *via* flow-cytometry-based intracellular staining (Figure 4.20A & B) and by Western blotting (Figure 4.20C & D), while GADD45A protein and gene (*GADD45A*) expression were detected *via* Western blot and RT-qPCR, respectively. Of note, 10 nM rapamycin treatment was included in the flow cytometry assay. Here, intracellular staining revealed increased γ-H2AX^{S139} abundance in unstimulated cultures compared to the CD40L untreated samples (Figure 4.20A & B), while western blotting indicated lower γ-H2AX^{S139} (Figure 4.20D). Nevertheless, AZD8055 treatment conferred a depletion of γ-H2AX^{S139} in data attained from either assay (Figure 4.20B & D). While ibrutinib treatment also induced a reduction in γ-H2AX^{S139} *via* western blot (Figure 4.20D), there was a significant difference in γ-H2AX^{S139} accumulation detected *via* intracellular staining between AZD8055, ibrutinib and AZD8055-ibrutinib combination treatments (Figure 4.20B), where western blotting showed no change in γ-H2AX^{S139} levels following combined AZD8055-ibrutinib treatment (Figure 4.20D). Corroborating these findings, treatment with rapamycin elicited a similar depletion of γ-H2AX^{S139} compared to that of AZD8055-treated conditions (Figure 4.20B). GADD45A protein (Figure 4.20C & E) and gene (Figure 4.20F) expression was significantly increased in long-term

CD40L co-cultures compared to the 'NTL' control. Further, although ibrutinib treatment induced no change in GADD45A expression (Figure 4.20E & F), AZD8055 alone or in combination with ibrutinib induced a significant decrease in *GADD45A* expression (Figure 4.20F), coincident with decreased protein expression (Figure 4.20E). These data are supported by an AZD8055-mediated downregulation of *GADD45A* in MEC1 cells (Figure 4.7). Collectively, these data allude to a CD40-mediated mechanism of expression of mTOR-AKT-FOXO-associated components of the DNA damage response (i.e. GADD45A) that are actively depleted by pharmacological BTK-mTOR inhibition.

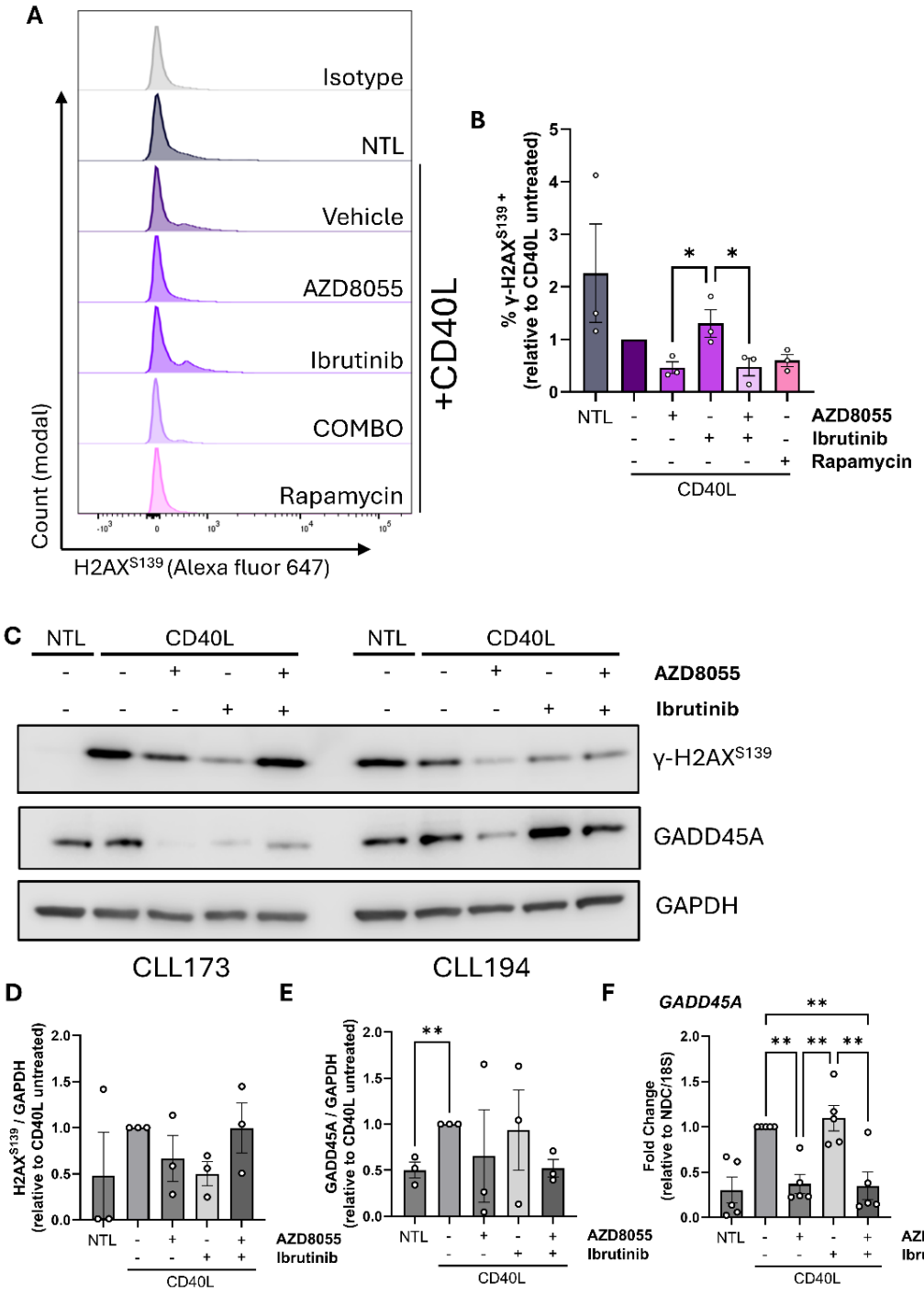

Figure 4.20: AZD8055 treatment depletes DNA-damage repair components in long-term CD40L co-cultures. Primary CLL cells were cultured for 8 days in CD40L co-culture (+10 ng/mL IL-4) ±100 nM AZD8055, 1 μM ibrutinib, alone or in combination, or 10 nM rapamycin single treatment. An unstimulated 'NTL' condition was also included. (A) CLL cells from 8-day CD40L co-cultures were isolated and stained with intracellular γ-H2AX^{S139} and visualised *via* flow cytometry (Alexa fluor 647). An Alexa fluor 647 isotype control was used to select cells positive for γ-H2AX^{S139} staining (presented in a FACS histogram). (B) Percentage of cells selected as γ-H2AX^{S139} positive, made relative to untreated cells on CD40L (n=3). (C) Western blot of protein lysates taken from 8-day CLL-CD40L co-cultures ±AZD8055 and/or ibrutinib to detect protein expression of γ-H2AX^{S139}, GADD45A and GAPDH. An unstimulated 'NTL' condition was also included. (D) Quantified protein expression of γ-H2AX^{S139}, normalised to GAPDH and made relative to untreated cells on CD40L. (E) Quantified expression of GADD45A, normalised to GAPDH and made relative to untreated cells on CD40L. (F) RT-qPCR of CLL cells following 8-day CD40L co-culture (+IL-4) to detect *GADD45A* transcript abundance, normalised to *18S* and presented as fold change relative to untreated cells on CD40L. Data points are depicted as white circles, and the data is represented as the mean ±SEM. All replicates are biological replicates from patient-derived CLL cells. Statistics were calculated using a Student's t-test for comparing samples ±CD40L, while one-way ANOVA was used to calculate statistics between CD40L-stimulated conditions, where * $p \leq 0.05$, ** $p \leq 0.01$.

4.3.16. FOXO-associated genes are regulated downstream of CD40 activation

As FOXOs regulate a plethora of transcriptional targets in a context- and cell-type-specific manner [429, 483, 484], we further investigated the expression of additional FOXO targets involved in discrete cellular functions in long-term CLL-CD40L co-culture: *IGF1R, MCL1, SESN3, CCNG2* and *BBC3* (Figure 4.21). *IGF1R* expression did not change following long-term CD40 stimulation (Figure 4.21A); AZD8055 and ibrutinib single/combination treatments induced an increase in *IGF1R* expression, albeit not significantly. *MCL1* was downregulated in CD40-stimulated cells, albeit not significantly (Figure 4.21B), where AZD8055 and/or ibrutinib did not affect *MCL1* expression (Figure 4.21B). However, *SESN3* expression was significantly increased in cells exposed to CD40L (Figure 4.21C) and was downregulated following combined AZD8055-ibrutinib treatment. Further, *CCNG2* expression was significantly induced in CD40-stimulated cells (Figure 4.21D) and was unaffected by AZD8055 and ibrutinib treatments. Unexpectedly, *BBC3* expression was significantly increased in CD40-stimulated cells (Figure 4.21E). While AZD8055 treatments significantly decreased *BBC3* expression, ibrutinib alone was unable to decrease *BBC3* expression (Figure 4.21E). These findings provide insight as to the expression of distinct FOXO target genes in following long-term CLL-CD40L interaction.

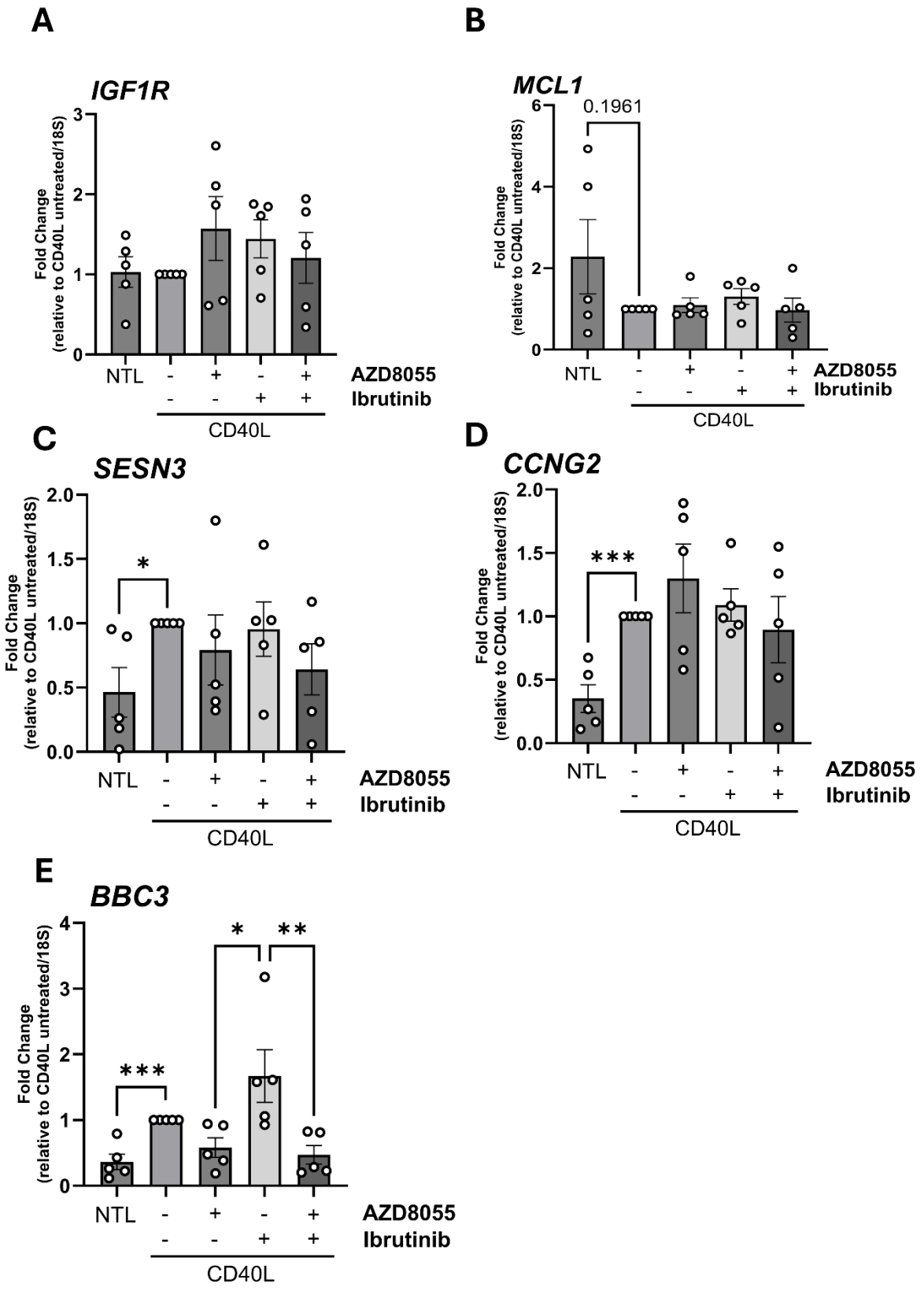

Figure 4.21: FOXO-associated genes are differentially regulated downstream of long-term CD40 stimulation. Primary CLL cells were cultured for 8 days in CD40L co-culture (+10 ng/mL IL-4) ±100 nM AZD8055 and/or 1 μM ibrutinib and were subsequently used to generate RNA samples to visualise gene expression *via* RT-qPCR. (A – E) Expression of *IGF1R* (A), *MCL1* (B), *SESN3* (C), *CCNG2* (D) and *BBC3* (E) was normalised to *18S* and presented as fold change relative to untreated cells on CD40L. Data points are depicted as white circles, and the data is represented as the mean ±SEM. All primary CLL replicates are derived from different patient samples. Statistics were calculated using a Student's t-

test comparing samples ±CD40L, while one-way ANOVA was used to calculate statistics between CD40L-stimulated conditions, where * $p \leq 0.05$, *** $p \leq 0.001$.

4.3.17. Selective FOXO1 inhibition attenuates an AZD8055-mediated block in CLL cell proliferation

To understand whether the anti-proliferative and anti-survival effects of AZD8055 are reliant on FOXO1 activity in CLL, we treated CLL cells with the FOXO1 inhibitor AS1842856 (Figure 4.22). Investigating the effect of 100 nM AZD8055 and 100 nM AS1842856 treatment, alone or in combination, on MEC1 (Figure 4.22A) and primary CLL (Figure 4.22B) proliferation *via* CTV staining, AZD8055 significantly blocked cell proliferation (Figure 4.22C). While AS8142856 single treatment did not affect MEC1 cell proliferation, AS1842856 pre-treatment attenuated an AZD8055-mediated block in MEC1 cell proliferation, demonstrated by a significant reduction in CTV MFI compared to AZD8055 single treatment (Figure 4.22C). In primary CLL co-cultures, CLL cell proliferation in the presence of CD40L with 10 ng/mL IL-4 (4.22D) or 15 ng/mL IL-21 (4.22E), was significantly blocked in cultures treated with AZD8055 alone (Figure 4.22 D & E). Interestingly, CLL cell proliferation was enhanced in cells treated with AS1842856 (Figure 4.22D & E), trending on significance for cells cultured with exogenous IL-4 ($p = 0.06$, Figure 4.22D). Mimicking results seen in MEC1 cultures (Figure 4.22C), AS1842856 pre-treatment attenuated a AZD8055-mediated block in primary CLL proliferation, regardless of exogenous cytokine, demonstrated by a significantly lower CTV MFI in AZD8055-AS1842856 combination treatment *vs.* AZD8055 single treatment (Figure 4.22D & E). These results are supported by changes in CLL cell count; MEC1 cells treated with AZD8055 had a significantly lower cell count than the vehicle control, which was significantly attenuated by AS1842856 pre-treatment (Figure 4.22F). In primary CLL cells, AZD8055 induced a modest reduction in cell count, albeit not significantly (Figure 4.22G), while AS1842856 treatment increased cell numbers. Of note, there was a significant difference in cell count between cells treated with AZD8055 and cells treated with AS1842856 (Figure 4.22G). Furthermore, AZD8055-AS1842856 combination treatment resulted in an average cell count reflecting that of untreated cells, demonstrating AS1842856's ability to rescue an AZD8055-mediated reduction in

cell count. Moreover, MEC1 cell apoptosis was significantly increased in cells treated with AZD8055 (supporting previous data in Figure 4.8) - a rise that was significantly attenuated by AS1842856 pre-treatment (Figure 4.22H). In contrast, AS1842856 treatment also increased MEC1 cell apoptosis (Figure 4.22H). This was defined more clearly in primary CLL cells, where AS1842856 treatment induced a significant reduction in cell viability when compared to the vehicle control (Figure 4.22I). Interestingly, primary cells treated with AS1842856 single treatment exhibited lower cell viability than cells treated with AZD8055, alone or in combination with AS1842856 (Figure 4.22I). These data demonstrate the ability of FOXO1 to induce cell cycle arrest and apoptosis downstream of pharmacological mTORC1/2 inhibition.

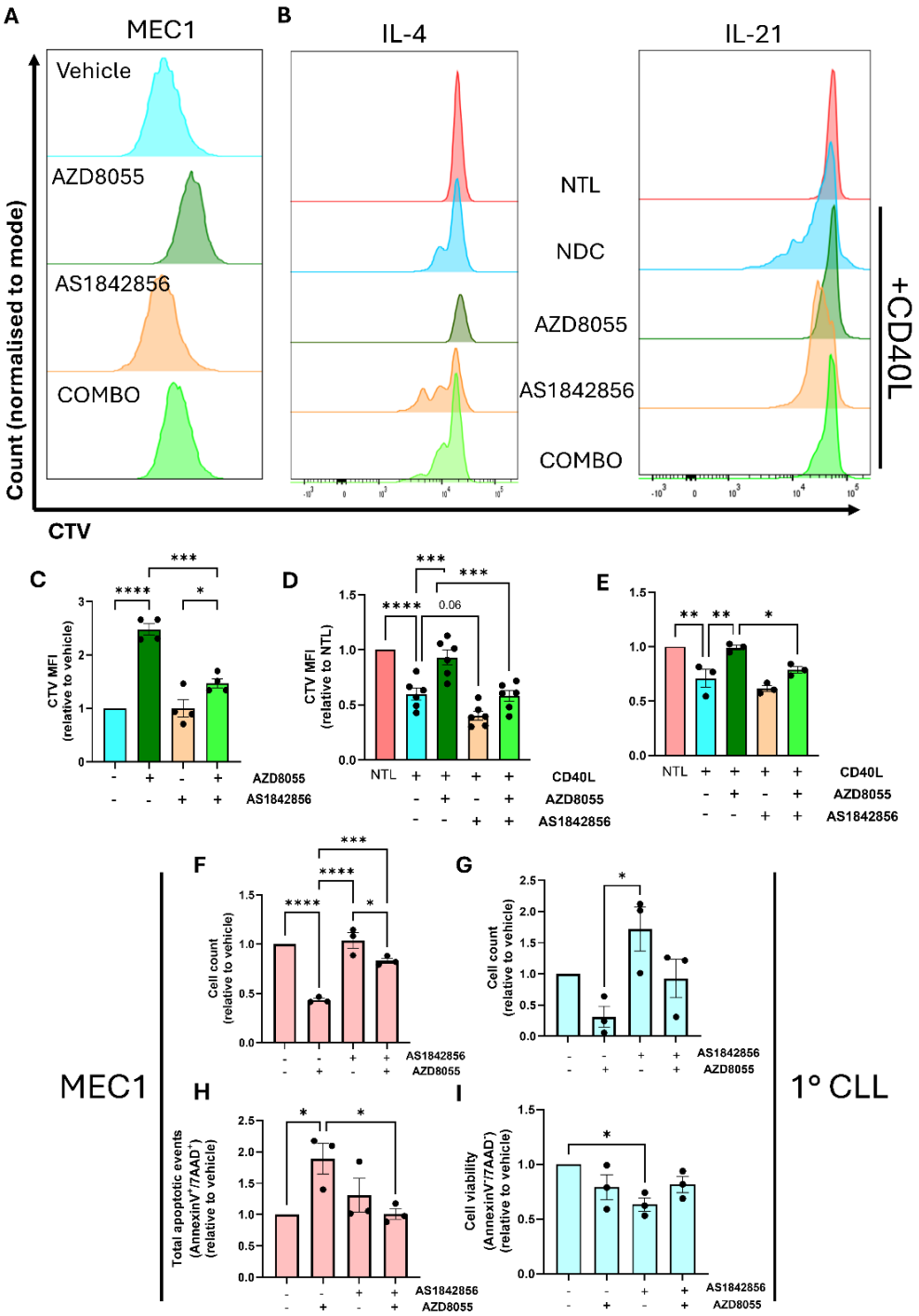

Figure 4.22: AS1842856 attenuates an AZD8055-mediated block in proliferation and reduction in MEC1 cell viability. (A) Representative histogram of CTV-stained MEC1 cells following 72 hr in culture ±100 nM AZD8055 and/or 100 nM AS1842856. Where applicable, cells were treated with AS1842856 30 min prior to addition of any other treatment. (B) Representative histogram of CTV-stained primary CLL cells in CD40L co-culture (+10 ng/mL IL-4 (left) or 15 ng/mL IL-21 (right)) following 5-14 days or 5 days in culture for IL-4 and IL-21 CD40L co-cultures, respectively. (C) Mean fluorescence intensity (MFI) of CTV in 72 hr MEC1 cultures ±AZD8055 and/or AS1842856, made relative to untreated cells (n=4). (D & E) CTV mean fluorescence intensities (MFI) of primary CLL cells following long-term CD40L co-culture +IL-4 (D) or IL-21 (E) ±AZD8055 and/or AS8142856, made relative to the unstimulated 'NTL' control (D: n=6, E: n=3). (F-G) Cell counts attained from MEC1 (F) and primary CD40L co-cultures (+10 ng/mL IL-4) using CountBright™ Absolute Counting Beads *via* flow cytometry analysis following 3 days (MEC1, F) or 3-5 days (primary CLL cells, G) in culture ±100 nM AZD8055 and/or 100 nM AS1842856. (H) Annexin/7AAD staining was conducted in MEC1 cells following 72 hr in culture ±AZD8055 and/or AS8142856 to determine cell apoptosis ($Annexin^{pos}/7AAD^{pos}$), made relative to untreated cells (n=3). (I) Primary CLL cells deemed 'viable' ($Annexin^{neg}/7AAD^{neg}$) following Annexin V/7AAD staining of 3–5-day primary CLL-CD40L co-cultures (+10 ng/mL IL-4), made relative to untreated cells (n=3). Data points are depicted as black circles, and the data is represented as the mean ±SEM. All primary CLL replicates are derived from different patient samples. Statistics were calculated using a one-way ANOVA, where * $p \leq 0.05$, ** $p \leq 0.01$, *** $p \leq 0.001$, **** $p \leq 0.0001$.

4.3.18. AS8142856 treatment affects FOXO family expression in long-term CD40L co-culture

As FOXOs are known to regulate other FOXO transcription factors [555], we addressed whether FOXO family expression is influenced by FOXO1 activity by treating 1- and 10-day CD40L co-cultures (+10 ng/mL IL-4) with 100 nM AS1842856. FOXO3 protein expression, which was significantly increased over the course of 10 days in CD40L co-culture (Figure 4.23A), was significantly attenuated by AS1842856 treatment (Figure 4.23B). On the other hand, FOXO1 protein expression did not exhibit any change in expression over 10 days (Figure 4.23C). AS1842856 treatment at 1 and 10 days did not influence FOXO1 protein expression (Figure 4.23C). Further, we investigated whether AS1842856 treatment affected the expression of *FOXO1, FOXO3, FOXO4* and *FOXO6* over 10 days in CD40L co-culture *via* RT-qPCR (Figure 4.23D-G). Here, *FOXO3* expression was unchanged over 10 days, irrespective of AS1842856 treatment (Figure 4.23D). Although FOXO1 protein expression exhibited nominal change (Figure 4.23C), *FOXO1* expression was significantly higher in CLL cells treated with AS1842856 for 10 days than in short-term, untreated cells (Figure 4.23E). Further, *FOXO4* expression was significantly increased in 10-day cultures compared to 1-day cultures, which was significantly attenuated by AS1842856 treatment (Figure 4.23F). Finally, *FOXO6* transcript abundance exhibited a slight

decrease over the course of 10 days, albeit not significantly, and was unaffected by AS1842856 treatment (Figure 4.23G). Of note, short-term CD40-CD40L engagement effectively downregulated *FOXO1, FOXO3, FOXO4* and *FOXO6* expression compared to the NTL control (Figure 4.23D-G, discussed in Figure 3.10).

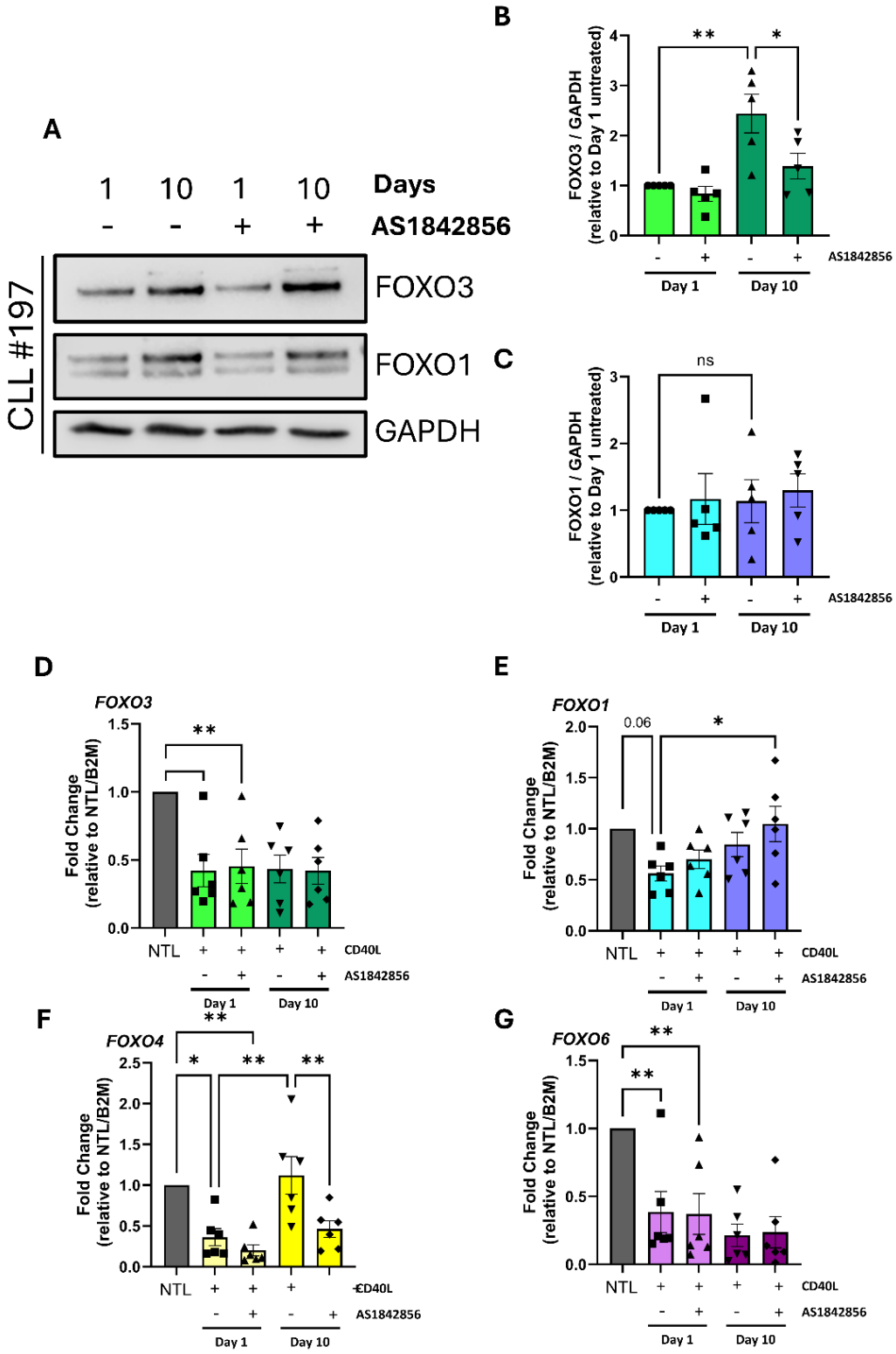

Figure 4.23: Differential FOXO expression in long-term CD40L co-cultures is affected by AS1842856 treatment. (A) Western blot of primary CLL cells co-cultured in CD40L co-culture for 1-10

days (+10 ng/mL IL-4) ±100 nM AS1842856 assessing the expression of FOXO3 and FOXO1. GAPDH was used as a loading control. (B & C) Quantified expression of FOXO3 and FOXO1 following 1 and 10 days in CD40L co-culture (+IL-4) ± AS1843856, normalised to GAPDH and made relative to untreated cells at day 1 (n=5). (D-G) RNA samples were generated from primary CLL cells in 1-10 day CD40L co-culture (+IL-4) ±100 nM AS1842856 to investigate the expression of *FOXO3* (D), *FOXO1* (E), *FOXO4* (F) and *FOXO6* (G) *via* RT-qPCR. An unstimulated 'NTL' sample was also collected at 24 hr (represented by the grey bar). *FOXO* expression values were normalised to *B2M* and presented as fold change relative to the unstimulated 24 hr control (n=6). Data points are depicted as black icons, and the data is represented as the mean ±SEM. All replicates are biological replicates from different patient samples. Statistics were calculated using a one-way ANOVA, where * $p \leq 0.05$, ** $p \leq 0.01$.

4.3.19. FOXO1 inhibition enhances AZD8055- and ibrutinib-mediated cytoplasmic depletion of FOXO4 in MEC1 cells

AS1842856 treatment has been shown not to affect the subcellular localisation of FOXO1 in CLL cells [49]. However, it is not known whether selective FOXO1 inhibition affects the activity and therefore subcellular localisation of other FOXO transcription factors, as functional redundancy may play a role in the rescue of FOXO dysfunction [428]. Therefore, we evaluated the effect of 100 nM AS1842856 treatment on cytoplasmic and nuclear localisation of FOXO4 in MEC1 (Figure 4.24A) and HG3 (Figure 4.24D) cells following short-term 100 nM AZD8055 and 1 μM ibrutinib treatment, alone or in combination. MEC1 cells exhibited significantly reduced cytoplasmic FOXO4 expression following treatment with AZD8055 and ibrutinib, enhanced in combination (Figure 4.24B), supporting previous findings (Figures 4.10 & 4.14). Further, AS1842856 alone significantly depleted cytoplasmic FOXO4, which was further enhanced with AZD8055-ibrutinib treatment (Figure 4.24B). These findings were corroborated by the nuclear localisation of FOXO4 in MEC1 cells, which was increased following drug treatment (Figure 4.24C).

HG3 cells exhibited a similar profile, where AZD8055 and ibrutinib treatments significantly depleted cytoplasmic FOXO4, alone or in combination, with combination treatment enhancing cytoplasmic FOXO4 depletion, trending towards significance ($p = 0.06$, Figure 4.24E). AS1842856 treatment also depleted cytoplasmic FOXO4 in HG3 cells (Figure 4.24E), though combining AS1842856 with AZD8055 and ibrutinib did not change cytoplasmic FOXO4 expression (Figure 4.24E). This was supported in FOXO4's nuclear localisation,

with AZD8055 and ibrutinib treatments enhancing FOXO4 nuclear expression (Figure 4.24F, supporting Figure 4.10), while AS1842856 treatment did not affect FOXO4 nuclear accumulation (Figure 4.24F).

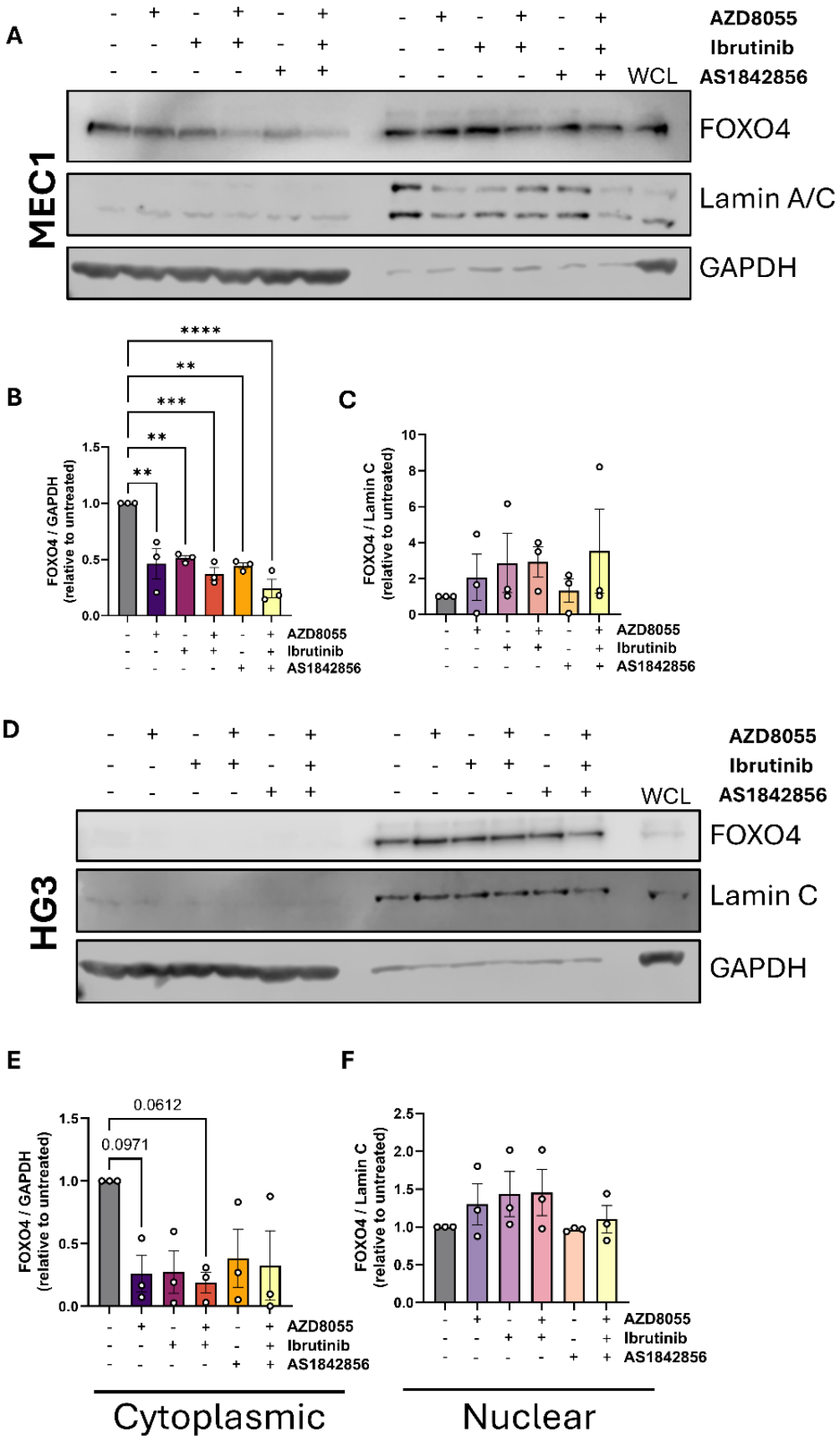

Figure 4.24: AS1842856 treatment depletes cytoplasmic FOXO4 expression. (A) Western blot to detect FOXO4 in MEC1 cytoplasmic and nuclear cell lysates generated *via* subcellular fractionation following 1 hr treatment with 100 nM AZD8055 and 1 μM ibrutinib, alone or in combination, or 100 nM AS1842856 treatment or AS1842856 combined with AZD8055 and ibrutinib. Where applicable, cells were treated with AS1842856 30 min prior to addition of any other treatment. Lamin A/C and GAPDH were used as nuclear and cytoplasmic loading controls, respectively. (B) Quantified expression of FOXO4 in MEC1 cytoplasmic compartments, normalised to GAPDH and made relative to untreated cells. (C) Quantified expression of FOXO4 in MEC1 nuclear compartments, normalised to Lamin A/C and made relative to untreated cells (n=3). (D) Western blot to detect FOXO4 in HG3 cytoplasmic and nuclear cell lysates generated *via* subcellular fractionation following 1 hr treatment with 100 nM AZD8055 and 1 μM ibrutinib, alone or in combination, or 100 nM AS1842856 treatment or AS1842856 combined with AZD8055 and ibrutinib. Lamin A/C and GAPDH were used as nuclear and cytoplasmic loading controls, respectively. (E) Quantified expression of FOXO4 in HG3 cytoplasmic compartments, normalised to GAPDH and made relative to untreated cells. (F) Quantified expression of FOXO4 in HG3 nuclear compartments, normalised to Lamin A/C and made relative to untreated cells (n=3). Data points are depicted as white circles, and the data is represented as the mean ±SEM. Statistics were calculated using a one-way ANOVA, where ** $p \leq 0.01$, *** $p \leq 0.001$, **** $p \leq 0.0001$.

4.4. Discussion

This chapter provides novel insight as to how BCR and CD40 engagement administer strict regulation of the expression and activity of FOXO3 and FOXO4 downstream of PI3K-AKT-mTOR signalling. Pharmacological mTORC1/2 inhibition induced upregulation of *FOXO3* and *FOXO4* in CLL cells, coincident with aberrant FOXO target gene expression, cell cycle arrest and cell death, strongly suggesting that the activity of the PI3K-AKT-mTOR axis is critical to induce CD40-mediated downregulation of FOXO family genes. Pharmacological mTORC1/2 inhibition demonstrated that FOXO3 and FOXO4 are regulated by mTORC2-AKT downstream of BCR and CD40 activation. Furthermore, pharmacological abrogation of AKT-mTOR-mediated signalling did not alleviate a block on FOXO nuclear localisation; rather, alleviation of AKT-mediated FOXO phosphorylation enhanced nuclear FOXO expression, supporting earlier findings that CLL cells harbour distinct nuclear FOXO3 and FOXO4 activity and alluding to a need for FOXO activity to control cell fate decisions irrespective of CLL-TME engagement. In addition, long-term CD40L co-cultures exhibited sustained CD40-mediated FOXO family gene expression and AKT-mediated FOXO4 inactivation, supporting a 'goldilocks' principle of FOXO expression and regulation which favours CLL cell survival while prohibiting tumour-suppressive FOXO activity induced by the abrogating survival signalling. Consistent pro-survival signalling in CLL-CD40L co-cultures was corroborated by sustained expression of BCL2-like proteins (BCL-XL, BIM and MCL1) in long-term cultures. Further, depletion of DNA-damage-associated markers *via* inhibition of mTORC1/2 signalling highlights the importance of CD40 activation in promoting survival by utilizing mechanisms of response to environmental stressors, perhaps mediated by FOXO activity. Finally, selective FOXO1 inhibition *via* AS1842856 treatment eliciting enhanced CLL cell proliferation supports published work that FOXO1 harbours tumour suppressive characteristics in CLL.

4.4.1. Pharmacological mTOR inhibition increases *FOXO3* and *FOXO4* expression

The bulk RNAseq dataset provided a wealth of data pertaining to changes in the CLL genomic landscape following CD40-CD40L engagement as well as the effect of pharmacologically abrogating downstream signals *via* AZD8055 and ibrutinib treatments in CD40-activated cells. It is worth noting that AZD8055 and ibrutinib were selected as a viable combination treatment due to exhibiting synergistic effects in primary CLL cells [284]. As well as following BCR activation, BTK is activated downstream of the CD40 receptor [569] and is purported to alter CD40-mediated signalling [570], indicating ibrutinib treatment as a viable strategy to prohibit CLL-TME interactions regardless of BCR or CD40 activation. These data are currently being utilised as part of bioinformatic analyses conducted within the group which could reveal potential new avenues of research concerning the tumour-suppressive effects of pharmacological mTOR inhibition in proliferating CLL cells.

Global heatmaps outlined how CD40L stimulation 'inversed' the distinct genetic profile of circulating CLL cells, of which was markedly influenced by AZD8055 treatment. Of note, the potency of AZD8055 was consistent between patients, irrespective of sample heterogeneity. PCA plotting of patient samples revealed distinct heterogeneous characteristics between samples highlighted by differences in sample variance. Of note, drug treatments did not affect sample variance. However, there was a clear separation of samples dependent on exposure to CD40L, reflecting how CD40 activation characteristically influences gene regulation downstream of multiple intracellular effectors [218, 220] - evidenced by a significant differential expression of 3733 genes. In cells exposed to CD40L, there was a marked impact on NFκB-associated genes including *BCL2A1* and *CD40LG*. Interestingly, these genes were also upregulated in a recent study investigating NF-κB transcriptional activity downstream of CLL-CD40 activation [237], illustrating the prominence of NF-κB activity downstream of CD40 activation [220]. In addition, distinct survival-associated genes such as *BCL2L1* and *MYC*, as well as genes involved in cytokine interactions (e.g. *CCR4,*

CCR7, CCL13, CCL22) were induced by CD40 stimulation, supporting previous findings in primary samples stimulated with exogenous IL-21 [223]. Increased *BCL2L1* expression corroborates findings in Figures 3.4 and 3.5, demonstrating a CD40-meditated favouring of survival protein expression [571]. Moreover, downstream of CD40-PI3K-AKT, there was also a marked downregulation of *FOXO3* and *FOXO4* expression, corroborating previous findings attained *via* RT-qPCR that CLL-CD40L co-cultures exhibit downregulation of genes encoding FOXO family members (Figures 3.4 & 3.5, discussed in section 3.3.2). Further, treatment with AZD8055 significantly increased *FOXO3* and *FOXO4* expression. These data support findings by Cosimo *et al*. revealing that AZD8055 treatment upregulates *FOXO1* and *FOXO4* expression following $F(ab')_2$-mediated BCR activation [284] and provide further insight concerning the regulation of FOXO4 downstream of CLL-TME interactions. Moreover, *FOXO4* upregulation following ibrutinib treatment illustrates how multiple downstream effectors of CD40 (e.g. activation of BTK [569]) collectively contribute to PI3K-AKT-mTOR activation. This is supported by *FOXO4* upregulation being enhanced in cells treated with AZD8055-ibrutinib combination treatment. In this context, the upregulation of genes encoding FOXO isoforms could be detrimental to cell function, akin to FOXO1 activity downstream of BCR ligation [284]. In mice with CLL-like disease, AZD8055's clinical analogue AZD2014 has been shown to synergise with ibrutinib to enhance ibrutinib's effectiveness in reducing tumour burden [284]. In DLBCL and subtypes of CNS lymphoma, AZD2014-ibrutinib combination therapy is synergistic and enhances apoptosis [572, 573]. Mechanistically, it is tempting to speculate that this could be due to the transcriptional programme governed by FOXO transcription factors. As FOXOs are known to regulate their own expression (and expression of other isoforms) [555], it could be that AZD8055 induces a positive feedback loop to upregulate FOXO isoform gene expression *via* AZD8055-mediated FOXO activity, though this remains to be elucidated. Nonetheless, the potency of AZD8055 treatment in altering the CLL genomic landscape downstream of CD40 activation to elicit anti-proliferative effects determines AZD8055 as the driver in 'synergistic' AZD8055-ibrutinib treatments, and that ibrutinib treatment serves to enhance effects elicited by AZD8055 in the short-term. This is also apparent in long-term cultures (Figures 4.17 – 4.21), further highlighting the potency of AZD8055 treatment in multiple *in vitro* contexts. In the context of FOXO signalling, this is as expected due to its ability to target

mTORC1/2 signals that directly regulate FOXO activity [284]. Although, ibrutinib treatments – along or in combination with AZD8055 - did serve to enhance FOXO3/4 transcript expression and nuclear import (e.g. Figure 4.6 & 4.14), coinciding with increased pro-apoptotic signalling (e.g. increased BIM in Figures 4.7 & 4.8), suggesting combination treatment is synergistic in certain contexts. Further, as MEC1 and HG3 cells exhibit constitutive signalling as opposed to PB-resident CLL cells, differences in gene expression may be cell-type- and context-specific [574], perhaps explaining cell-type-specific differences in *CDKN1B*, *GADD45A* and *SESN3* expression. Nevertheless, an AZD8055-mediated depletion of *SESN3* in HG3 cells and *GADD45A* depletion in MEC1 cells could infer tumour-suppressive FOXO behaviour, diminishing components of intracellular oxidative and DNA damage repair to facilitate CLL cell death [575, 576].

4.4.2. AZD8055 and ibrutinib reduce CLL cell viability, coincident with FOXO4 depletion

The synergistic effect of AZD8055 and ibrutinib highlighted by Cosimo *et al*. and Michael Moles [49, 284] highlight therapeutic potential in the joint targeting of BTK and mTORC1/2 signals. Here, our data reinforce the synergistic effect of AZD8055 and ibrutinib at inducing active FOXO evidenced by a block in MEC1 proliferation and induction of cell death coinciding with *CCND1* downregulation [577], decreased cell count and increased BIM expression. However, while AZD8055 increases FOXO family gene expression in CLL cell line and patient samples (revealed by the RNA-Seq dataset) in the short-term, long-term MEC1 and HG3 cultures exhibited a depletion of FOXO4 protein expression. In multiple cancers, FOXO expression and subsequent activity is associated with disease prognosis [574] and, in certain cancer contexts, heightened FOXO expression is associated with drug resistance. For example, in non-small cell lung cancer (NSCLC), Bing *et al*. demonstrated an association of FOXO3 upregulation with resistance to gefitinib TKI treatment [578]. In leukaemic cells, Hui *et al*. revealed that FOXO3 is necessary to promote enhanced PI3K-AKT signalling in CML cells, subsequently driving drug resistance [579]. Further, as previously mentioned, FOXO4 expression is required to promote self-renewal, drug

resistance and colony formation in DLBCL [545]. These findings allow us to speculate that, while AZD8055 treatment elicits tumour suppressive effects *via* downstream FOXO1 activity in the short-term [284], another mechanism of action of AZD8055 treatment could result in a depletion of FOXO4 protein expression, thereby repressing the maintenance of cells potentially governed by other FOXO isoforms such as FOXO4. In soft tissue sarcoma, AML and breast cancer, FOXO1 downregulation is associated with reduced survival [517, 580, 581], demonstrating that distinct FOXO family members can modulate survival in a cell-type and context-specific manner. To investigate this further, it would be worth exploring whether *FOXO4* gene expression is disrupted by combined AZD8055-ibrutinib treatment at later timepoints.

4.4.3. Pharmacological BTK and/or mTORC1/2 inhibition induces FOXO3 and FOXO4 nuclear shuttling in CLL

The PI3K-AKT axis is perhaps the most well defined regulator of FOXO activity in normal and pathophysiological scenarios, where AKT-mediated FOXO phosphorylation marks FOXO for nuclear export *via* binding of the phospho-binding protein 14-3-3, typically associated with enhanced cell proliferation and survival [428]. Previous investigation within our group demonstrated that FOXO1 is actively phosphorylated downstream of AKT activity in the context of CD40-CD40L engagement. Here, we demonstrated that the abrogation of BTK and mTORC1/2 activity *via* ibrutinib and AZD8055 treatment increased the nuclear abundance of FOXO3 and FOXO4. Previous study in hepatocarcinoma cells by Patra *et al*. revealed AZD8055 treatment effectively induced FOXO3 nuclear localisation and an enhancement of pro-apoptotic BIM expression [582]. Further, work by Jimenez *et al*. revealed that AZD8055 mediates the nuclear shuttling of FOXO1, FOXO3 and FOXO4 in neuroblastoma and osteosarcoma cell lines [583]. In Figure 4.10, AZD8055 and ibrutinib combination treatment depleted AKT-mediated FOXO4 phosphorylation ($FOXO4^{S193}$) in MEC1 and HG3 cells, coincident with significantly increased nuclear FOXO4 expression in HG3 cells. These findings illustrate the capability of AZD8055 in prohibiting mTOR-AKT-mediated

regulation of FOXO3 and FOXO4 in different disease contexts, including CLL. However, study of AKT-mediated FOXO regulation in CLL cell lines was limited by a lack of detection of FOXO3 in HG3 cells and, in MEC1 cells, combined AZD8055-ibrutinib treatment did not affect FOXO3^{S253} levels. These effects have been seen in other cancer cell lines; for example, in adenocarcinoma cells, AZD8055 treatment effectively depletes AKT^{S473} while only transiently affecting the phosphorylation of AKT effectors, including FOXO1 and FOXO3 [406], demonstrating a cell-type-specific response of AKT effectors to AZD8055 treatment. As such, we focused on elucidating AKT-mediated FOXO3 and FOXO4 phosphorylation downstream of BCR and CD40-mediated signals in primary patient cells. While AZD8055 and ibrutinib treatments diminished FOXO3^{S253}, FOXO3 is constitutively expressed in the nucleus, indicating that FOXO3 exhibits activity regardless of BCR ligation. This could be due to positive feedback loops reinforcing FOXO activity such as AMPK or JNK [445, 446] which have yet to be explored. FOXO4^{S193} levels were also increased following F(ab')$_2$-mediated BCR activation, indicating that AKT does regulate the wider FOXO family downstream of BCR signalling. These experiments revealed an abundance of FOXO4 in the nucleus of PB-resident CLL cells actively shuttled to the cytoplasm upon BCR activation, where AZD8055 treatment induced further FOXO4 nuclear localisation, supporting previous findings that AKT directly phosphorylated and regulated FOXO4 localisation in MEC1 cells (Figure 3.9).

These results are mimicked in cells engaged in the CD40L(+IL-4) co-culture model, demonstrating FOXO regulation downstream of PI3K-AKT activation in multiple contexts [247]. Moreover, FOXO4^{S193} levels were effectively depleted by combined AZD8055 and ibrutinib treatment. Interestingly, FOXO4 nuclear abundance was most prevalent in cells treated with ibrutinib, while AZD8055 potentiated an ibrutinib-mediated increase in FOXO3 nuclear abundance in CLL-CD40L co-cultures. As previously mentioned, CD40 can indirectly activate BTK irrespective of BCR activation [569] so, in this context, an increase in nuclear FOXO4 aligns with a potential mechanism of ibrutinib treatment. The RNA-Seq dataset indicated that ibrutinib treatment had little effect on the genomic landscape of CLL cells in CD40L co-culture. However, it did lead to an upregulation of *FOXO4* (Figure 4.4). These findings support a mechanism of FOXO expression, nuclear abundance and subsequent activity downstream of

pharmacological BCR- and CD40-BTK inhibition in CLL cells. FOXOs are known to be critical regulators of cell migration and cancer metastasis (reviewed in [424]); therefore, we speculate that one mechanism through which ibrutinib induces transient lymphocytosis in TME-resident CLL cells is by attenuating BTK-PI3K-AKT signalling and subsequent activation and upregulation of FOXO transcription factors, thereby facilitating FOXO-mediated cell migration to PB compartments. As well as in the context of lymphocytosis, constitutive FOXO activity could be necessary for facilitating CLL cell re-entry to proliferative lymphoid tissue compartments. Work by Seda *et al*. demonstrated a capability of FOXO1 to induce *GAB1* expression, subsequently promoting GAB1-mediated migration of circulating CLL cells to lymphoid tissues [502]. Of note, this work also revealed heightened expression of *FOXO1* and *FOXO3* in CLL cells harbouring a phenotype indicative of long-term PB circulation ($CXCR4^{bright}/CD5^{dim}$) compared with PB CLL cells that have recently entered the PB compartment ($CXCR4^{dim}/CD5^{bright}$) [502], supporting a downregulation of FOXO activity mediated by TME signals (as discussed in section 3.3.2), but also of FOXO1/3 activity in circulating CLL populations. These findings allude to FOXO1, FOXO3 and potentially FOXO4 expression being required as part of the PB-CLL phenotype to facilitate homeostasis, maintenance of quiescence and possibly cell migration. Further investigation would need to be conducted to understand the intricacies of FOXO biology in the context of CLL cell migration. Nevertheless, unpublished work as part of our lab reveal that, downstream of CD40 activation, modulating discrete FOXO expression affects the secretion of chemotaxis-promoting chemokines such as CCL20 (Jodie Hay, unpublished). Supporting this, in hepatocellular carcinoma (HCC) cells, FOXO1 drives CCL20 transcription by enhancing NF-κB binding to the *CCL20* promoter [518] - a mechanism that could exist in CLL cells *via* the CD40-NF-κB axis [220]. Indeed, these findings support the idea of a context-dependent expression of FOXOs leading to either supportive or detrimental cellular outcomes, where FOXO quiescent populations require FOXO expression while FOXO activation in BCR-activated LN-CLL cell populations could induce detrimental outcomes [284].

In long-term CLL-CD40L co-cultures, AKT-mediated phosphorylation of FOXO3 and the distinct regulation of *FOXO1, FOXO3* and *FOXO4* was sustained, demonstrating that CD40-mediated FOXO regulation is a necessary consequence

of CLL-CD40L engagement, regardless of time spent in culture. This is akin to that of powerful FOXO regulation as seen in GC-resident B-cells [463], highlighting the importance of FOXO activity in a context-dependent manner, where tight regulation of FOXOs by major intracellular signalling axes skews the activity of FOXO family members to favour proliferation and survival while simultaneously negating their distinct tumour suppressive capabilities.

4.4.4. mTOR inhibition induces cellular dysfunction associated with FOXO target gene regulation

Using the established CD40L+IL-4 system, primary patient cells exhibited significant proliferative capacity, albeit at later time points than samples cultured with exogenous IL-21. IL-4 and IL-21 induce unique downstream effects within B-cells: IL-4 binds to the IL-4R, initiating JAK1/3-mediated STAT6 phosphorylation, which then undergoes nuclear translocation and promotes anti-apoptotic gene transcription [584]. In contrast, IL-21 binds to IL-21R, activating STAT1, 3 and 5, which can facilitate both pro- and anti-apoptotic effects [585]. IL-21 has been shown to induce subsequent activation of BIM [586], inferring a cytokine-dependent regulation of FOXO activity. The functional differences of IL-4 and IL-21 in CLL disease biology may explain the differences in CLL cell proliferation and expression of BCL-XL (*BCL2L1*) and BIM (*BCL2L11*) as seen in Figures 3.4 & 3.5. Nevertheless, AZD8055 treatment effectively prohibited proliferation, irrespective of exogenous cytokine. Furthermore, upregulation of *CCND2* and *CDKN1A* ($p21^{cip1}$) in cells exposed to CD40L alludes to disparate FOXO activity, as FOXOs are known to repress *CCND2* while inducing *CKDN1A* expression. Specifically, *CCND2* (Cylin D2) is responsible for facilitating cell proliferation, while *CDKN1A* ($p21^{cip1}$) typically acts as an inhibitor of cell cycle progression [559, 560]. Increased $p21^{cip1}$ therefore appears counterintuitive downstream of CD40 activation. However, $p21^{cip1}$ upregulation has been reported as a necessary downstream effect of CD40 activation in resting B-cells to facilitate cyclin D family nuclear translocation [521]. This is corroborated in MM cells, where both p53 and $p21^{cip1}$ are induced downstream of CD40 [587]. These

results outline a bi-modal role for the FOXO target $p21^{cip1}$ (*CDKN1A*) in facilitating and prohibiting cell cycle progression in a context-dependent manner. Of note, CD40-mediated *CCND2* and *CDKN1A* expression were also observed in short-term CLL-CD40L co-cultures (Figure 4.2), corroborating these findings. Further, $p27^{kip1}$, another potent cell cycle inhibitor and FOXO target [588], was depleted following long-term CD40L co-culture - an effect also observed in resting B-cells [521], outlining how CD40-mediated FOXO phosphorylation and downregulation dampens tumour-suppressive effects elicited by FOXO family members such as upregulating $p27^{kip1}$. Although AZD8055 effectively prohibited long-term CLL cell proliferation, the effect of AZD8055 and ibrutinib treatment on *CCND2*, *CDKN1A* and *CDKN1B* expression was highly sample variant, so no conclusions can yet be drawn from these results. *CCNG2* was also upregulated in CLL-CD40L co-culture, indicative of an increase in both positive and negative regulators of cell cycle progression regulated by FOXOs [589], though more work will be needed to elucidate the behaviour of the FOXO signalling pathway in long-term CLL-CD40L co-cultures.

PI staining highlighted the importance of PI3K-AKT-mTOR-mediated signalling in proliferating CLL cells, whereby pharmacological abrogation of mTOR-mediated signalling prohibited G_0/G_1-S phase transition, reflected by a significant depletion of the S-phase population. As an mTORC1 inhibitor, rapamycin is known to mechanistically suppress p70-S6K activity, thereby prohibiting G_1-S transition [590]. Hashemolhosseini *et al*. found that rapamycin prevented the accumulation of cyclin D family proteins [591], indicative of FOXO activity downstream of selective mTORC1 inhibition. However, study in colon cancer cells revealed that FOXO1 is inactivated downstream of rapamycin treatment [592], inferring an alternative mechanism of rapamycin-mediated G_1 growth arrest in proliferating CLL cells. This is supported by work from our group describing that AKT-mediated phosphorylation of FOXO1 and subsequent cytoplasmic shuttling occurs irrespective of rapamycin treatment [49]. Further work should elucidate whether selective abrogation of mTORC1-mediated signals affect the subcellular localisation and subsequent activity of FOXO3 and FOXO4 in CLL cells. However, a similar profile of cell cycle arrest exhibited by AZD8055 and rapamycin treatment determine that the effects pertaining to drug-mediated cell cycle arrest emanate specifically from mTOR1-mediated effectors such as S6K and not

from mTORC2-AKT. AZD8055 also induced cell death in CLL-CD40L co-cultures, coincident with BCL-XL (*BCL2L1*) depletion and BIM (*BCL2L11*) upregulation, highlighting that sustained anti-apoptotic signalling by these factors is essential for mediating cell survival in proliferating CLL cells. In contrast, the FOXO target gene *BBC3* [593] was upregulated following CD40 activation. The *BBC3* gene codes for the BH3-only protein PUMA – a pro-apoptotic BCL2 family member that functions by facilitating BAX/BAK-mediated cytochrome C release and subsequent caspase-induced cell death – a similar mechanism to that elicited by the FOXO-BIM axis [363, 594]. However, Clybouw *et* al. revealed *in vivo* and *in vitro* that PUMA expression is essential for regulating B-cell immune activation by T-cells [595], illustrating an alternative paradigm for *BBC3* expression in CLL, perhaps orchestrated by FOXO activity. These findings are partnered with sustained *MCL1* gene downregulation; the MCL1 protein is known to harbour pro- and anti-apoptotic tendencies (reviewed in [596]), which could explain a depletion of *MCL1* gene expression following CD40L engagement.

Next, we revealed that the expression of distinct DNA-damage-associated markers were induced in cells engaged in long-term CD40L interactions. PARP is a critical component of DNA damage repair, with its cleavage being associated with programmed cell death [597]. Here, both total and cleaved forms of PARP were expressed downstream of CD40 activation. High expression of cleaved PARP contrasts the pro-survival nature surrounding CD40 activation; one explanation is that PARP is reported as a cofactor to promote NF-κB-dependent gene expression [598]; NF-κB signalling is strongly activated downstream of CD40 ligation [599], so it is likely that, as well as regulating distinct cellular fate decisions, PARP is required to mediate NF-κB transcriptional activity. Additionally, PARP has been reported to associate with p21 to control fork progression and subsequent DNA replication [600], which could explain an association and potential coexpression of PARP and $p21^{cip1}$ expression downstream of long-term CD40L activation in the context of replication stress. Indeed, PARP upregulation could explain an abundance of its cleaved form.

Furthermore, increases in γ-$H2AX^{S139}$ and GADD45A expression were noted in proliferating CLL cells. γ-$H2AX^{S139}$ actively accumulates at sites of double histone breaks [601], acting as a foundation for assembling repair foci [602]. As such, it is a suitable marker for assessing DNA damage accumulation. Pharmacological

mTOR inhibition by AZD8055 and rapamycin prohibited γ-H2AX accumulation in long-term CD40L co-cultures, suggesting an mTOR-mediated mechanism of DNA damage repair in CLL cells. Silvera *et al*. discovered in breast cancer cells that mTORC1/2 activity orchestrated both DNA damage repair and cell survival [603]. Furthermore, Chen *et al*. revealed in the MCF7 breast cancer cell line that rapamycin suppressed double-strand break repair [604], suggesting that γ-H2AX^{S139} depletion induced by pharmacological mTOR inhibition could indicate a reduction of mTOR-mediated DNA damage repair components without fully alleviating DNA damage. Literature investigating the consequences of AZD8055 treatment on intracellular γ-H2AX^{S139} accumulation are conflicting; Huang *et al*. demonstrated that AZD8055 treatment attenuated γ-H2AX^{S139} accumulation in colon cancer cells; however, in rhabdomyosarcoma, Zhou *et al*. revealed that AZD8055 treatment induced γ-H2AX^{S139} accumulation [605, 606]. While the implications of pharmacological mTORC1/2 inhibition are not fully clear, these data highlight the importance of mTOR activity in regulating DNA damage repair mechanisms, perhaps *via* the regulation of FOXO transcription factors. Further assessment *via* immunofluorescent staining would serve to determine whether γ-H2AX^{S139} accumulation seen *via* flow cytometry coincides with the generation of actual γ-H2AX foci that can be used to recruit DSB repair components.

GADD45A - a known FOXO target [439] - was significantly upregulated downstream of long-term CD40 engagement. Irrespective of AKT-mediated phosphorylation, this could infer that FOXO activity mediates distinct cellular functions downstream of CD40 such as the DNA damage response. Although, GADD45 activity may stem from CD40-NF-κB (reviewed in [607]), which has been shown to occur in CLL cells downstream of CD40 activation [237], albeit in GADD45 family members that are not FOXO targets. Wingert *et al*. found that *GADD45A* is constitutively expressed in HSCs and their progeny [608], revealing a role for GADD45A in promoting cell maintenance and development. GADD45A has also been implicated in promoting DNA damage repair by promoting DNA methylation *via* direct interactions with histones [609]. However, it is also a major driver of checkpoint arrest at the S- and G_2/M phases of the cell cycle [610, 611]. As we see that AZD8055 significantly depleted *GADD45A* transcript abundance, we could speculate that a mechanism of action of AZD8055 involves abrogating mTORC2-AKT-mediated FOXO phosphorylation, leading to FOXO-

mediated *GADD45A* downregulation which in-turn reduces S-phase cell populations, as seen following AZD8055 treatment in long-term CD40L co-cultures (Figure 4.17). Another mechanism could be that GADD45A and γ-H2AX act as indicators of replication stress and, with an AZD8055-mediated abrogation of a transition into the S-phase, DNA replication stress is reduced, thus depleting intracellular γ-H2AX and GADD45A [612]. Indeed, further replicates would need to be conducted to determine the significance of CD40- and AZD8055-ibrutinib-mediated regulation of PARP, γ-H2AX^{S139} accumulation and GADD45A, as well as the wider implications surrounding mTOR signal abrogation and the DNA damage response. Nevertheless, these results reveal a potential for mTOR- and FOXO-mediated signals to orchestrate distinct components of DNA damage repair in CLL.

Long-term CD40 engagement also increased expression of the FOXO target gene *SESN3*. Sestrin 3 is important for promoting oxidative damage repair and, unlike other sestrin isoforms, current evidence suggests that its expression is exclusively induced by FOXO transcription factors [575, 613] – supporting a regulatory network of cellular homeostasis and maintenance governed by FOXO activity in proliferating CLL cells.

4.4.5. Selective FOXO1 inhibition negates tumour suppression and reveals FOXO-FOXO transcriptional regulation

AS1842856 selectively inhibits FOXO1 *via* direct binding to 'active', dephosphorylated FOXO1, thereby preventing FOXO1-mediated gene transactivation [614]. Investigating AS1842856 treatment within the CD40L (+IL-4) system and its effect on the potency of AZD8055 on inducing cell cycle arrest showed enhanced proliferation in AS1842856-treated cells. Furthermore, AS1842856 pre-treatment attenuated an AZD8055-mediated block in proliferation, supporting that selective FOXO1 inhibition favours cell proliferation. This suggests that FOXO1 is responsible for the tumour-suppressive effects elicited by AZD8055 treatment in CLL, corroborating previous findings [49, 284]. However, irrespective of a rescue of cell viability in AZD8055-treated

MEC1 cells, reduced cell viability in AS1842856-treated primary cells infers a potential for FOXO1 in promoting cell survival, as well as having activity in promoting cell cycle arrest. Indeed, selective FOXO1 inhibition could inhibit the activity of nuclear-resident FOXO1, prohibiting FOXO1-mediated positive and negative functional outcomes. FOXOs are known to induce cell quiescence in a context-dependent manner [486], alluding to the possibility that FOXO1 activation following AZD8055 treatment leads to cell cycle arrest as a mechanism to perhaps mitigate further cell death in this context. Of note, AS1842856 treatment has been reported to induce cell death in multiple cancer models where FOXO1 expression is a known disease driver including GBM, BL and AML [615-617], reinforcing the necessity of FOXO1 expression in multiple disease contexts.

Pharmacological FOXO1 inhibition affected the distinct regulation of FOXO3 protein and *FOXO4* gene expression in long-term CLL-CD40L co-cultures. These data suggest that FOXO1 could be responsible for regulating the expression of FOXO3 and *FOXO4* in long-term cultures, further supporting the capability of FOXOs in regulating their own genes as well as those of other isoforms [555]. The complexity surrounding pharmacological FOXO inhibition is increased further by study in FOXO1-deficient MM cells showing that AS1842856 treatment attenuated FOXO3-mediated cell death [618], suggesting that AS8142856 could possess affinity for other FOXO isoforms. Supporting this, Nagashima *et al*. found that AS1842856 can inhibit the transcriptional activity of both FOXO3 and FOXO4 in HCC cells at concentrations >100 nM, although not to the same degree as FOXO1, inferring a non-specific targeting of other FOXO isoforms in CLL [614]. Specifically, AS1842856 was found to affect the promoter activity of FOXO3 and FOXO4 by 3% and 20%, respectively [614]; notable differences in affinity for other family isoforms could explain how *FOXO4*-depleted cells are susceptible to apoptosis induced by AS1842856 treatment, reflected by increased significance of a reduction in cell viability in AS1842856-treated, *FOXO4*-depleted cells (presented in Figure 5.27). A mechanistic explanation could be that, in the context of functional redundancy (discussed extensively in [619]), FOXO4 could compensate for dysfunctional FOXO1 activity. These findings could also infer that AS1842856 treatment alters the expression of other FOXO isoforms, providing another explanation for how AS1842856 attenuated an increase in FOXO

expression in CLL-CD40L co-cultures. Supporting this hypothesis, recent study in AML cells has revealed that AS1842856 treatment suppresses the expression of both *FOXO1* and *FOXO3* [617]. These data demonstrate the importance of FOXO activity in regulating FOXO expression in CD40-activated CLL cells, akin to dynamic FOXO expression of FOXO at different stages of B-cell development and maturation [463]. As developed for FOXO1, the generation of novel compounds that specifically target the activity of other FOXO isoforms would provide an effective, direct method to determine the distinct characteristics of discrete FOXO isoforms in normal and malignant contexts.

5. The impact of modulating FOXO3/4 expression on CLL cell proliferation and survival

5.1. Introduction

In previous chapters, it was revealed that *ex vivo* CLL cells exhibited greater levels of FOXO3 and FOXO4 than healthy B-cell populations (Figure 3.3). These data, along with disparate FOXO3/4 expression in MEC1 and HG3 cells, highlight a potential requirement for FOXO3/4 expression in the pathophysiology of CLL. These findings also highlight how disparate cytogenetics may influence FOXO isoform expression and subsequent activity in CLL cells as seen in other cancer contexts. For example, classical Hodgkin's Lymphoma (cHL) patients harbouring 13q14 chromosomal deletions resultantly lack typical FOXO1 expression, which could explain a depletion of FOXO1 seen in CLL patient samples harbouring 13q deletions. It is worth noting that genes encoding the different FOXO family isoforms are located on separate chromosomes in humans; *FOXO1, FOXO3, FOXO4* and *FOXO6* are located on chromosomes 13, 6, X and 1, respectively [620]. Though it lacks sufficient investigation, it is likely that cytogenetic aberrations affecting these chromosomes could elicit aberrant FOXO expression and, therefore, activity. Interestingly, while 13q, 11q, 17p and trisomy 12 are the most frequent genomic aberrations in CLL [5], cytogenetic analyses conducted by Vajen *et al*. revealed that, from 1298 patients exhibiting chromosomal aberrations, 3% of patients exhibited aberrations involving the X chromosome. Within this cohort, a loss or gain of an X chromosome was detected in 69% and 31% of patient CLL, respectively [621]. While only prevalent in a small subset of CLL patients, these data speculate a link between cytogenetics and potential dysfunction of FOXO4. Furthermore, *FOXO3* expression is abrogated by the chromosomal 6q21 deletion – a more common genomic aberration in CLL conferring poor prognosis [622]. Nonetheless, these findings do not discount an association between high *FOXO3* expression and poor prognosis as seen in this work and in other cancer neoplasms [526, 575, 578, 579, 623],

where an imbalance of typical *FOXO3* expression could favour disease progression in a context-dependent manner. In BCP-ALL, FOXO1 and FOXO3 are characterised as favourable and detrimental to disease progression, respectively [624], highlighting how atypical FOXO activity elicits multiple outcomes in an isoform- and context-dependent manner [463]. As FOXO1 exhibits tumour suppressor capabilities in CLL [49, 284], it could be that FOXO3 also exhibits inverse characteristics in mature B-cells compared with malignancies emanating from pre-B-cell populations, and so could contribute to CLL pathophysiology. As previously stated, FOXO4 expression is important for promoting colony forming and drug resistance in DLBCL cells [545], supporting a requirement for FOXO4 in the pathophysiology of mature B-cell neoplasms.

5.1.1. Aims

1. Determine the capability of depleting *FOXO3* and *FOXO4* in CLL cells

2. Characterise CLL cell functionality and chemosensitivity in the absence of *FOXO3/4*

3. Elucidate the expression and subsequent function of FOXO target genes in the absence of *FOXO3/4* in CLL

5.2. Results

5.2.1. Optimisation of the shRNA-mediated knockdown of *FOXO3* and *FOXO4* in MEC1 and HG3 cells

To further profile the characteristics of FOXO behaviour in CLL, shRNA-mediated knockdown of *FOXO3* was performed in MEC1 and HG3 cells. Knockdown of *FOXO3* in HG3 cells was unachievable, so the method was focused within MEC1 cells (Figure 5.1). This was deemed appropriate, as previous studies determined that FOXO3 gene and protein expression was more readily detected in MEC1 cells (Figures 3.1 & 4.10). Lentiviral transduction of 5 different *FOXO3* shRNA constructs was conducted in MEC1 cells (Figure 5.1A). ShRNA construct #1 elicited a significant knockdown of *FOXO3* expression (achieving a mean downregulation of ~38% compared to the 'scrambled' (SCR) control, Figure 5.1A). Constructs #2, #3 achieved a knockdown of ~15-20%, while constructs #4 and #5 were not effective in reducing *FOXO3* expression. Cells from positively selected sh*FOXO3* construct 1 (named 'shFOXO3-1') were then assessed for relative FOXO3 protein expression (Figure 5.1B & C). Construct #1 elicited a significant knockdown of FOXO3 at protein level compared to the SCR control (Figure 5.1C) and was therefore selected for *in vitro* study.

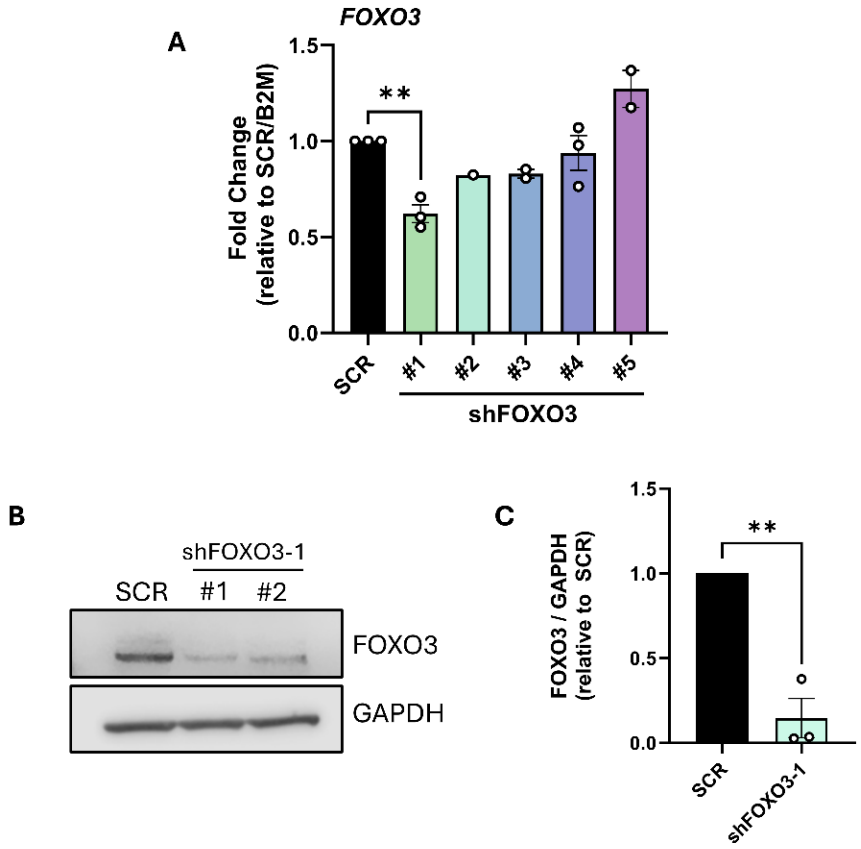

Figure 5.1: shRNA-mediated knockdown effectively diminishes FOXO3 expression in MEC1 cells. (A) RT-qPCR was used to assess transcript abundance of *FOXO3* in MEC1 cells that were positively selected following lentiviral transduction using five different shRNA DNA constructs (#1-#5) and a SCR control (does not affect target gene transcript expression). *FOXO3* expression values were normalised to *B2M* and presented as 'fold change' relative to the SCR control (#1 n=3, #2 n=1, #3 n=2, #4 n=3, #5 n=2). (B) Successful depletion of *FOXO3* in construct #1 led to further analysis of FOXO3 protein expression in this construct *via* Western blot (#1 and #2 being two repeats of construct #1-mediated FOXO3 knockdown). GAPDH was used as a loading control. (C) Quantified expression of FOXO3 in MEC1 cells transduced with construct #1 compared to a SCR control, normalised to GAPDH and made relative to the SCR control (n=3). Data points are depicted as white circles, and the data is represented as the mean ±SEM. Statistics were calculated using a Student's t-test, where ** $p \leq 0.01$.

Lentiviral knockdown was also conducted to investigate the implications of diminishing *FOXO4* expression in the context of CLL proliferation and survival (Figure 5.2). shRNA-mediated knockdown of *FOXO4* was first assessed in MEC1 cells using three separate sh*FOXO4* constructs, with all three constructs achieving a significant downregulation of *FOXO4* following positive selection with puromycin (Figure 5.2A). Of these three constructs, the most effective and significant *FOXO4* downregulation was seen using construct #3 (average knockdown of ~86% compared to the SCR control), which also elicited an effective depletion of FOXO4 protein (Figure 5.2B). Constructs #1 and #2 achieved average knockdowns of ~76% and ~40%, respectively (Figure 5.2A). Therefore, construct #3 (termed 'sh*FOXO4*-3) was selected for *in vitro* study.

Further, the three constructs were assessed for their selectivity in depleting *FOXO4* by investigating the expression of additional FOXO family members (Figure 5.2C-E). *FOXO1* expression was unaffected, regardless of the construct used (Figure 5.2C). *FOXO3*, however, was significantly depleted in constructs #1 and #3, while construct #2 did not affect *FOXO3* expression (Figure 5.2D). *FOXO6* expression was not affected by shRNA-mediated *FOXO4* depletion (Figure 5.2E).

We additionally assessed the effectiveness of sh*FOXO4*-3 at depleting *FOXO4* in HG3 cells (Figure 5.2F-J). Following lentiviral transduction, *FOXO4* expression was significantly diminished by sh*FOXO4*-3 (Figure 5.2F). After positive selection with puromycin, the abundance of the FOXO4 protein was also significantly depleted in HG3 cells (Figure 5.2G & H), demonstrating further effectiveness of depleting FOXO4 in HG3 cells. Assessing the expression of *FOXO1* and *FOXO3* expression following shRNA-mediated *FOXO4* knockdown, *FOXO1* expression was increased, albeit not significantly (Figure 5.2I). Interestingly, *FOXO3* expression was significantly increased in *FOXO4*-depleted HG3 cells (Figure 5.2J), an inverse result to that of *FOXO4*-depleted MEC1 cells (Figure 5.2D).

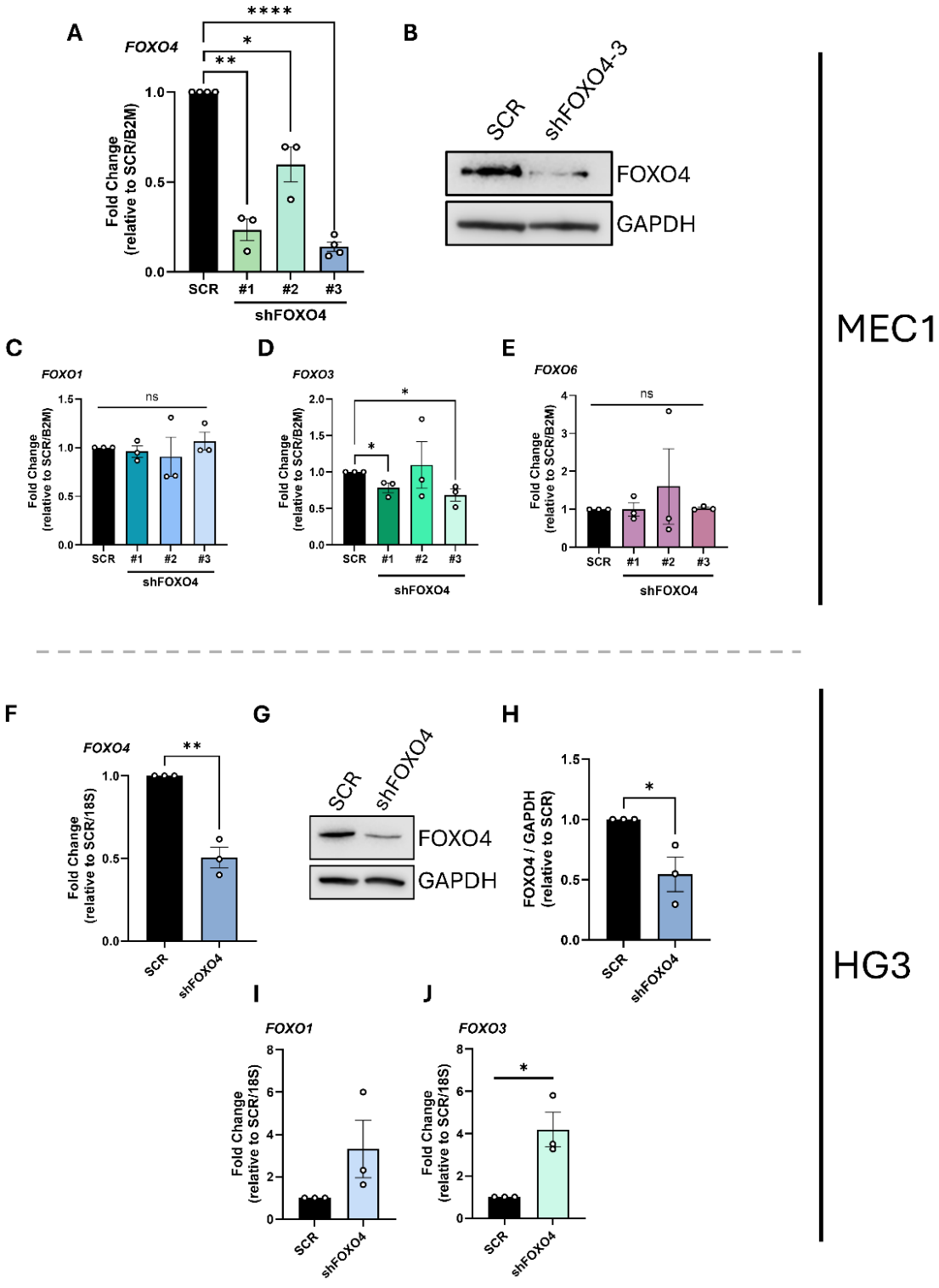

Figure 5.2: shRNA-mediated knockdown effectively depletes FOXO4 in MEC1 and HG3 cells. Initial shRNA-mediated knockdown of *FOXO4* was conducted in MEC1 cells using three different sh*FOXO4* constructs. (A) RT-qPCR was conducted to assess *FOXO4* transcript abundance following successful positive selection of MEC1 cells using 2 µg/mL puromycin in the three constructs (#1, #2, #3) compared to a SCR control. *FOXO4* expression values were normalised to *B2M* and made relative to the SCR control (#1 & #2 n=3, #3 n=4). (B) Western blot depicting expression of FOXO4 in MEC1 cells transduced with sh*FOXO4* construct #3. GAPDH was used as a loading control. (C-E) RT-qPCR was used to detect the transcript abundance of the other FOXO family members: *FOXO1* (A), *FOXO3* (D) and *FOXO4* (E) following shRNA-mediated *FOXO4* knockdown using the three sh*FOXO4* constructs (n=3). (F) Effective depletion of *FOXO4* using construct #3 led it to be used in HG3 cells, where RT-qPCR was used to detect *FOXO4* transcript abundance following puromycin selection. *FOXO4* expression values were normalised to *18S* and made relative to the SCR control (n=3). (G) Western

blotting of HG3 cells transduced with sh*FOXO4* construct #3 to assess FOXO4 protein expression. GAPDH was used as a loading control. (H) Quantified FOXO4 protein expression in *FOXO4*-depleted HG3 cells, normalised to GAPDH and made relative to the SCR control (n=3). (I & J) Transcript abundance of *FOXO1* (I) and *FOXO3* (J) in sh*FOXO4*-transduced HG3 cells detected *via* RT-qPCR, normalised to *18S* and made relative to the SCR control. Data points are depicted as white circles, and the data is represented as the, ** $p \leq 0.01$ mean ±SEM. Statistics were calculated using a Student's t-test, where * $p \leq 0.05$, **** $p \leq 0.0001$.

5.2.2. *FOXO3*- and *FOXO4*-depleted MEC1 cells exhibit correlational increases in FOXO1 and BIM expression

FOXOs harbour DNA binding affinity for their own family member genes as well as other FOXO genes [555]. Such a regulatory FOXO network is worth investigating, as FOXOs exhibit functional redundancy, thereby rescuing the roles of other FOXOs in a context-dependent manner [429]. As such, we investigated the protein expression of FOXO3 and FOXO1 in *FOXO3* (3KD)- and *FOXO4* (4KD)-depleted MEC1 cells, as well as the expression of the pro-apoptotic FOXO target BIM (Figure 5.3). Of note, FOXO3 and FOXO1 were assessed due to findings that *FOXO3* and *FOXO1* were aberrantly expressed in *FOXO4*-depleted cells in long-term cultures (Figure 5.2, discussed later in section 5.2.7).

The expression of FOXO3 was significantly depleted in MEC1 cells harbouring a *FOXO3* or *FOXO4* knockdown (Figure 5.3A). Comparatively, although shRNA-mediated *FOXO4* knockdown depleted FOXO3 expression (Figure 5.3A), *FOXO3*-depleted cells retained a stronger depletion of FOXO3 at protein level than *FOXO4*-depleted cells, trending towards significance ($p = 0.09$, Figure 5.3B). Inversely, FOXO1 expression was significantly increased in both *FOXO3*- and *FOXO4*-depleted cells (Figure 5.3C). Coincident with FOXO1 upregulation, *FOXO3*-depleted MEC1 cells exhibited increased FOXO1 DNA binding activity (Figure 5.3D), indicating an increase in FOXO1 activity. Corroborating this, *FOXO3*- and *FOXO4*-depleted MEC1 cells exhibited increased expression of each BIM isoform (BIM_{EL}, BIM_{L}, BIM_{S}); BIM_{EL} expression was significantly increased in both *FOXO3*- and *FOXO4*-depleted cells, and was higher in *FOXO4*-depleted cells (Figure 5.3E), coincident with elevated FOXO1 (Figure 5.3C). Supporting this,

BIM_L (Figure 5.3F) and BIM_S (Figure 5.3G) expression were also higher in *FOXO4*-depleted MEC1 cells than in cells lacking *FOXO3*.

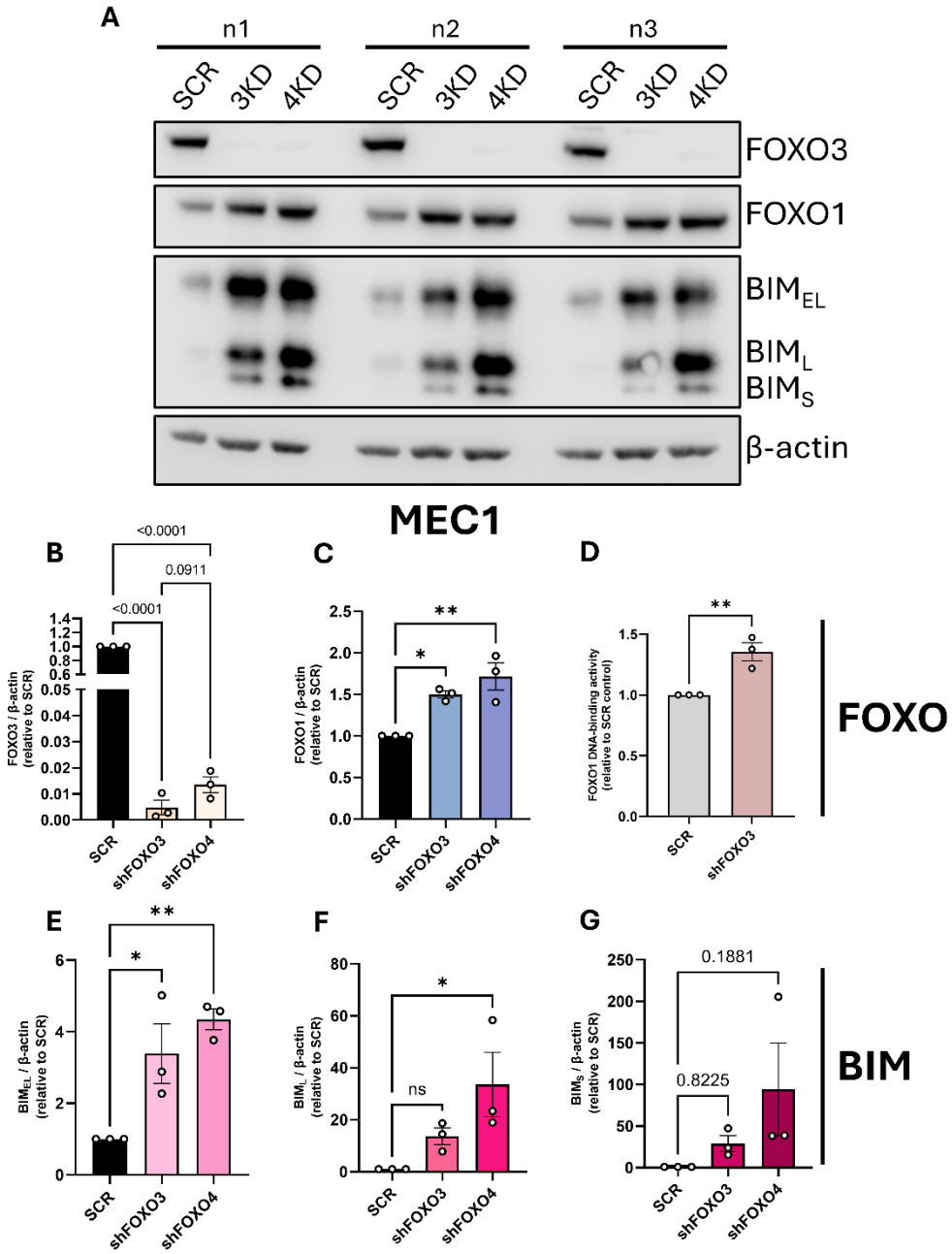

Figure 5.3: FOXO3 and FOXO4 knockdown increases FOXO1 and BIM expression in MEC1 cells. (A) Western blot of lysates generated from MEC1 cells cultured in media containing 1 µg/mL puromycin harbouring a FOXO3 or FOXO4 knockdown (3KD or 4KD respectively), compared to a SCR control. Western blot was conducted to assess the expression of FOXO3, FOXO1 and BIM isoforms (BIM_{EL}, BIM_L and BIM_S). β-actin was used as a loading control. (B) Quantified expression of FOXO3 in SCR, 3KD and 4KD cells, normalised to β-actin and made relative to the SCR control. (C) Quantified FOXO1 protein expression in SCR, 3KD and 4KD MEC1 cells, normalised to β-actin and made relative to the SCR control. (D) DNA-binding activity of FOXO1 was assessed using a FOXO1 DNA-binding ELISA in *FOXO3*-depleted cells, where FOXO1 binding activity is associated with a colorimetric reaction, relative to the SCR control. (E-G) Expression of the BIM isoforms BIM_{EL} (E), BIM_L (F) and BIM_S (G) in *FOXO3*- and *FOXO4*-depleted MEC1 cells, normalised to β-actin and made relative to the SCR control. Data points are depicted as white circles, and the data is represented as the mean ±SEM. Statistics were calculated using one-way ANOVA, where * $p \leq 0.05$, ** $p \leq 0.01$.

5.2.3. *FOXO4* depletion affects MEC1 cell proliferation

In Figure 5.4, we addressed the proliferative capacity of MEC1 and HG3 cells lacking *FOXO4* expression by using AZD8055 (100 nM) and/or ibrutinib (1 μM) treatment as controls to facilitate a block in proliferation. Of note, in Figures 5.4, 5.6-5.8, AZD8055 and ibrutinib treatments were conducted in combination in MEC1 cells (COMBO), while single treatments were also included for HG3 cells. Assessing proliferation *via* CTV staining (flow cytometry) at 72 hr, *FOXO4*-depleted MEC1 cells exhibited a significant reduction in proliferation, whereas *FOXO4*-depleted HG3 cells exhibited no change in proliferative capacity, when compared to their respective SCR controls (Figure 5.4B & C). AZD8055 and ibrutinib treatments facilitated a further decrease in MEC1 cell proliferation, irrespective of *FOXO4* expression (Figure 5.4B), although not significantly. In HG3 cells, ibrutinib treatment induced a significant block in proliferation in the SCR control which was absent in *FOXO4*-depleted cells (Figure 5.4C), while AZD8055 – alone or in combination with ibrutinib - elicited a significant block in proliferation, irrespective of *FOXO4* expression (Figure 5.4C). These data suggest that *FOXO4* depletion affects CLL cell proliferation in a cell-type-specific manner.

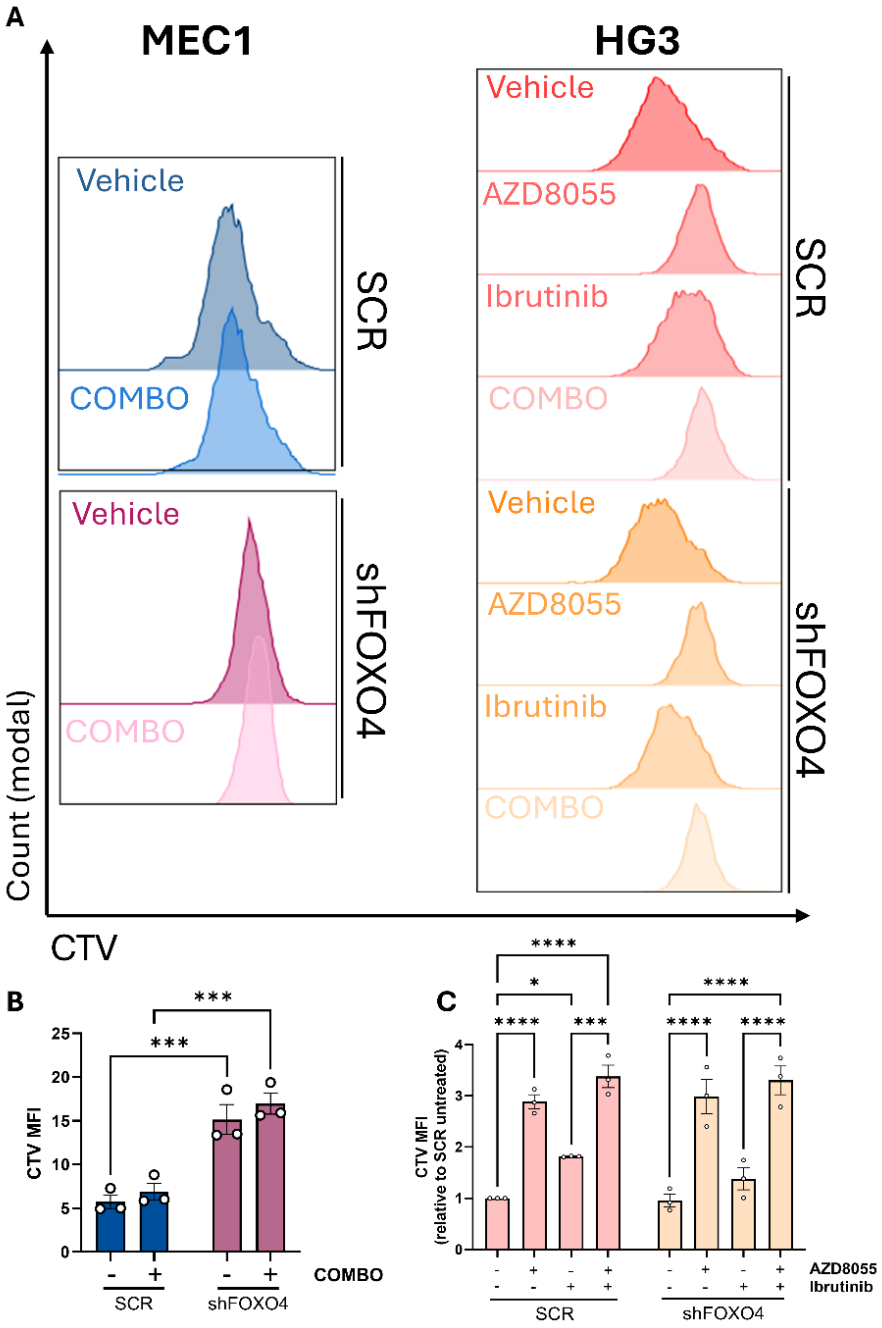

Figure 5.4: FOXO4 depletion negatively affects MEC1 cell proliferation. (A) Representative FACS histograms of MEC1 (left) and HG3 (right) cells 72 hr after CTV staining ±AZD8055 (100 nM) and ibrutinib (1 μM) treatment, alone or in combination (for HG3 cells, strictly COMBO for MEC1 cells). (B) Mean fluorescence intensity of CTV for SCR and *FOXO4*-depleted MEC1 cells following 72 hr in culture ±COMBO. (C) Mean fluorescence intensities for SCR and *FOXO4*-depleted HG3 cells following 72 hr in culture ±AZD8055 and/or ibrutinib, made relative to untreated SCR cells (n=3). Data points are depicted as white circles, and the data is represented as the mean ±SEM. Statistics were calculated using two-way ANOVA, where *** $p \leq 0.001$, **** $p \leq 0.0001$.

5.2.4. *FOXO4* depletion elicits changes in cell cycle progression, coincident with aberrant $p27^{kip1}$ and $p21^{cip1}$ expression

The fact that *FOXO4* depletion affects MEC1 cell proliferation suggests an alteration of cell cycle progression in cells with ablated *FOXO4*. Thus, we addressed whether sh*FOXO4* knockdown altered cell cycle progression of MEC1 and HG3 cells, alone or in response to AZD8055 (100 nM) and/or ibrutinib (1 μM) treatment. Of note, there was movement in the G_0/G_1 peak in MEC1 cells with ablated *FOXO4*, likely due to aberrant cell size in these populations (discussed in Figure 5.19). MEC1 G_0/G_1 populations were increased in shFOXO4 MEC1 cells compared to the SCR control (Figure 5.5B, top), coinciding with a significant decrease in MEC1 S phase (Figure 5.5C, top) and G2 phase (Figure 5.5D, top) populations. Furthermore, long-term treatment with AZD8055, alone or in combination with ibrutinib, significantly increased SCR G_0/G_1 populations (Figure 5.5B), corroborated by AZD8055 and/or ibrutinib treatment significantly depleting MEC1 SCR cell S and G2 phase populations (Figure 5.5B-D, top). A significant rise in the MEC1 G_0/G_1 population was lost following *FOXO4* depletion (Figure 5.5B, top), perhaps due to increased basal G1/G0 populations in *FOXO4*-depleted cells. Further, AZD8055-mediated S phase and G2 phase depletion in MEC1 cells lacking *FOXO4* resulted in reduced significance compared to the SCR control (Figure 5.5C & D, top). In contrast, HG3 G_0/G_1, S and G2 phase populations were unaffected by *FOXO4* knockdown (Figure 5.5B-D, bottom), supporting that *FOXO4* depletion has little effect on the proliferative capacity of HG3 cells (Figure 5.4). However, AZD8055 and ibrutinib treatments significantly enhanced HG3 G1/G0 phase arrest when compared to the SCR control, demonstrated by an increase in significance in G_0/G_1 phase abundance and reduced S/G2 phase populations (Figure 5.5D). Additionally, enhanced G_0/G_1 arrest was supported by AZD8055 and ibrutinib treatment exclusively diminishing G2 cell populations in *FOXO4*-depleted HG3 cells (Figure 5.5D, bottom).

These results are linked the disparate expression of $p27^{kip1}$ and $p21^{cip1}$ in *FOXO4*-depleted MEC1 and HG3 cells (Figure 5.5E). shRNA-mediated knockdown elicited a significant increase in $p27^{kip}$ expression in MEC1 cells, while $p27^{kip1}$ expression

was significantly reduced in *FOXO4*-depleted HG3 cells (Figure 5.5F). Unexpectedly, p21^{cip1} expression was reduced in shFOXO4 MEC1 and HG3 cell cultures, trending towards significance in HG3 cells (p = 0.06, Figure 5.5G). These data suggest that FOXO4 expression is required for cell cycle progression in a cell-type-specific manner.

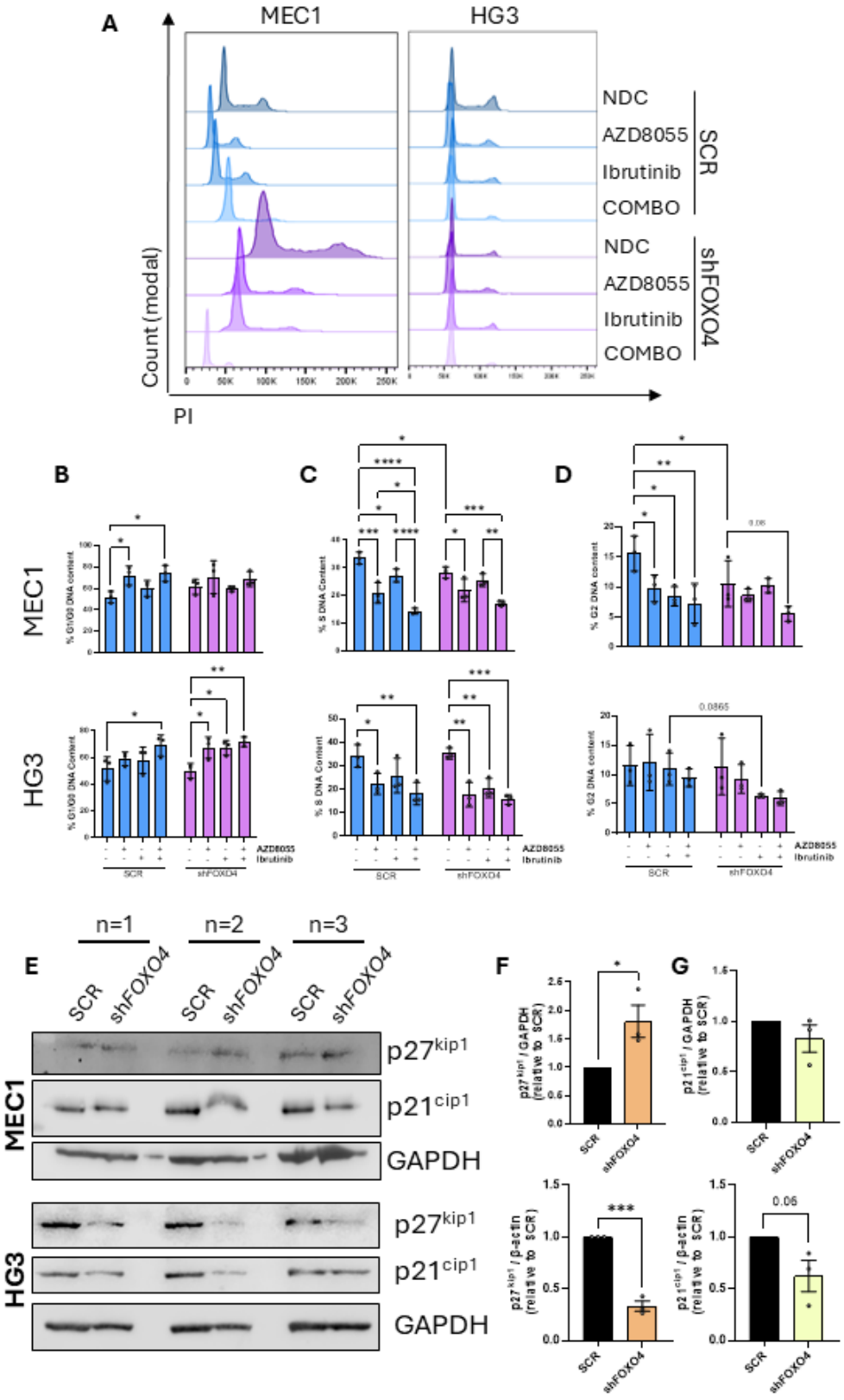

Figure 5.5: FOXO4 knockdown elicits cell-specific changes in MEC1 and HG3 cell cycle progression, partnered with differential p27kip1 and p21cip expression. (A) Representative FACS histograms of SCR and *FOXO4*-depleted MEC1 (left) and HG3 (right) cells stained with PI following 48 hr in culture ±100 nM AZD8055 and/or 1 μM ibrutinib. (B-D) Percentages of MEC1 (top) and HG3 (bottom) DNA content associated with G_0/G_1 (B), S (C) and G2 phases (D) was calculated using in-house FlowJo cell cycle software (n=3). (E) Western blots of *FOXO4*-depleted MEC1 (top) and HG3 (bottom) cells in cultures treated with 1 μg/mL puromycin assessing the expression of $p27^{kip1}$ and $p21^{cip1}$ compared to their respective SCR controls. GAPDH was used as a loading control. (F & G) Quantified expression of $p27^{kip1}$ (F) and $p21^{cip1}$ (G) in *FOXO4*-depleted MEC1 (top) and HG3 (bottom) cells, normalised to GAPDH and made relative to their respective SCR controls. Data points are depicted as white circles, and the data is represented as the mean ±SEM. Statistics were calculated using a two-way ANOVA for PI analysis, while an unpaired Student's t-test was used to compare $p27^{kip1}$ and $p21^{cip1}$ expression. * $p \leq 0.05$, ** $p \leq 0.01$, *** $p \leq 0.001$, **** $p \leq 0.0001$.

5.2.5. CLL cells lacking *FOXO4* exhibit increased chemosensitivity to AZD8055-ibrutinib treatment

Due to FOXO expression being associated with drug resistance in other B-cell malignancies [545], we explored whether the ablation of *FOXO4* affects CLL cell chemosensitivity, particularly in response to AZD8055 (100 nM) and ibrutinib (1 μM) treatment. In HG3 cells, Annexin/7AAD staining (Figure 5.6A) revealed a significant decrease in cell viability in *FOXO4*-depleted cells (Figure 5.6B), reflected by an increase in apoptosis in the absence of drug treatment (Figure 5.6C). Moreover, both the SCR control and *FOXO4*-depleted HG3 cells exhibited a significant increase in apoptosis following combined AZD8055-ibrutinib treatment, which was potentiated further by *FOXO4* depletion (Figure 5.6C), suggesting an enhancement of AZD8055-ibrutinib-mediated cell death in the absence of *FOXO4*. In MEC1 cells, there was no difference in cell viability following *FOXO4* ablation (Figure 5.6E). However, *FOXO4*-depleted MEC1 cells exhibited enhanced cell death following COMBO treatment compared to the SCR control (Figure 5.6F), complimented by a significant decrease in cell viability (Figure 5.6E). Next, we addressed how shRNA-mediated *FOXO4* depletion affected the viability of primary cells in CD40L co-culture (Figure 5.6G). Following 96 hr culture on CD40L (+10 ng/μL IL-4), primary CLL cells exposed to sh*FOXO4*-3-containing lentivirus exhibited higher levels of apoptosis than the SCR control (Figure 5.6G). These data highlight a suppressive role for FOXO4 in CLL in

the context of chemosensitivity, where depleting endogenous *FOXO4* increases susceptibility to drug-induced apoptosis.

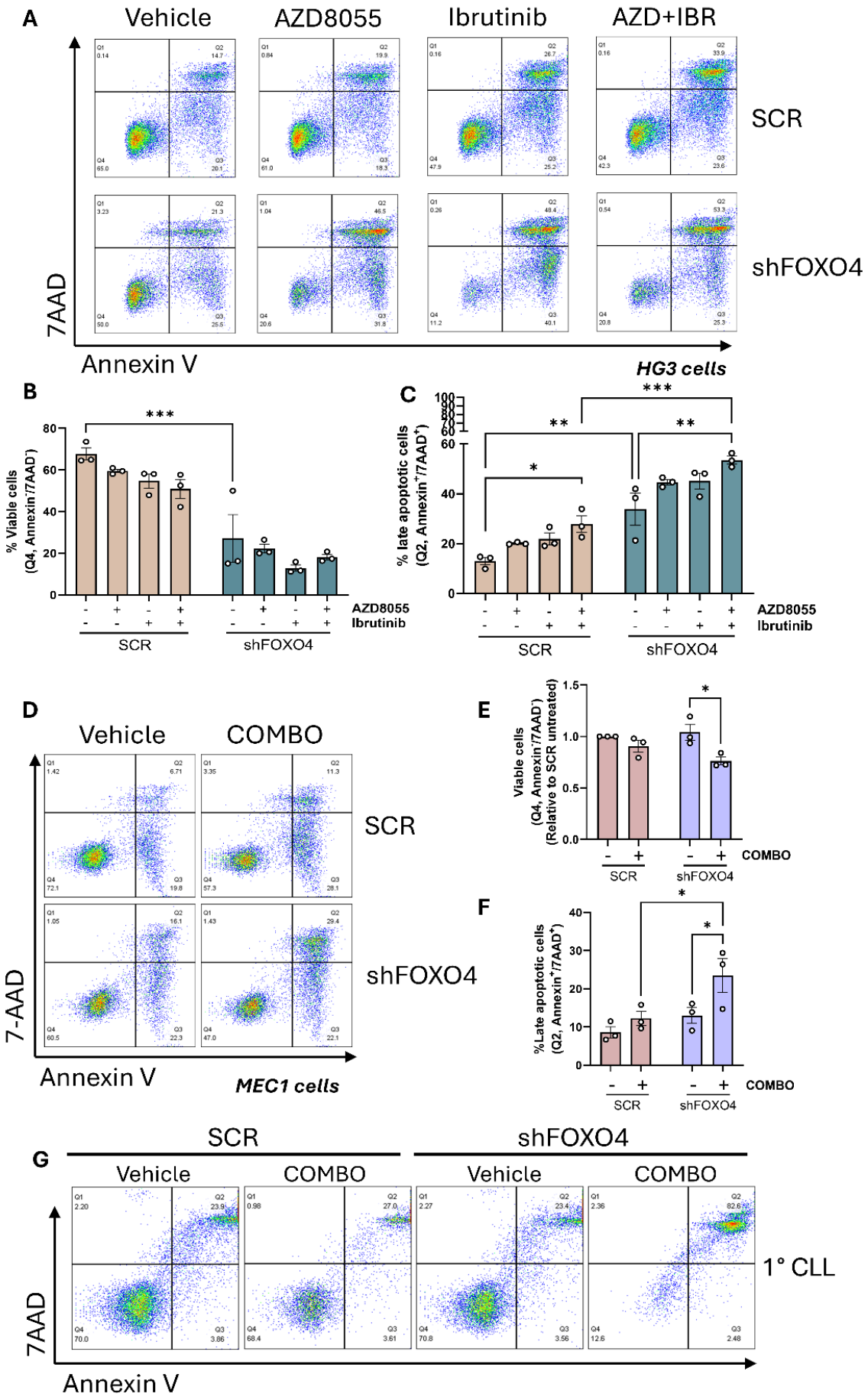
A
Vehicle
AZD8055
Ibrutinib
AZD+IBR
SCR
shFOXO4
7AAD
Annexin V
HG3 cells
B
% Viable cells (Q4, Annexin⁻/7AAD⁻)
AZD8055
Ibrutinib
SCR
shFOXO4
C
% late apoptotic cells (Q2, Annexin⁺/7AAD⁺)
AZD8055
Ibrutinib
SCR
shFOXO4
D
Vehicle
COMBO
SCR
shFOXO4
7-AAD
Annexin V
MEC1 cells
E
Viable cells (Q4, Annexin⁻/7AAD⁻) (Relative to SCR untreated)
COMBO
SCR
shFOXO4
F
%Late apoptotic cells (Q2, Annexin⁺/7AAD⁺)
COMBO
SCR
shFOXO4
G
SCR
shFOXO4
Vehicle
COMBO
Vehicle
COMBO
7AAD
Annexin V
1° CLL

Figure 5.6: Diminishing FOXO4 negatively affects CLL cell viability and chemosensitivity. sh*FOXO4* HG3 and MEC1 cells were cultured for 48 hr with their respective SCR controls ±100 nM AZD8055 and/or 1 μM ibrutinib (for HG3 cells, strictly COMBO for MEC1 cells). (A) Representative FACS plot of SCR and *FOXO4*-depleted HG3 cells stained with Annexin and 7AAD following 48 hr in culture ±AZD8055 and/or ibrutinib. (B) Percentage of SCR and *FOXO4*-depleted HG3 cells deemed 'viable' (Annexin^{neg}/7AAD^{neg}) following 48 hr in culture ±AZD8055 and/or ibrutinib. (C) percentage of SCR and *FOXO4*-depleted HG3 cells that are undergoing 'late' stages of apoptosis (Annexin^{pos}/7AAD^{pos}) following 48 hr in culture ±AZD8055 and/or ibrutinib (n=3). (D) Representative FACS plot of Annexin/7AAD-stained, *FOXO4*-depleted MEC1 cells following 48 hr in culture ±COMBO treatment. (E) Percentage of 'viable' (Annexin^{neg}/7AAD^{neg}) SCR and *FOXO4*-depleted MEC1 cells following 48 hr in culture, made relative to untreated SCR cells. (F) Percentage of SCR and *FOXO4*-depleted MEC1 cells undergoing late-stage apoptosis (Annexin^{pos}/7AAD^{pos}) following 48 hr in culture (n=3). (G) Annexin/7AAD FACS plot of primary CLL cells (CLL #132) on CD40L (+10 ng/mL IL-4) 96 hr post induction with SCR or shFOXO4 lentivirus ±COMBO treatment (n=1). In all cases, a 'vehicle', untreated control was included. Data points are depicted as white circles, and the data is represented as the mean ±SEM. Statistics were calculated using two-way ANOVA, where * $p \leq 0.05$, ** $p \leq 0.01$, *** $p \leq 0.001$.

5.2.6. Gene expression is altered following *FOXO4* knockdown and subsequent mTOR/BTK inhibition in MEC1 and HG3 cells

We explored the expression of FOXO-associated genes involved in CLL survival (*BBC3*, *BCL2L1*, *BCL2L11, MCL1, TP53*), cell cycle progression (*CCND2, CDKN1A, CDKN1B*, *GADD45A*), mechanisms of damage repair (*GADD45A* & *SESN3*) and growth factor signalling (*IGF1R*) to elucidate whether alterations in *FOXO4* expression affect the distinct expression of different FOXO-associated functional components downstream of AZD8055 and/or ibrutinib treatment (Figure 5.7). Of note, *TP53* expression was only investigated in HG3 cells due to MEC1 cells harbouring a *TP53* deletion [625]. *BCL2L1* expression exhibited a modest decrease in *FOXO4*-depleted HG3 cells which was significantly increased following AZD8055 and ibrutinib combination treatment, regardless of *FOXO4* expression. However, increases were muted in *FOXO4*-depleted HG3 cells than in the SCR control (Figure 5.7A). In contrast, *BCL2L1* expression was significantly reduced in COMBO-treated MEC1 cells (Figure 5.7G), reflecting AZD8055-ibrutinib-mediated *BCL2L1* downregulation demonstrated in Figure 4.7 (and BCL-XL, Figure 5.8). Furthermore, *BCL2L1* expression was reduced in *FOXO4*-depleted MEC1 cells compared to the SCR control, resulting in reduced significance of COMBO-induced *BCL2L1* downregulation ($p = 0.003$ *vs* 0.01, Figure 5.7G). *BCL2L11* expression did not change significantly following AZD8055 and ibrutinib

treatments in SCR and shFOXO4 HG3 cells (Figure 5.7B). Reflecting BIM expression in MEC1 cells with depleted *FOXO4* (Figure 5.8), *BCL2L11* expression was modestly increased in cells with *FOXO4* knockdown, which was significantly increased in COMBO-treated cells (Figure 5.7H). When compared to the AZD8055-ibrutinib-treated SCR control, *BCL2L11* expression was significantly higher in COMBO-treated, *FOXO4*-depleted MEC1 cells (Figure 5.7H). The expression of *CDKN1B* was significantly increased in *FOXO4*-depleted HG3 cells, and was significantly attenuated following ibrutinib treatment, alone or in combination with AZD8055 (Figure 5.7C). In contrast, although shFOXO4 MEC1 cells exhibited a slight increase in *CDKN1B*, AZD8055-ibrutinib treatment significantly increased *CDKN1B* expression (Figure 5.7C), highlighting cell-specific, drug-mediated *CDKN1B* regulation.

Interestingly, *GADD45A* expression was significantly downregulated in *FOXO4*-depleted MEC1 and HG3 cells (Figure 5.7D & J), rendering *FOXO4*-depleted cells insensitive to AZD8055-mediated *GADD45A* depletion as seen in SCR cells, perhaps due to its low expression (Figure 5.7D & J). *FOXO4*-depleted MEC1 and HG3 cells also exhibited diminished *SESN3* expression, which was insensitive to a significant AZD8055-mediated depletion seen in SCR cells (alone or in combination with ibrutinib, Figure 5.7E & K). Inversely, *FOXO4*-depleted cells exhibited a marked significant increase in *SESN3* following COMBO treatment (Figure 5.7K). Further, *TP53* expression was markedly reduced by either AZD8055 and ibrutinib treatment, alone or in combination (for the SCR control), or by *FOXO4* depletion, which led to a lack of AZD8055-ibrutinib-mediated *TP53* depletion – perhaps due to its absence in *FOXO4*-depleted cells (Figure 5.7F). In MEC1 cells, *IGF1R* expression was increased following COMBO treatment, irrespective of *FOXO4* expression (Figure 5.7L). *CDKN1A* expression was significantly decreased in *FOXO4*-depleted cells, where COMBO treatment significantly increased *CDKN1A* expression, rather than significantly reducing *CDKN1A* expression as in the SCR control (Figure 5.7M). Moreover, *CCND2* exhibited variable expression in *FOXO4*-depleted MEC1 cells. Although a median rise in *CCND2* elicited a COMBO-mediated significant depletion of *CCND2*, said depletion was not significant (Figure 5.7N). Finally, *BBC3* expression was significantly increased following COMBO treatment, irrespective of *FOXO4* expression status (Figure 5.7O). These findings highlight the impact of FOXO4 in

driving transcription of canonical genes associated with the FOXO signalling pathway.

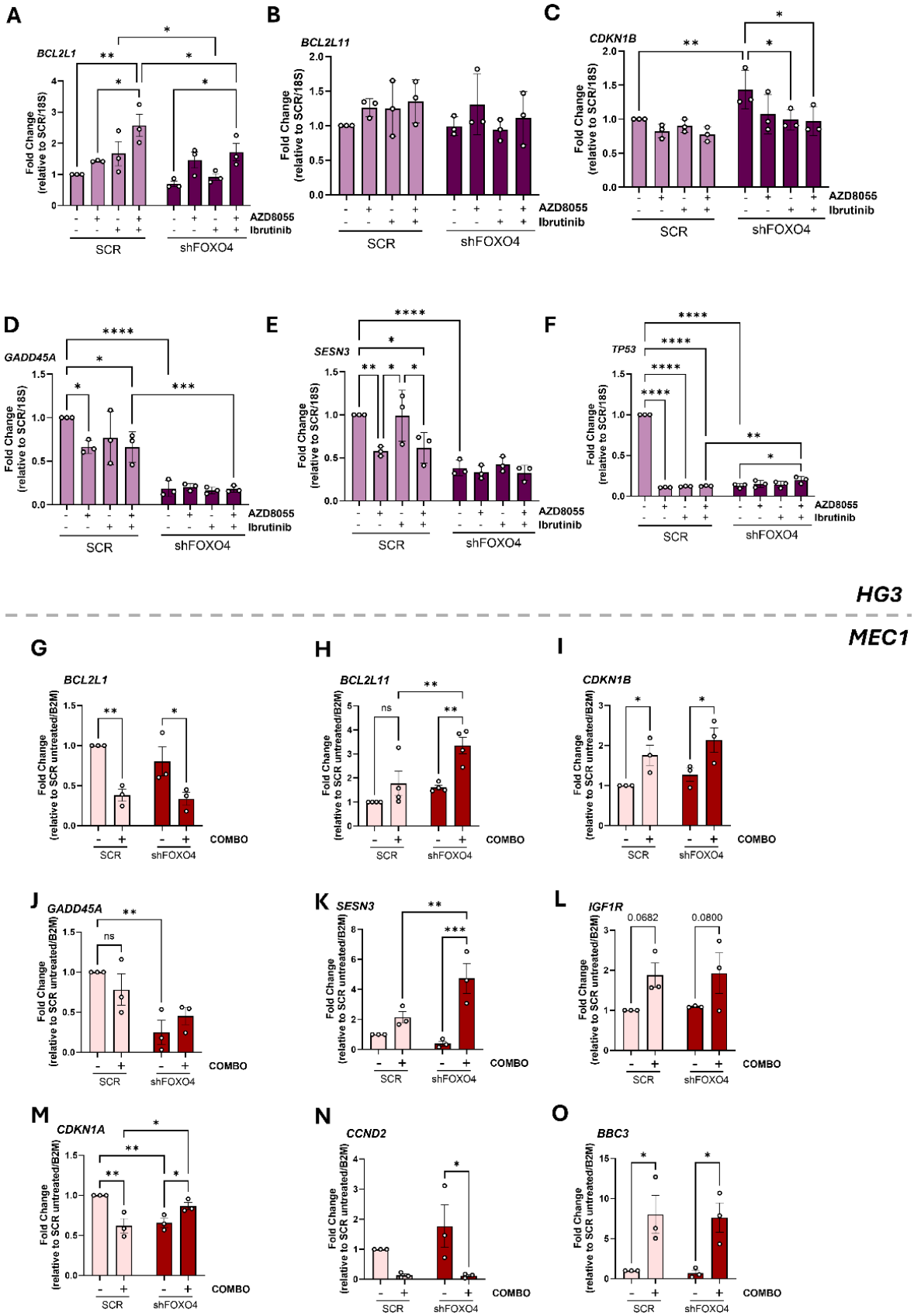

Figure 5.7: FOXO target genes are aberrantly expressed following shRNA-mediated FOXO4 knockdown. RT-qPCR was conducted in *FOXO4*-depleted HG3 and MEC1 cells following 24 hr in culture ±100 nM AZD8055 and/or 1 μM ibrutinib (HG3) or COMBO (MEC1) treatment, assessing the

transcript abundance of various FOXO target genes compared to their respective SCR controls. (A-F) Transcript abundance of *BCL2L1, BCL2L11, CDKN1B, GADD45A, SESN3* and *TP53* in *FOXO4*-depleted HG3 cells ±AZD8055 and/or ibrutinib treatment, normalised to 18S and presented as fold change relative to untreated SCR cells. (G-O) Transcript abundance of *BBC3, BCL2L1, BCL2L11, CCND2, CDKN1A, CDKN1B, GADD45A, IGF1R* and *SESN3* in *FOXO4*-depleted MEC1 cells ±COMBO treatment, normalised to *B2M* and presented as fold change relative to untreated SCR cells (n=3, n=4 for *BCL2L11* in MEC1 cells (H)). Data points are depicted as white circles, and the data is represented as the mean ±SEM. Statistics were calculated using two-way ANOVA (A-G) and a Student's t-test (H & I), where * $p \leq 0.05$, ** $p \leq 0.01$, *** $p \leq 0.001$, **** $p \leq 0.0001$.

5.2.7. *FOXO4* depletion induces BIM upregulation in MEC1 and HG3 cells

We next explored the expression of survival-associated proteins in long-term cultures following *FOXO4* knockdown. Cells were analysed for changes in MCL1, BCL-XL, BIM expression, and levels of AKT^{S473}, with or without AZD8055 (100 nM) and/or ibrutinib (1 μM) treatments (Figure 5.8). As expected, AKT^{S473} levels were effectively depleted in AZD8055-treated cells, alone or in combination with ibrutinib - indicative of successful mTOR inhibition (Figure 5.8A & B). Interestingly, MCL1 and BCL-XL exhibited cell-specific expression; HG3 cells exhibited increased MCL1 and BCL-XL expression in *FOXO4*-depleted, AZD8055-ibrutinib-treated cells (Figure 5.8C & D, left) and BCL-XL expression following COMBO treatment was significantly higher than in the SCR control (Figure 5.8D, left). In contrast, while MCL1 expression was unchanged in MEC1 cells with ablated *FOXO4*, (Figure 5.8C, right), a reduction in BCL-XL expression in SCR MEC1 cells following AZD8055-ibrutinib treatment was reversed in *FOXO4*-depleted MEC1 cells, as BCL-XL expression was lower than in untreated SCR cells (Figure 5.8D, right). Supporting increased apoptosis, BIM_{EL} (Figure 5.8E), BIM_L (Figure 5.8F) and BIM_S (Figure 5.8G) were all increased in HG3 and MEC1 cells with combined AZD8055-ibrutinib treatment (supporting Figures 4.7 & 4.8). Interestingly, the expression of each BIM isoform was further enhanced in *FOXO4*-depleted cells following AZD8055 and ibrutinib treatments (Figure 5.8E-G), where *FOXO4*-depleted cells exhibited a significant increase in BIM_{EL} expression with single ibrutinib treatment (Figure 5.8E). MEC1 cells exhibited a similar BIM profile, where *FOXO4* depletion increased BIM_L and BIM_S expression (Figure 5.8F & G). Furthermore, BIM_{EL} expression was significantly increased in

COMBO-treated MEC1 cells - this was significantly greater than BIM_{EL} expression following long-term COMBO treatment in the SCR control (Figure 5.8E).

FOXO4 depletion elicited a cell-specific elevation in apoptosis, where HG3 cells exhibited higher basal levels of apoptosis compared to MEC1 cells (Figure 5.6). These CLL cell lines exhibit different cytogenetic profiles; specifically, HG3 cells differ from MEC1 cells in their expression of *TP53* [514]. Indeed, FOXO4 is known to be co-expressed with p53 to mediate transactivation involved in numerous cellular processes – a characteristic exclusive to the FOXO4 isoform [626]. As such, we investigated whether *FOXO4* depletion affected p53 expression in HG3 cells (Figure 5.8H & I). While *TP53* expression was decreased following *FOXO4* depletion (Figure 5.8F), *FOXO4*-ablated HG3 cells exhibited increased p53 expression, verging on significance (Figure 5.8I, $p = 0.051$). These findings demonstrate increased apoptotic signalling in the absence of *FOXO4* expression, supporting a cell-type-specific increase in apoptosis in CLL cells with ablated *FOXO4* (Figure 5.6).

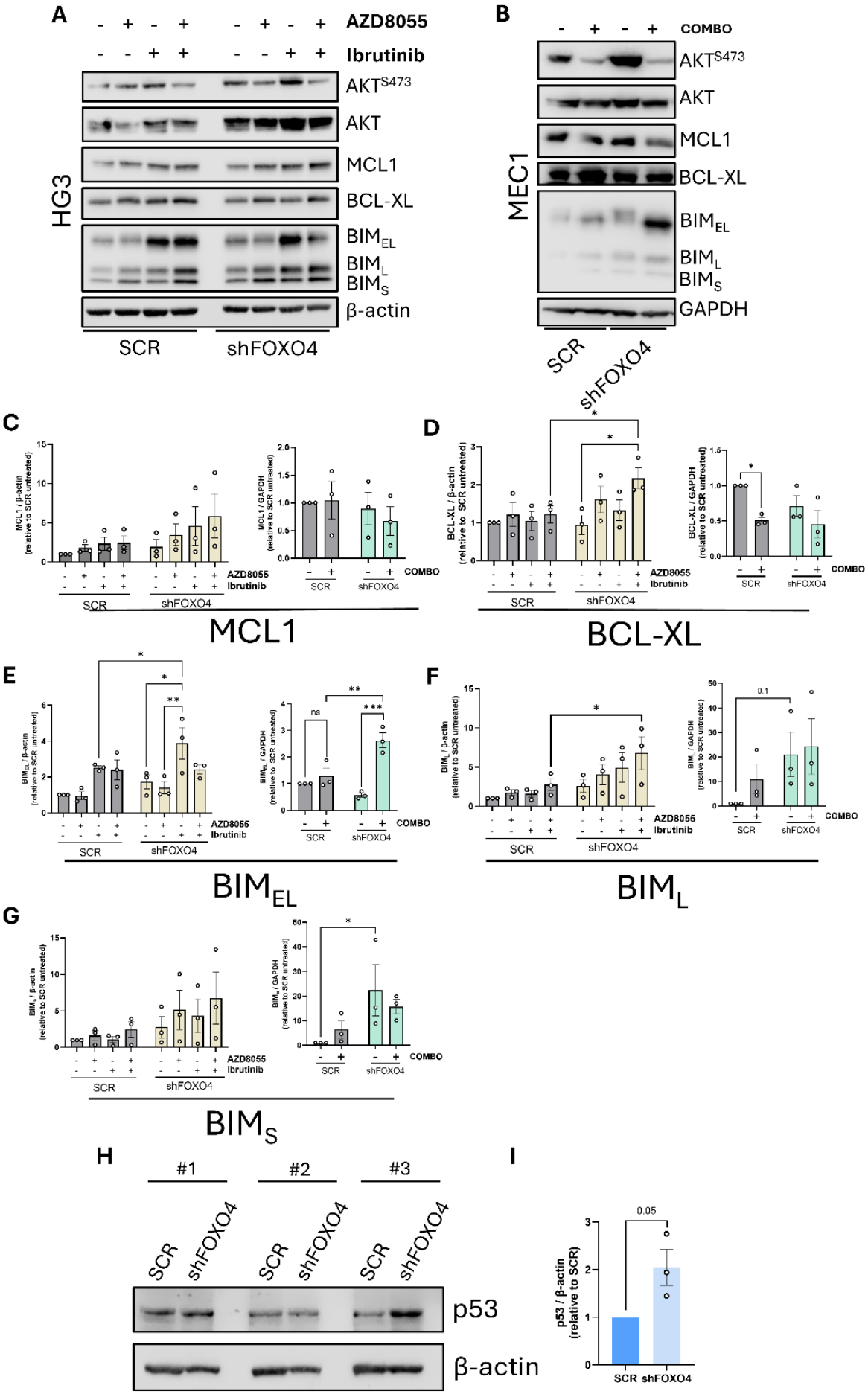
A
AZD8055
Ibrutinib
AKT^S473
AKT
MCL1
BCL-XL
BIM_EL
BIM_L
BIM_S
β-actin
HG3
SCR
shFOXO4
B
COMBO
AKT^S473
AKT
MCL1
BCL-XL
BIM_EL
BIM_L
BIM_S
GAPDH
MEC1
SCR
shFOXO4
C
MCL1
D
BCL-XL
E
BIM_EL
F
BIM_L
G
BIM_S
H
#1
#2
#3
SCR
shFOXO4
p53
β-actin
I
p53 / β-actin (relative to SCR)
0.05
SCR
shFOXO4

Figure 5.8: Pro-apoptotic marker expression is enhanced in drug-treated, FOXO4-depleted CLL cells. (A & B) Western blots of SCR and *FOXO4*-depleted HG3 (A) and MEC1 (B) cells following 48 hr in culture ±100 nM AZD8055 and/or 1 µM ibrutinib (for HG3 cells, strictly COMBO for MEC1 cells), assessing the expression of AKT^{S473}, AKT, MCL1, BCL-XL, BIM_{EL}, BIM_L and BIM_S. β-actin and GAPDH were used as loading controls for HG3 and MEC1 cells, respectively. (C & D) Quantified expression of MCL1 (C) and BCL-XL (D) in *FOXO4*-depleted HG3 (left) and MEC1 (right) cells, normalised to β-actin/GAPDH (HG3/MEC1) and made relative to untreated SCR cells. (E-G) Quantified expression of the BIM isoforms BIM_{EL} (E), BIM_L (F) and BIM_S (G) in *FOXO4*-depleted HG3 (left) and MEC1 (right) cells, normalised to their respective loading controls and made relative to untreated SCR cells (n=3). (H) Western blot assessing p53 expression in *FOXO4*-depleted HG3 cells in cultures treated with 1 µg/mL puromycin. β-actin was used as a loading control. (I) Quantified expression of p53 in *FOXO4*-depleted HG3 cells, normalised to β-actin and made relative to the SCR control (n=3). Data points are depicted as white circles, and the data is represented as the mean ±SEM. Statistics were calculated using two-way ANOVA (A-G) and a Student's t-test (H & I), where * $p \leq 0.05$, ** $p \leq 0.01$.

5.2.8. FOXO3 expression is increased in long-term cultures of *FOXO4*-depleted CLL cell lines

Due to the aspect of functional redundancy existing in FOXO biology [483], we explored whether *FOXO4* knockdown affected FOXO3/1 expression in MEC1 and HG3 cells, and whether distinct FOXO3/1 expression was altered by AZD8055 and/or ibrutinib treatments (Figure 5.9). Following 48 hr culture, FOXO3 expression was significantly increased in MEC1 cells lacking *FOXO4* expression (Figure 5.9A & B). Interestingly, this increase was significantly attenuated by combined AZD8055-ibrutinib treatment (Figure 5.9B). Increased FOXO3 expression was supported by 24 hr RT-qPCR investigating *FOXO3* expression, where proliferating, *FOXO4*-depleted MEC1 cells exhibited significantly increased *FOXO3* expression (Figure 5.9C). In comparison, although FOXO1 was significantly increased in *FOXO4*-depleted MEC1 cells in initial study (Figure 5.3), FOXO1 protein and gene expression was unchanged in *FOXO4*-depleted cells in long-term cultures (figure 5.9D & E).

HG3 cells exhibited a similar expression to that of MEC1 cells in long-term culture (Figure 5.9F); FOXO3 protein expression was increased in *FOXO4*-depleted cells (Figure 5.9G), albeit not significantly. However, 24 hr culture revealed a significant increase in *FOXO3* expression in HG3 cells with diminished *FOXO4* (Figure 5.9H), supporting increased *FOXO3* expression seen in MEC1 cells lacking *FOXO4* (Figure 5.9A-E). Further, AZD8055 and ibrutinib treatments had no effect on FOXO3 protein expression in HG3 cells (Figure 5.9G). For FOXO1,

protein expression was unaffected by *FOXO4* depletion in HG3 cells (Figure 5.9I). AZD8055-ibrutinib treatments exhibited a slight increase in FOXO1 protein expression in *FOXO4*-depleted cells, though results were variable between replicates (Figure 5.9I). The expression of FOXO1 in the SCR control was unaffected by AZD8055-ibrutinib treatment (Figure 5.9I). *FOXO1* gene expression, though increased in HG3 cells lacking *FOXO4* (Figure 5.9J), was not significant. These data perhaps highlight a mechanism through which CLL cells overcome genomic pressures induced by a lack of *FOXO4* expression *via* the overexpression of FOXO3 and FOXO1.

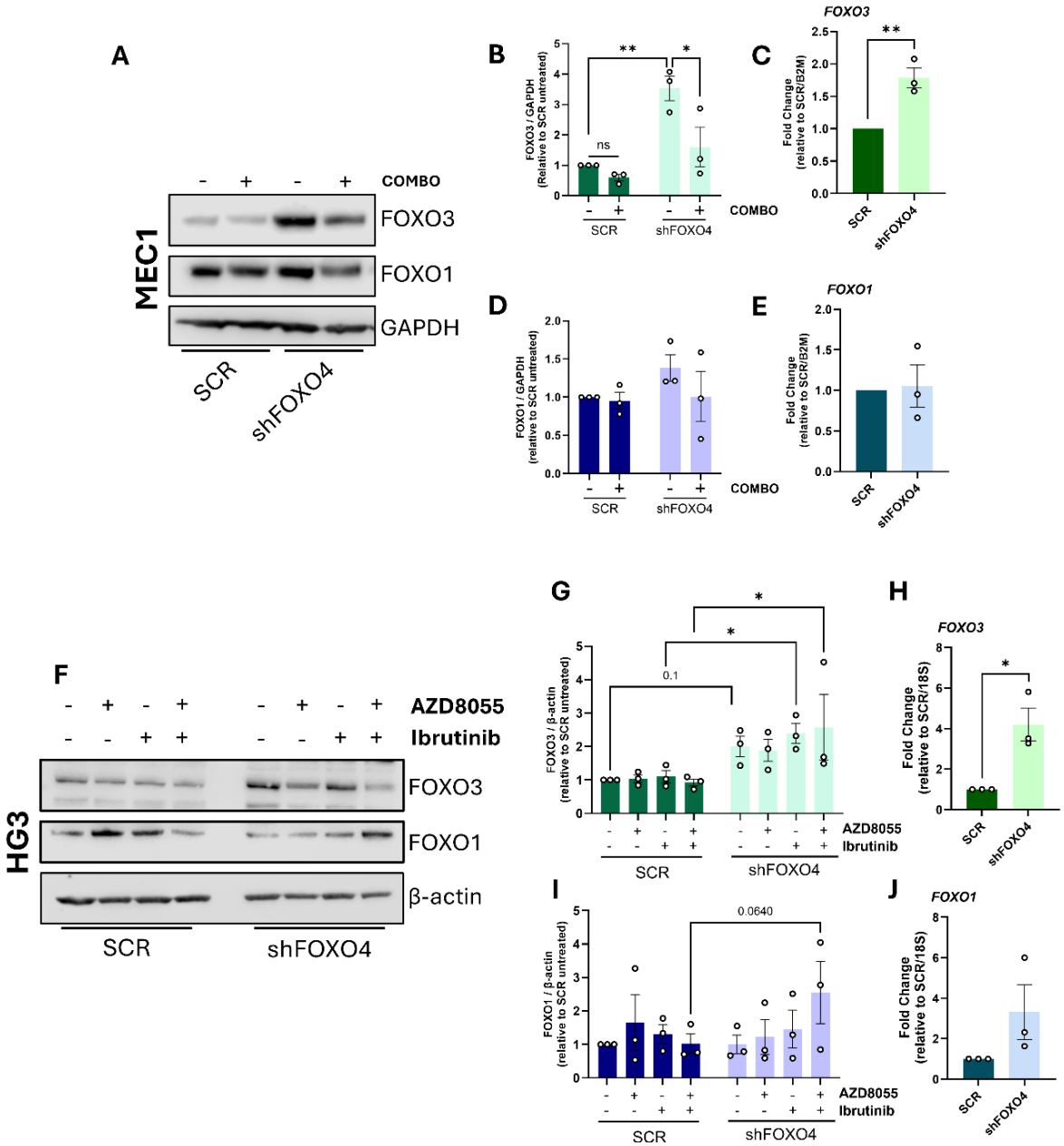

Figure 5.9: FOXO3 expression is elevated in long-term culture of FOXO4-depleted CLL cells. (A) Western blot of SCR and shFOXO4 MEC1 cells following 48 hr in culture ±COMBO (100 nM AZD8055 and 1 μM ibrutinib treatment) assessing the expression of FOXO3 and FOXO1. GAPDH was used as a loading control. (B) Quantified expression of FOXO3 in *FOXO4*-depleted MEC1 cells in 48 hr cultures ±COMBO, normalised to GAPDH and made relative to untreated SCR cells. (C) Transcript abundance

of *FOXO3* in shFOXO4 MEC1 cells attained *via* RT-qPCR, normalised to *B2M* and presented as fold change relative to SCR cells. (D) Quantified expression of FOXO1 in SCR and shFOXO4 MEC1 cells following 48 hr in culture ±COMBO treatment, normalised to GAPDH and made relative to untreated SCR cells. (E) Transcript abundance of *FOXO1* in SCR and shFOXO4 MEC1 cells following 24 hr in culture, normalised to *B2M* and presented as fold change relative to SCR cells. (F) Western blot of SCR and shFOXO4 HG£ cells following 48 hr in culture ±AZD8055 and/or ibrutinib treatment assessing the expression of FOXO3 and FOXO1. β-actin was used as a loading control. (G) Quantified FOXO3 expression in SCR and shFOXO4 HG3 cells ±AZD8055 and/or ibrutinib, normalised to β-actin and made relative to untreated SCR cells. (H) Transcript abundance of *FOXO3* in SCR and shFOXO4 HG3 cells after 24 hr in culture, normalised to *18S* and presented as fold change relative to the SCR control. (I) Quantified expression of FOXO1 in SCR and shFOXO4 HG3 cells, normalised to β-actin and made relative to untreated SCR cells. (J) *FOXO1* transcript abundance in SCR and shFOXO4 HG3 cells, normalised to *18S* and presented as fold change relative to the SCR control (n=3). Data points are depicted as white circles, and the data is represented as the mean ±SEM. Statistics were calculated using two-way ANOVA for protein expression and an unpaired student's t-test for gene fold change, where * $p \leq 0.05$, ** $p \leq 0.01$.

5.2.9. mTOR inhibition reverses a *FOXO3*-depletion-mediated loss in MEC1 cell viability

To investigate whether reducing *FOXO3* expression affected MEC1 cell viability and sensitivity to mTOR and BTK inhibition, MEC1 cells were stained with Annexin V/DAPI and assessed for changes in viability *via* flow cytometry (Figure 5.10A). MEC1 cells exhibited a significant reduction in viability following *FOXO3* knockdown (Figure 5.10B), coincident with a significant increase in apoptosis (Figure 5.10C). Ibrutinib, alone or in combination with AZD8055, elicited a decrease in MEC1 cell viability in the SCR control, albeit not significantly (Figure 5.10B). In contrast, viability was significantly increased following AZD8055 treatment, alone or in combination with ibrutinib on *FOXO3* knockdown, while ibrutinib monotherapy elicited no significant difference in viability (Figure 5.10B). This was supported by a significant decrease in MEC1 cell apoptosis in AZD8055 and AZD8055-ibrutinib-treated MEC1 cells harbouring *FOXO3* knockdown (Figure 5.10C). Of note, although these treatments reduced the population of *FOXO3*-depleted cells undergoing apoptosis, MEC1 cell viability was still lower than that of the SCR control (Figure 5.10B & C). These findings highlight a role for FOXO3 in CLL cell maintenance (perhaps *via* inducing *IGF1R* expression) and the pro-apoptotic response to AZD8055-ibrutinib treatment.

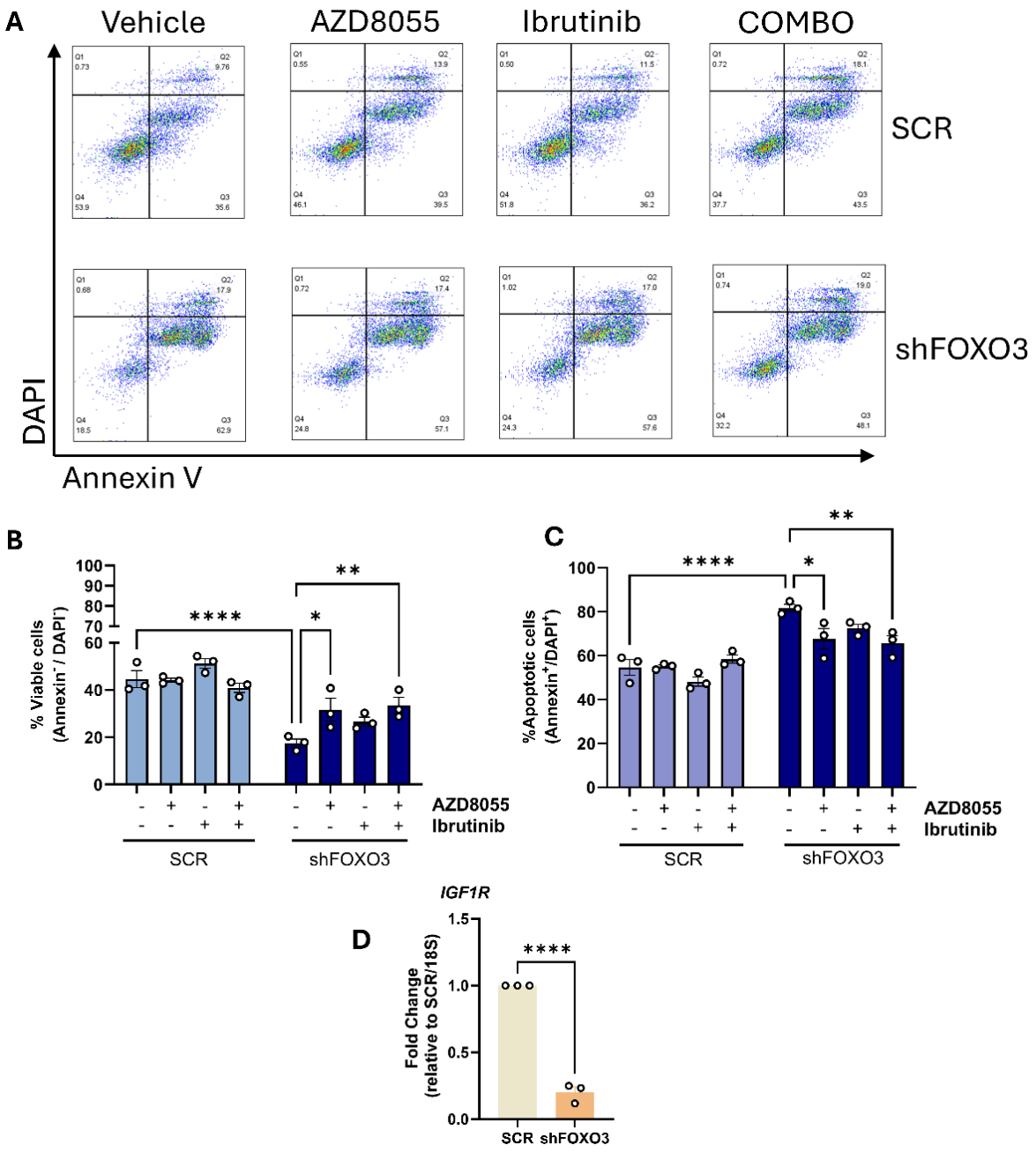

Figure 5.10: AZD8055 treatment rescues a FOXO3-knockdown-mediated loss in MEC1 cell viability. (A) Representative FACS plot of MEC1 cells following 48 hr in culture ±100 nM AZD8055 and/or 1 µM treatment and subsequent visualisation of cell viability *via* Annexin/7AAD staining. (B) Percentage of SCR and shFOXO3 MEC1 cells deemed 'viable' (Annexin^{neg}/7AAD^{neg}, Q4) following 48 hr in culture ±AZD8055 and/or ibrutinib treatment. (C) Percentage of total apoptotic SCR and shFOXO3 cells (Annexin^{pos}/7AAD^{pos}, Q2 & Q3) following 48 hr in culture ±AZD8055 and/or ibrutinib treatment. (D) Transcript abundance of *IGF1R* in SCR and shFOXO3 MEC1 cells detected *via* RT-qPCR, normalised to *18S* and presented as fold change relative to SCR cells (n=3). Data points are depicted as white circles, and the data is represented as the mean ±SEM. Statistics were calculated using two-way ANOVA for analysing cell viability and a student's t-test for gene fold change, where * $p \leq 0.05$, ** $p \leq 0.01$, **** $p \leq 0.0001$.

5.2.10. Proliferation and cell cycle progression are hindered in *FOXO3*-depleted MEC1 cells

In Figure 5.11, we investigated the impact of shRNA-mediated *FOXO3* knockdown on MEC1 cell proliferation and cell cycle progression using CTV (Figure 5.11A) and PI (Figure 5.11C) assays, respectively, and whether *FOXO3* knockdown affected the potency of combined AZD8055-ibrutinib-mediated cell cycle arrest as seen in MEC1 cells [49]. MEC1 cell proliferation was reduced in cells lacking *FOXO3* expression (Figure 5.11B), trending towards significance ($p = 0.1$, Figure 5.11B), suggesting a requirement for *FOXO3* (and *FOXO4,* Figure 5.4) to promote MEC1 cell proliferation. PI staining revealed distinct changes in cell cycle progression mediated by *FOXO3* knockdown; as expected, regardless of *FOXO3* expression, AZD8055 treatment induced a significant G1 arrest, which was enhanced in combination with ibrutinib (Figure 5.11D); *FOXO3* knockdown did not affect MEC1 G_0/G_1 populations (Figure 5.11D). Consistent with increased G_0/G_1, AZD8055 treatment depleted S phase MEC1 cell populations, which was enhanced in combination with ibrutinib (Figure 5.11E). Interestingly, *FOXO3*-depletion significantly reduced S phase cell populations in the presence and absence of drug treatment (Figure 5.11E), coinciding with increased G_0/G_1 DNA content (Figure 5.11D). Moreover, G2 DNA content exhibited little change in response to AZD8055 and/or ibrutinib treatment in the SCR control (Figure 5.11F). However, *FOXO3*-depleted cells exhibited a significant increase in MEC1 G2 DNA content (Figure 5.11F), which was significantly attenuated by AZD8055 treatment - alone or in combination with ibrutinib (Figure 5.11F). These data allude to a role for FOXO3 in the positive regulation of the cell cycle.

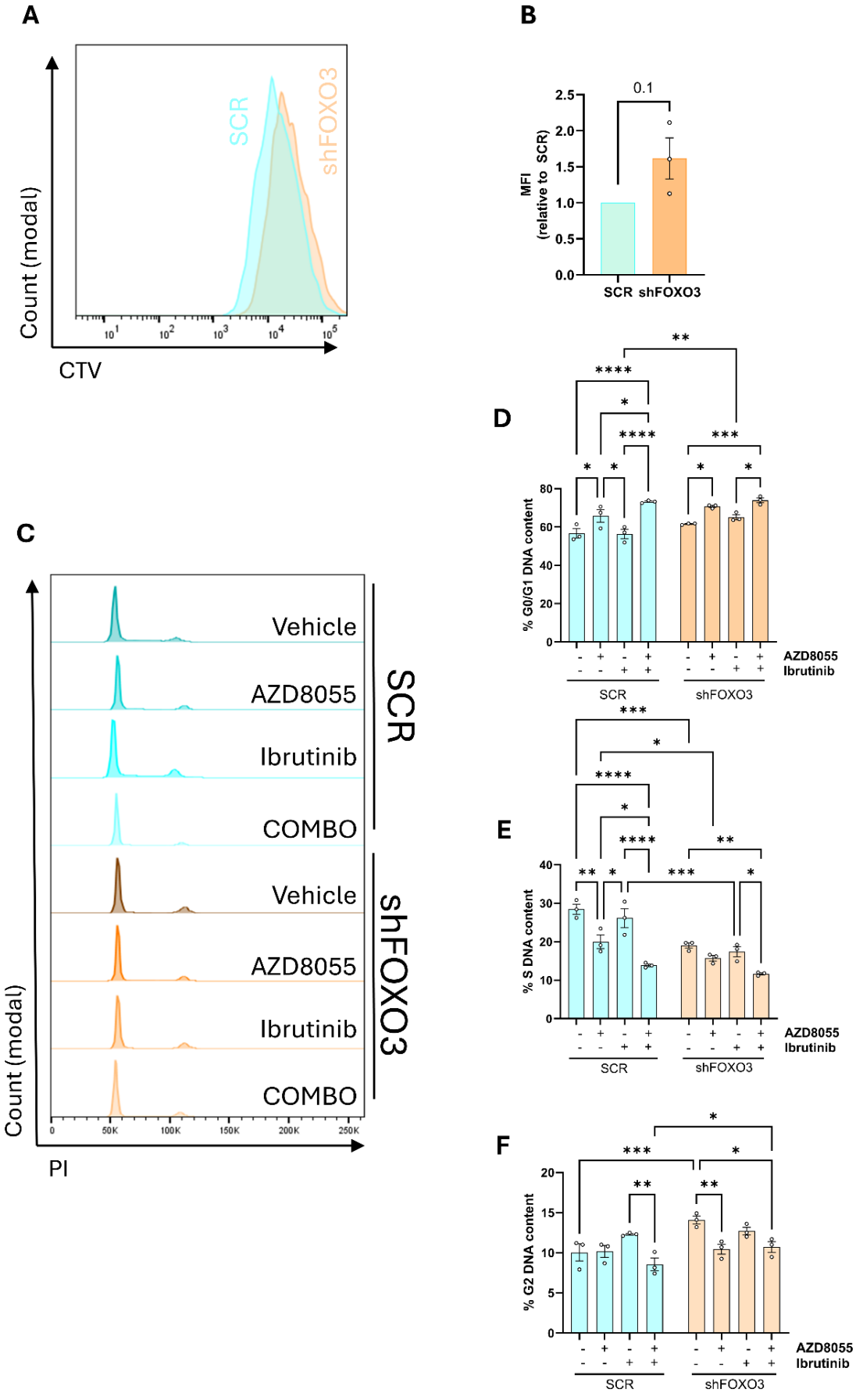

Figure 5.11: FOXO3 knockdown elicits a reduction in MEC1 proliferative capacity and aberrant cell cycle progression. (A) Representative FACS CTV histogram of SCR and shFOXO3 MEC1 cells following 72 hr in culture after being stained with CellTrace Violet™. The CTV mean fluorescence intensity was

subsequently calculated and made relative to the SCR control (B). (C) Representative PI histogram of SCR and shFOXO4 MEC1 cells that were fixed, permeabilised, subsequently stained with PI and visualised by flow cytometry following 48 hr in culture ±100 nM AZD8055 and/or 1 μM ibrutinib. (D-F) The percentage DNA content of SCR and shFOXO3 cells in G_0/G_1 (D), S (E) and G2 (F) phases were calculated using in-house FlowJo cell cycle software (n=3). Data points are depicted as white circles, and the data is represented as the mean ±SEM. Statistics were calculated using a Student's t-test to compare SCR and shFOXO4 proliferation, while a two-way ANOVA was conducted for PI analysis, where * $p \leq 0.05$, ** $p \leq 0.01$, *** $p \leq 0.001$, **** $p \leq 0.0001$.

5.2.11. FOXO target genes are differentially expressed in *FOXO3*-depleted MEC1 cells

To address how *FOXO3* knockdown in MEC1 cells affects the expression of other FOXOs (*FOXO1* and *FOXO4*) and distinct FOXO target genes involved in regulating cell survival (*BBC3, BCL2L1, BCL2L11*), cell cycle progression (*CCND2, CDKN1B*), DNA damage repair (*GADD45A*) and regulation of cell growth and/or oxidative damage (*SESN3*), we assessed the changes to these specific genes in the presence and absence of 24 hr drug treatment (Figure 5.12). No significant changes were seen in *FOXO1* or *FOXO4* expression in *FOXO3*-depleted cells (Figure 5.12A & B). However, AZD8055 treatments experienced an upregulation of *FOXO4*, which was enhanced in combination with ibrutinib (Figure 5.12B), supporting previous findings (Figures 4.2-4.5, 4.7, 4.15, [49, 284]).

Survival-associated genes were also affected by *FOXO3* depletion (Figure 5.12C-E). Specifically, although endogenous *BBC3* expression was unaffected by *FOXO3* depletion, *BBC3* exhibited a significant AZD8055-mediated upregulation, which was enhanced further in combination with ibrutinib (Figure 5.12C). This enhancement was greater in *FOXO3*-depleted cells than the SCR control (Figure 5.12C). AZD8055 and/or ibrutinib treatments significantly downregulated *BCL2L1* expression in MEC1 cells (Figure 5.12D, supporting Figures 4.7 & 5.7). Furthermore, *BCL2L1* expression was significantly depleted in MEC1 cells with depleted *FOXO3,* leading to a reduction of AZD8055-ibrutinib-mediated *BCL2L1* depletion compared to the SCR control (Figure 5.12D). On the other hand, *BCL2L11* expression was increased following AZD8055 and/or ibrutinib treatment in the SCR control, while *FOXO3*-depleted MEC1 cells exhibited diminished upregulation of *BCL2L11* in AZD8055- and/or ibrutinib-treated cells (Figure 5.12E). In the SCR control, *CCND2* expression was downregulated following

AZD8055 and ibrutinib treatment, alone or in combination (Figure 5.12F). Further, *FOXO3*-depletion elicited a significant downregulation of *CCND2* compared to that of the SCR control (Figure 5.12F), which was further downregulated by AZD8055 treatment and enhanced in combination with ibrutinib (Figure 5.12F). *CCND2* downregulation was significantly higher in *FOXO3*-depleted cells than in the SCR control (Figure 5.12F). Further, *CDKN1B* expression was increased in the SCR control following AZD8055 treatment and was enhanced in combination with ibrutinib (Figure 5.12E, supporting Figures 4.7, 4.16, 5.7, [49, 284]). Moreover, *FOXO3* depletion enhanced AZD8055-ibrutinib-mediated *CDKN1B* upregulation, trending towards significance ($p = 0.08$, Figure 5.12E). *GADD45A* expression was effectively diminished in AZD8055-treated SCR cells, alone or in combination with ibrutinib (Figure 5.12H), supporting Figures 4.7 & 4.20). Akin to *GADD45A* expression in *FOXO4*-depleted MEC1 cells (Figure 5.7), *GADD45A* expression was abrogated following *FOXO3* depletion in MEC1 cells, trending towards significance (Figure 5.12H), rendering *GADD45A* ineffective to further AZD8055-mediated downregulation (Figure 5.12H). Finally, ibrutinib treatment, alone or in combination with AZD8055, nominally increased *SESN3* expression, regardless of *FOXO3* expression (Figure 5.12I, supporting Figures 4.7 & 5.7). These findings highlight the importance of FOXO3 in regulating FOXO target genes involved in numerous cellular processes.

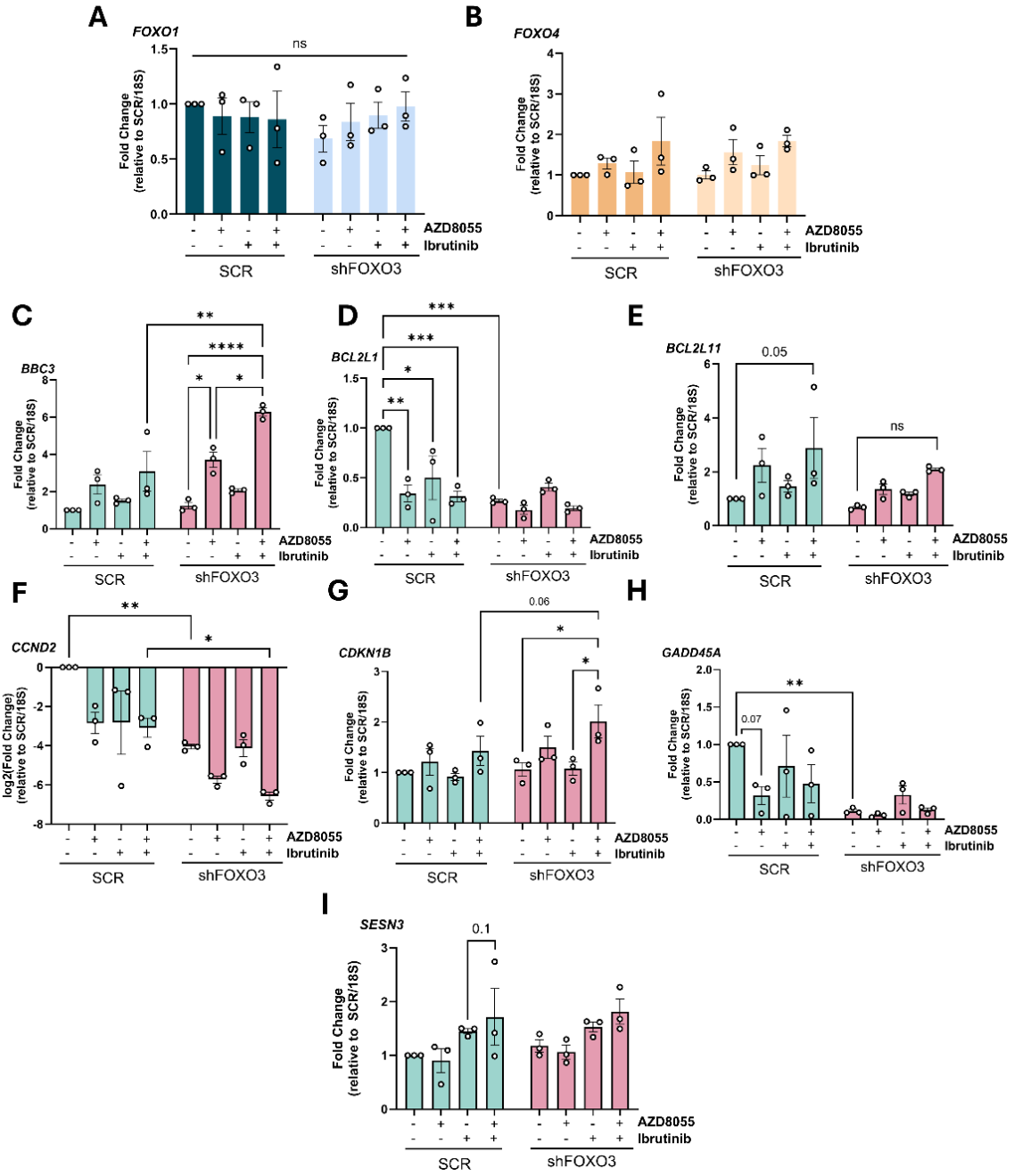

Figure 5.12: Distinct FOXO target genes are aberrantly expressed endogenously or in response to AZD8055-ibrutinib treatment in FOXO3-depleted MEC1 cells. (A-I) *FOXO3*-depleted MEC1 cells were cultured for 24 hr ±100 nM AZD8055 and/or 1 μM ibrutinib. Samples were then collected to generate RNA to use in RT-qPCR to detect the transcript abundance of *BBC3* (A), *BCL2L1* (B), *BCL2L11* (C), *CCND2* (D), *CDKN1B* (E), *GADD45A* (F) and *SENS3* (G). Expression values were normalised to *18S* and presented as fold change relative to the SCR control (n=3). Data points are depicted as white circles, and the data is represented as the mean ±SEM. Statistics were calculated using a two-way ANOVA, where * $p \leq 0.05$, ** $p \leq 0.01$, *** $p \leq 0.001$, **** $p \leq 0.0001$.

5.2.12. shRNA-mediated *FOXO3* knockdown does not affect FOXO-associated protein expression

As was conducted for cells with diminished *FOXO4*, we investigated whether shRNA-mediated *FOXO3* knockdown affected the expression of FOXO family members as well as distinct FOXO targets in the presence and absence of drug treatments. FOXO1 expression was unaffected by *FOXO3* depletion, either alone or in the presence of AZD8055 and ibrutinib treatments (Figure 5.13A & B). Interestingly, while *FOXO3*-depleted cells exhibited varying levels of FOXO4, AZD8055 and ibrutinib treatments depleted FOXO4 expression in MEC1 cells, regardless of *FOXO3* expression (Figure 5.13C, supporting Figure 4.8). MCL1, BCL-XL and $p21^{kip1}$ expression varied between samples and was unaffected by *FOXO3* depletion, where AZD8055 and ibrutinib treatments elicited little change in expression (Figure 5.13D-F). GADD45A expression was significantly depleted in the SCR control following combined AZD8055-ibrutinib treatment (Figure 5.13G), supporting GADD45A depletion exhibited by AZD8055-treated MEC1 and primary CLL cells (Figures 4.7 & 4.20). AZD8055-mediated *GADD45A* depletion was also apparent in *FOXO3*-depleted cells. However, due to sample variability in this context, it lacked significance (Figure 5.13A & G). Furthermore, BIM_{EL} expression was significantly increased following AZD8055-ibrutinib treatment, regardless of *FOXO3* expression status (Figure 5.13H) indicating that, in long-term MEC1 cultures, BIM expression is unaffected by *FOXO3* depletion, while short-term study indicated that *FOXO3* depletion induced BIM upregulation (Figure 5.3). leading to reduced MEC1 cell viability (Figure 5.10).

PUMA, a pro-apoptotic FOXO3 target encoded by *BBC3* [593], was differentially expressed and regulated by AZD8055 (alone or in combination) in cells lacking *FOXO3* expression (Figure 5.13I); PUMA expression was increased following *FOXO3* depletion (Figure 5.13J); and drug treatments enhanced PUMA expression, where the strongest PUMA expression was exhibited in shFOXO3 cells treated with AZD8055-ibrutinib (Figure 5.13J).

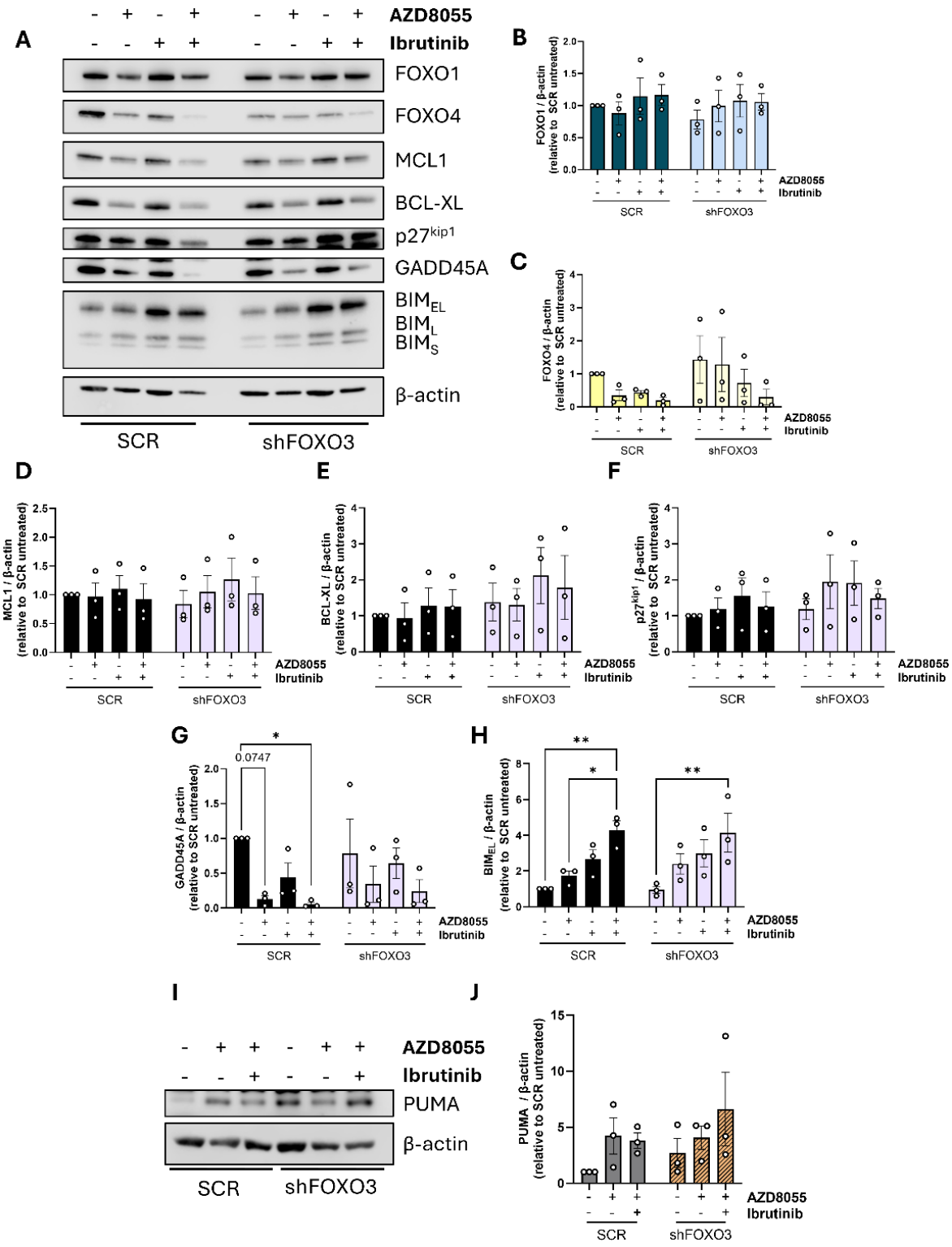

Figure 5.13: FOXO-associated proteins are unaffected by shRNA-mediated FOXO3 knockdown. (A) Western blot of lysates attained following 48 hr culture of SCR and shFOXO3 MEC1 cells ±100 nM AZD8055 and/or 1 μM ibrutinib, assessing the expression of FOXO1, FOXO4, MCL1, BCL-XL, $p27^{kip1}$, GADD45A and BIM. β-actin was used as a loading control. (B-H) Quantified expression of FOXO1 (B), FOXO3 (C), MCL1 (D), BCL-XL (E), $p27^{kip1}$ (F), GADD45A (G) and BIM_{EL} (H) in shFOXO3 cells compared to the SCR control following 48 hr culture ±AZD8055 and/or ibrutinib. Expression values were normalised to β-actin and made relative to the SCR control (n=3). (I) Western blot analysing the expression of PUMA in shFOXO3 MEC1 cells following 48 hr in culture ±100 nM AZD8055, alone or in combination with 1 μM ibrutinib. β-actin was used as a loading control. (J) Quantified expression of PUMA following 48 hr culture of shFOXO3 MEC1 cells ±AZD8055, alone or in combination with ibrutinib, normalised to

β-actin and made relative to untreated SCR cells (n=3). Data points are depicted as white circles, and the data is represented as the mean ±SEM. Statistics were calculated using a two-way ANOVA, where * $p \leq 0.05$, ** $p \leq 0.01$.

5.2.13. GADD45A is diminished in *FOXO3*- and *FOXO4*-depleted MEC1 cells

GADD45 proteins are typically known for being induced in response to elevated DNA damage (reviewed in [627]). As *GADD45* genes are FOXO targets [439], we hypothesised that a depletion of *FOXO3/4*, and subsequently of *GADD45A*, would be indicative of a reduced repair mechanism to combat DNA damage. Therefore, we investigated the expression of GADD45A in MEC1 cells lacking *FOXO3* and *FOXO4* expression, and changes in γ-H2AX^{S139} abundance following *FOXO3* ablation, with a focus on whether drug treatments affected the intracellular accumulation of γ-H2AX^{S139}. Detected *via* Western blot (Figure 5.14A), GADD45A expression was significantly reduced in MEC1 cells deficient in either *FOXO3* or *FOXO4* compared to the SCR control (Figure 5.15B), supporting earlier gene profiling of *GADD45A* in *FOXO3*- and *FOXO4*-depleted MEC1 cells (Figures 5.7 & 5.12). Furthermore, GADD45A protein expression was significantly reduced in MEC1 cultures lacking *FOXO3* expression compared to cells lacking *FOXO4* expression (Figure 5.14B). These data were corroborated by reduced *GADD45A* gene expression in sh*FOXO3* and sh*FOXO4* MEC1 cells (Figure 5.14C). *GADD45A* downregulation in *FOXO4*-depleted MEC1 cells was more profound than in *FOXO3*-depleted cells, and so exhibited increased significance (Figure 5.14C). Investigating γ-H2AX^{S139} accumulation *via* intracellular staining (Figure 5.14D & E), γ-H2AX^{S139} status was not affected by AZD8055 and/or ibrutinib treatments in the SCR control. Moreover, *FOXO3* depletion did not affect endogenous γ-H2AX^{S139}. However, AZD8055 treatments, alone or in combination with ibrutinib, did increase intracellular γ-H2AX^{S139} (Figure 5.14E). Notably, combined AZD8055-ibrutinib treatment aggregated greater levels of γ-H2AX^{S139}, more than that of combined AZD8055-ibrutinib treatment in the SCR control, which elicited no increase in γ-H2AX^{S139} abundance ($p = 0.08$, Figure 5.14E). These findings indicate that mTOR inhibition induces increased DNA damage in cells lacking *FOXO3* expression, perhaps due to a lack of DNA damage regulation mediated by FOXO3-GADD45A.

-H

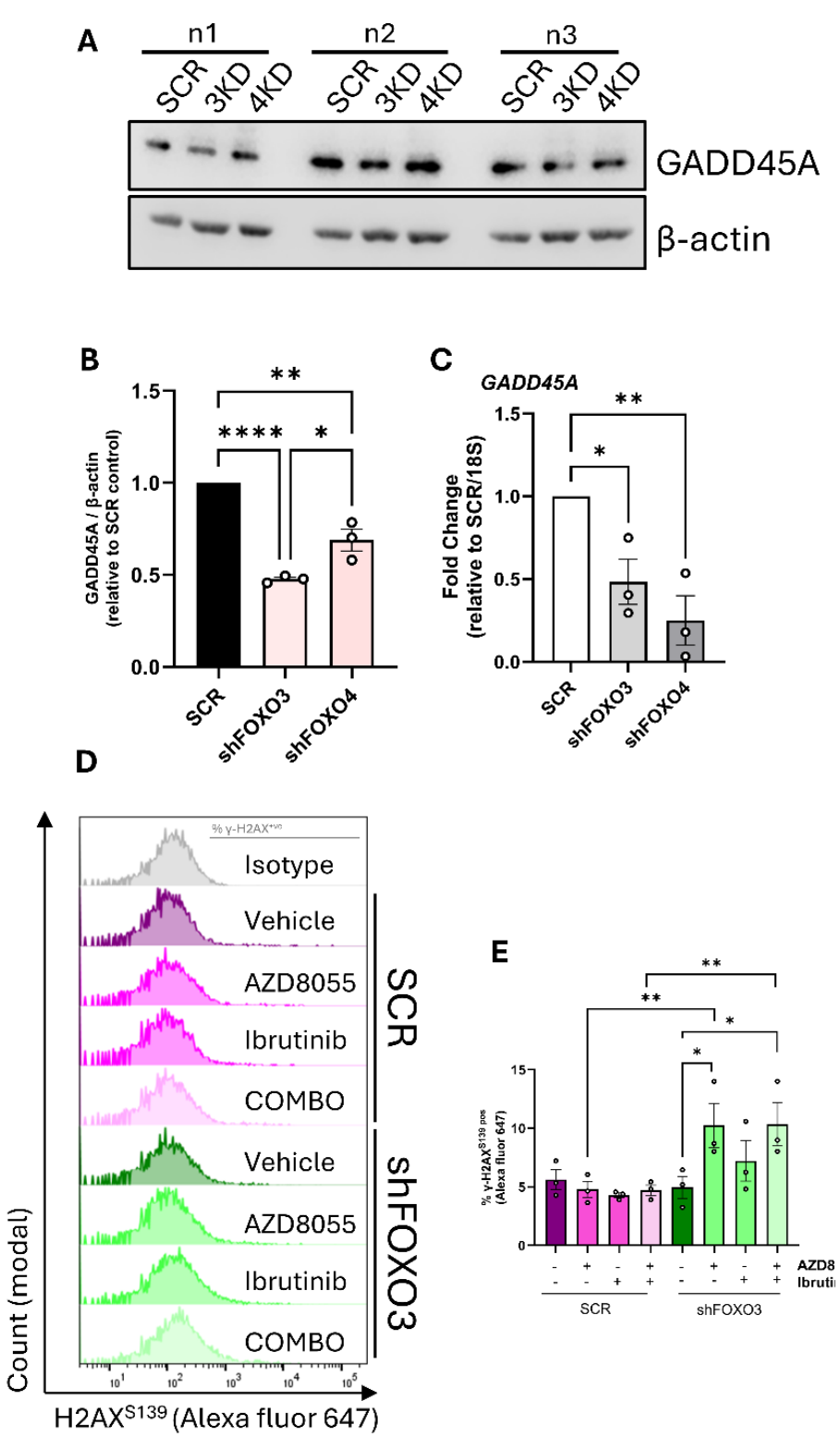

Figure 5.14: FOXO3- and FOXO4-depleted MEC1 cells exhibit diminished GADD45A expression, coinciding with increased γ-H2AX^{S139} expression in cells following AZD8055 treatment. (A) Western blot of SCR, shFOXO3 (3KD) and shFOXO4 (4KD) MEC1 cells following 24 hr in culture, assessing the expression of GADD45A. β-actin was used as a loading control. (B) Quantified expression of GADD45A in SCR, 3KD and 4KD cells, normalised to β-actin and made relative to the SCR control. (C) Transcript abundance of *GADD45A* in SCR, 3KD and 4KD cells, detected *via* RT-qPCR after 48 hr in culture. Expression values are normalised to *18S* and presented as fold change relative to the SCR control (n=3). (D) Representative FACS histogram of γ-H2AX^{S139} levels in SCR and shFOXO3 MEC1 cells following 48 hr in culture ±100 nM AZD8055 and/or 1 μM ibrutinib. Intracellular staining was performed to detect intracellular γ-H2AX^{S139} levels as a percentage following removal of background using the

isotype control (gate shown). Of note, an isotype control was used to select cells positive for γ-H2AX^{S139} expression. (E) Expression of γ-H2AX^{S139} taken as a percentage of the total MEC1 cell population in SCR and shFOXO3 MEC1 cells following 48 hr in culture ±AZD8055 and/or ibrutinib (n=3). Data points are depicted as white circles, and the data is represented as the mean ±SEM. Statistics were calculated using a one-way ANOVA for comparing GADD45A expression, while a two-way ANOVA was used for comparing γ-H2AX^{S139} levels. * p ≤ 0.05, ** p ≤ 0.01, **** p ≤ 0.0001.

5.2.14. γ-H2AX accumulation is increased in *FOXO4*-depleted CLL cell lines following mTOR inhibition

Next, we explored whether γ-H2AX^{S139} accumulation existed in MEC1 and HG3 cells harbouring shRNA-mediated *FOXO4* knockdowns, and whether AZD8055 (100 nM) and/or ibrutinib (1 μM) treatment affected intracellular γ-H2AX^{S139} accumulation in cells lacking *FOXO4*. Detecting γ-H2AX^{S139} levels *via* flow cytometry after 48 hr in culture (Figure 5.15A & C), endogenous levels of γ-H2AX^{S139} in MEC1 and HG3 cells exhibited nominal change due to shRNA-mediated *FOXO4* knockdown (Figure 5.15B & D). Further, AZD8055 and ibrutinib treatments elicited only a modest increase in γ-H2AX^{S139} levels in MEC1 and HG3 SCR controls (Figure 5.15B & D). In contrast, γ-H2AX^{S139} levels were elevated in *FOXO4*-depleted MEC1 cells following single treatments with AZD8055 and ibrutinib, while AZD8055-ibrutinib combination treatment significantly increased γ-H2AX^{S139} accumulation in MEC1 cells (Figure 5.15B). Furthermore, γ-H2AX^{S139} levels were significantly increased in HG3 cells following AZD8055 treatment, alone or in combination with ibrutinib (Figure 5.15D). Significant elevations of γ-H2AX^{S139} in *FOXO4*-depleted cells were significantly higher than that of their respective SCR counterparts (Figure 5.15B & D). Collectively, Figures 5.14 and 5.15 allude to a role for FOXO3 and FOXO4 in inducing *GADD45A* expression, where an absence of *FOXO3* or *FOXO4* expression increases CLL cell susceptibility to AZD8055-ibrutinib-mediated stress, such as accumulation of double-strand breaks (indicated by elevated γ-H2AX^{S139}).

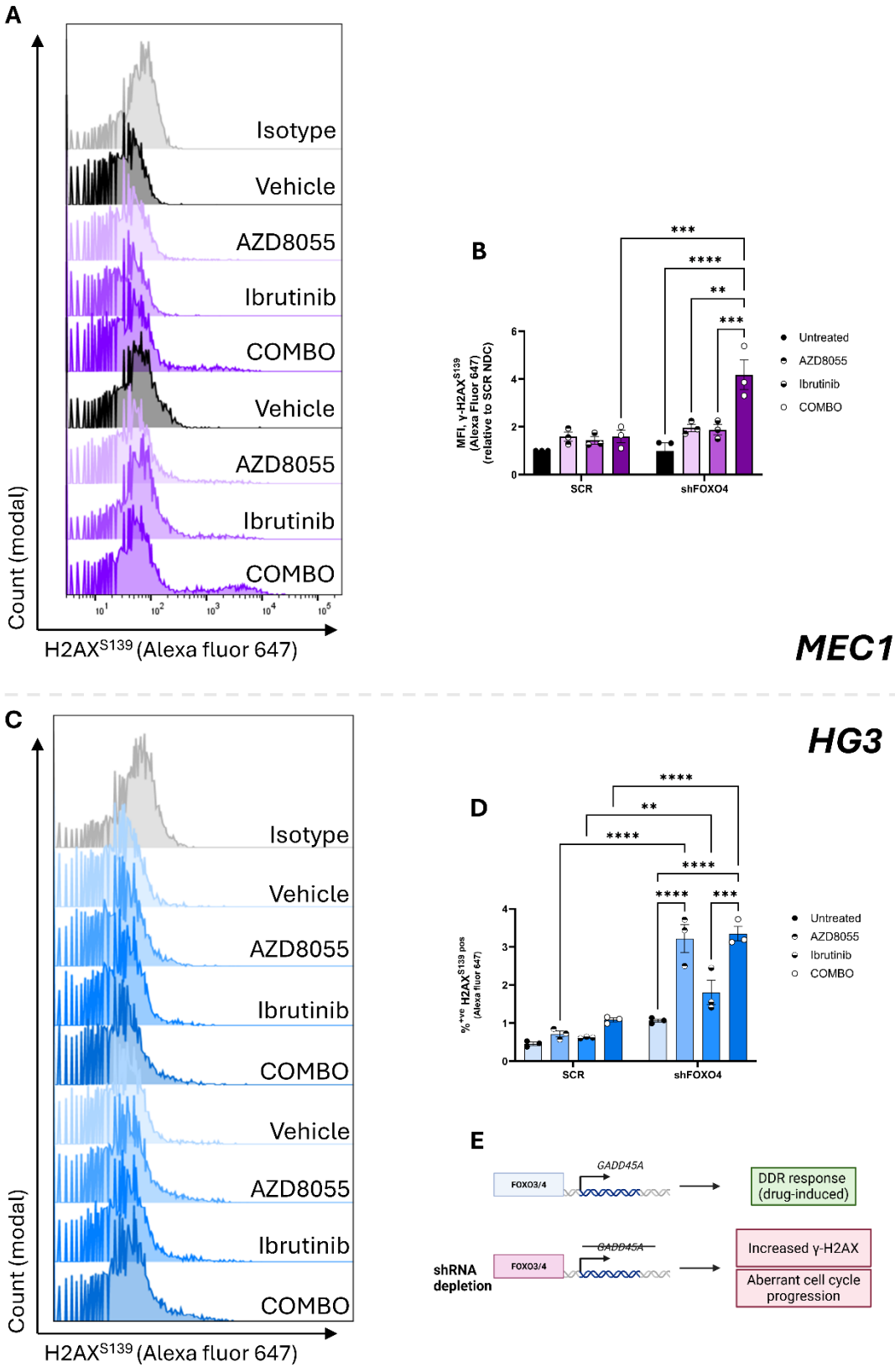

Figure 5.15: FOXO4-depleted MEC1 and HG3 cells exhibit a drug-mediated increase in γ-H2AX^{S139} accumulation. MEC1 and HG3 cells were cultured for 48 hr ±100 nM AZD8055 and/or 1 μM ibrutinib and were then fixed and permeabilised and stained to detect intracellular γ-H2AX^{S139}. Isotype controls were used to select for cells positive for γ-H2AX^{S139} accumulation. (A) Representative FACS histogram of SCR and shFOXO4 MEC1 cells following 48 hr in culture intracellular staining to detect γ-H2AX^{S139}

±AZD8055 and/or ibrutinib. (B) The mean fluorescence intensity (MFI) of γ-H2AX^{S139} accumulation in SCR and shFOXO4 MEC1 cells was attained from FACS histograms and made relative to untreated SCR cells (n=3). (C) Representative FACS histogram of HG3 cells following 48 hr culture ±AZD8055 and/or ibrutinib and subsequent intracellular staining to detect for γ-H2AX^{S139}. Gating is shown. (D) γ-H2AX^{S139} accumulation in *FOXO4*-depleted cells was calculated as a percentage of the total population, made relative to the SCR control (n=3). (E) Proposed schematic for the relationship between FOXO3/4 depletion, GADD45A expression and subsequent aberrant cell cycle progression and drug-induced accumulation of γ-H2AX^{S193} in MEC1 and HG3 cells. Data points are depicted as patterned circles (see key), and the data is represented as the mean ±SEM. Statistics were calculated using a two-way ANOVA, where ** $p \leq 0.01$, *** $p \leq 0.001$, **** $p \leq 0.0001$.

5.2.15. *FOXO4*-depleted MEC1 and HG3 cells are sensitised to venetoclax treatment in a dose-dependent manner

The increased chemosensitivity exhibited by MEC1 and HG3 cells due to *FOXO4* depletion (Figure 5.6) suggests an increased susceptibility of CLL cells to other targeted agents. Therefore, in the context of other CLL therapies, we treated HG3 and MEC1 cells with venetoclax dose increments (1-1000 nM, as indicated in Figure 5.16) following shRNA-mediated *FOXO4* knockdown, and compared relative levels of apoptosis in *FOXO4*-depleted cells to a SCR control *via* Annexin/DAPI staining. HG3 cell viability was significantly reduced in *FOXO4*-depleted cells compared to the SCR control ($p = 0.003$, Figure 5.16A & B). Interestingly, as venetoclax concentration increased, *FOXO4*-depeleted HG3 cells exhibited a more significant reduction in cell viability compared to the SCR control. In contrast, *FOXO4*-depleted MEC1 cells exhibited similar cell viability to that of the SCR control (Figure 5.16C). Nonetheless, MEC1 cell viability was significantly reduced in *FOXO4*-depleted MEC1 cells compared to the SCR control and achieved significance when venetoclax concentration was increased ≥10 nM (10 nM: $p = 0.0149$, 100 nM: $p = 0.0073$, 1000 nM: $p = 0.0022$). Furthermore, between 10 and 1000 nM venetoclax, there were significant, dose-dependent reductions in cell viability in *FOXO4*-depleted MEC1 and HG3 cells that were absent in their respective SCR controls (HG3: $p = <0.0001$, MEC1: $p = 0.0124$, Figure 5.16B & C). These findings highlight a dose-dependent increase in

susceptibility to venetoclax following ablation of *FOXO4* and reinforce a need for *FOXO4* expression to promote resistance in CLL cells in multiple drug contexts.

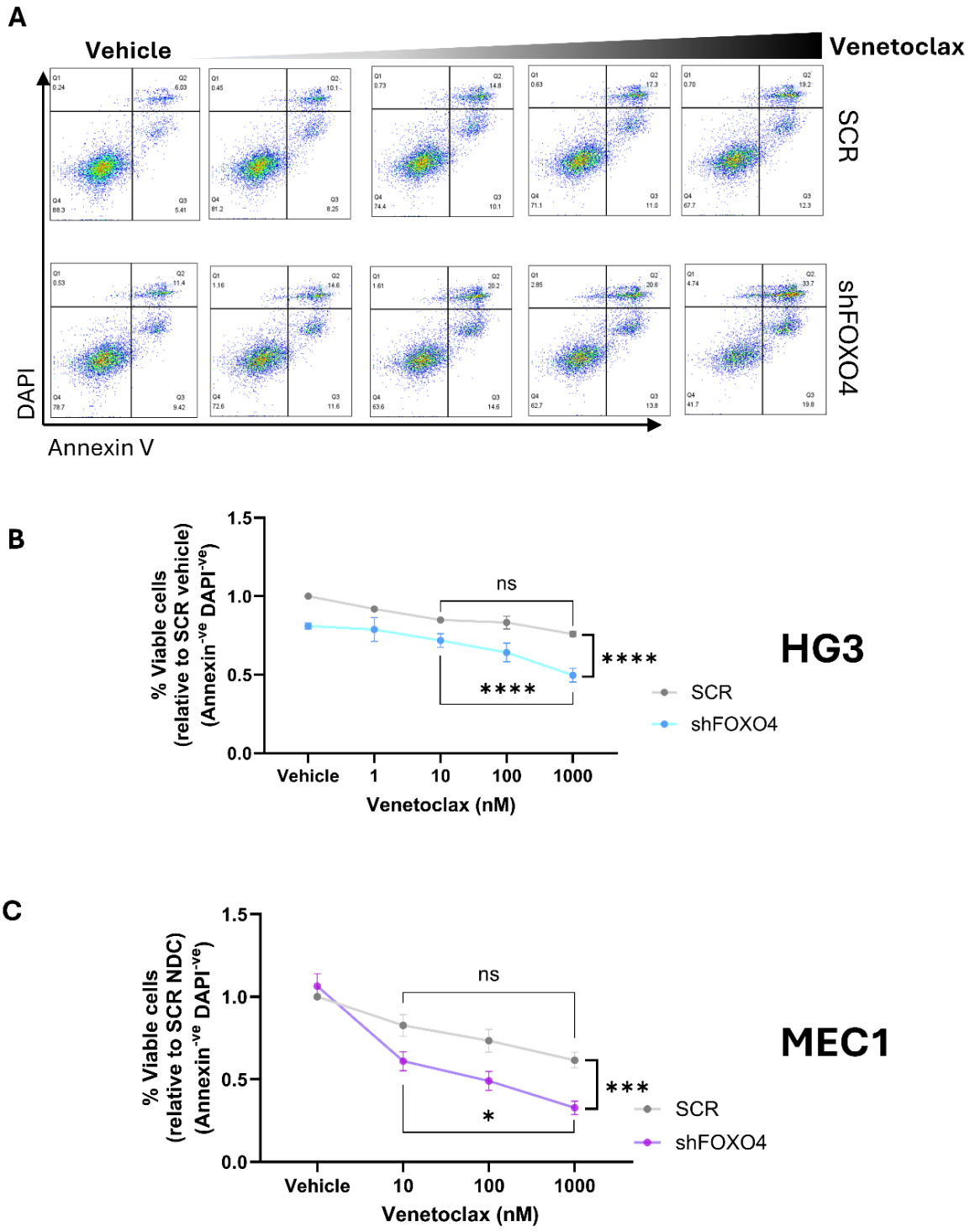

Figure 5.16: shRNA-mediated FOXO4 knockdown sensitises HG3 and MEC1 cells to dose-dependent venetoclax treatment. HG3 and MEC1 cells were cultured for 48 hr in the presence of increasing dosages of venetoclax (0 'vehicle' – 1000 nM) and were subsequently stained with Annexin/DAPI and visualised *via* flow cytometry to detect for dose-dependent CLL cell death. (A) Representative FACS plot of SCR and shFOXO4 HG3 cells cultured with different dosages of venetoclax, with increased venetoclax dosage indicated by a darkening gradient (top). AnnexinV/DAPI staining was used to detect cell death. (B & C) Line graphs quantifying the percentage of 'viable' (Annexin^{neg}/DAPI^{neg}) SCR (grey) and shFOXO4 (HG3: blue, MEC1: purple) cells exposed to dose-dependent venetoclax treatment, made relative to untreated SCR cells. Of note, HG3 cells were

treated in the range of 1 – 1000 nM venetoclax, while MEC1 cells were treated in a range of 10 – 1000 nM venetoclax. Data points are depicted as coloured circles, and the data is represented as the mean ±SEM. Statistics were calculated using a two-way ANOVA, where * $p \leq 0.05$, *** $p \leq 0.001$, **** $p \leq 0.0001$.

5.2.16. Venetoclax sensitivity is partnered with aberrant PARP and BCL2 family expression in *FOXO4*-depleted cells

FOXO-mediated regulation of venetoclax sensitivity has been reported in DLBCL [628]. Furthermore, FOXO activity has been associated with the regulation of other BCL2 family members [618, 629], highlighting an intricate network through which FOXO proteins regulate cell survival, and inferring that venetoclax sensitivity could be associated with FOXO activity in CLL. In Figure 5.17, we investigated the distinct expression of PARP and BCL2 family proteins to understand how *FOXO4* depletion affects the expression of such anti-apoptotic proteins in response to dose-dependent venetoclax treatment in MEC1 and primary CLL cells (Figure 5.17A & B, respectively). Endogenous PARP was higher in *FOXO4*-depleted MEC1 cells, and its expression was further enhanced with venetoclax treatment in a dose-dependent manner (Figure 5.17C). This was reflected in primary CLL cells where, although endogenous PARP was lower than in the SCR control, PARP exhibited a dose-dependent increase in cells lacking *FOXO4*, as well as the expression of cleaved (c-)PARP (Figure 5.17B). Further, SCR MEC1 cells elicited a dose-dependent increase in MCL1 and BCL-XL, both of which achieved significance in cells treated with 1000 nM venetoclax ($p = 0.032$ and 0.0006, respectively, Figure 5.17D & E). While, in primary CLL cells, MCL1 and BCL-XL were reduced in the SCR control in a dose-dependent manner (Figure 5.17B). However, MCL1 expression was significantly increased in *FOXO4*-depleted MEC1 cells, in cells treated with 100 and 1000 nM venetoclax (Figure 5.17D). Furthermore, MCL1 expression in *FOXO4*-depleted MEC1 cells treated with 1000 nM venetoclax was significantly higher than in the SCR control (Figure 5.17D). In primary CLL cells, however, MCL1 expression was reduced in cells lacking *FOXO4* expression (Figure 5.17B). Conversely, *FOXO4* depletion attenuated a dose-dependent increase in BCL-XL, where *FOXO4*-depleted MEC1 cells treated with

1000 nM venetoclax expressed significantly less BCL-XL than SCR cells treated with 1000 nM venetoclax (Figure 5.17E). This was reflected in primary CLL cells, where *FOXO4*-depleted cells exhibited diminished BCL-XL expression (Figure 5.17B). Finally, BCL2 expression was elevated in *FOXO4*-depleted MEC1 cells, which was increased further following dose-dependent venetoclax treatment (Figure 5.17F). Of note, BCL2 expression was not detected in primary CLL cells due to difficulties in chemiluminescent detection (Figure 5.17B). These data support a role for FOXO4 in promoting drug resistance in CLL cells.

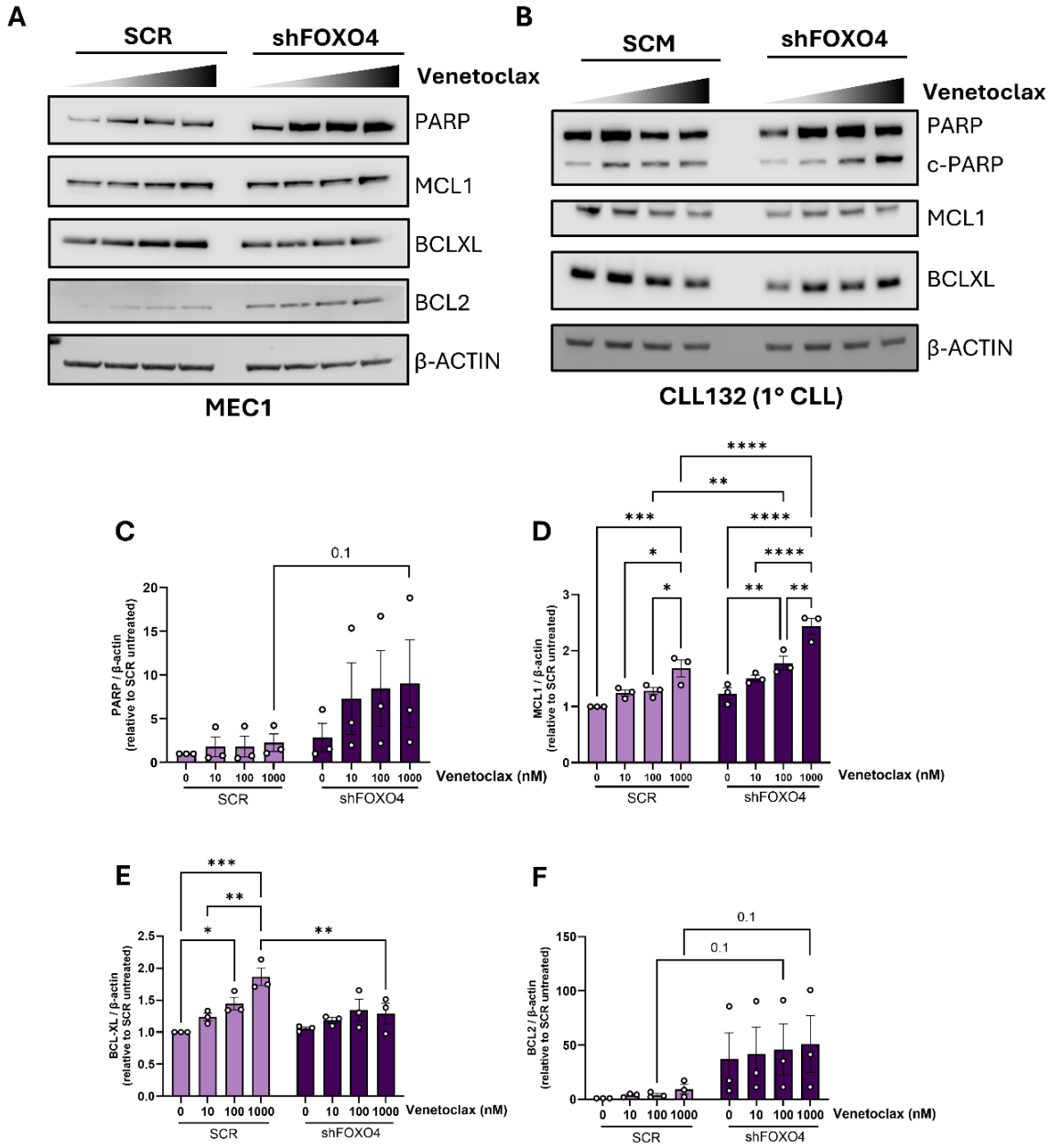

Figure 5.17: Increased venetoclax sensitivity in MEC1 cells coincides with the aberrant expression of PARP and the BCL2 family members. (A) Western blot assessing the expression of PARP, MCL1, BCL-XL, BCL2 in SCR and shFOXO4 MEC1 cells subject to varying dosages of venetoclax for 48 hr (0 – 1000 nM, represented by a darkening gradient). (B) Western blot assessing the expression of PARP, cleaved PARP (c-PARP), MCL1 and BCLXL in SCR and *FOXO4*-depleted CLL patient sample

#132, following lentiviral knockdown and subsequent CD40L co-culture for 48 hr ±10 – 1000 nM venetoclax (n=1). In both cases, β-actin was used as a loading control. (C-F) Quantified expression of PARP (C), MCL1 (D), BCL-XL (E) and BCL2 (F) in SCR and shFOXO4 MEC1 cells following 48 hr in culture ±10 – 1000 nM venetoclax, normalised to β-actin and made relative to the SCR control. Data points are depicted as white circles, and the data is represented as the mean ±SEM. Statistics were calculated using a two-way ANOVA, where * $p \leq 0.05$, ** $p \leq 0.01$, *** $p \leq 0.001$ **** $p \leq 0.0001$.

5.2.17. FOXO-associated genes are differentially regulated in *FOXO4*-depleted primary CLL cells

In Figure 5.18, we investigated whether *FOXO4* knockdown affects FOXO isoform and FOXO target gene expression in primary CLL cells in CD40L co-culture (+10 ng/mL IL-4). Primary CLL cells were transduced with shFOXO4 lentivirus and were then cultured in CD40L co-cultures for 24 hr, where we then investigated the expression of *FOXO4, FOXO1, FOXO3, CCND2, CDKN1B, BCL2L1, MCL1* and *BCL2L11*. Of note, expression data for AZD8055 and/or ibrutinib treatment is only included for *BCL2L11* as no obvious changes were seen for the other targets in response to drug treatment. Initial profiling the cells for *FOXO4* expression determined that a modest, yet effective knockdown was achieved in CD40L co-cultures (~30%, Figure 5.18A). *FOXO1* and *FOXO3* were also significantly reduced (Figure 5.18B & C). Further, *CCND2* expression was reduced, trending towards significance ($p = 0.06$, Figure 5.18D). *CDKN1B* expression was also significantly decreased (Figure 5.18E), supporting a loss in $p27^{kip1}$ expression seen in long-term HG3 cell cultures with ablated *FOXO4* (Figure 5.5). Pro-survival BCL2 family gene expression was also significantly reduced in primary cells harbouring *FOXO4* knockdowns, including *BCL2L1* and *MCL1* (Figure 5.18F-G), supporting reduced *BCL2L1* and BCL-XL expression seen in *FOXO4*-depleted MEC1 cells (Figures 5.7-5.8). Of note, shRNA-mediated knockdown did not affect endogenous *BCL2L11* expression in primary CLL cell co-cultures (Figure 5.18H). However, *BCL2L11* expression was significantly increased in *FOXO4*-depleted cells treated with AZD8055 and ibrutinib, leading to a significantly higher expression than SCR cells treated with AZD8055 and ibrutinib, thereby mimicking *BCL2L11*/BIM expression exhibited by *FOXO4*-depleted HG3 and MEC1 cell cultures following AZD8055-ibrutinib combination treatment (Figures 5.7 & 5.8) and confirming an increased presence of a pro-apoptotic gene signature in primary CLL cells in the absence of

proper *FOXO4* expression. A collective decrease in pro-survival gene expression combined with increased *BCL2L11* expression could perhaps explain the increased sensitivity to COMBO-treatment-induced cell death (Figure 5.6) in *FOXO4*-depleted primary CLL cells.

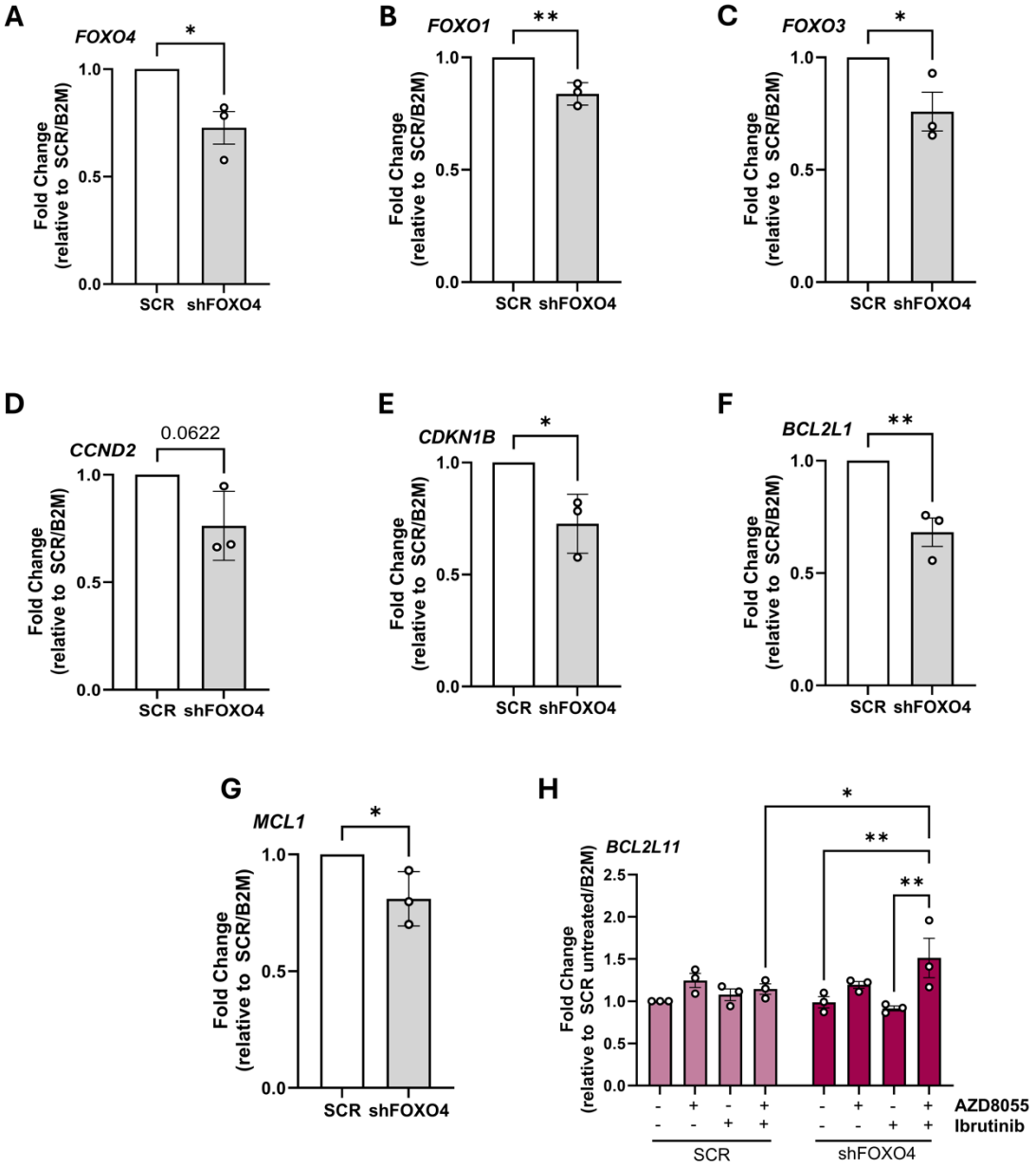

Figure 5.18: shRNA-mediated FOXO4 knockdown affects FOXO1/3 and FOXO target gene expression in primary CLL cells. Primary CLL cells were exposed to sh*FOXO4*-containing lentivirus for 72 hr on a supportive 'NTL' monolayer, followed by overnight equilibration on CD40L-expressing stroma (+10 ng/mL IL-4). Primary CLL cells were then cultured for 24 hr ±100 nM AZD8055 and/or 1 μM ibrutinib (drug treatment data only shown for H) followed by the generation of RNA to be used in RT-qPCR. (A-G) The expression of *FOXO4* (A), *FOXO1* (B), *FOXO3* (C), *CCND2* (D), *CDKN1B* (E), *BCL2L1* (F) and *MCL1* (G) in *FOXO4*-depleted primary CLL cells, normalised to *B2M* and presented as fold change relative to the SCR control. (H) *BCL2L11* transcript abundance in *FOXO4*-depleted primary CLL cells following 24 hr in CD40L co-culture (+IL-4) ±AZD8055 and/or ibrutinib, normalised to *18S* and presented as fold change relative to the SCR control. Data points are depicted as white circles, and

the data is represented as the mean ±SEM. Statistics were calculated using a Student's t-test for A-G, while a two-way ANOVA was used to calculate significance for *BCL2L11* expression using drug treatments. * p ≤ 0.05, ** p ≤ 0.01.

5.2.18. shRNA-mediated *FOXO4* knockdown increases MEC1 cell size

FOXO activity can directly and indirectly regulate mTORC1 activity [437, 438]. These findings demonstrate multiple avenues through which FOXOs could regulate phenotypic changes in CLL. We identified that, when gating for 'viable' cell populations using FSC-A and SSC-A, *FOXO4*-depleted MEC1 cell FSC values were significantly higher than that of the SCR control (Figure 5.19A & C), demonstrating that *FOXO4* ablation increased MEC1 cell size. As expected, combined AZD8055-ibrutinib treatment (COMBO) significantly reduced MEC1 cell size, irrespective of *FOXO4* expression status (figure 5.19C), although COMBO-treated *FOXO4*-depleted cells retained a higher cell size compared to COMBO-treated SCR cells, albeit not significantly (p = 0.13, Figure 5.19C). Increased cell size in the absence of *FOXO4* expression supports a role for FOXO4 in the maintenance of CLL cells.

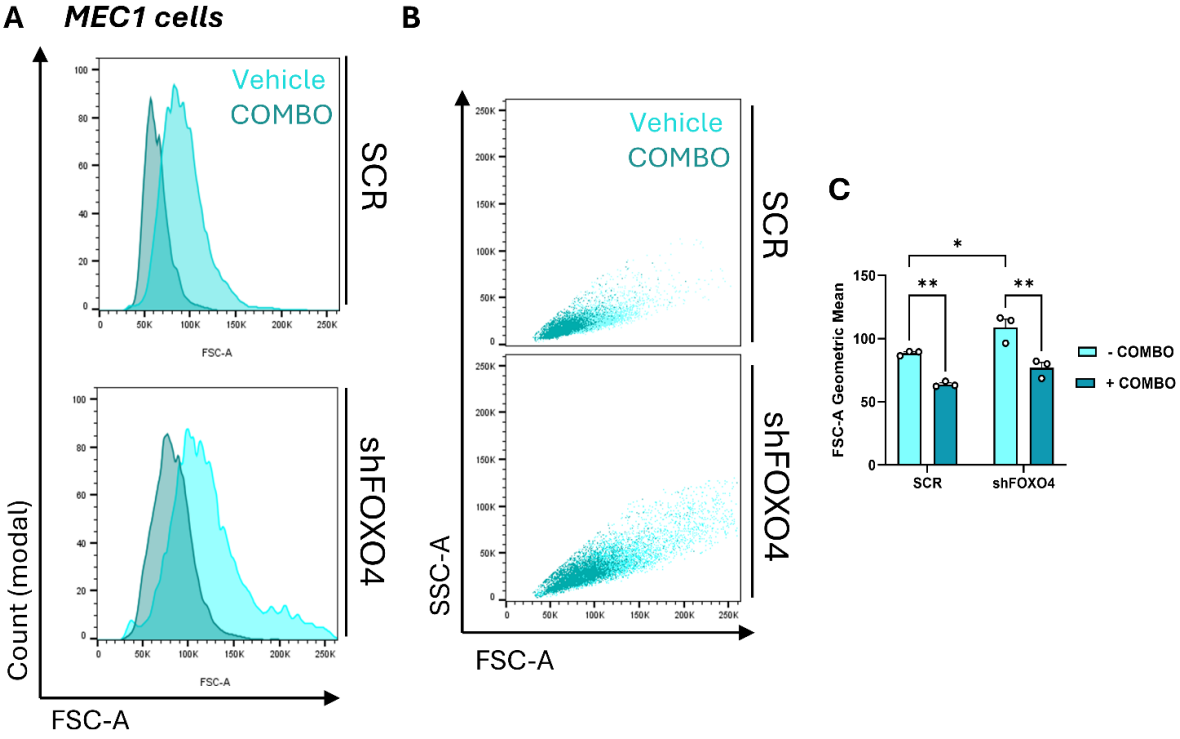

Figure 5.19: FOXO4-depleted MEC1 cells exhibit increased cell size. SCR and shFOXO4 MEC1 cells were cultured for 48 hr ±COMBO (100 nM AZD8055 + 1 μM ibrutinib) treatment and visualised *via* flow cytometry. (A) FACS histogram plotting cell count with forward scatter (FSC-A), comparing cell size in

SCR and shFOXO4 cells with (dark blue) or without (light blue) COMBO treatment. (B) FACS scatter plot visualising SCR and shFOXO4 MEC1 cell side scatter (SSC-A) with forward scatter (FSC-A), looking at the same comparisons in cell size as described in (A). (C) Quantified geometric mean of SCR and shFOXO4 MEC1 cell forward scatter (FSC-A) ±COMBO treatment (n=3). Data points are depicted as white circles, and the data is represented as the mean ±SEM. Statistics were calculated using a two-way ANOVA, where * $p \leq 0.05$, ** $p \leq 0.01$.

5.2.19. Genes coding major mTOR components are upregulated in *FOXO4*-depleted cells

FOXO activity can provide a negative feedback mechanism to further inhibit mTORC1 activity by regulating *RICTOR* and *SESN3* expression [437, 438]. In this work, we have identified that *SESN3* was differentially regulated in HG3 and MEC1 cells following shRNA-mediated *FOXO4* knockdown (Figure 5.7). In Figure 5.20, we investigated whether *FOXO4* depletion affected the gene expression of major components of the two mTOR complexes in MEC1 and HG3 cells. *MTOR* expression was increased in both MEC1 and HG3 cells with diminished *FOXO4* expression (Figure 5.20A & D). This increase was significant in HG3 cells (Figure 5.20D), while it was trending towards significance in MEC1 cells ($p = 0.06$, Figure 5.20A). Interestingly, *RICTOR* expression was also increased in *FOXO4*-depleted cells (Figure 5.20B & E), where *RICTOR* was significantly upregulated in *FOXO4*-depleted HG3 cells compared to the SCR control (Figure 5.20E). Concomitantly, *RAPTOR* expression was also upregulated in *FOXO4*-depleted MEC1 and HG3 cells (Figure 5.20C & F; $p = 0.11$ in *FOXO4*-depleted HG3 cells).

In addition to mTOR components, we investigated the expression of *SESN3* following the depletion of *FOXO3* or *FOXO4* in MEC1 (Figure 5.20G) and HG3 (Figure 5.20H) cells. Interestingly, *SESN3* was significantly downregulated in *FOXO4*-depleted MEC1 and HG3 cells compared to the SCR control (Figure 5.20G & H). Additionally, *FOXO3* depletion also induced a significant downregulation of *SESN3* in MEC1 cells, though not to the same degree as in *FOXO4*-depleted cells (Figure 5.20G). These findings allude to a mechanism of regulation of mTORC1/2 *via* FOXO activity, perhaps indirectly through the induction of *SESN3*.

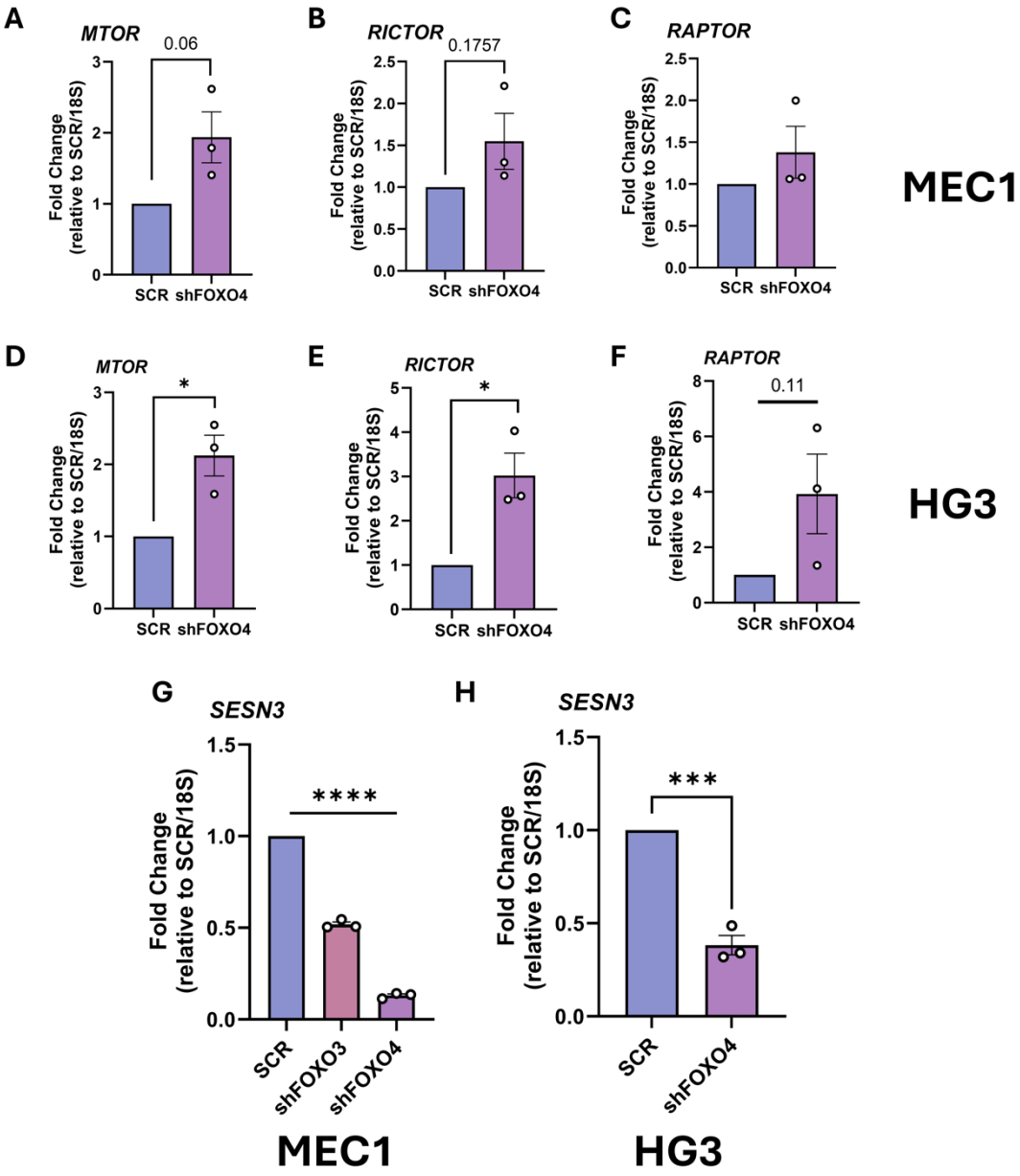

Figure 5.20: Gene expression of mTORC1/2 components are elevated in FOXO4-depleted MEC1 and HG3 cells, coinciding with diminished SESN3 expression. (A-H) RNA samples were generated from SCR and shFOXO4 MEC1 (A-C, G) and HG3 cells (D-F, H) following 24 hr in culture to assess the transcript abundance of *MTOR* (A & D), *RICTOR* (B & E) and *RAPTOR*. (G & H) In separate experiments, *SESN3* expression was assessed in SCR, shFOXO3 and shFOXO4 MEC1 cells (G) as well as in SCR and shFOXO4 HG3 cells (H) following 24 hr in culture. In all cases, expression values were normalised to *18S* and presented as fold change relative to the SCR control. Data points are depicted as white circles, and the data is represented as the mean ±SEM. Statistics were calculated using a Student's t-test, where * $p \leq 0.05$, *** $p \leq 0.001$, **** $p \leq 0.0001$.

5.2.20. *FOXO4*-depleted cells exhibit distinct hyperactivation of mTORC1/2 signalling components

Increased expression of major mTORC1/2 components suggests dysfunctional activity of mTORC1/2 following shRNA-mediated *FOXO4* knockdown in CLL cells. Han *et al*. have previously demonstrated that *FOXO4* overexpression resulted in reduced activity of the mTORC1 components mTOR, p70 S6K and S6 in T-helper cell populations [630], arguing that mTORC1 activity may be regulated by distinct *FOXO4* expression. We addressed whether *FOXO4* depletion affects the phosphorylation status of mTORC1/2 components in HG3 (Figure 5.21) and MEC1 (Figure 5.22) cells, cultured long-term in the presence or absence of AZD8055 (100 nM). Here, in HG3 cells, *FOXO4*-depleted cells elicited increased Rictor^{T1135} expression close to significance ($p = 0.07$), which was significantly attenuated by AZD8055 treatment, whereas Rictor^{T1135} was unaffected by AZD8055 treatment in the SCR control (Figure 5.21B). Although AZD8055 depleted PRAS40^{T246} levels in both the SCR control and *FOXO4*-depleted HG3 cells, the increased abundance of PRAS40^{T246} in *FOXO4*-depleted cells ($p = 0.08$) led to an increase in significance of AZD8055-mediated PRAS40^{T246} depletion ($p = 0.0014$ *vs*. $p = <0.0001$), which was significantly lower than in AZD8055-treated SCR cells (Figure 5.21C). p70-S6K phosphorylation (S6K^{T389}) was significantly increased in cells lacking *FOXO4* expression (Figure 5.21D) which led to an increase in significance of AZD8055-mediated S6K^{T389} depletion compared to the SCR control ($p = 0.0003$ *vs*. $p = 0.03$, respectively, Figure 5.21D). Downstream of S6K, PDCD4 expression was also significantly increased in *FOXO4*-depleted HG3 cells, coincident with increased S6K activity (Figure 5.21D & E). The activity of the canonical S6K target, S6 (S6$^{S235/236}$), was significantly increased in *FOXO4*-depleted HG3 cells (Figure 5.21F), and significantly attenuated by AZD8055 treatment. Inversely, AZD8055 did not affect S6$^{S235/236}$ levels in the SCR control (Figure 5.21F). 4E-BP1$^{T37/46}$ expression was significantly reduced in *FOXO4*-depleted HG3 cells, negating an AZD8055-mediated 4E-BP1$^{T37/46}$ depletion induced in the SCR control

(Figure 5.21G). Finally, eIF4E expression was unaffected by either shRNA-mediated *FOXO4* knockdown or AZD8055 treatment (Figure 5.21H).

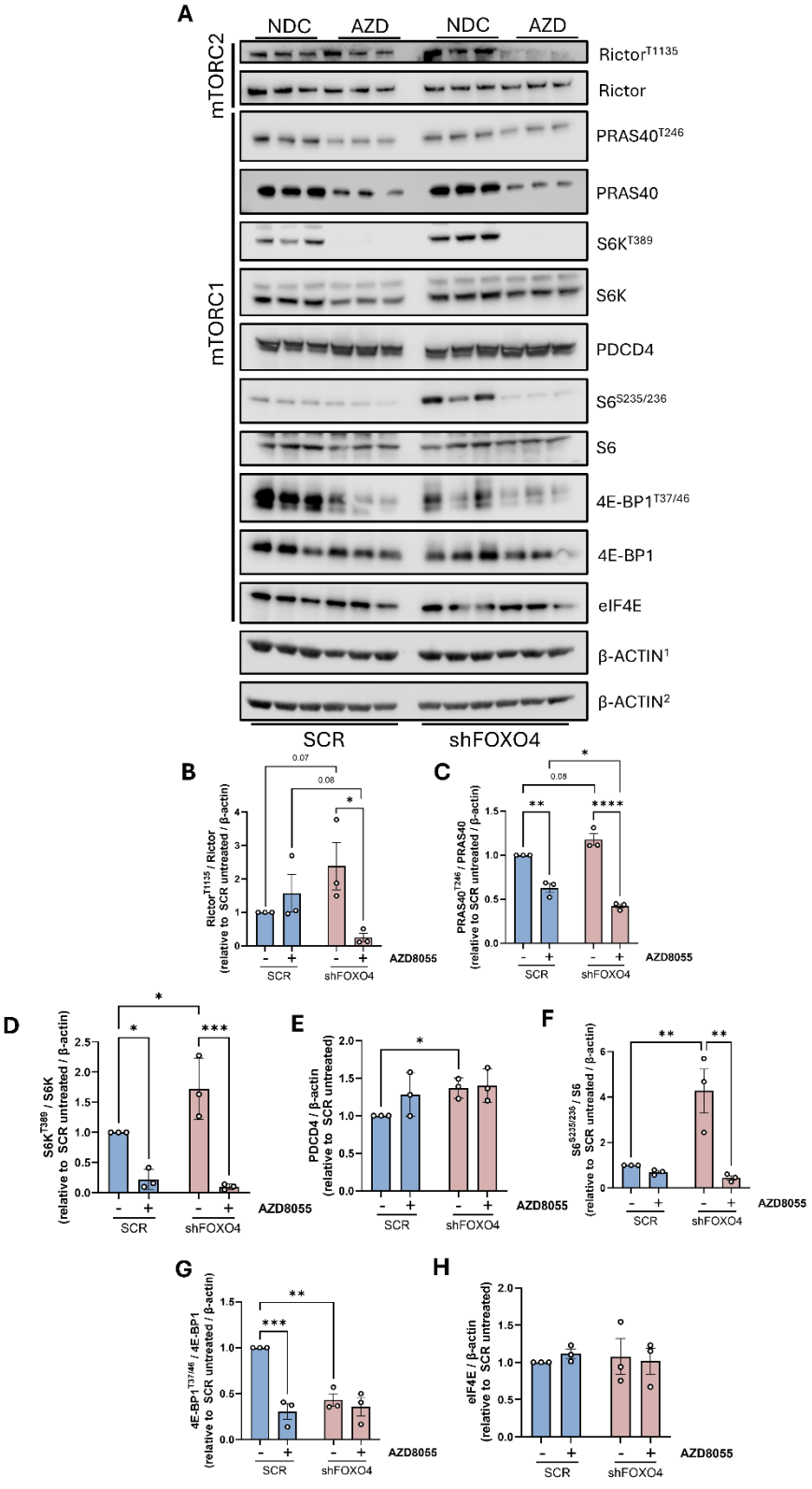

Figure 5.21: mTORC1 signalling is enhanced in FOXO4-depleted HG3 cells. (A) Western blot of SCR and shFOXO4 HG3 cells cultured for 48 hr ±100 nM AZD8055 to assess the expression of Rictor^{T1135}, Rictor, PRAS40^{T246}, PRAS40, S6K^{T389}, S6K, PDCD4, S6$^{S235/236}$, S6, 4E-BP1$^{T37/46}$, 4E-BP1 and eIF4E. β-actin was used as a loading control. (B) Quantified expression of Rictor^{T1135} compared to total rictor expression. (C) Quantified expression of PRAS40^{T246} compared to total PRAS40 protein. (D) Quantified expression of S6K^{T389} compared to total S6K protein. (E) Quantified expression of PDCD4. (F) Quantified expression of S6$^{S235/236}$ compared to total S6 protein. (G) Quantified expression of 4E-BP1$^{T37/46}$ compared to total 4E-BP1 protein. (H) Quantified expression of eIF4E. In all cases, expression values are normalised to β-actin and made relative to the SCR control. Data points are depicted as white circles, and the data is represented as the mean ±SEM. Statistics were calculated using a two-way ANOVA, where * $p \leq 0.05$, ** $p \leq 0.01$, *** $p \leq 0.001$, **** $p \leq 0.0001$.

A similar network of mTORC1/2 activity was observed MEC1 cells following *FOXO4* ablation (Figure 5.22). Focusing on the specific mTORC1/2 components that were affected as a result of *FOXO4* depletion in HG3 cells (Figure 5.22), Rictor^{T1135} phosphorylation was significantly increased in *FOXO4*-depleted MEC1 cells, attenuated by AZD8055 treatment (Figure 5.22B) and, unlike HG3 cells, total Rictor was also enhanced by *FOXO4* depletion, albeit not significantly (Figure 5.22C). Further, AZD8055 treatment enhanced Rictor expression in SCR and shFOXO4 MEC1 cells, trending towards significance in the SCR control ($p = 0.06$, Figure 5.22C). Supporting *FOXO4* depletion in HG3 cells, MEC1 cells also exhibited significantly increased PRAS40^{T246} expression following *FOXO4* ablation, which led to an increase in the significance of AZD8055-mediated PRAS40^{T246} depletion compared to the SCR control (Figure 5.22D). Further, *FOXO4*-depleted MEC1 cells exhibited a significant increase in S6$^{S235/236}$ levels (Figure 5.22E), significantly depleted by AZD8055 treatment, regardless of *FOXO4* expression status (Figure 5.22E). Interestingly, although S6$^{S235/236}$ was increased following *FOXO4* depletion, AZD8055-treated, *FOXO4*-depleted MEC1 cells exhibited significantly lower S6$^{S235/236}$ levels compared to AZD8055-treated SCR cells (Figure 5.22E) - a trend also observed in HG3 cells (Figure 5.21F). Finally, 4E-BP1$^{T37/46}$ levels were unaltered in *FOXO4*-depleted MEC1 cells, while AZD8055 treatment significantly reduced 4E-BP1$^{T37/46}$, regardless of *FOXO4* expression (Figure 5.22F).

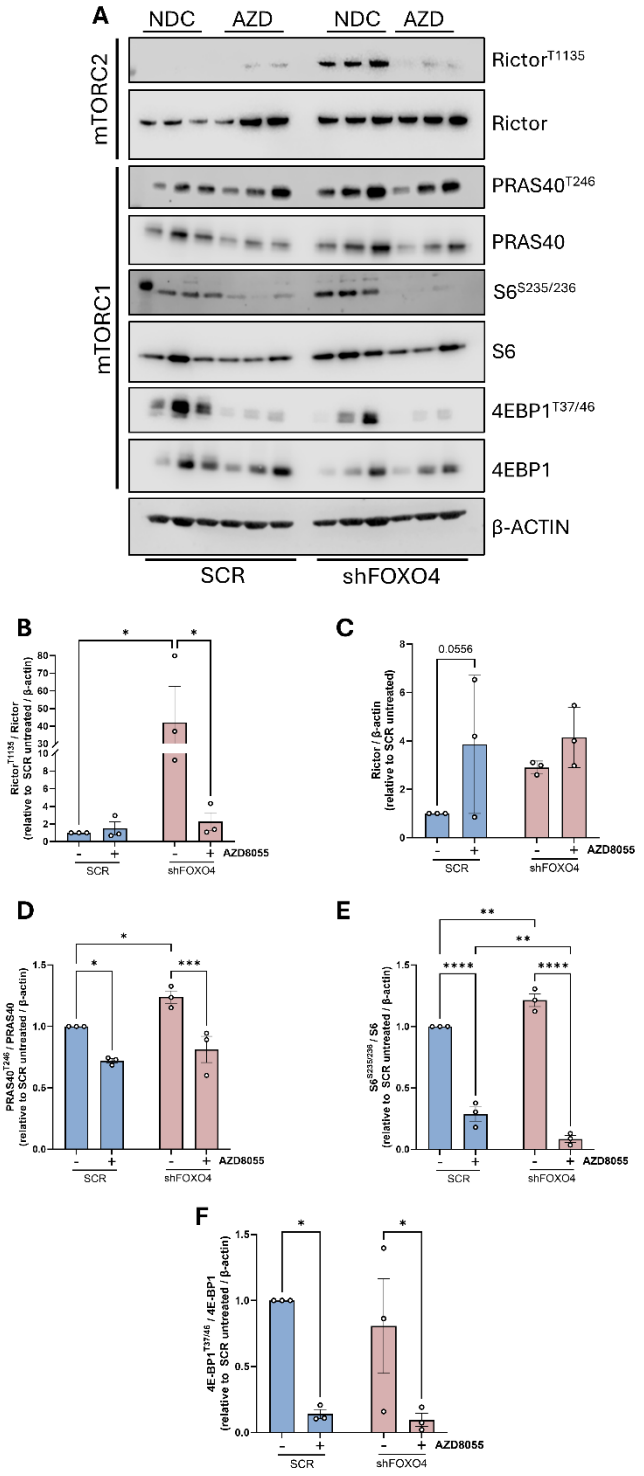

Figure 5.22: FOXO4-depleted MEC1 cells also exhibit mTORC1 hyperactivity. (A) Western blot of SCR and shFOXO4 MEC1 cells cultured for 48 hr ±100 nM AZD8055 (NDC vs AZD), assessing the expression of Rictor^{T1135}, Rictor, PRAS40^{T246}, PRAS40, S6$^{S235/236}$, S6, 4E-BP1$^{T37/46}$ and 4E-BP1. β-actin was used as a loading control. (B) Quantified expression of Rictor^{T1135} compared with total Rictor protein, normalised to β-actin and made relative to the SCR control. (C) Expression of total Rictor protein, normalised to β-actin and made relative to the SCR control. (D-F) Quantified expression of PRAS40^{T236} (D), S6$^{S235/236}$ (E) and 4E-BP1$^{T37/46}$ (F) compared to their respective total protein, normalised to β-actin and made relative to the SCR control (n=3). Data points are depicted as white circles, and the data is represented as the mean ±SEM. Statistics were calculated using a two-way ANOVA, where * p ≤ 0.05, ** p ≤ 0.01, *** p ≤ 0.001, **** p ≤ 0.0001.

5.2.21. AKT loses rapamycin sensitivity following *FOXO4* depletion in MEC1 cells

The increased mTORC1 activity and sensitivity of mTORC1/2 components to AZD8055 treatment in CLL cells harbouring *FOXO4* knockdowns (Figures 5.21 & 5.22) justified further investigation of mTORC1/2 component sensitivity to other targeted agents that affected mTOR activity. We sought to elucidate whether AZD8055 (100 nM), rapamycin (10 nM) or ibrutinib (alone or in combination) affected the phosphorylation status of Rictor^{T1135}, AKT^{S473}, eEF2^{T56}, S6$^{S235/236}$ and 4E-BP1$^{T37/46}$ in *FOXO4*-depleted long-term MEC1 cultures (Figure 5.23A). Rictor phosphorylation and expression were both increased in *FOXO4*-depleted MEC1 cells, trending towards significance ($p = 0.07$, Figure 5.23A-C). Further, AZD8055 and rapamycin treatments strongly diminished Rictor^{T1135} in shFOXO4 MEC1 cells, although SCR cells also exhibited a modest rapamycin-induced Rictor^{T1135} depletion (Figure 5.23B). Furthermore, AZD8055, rapamycin and ibrutinib treatments enhanced Rictor expression in *FOXO4*-depleted cells compared to SCR cells (Figure 5.23C). AKT^{S473} levels were decreased in *FOXO4*-depleted MEC1 cells compared to the SCR control, leading to a loss of significance of AZD8055-mediated AKT^{S473} depletion as seen in the SCR control (Figure 5.23D). Although rapamycin and ibrutinib treatments diminished AKT^{S473} levels in the SCR control (Figure 5.23D), they did not reduce AKT^{S473} levels in *FOXO4*-depleted MEC1 cells. Instead, AKT^{S473} was higher in rapamycin-treated, *FOXO4* depleted MEC1 cells, trending towards significance ($p = 0.08$, Figure 5.23D), and was significantly higher in ibrutinib and rapamycin-ibrutinib-treated shFOXO4 cells compared to their SCR counterparts (Figure 5.23D). Furthermore, we assessed eEF2^{T56} phosphorylation as eEF2 has a role in promoting translation elongation downstream of mTORC1-S6K [300]. Here, there were no significant differences in eEF2 phosphorylation (T56) or expression between SCR and *FOXO4* knockdown MEC1 cells (Figure 5.23E).

4E-BP1$^{T37/46}$ exhibited a modest increase in *FOXO4*-depleted MEC1 cells, albeit not significantly (Figure 5.23F). As expected, AZD8055 treatment effectively diminished 4E-BP1$^{T37/46}$ in SCR and shFOXO4 cells, while ibrutinib and rapamycin did not (Figure 5.23F). S6$^{S235/S236}$ abundance was significantly increased in

FOXO4-depleted MEC1 cells (Figure 5.23G), supporting Figures 5.21 and 5.22. Furthermore, a significant rise in $S6^{S235/236}$ led to a significant reduction of $S6^{S235/236}$ in *FOXO4*-depleted MEC1 cells mediated by AZD8055 or rapamycin treatment (alone or in combination with ibrutinib) (Figure 5.23G).

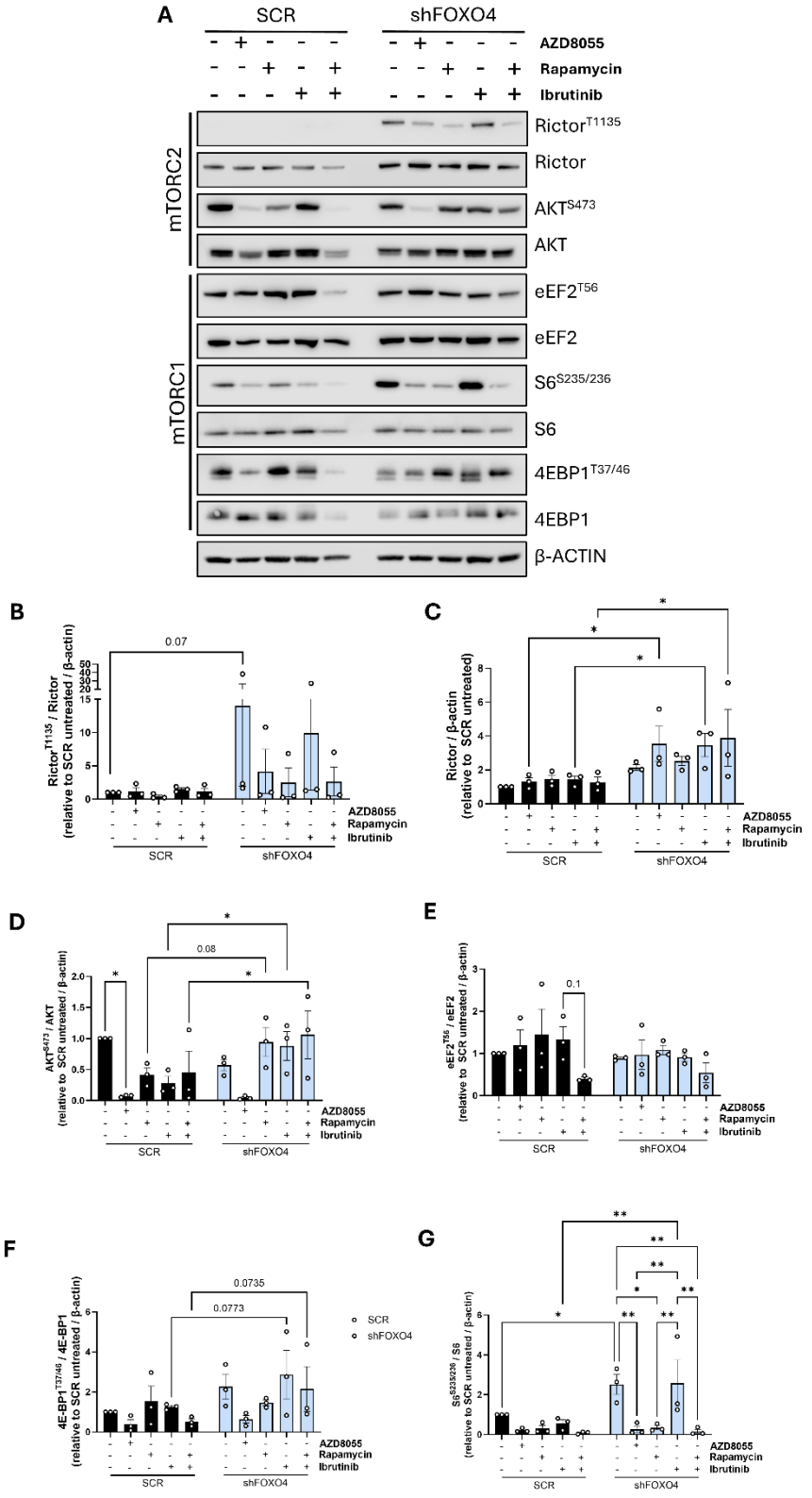

Figure 5.23: AKT exhibits decreased sensitivity to rapamycin and ibrutinib treatment in FOXO4-depleted MEC1 cells. (A) Western blot of SCR and shFOXO4 MEC1 cells cultured for 48 hr ±100 nM AZD8055 alone or in combination 10 nM rapamycin or 1 μM ibrutinib treatment, assessing the expression of Rictor^{T1135}, Rictor, AKT^{S473}, AKT, eEF2^{T56}, eEF2, S6$^{S235/236}$, S6, 4E-BP1$^{T37/46}$ and 4E-BP1. β-actin was used as a loading control. (B) Quantified expression of Rictor^{T1135} compared with Rictor, normalised to β-actin and made relative to the SCR control. (C) Quantified expression of Rictor, normalised to β-actin and made relative to the SCR control. (D-G) Quantified expression of AKT^{S473} (D), eEF2^{T56} (E), 4E-BP1$^{T37/46}$ (F) and S6$^{S235/236}$ compared with expression of their total proteins, normalised to β-actin and relative to the SCR control (n=3). Data points are depicted as white circles, and the data is represented as the mean ±SEM. Statistics were calculated using a two-way ANOVA, where * p ≤ 0.05, ** p ≤ 0.01.

5.2.22. *FOXO4*-depleted cells exhibit increased sensitivity to combined rapamycin-ibrutinib treatment

Next, we assessed the impact of rapamycin (10 nM) and ibrutinib (1 μM) single or combination treatments on CLL cell proliferation and survival in *FOXO4*-depleted MEC1 and HG3 cells. AZD8055 treatment (100 nM) was included as a positive control. Investigating MEC1 cell proliferation *via* CTV staining (Figure 5.24A), *FOXO4*-depleted MEC1 cells exhibited reduced proliferative capacity compared to the SCR control (Figure 5.24B). Further, although AZD8055 treatment significantly reduced the proliferation of both SCR and shFOXO4 MEC1 cells, MEC1 cell proliferation was impacted more negatively in AZD8055-treated, *FOXO4*-depleted cells, evidenced by an increase in significance higher in shFOXO4 than in SCR cells (Figure 5.24B, supporting Figure 5.4A & B). *FOXO4*-depleted MEC1 cells exhibited a stronger rapamycin-mediated proliferative block, with a significant increase in CTV MFI higher than in the rapamycin-treated control (Figure 5.24B). While ibrutinib treatments did little to impact cell proliferation, rapamycin in combination with ibrutinib significantly increased CTV MFI in both SCR and *FOXO4*-depleted cells, though again CTV MFI was significantly higher following rapamycin-ibrutinib treatment in *FOXO4*-depleted cells (Figure 5.24). Furthermore, ibrutinib significantly enhanced a rapamycin-induced block in proliferation in *FOXO4*-depleted MEC1 cells – an effect not seen in the SCR control (Figure 5.24B). *FOXO4*-depleted HG3 cells exhibited similar characteristics as *FOXO4*-depleted MEC1 cells (Figure 5.24C).

Addressing whether *FOXO4*-depleted MEC1 and HG3 cells were more sensitive to drug-induced cell death by Annexin/7AAD staining of long-term cultures, following 48 hr in culture, rapamycin and ibrutinib treatments had no affect MEC1 cell viability in the SCR control (Figure 5.24). However, *FOXO4*-depleted MEC1 cells exhibited a modest decrease in cell viability following rapamycin and ibrutinib single treatments, further enhanced in combination ($p = 0.05$, Figure 5.24E). Rapamycin alone decreased shFOXO4 cell viability more than in the SCR control, trending towards significance ($p = 0.1$, Figure 5.24E). Combining

rapamycin and ibrutinib depleted cell viability in shFOXO4 MEC1 cells significantly more than in rapamycin-ibrutinib-treated SCR cells (Figure 5.24E). In contrast, HG3 SCR cells were more sensitive to AZD8055, rapamycin and/or ibrutinib treatment, though drug-induced reductions in cell viability were not significant (Figure 5.24F). Collectively, Figures 5.21 – 5.24 demonstrate that FOXO4 provides positive feedback to regulate mTORC1/2 function and responsiveness to pharmacological mTOR inhibition *via* AZD8055 or rapamycin treatment, perhaps indirectly *via SESN3* expression (Figure 5.20).

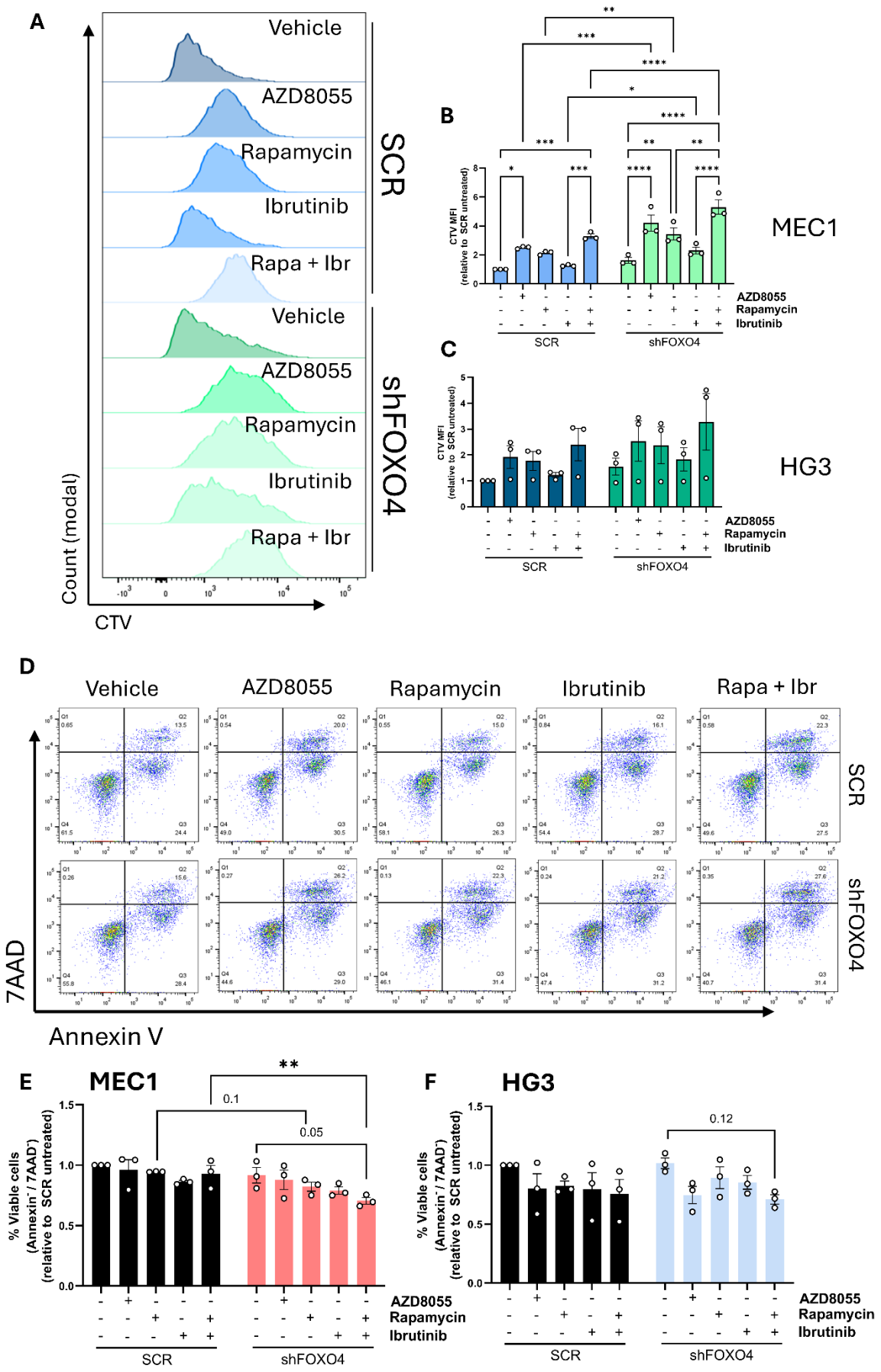

Figure 5.24: Rapamycin and ibrutinib combination treatment diminishes proliferative capacity and cell viability in FOXO4-depleted MEC1 and HG3 cells. (A) Representative FACS histogram of CTV-stained SCR and shFOXO4 MEC1 cells following 96 hr in culture ±100 nM AZD8055, or single or combination treatment with 10 nM rapamycin and 1 μM ibrutinib (rapa + ibr). (B & C) CTV mean

fluorescence intensities (MFI) of MEC1 (B) and HG3 (C) SCR and shFOXO4 cells following 96 hr in culture ±AZD8055 single or rapamycin and/or ibrutinib treatment, made relative to untreated SCR cells. (D) Representative FACS plot of Annexin V/7AAD staining of SCR and shFOXO4 MEC1 cells following 48 hr in culture ±100 nM AZD8055 alone or single or combination treatment with 10 nM rapamycin and 1 μM ibrutinib. (E & F) Percentage 'viable' (Annexin^{neg}/7AAD^{neg}) SCR and shFOXO4 MEC1 (E) and HG3 (F) cells following 48 hr in culture ±AZD8055, rapamycin and/or ibrutinib treatment, made relative to the SCR control. Data points are depicted as white circles, and the data is represented as the mean ±SEM. Statistics were calculated using a two-way ANOVA, where * $p \leq 0.05$, ** $p \leq 0.01$, *** $p \leq 0.001$, **** $p \leq 0.0001$.

5.2.23. shRNA-mediated knockdown of FOXO family members differentially regulates mTORC1 activity

To elucidate whether aberrant mTORC1/2 activity was exclusive to shFOXO4 cells, we also investigated the phosphorylation status of Rictor^{T1135}, eEF2^{T56}, S6$^{S235/236}$, 4E-BP1$^{T37/46}$ and AKT^{S473} compared with total protein expression (Figure 5.25A) in cells harbouring *FOXO1* or *FOXO3* knockdown. Here, depletion of individual FOXO genes increased Rictor^{T1135} phosphorylation, with *FOXO3*-depleted MEC1 cells exhibiting a significant increase in Rictor^{T1135} compared to the SCR control (Figure 5.25B). Further, AZD8055 treatment effectively diminished Rictor^{T1135} in *FOXO*-depleted cells, which was significant in *FOXO3*-depleted cells and trending towards significance for *FOXO1*-depleted cells (Figure 5.25B). Total Rictor expression was also increased following depletion of each isoform, which was further increased in shFOXO1/3/4 cells treated with AZD8055 (supporting previous findings in Figures 5.22 & 5.23). *FOXO3*- and *FOXO4*-depleted MEC1 cells exhibited the highest increases in Rictor expression following AZD8055 treatment, trending towards significance (shFOXO3: $p = 0.06$, shFOXO4: $p = 0.09$, Figure 5.25C), and was highest in *FOXO4*-depleted MEC1 cells following AZD8055 treatment. These values were significantly higher than in AZD8055-treated SCR cells (Figure 5.25C). Rictor expression was also higher in *FOXO3*-depleted cells following AZD8055 treatment, trending towards significance compared to AZD8055-treated SCR cells ($p = 0.05$, Figure 5.25C).

eEF2^{T56} expression was reduced in shFOXO1/3/4 cells, with *FOXO4*-depleted cells exhibiting the lowest abundance of eEF2^{T56} (Figure 5.25D). Additionally, AZD8055 treatment reduced eEF2^{T56} levels more efficiently in *FOXO3*-depleted cells

compared to the SCR control, trending towards significance (p = 0.1, Figure 5.25D). Total eEF2 expression did not change following depletion of any FOXO isoform (Figure 5.25E).

$S6^{S235/236}$ levels were unaffected in shFOXO1/3/4 cells (Figure 5.25F). AZD8055 treatment effectively depleted $S6^{S235/236}$, which was significant in *FOXO1*-depleted cells (Figure 5.25F). Further, total S6 expression was increased slightly in *FOXO3*- and *FOXO4*-depleted cells (Figure 5.25G). 4E-$BP1^{T37/46}$ abundance was enhanced in shFOXO1/3/4 cells, trending towards significance for *FOXO4*-depleted cells (p = 0.09, Figure 5.25H). 4E-$BP1^{T37/46}$ enhancement led to effective AZD8055-mediated 4E-$BP1^{T37/46}$ inhibition in shFOXO1/3/4 cells, which was significant for *FOXO3*- and *FOXO4*-depleted cells (Figure 5.25H). While total 4E-BP1 protein was unaffected by *FOXO1/3/4* depletion, AZD8055 treatment induced an increase in 4E-BP1 expression, regardless of *FOXO1/3/4* expression (SCR: p = 0.11, Figure 5.25I). AKT^{S473} levels exhibited a modest increase following *FOXO1/3/4* depletion; this led to a significant depletion in AKT^{S473} in shFOXO1/3/4 cells mediated by AZD8055 that was not exhibited by the SCR control (Figure 5.25J). Further, total AKT expression was not affected by *FOXO1/3/4* knockdown, though cells lacking *FOXO3* exhibited an AZD8055-mediated decrease in total AKT, trending towards significance (p = 0.1, Figure 5.25K). These findings further demonstrate the necessity of FOXO gene expression to maintain functional mTORC1/2 signalling in CLL cells.

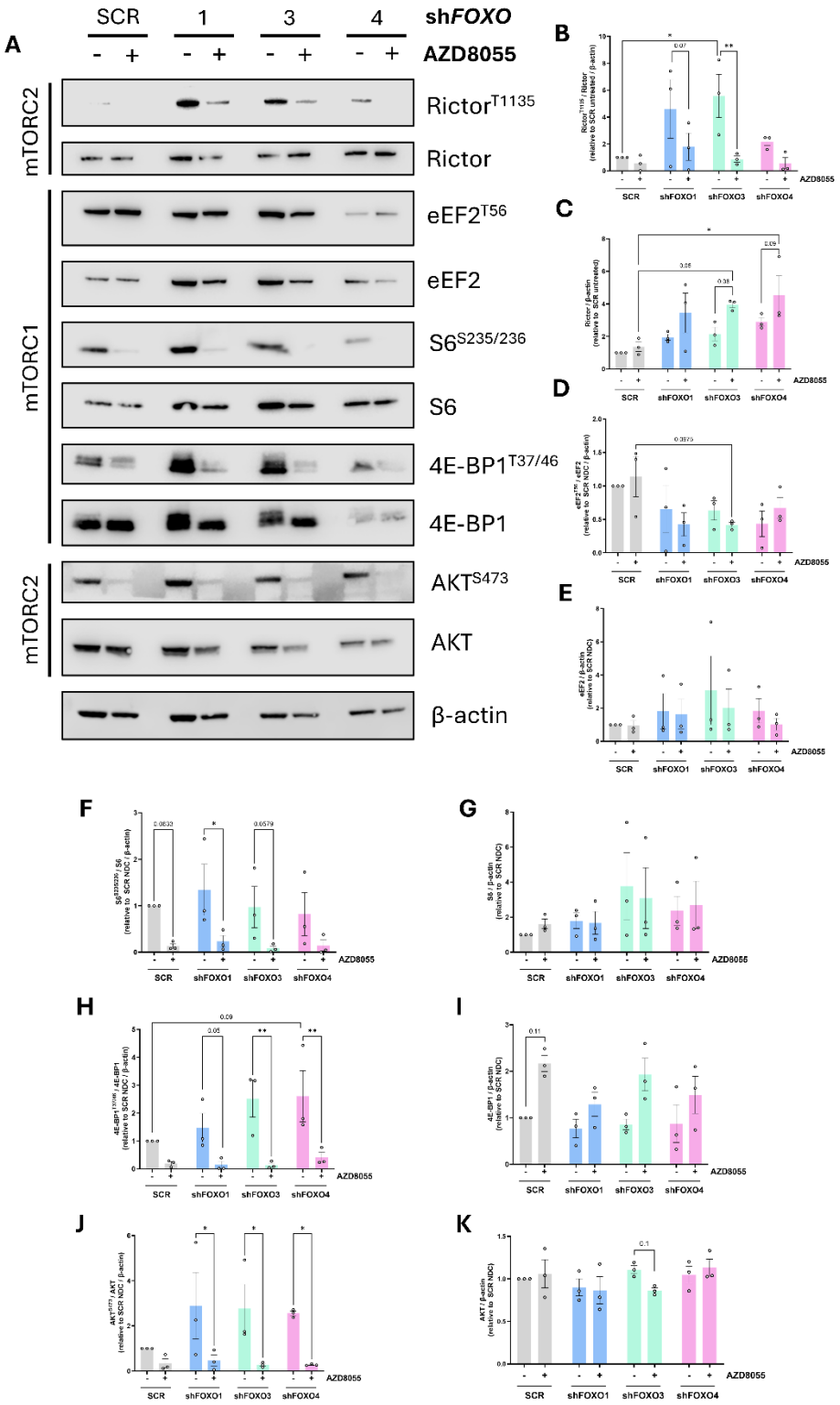

Figure 5.25: mTOR activity is altered following depletion of FOXO1, FOXO3 and FOXO4. (A) Western blot of SCR and shFOXO1, 3 and 4 cells following 48 hr in culture ±100 nM AZD8055, assessing the expression Rictor^{T1135}, Rictor, eEF2^{T56}, eEF2, S6$^{S235/236}$, S6, 4E-BP1$^{T37/46}$, 4E-BP1, AKT^{S473} and AKT. β-actin was used as a loading control. (B-C) Quantified expression of Rictor^{T1135} compared with total Rictor protein (B) and quantified expression of total Rictor protein (C), normalised to β-actin and made relative to the SCR control. (D-E) Quantified expression of eEF2^{T56} compared with total eEF2 protein (D) as well as total eEF2 expression (E), normalised to β-actin and made relative to the SCR control. (F-G) Quantified expression of S6$^{S235/236}$ compared with total S6 protein (F) as well as total S6 expression (G), normalised to β-actin and made relative to the SCR control. (H-I) Quantified expression of 4E-BP1$^{T37/46}$ compared with total 4E-BP1 protein (H) as well as total 4E-BP1 expression (I), normalised to β-actin

and made relative to the SCR control. (J-K) Quantified expression of AKT^{S473} compared with total AKT protein (J), as well as total AKT expression (K) (n=3). Data points are depicted as white circles, and the data is represented as the mean ±SEM. Statistics were calculated using a two-way ANOVA, where * $p \leq 0.05$, ** $p \leq 0.01$

These results shed light on an intricate network of FOXO-mediated regulation of upstream mTORC1/2 activity existing within CLL, particularly with regards to FOXO4 expression, and how this influences sensitivity to mTORC1 inhibition, either *via* rapamycin or AZD8055 treatment. A summarised model of FOXO4-mediated regulation of mTORC1/2 activity can be found below (Figure 5.26):

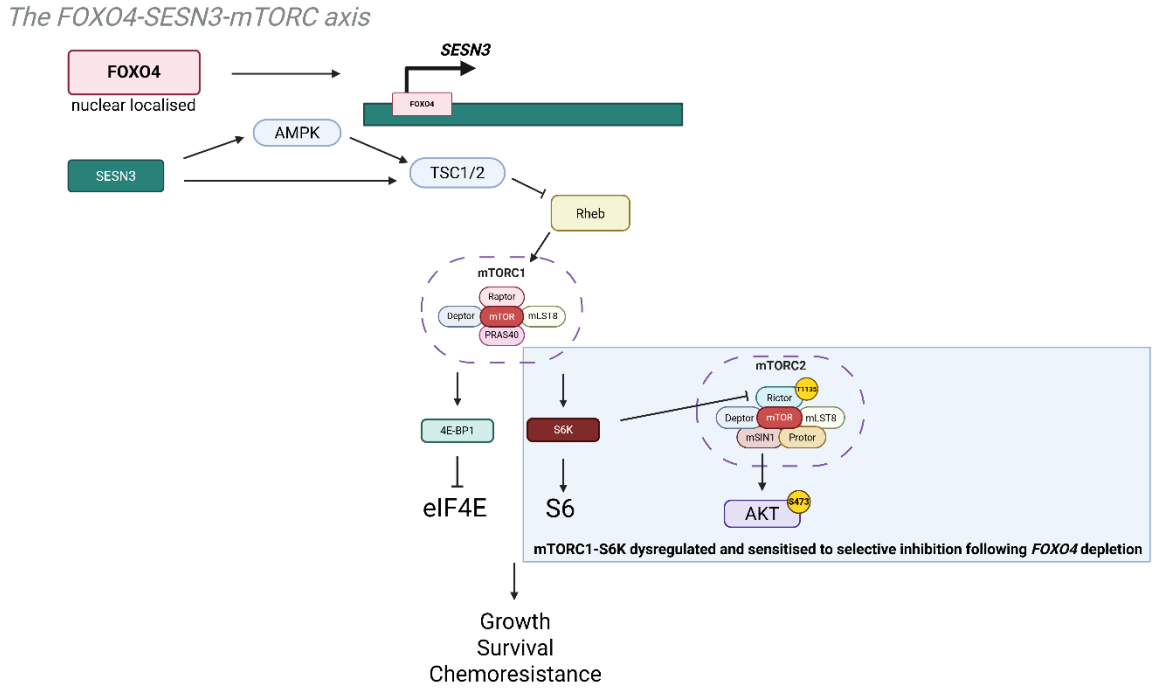

Figure 5.26: Proposed model of FOXO4-mediated regulation of mTORC1/2 activity in CLL. Proposed in this thesis, FOXO4 has the capacity to directly (*via* regulation of *RICTOR* transcript expression or indirectly (proposed within this model) *via* induction of expression of *SESN3*. *SESN3* expression mediates activation of TSCs to promote regulation of mTORC1 activity and downstream S6K activity, which negatively regulates mTORC2 *via* phosphorylation of Rictor^{T1135}. Abolishing *FOXO4* expression is detrimental to mTORC1 activity, reflected by S6K/S6 hyperphosphorylation and hypersensitivity to targeted mTORC1 inhibition.

5.2.24. *FOXO4* depletion increases MEC1 sensitivity to selective FOXO1 inhibition

The increase in FOXO1 expression exhibited in *FOXO4*-depleted cells (Figure 5.3) alludes to an increased reliance on FOXO1 to rescue functions typically carried out by FOXO4. That, and the increased chemosensitivity of shFOXO4 CLL cels,

led us to investigate whether shRNA *FOXO4* MEC1 cells were more sensitive to AZD8055 (100 nM) and AS1842856 (100 nM) treatment in long-term culture (Figure 5.27). MEC1 cell viability following 48 hr in culture with AZD8055 and/or AS1842856 was significantly reduced in cells lacking *FOXO4* expression (Figure 5.27A & B), supporting previous data (Figure 5.6). Furthermore, AZD8055 treatment led to a modest decrease in cell viability in both SCR and shFOXO4 MEC1 cells (Figure 5.27B), which was enhanced in combination with AS1842856 in SCR cells, albeit not significantly (Figure 5.27B). Interestingly, shFOXO4 MEC1 cell viability was reduced further following AS1842856 treatment, which was significantly lower than AS1842856-treated SCR cells (Figure 5.27B). AZD8055-AS1842856 combination resulted in a similar decrease in cell viability as AS8142856 single treatments in *FOXO4*-depleted MEC1 cells (Figure 5.27B). These findings suggest enhanced FOXO1 activity in shFOXO4 CLL cells (potentially due to increased FOXO1 expression (Figure 5.3)), perhaps explaining an increase in shFOXO4 MEC1 cell sensitivity to AS1842856 treatment.

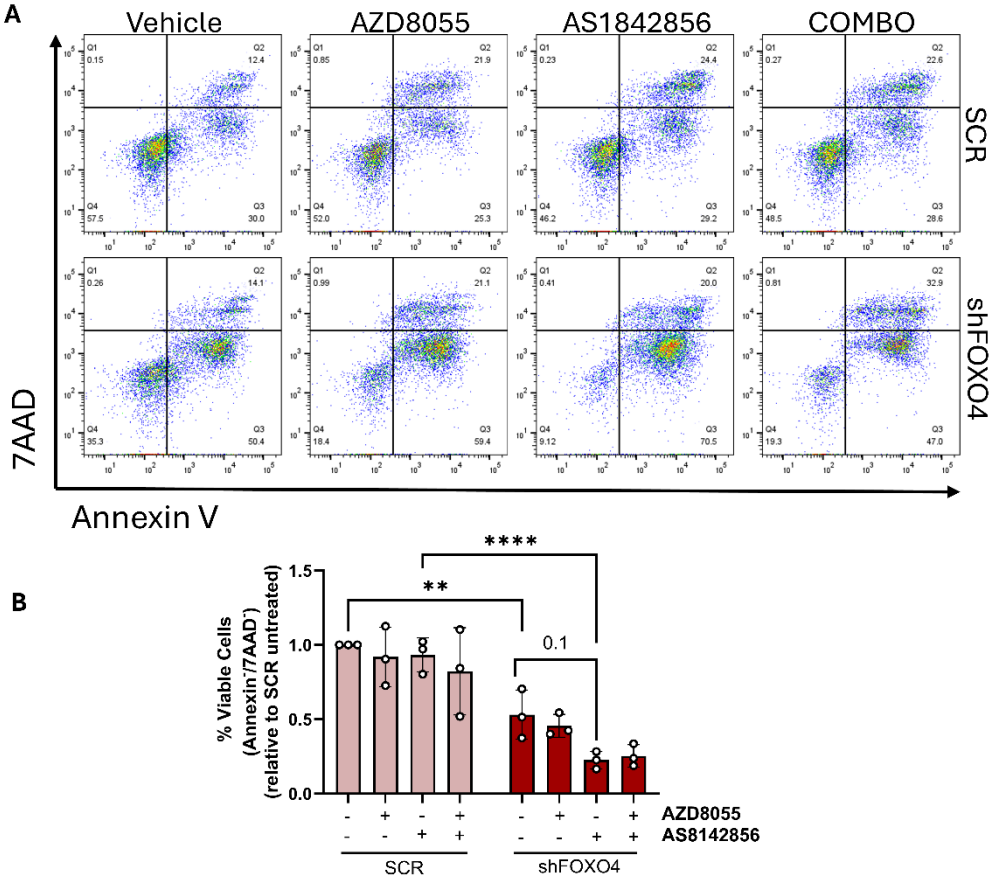

Figure 5.27: shRNA-mediated FOXO4 knockdown increases susceptibility to AS1842856-induced cell death in MEC1 cells. (A) Representative FACS plot of Annexin V/7AAD staining in SCR and shFOXO4 MEC1 cells following 48 hr in culture ±100 nM AZD8055 and/or 100 nM AS1842856. (B) SCR and shFOXO4 cells deemed 'viable' (Annexin^{neg}/7AAD^{neg}) following 48 hr in culture ±AZD8055 and/or AS1842856, made relative to untreated SCR cells (n=3). Data points are depicted as white circles, and

the data is represented as the mean ±SEM. Statistics were calculated using a two-way ANOVA, where ** $p \leq 0.01$, **** $p \leq 0.0001$.

5.3. Discussion

We observed constitutive expression of FOXO3 and FOXO4 in the nucleus of proliferating CLL cells (MEC1, HG3 and primary CLL cells in the presence or absence of BCR or CD40 ligation), suggesting that 'active' nuclear FOXO3 and FOXO4 could be required to orchestrate functional responses in CLL, irrespective of upstream PI3K-AKT activity. This has been reported in several CLL model systems ([49, 284] & Jodie Hay, unpublished data) demonstrating that, although FOXO expression and activity are regulated by PI3K-AKT-mTOR, a basal level of FOXO expression and nuclear localisation has the capacity to promote CLL proliferation and survival. Supporting this, a previous study in BL and BCP-ALL cells revealed a requirement for FOXO-mediated signalling events to drive disease progression [540, 541]. Moreover, supporting findings in this thesis, Kapoor *et al*. highlighted that MEC1 cells exhibit dynamic nuclear FOXO3 activity even in the presence of AKT^{S473} phosphorylation [524]. Collectively, these data stress the importance of the expression of discrete FOXO isoforms to promote cellular maintenance in CLL, akin to that of FOXO behaviour in other mature B-cell malignancies and more distant neoplasms. In this chapter, we assessed the importance of *FOXO3* and *FOXO4* expression in proliferating CLL cells *via* shRNA-mediated knockdown, investigating the functional impact of ablating *FOXO3* and *FOXO4* expression as well as the responsiveness to targeted agents including AZD8055, ibrutinib and venetoclax. Aberrant expression of BCL2 family members following treatment with the targeted agents AZD8055, ibrutinib and venetoclax demonstrate a FOXO4-mediated mechanism of drug resistance in CLL as seen in other cancer contexts [549, 550], where FOXO4 can regulate the transcriptional activation of genes required for promoting chemoresistance. Indeed, these negative effects could be amplified further *via* an upregulation of FOXO1 [284]. GADD45A downregulation in MEC1 and HG3 cells with diminished *FOXO3/4* allude to a FOXO3/4-mediated mechanism of DNA damage repair in CLL [439], where a

lack of GADD45A expression is associated with increased susceptibility to DNA damage *via* AZD8055-ibrutinib treatment, phenotypically reflected by an elevation of γ-H2AX^{S139} and aberrant cell cycle progression. Finally, we report that *FOXO*4 depletion induced selective, hyperactive mTORC1 signalling in MEC1 and HG3 cells; this was associated with diminished *SESN3* expression, highlighting a novel role for FOXO4 in regulating upstream mTORC1/2 activity (akin to that of FOXO1 in 'normal' and malignant scenarios [317, 541]) and potentially explaining how *FOXO4*-depletion sensitises CLL cells to AZD8055 and rapamycin treatment.

5.3.1. FOXO3/4 knockdown differentially affects CLL cell proliferation, viability and drug responsiveness

As described extensively within this thesis, FOXO activity has been historically associated with tumour suppression *via* the regulation of key effectors involved in modulating cell fate decisions [429]. In other disease models, depending on the context, downregulation of the gene expression of FOXO family members has contrasting effects. For example, in renal cell carcinoma, *FOXO3* downregulation is associated with tumour metastasis, indicating tumour-suppressive FOXO3 activity [631]. Further, siRNA knockdown of *FOXO3* in urinary bladder carcinoma cells enhanced cell proliferation and drug resistance, demonstrating the capability of FOXO3 to instruct detrimental cell fate decisions [632]. In colon cancer cells, Li *et al*. found that siRNA-mediated *FOXO3* knockdown led to dysfunctional NF-κB signalling [633], suggesting that FOXO3 activity is required to regulate specific upstream signals. In the context of leukaemia, Pellicano *et al*. revealed - *via* shRNA-mediated *FOXO3* knockdown in CML cells - that depleting *FOXO3* expression abrogates FOXO3-associated quiescence and increases CML cell sensitivity to TKI therapy [486] suggesting that, unlike in urinary bladder carcinoma [632], FOXO3 is required for disease maintenance and chemoprotection. Compared to FOXO3 and FOXO1, limited literature is available with regards to the functional effect of modulating *FOXO4* expression in cancer model systems. Nevertheless, Su *et al*. demonstrated that siRNA-mediated

FOXO4 knockdown promotes the growth and metastasis of gastric cancer cells [634]. Similar findings were described *via FOXO4* overexpression, which inhibited CRC cell migration and metastasis and induced apoptosis in clear-cell renal carcinoma cells, respectively [530, 635]. Recent findings by Zhong *et al*. demonstrate that shRNA-mediated knockdown of *FOXO4* increases colony formation and cell migration in NSCLC cells [636]. Collectively, these findings suggest that *FOXO4* expression hinders the core oncogenic programmes that contribute to multiple cancer hallmarks [262]. However, it is important to note that these findings are in cancer neoplasms that express diminished *FOXO4* compared to 'normal' cell populations [530, 634-637]. We have established that FOXO3 and FOXO4 are highly expressed in CLL cell populations, inferring a need for FOXO expression and subsequent activity that may be absent in other malignant contexts [530, 634-637]. Modulating *FOXO3* and *FOXO4* expression in CLL cells may elicit different functional effects. Therefore, we will proceed by discussing the effect of *FOXO3* and *FOXO4* knockdown in CLL cells with regards to specific cell functions and intracellular mechanisms associated with dysfunctional regulation of FOXO family members and distinct FOXO target genes.

5.3.1.1. Proliferation

shRNA-mediated knockdown of *FOXO4* reduced the proliferative capacity of MEC1 cells, reflected by diminished S- and G2-phase populations. Concurrently, regardless of *FOXO4* expression, AZD8055 and ibrutinib treatments maintained their effectiveness in inducing cell cycle arrest in proliferating MEC1 and HG3 cells in a cell-type-specific manner, suggesting that the potency of mTORC1/2 inhibition at inducing cell cycle arrest does not emanate from FOXO4 activity. A reduction in significance of AZD8055-ibrutinib-mediated cell cycle arrest in MEC1 cells is likely due to increased G_0/G1 cell populations. While shFOXO4 depletion did not hinder HG3 proliferation, an increased sensitivity in *FOXO4*-depleted cells to AZD8055 and/or ibrutinib-mediated cell cycle arrest, suggests that *FOXO4* is regulated in a cell-type-specific manner. This cell-type-specific regulation could be mediated by FOXO target genes $p21^{cip1}$ and $p27^{kip1}$. An

elevation of endogenous $p27^{kip1}$ in *FOXO4*-depleted MEC1 cells could possibly allude to a $p27^{kip1}$-mediated mechanism of cell cycle arrest in *FOXO4*-depleted cells, while diminished $p27^{kip1}$ in HG3 cells lacking *FOXO4* expression may indicate a mechanism through which proliferative capacity is maintained in HG3 cells. Of note, this was coincident with $p21^{cip1}$ depletion in *FOXO4*-depleted cells, irrespective of the cell type. *CDKN1A* ($p21^{cip1}$) is upregulated in a FOXO4-mediated programme of cell senescence [638], so it is likely that diminishing *FOXO4* expression could hinder FOXO4-dependent p21 transcription. These findings indicate that *FOXO4* expression promotes proliferation *via* regulation of distinct effectors associated with cell cycle progression.

In the same vein, shFOXO3 knockdown reduced the proliferative capacity of MEC1 cells, demonstrating that MEC1 cell proliferation is sensitive to changes in expression to both *FOXO3* and *FOXO4*. This is in contrast to diminishing *FOXO1* expression, which elicited no change to MEC1 cell proliferation [49]. These results were complemented by cell cycle analysis, revealing reduced S- and increased G2-phase populations following *FOXO3* ablation. Hornsveld *et al*. recently reported that FOXO3 is required for mediating G2 cell cycle exit following activation due to replication stress [639], which could explain an increase in G2 populations in the absence of *FOXO3*. Like with *FOXO4*, *FOXO3* depletion also reduced the S phase populace, albeit without affecting the potency of AZD8055-ibrutinib-mediated G1 growth arrest, demonstrating that the anti-proliferative effect of BTK and mTORC1/2 inhibition in the context of FOXO activity could emanate solely from FOXO1.

Aberrant cell cycle progression in shFOXO3 MEC1 cells was supported by decreased *CCND2* expression and increased AZD8055-ibrutinib-mediated *CDKN1B* expression. As FOXO activity represses expression of cyclin D family members, it is unlikely that *CCND2* is regulated by FOXO3 in this context. Instead, it could be that these FOXO target genes are manipulated by enhanced FOXO1 expression. In Figure 5.3, the endogenous levels of FOXO1 were elevated in MEC1 cells following *FOXO3* an *FOXO4* depletion, where MEC1 cells lacking *FOXO3* expression exhibited increased FOXO1 DNA binding activity. The complexity of FOXO biology in their regulation of other FOXO isoforms [555], as well the existence of functional redundancy [483], could explain a significant increase in FOXO1 expression in the absence of *FOXO3* or *FOXO4* in MEC1 cells. As FOXO1

harbours tumour suppressive characteristics in CLL [284], it becomes tempting to speculate that, while FOXO1 may rescue the functions of other FOXO family members when expression is scarce, increased FOXO1 transcriptional activity may lead to further upregulation of FOXO1 target genes associated with detrimental effects including cell cycle arrest and cell death. This may explain an increase of $p27^{kip1}$ observed in *FOXO4*-depleted MEC1 cells, increased *CDKN1B* expression observed in *FOXO4*-depleted HG3 cells, as well as reduced *CCND2* expression and enhanced *CDKN1B* expression following AZD8055-ibrutinib treatment in *FOXO3*-depleted MEC1 cells. Further work is required to address the implications of depleting *FOXO3* or *FOXO4* on the transcriptional activity of other FOXO isoforms.

As previously mentioned, FOXO transcription factors actively regulate the expression of GADD45A – a member of the GADD45 family responsible for mediating several mechanisms in response to intracellular DNA damage. As well as being a potential indicator of DNA damage repair components in CLL cells (discussed in section 5.3.1.4), GADD45A also functions as a mediator of G2 growth arrest and is highly expressed during the S-phase of the cell cycle [567]. Explanations for a depletion of GADD45A in MEC1 cells with diminished *FOXO3/4* are threefold: (1) Due to its accumulation in the S-phase as a contributing factor to DNA damage repair, GADD45A expression may serve as a molecular indicator of the S-phase cell population, possibly explaining a reduction in GADD45A expression following AZD8055-mediated S-phase depletion; (2) FOXO-mediated GADD45A expression is required for modulating cell cycle progression in CLL cells [439], primarily in the context of DNA damage repair at the G2-M checkpoint, which could explain increased G2 phase populations and reduced S phase populations in *FOXO3*-depleted MEC1 cells; and (3) *GADD45A* could serve as an indicator of $\gamma H2AX^{S139}$ accumulation in CLL cells, as $\gamma H2AX^{S139}$ levels have been shown to directly affect FOXO3 target gene expression in mouse fibroblasts [640]. GADD45A has also been reported as an inducer of G1 growth arrest [641, 642], which could explain aberrant cell cycle progression exhibited by *FOXO4*-depleted MEC1 cells. Figure 5.3 revealed that *FOXO4*-depleted cells expressed a concomitant depletion of *FOXO3* (also seen in primary CLL cells in Figure 5.18), while *FOXO3*-depleted cells exhibited no change in *FOXO4* expression, alluding *GADD45A* expression being induced by FOXO3, though more work will be needed

to determine this. These data provide a novel insight into FOXO-mediated regulation of the cell cycle and DNA damage in CLL cells, where depletion of FOXO leads to detrimental effects on cell cycle progression *via* downregulation of crucial effectors such as *GADD45A*, thereby eliciting aberrant cell cycle progression and a depletion of critical components of the DNA damage response.

5.3.1.2. Viability and chemosensitivity

As AZD8055 and ibrutinib synergistically promote CLL cell death [284], we addressed how *FOXO3/4* depletion affects CLL cell viability and sensitivity to these targeted agents. *FOXO4* depletion in MEC1 cells did not affect overall cell viability. However, HG3 cells expressing *FOXO4* knockdown exhibited reduced cell viability. Further, MEC1 cells harbouring a *FOXO3* knockdown were less viable in culture. As depletion of FOXO isoform expression in other cancer contexts promotes cell functionality when endogenous levels are low [530, 634-637], we speculate that a reduction in viability associated with *FOXO3/4* depletion is tied to their disparate expression in a cell-type-specific manner, supporting a cell-type-specific expression of FOXO family members in CLL. Nevertheless, irrespective of cell viability in the control population, lower FOXO4 expression does not discount FOXO4-mediated regulation of cell viability in MEC1 cells, evidenced by *FOXO4*-depleted MEC1 cells exhibiting increased sensitivity to AZD8055-ibrutinib treatment [545].

These data coincide with a significant increase in BIM isoform expression following AZD8055-ibrutinib or ibrutinib treatment, indicative of increased drug-mediated pro-apoptotic signalling in FOXO4-depleted cells. As FOXO4 nuclear expression was enhanced following ibrutinib treatment in CLL cells (Figures 4.10 & 4.14), we could speculate that FOXO4 may hinder ibrutinib-mediated BIM expression mediated by other FOXO transcription factors, though more work is needed to fully elucidate this. Indeed, Wagle *et al.* found that tyrosine kinase inhibitor resistance is induced by FOXO1 activity in CML cells [550], supporting that FOXOs could mediate resistance to targeted agents in leukaemic cells. MEC1 and HG3 cells exhibited disparate *BCL2L1* expression in a cell-type-specific manner. Specifically, COMBO-treated, *FOXO4*-depleted MEC1 and HG3 cells

expressed lower levels of *BCL2L1* than the SCR control. Mechanistically, FOXO4 can indirectly influence *BCL2L1* regulation *via* regulation of *BCL6* [629], which could explain a reduction in *BCL2L1* and BCL-XL observed in MEC1, HG3 and primary CLL cells with ablated *FOXO4*, though the expression status of *BCL6* in this context remains to be elucidated. MCL1 is purported to be directly inhibited by FOXO4 [643], which could explain an increase in MCL1 seen in HG3 cells. Nevertheless, an imbalance in BCL2 family protein expression seen following *FOXO4* depletion in CLL cells demonstrates a clear mechanism through which CLL cells with deficient *FOXO4* expression exhibited reduced cell viability and increased sensitivity to synergistic AZD8055-ibrutinib therapy, reinforcing FOXO4 as a key modulator of CLL cell survival.

FOXO4, as well as being a transcription factor, has been shown to bind to and antagonise p53 transcriptional activity [644], which could explain a p53-mediated depletion of cell viability that is absent in CLL cells with del(17p). FOXO4 also binds to p53 at sites of DNA damage repair [645], further supporting FOXO4 as a critical regulator of the DNA damage response. Interestingly, while *TP53* expression was reduced, p53 protein expression was significantly increased in HG3 cells, alluding to increased p53 activity in the absence of *FOXO4* expression; a decrease in *TP53* transcript expression may be due to more translated p53 in the absence of FOXO4, though these results are unclear and would need to be validated further. Future work investigating an association between FOXO4 and p53 in CLL would be critical to develop our understanding of the distinctive characteristics of CLL cells in discrete prognostic subsets.

FOXO3 knockdown also significantly reduced cell viability. FOXOs are known to induce the transcription of multiple growth factor receptors, including IGF1R, which facilitates cell survival *via* upregulation of PI3K-AKT signalling [501]. As *IGF1R* expression was diminished in cells with ablated *FOXO3*, this could explain a context-dependent reduction in cell viability. Moreover, *BCL2L1* expression was reduced in cells lacking *FOXO3* expression. As well as FOXO4 [629], FOXO3 is a known regulator of *BCL6* expression in CML cells [646], demonstrating a potential role for FOXO3 to indirectly regulate survival *via* BCL-XL. Increased FOXO1 expression and activity present in cells with ablated *FOXO3* and *FOXO4* could also be a reason for *BCL2L1* downregulation. While AZD8055 and ibrutinib enhanced CLL cell death in cells lacking *FOXO4* expression, shFOXO3-mediated

MEC1 cell death was attenuated by AZD8055-ibrutinib treatment, potentially highlighting a mechanism of FOXO3-induced apoptosis downstream of mTORC1/2 inhibition in CLL cells. Of note, mTOR inhibition has been shown to markedly increase PI3K activation and subsequent AKT^{T308} phosphorylation, promoting cell survival [406]. Further, AZD8055 has been known to promote cell autophagy [403], subsequently demonstrating how mTOR inhibition can promote cancer cell survival in multiple contexts. Considering these findings, AZD8055 treatment in the absence of FOXO3 expression may favour a positive feedback loop promoting CLL cell survival *via* enhanced PI3K-AKT signalling. More work is needed to elucidate this. However, a reduction in *BCL2L11* expression in *FOXO3*-depleted cells suggests a reduction in BIM-mediated apoptosis downstream of FOXO3 activity, which is established as a FOXO3-mediated response in several cancer models [647-650], supporting a crucial role for FOXO3 in regulating cell function and outcomes. In contrast, *BBC3* expression was enhanced following AZD8055-ibrutinib treatment in *FOXO3*-depleted MEC1 cells. *BBC3* (PUMA) is known to induce apoptosis downstream of FOXO3 activity [593]. Yun *et al*. have demonstrated that PUMA can be expressed independently of FOXO3, where dual mTORC1/2 inhibition induces PUMA *via* pharmacological inhibition of 4E-BP1, subsequently promoting translation initiation and preventing c-MYC-mediated *BBC3* repression [651]. FOXO expression can also modulate mTORC1 signalling capacity [547], which could lead to increased mTORC1 sensitivity to targeted inhibition by AZD8055, therefore potentiating *BBC3* expression (supported by an increase in PUMA expression in *FOXO3*-depleted MEC1 cells treated with AZD8055 and ibrutinib – Figure 5.13). In Figure 5.27, AZD8055-mediated abrogation of 4E-BP1$^{T37/46}$ phosphorylation was significantly enhanced in MEC1 cells with diminished *FOXO3*, demonstrating both indirect and direct mechanisms of FOXO3-mediated *BBC3* regulation in CLL cells. No change in protein expression could be explained by functional redundancy exhibited by FOXO1 and FOXO4 in *FOXO3*-depleted cells. Of note, consistent *BBC3* expression in *FOXO4*-depleted cells suggests a FOXO3-specific regulation of *BBC3*. Further work would serve to elucidate the expression and function of discrete FOXO3 targets in this context.

FOXO-mediated venetoclax sensitivity has been reported in investigative study in DLBCL *via* pharmacologically mediated FOXO1 activation and subsequent upregulation of *BCL2* [628]. We confirmed that *FOXO4* knockdown induces

chemosensitivity in MEC1 and HG3 cells to ibrutinib treatment, coincident with the aberrant expression of BCL2 family members. Furthermore, we demonstrated that shFOXO4 knockdown sensitises CLL cells to venetoclax treatment in a dose-dependent manner. Further investigation in MEC1 cells revealed that *FOXO4* depletion induces a dose-dependent enhancement in PARP, MCL1 and BCL2 expression. PARP-dependent apoptosis is a well-established effector of cell death [652], so a dose-dependent increase in PARP in *FOXO4*-depleted cells could be indicative of detrimental cell function. As previously mentioned, FOXO1 is known to mediate increased *BCL2* expression [628]; due to an abundance of FOXO1 in MEC1 cells, and venetoclax sensitivity being associated with intracellular levels of BCL2 [653], an increase in venetoclax sensitivity exhibited by *FOXO4*-depleted MEC1 cells may be potentiated by increased FOXO1 expression, though this remains to be elucidated. Interestingly, *FOXO4*-depleted MEC1 cells exhibited a dose-dependent enhancement of MCL1 expression. Upregulation of MCL1 with venetoclax treatment is associated with resistance to targeted therapy in lymphoid malignancies [654], so an upregulation of MCL1 could be a rescue mechanism to mitigate venetoclax-mediated cytotoxicity [655]. Concomitant with increased BCL2, lack of dose-dependent BCL-XL expression in cells lacking *FOXO4* may contribute to venetoclax sensitivity *via* aberrant pro-survival signalling and could also explain a dose-dependent enhancement of MCL1 in the absence of BCL-XL. In AML cells, BCL-XL degradation is associated with enhanced MCL1 expression [656], suggesting a compensatory mechanism is perhaps shared by these two BCL2-like proteins in CLL. Despite this, Yu *et al*. demonstrated that venetoclax induces apoptosis primarily in the absence of BCL-XL expression [657], supporting that an absence of BCL-XL upregulation is a causative factor for an increase in dose-dependent cell death. Primary CLL cells exhibited a dose-dependent increase in PARP cleavage, coincident with a depletion in MCL1 and BCL-XL expression. Primary CLL cell co-cultures are short-lived, lack hyperactive signalling exhibited by MEC1 cells and could therefore lack compensatory mechanisms in the context of MCL1 and BCL-XL expression. However, a reduction in MCL1 and BCL-XL gene and protein expression, as well as an increase in PARP cleavage in *FOXO4*-depleted primary CLL cells could suggest decreased cell viability and increased sensitivity to venetoclax. As part of future study, further sh-*FOXO4* knockdown and analysis of cell viability following dose-dependent venetoclax treatment

using cell staining methods would be pivotal in elucidating the impact of FOXO4 activity in CLL cell maintenance and could provide essential knowledge into distinct resistance mechanisms to first-line therapy.

5.3.1.3. FOXO3 upregulation in *FOXO4*-depleted CLL cells

The complexity surrounding FOXO regulation in disease biology is demonstrated by the existence of functional redundancy, whereby dysfunctional FOXO activity can be attenuated via rescue by other FOXO isoforms [427, 428, 483]. Highlighted by aberrant FOXO3 and FOXO4 depletion resulting in FOXO1 overexpression in MEC1 cells (Figure 5.3), these data point to either of these mechanisms existing within CLL cells. Moreover, as we show that FOXO isoform expression exhibited dynamic regulation over time in culture (Figure 3.10), it was of interest to understand how alterations in FOXO4 expression affect the expression of FOXO1 and FOXO3 during the culture of MEC1 and HG3 cells. In long-term cultures, FOXO4-depleted cells exhibited a significant increase in FOXO3 gene and protein expression. Considering FOXO3-mediated regulation of FOXO4 in this context, Essaghir et al. revealed that FOXO transcription factors exhibit distinct regulation by FOXO family isoforms; the FOXO1 promoter sequence harbours a consensus FOXO-binding region, demonstrating binding affinity for FOXO1 and FOXO3, confirming that FOXO1 is regulated by FOXO3 and by its own isoform, albeit to a lesser degree. Contrary to FOXO1, the FOXO4 promoter sequence lacks a consensus FOXO-binding site, arguing that FOXO4 cannot regulate the expression of its own isoform. Regardless, FOXO4 was also shown to be regulated by FOXO3 [555], demonstrating a capability of FOXO3 to regulate other discrete FOXO isoforms. FOXO3 can also regulate its own expression via FOXO3-mediated positive feedback loops in different disease contexts [658, 659]. Indeed, much of the literature surrounding FOXO expression in disease pathophysiology focuses on tissue-specific FOXO expression. Thus, a limiting factor in understanding FOXO behaviour is the lack of comparison of FOXO isoform characteristics [620]. Nevertheless, we could speculate that, in long-term culture, FOXO3 is upregulated as a compensatory mechanism to drive FOXO4 expression. Furthermore, COMBO-mediated attenuation of FOXO3 expression in

FOXO4-depleted MEC1 cells could be due to decreased mTOR activity. As FOXO activity regulates mTORC2-AKT activity in a positive feedback loop, a depletion of FOXO3 could be a mechanistic consequence of long-term abrogation of mTORC2-AKT-medited signals in MEC1 cells exhibiting constitutive PI3K-AKT signalling due to a lack of positive feedback loop promoting both AKT and FOXO3 activity. Supporting this, FOXO3 facilitates PI3K-AKT activation via upregulation of *PIK3CA* [548]. Moreover, mTOR inhibition has been shown to enhance protein degradation via the ubiquitin proteasome [660]. In contrast, our RNA-Seq dataset revealed decreased expression of proteasomal gene signatures (e.g. PSMD genes) following dual mTOR inhibition (Figures 4.3 & 4.5), suggesting mTOR signal abrogation impedes proteasomal function in primary CLL cells. PSMD expression has been associated with tumourigenesis in other cancer models [661], suggesting that AZD8055 can facilitate tumour suppression via PSMD family downregulation. Nevertheless, other studies have revealed that mTOR inhibition can facilitate or prohibit proteasomal activity in a context-dependent manner [308, 310, 662], which could explain a cell-type-specific depletion of FOXO3 and FOXO4 (Figure 4.8) in MEC1 cells after AZD8055 treatment, irrespective of mechanistic upregulation of FOXO induced by AZD8055. Additionally, FOXOs have been shown to regulate distinct components of the proteasome [663, 664], further reinforcing the importance of FOXO-mediated gene regulation in promoting cell maintenance.

5.3.1.4. The DNA damage response

FOXOs are established as mediators of damage response mechanisms, including the DNA damage response, primarily by inducing GADD45 protein expression [439]. Consistently, we observed that GADD45A expression was depleted in cells lacking *FOXO3* or *FOXO4* expression, suggesting that depleting *FOXO3/4* compromises a crucial mechanism of GADD45-mediated response to DNA damage in CLL cells, reflected by aberrant cell cycle progression (Figure 5.5 & 5.11) – coincident with GADD45A downregulation. Using γH2AX^{S139} intracellular staining, we showed that, while γH2AX^{S139} levels were unaffected by shRNA-mediated *FOXO3/4* knockdown, AZD8055 treatments conferred a significant rise in intracellular γH2AX^{S139} in cells lacking *FOXO3* or *FOXO4*. These findings infer an

increase in drug-mediated DNA damage in CLL cells in the absence of *FOXO3/4* expression. Multiple studies have shown that FOXO3 activity promotes DNA damage repair and facilitates drug resistance (reviewed in [665]). As we have shown that pharmacologically abrogating PI3K-AKT-mTOR-mediated signals induced FOXO expression and nuclear localisation in multiple *in vitro* contexts, it is safe to assume that FOXO activity facilitates a mechanism of DNA damage repair reflected by a reduction in intracellular γ-H2AX^{S139} (as seen in long-term CLL-CD40L co-cultures – Figure 4.20) in cells treated with AZD8055, while an absence of *FOXO3/4* expression conferred drug-induced DNA damage and a concomitant increase in intracellular γH2AX^{S139}. These data are supported in work by Liu *et al.*, demonstrating that GADD45A downregulation enhances chemosensitivity in melanoma cells, subsequently increasing intracellular γH2AX^{S139} [666]. Furthermore, Hassan *et al*. recently demonstrated that targeted deletion of *GADD45A* induced heightened levels of endogenous DNA damage in AML leukaemic stem cells (LSCs) [667]. Further investigation into other damage repair components, such as the accumulation of 53BP1 foci – a key determining factor in the repair of DSBs [668] - would help to determine whether an absence of FOXO3/4 – and therefore GADD45A – truly negatively influences the CLL DNA damage response. Nevertheless, these findings demonstrate FOXO-mediated GADD45A activity as a key determinant of DNA damage repair in CLL cells and reinforce the need for FOXO activity to mediate resistance to targeted therapies.

5.3.2. FOXO3/4 as novel regulators of mTORC1/2 signalling in CLL

As well as eliciting downstream effects, it is well known that FOXO activity can provide a modulatory feedback loop to negatively regulate mTORC1/2 function, both directly (*via RICTOR* upregulation) or indirectly (*via SESN3* upregulation) [437, 438]. Initial findings that *FOXO4*-depleted MEC1 cells exhibited increased cell size (Figure 5.19). As effectors of mTORC1 signalling are known regulators of mammalian cell size [669], we investigated whether ablation of *FOXO4* influenced upstream mTOR signalling in CLL. In MEC1 and HG3 cells, sh-*FOXO3/4*

knockdown induced a significant downregulation of *SESN3*, indicative of an absence of Sesn3-mediated negative regulation of mTORC1 activity. Concurrently, genes encoding mTORC1/2 components (*MTOR, RICTOR* and *RAPTOR*) were upregulated, suggesting enhanced expression of mTORC1/2 components in CLL cells lacking *FOXO3/4*. Further investigation revealed that distinct mTORC1 components were activated in *FOXO4*-depleted MEC1 and HG3 cells demonstrating that, while *RICTOR* upregulation inhibits mTORC1 activity, mTORC1 signalling is favoured in *FOXO4*-depleted cells, perhaps due to shFOXO4-mediated *SESN3* depletion. In CML cells, Vakana *et al*. revealed that *SESN3* overexpression elicits an inhibitory effect on mTORC1/2 signalling, primarily with regards to downstream S6 activity [670], demonstrating a practical application of SESN3-mediated regulation of mTORC1 activity as reported downstream of FOXO1 and FOXO3 [547]. In this work, skew of mTORC1/2 activity towards mTORC1 was further demonstrated by constitutive expression of Rictor^{T1135} in *FOXO4*-depleted cells. Rictor^{T1135} is a designated marker of mTORC1 component activity as it is directly phosphorylated by S6K, thus leading to mTORC2 inactivation as part of a negative feedback loop [306]. Increased phosphorylation of p70-S6K in *FOXO4*-depleted HG3 cells, as well as increased S6$^{S235/236}$ levels in HG3 and MEC1 cells reinforce mTORC1-mediated inactivation of mTORC2 in *FOXO4*-depleted cells, supported by reduced AKT^{S473} seen following further investigation (Figure 5.23). Moreover, increased S6$^{S235/236}$ phosphorylation could explain a phenotypic change in cell size [671]. *FOXO4* depletion also elicited aberrant 4E-BP1$^{T37/46}$ phosphorylation in a cell-type-specific manner; although 4E-BP1$^{T37/46}$ levels were unaffected in MEC1 cells, HG3 cells exhibited a depletion of 4E-BP1$^{T37/46}$ alongside *FOXO4* depletion. Shull *et al*. previously found that 4E-BP1 dephosphorylation is associated with apoptosis in CLL [672], which could be a factor contributing to decreased cell viability evident in *FOXO4*-depleted HG3 cells. Nevertheless, an abundance of p70-S6K and S6 activity co-occurring with reduced 4E-BP1$^{T37/46}$ and significantly increased PDCD4 suggest that, while *FOXO4* depletion confers an increase in activity of distinct mTORC1 components, mTORC1 hyperactivity in this context is dysfunctional and therefore does not contribute to the oncogenic programme as it does in other disease contexts [437]. Interestingly, supportive work by Han *et al*. revealed that *FOXO4* overexpression induced a context-dependent dephosphorylation of selective mTORC1 components including S6K and S6 *via* increased AMPK activity

in T-helper cells [630], supporting FOXO4 as a critical regulator of mTOR activity in leukocyte populations.

An alternative paradigm exists in which hyperactivation of mTOR-mediated signalling can also sensitise cells to apoptosis (reviewed in [673]). Here, dysfunctional mTORC1 hyperactivation in the context of shFOXO4 knockdown was demonstrated by a contrasting phenotype in which *FOXO4*-depleted cells exhibited diminished proliferation and survival. This significant increase in mTORC1 signalling/dysfunction and sensitivity to targeted mTORC1/2 inhibition could explain CLL cell sensitivity to mTORC1/2 inhibition in the absence of *FOXO4*. As this was more profound in mTORC1, we investigated the functional implications of selective mTORC1 treatment with rapamycin, alone or in combination with ibrutinib (as ibrutinib is known to synergistically enhance the efficacy of rapamycin in CLL [409]). Rictor^{T1135} phosphorylation in *FOXO4*-depleted cells was effectively diminished by AZD8055 and rapamycin treatments, while Rictor^{T1135} was unaffected by mTORC1/2 inhibition in the SCR control. As expected, AKT^{S473} was diminished with AZD8055 treatment irrespective of *FOXO4* expression. However, a depletion of AKT^{S473} by rapamycin and ibrutinib treatment seen in the SCR control (and in published data in CLL [409]) was lost in *FOXO4*-depleted cells. This is perhaps due to an increase in sensitivity of S6K - and therefore Rictor^{T1135} - to these agents, thereby promoting mTORC2 and subsequent AKT^{S473} activity [674]. These findings could also explain how rapamycin and ibrutinib treatments have an increased negative effect on CLL cell proliferation and survival in cells lacking *FOXO4* expression. Additional work investigating the activity of TSC1/2 would provide a crucial link between FOXO downregulation and subsequent *SESN3* downregulation to mTORC1/2 activity [438]. As *SESN3* is also known to contribute to oxidative damage repair downstream of FOXO activity [675], it would also be worth investigating the impact of *FOXO4* depletion on ROS accumulation in CLL cells, given that FOXOs are known to regulate other ROS defence components including catalase (CAT) [676] and manganese superoxide dismutase (MnSOD) [554], and are themselves regulated by intracellular ROS [677].

Nonetheless, these data demonstrate a dependency of CLL cells on the expression and subsequent activity of FOXO4 to administer tight regulation over the expression and signalling of mTORC1/2 components to promote proliferation,

survival and resistance to selective agents. Of note, this does not seem to be entirely exclusive to *FOXO4* expression, as further investigation in MEC1 cells harbouring an shRNA-mediated knockdown of *FOXO1* or *FOXO3* also revealed aberrant expression and activity of mTORC1/2 components, demonstrating that the activity of the wider FOXO family may regulate mTORC1/2-mediated signalling in CLL; more work would need to be conducted to elucidate this further. These data also inversely reflect mTORC1/2 activity observed in poor prognostic CLL patients [284], reinforcing the clinical relevance of FOXO3/4 expression in regulating mTOR-mediated signals to facilitate disease progression.

6. General discussion

6.1. The dichotomy of FOXO behaviour

FOXOs have traditionally been regarded as tumour suppressors, not only due to their canonical activity being associated with detrimental cellular fate (e.g. cell cycle arrest and apoptosis) [429], but also due to deletion of *FOXO1/3/4* in adult mice leading to tumour formation [483]. Supporting this, as discussed in this thesis, a number of studies have demonstrated that FOXO function is diminished in B cell malignancies either by reducing FOXO expression [500, 511, 512], or by FOXO inactivation within distinct cellular environments [284, 285, 513]. However, as presented in this thesis, FOXO family members can also promote tumorigenesis, and this can occur in a disease- and cell lineage-dependent manner, as observed in B-cell malignancies [501, 678] and in solid tumours; high expression of *FOXO3* is associated with glioblastoma progression, pancreatic ductal adenocarcinoma, and poor survival rates in breast and colorectal cancers (CRC) [623]. Furthermore, mutations leading to constitutive activation of FOXO1 are associated with B-cell disease progression, particularly in DLBCL [679] and BL [540], impacting on the transcriptional activity of FOXO family members and implicating a plethora of avenues by which disease can exploit FOXO expression to promote cell survival and proliferation. In addition to the well documented roles of FOXO1 and FOXO3 in regulating B-cell malignancies, lower expression levels of *FOXO4,* and perhaps *FOXO6,* do not preclude these family members having a role in lymphomagenesis. In DLBCL, *FOXO4* expression is important for maintaining colony formation and drug resistance [545]. As CLL is closely related to DLBCL, the work described in this thesis strongly suggest that FOXO4 exhibits similar characteristics in CLL. This study in DLBCL aligns with findings that FOXO3 activity is important for maintenance of leukaemia-initiating cells in myeloid leukaemias [485-487], reinforcing that individual FOXOs may perform specific functions in a lineage-dependent manner. These data complement findings discussed in this thesis, as modulating *FOXO3/4* expression had notable

influence on distinct cellular outcomes, coincident with the aberrant expression of distinct FOXO target genes, all of which are tightly regulated by upstream signals to facilitate cell function. Indeed, FOXO4's role in B-cell development and maturation has yet to be fully elucidated [463]; it could be that, in conjunction with FOXO1 and FOXO3, FOXO4 plays a role in mediating these processes, perhaps explaining why B-cell malignancies such as DLBCL [545] and CLL require its expression to promote proliferation, survival and resistance to targeted therapies.

6.2. Therapeutic targeting of FOXO activity

Attempts to pharmacologically manipulate FOXO activity have strong clinical relevance due to their interest as a novel therapeutic targets in multiple disease contexts [574]. As well as pharmacologically targeting effectors upstream of FOXO, agents have been developed to specifically target the distinct characteristics of FOXO isoforms - carbenoxolone is an example of one such compound that directly target the DNA-binding capability of FOXO isoforms [680]. In addition, targeted therapeutics have been developed that perturb interactions of FOXO transcription factors with distinct binding partners. As a notable example, FOXO4 has been reported to maintain cell senescence *via* binding to - and prohibiting the tumour-suppressive characteristics of - p53. As such, Baar *et al*. developed a cell-penetrating peptide that exclusively has affinity for FOXO4 and prevents the FOXO4-p53 interaction, subsequently inducing p53-mediated cell death in senescent, disease-associated cell populations [681]. As p53 expression and activity are heavily associated with prognosis in CLL [50], it would be interesting to investigate the outcomes of pharmacologically modulating the FOXO4-p53 interaction and how this differs to CLL cells harbouring del(17p)/*TP53* mutations. Indeed, depleting *FOXO4* could perhaps explain a p53-mediated reduction in HG3 cell viability that is absent in MEC1 cells (Figure 5.6), reinforcing FOXO4 as a positive regulator of cell survival.

In the context of diabetes, small molecule inhibitors have been shown to prevent interactions of FOXO1 with SIN3A, thereby preventing FOXO1-mediated

gluconeogenesis associated with hyperglycaemia [682]. These data provide more evidence as to the complexity of FOXO biology in that FOXO isoforms regulate – and are regulated by - distinct protein-protein interactions that are perhaps dysregulated in cancer neoplasms. Targeting other interaction partners that promote FOXO activity - such as ß-catenin [683] - could provide an alternate method of repressing FOXO activity to further increase our understanding of how discrete FOXO isoforms contribute to disease pathophysiology. Moreover, multiple compounds have been developed that disrupt FOXO nuclear export, the most advanced of these being selective inhibitors of nuclear export (SINE) inhibitors. SINE inhibitors function by reversibly binding to CRM1 (XPO1), thereby preventing CRM1-mediated FOXO nuclear export [684]. CRM1 is known to be upregulated in haematological malignancies including CLL [685], potentially increasing export of transcription factors associated with tumour suppression, including FOXOs. It is worth noting that the therapeutic benefit of Selinexor treatment has been highlighted in phase I clinical trial in multiple haematological malignancies (described in [686]); is clinically approved for the treatment of R/R DLBCL [687]; and is under extensive further investigation in CLL, with recent results by Vitale *et al*. showing that Selinexor-mediated nuclear retention of FOXO3 potentiates cytotoxicity to idelalisib treatment [688]. In a recent phase I trial for CLL patients (NCT02303392), Selinexor treatment induced effective treatment response in combination with ibrutinib [689], demonstrating that a context-dependent prevention of FOXO nuclear export could sensitise cells to targeted inhibitor treatment, as previously reported by Kapoor *et al*. in CLL and DLBCL [524]. In this regard, it would be of interest to elucidate how Selinexor treatment affects the nuclear localisation of other FOXO isoforms in CLL. Moreover, multiple 14-3-3 inhibitors have been developed that resensitise malignant cells to targeted therapies (described in [690]), perhaps as a consequence of impeding 14-3-3-mediated FOXO nuclear export. Collectively, these findings demonstrate how disrupting the regulation of FOXO activity in CLL and wider cancer contexts could induce tumour suppressive effects to overcome drug resistance in leukaemic cells, highlighting the importance of tightly controlling FOXO expression, subcellular localisation and subsequent activity to promote survival. This is evident for FOXO1, whose pharmacological activation is associated with cell cycle arrest and cell death in CLL following pharmacological abrogation of mTORC1/2- and BTK-mediated signals *via* AZD8055 and ibrutinib

treatment, even though untreated CLL cells harbour nuclear FOXO1 expression [284]. Indeed, these findings do not discount a role for FOXO transcription factors in promoting proliferation and survival in the absence of dysfunctional FOXO nuclear/cytoplasmic shuttling. An extensive overview of therapeutics targeting FOXO activity for the treatment of cancer and wider disease can be found in [574].

6.3. FOXOs as disease biomarkers

In the broader context, studies investigating FOXO expression as a prognostic biomarker have contrasting results. In CRC, low expression of FOXO3 is associated with cancer progression in specimens with normal tissue [691], while high FOXO3 expression is purported to promote CRC progression in cells with high expression of ß-catenin [623], further demonstrating the dichotomy of FOXO behaviour depending on the distinct context of the cellular environment. Further, FOXO1 expression is associated with good prognosis in prostate and breast cancers [516, 517]. In B-cell malignancy, FOXO1 mutations are used as an indicator of FL progression [692]. These mutations are also evident in BL and DLBCL and are associated with poorer disease outcomes [494], demonstrating a potential use of FOXO1 as biomarker in specific B-cell malignancies. Indeed, *ex vivo* patient samples exhibited disparate expression of FOXO isoforms, all of which were elevated in CLL samples compared with B-cell donor samples. Notably, FOXO1, FOXO3 and FOXO4 were differentially expressed in different prognostic subsets, which could have potential for defining patient prognostics and outcomes. Though, due to a lack of mutation of FOXO transcription factors in CLL [463], their nuclear activity remains poorly defined. Nevertheless, little is known with regards to the mutational status of FOXO4 in CLL and in wider B-cell malignancies [463]. As subcellular fractionation studies demonstrated that FOXO4 was consistently expressed in the CLL cell nucleus, these findings allude to potential activating mutations and/or components regulating FOXO4 activity that have yet to be elucidated which – combined with FOXO4's role in CLL cell maintenance and drug resistance – could warrant a use for FOXO4 as a potential predictive biomarker of resistance to targeted therapy. Indeed, the uncertainty

of transcription factor behaviour and the differential nature of FOXO activity in different CLL-relevant contexts – such as those described in this thesis – beckons further investigation to determine their potential as prognostic or predictive biomarkers.

While considering the expression levels of specific FOXO family members (or their mutational status) as biomarkers, it may also be interesting to consider the utility of FOXO activity. While FOXO family members can be inactivated as a result of microenvironmental factors that impinge on the tumour cell, drugs targeting protein/pathways upstream of FOXO can lead to a reactivation and promotion of its tumour suppressor role [284, 525, 693, 694]. Supporting this, our data revealed a 'dampening' of FOXO expression and activity downstream of BCR and CD40 receptor activation, alluding further to a 'goldilocks' state of FOXO activity to tilt their function towards promoting proliferation and survival, while shRNA-mediated depletion of *FOXO3*/*FOXO4* expression was detrimental to cell viability and function. The resultant change in FOXO activity can be exploited for the development of novel, tumour-specific FOXO-gene signatures. Indeed, repression of FOXO1/3-regulated genes in MM patients has prognostic significance, being associated with reduced overall survival [513]. Therefore, gaining a deeper understanding of FOXO family regulation, in addition to providing targeting opportunities for the development of novel, FOXO-specific therapies, may reveal robust pharmacological/prognostic biomarkers to enhance the clinical management and survival prospects of patients.

6.4. Conclusive remarks

In this thesis, we have explored the characteristics of FOXO3 and FOXO4 to define their importance in promoting or repressing CLL proliferation and survival. This work has challenged the conventional dogma that FOXO transcription factors behave as typical 'tumour suppressors' by detailing the extent to which discrete FOXO expression, regulation and subsequent activity negatively influence cell function, survival and sensitivity to targeted agents. In doing so, this thesis revises our view of the characteristics of FOXO behaviour in

the context of CLL, indicating that discrete FOXO isoforms exhibit disparate behaviour by regulating distinct processes both beneficial and detrimental to cell function. Alongside previous work conducted by our group, the findings described in this thesis contribute to our understanding of FOXO biology in CLL and, consequently, in the wider context of disease. While we define that FOXO isoform expression and activity are regulated by canonical PI3K-AKT-mTOR signalling, the persistence of nuclear FOXO expression suggests the need for FOXO expression in CLL - the upstream components regulating this have yet to be elucidated.

The ever-growing list of therapeutics that serve to modulate FOXO transcriptional activity have promising outcomes that could be refined for clinical use (e.g. Selinexor) in conjunction with current clinical strategies (e.g. BTKi therapy). Yet, as the findings in this thesis and discoveries in other cancer neoplasms make apparent, the multidimensional complexity surrounding FOXO regulation in disease pathophysiology is ever-growing. Therefore, to truly determine whether targeting FOXO activity has therapeutic benefit, we must consider investigating other avenues through which FOXO activity is modulated, as well as developing on our current understanding by utilising a wider array of model systems. Nonetheless, this thesis provides a novel understanding of FOXO behaviour in CLL disease biology, harbouring potential to contribute to future pre-clinical investigations to aid in the development of novel therapeutics to ultimately improve CLL patient outcomes.

7. List of references

1. Kipps, T.J., et al., *Chronic lymphocytic leukaemia.* Nat Rev Dis Primers, 2017. **3**: p. 17008.

2. Chiorazzi, N., S.S. Chen, and K.R. Rai, *Chronic Lymphocytic Leukemia.* Cold Spring Harb Perspect Med, 2021. **11**(2): p. a035220.

3. Klein, U., et al., *Gene expression profiling of B cell chronic lymphocytic leukemia reveals a homogeneous phenotype related to memory B cells.* J Exp Med, 2001. **194**(11): p. 1625-38.

4. Zhang, S. and T.J. Kipps, *The pathogenesis of chronic lymphocytic leukemia.* Annu Rev Pathol, 2014. **9**: p. 103-18.

5. Dohner, H., et al., *Genomic aberrations and survival in chronic lymphocytic leukemia.* N Engl J Med, 2000. **343**(26): p. 1910-6.

6. Damle, R.N., et al., *Ig V gene mutation status and CD38 expression as novel prognostic indicators in chronic lymphocytic leukemia.* Blood, 1999. **94**(6): p. 1840-7.

7. Hamblin, T.J., et al., *Unmutated Ig V(H) genes are associated with a more aggressive form of chronic lymphocytic leukemia.* Blood, 1999. **94**(6): p. 1848-54.

8. Crespo, M., et al., *ZAP-70 expression as a surrogate for immunoglobulin-variable-region mutations in chronic lymphocytic leukemia.* N Engl J Med, 2003. **348**(18): p. 1764-75.

9. Wiestner, A., et al., *ZAP-70 expression identifies a chronic lymphocytic leukemia subtype with unmutated immunoglobulin genes, inferior clinical outcome, and distinct gene expression profile.* Blood, 2003. **101**(12): p. 4944-51.

10. Hallek, M., et al., *iwCLL guidelines for diagnosis, indications for treatment, response assessment, and supportive management of CLL.* Blood, 2018. **131**(25): p. 2745-2760.

11. Ten Hacken, E. and J.A. Burger, *Microenvironment interactions and B-cell receptor signaling in Chronic Lymphocytic Leukemia: Implications for disease pathogenesis and treatment.* Biochim Biophys Acta, 2016. **1863**(3): p. 401-413.

12. Hallek, M., *Chronic lymphocytic leukemia: 2020 update on diagnosis, risk stratification and treatment.* Am J Hematol, 2019. **94**(11): p. 1266-1287.

13. Pula, B., et al., *Overcoming Ibrutinib Resistance in Chronic Lymphocytic Leukemia.* Cancers (Basel), 2019. **11**(12): p. 1834.

14. UK, C.R. *Chronic Lymphocytic Leukaemia Statistics*. 2017; Available from: https://www.cancerresearchuk.org/health-professional/cancer-statistics/statistics-by-cancer-type/leukaemia-cll#heading-Three.

15. HMRN CLL survival statistics. 2010-2022. Available from: https://hmrn.org/statistics/survival

16. Catovsky, D., R. Wade, and M. Else, *The clinical significance of patients' sex in chronic lymphocytic leukemia.* Haematologica, 2014. **99**(6): p. 1088-94.

17. Goldin, L.R., et al., *Familial risk of lymphoproliferative tumors in families of patients with chronic lymphocytic leukemia: results from the Swedish Family-Cancer Database.* Blood, 2004. **104**(6): p. 1850-4.

18. Gale, R.P., et al., *Decreased chronic lymphocytic leukemia incidence in Asians in Los Angeles County.* Leuk Res, 2000. **24**(8): p. 665-9.

19. Law, P.J., et al., *Genome-wide association analysis implicates dysregulation of immunity genes in chronic lymphocytic leukaemia.* Nat Commun, 2017. **8**: p. 14175.

20. Went, M., et al., *Genetic correlation between multiple myeloma and chronic lymphocytic leukaemia provides evidence for shared aetiology.* Blood Cancer J, 2018. **9**(1): p. 1.

21. Anderson, L.A., O. Landgren, and E.A. Engels, *Common community acquired infections and subsequent risk of chronic lymphocytic leukaemia.* Br J Haematol, 2009. **147**(4): p. 444-9.

22. Landgren, O., et al., *Acquired immune-related and inflammatory conditions and subsequent chronic lymphocytic leukaemia.* Br J Haematol, 2007. **139**(5): p. 791-8.

23. Landgren, O., et al., *Respiratory tract infections and subsequent risk of chronic lymphocytic leukemia.* Blood, 2007. **109**(5): p. 2198-201.

24. Lenders, J.W., et al., *Combined immunodeficiency preceding chronic lymphocytic leukemia.* Blut, 1984. **48**(3): p. 171-5.

25. Tsai, H.T., et al., *Evidence of serum immunoglobulin abnormalities up to 9.8 years before diagnosis of chronic lymphocytic leukemia: a prospective study.* Blood, 2009. **114**(24): p. 4928-32.

26. Leon, M.E., et al., *Pesticide use and risk of non-Hodgkin lymphoid malignancies in agricultural cohorts from France, Norway and the USA: a pooled analysis from the AGRICOH consortium.* Int J Epidemiol, 2019. **48**(5): p. 1519-1535.

27. Mescher, C., et al., *The impact of Agent Orange exposure on prognosis and management in patients with chronic lymphocytic leukemia: a National Veteran Affairs Tumor Registry Study.* Leuk Lymphoma, 2018. **59**(6): p. 1348-1355.

28. Schwartz, G.G. and M.G. Klug, *Incidence rates of chronic lymphocytic leukemia in US states are associated with residential radon levels.* Future Oncol, 2016. **12**(2): p. 165-74.

29. Preston, D.L., et al., *Cancer incidence in atomic bomb survivors. Part III. Leukemia, lymphoma and multiple myeloma, 1950-1987.* Radiat Res, 1994. **137**(2 Suppl): p. S68-97.

30. Gluzman, D., et al., *Patterns of hematological malignancies in Chernobyl clean-up workers (1996-2005).* Exp Oncol, 2006. **28**(1): p. 60-3.

31. Chumak, V.V., et al., *The Ukrainian-American study of leukemia and related disorders among Chornobyl cleanup workers from Ukraine: II. Estimation of bone marrow doses.* Radiat Res, 2008. **170**(6): p. 698-710.

32. Kesminiene, A., et al., *Risk of hematological malignancies among Chernobyl liquidators.* Radiat Res, 2008. **170**(6): p. 721-35.

33. Rawstron, A.C., et al., *Reproducible diagnosis of chronic lymphocytic leukemia by flow cytometry: An European Research Initiative on CLL (ERIC) & European Society for Clinical Cell Analysis (ESCCA) Harmonisation project.* Cytometry B Clin Cytom, 2018. **94**(1): p. 121-128.

34. Binet, J.L., et al., *A new prognostic classification of chronic lymphocytic leukemia derived from a multivariate survival analysis.* Cancer, 1981. **48**(1): p. 198-206.

35. Rai, K.R., et al., *Clinical staging of chronic lymphocytic leukemia.* Blood, 1975. **46**(2): p. 219-34.

36. Hallek, M. and O. Al-Sawaf, *Chronic lymphocytic leukemia: 2022 update on diagnostic and therapeutic procedures.* Am J Hematol, 2021. **96**(12): p. 1679-1705.

37. Rai, K.R., *Rai KR. A critical analysis of staging in CLL. In: RP Gale, KR Rai, eds. Chronic Lymphocytic Leukemia: Recent Progress and Future Directions. Alan R.Liss;* 1987: 253-264.

38. UK, B.C. *Staging CLL*. 2024; Available from: https://bloodcancer.org.uk/understanding-blood-cancer/leukaemia/chronic-lymphocytic-leukaemia-cll/cll-symptoms-diagnosis/staging-cll/.

39. Pflug, N., et al., *Development of a comprehensive prognostic index for patients with chronic lymphocytic leukemia.* Blood, 2014. **124**(1): p. 49-62.

40. International, C.L.L.I.P.I.w.g., *An international prognostic index for patients with chronic lymphocytic leukaemia (CLL-IPI): a meta-analysis of individual patient data.* Lancet Oncol, 2016. **17**(6): p. 779-790.

41. Cortese, D., et al., *On the way towards a 'CLL prognostic index': focus on TP53, BIRC3, SF3B1, NOTCH1 and MYD88 in a population-based cohort.* Leukemia, 2014. **28**(3): p. 710-3.

42. Shanafelt, T.D., et al., *Validation of a new prognostic index for patients with chronic lymphocytic leukemia.* Cancer, 2009. **115**(2): p. 363-72.

43. Wierda, W.G., et al., *Prognostic nomogram and index for overall survival in previously untreated patients with chronic lymphocytic leukemia.* Blood, 2007. **109**(11): p. 4679-85.

44. *Chemotherapeutic options in chronic lymphocytic leukemia: a meta-analysis of the randomized trials. CLL Trialists' Collaborative Group.* J Natl Cancer Inst, 1999. **91**(10): p. 861-8.

45. Dighiero, G., et al., *Chlorambucil in indolent chronic lymphocytic leukemia. French Cooperative Group on Chronic Lymphocytic Leukemia.* N Engl J Med, 1998. **338**(21): p. 1506-14.

46. Spanish Cooperative Group, P., *Treatment of Chronic Lymphocytic Leukemia: A Preliminary Report of Spanish (Pethema) Trials.* Leuk Lymphoma, 1991. **5 Suppl 1**: p. 89-91.

47. Molica, S., et al., *The chronic lymphocytic leukemia international prognostic index predicts time to first treatment in early CLL: Independent validation in a prospective cohort of early stage patients.* Am J Hematol, 2016. **91**(11): p. 1090-1095.

48. Munoz-Novas, C., et al., *The International Prognostic Index for Patients with Chronic Lymphocytic Leukemia Has the Higher Value in Predicting Overall Outcome Compared with the Barcelona-Brno Biomarkers Only Prognostic Model and the MD Anderson Cancer Center Prognostic Index.* Biomed Res Int, 2018. **2018**: p. 9506979.

49. Moles, M.W., *Investigating mTORC2/AKT-mediated regulation of FOXO1: a novel therapeutic strategy for chronic lymphocytic leukaemia?* 2021, University of Glasgow. PhD thesis.

50. Gaidano, G. and D. Rossi, *The mutational landscape of chronic lymphocytic leukemia and its impact on prognosis and treatment.* Hematology Am Soc Hematol Educ Program, 2017. **2017**(1): p. 329-337.

51. Pieper, K., B. Grimbacher, and H. Eibel, *B-cell biology and development.* J Allergy Clin Immunol, 2013. **131**(4): p. 959-71.

52. D'Avola, A., et al., *Surface IgM expression and function are associated with clinical behavior, genetic abnormalities, and DNA methylation in CLL.* Blood, 2016. **128**(6): p. 816-26.

53. Parikh, S.A., et al., *Should IGHV status and FISH testing be performed in all CLL patients at diagnosis? A systematic review and meta-analysis.* Blood, 2016. **127**(14): p. 1752-60.

54. Cahill, N., et al., *IGHV3-21 gene frequency in a Swedish cohort of patients with newly diagnosed chronic lymphocytic leukemia.* Clin Lymphoma Myeloma Leuk, 2012. **12**(3): p. 201-6.

55. Pepper, C., et al., *Defining the prognosis of early stage chronic lymphocytic leukaemia patients.* Br J Haematol, 2012. **156**(4): p. 499-507.

56. Rossi, D., et al., *Mutations of NOTCH1 are an independent predictor of survival in chronic lymphocytic leukemia.* Blood, 2012. **119**(2): p. 521-9.

57. Sigmund, A.M. and A.S. Kittai, *Richter's Transformation.* Curr Oncol Rep, 2022. **24**(8): p. 1081-1090.

58. Seifert, M., et al., *Cellular origin and pathophysiology of chronic lymphocytic leukemia.* J Exp Med, 2012. **209**(12): p. 2183-98.

59. Chen, L., et al., *Expression of ZAP-70 is associated with increased B-cell receptor signaling in chronic lymphocytic leukemia.* Blood, 2002. **100**(13): p. 4609-14.

60. Hoogeboom, R., et al., *A mutated B cell chronic lymphocytic leukemia subset that recognizes and responds to fungi.* J Exp Med, 2013. **210**(1): p. 59-70.

61. Ten Hacken, E., et al., *The importance of B cell receptor isotypes and stereotypes in chronic lymphocytic leukemia.* Leukemia, 2019. **33**(2): p. 287-298.

62. Agathangelidis, A., et al., *Stereotyped B-cell receptors in one-third of chronic lymphocytic leukemia: a molecular classification with implications for targeted therapies.* Blood, 2012. **119**(19): p. 4467-75.

63. Del Giudice, I., et al., *Stereotyped subset #1 chronic lymphocytic leukemia: a direct link between B-cell receptor structure, function, and patients' prognosis.* Am J Hematol, 2014. **89**(1): p. 74-82.

64. Landau, D.A., et al., *Evolution and impact of subclonal mutations in chronic lymphocytic leukemia.* Cell, 2013. **152**(4): p. 714-26.

65. Landau, D.A., et al., *Mutations driving CLL and their evolution in progression and relapse.* Nature, 2015. **526**(7574): p. 525-30.

66. Puente, X.S., et al., *Non-coding recurrent mutations in chronic lymphocytic leukaemia.* Nature, 2015. **526**(7574): p. 519-24.

67. Puente, X.S., et al., *Whole-genome sequencing identifies recurrent mutations in chronic lymphocytic leukaemia.* Nature, 2011. **475**(7354): p. 101-5.

68. Quesada, V., et al., *Exome sequencing identifies recurrent mutations of the splicing factor SF3B1 gene in chronic lymphocytic leukemia.* Nat Genet, 2011. **44**(1): p. 47-52.

69. Schuh, A., et al., *Monitoring chronic lymphocytic leukemia progression by whole genome sequencing reveals heterogeneous clonal evolution patterns.* Blood, 2012. **120**(20): p. 4191-6.

70. Rossi, D., et al., *Integrated mutational and cytogenetic analysis identifies new prognostic subgroups in chronic lymphocytic leukemia.* Blood, 2013. **121**(8): p. 1403-12.

71. Rossi, D., et al., *Different impact of NOTCH1 and SF3B1 mutations on the risk of chronic lymphocytic leukemia transformation to Richter syndrome.* Br J Haematol, 2012. **158**(3): p. 426-9.

72. Burger, J.A., et al., *Ibrutinib as Initial Therapy for Patients with Chronic Lymphocytic Leukemia.* N Engl J Med, 2015. **373**(25): p. 2425-37.

73. O'Brien, S., et al., *Ibrutinib for patients with relapsed or refractory chronic lymphocytic leukaemia with 17p deletion (RESONATE-17): a phase 2, open-label, multicentre study.* Lancet Oncol, 2016. **17**(10): p. 1409-1418.

74. Coutre, S.e.a., *Clinical Activity Of Idelalisib (GS-1101), a Selective Inhibitor Of PI3Kδ, In Phase 1 and 2 Trials In Chronic Lymphocytic Leukemia (CLL): Effect Of Del(17p)/TP53 Mutation, Del(11q), IGHV Mutation, and NOTCH1 Mutation.* Blood, 2013 (Poster).

75. Villamor, N., et al., *NOTCH1 mutations identify a genetic subgroup of chronic lymphocytic leukemia patients with high risk of transformation and poor outcome.* Leukemia, 2013. **27**(5): p. 1100-6.

76. Else, M., et al., *The long-term outcome of patients in the LRF CLL4 trial: the effect of salvage treatment and biological markers in those surviving 10 years.* Br J Haematol, 2016. **172**(2): p. 228-37.

77. Goede, V., et al., *Obinutuzumab plus chlorambucil in patients with CLL and coexisting conditions.* N Engl J Med, 2014. **370**(12): p. 1101-10.

78. Stilgenbauer, S., et al., *Gene mutations and treatment outcome in chronic lymphocytic leukemia: results from the CLL8 trial.* Blood, 2014. **123**(21): p. 3247-54.

79. Estenfelder, S. *et al.*, *Gene Mutations and Treatment Outcome in the Context of Chlorambucil (Clb) without or with the Addition of Rituximab (R) or Obinutuzumab (GA-101, G) - Results of an Extensive Analysis of the Phase III Study CLL11 of the German CLL Study Group.* Blood, 2016. **642. CLL: Therapy, excluding Transplantation: Poster II**.

80. Woyach, J.A., et al., *BTK(C481S)-Mediated Resistance to Ibrutinib in Chronic Lymphocytic Leukemia.* J Clin Oncol, 2017. **35**(13): p. 1437-1443.

81. Gaballa, S. and J. Pinilla-Ibarz, *BTK Inhibitors in Chronic Lymphocytic Leukemia.* Curr Hematol Malig Rep, 2021. **16**(5): p. 422-432.

82. Calin, G.A., et al., *Frequent deletions and down-regulation of micro- RNA genes miR15 and miR16 at 13q14 in chronic lymphocytic leukemia.* Proc Natl Acad Sci U S A, 2002. **99**(24): p. 15524-9.

83. Klein, U., et al., *The DLEU2/miR-15a/16-1 cluster controls B cell proliferation and its deletion leads to chronic lymphocytic leukemia.* Cancer Cell, 2010. **17**(1): p. 28-40.

84. Cimmino, A., et al., *miR-15 and miR-16 induce apoptosis by targeting BCL2.* Proc Natl Acad Sci U S A, 2005. **102**(39): p. 13944-9.

85. Roberts, A.W., et al., *Targeting BCL2 with Venetoclax in Relapsed Chronic Lymphocytic Leukemia.* N Engl J Med, 2016. **374**(4): p. 311-22.

86. Zimmermann, M., et al., *CRISPR screens identify genomic ribonucleotides as a source of PARP-trapping lesions.* Nature, 2018. **559**(7713): p. 285-289.

87. Anderson, M.A., et al., *The BCL2 selective inhibitor venetoclax induces rapid onset apoptosis of CLL cells in patients via a TP53-independent mechanism.* Blood, 2016. **127**(25): p. 3215-24.

88. Chigrinova, E., et al., *Two main genetic pathways lead to the transformation of chronic lymphocytic leukemia to Richter syndrome.* Blood, 2013. **122**(15): p. 2673-82.

89. Chatzikonstantinou, T., C. Demosthenous, and P. Baliakas, *Biology and Treatment of High-Risk CLL: Significance of Complex Karyotype.* Front Oncol, 2021. **11**: p. 788761.

90. Juliusson, G., et al., *Prognostic information from cytogenetic analysis in chronic B-lymphocytic leukemia and leukemic immunocytoma.* Blood, 1985. **65**(1): p. 134-41.

91. Baliakas, P., et al., *Chromosomal translocations and karyotype complexity in chronic lymphocytic leukemia: a systematic reappraisal of classic cytogenetic data.* Am J Hematol, 2014. **89**(3): p. 249-55.

92. Baliakas, P., et al., *Cytogenetic complexity in chronic lymphocytic leukemia: definitions, associations, and clinical impact.* Blood, 2019. **133**(11): p. 1205-1216.

93. O'Brien, S., et al., *Single-agent ibrutinib in treatment-naive and relapsed/refractory chronic lymphocytic leukemia: a 5-year experience.* Blood, 2018. **131**(17): p. 1910-1919.

94. Furman, R.R., et al., *Idelalisib and rituximab in relapsed chronic lymphocytic leukemia.* N Engl J Med, 2014. **370**(11): p. 997-1007.

95. Kater, A.P., et al., *Venetoclax Plus Rituximab in Relapsed Chronic Lymphocytic Leukemia: 4-Year Results and Evaluation of Impact of Genomic Complexity and Gene Mutations From the MURANO Phase III Study.* J Clin Oncol, 2020. **38**(34): p. 4042-4054.

96. Vaisitti, T., et al., *CD38 increases CXCL12-mediated signals and homing of chronic lymphocytic leukemia cells.* Leukemia, 2010. **24**(5): p. 958-69.

97. Orchard, J.A., et al., *ZAP-70 expression and prognosis in chronic lymphocytic leukaemia.* Lancet, 2004. **363**(9403): p. 105-11.

98. Rassenti, L.Z., et al., *ZAP-70 compared with immunoglobulin heavy-chain gene mutation status as a predictor of disease progression in chronic lymphocytic leukemia.* N Engl J Med, 2004. **351**(9): p. 893-901.

99. Chen, J., A. Moore, and I. Ringshausen, *ZAP-70 Shapes the Immune Microenvironment in B Cell Malignancies.* Front Oncol, 2020. **10**: p. 595832.

100. Gobessi, S., et al., *ZAP-70 enhances B-cell-receptor signaling despite absent or inefficient tyrosine kinase activation in chronic lymphocytic leukemia and lymphoma B cells.* Blood, 2007. **109**(5): p. 2032-9.

101. Schroers, R., et al., *Combined analysis of ZAP-70 and CD38 expression as a predictor of disease progression in B-cell chronic lymphocytic leukemia.* Leukemia, 2005. **19**(5): p. 750-8.

102. Herishanu, Y., et al., *The lymph node microenvironment promotes B-cell receptor signaling, NF-kappaB activation, and tumor proliferation in chronic lymphocytic leukemia.* Blood, 2011. **117**(2): p. 563-74.

103. Herndon, T.M., et al., *Direct in vivo evidence for increased proliferation of CLL cells in lymph nodes compared to bone marrow and peripheral blood.* Leukemia, 2017. **31**(6): p. 1340-1347.

104. Collins, R.J., et al., *Spontaneous programmed death (apoptosis) of B-chronic lymphocytic leukaemia cells following their culture in vitro.* Br J Haematol, 1989. **71**(3): p. 343-50.

105. Burger, J.A., et al., *Blood-derived nurse-like cells protect chronic lymphocytic leukemia B cells from spontaneous apoptosis through stromal cell-derived factor-1.* Blood, 2000. **96**(8): p. 2655-63.

106. Caligaris-Cappio, F. and P. Ghia, *Novel insights in chronic lymphocytic leukemia: are we getting closer to understanding the pathogenesis of the disease?* J Clin Oncol, 2008. **26**(27): p. 4497-503.

107. Koehrer, S. and J.A. Burger, *Chronic Lymphocytic Leukemia: Disease Biology.* Acta Haematol, 2024. **147**(1): p. 8-21.

108. Messmer, B.T., et al., *In vivo measurements document the dynamic cellular kinetics of chronic lymphocytic leukemia B cells.* J Clin Invest, 2005. **115**(3): p. 755-64.

109. Burkle, A., et al., *Overexpression of the CXCR5 chemokine receptor, and its ligand, CXCL13 in B-cell chronic lymphocytic leukemia.* Blood, 2007. **110**(9): p. 3316-25.

110. de Rooij, M.F., et al., *The clinically active BTK inhibitor PCI-32765 targets B-cell receptor- and chemokine-controlled adhesion and migration in chronic lymphocytic leukemia.* Blood, 2012. **119**(11): p. 2590-4.

111. Vom Stein, A.F., M. Hallek, and P.H. Nguyen, *Role of the tumor microenvironment in CLL pathogenesis.* Semin Hematol, 2023. **61**(3): p. 142-54.

112. Ding, W., et al., *Platelet-derived growth factor (PDGF)-PDGF receptor interaction activates bone marrow-derived mesenchymal stromal cells derived from chronic lymphocytic leukemia: implications for an angiogenic switch.* Blood, 2010. **116**(16): p. 2984-93.

113. Lutzny, G., et al., *Protein kinase c-beta-dependent activation of NF-kappaB in stromal cells is indispensable for the survival of chronic lymphocytic leukemia B cells in vivo.* Cancer Cell, 2013. **23**(1): p. 77-92.

114. Mangolini, M., et al., *Notch2 controls non-autonomous Wnt-signalling in chronic lymphocytic leukaemia.* Nat Commun, 2018. **9**(1): p. 3839.

115. Vom Stein, A.F., et al., *LYN kinase programs stromal fibroblasts to facilitate leukemic survival via regulation of c-JUN and THBS1.* Nat Commun, 2023. **14**(1): p. 1330.

116. Dubois, N., et al., *Importance of Crosstalk Between Chronic Lymphocytic Leukemia Cells and the Stromal Microenvironment: Direct Contact, Soluble Factors, and Extracellular Vesicles.* Front Oncol, 2020. **10**: p. 1422.

117. Boissard, F., et al., *Nurse like cells: chronic lymphocytic leukemia associated macrophages.* Leuk Lymphoma, 2015. **56**(5): p. 1570-2.

118. Domagala, M., et al., *IL-10 Rescues CLL Survival through Repolarization of Inflammatory Nurse-like Cells.* Cancers (Basel), 2021. **14**(1). p. 16.

119. Jia, L., et al., *Extracellular HMGB1 promotes differentiation of nurse-like cells in chronic lymphocytic leukemia.* Blood, 2014. **123**(11): p. 1709-19.

120. Burger, J.A., M. Burger, and T.J. Kipps, *Chronic lymphocytic leukemia B cells express functional CXCR4 chemokine receptors that mediate spontaneous migration beneath bone marrow stromal cells.* Blood, 1999. **94**(11): p. 3658-67.

121. Mohle, R., et al., *Overexpression of the chemokine receptor CXCR4 in B cell chronic lymphocytic leukemia is associated with increased functional*

response to stromal cell-derived factor-1 (SDF-1). Leukemia, 1999. **13**(12): p. 1954-9.

122. Calissano, C., et al., *Intraclonal complexity in chronic lymphocytic leukemia: fractions enriched in recently born/divided and older/quiescent cells.* Mol Med, 2011. **17**(11-12): p. 1374-82.

123. Cols, M., et al., *Stromal endothelial cells establish a bidirectional crosstalk with chronic lymphocytic leukemia cells through the TNF-related factors BAFF, APRIL, and CD40L.* J Immunol, 2012. **188**(12): p. 6071-83.

124. Nishio, M., et al., *Nurselike cells express BAFF and APRIL, which can promote survival of chronic lymphocytic leukemia cells via a paracrine pathway distinct from that of SDF-1alpha.* Blood, 2005. **106**(3): p. 1012-20.

125. Endo, T., et al., *BAFF and APRIL support chronic lymphocytic leukemia B-cell survival through activation of the canonical NF-kappaB pathway.* Blood, 2007. **109**(2): p. 703-10.

126. Paiva, C., et al., *SYK inhibition thwarts the BAFF - B-cell receptor crosstalk and thereby antagonizes Mcl-1 in chronic lymphocytic leukemia.* Haematologica, 2017. **102**(11): p. 1890-1900.

127. Schleiss, C., et al., *BCR-associated factors driving chronic lymphocytic leukemia cells proliferation ex vivo.* Sci Rep, 2019. **9**(1): p. 701.

128. Gupta, R., et al., *Mechanistic Insights into CpG DNA and IL-15 Synergy in Promoting B Cell Chronic Lymphocytic Leukemia Clonal Expansion.* J Immunol, 2018. **201**(5): p. 1570-1585.

129. Aguilar-Hernandez, M.M., J.C. Rincon Camacho, and G. Galicia Garcia, *Extracellular vesicles and their associated miRNAs as potential prognostic biomarkers in chronic lymphocytic leukemia.* Curr Oncol Rep, 2021. **23**(6): p. 66.

130. Ghia, P., et al., *Chronic lymphocytic leukemia B cells are endowed with the capacity to attract CD4+, CD40L+ T cells by producing CCL22.* Eur J Immunol, 2002. **32**(5): p. 1403-13.

131. Bianco, M., et al., *Inhibition of chronic lymphocytic leukemia progression by full-length chromogranin A and its N-terminal fragment in mouse models.* Oncotarget, 2016. **7**(27): p. 41725-41736.

132. Paggetti, J., et al., *Exosomes released by chronic lymphocytic leukemia cells induce the transition of stromal cells into cancer-associated fibroblasts.* Blood, 2015. **126**(9): p. 1106-17.

133. Panayiotidis, P., et al., *Human bone marrow stromal cells prevent apoptosis and support the survival of chronic lymphocytic leukaemia cells in vitro.* Br J Haematol, 1996. **92**(1): p. 97-103.

134. Bottcher, M., et al., *Control of PD-L1 expression in CLL-cells by stromal triggering of the Notch-c-Myc-EZH2 oncogenic signaling axis.* J Immunother Cancer, 2021. **9**(4). p. e001889.

135. Gibson, S.E., et al., *Proliferation centres of chronic lymphocytic leukaemia/small lymphocytic lymphoma have enhanced expression of MYC protein, which does not result from rearrangement or gain of the MYC gene.* Br J Haematol, 2016. **175**(1): p. 173-5.

136. Sun, C., et al., *The immune microenvironment shapes transcriptional and genetic heterogeneity in chronic lymphocytic leukemia.* Blood Adv, 2023. **7**(1): p. 145-158.

137. Park, E., et al., *Stromal cell protein kinase C-beta inhibition enhances chemosensitivity in B cell malignancies and overcomes drug resistance.* Sci Transl Med, 2020. **12**(526).

138. Pozzo, F., et al., *Multiple Mechanisms of NOTCH1 Activation in Chronic Lymphocytic Leukemia: NOTCH1 Mutations and Beyond.* Cancers (Basel), 2022. **14**(12). p. 2997.

139. Arruga, F., et al., *Functional impact of NOTCH1 mutations in chronic lymphocytic leukemia.* Leukemia, 2014. **28**(5): p. 1060-70.

140. Onaindia, A., et al., *Chronic lymphocytic leukemia cells in lymph nodes show frequent NOTCH1 activation.* Haematologica, 2015. **100**(5): p. e200-3.

141. Deaglio, S., et al., *CD38 and CD100 lead a network of surface receptors relaying positive signals for B-CLL growth and survival.* Blood, 2005. **105**(8): p. 3042-50.

142. Alankus, B., et al., *Pathological RANK signaling in B cells drives autoimmunity and chronic lymphocytic leukemia.* J Exp Med, 2021. **218**(2). p. e20200517.

143. Scielzo, C. and P. Ghia, *Modeling the Leukemia Microenviroment In Vitro.* Front Oncol, 2020. **10**: p. 607608.

144. Stein, H., et al., *Immunohistologic analysis of the organization of normal lymphoid tissue and non-Hodgkin's lymphomas.* J Histochem Cytochem, 1980. **28**(8): p. 746-60.

145. Vaca, A.M., et al., *Activation and expansion of T-follicular helper cells in chronic lymphocytic leukemia nurselike cell co-cultures.* Leukemia, 2022. **36**(5): p. 1324-1335.

146. Burger, J.A., et al., *Leukemia cell proliferation and death in chronic lymphocytic leukemia patients on therapy with the BTK inhibitor ibrutinib.* JCI Insight, 2017. **2**(2): p. e89904.

147. Melchers, F., *Checkpoints that control B cell development.* J Clin Invest, 2015. **125**(6): p. 2203-10.

148. Ghia, P., et al., *Ordering of human bone marrow B lymphocyte precursors by single-cell polymerase chain reaction analyses of the rearrangement status of the immunoglobulin H and L chain gene loci.* J Exp Med, 1996. **184**(6): p. 2217-29.

149. Shapiro-Shelef, M. and K. Calame, *Regulation of plasma-cell development.* Nat Rev Immunol, 2005. **5**(3): p. 230-42.

150. Watson, C.T., et al., *Complete haplotype sequence of the human immunoglobulin heavy-chain variable, diversity, and joining genes and characterization of allelic and copy-number variation.* Am J Hum Genet, 2013. **92**(4): p. 530-46.

151. Chi, X., Y. Li, and X. Qiu, *V(D)J recombination, somatic hypermutation and class switch recombination of immunoglobulins: mechanism and regulation.* Immunology, 2020. **160**(3): p. 233-247.

152. Kraus, M., et al., *Survival of resting mature B lymphocytes depends on BCR signaling via the Igalpha/beta heterodimer.* Cell, 2004. **117**(6): p. 787-800.

153. Chiorazzi, N. and M. Ferrarini, *Cellular origin(s) of chronic lymphocytic leukemia: cautionary notes and additional considerations and possibilities.* Blood, 2011. **117**(6): p. 1781-91.

154. Dono, M., et al., *Evidence for progenitors of chronic lymphocytic leukemia B cells that undergo intraclonal differentiation and diversification.* Blood, 1996. **87**(4): p. 1586-94.

155. Rubartelli, A., et al., *Differentiation of chronic lymphocytic leukemia cells: correlation between the synthesis and secretion of immunoglobulins and the ultrastructure of the malignant cells.* Blood, 1983. **62**(2): p. 495-504.

156. Hombach, J., et al., *Molecular components of the B-cell antigen receptor complex of the IgM class.* Nature, 1990. **343**(6260): p. 760-2.

157. Xie, W., K. Wucherpfennig, and D.J. Patel, *A structural platform for B cell receptor signaling.* Cell Res, 2023. **33**(2): p. 95-96.

158. Schamel, W.W. and M. Reth, *Monomeric and oligomeric complexes of the B cell antigen receptor.* Immunity, 2000. **13**(1): p. 5-14.

159. Treanor, B., *B-cell receptor: from resting state to activate.* Immunology, 2012. **136**(1): p. 21-7.

160. Reth, M., *Antigen receptor tail clue.* Nature, 1989. **338**(6214): p. 383-4.

161. Li, Y., et al., *Structural insights into immunoglobulin M.* Science, 2020. **367**(6481): p. 1014-1017.

162. Radaev, S., et al., *Structural and functional studies of Igalphabeta and its assembly with the B cell antigen receptor.* Structure, 2010. **18**(8): p. 934-43.

163. Dong, Y., et al., *Structural principles of B cell antigen receptor assembly.* Nature, 2022. **612**(7938): p. 156-161.

164. Ma, X., et al., *Cryo-EM structures of two human B cell receptor isotypes.* Science, 2022. **377**(6608): p. 880-885.

165. Su, Q., et al., *Cryo-EM structure of the human IgM B cell receptor.* Science, 2022. **377**(6608): p. 875-880.

166. Thomas, C. and R. Tampe, *Structure and mechanism of immunoreceptors: New horizons in T cell and B cell receptor biology and beyond.* Curr Opin Struct Biol, 2023. **80**: p. 102570.

167. Ubelhart, R., et al., *Responsiveness of B cells is regulated by the hinge region of IgD.* Nat Immunol, 2015. **16**(5): p. 534-43.

168. Harwood, N.E. and F.D. Batista, *New insights into the early molecular events underlying B cell activation.* Immunity, 2008. **28**(5): p. 609-19.

169. Harwood, N.E. and F.D. Batista, *Early events in B cell activation.* Annu Rev Immunol, 2010. **28**: p. 185-210.

170. Sohn, H.W., P. Tolar, and S.K. Pierce, *Membrane heterogeneities in the formation of B cell receptor-Lyn kinase microclusters and the immune synapse.* J Cell Biol, 2008. **182**(2): p. 367-79.

171. Khan, W.N., et al., *The role of Bruton's tyrosine kinase in B-cell development and function in mice and man.* Ann N Y Acad Sci, 1995. **764**: p. 27-38.

172. Nishizumi, H., et al., *Impaired proliferation of peripheral B cells and indication of autoimmune disease in lyn-deficient mice.* Immunity, 1995. **3**(5): p. 549-60.

173. Turner, M., et al., *Perinatal lethality and blocked B-cell development in mice lacking the tyrosine kinase Syk.* Nature, 1995. **378**(6554): p. 298-302.

174. Dal Porto, J.M., et al., *B cell antigen receptor signaling 101.* Mol Immunol, 2004. **41**(6-7): p. 599-613.

175. Pal Singh, S., F. Dammeijer, and R.W. Hendriks, *Role of Bruton's tyrosine kinase in B cells and malignancies.* Mol Cancer, 2018. **17**(1): p. 57.

176. Fujimoto, M., et al., *CD19 regulates Src family protein tyrosine kinase activation in B lymphocytes through processive amplification.* Immunity, 2000. **13**(1): p. 47-57.

177. Tanaka, S. and Y. Baba, *B Cell Receptor Signaling.* Adv Exp Med Biol, 2020. **1254**: p. 23-36.

178. Aiba, Y., et al., *Regulation of B-cell development by BCAP and CD19 through their binding to phosphoinositide 3-kinase.* Blood, 2008. **111**(3): p. 1497-503.

179. Limon, J.J. and D.A. Fruman, *Akt and mTOR in B Cell Activation and Differentiation.* Front Immunol, 2012. **3**: p. 228.

180. Carter, R.H. and D.T. Fearon, *CD19: lowering the threshold for antigen receptor stimulation of B lymphocytes.* Science, 1992. **256**(5053): p. 105-7.

181. Liu, C., et al., *A balance of Bruton's tyrosine kinase and SHIP activation regulates B cell receptor cluster formation by controlling actin remodeling.* J Immunol, 2011. **187**(1): p. 230-9.

182. Mkaddem, S.B., et al., *Lyn and Fyn function as molecular switches that control immunoreceptors to direct homeostasis or inflammation.* Nat Commun, 2017. **8**(1): p. 246.

183. Zonta, F., et al., *Lyn sustains oncogenic signaling in chronic lymphocytic leukemia by strengthening SET-mediated inhibition of PP2A.* Blood, 2015. **125**(24): p. 3747-55.

184. Wodarz, D., et al., *Kinetics of CLL cells in tissues and blood during therapy with the BTK inhibitor ibrutinib.* Blood, 2014. **123**(26): p. 4132-5.

185. Damle, R.N., et al., *B-cell chronic lymphocytic leukemia cells express a surface membrane phenotype of activated, antigen-experienced B lymphocytes.* Blood, 2002. **99**(11): p. 4087-93.

186. Muzio, M., et al., *Constitutive activation of distinct BCR-signaling pathways in a subset of CLL patients: a molecular signature of anergy.* Blood, 2008. **112**(1): p. 188-95.

187. Buchner, M., et al., *Spleen tyrosine kinase is overexpressed and represents a potential therapeutic target in chronic lymphocytic leukemia.* Cancer Res, 2009. **69**(13): p. 5424-32.

188. Contri, A., et al., *Chronic lymphocytic leukemia B cells contain anomalous Lyn tyrosine kinase, a putative contribution to defective apoptosis.* J Clin Invest, 2005. **115**(2): p. 369-78.

189. Hay, J., et al., *PKCbeta Facilitates Leukemogenesis in Chronic Lymphocytic Leukaemia by Promoting Constitutive BCR-Mediated Signalling.* Cancers (Basel), 2022. **14**(23). p. 6006.

190. Shorer Arbel, Y., et al., *Spatial organization and early signaling of the B-cell receptor in CLL.* Front Immunol, 2022. **13**: p. 953660.

191. Duhren-von Minden, M., et al., *Chronic lymphocytic leukaemia is driven by antigen-independent cell-autonomous signalling.* Nature, 2012. **489**(7415): p. 309-12.

192. Minici, C., et al., *Distinct homotypic B-cell receptor interactions shape the outcome of chronic lymphocytic leukaemia.* Nat Commun, 2017. **8**: p. 15746.

193. Mazzarello, A.N., et al., *B cell receptor isotypes differentially associate with cell signaling, kinetics, and outcome in chronic lymphocytic leukemia.* J Clin Invest, 2022. **132**(2). p. e149308.

194. Lanham, S., et al., *Differential signaling via surface IgM is associated with VH gene mutational status and CD38 expression in chronic lymphocytic leukemia.* Blood, 2003. **101**(3): p. 1087-93.

195. Mockridge, C.I., et al., *Reversible anergy of sIgM-mediated signaling in the two subsets of CLL defined by VH-gene mutational status.* Blood, 2007. **109**(10): p. 4424-31.

196. Krysov, S., et al., *Surface IgM stimulation induces MEK1/2-dependent MYC expression in chronic lymphocytic leukemia cells.* Blood, 2012. **119**(1): p. 170-9.

197. Ten Hacken, E., et al., *Functional Differences between IgM and IgD Signaling in Chronic Lymphocytic Leukemia.* J Immunol, 2016. **197**(6): p. 2522-31.

198. Binder, M., et al., *Stereotypical chronic lymphocytic leukemia B-cell receptors recognize survival promoting antigens on stromal cells.* PLoS One, 2010. **5**(12): p. e15992.

199. Chu, C.C., et al., *Many chronic lymphocytic leukemia antibodies recognize apoptotic cells with exposed nonmuscle myosin heavy chain IIA: implications for patient outcome and cell of origin.* Blood, 2010. **115**(19): p. 3907-15.

200. Lanemo Myhrinder, A., et al., *A new perspective: molecular motifs on oxidized LDL, apoptotic cells, and bacteria are targets for chronic lymphocytic leukemia antibodies.* Blood, 2008. **111**(7): p. 3838-48.

201. Jimenez de Oya, N., et al., *Pathogen-specific B-cell receptors drive chronic lymphocytic leukemia by light-chain-dependent cross-reaction with autoantigens.* EMBO Mol Med, 2017. **9**(11): p. 1482-1490.

202. Kostareli, E., et al., *Molecular evidence for EBV and CMV persistence in a subset of patients with chronic lymphocytic leukemia expressing stereotyped IGHV4-34 B-cell receptors.* Leukemia, 2009. **23**(5): p. 919-24.

203. Ruuskanen, O., et al., *Staphylococcus aureus Cowan I-induced immunoglobulin production in human cord blood lymphocytes.* J Immunol, 1980. **125**(1): p. 411-3.

204. Bernal, A., et al., *Survival of leukemic B cells promoted by engagement of the antigen receptor.* Blood, 2001. **98**(10): p. 3050-7.

205. Nedellec, S., et al., *B cell response to surface IgM cross-linking identifies different prognostic groups of B-chronic lymphocytic leukemia patients.* J Immunol, 2005. **174**(6): p. 3749-56.

206. Guarini, A., et al., *BCR ligation induced by IgM stimulation results in gene expression and functional changes only in IgV H unmutated chronic lymphocytic leukemia (CLL) cells.* Blood, 2008. **112**(3): p. 782-92.

207. Rombout, A., et al., *Mimicking the tumour microenvironment of chronic lymphocytic leukaemia in vitro critically depends on the type of B-cell receptor stimulation.* Br J Cancer, 2016. **114**(6): p. 704-12.

208. Burger, J.A., et al., *High-level expression of the T-cell chemokines CCL3 and CCL4 by chronic lymphocytic leukemia B cells in nurselike cell cocultures and after BCR stimulation.* Blood, 2009. **113**(13): p. 3050-8.

209. Elgueta, R., et al., *Molecular mechanism and function of CD40/CD40L engagement in the immune system.* Immunol Rev, 2009. **229**(1): p. 152-72.

210. Quezada, S.A., et al., *CD40/CD154 interactions at the interface of tolerance and immunity.* Annu Rev Immunol, 2004. **22**: p. 307-28.

211. Os, A., et al., *Chronic lymphocytic leukemia cells are activated and proliferate in response to specific T helper cells.* Cell Rep, 2013. **4**(3): p. 566-77.

212. van Kooten, C. and J. Banchereau, *CD40-CD40 ligand.* J Leukoc Biol, 2000. **67**(1): p. 2-17.

213. van Kooten, C. and J. Banchereau, *Functions of CD40 on B cells, dendritic cells and other cells.* Curr Opin Immunol, 1997. **9**(3): p. 330-7.

214. Karpusas, M., et al., *2 A crystal structure of an extracellular fragment of human CD40 ligand.* Structure, 1995. **3**(12): p. 1426.

215. Carbone, E., et al., *A new mechanism of NK cell cytotoxicity activation: the CD40-CD40 ligand interaction.* J Exp Med, 1997. **185**(12): p. 2053-60.

216. Laidlaw, B.J. and J.G. Cyster, *Transcriptional regulation of memory B cell differentiation.* Nat Rev Immunol, 2021. **21**(4): p. 209-220.

217. Chen, Z. and J.H. Wang, *How the Signaling Crosstalk of B Cell Receptor (BCR) and Co-Receptors Regulates Antibody Class Switch Recombination: A New*

Perspective of Checkpoints of BCR Signaling. Front Immunol, 2021. **12**: p. 663443.

218. Bishop, G.A., et al., *TRAF proteins in CD40 signaling*. Adv Exp Med Biol, 2007. **597**: p. 131-51.

219. Yamamoto, M., et al., *TNF receptor-associated factor 6 (TRAF6) plays crucial roles in multiple biological systems through polyubiquitination-mediated NF-kappaB activation*. Proc Jpn Acad Ser B Phys Biol Sci, 2021. **97**(4): p. 145-160.

220. Guldenpfennig, C., E. Teixeiro, and M. Daniels, *NF-kB's contribution to B cell fate decisions*. Front Immunol, 2023. **14**: p. 1214095.

221. Tsukamoto, N., et al., *Two differently regulated nuclear factor kappaB activation pathways triggered by the cytoplasmic tail of CD40*. Proc Natl Acad Sci U S A, 1999. **96**(4): p. 1234-9.

222. Bonizzi, G. and M. Karin, *The two NF-kappaB activation pathways and their role in innate and adaptive immunity*. Trends Immunol, 2004. **25**(6): p. 280-8.

223. Pascutti, M.F., et al., *IL-21 and CD40L signals from autologous T cells can induce antigen-independent proliferation of CLL cells*. Blood, 2013. **122**(17): p. 3010-9.

224. Hartmann, E.M., et al., *CCL3 chemokine expression by chronic lymphocytic leukemia cells orchestrates the composition of the microenvironment in lymph node infiltrates*. Leuk Lymphoma, 2016. **57**(3): p. 563-71.

225. Vardi, A., et al., *Restrictions in the T-cell repertoire of chronic lymphocytic leukemia: high-throughput immunoprofiling supports selection by shared antigenic elements*. Leukemia, 2017. **31**(7): p. 1555-1561.

226. Ramsay, A.G., et al., *Chronic lymphocytic leukemia T cells show impaired immunological synapse formation that can be reversed with an immunomodulating drug*. J Clin Invest, 2008. **118**(7): p. 2427-37.

227. Bagnara, D., et al., *A novel adoptive transfer model of chronic lymphocytic leukemia suggests a key role for T lymphocytes in the disease*. Blood, 2011. **117**(20): p. 5463-72.

228. Hagn, M., et al., *B-CLL cells acquire APC- and CTL-like phenotypic characteristics after stimulation with CpG ODN and IL-21*. Int Immunol, 2014. **26**(7): p. 383-95.

229. Vlachonikola, E., K. Stamatopoulos, and A. Chatzidimitriou, *T Cells in Chronic Lymphocytic Leukemia: A Two-Edged Sword*. Front Immunol, 2020. **11**: p. 612244.

230. Furman, R.R., et al., *Modulation of NF-kappa B activity and apoptosis in chronic lymphocytic leukemia B cells*. J Immunol, 2000. **164**(4): p. 2200-6.

231. Xu, Z.S., et al., *Constitutive activation of NF-kappaB signaling by NOTCH1 mutations in chronic lymphocytic leukemia*. Oncol Rep, 2015. **33**(4): p. 1609-14.

232. Parente-Ribes, A., et al., *Spleen tyrosine kinase inhibitors reduce CD40L-induced proliferation of chronic lymphocytic leukemia cells but not normal B cells.* Haematologica, 2016. **101**(2): p. e59-62.

233. Ying, H., et al., *Syk mediates BCR- and CD40-signaling integration during B cell activation.* Immunobiology, 2011. **216**(5): p. 566-70.

234. Schattner, E.J., *CD40 ligand in CLL pathogenesis and therapy.* Leuk Lymphoma, 2000. **37**(5-6): p. 461-72.

235. Haselager, M., et al., *Regulation of Bcl-XL by non-canonical NF-kappaB in the context of CD40-induced drug resistance in CLL.* Cell Death Differ, 2021. **28**(5): p. 1658-1668.

236. Slinger, E., et al., *Targeting antigen-independent proliferation in chronic lymphocytic leukemia through differential kinase inhibition.* Leukemia, 2017. **31**(12): p. 2601-2607.

237. Burley, T.A., et al., *Targeting the Non-Canonical NF-kappaB Pathway in Chronic Lymphocytic Leukemia and Multiple Myeloma.* Cancers (Basel), 2022. **14**(6). p. 1489.

238. Vonderheide, R.H., et al., *Clinical activity and immune modulation in cancer patients treated with CP-870,893, a novel CD40 agonist monoclonal antibody.* J Clin Oncol, 2007. **25**(7): p. 876-83.

239. Law, C.L., et al., *Preclinical antilymphoma activity of a humanized anti-CD40 monoclonal antibody, SGN-40.* Cancer Res, 2005. **65**(18): p. 8331-8.

240. Piechutta, M. and A.S. Berghoff, *New emerging targets in cancer immunotherapy: the role of Cluster of Differentiation 40 (CD40/TNFR5).* ESMO Open, 2019. **4**(Suppl 3): p. e000510.

241. Planken, E.V., et al., *Proliferation of B cell malignancies in all stages of differentiation upon stimulation in the 'CD40 system'.* Leukemia, 1996. **10**(3): p. 488-93.

242. Crassini, K., et al., *Modeling the chronic lymphocytic leukemia microenvironment in vitro.* Leuk Lymphoma, 2017. **58**(2): p. 266-279.

243. Banchereau, J. and F. Rousset, *Growing human B lymphocytes in the CD40 system.* Nature, 1991. **353**(6345): p. 678-9.

244. Neron, S., et al., *Tuning of CD40-CD154 interactions in human B-lymphocyte activation: a broad array of in vitro models for a complex in vivo situation.* Arch Immunol Ther Exp (Warsz), 2011. **59**(1): p. 25-40.

245. Hamilton, E., et al., *Mimicking the tumour microenvironment: three different co-culture systems induce a similar phenotype but distinct proliferative signals in primary chronic lymphocytic leukaemia cells.* Br J Haematol, 2012. **158**(5): p. 589-99.

246. Woyach, J.A., A.J. Johnson, and J.C. Byrd, *The B-cell receptor signaling pathway as a therapeutic target in CLL.* Blood, 2012. **120**(6): p. 1175-84.

247. Chapman, E.A., et al., *Delineating the distinct role of AKT in mediating cell survival and proliferation induced by CD154 and IL-4/IL-21 in chronic lymphocytic leukemia.* Oncotarget, 2017. **8**(61): p. 102948-102964.

248. Glaviano, A., et al., *PI3K/AKT/mTOR signaling transduction pathway and targeted therapies in cancer.* Mol Cancer, 2023. **22**(1): p. 138.

249. Zhao, L. and P.K. Vogt, *Class I PI3K in oncogenic cellular transformation.* Oncogene, 2008. **27**(41): p. 5486-96.

250. Engelman, J.A., *Targeting PI3K signalling in cancer: opportunities, challenges and limitations.* Nat Rev Cancer, 2009. **9**(8): p. 550-62.

251. Cantrell, D.A., *Phosphoinositide 3-kinase signalling pathways.* J Cell Sci, 2001. **114**(Pt 8): p. 1439-45.

252. Castellano, E. and J. Downward, *RAS Interaction with PI3K: More Than Just Another Effector Pathway.* Genes Cancer, 2011. **2**(3): p. 261-74.

253. Ramadani, F., et al., *The PI3K isoforms p110alpha and p110delta are essential for pre-B cell receptor signaling and B cell development.* Sci Signal, 2010. **3**(134): p. ra60.

254. Calderon, L., et al., *Pax5 regulates B cell immunity by promoting PI3K signaling via PTEN down-regulation.* Sci Immunol, 2021. **6**(61). p. eabg5003.

255. Abdelrasoul, H., et al., *PI3K induces B-cell development and regulates B cell identity.* Sci Rep, 2018. **8**(1): p. 1327.

256. Davids, M.S. and J.R. Brown, *Phosphoinositide 3'-kinase inhibition in chronic lymphocytic leukemia.* Hematol Oncol Clin North Am, 2013. **27**(2): p. 329-39.

257. Srinivasan, L., et al., *PI3 kinase signals BCR-dependent mature B cell survival.* Cell, 2009. **139**(3): p. 573-86.

258. Castello, A., et al., *Nck-mediated recruitment of BCAP to the BCR regulates the PI(3)K-Akt pathway in B cells.* Nat Immunol, 2013. **14**(9): p. 966-75.

259. Delgado, P., et al., *Essential function for the GTPase TC21 in homeostatic antigen receptor signaling.* Nat Immunol, 2009. **10**(8): p. 880-8.

260. Yang, G., et al., *A Positive Feedback Loop between Akt and mTORC2 via SIN1 Phosphorylation.* Cell Rep, 2015. **12**(6): p. 937-43.

261. Manning, B.D. and A. Toker, *AKT/PKB Signaling: Navigating the Network.* Cell, 2017. **169**(3): p. 381-405.

262. Hanahan, D. and R.A. Weinberg, *Hallmarks of cancer: the next generation.* Cell, 2011. **144**(5): p. 646-74.

263. Brunet, A., et al., *Akt promotes cell survival by phosphorylating and inhibiting a Forkhead transcription factor.* Cell, 1999. **96**(6): p. 857-68.

264. Chow, L.M. and S.J. Baker, *PTEN function in normal and neoplastic growth.* Cancer Lett, 2006. **241**(2): p. 184-96.

265. Suzuki, A., et al., *Critical roles of Pten in B cell homeostasis and immunoglobulin class switch recombination.* J Exp Med, 2003. **197**(5): p. 657-67.

266. Helgason, C.D., et al., *A dual role for Src homology 2 domain-containing inositol-5-phosphatase (SHIP) in immunity: aberrant development and enhanced function of b lymphocytes in ship -/- mice.* J Exp Med, 2000. **191**(5): p. 781-94.

267. Maxwell, M.J., et al., *Genetic segregation of inflammatory lung disease and autoimmune disease severity in SHIP-1-/- mice.* J Immunol, 2011. **186**(12): p. 7164-75.

268. Bou Zeid, N. and V. Yazbeck, *PI3k Inhibitors in NHL and CLL: An Unfulfilled Promise*. Blood Lymphat Cancer, 2023. **13**: p. 1-12.

269. Hillmann, P. and D. Fabbro, *PI3K/mTOR Pathway Inhibition: Opportunities in Oncology and Rare Genetic Diseases.* Int J Mol Sci, 2019. **20**(22). p. 5792.

270. Ringshausen, I., et al., *Constitutively activated phosphatidylinositol-3 kinase (PI-3K) is involved in the defect of apoptosis in B-CLL: association with protein kinase Cdelta.* Blood, 2002. **100**(10): p. 3741-8.

271. Kienle, D., et al., *Distinct gene expression patterns in chronic lymphocytic leukemia defined by usage of specific VH genes.* Blood, 2006. **107**(5): p. 2090-3.

272. Guarente, V. and P. Sportoletti, *Lessons, Challenges and Future Therapeutic Opportunities for PI3K Inhibition in CLL*. Cancers (Basel), 2021. **13**(6). p. 1280.

273. Platonova, N., et al., *PI3K/AKT signaling inhibits NOTCH1 lysosome-mediated degradation.* Genes Chromosomes Cancer, 2015. **54**(8): p. 516-526.

274. Kohlhaas, V., et al., *Active Akt signaling triggers CLL toward Richter transformation via overactivation of Notch1.* Blood, 2021. **137**(5): p. 646-660.

275. Chunfang Kong, M.W., Qilin Lu, Bo Ke, Jianhui Xie, Anna Li, *PI3K/AKT confers intrinsic and acquired resistance to pirtobrutinib in chronic lymphocytic leukemia.* Leukemia Research, 2024. p. 107548.

276. Scala, S., *Molecular Pathways: Targeting the CXCR4-CXCL12 Axis--Untapped Potential in the Tumor Microenvironment.* Clin Cancer Res, 2015. **21**(19): p. 4278-85.

277. Ali, A.Y., et al., *Distinct roles for phosphoinositide 3-kinases gamma and delta in malignant B cell migration.* Leukemia, 2018. **32**(9): p. 1958-1969.

278. Annika Scheffold, B.S.H., Philipp Roeßner, Yasmin Demerdash, Billy Michael Chelliah Jebaraj, Peter Lichter, Stephan Stilgenbauer, Martina Seiffert, *PI3K-δ Inhibition Influences T-Cell Populations and Anti-Tumoral Immune Function in Preclinical Models.* Blood, 2017. **130**: p. 2998.

279. Ladygina, N., et al., *PI3Kgamma kinase activity is required for optimal T-cell activation and differentiation.* Eur J Immunol, 2013. **43**(12): p. 3183-96.

280. Solinas, G. and B. Becattini, *The role of PI3Kgamma in metabolism and macrophage activation.* Oncotarget, 2017. **8**(63): p. 106145-106146.

281. Ecker, V., et al., *Targeted PI3K/AKT-hyperactivation induces cell death in chronic lymphocytic leukemia.* Nat Commun, 2021. **12**(1): p. 3526.

282. Longo, P.G., et al., *The Akt/Mcl-1 pathway plays a prominent role in mediating antiapoptotic signals downstream of the B-cell receptor in chronic lymphocytic leukemia B cells.* Blood, 2008. **111**(2): p. 846-55.

283. Zhuang, J., et al., *Akt is activated in chronic lymphocytic leukemia cells and delivers a pro-survival signal: the therapeutic potential of Akt inhibition.* Haematologica, 2010. **95**(1): p. 110-8.

284. Cosimo, E., et al., *AKT/mTORC2 Inhibition Activates FOXO1 Function in CLL Cells Reducing B-Cell Receptor-Mediated Survival.* Clin Cancer Res, 2019. **25**(5): p. 1574-1587.

285. Ticchioni, M., et al., *Homeostatic chemokines increase survival of B-chronic lymphocytic leukemia cells through inactivation of transcription factor FOXO3a.* Oncogene, 2007. **26**(50): p. 7081-91.

286. Szwed, A., E. Kim, and E. Jacinto, *Regulation and metabolic functions of mTORC1 and mTORC2.* Physiol Rev, 2021. **101**(3): p. 1371-1426.

287. Liu, G.Y. and D.M. Sabatini, *mTOR at the nexus of nutrition, growth, ageing and disease.* Nat Rev Mol Cell Biol, 2020. **21**(4): p. 183-203.

288. Garami, A., et al., *Insulin activation of Rheb, a mediator of mTOR/S6K/4E-BP signaling, is inhibited by TSC1 and 2.* Mol Cell, 2003. **11**(6): p. 1457-66.

289. Gwinn, D.M., et al., *AMPK phosphorylation of raptor mediates a metabolic checkpoint.* Mol Cell, 2008. **30**(2): p. 214-26.

290. Fu, W. and G. Wu, *Targeting mTOR for Anti-Aging and Anti-Cancer Therapy.* Molecules, 2023. **28**(7). p. 3157.

291. Guertin, D.A. and D.M. Sabatini, *The pharmacology of mTOR inhibition.* Sci Signal, 2009. **2**(67): p. pe24.

292. Saxton, R.A. and D.M. Sabatini, *mTOR Signaling in Growth, Metabolism, and Disease.* Cell, 2017. **169**(2): p. 361-371.

293. Sancak, Y., et al., *PRAS40 is an insulin-regulated inhibitor of the mTORC1 protein kinase.* Mol Cell, 2007. **25**(6): p. 903-15.

294. Ma, X.M. and J. Blenis, *Molecular mechanisms of mTOR-mediated translational control.* Nat Rev Mol Cell Biol, 2009. **10**(5): p. 307-18.

295. Jacinto, E. and M.N. Hall, *Tor signalling in bugs, brain and brawn.* Nat Rev Mol Cell Biol, 2003. **4**(2): p. 117-26.

296. Nojima, H., et al., *The mammalian target of rapamycin (mTOR) partner, raptor, binds the mTOR substrates p70 S6 kinase and 4E-BP1 through their TOR signaling (TOS) motif.* J Biol Chem, 2003. **278**(18): p. 15461-4.

297. Burnett, P.E., et al., *RAFT1 phosphorylation of the translational regulators p70 S6 kinase and 4E-BP1.* Proc Natl Acad Sci U S A, 1998. **95**(4): p. 1432-7.

298. Raught, B., et al., *Phosphorylation of eucaryotic translation initiation factor 4B Ser422 is modulated by S6 kinases.* EMBO J, 2004. **23**(8): p. 1761-9.

299. Dorrello, N.V., et al., *S6K1- and betaTRCP-mediated degradation of PDCD4 promotes protein translation and cell growth.* Science, 2006. **314**(5798): p. 467-71.

300. Browne, G.J. and C.G. Proud, *Regulation of peptide-chain elongation in mammalian cells.* Eur J Biochem, 2002. **269**(22): p. 5360-8.

301. Gingras, A.C., et al., *Regulation of 4E-BP1 phosphorylation: a novel two-step mechanism.* Genes Dev, 1999. **13**(11): p. 1422-37.

302. Battaglioni, S., et al., *mTOR substrate phosphorylation in growth control.* Cell, 2022. **185**(11): p. 1814-1836.

303. Wang, Y., et al., *Inactivation of mTORC1 Signaling in Osterix-Expressing Cells Impairs B-cell Differentiation.* J Bone Miner Res, 2018. **33**(4): p. 732-742.

304. Tang, J., et al., *The role of Raptor in lymphocytes differentiation and function.* Front Immunol, 2023. **14**: p. 1146628.

305. Malik, N., et al., *mTORC1 activity is essential for erythropoiesis and B cell lineage commitment.* Sci Rep, 2019. **9**(1): p. 16917.

306. Dibble, C.C., J.M. Asara, and B.D. Manning, *Characterization of Rictor phosphorylation sites reveals direct regulation of mTOR complex 2 by S6K1.* Mol Cell Biol, 2009. **29**(21): p. 5657-70.

307. Harrington, L.S., et al., *The TSC1-2 tumor suppressor controls insulin-PI3K signaling via regulation of IRS proteins.* J Cell Biol, 2004. **166**(2): p. 213-23.

308. Shah, O.J., Z. Wang, and T. Hunter, *Inappropriate activation of the TSC/Rheb/mTOR/S6K cassette induces IRS1/2 depletion, insulin resistance, and cell survival deficiencies.* Curr Biol, 2004. **14**(18): p. 1650-6.

309. Hsu, P.P., et al., *The mTOR-regulated phosphoproteome reveals a mechanism of mTORC1-mediated inhibition of growth factor signaling.* Science, 2011. **332**(6035): p. 1317-22.

310. Yu, Y., et al., *Phosphoproteomic analysis identifies Grb10 as an mTORC1 substrate that negatively regulates insulin signaling.* Science, 2011. **332**(6035): p. 1322-6.

311. Baudler, S., et al., *Insulin-like growth factor-1 controls type 2 T cell-independent B cell response.* J Immunol, 2005. **174**(9): p. 5516-25.

312. Makhijani, P., et al., *Regulation of the immune system by the insulin receptor in health and disease.* Front Endocrinol (Lausanne), 2023. **14**: p. 1128622.

313. Liu, P., et al., *PtdIns(3,4,5)P3-Dependent Activation of the mTORC2 Kinase Complex.* Cancer Discov, 2015. **5**(11): p. 1194-209.

314. Manning, B.D., et al., *Identification of the tuberous sclerosis complex-2 tumor suppressor gene product tuberin as a target of the phosphoinositide 3-kinase/akt pathway.* Mol Cell, 2002. **10**(1): p. 151-62.

315. Cross, D.A., et al., *Inhibition of glycogen synthase kinase-3 by insulin mediated by protein kinase B.* Nature, 1995. **378**(6559): p. 785-9.

316. Lee, K., et al., *Requirement for Rictor in homeostasis and function of mature B lymphoid cells*. Blood, 2013. **122**(14): p. 2369-79.

317. Zhang, Y., et al., *Rictor is required for early B cell development in bone marrow*. PLoS One, 2014. **9**(8): p. e103970.

318. Farrerasvalenti, P., C. Rozman, and F. Blanco, *[Treatment of Chronic Lymphatic Leukemia with a New Alkylating Agent, Cyclophosphamide]*. Rev Clin Esp, 1963. **91**: p. 17-22.

319. Galton, D.A., et al., *The use of chlorambucil and steroids in the treatment of chronic lymphocytic leukaemia*. Br J Haematol, 1961. **7**: p. 73-98.

320. Keating, M.J., et al., *Long-term follow-up of patients with chronic lymphocytic leukemia (CLL) receiving fludarabine regimens as initial therapy*. Blood, 1998. **92**(4): p. 1165-71.

321. Rai, K.R., et al., *Fludarabine compared with chlorambucil as primary therapy for chronic lymphocytic leukemia*. N Engl J Med, 2000. **343**(24): p. 1750-7.

322. Bellosillo, B., et al., *In vitro evaluation of fludarabine in combination with cyclophosphamide and/or mitoxantrone in B-cell chronic lymphocytic leukemia*. Blood, 1999. **94**(8): p. 2836-43.

323. Bosch, F., et al., *Fludarabine, cyclophosphamide and mitoxantrone in the treatment of resistant or relapsed chronic lymphocytic leukaemia*. Br J Haematol, 2002. **119**(4): p. 976-84.

324. O'Brien, S.M., et al., *Results of the fludarabine and cyclophosphamide combination regimen in chronic lymphocytic leukemia*. J Clin Oncol, 2001. **19**(5): p. 1414-20.

325. Scheffold, A. and S. Stilgenbauer, *Revolution of Chronic Lymphocytic Leukemia Therapy: the Chemo-Free Treatment Paradigm*. Curr Oncol Rep, 2020. **22**(2): p. 16.

326. Eichhorst, B., et al., *First-line chemoimmunotherapy with bendamustine and rituximab versus fludarabine, cyclophosphamide, and rituximab in patients with advanced chronic lymphocytic leukaemia (CLL10): an international, open-label, randomised, phase 3, non-inferiority trial*. Lancet Oncol, 2016. **17**(7): p. 928-942.

327. Keating, M.J., et al., *Early results of a chemoimmunotherapy regimen of fludarabine, cyclophosphamide, and rituximab as initial therapy for chronic lymphocytic leukemia*. J Clin Oncol, 2005. **23**(18): p. 4079-88.

328. Fischer, K., et al., *Long-term remissions after FCR chemoimmunotherapy in previously untreated patients with CLL: updated results of the CLL8 trial*. Blood, 2016. **127**(2): p. 208-15.

329. Hallek, M., et al., *Addition of rituximab to fludarabine and cyclophosphamide in patients with chronic lymphocytic leukaemia: a randomised, open-label, phase 3 trial*. Lancet, 2010. **376**(9747): p. 1164-74.

330. Thompson, P.A., et al., *Fludarabine, cyclophosphamide, and rituximab treatment achieves long-term disease-free survival in IGHV-mutated chronic lymphocytic leukemia*. Blood, 2016. **127**(3): p. 303-9.

331. Patz, M., et al., *Comparison of the in vitro effects of the anti-CD20 antibodies rituximab and GA101 on chronic lymphocytic leukaemia cells.* Br J Haematol, 2011. **152**(3): p. 295-306.

332. Cartron, G., et al., *Obinutuzumab (GA101) in relapsed/refractory chronic lymphocytic leukemia: final data from the phase 1/2 GAUGUIN study.* Blood, 2014. **124**(14): p. 2196-202.

333. Goede, V., et al., *Obinutuzumab as frontline treatment of chronic lymphocytic leukemia: updated results of the CLL11 study.* Leukemia, 2015. **29**(7): p. 1602-4.

334. Benjamini, O., et al., *Second cancers in patients with chronic lymphocytic leukemia who received frontline fludarabine, cyclophosphamide and rituximab therapy: distribution and clinical outcomes.* Leuk Lymphoma, 2015. **56**(6): p. 1643-50.

335. Hampel, P.J. and S.A. Parikh, *Chronic lymphocytic leukemia treatment algorithm 2022.* Blood Cancer J, 2022. **12**(11): p. 161.

336. Burger, J.A., et al., *Long-term efficacy and safety of first-line ibrutinib treatment for patients with CLL/SLL: 5 years of follow-up from the phase 3 RESONATE-2 study.* Leukemia, 2020. **34**(3): p. 787-798.

337. Bond, D.A. and J.A. Woyach, *Targeting BTK in CLL: Beyond Ibrutinib.* Curr Hematol Malig Rep, 2019. **14**(3): p. 197-205.

338. Spaargaren, M., et al., *The B cell antigen receptor controls integrin activity through Btk and PLCgamma2.* J Exp Med, 2003. **198**(10): p. 1539-50.

339. Ponader, S., et al., *The Bruton tyrosine kinase inhibitor PCI-32765 thwarts chronic lymphocytic leukemia cell survival and tissue homing in vitro and in vivo.* Blood, 2012. **119**(5): p. 1182-9.

340. Herman, S.E., et al., *Bruton tyrosine kinase represents a promising therapeutic target for treatment of chronic lymphocytic leukemia and is effectively targeted by PCI-32765.* Blood, 2011. **117**(23): p. 6287-96.

341. Herman, S.E., et al., *Ibrutinib inhibits BCR and NF-kappaB signaling and reduces tumor proliferation in tissue-resident cells of patients with CLL.* Blood, 2014. **123**(21): p. 3286-95.

342. Byrd, J.C., et al., *Targeting BTK with ibrutinib in relapsed chronic lymphocytic leukemia.* N Engl J Med, 2013. **369**(1): p. 32-42.

343. Futatani, T., et al., *Bruton's tyrosine kinase is present in normal platelets and its absence identifies patients with X-linked agammaglobulinaemia and carrier females.* Br J Haematol, 2001. **114**(1): p. 141-9.

344. Byrd, J.C., et al., *Ibrutinib versus ofatumumab in previously treated chronic lymphoid leukemia.* N Engl J Med, 2014. **371**(3): p. 213-23.

345. Woyach, J.A., et al., *Ibrutinib Regimens versus Chemoimmunotherapy in Older Patients with Untreated CLL.* N Engl J Med, 2018. **379**(26): p. 2517-2528.

346. Moreno, C., et al., *Ibrutinib plus obinutuzumab versus chlorambucil plus obinutuzumab in first-line treatment of chronic lymphocytic leukaemia*

(iLLUMINATE): a multicentre, randomised, open-label, phase 3 trial. Lancet Oncol, 2019. **20**(1): p. 43-56.

347. Shanafelt, T.D., et al., *Ibrutinib-Rituximab or Chemoimmunotherapy for Chronic Lymphocytic Leukemia.* N Engl J Med, 2019. **381**(5): p. 432-443.

348. Sharman, J.P., et al., *Acalabrutinib with or without obinutuzumab versus chlorambucil and obinutuzmab for treatment-naive chronic lymphocytic leukaemia (ELEVATE TN): a randomised, controlled, phase 3 trial.* Lancet, 2020. **395**(10232): p. 1278-1291.

349. Ghia, P., et al., *ASCEND: Phase III, Randomized Trial of Acalabrutinib Versus Idelalisib Plus Rituximab or Bendamustine Plus Rituximab in Relapsed or Refractory Chronic Lymphocytic Leukemia.* J Clin Oncol, 2020. **38**(25): p. 2849-2861.

350. Tam, C.S., et al., *Phase 1 study of the selective BTK inhibitor zanubrutinib in B-cell malignancies and safety and efficacy evaluation in CLL.* Blood, 2019. **134**(11): p. 851-859.

351. P. Hillmen, B.E., J.R. Brown, N. Lamanna, S. O'Brien, C.S. Tam, et al., *First interim analysis of alpine study: Results of a phase 3 randomized study of zanubrutinib vs ibrutinib in patients with relapsed/refractory chronic lymphocytic leukemia/small lymphocytic lymphoma.* European Hematology Association Congress, 2021.

352. Brown, J.R., et al., *Zanubrutinib or Ibrutinib in Relapsed or Refractory Chronic Lymphocytic Leukemia.* N Engl J Med, 2023. **388**(4): p. 319-332.

353. Reiff, S.D., et al., *The BTK Inhibitor ARQ 531 Targets Ibrutinib-Resistant CLL and Richter Transformation.* Cancer Discov, 2018. **8**(10): p. 1300-1315.

354. Mato, A.R., et al., *Pirtobrutinib in relapsed or refractory B-cell malignancies (BRUIN): a phase 1/2 study.* Lancet, 2021. **397**(10277): p. 892-901.

355. Brandhuber, B., et al., *LOXO-305, A Next Generation Reversible BTK Inhibitor, for Overcoming Acquired Resistance to Irreversible BTK Inhibitors.* Clinical Lymphoma Myeloma and Leukemia, 2018. **18**(1): S216.

356. Nakhoda, S., A. Vistarop, and Y.L. Wang, *Resistance to Bruton tyrosine kinase inhibition in chronic lymphocytic leukaemia and non-Hodgkin lymphoma.* Br J Haematol, 2023. **200**(2): p. 137-149.

357. Wang, E., et al., *Mechanisms of Resistance to Noncovalent Bruton's Tyrosine Kinase Inhibitors.* N Engl J Med, 2022. **386**(8): p. 735-743.

358. Brown, J.R., et al., *Idelalisib, an inhibitor of phosphatidylinositol 3-kinase p110delta, for relapsed/refractory chronic lymphocytic leukemia.* Blood, 2014. **123**(22): p. 3390-7.

359. Hoellenriegel, J., et al., *The phosphoinositide 3'-kinase delta inhibitor, CAL-101, inhibits B-cell receptor signaling and chemokine networks in chronic lymphocytic leukemia.* Blood, 2011. **118**(13): p. 3603-12.

360. Eichhorst, B., et al., *Chronic lymphocytic leukaemia: ESMO Clinical Practice Guidelines for diagnosis, treatment and follow-up.* Ann Oncol, 2021. **32**(1): p. 23-33.

361. Burger, J.A., *Treatment of Chronic Lymphocytic Leukemia.* N Engl J Med, 2020. **383**(5): p. 460-473.

362. Flinn, I.W., et al., *The phase 3 DUO trial: duvelisib vs ofatumumab in relapsed and refractory CLL/SLL.* Blood, 2018. **132**(23): p. 2446-2455.

363. Campbell, K.J. and S.W.G. Tait, *Targeting BCL-2 regulated apoptosis in cancer.* Open Biol, 2018. **8**(5). p. 180002.

364. Robertson, L.E., et al., *Bcl-2 expression in chronic lymphocytic leukemia and its correlation with the induction of apoptosis and clinical outcome.* Leukemia, 1996. **10**(3): p. 456-9.

365. Pekarsky, Y., V. Balatti, and C.M. Croce, *BCL2 and miR-15/16: from gene discovery to treatment.* Cell Death Differ, 2018. **25**(1): p. 21-26.

366. Allegra, D., et al., *Defective DROSHA processing contributes to downregulation of MiR-15/-16 in chronic lymphocytic leukemia.* Leukemia, 2014. **28**(1): p. 98-107.

367. Oltersdorf, T., et al., *An inhibitor of Bcl-2 family proteins induces regression of solid tumours.* Nature, 2005. **435**(7042): p. 677-81.

368. Park, C.M., et al., *Discovery of an orally bioavailable small molecule inhibitor of prosurvival B-cell lymphoma 2 proteins.* J Med Chem, 2008. **51**(21): p. 6902-15.

369. Gandhi, L., et al., *Phase I study of Navitoclax (ABT-263), a novel Bcl-2 family inhibitor, in patients with small-cell lung cancer and other solid tumors.* J Clin Oncol, 2011. **29**(7): p. 909-16.

370. Mason, K.D., et al., *Programmed anuclear cell death delimits platelet life span.* Cell, 2007. **128**(6): p. 1173-86.

371. Hafezi, S. and M. Rahmani, *Targeting BCL-2 in Cancer: Advances, Challenges, and Perspectives.* Cancers (Basel), 2021. **13**(6). p. 1292.

372. Trudel, S., et al., *Preclinical studies of the pan-Bcl inhibitor obatoclax (GX015-070) in multiple myeloma.* Blood, 2007. **109**(12): p. 5430-8.

373. Schimmer, A.D., et al., *A phase I study of the pan bcl-2 family inhibitor obatoclax mesylate in patients with advanced hematologic malignancies.* Clin Cancer Res, 2008. **14**(24): p. 8295-301.

374. Opferman, J.T., et al., *Obligate role of anti-apoptotic MCL-1 in the survival of hematopoietic stem cells.* Science, 2005. **307**(5712): p. 1101-4.

375. Wilson, W.H., et al., *Navitoclax, a targeted high-affinity inhibitor of BCL-2, in lymphoid malignancies: a phase 1 dose-escalation study of safety, pharmacokinetics, pharmacodynamics, and antitumour activity.* Lancet Oncol, 2010. **11**(12): p. 1149-59.

376. Souers, A.J., et al., *ABT-199, a potent and selective BCL-2 inhibitor, achieves antitumor activity while sparing platelets.* Nat Med, 2013. **19**(2): p. 202-8.

377. Yoshino, T., et al., *Bcl-2 expression as a predictive marker of hormone-refractory prostate cancer treated with taxane-based chemotherapy.* Clin Cancer Res, 2006. **12**(20 Pt 1): p. 6116-24.

378. Stilgenbauer, S., et al., *Venetoclax in relapsed or refractory chronic lymphocytic leukaemia with 17p deletion: a multicentre, open-label, phase 2 study.* Lancet Oncol, 2016. **17**(6): p. 768-778.

379. Deeks, E.D., *Venetoclax: First Global Approval.* Drugs, 2016. **76**(9): p. 979-87.

380. Seymour, J.F., et al., *Venetoclax plus rituximab in relapsed or refractory chronic lymphocytic leukaemia: a phase 1b study.* Lancet Oncol, 2017. **18**(2): p. 230-240.

381. Seymour, J.F., et al., *Venetoclax-Rituximab in Relapsed or Refractory Chronic Lymphocytic Leukemia.* N Engl J Med, 2018. **378**(12): p. 1107-1120.

382. Fischer, K., et al., *Venetoclax and Obinutuzumab in Patients with CLL and Coexisting Conditions.* N Engl J Med, 2019. **380**(23): p. 2225-2236.

383. Yang, X., et al., *Treatment Patterns, Healthcare Resource Utilization, and Costs of Patients With Chronic Lymphocytic Leukemia or Small Lymphocytic Lymphoma in the US.* Oncologist, 2024. **29**(3): p. e360-e371.

384. Strati, P., et al., *Eradication of bone marrow minimal residual disease may prompt early treatment discontinuation in CLL.* Blood, 2014. **123**(24): p. 3727-32.

385. Woyach, J.A., et al., *Prolonged lymphocytosis during ibrutinib therapy is associated with distinct molecular characteristics and does not indicate a suboptimal response to therapy.* Blood, 2014. **123**(12): p. 1810-7.

386. Blombery, P., et al., *Acquisition of the Recurrent Gly101Val Mutation in BCL2 Confers Resistance to Venetoclax in Patients with Progressive Chronic Lymphocytic Leukemia.* Cancer Discov, 2019. **9**(3): p. 342-353.

387. Thijssen, R. and A.W. Roberts, *Venetoclax in Lymphoid Malignancies: New Insights, More to Learn.* Cancer Cell, 2019. **36**(4): p. 341-343.

388. Halford, B.C.E.B. *Rapamycin's secrets unearthed*. 2016. **94**, 26-30.

389. Brown, E.J., et al., *A mammalian protein targeted by G1-arresting rapamycin-receptor complex.* Nature, 1994. **369**(6483): p. 756-8.

390. Chiu, M.I., H. Katz, and V. Berlin, *RAPT1, a mammalian homolog of yeast Tor, interacts with the FKBP12/rapamycin complex.* Proc Natl Acad Sci U S A, 1994. **91**(26): p. 12574-8.

391. Sabatini, D.M., et al., *RAFT1: a mammalian protein that binds to FKBP12 in a rapamycin-dependent fashion and is homologous to yeast TORs.* Cell, 1994. **78**(1): p. 35-43.

392. Aylett, C.H., et al., *Architecture of human mTOR complex 1.* Science, 2016. **351**(6268): p. 48-52.

393. Scaiola, A., et al., *The 3.2-A resolution structure of human mTORC2.* Sci Adv, 2020. **6**(45). p. eabc1251.

394. Sarbassov, D.D., et al., *Prolonged rapamycin treatment inhibits mTORC2 assembly and Akt/PKB.* Mol Cell, 2006. **22**(2): p. 159-68.

395. Selvarani, R., S. Mohammed, and A. Richardson, *Effect of rapamycin on aging and age-related diseases-past and future*. Geroscience, 2021. **43**(3): p. 1135-1158.

396. Shams, R., et al., *In Silico and In Cell Hybrid Selection of Nonrapalog Ligands to Allosterically Inhibit the Kinase Activity of mTORC1.* J Med Chem, 2022. **65**(2): p. 1329-1341.

397. Dowling, R.J., et al., *Dissecting the role of mTOR: lessons from mTOR inhibitors*. Biochim Biophys Acta, 2010. **1804**(3): p. 433-9.

398. Chresta, C.M., et al., *AZD8055 is a potent, selective, and orally bioavailable ATP-competitive mammalian target of rapamycin kinase inhibitor with in vitro and in vivo antitumor activity.* Cancer Res, 2010. **70**(1): p. 288-98.

399. Hu, W., et al., *Anti-tumor effect of AZD8055 against bladder cancer and bladder cancer-associated macrophages*. Heliyon, 2023. **9**(3): p. e14272.

400. Kauffman, E.C., et al., *Preclinical efficacy of dual mTORC1/2 inhibitor AZD8055 in renal cell carcinoma harboring a TFE3 gene fusion*. BMC Cancer, 2019. **19**(1): p. 917.

401. Khan, S., et al., *Co-targeting BCL-X(L) and MCL-1 with DT2216 and AZD8055 synergistically inhibit small-cell lung cancer growth without causing on-target toxicities in mice*. Cell Death Discov, 2023. **9**(1): p. 1.

402. Ni, Z., et al., *Comparison of dual mTORC1/2 inhibitor AZD8055 and mTORC1 inhibitor rapamycin on the metabolism of breast cancer cells using proton nuclear magnetic resonance spectroscopy metabolomics*. Invest New Drugs, 2022. **40**(6): p. 1206-1215.

403. Willems, L., et al., *The dual mTORC1 and mTORC2 inhibitor AZD8055 has anti-tumor activity in acute myeloid leukemia*. Leukemia, 2012. **26**(6): p. 1195-202.

404. Mao, B., et al., *Overview of Research into mTOR Inhibitors*. Molecules, 2022. **27**(16). p. 5295.

405. Gupta, M., et al., *Dual mTORC1/mTORC2 inhibition diminishes Akt activation and induces Puma-dependent apoptosis in lymphoid malignancies*. Blood, 2012. **119**(2): p. 476-87.

406. Rodrik-Outmezguine, V.S., et al., *mTOR kinase inhibition causes feedback-dependent biphasic regulation of AKT signaling*. Cancer Discov, 2011. **1**(3): p. 248-59.

407. Dobashi, Y., et al., *Mammalian target of rapamycin: a central node of complex signaling cascades*. Int J Clin Exp Pathol, 2011. **4**(5): p. 476-95.

408. Stemke-Hale, K., et al., *An integrative genomic and proteomic analysis of PIK3CA, PTEN, and AKT mutations in breast cancer.* Cancer Res, 2008. **68**(15): p. 6084-91.

409. Malik, N., et al., *mTORC1-selective activation of translation elongation promotes disease progression in chronic lymphocytic leukemia*. Leukemia, 2023. **37**(12): p. 2414-2425.

410. Decker, T., et al., *Rapamycin-induced G1 arrest in cycling B-CLL cells is associated with reduced expression of cyclin D3, cyclin E, cyclin A, and survivin.* Blood, 2003. **101**(1): p. 278-85.

411. Aleskog, A., et al., *Rapamycin shows anticancer activity in primary chronic lymphocytic leukemia cells in vitro, as single agent and in drug combination.* Leuk Lymphoma, 2008. **49**(12): p. 2333-43.

412. Zent, C.S., et al., *The treatment of recurrent/refractory chronic lymphocytic leukemia/small lymphocytic lymphoma (CLL) with everolimus results in clinical responses and mobilization of CLL cells into the circulation.* Cancer, 2010. **116**(9): p. 2201-7.

413. Feng, Y., et al., *The Role of mTOR Inhibitors in Hematologic Disease: From Bench to Bedside.* Front Oncol, 2020. **10**: p. 611690.

414. Witzens-Harig, M., et al., *A phase I/II trial to evaluate the safety, feasibility and activity of salvage therapy consisting of the mTOR inhibitor Temsirolimus added to standard therapy of Rituximab and DHAP for the treatment of patients with relapsed or refractory diffuse large cell B-Cell lymphoma - the STORM trial.* BMC Cancer, 2013. **13**: p. 308.

415. Smith, S.M., et al., *Temsirolimus has activity in non-mantle cell non-Hodgkin's lymphoma subtypes: The University of Chicago phase II consortium.* J Clin Oncol, 2010. **28**(31): p. 4740-6.

416. Huntington, S.F., et al., *DTRMWXHS-12, a novel Bruton tyrosine kinase inhibitor, in combination with everolimus and pomalidomide in patients with relapsed/refractory lymphomas: An open-label, multicenter, phase 1a/1b study.* Am J Hematol, 2023. **98**(5): p. 739-749.

417. Sun, S.Y., et al., *Activation of Akt and eIF4E survival pathways by rapamycin-mediated mammalian target of rapamycin inhibition.* Cancer Res, 2005. **65**(16): p. 7052-8.

418. Herman, L., A.L. Todeschini, and R.A. Veitia, *Forkhead Transcription Factors in Health and Disease.* Trends Genet, 2021. **37**(5): p. 460-475.

419. Galili, N., et al., *Fusion of a fork head domain gene to PAX3 in the solid tumour alveolar rhabdomyosarcoma.* Nat Genet, 1993. **5**(3): p. 230-5.

420. Schmitt-Ney, M. and G. Camussi, *The PAX3-FOXO1 fusion protein present in rhabdomyosarcoma interferes with normal FOXO activity and the TGF-beta pathway.* PLoS One, 2015. **10**(3): p. e0121474.

421. Borkhardt, A., et al., *Cloning and characterization of AFX, the gene that fuses to MLL in acute leukemias with a t(X;11)(q13;q23).* Oncogene, 1997. **14**(2): p. 195-202.

422. Parry, P., Y. Wei, and G. Evans, *Cloning and characterization of the t(X;11) breakpoint from a leukemic cell line identify a new member of the forkhead gene family.* Genes Chromosomes Cancer, 1994. **11**(2): p. 79-84.

423. Hillion, J., et al., *AF6q21, a novel partner of the MLL gene in t(6;11)(q21;q23), defines a forkhead transcriptional factor subfamily.* Blood, 1997. **90**(9): p. 3714-9.

424. Jiramongkol, Y. and E.W. Lam, *FOXO transcription factor family in cancer and metastasis*. Cancer Metastasis Rev, 2020. **39**(3): p. 681-709.

425. Fu, Z. and D.J. Tindall, *FOXOs, cancer and regulation of apoptosis*. Oncogene, 2008. **27**(16): p. 2312-9.

426. Calnan, D.R. and A. Brunet, *The FoxO code*. Oncogene, 2008. **27**(16): p. 2276-88.

427. Hosaka, T., et al., *Disruption of forkhead transcription factor (FOXO) family members in mice reveals their functional diversification.* Proc Natl Acad Sci U S A, 2004. **101**(9): p. 2975-80.

428. Tzivion, G., M. Dobson, and G. Ramakrishnan, *FoxO transcription factors; Regulation by AKT and 14-3-3 proteins.* Biochim Biophys Acta, 2011. **1813**(11): p. 1938-45.

429. Hornsveld, M., et al., *Re-evaluating the role of FOXOs in cancer.* Semin Cancer Biol, 2018. **50**: p. 90-100.

430. Eijkelenboom, A. and B.M. Burgering, *FOXOs: signalling integrators for homeostasis maintenance*. Nat Rev Mol Cell Biol, 2013. **14**(2): p. 83-97.

431. van der Heide, L.P., et al., *FoxO6 transcriptional activity is regulated by Thr26 and Ser184, independent of nucleo-cytoplasmic shuttling*. Biochem J, 2005. **391**(Pt 3): p. 623-9.

432. Yaffe, M.B., et al., *The structural basis for 14-3-3:phosphopeptide binding specificity.* Cell, 1997. **91**(7): p. 961-71.

433. Silhan, J., et al., *14-3-3 protein masks the DNA binding interface of forkhead transcription factor FOXO4.* J Biol Chem, 2009. **284**(29): p. 19349-60.

434. Brunet, A., et al., *14-3-3 transits to the nucleus and participates in dynamic nucleocytoplasmic transport*. J Cell Biol, 2002. **156**(5): p. 817-28.

435. Obsilova, V., et al., *14-3-3 Protein interacts with nuclear localization sequence of forkhead transcription factor FoxO4.* Biochemistry, 2005. **44**(34): p. 11608-17.

436. Yadav, R.K., et al., *FoxO transcription factors in cancer metabolism*. Semin Cancer Biol, 2018. **50**: p. 65-76.

437. Laplante, M. and D.M. Sabatini, *mTOR signaling in growth control and disease*. Cell, 2012. **149**(2): p. 274-93.

438. Lee, D.F., et al., *IKK beta suppression of TSC1 links inflammation and tumor angiogenesis via the mTOR pathway.* Cell, 2007. **130**(3): p. 440-55.

439. Tran, H., et al., *DNA repair pathway stimulated by the forkhead transcription factor FOXO3a through the Gadd45 protein.* Science, 2002. **296**(5567): p. 530-4.

440. Yang, J.Y., et al., *ERK promotes tumorigenesis by inhibiting FOXO3a via MDM2-mediated degradation.* Nat Cell Biol, 2008. **10**(2): p. 138-48.

441. Yang, J.Y., et al., *Activation of FOXO3a is sufficient to reverse mitogen-activated protein/extracellular signal-regulated kinase kinase inhibitor chemoresistance in human cancer.* Cancer Res, 2010. **70**(11): p. 4709-18.

442. Huang, H., et al., *CDK2-dependent phosphorylation of FOXO1 as an apoptotic response to DNA damage.* Science, 2006. **314**(5797): p. 294-7.

443. Rena, G., et al., *Two novel phosphorylation sites on FKHR that are critical for its nuclear exclusion.* EMBO J, 2002. **21**(9): p. 2263-71.

444. Rena, G., et al., *D4476, a cell-permeant inhibitor of CK1, suppresses the site-specific phosphorylation and nuclear exclusion of FOXO1a.* EMBO Rep, 2004. **5**(1): p. 60-5.

445. Essers, M.A., et al., *FOXO transcription factor activation by oxidative stress mediated by the small GTPase Ral and JNK.* EMBO J, 2004. **23**(24): p. 4802-12.

446. Yun, H., et al., *AMP-activated protein kinase mediates the antioxidant effects of resveratrol through regulation of the transcription factor FoxO1.* FEBS J, 2014. **281**(19): p. 4421-38.

447. Orea-Soufi, A., et al., *FOXO transcription factors as therapeutic targets in human diseases.* Trends Pharmacol Sci, 2022. **43**(12): p. 1070-1084.

448. Brown, A.K. and A.E. Webb, *Regulation of FOXO Factors in Mammalian Cells.* Curr Top Dev Biol, 2018. **127**: p. 165-192.

449. Brunet, A., et al., *Stress-dependent regulation of FOXO transcription factors by the SIRT1 deacetylase.* Science, 2004. **303**(5666): p. 2011-5.

450. Calnan, D.R., et al., *Methylation by Set9 modulates FoxO3 stability and transcriptional activity.* Aging (Albany NY), 2012. **4**(7): p. 462-79.

451. Fukuoka, M., et al., *Negative regulation of forkhead transcription factor AFX (Foxo4) by CBP-induced acetylation.* Int J Mol Med, 2003. **12**(4): p. 503-8.

452. Motta, M.C., et al., *Mammalian SIRT1 represses forkhead transcription factors.* Cell, 2004. **116**(4): p. 551-63.

453. van der Horst, A., et al., *FOXO4 transcriptional activity is regulated by monoubiquitination and USP7/HAUSP.* Nat Cell Biol, 2006. **8**(10): p. 1064-73.

454. Guttilla, I.K. and B.A. White, *Coordinate regulation of FOXO1 by miR-27a, miR-96, and miR-182 in breast cancer cells.* J Biol Chem, 2009. **284**(35): p. 23204-16.

455. Welinder, E., et al., *The transcription factors E2A and HEB act in concert to induce the expression of FOXO1 in the common lymphoid progenitor.* Proc Natl Acad Sci U S A, 2011. **108**(42): p. 17402-7.

456. Ushmorov, A. and T. Wirth, *FOXO in B-cell lymphopoiesis and B cell neoplasia.* Semin Cancer Biol, 2018. **50**: p. 132-141.

457. Amin, R.H. and M.S. Schlissel, *Foxo1 directly regulates the transcription of recombination-activating genes during B cell development.* Nat Immunol, 2008. **9**(6): p. 613-22.

458. Dengler, H.S., et al., *Distinct functions for the transcription factor Foxo1 at various stages of B cell differentiation.* Nat Immunol, 2008. **9**(12): p. 1388-98.

459. Cooper, A.B., et al., *A unique function for cyclin D3 in early B cell development*. Nat Immunol, 2006. **7**(5): p. 489-97.

460. Baracho, G.V., et al., *Emergence of the PI3-kinase pathway as a central modulator of normal and aberrant B cell differentiation*. Curr Opin Immunol, 2011. **23**(2): p. 178-83.

461. Hinman, R.M., et al., *Foxo3-/- mice demonstrate reduced numbers of pre-B and recirculating B cells but normal splenic B cell sub-population distribution*. Int Immunol, 2009. **21**(7): p. 831-42.

462. Pena-Perez, L., et al., *FOXO Dictates Initiation of B Cell Development and Myeloid Restriction in Common Lymphoid Progenitors*. Front Immunol, 2022. **13**: p. 880668.

463. Lees, J., et al., *The discrete roles of individual FOXO transcription factor family members in B-cell malignancies*. Front Immunol, 2023. **14**: p. 1179101.

464. Hinman, R.M., et al., *B cell receptor signaling down-regulates forkhead box transcription factor class O 1 mRNA expression via phosphatidylinositol 3-kinase and Bruton's tyrosine kinase*. J Immunol, 2007. **178**(2): p. 740-7.

465. Yusuf, I., et al., *Optimal B-cell proliferation requires phosphoinositide 3-kinase-dependent inactivation of FOXO transcription factors*. Blood, 2004. **104**(3): p. 784-7.

466. Srinivasan, L., et al., *PI3 kinase signals BCR-dependent mature B cell survival*. Cell, 2009. **139**: p. 573-86.

467. Vandenberg, C.J., N. Motoyama, and S. Cory, *FoxO3 suppresses Myc-driven lymphomagenesis*. Cell Death Dis, 2016. **6**(1): p. e2046.

468. De Silva, N.S. and U. Klein, *Dynamics of B cells in germinal centres*. Nat Rev Immunol, 2015. **15**(3): p. 137-48.

469. Basso, K. and R. Dalla-Favera, *Germinal centres and B cell lymphomagenesis*. Nat Rev Immunol, 2015. **15**(3): p. 172-84.

470. Pae, J., et al., *Cyclin D3 drives inertial cell cycling in dark zone germinal center B cells*. J Exp Med, 2021. **218**(4).

471. Muramatsu, M., et al., *Class switch recombination and hypermutation require activation-induced cytidine deaminase (AID), a potential RNA editing enzyme*. Cell, 2000. **102**(5): p. 553-63.

472. Revy, P., et al., *Activation-induced cytidine deaminase (AID) deficiency causes the autosomal recessive form of the Hyper-IgM syndrome (HIGM2)*. Cell, 2000. **102**(5): p. 565-75.

473. Dominguez-Sola, D., et al., *The FOXO1 Transcription Factor Instructs the Germinal Center Dark Zone Program*. Immunity, 2015. **43**(6): p. 1064-74.

474. Dominguez-Sola, D., et al., *The proto-oncogene MYC is required for selection in the germinal center and cyclic reentry*. Nat Immunol, 2012. **13**(11): p. 1083-91.

475. Tunyaplin, C., et al., *Direct repression of prdm1 by Bcl-6 inhibits plasmacytic differentiation*. J Immunol, 2004. **173**(2): p. 1158-65.

476. Sander, S., et al., *PI3 Kinase and FOXO1 Transcription Factor Activity Differentially Control B Cells in the Germinal Center Light and Dark Zones.* Immunity, 2015. **43**: p. 1075-86.

477. Zhu, Z., et al., *The AKT isoforms 1 and 2 drive B cell fate decisions during the germinal center response.* Life Sci Alliance, 2019. **2**(6). p. e201900506.

478. Inoue, T., et al., *The transcription factor Foxo1 controls germinal center B cell proliferation in response to T cell help.* J Exp Med, 2017. **214**(4): p. 1181-1198.

479. Luo, W., F. Weisel, and M.J. Shlomchik, *B Cell Receptor and CD40 Signaling Are Rewired for Synergistic Induction of the c-Myc Transcription Factor in Germinal Center B Cells.* Immunity, 2018. **48**(2): p. 313-326 e5.

480. Ramezani-Rad, P., et al., *Cyclin D3 Governs Clonal Expansion of Dark Zone Germinal Center B Cells.* Cell Rep, 2020. **33**(7): p. 108403.

481. Crotty, S., *T follicular helper cell differentiation, function, and roles in disease.* Immunity, 2014. **41**(4): p. 529-42.

482. Qi, H., et al., *Foxo3 Promotes the Differentiation and Function of Follicular Helper T Cells.* Cell Rep, 2020. **31**(6): p. 107621.

483. Paik, J.H., et al., *FoxOs are lineage-restricted redundant tumor suppressors and regulate endothelial cell homeostasis.* Cell, 2007. **128**(2): p. 309-23.

484. Tothova, Z., et al., *FoxOs are critical mediators of hematopoietic stem cell resistance to physiologic oxidative stress.* Cell, 2007. **128**(2): p. 325-39.

485. Naka, K., et al., *TGF-beta-FOXO signalling maintains leukaemia-initiating cells in chronic myeloid leukaemia.* Nature, 2010. **463**(7281): p. 676-80.

486. Pellicano, F., et al., *The antiproliferative activity of kinase inhibitors in chronic myeloid leukemia cells is mediated by FOXO transcription factors.* Stem Cells, 2014. **32**(9): p. 2324-37.

487. Sykes, S.M., et al., *AKT/FOXO signaling enforces reversible differentiation blockade in myeloid leukemias.* Cell, 2011. **146**(5): p. 697-708.

488. Zehir, A., et al., *Mutational landscape of metastatic cancer revealed from prospective clinical sequencing of 10,000 patients.* Nat Med, 2017. **23**(6): p. 703-713.

489. Ma, M.C.J., et al., *Pathognomonic and epistatic genetic alterations in B-cell non-Hodgkin lymphoma.* bioRxiv, 2019: p. 674259.

490. Reddy, A., et al., *Genetic and Functional Drivers of Diffuse Large B Cell Lymphoma.* Cell, 2017. **171**(2): p. 481-494 e15.

491. Chakravarty, D., et al., *OncoKB: A Precision Oncology Knowledge Base.* JCO Precision Oncology, 2017(1): p. 1-16.

492. Chang, M.T., et al., *Accelerating Discovery of Functional Mutant Alleles in Cancer.* Cancer Discov, 2018. **8**(2): p. 174-183.

493. Roberto, M.P., et al., *Mutations in the transcription factor FOXO1 mimic positive selection signals to promote germinal center B cell expansion and lymphomagenesis*. Immunity, 2021. **54**(8): p. 1807-1824 e14.

494. Sablon, A., et al., *FOXO1 forkhead domain mutants in B-cell lymphoma lack transcriptional activity.* Sci Rep, 2022. **12**(1): p. 1309.

495. Yuan, C., et al., *The function of FOXO1 in the late phases of the cell cycle is suppressed by PLK1-mediated phosphorylation*. Cell Cycle, 2014. **13**(5): p. 807-19.

496. Thelander, E.F., et al., *Characterization of 6q deletions in mature B cell lymphomas and childhood acute lymphoblastic leukemia*. Leuk Lymphoma, 2008. **49**(3): p. 477-87.

497. Offit, K., et al., *6q deletions define distinct clinico-pathologic subsets of non-Hodgkin's lymphoma*. Blood, 1993. **82**(7): p. 2157-62.

498. Katzenberger, T., et al., *Delineation of distinct tumour profiles in mantle cell lymphoma by detailed cytogenetic, interphase genetic and morphological analysis*. Br J Haematol, 2008. **142**(4): p. 538-50.

499. Ramsay, A.J., et al., *Next-generation sequencing reveals the secrets of the chronic lymphocytic leukemia genome*. Clin Transl Oncol, 2013. **15**(1): p. 3-8.

500. Palacios, F., et al., *Activation of the PI3K/AKT pathway by microRNA-22 results in CLL B-cell proliferation*. Leukemia, 2015. **29**(1): p. 115-25.

501. Scheffold, A., et al., *IGF1R as druggable target mediating PI3K-delta inhibitor resistance in a murine model of chronic lymphocytic leukemia*. Blood, 2019. **134**(6): p. 534-547.

502. Seda, V., et al., *FoxO1-GAB1 axis regulates homing capacity and tonic AKT activity in chronic lymphocytic leukemia*. Blood, 2021. **138**(9): p. 758-772.

503. Hay, J., et al., *Subcellular Fractionation of Primary Chronic Lymphocytic Leukemia Cells to Monitor Nuclear/Cytoplasmic Protein Trafficking*. J Vis Exp, 2019(152).

504. *DSMZ. MEC1*. Available from: https://www.dsmz.de/collection/catalogue/details/culture/ACC-497.

505. *DSMZ. HG3*. Available from: https://www.dsmz.de/collection/catalogue/details/culture/ACC-765.

506. *ATCC. L cells* Available from: https://www.lgcstandards-atcc.org/products/all/CRL-2648.aspx?geo_country=de.

507. *ATCC. HEK293T cells*. Available from: https://www.lgcstandards-atcc.org/products/all/crl-3216.aspx?geo_country=de#culturemethod.

508. ThermoFisher. *CellTrace™ Violet Cell Proliferation Assay*. 2025; Available from: https://www.thermofisher.com/order/catalog/product/C34557.

509. Livak, K.J. and T.D. Schmittgen, *Analysis of relative gene expression data using real-time quantitative PCR and the 2(-Delta Delta C(T)) Method*. Methods, 2001. **25**(4): p. 402-8.

510. Addgene. *pLKO.1 - TRC Cloning Vector 2006*. Available from: https://www.addgene.org/protocols/plko/.

511. Chen, Y.J., et al., *A conserved phosphorylation site within the forkhead domain of FoxM1B is required for its activation by cyclin-CDK1.* J Biol Chem, 2009. **284**(44): p. 30695-707.

512. Zheng, X., et al., *Proliferation and Apoptosis of B-Cell Lymphoma Cells under Targeted Regulation of FOXO3 by miR-155.* Mediterr J Hematol Infect Dis, 2020. **12**(1): p. e2020073.

513. De Bruyne, E., et al., *IGF-1 suppresses Bim expression in multiple myeloma via epigenetic and posttranslational mechanisms.* Blood, 2010. **115**(12): p. 2430-40.

514. Rosen, A., et al., *Lymphoblastoid cell line with B1 cell characteristics established from a chronic lymphocytic leukemia clone by in vitro EBV infection.* Oncoimmunology, 2012. **1**(1): p. 18-27.

515. Stacchini, A., et al., *MEC1 and MEC2: two new cell lines derived from B-chronic lymphocytic leukaemia in prolymphocytoid transformation.* Leuk Res, 1999. **23**(2): p. 127-36.

516. Zhang, H., et al., *FOXO1 inhibits Runx2 transcriptional activity and prostate cancer cell migration and invasion.* Cancer Res, 2011. **71**(9): p. 3257-67.

517. Wu, Y., et al., *Expression of FOXO1 is associated with GATA3 and Annexin-1 and predicts disease-free survival in breast cancer.* Am J Cancer Res, 2012. **2**(1): p. 104-15.

518. Miao, H., et al., *FOXO1 increases CCL20 to promote NF-kappaB-dependent lymphocyte chemotaxis.* Mol Endocrinol, 2012. **26**(3): p. 423-37.

519. Homey, B., et al., *Up-regulation of macrophage inflammatory protein-3 alpha/CCL20 and CC chemokine receptor 6 in psoriasis.* J Immunol, 2000. **164**(12): p. 6621-32.

520. Gao, Y., H. Kazama, and S. Yonehara, *Bim regulates B-cell receptor-mediated apoptosis in the presence of CD40 signaling in CD40-pre-activated splenic B cells differentiating into plasma cells.* Int Immunol, 2012. **24**(5): p. 283-92.

521. Mullins, M.W., B.T. Pittner, and E.C. Snow, *CD40-mediated induction of p21 accumulation in resting and cycling B cells.* Mol Immunol, 1998. **35**(10): p. 567-80.

522. Davies, B.R., et al., *Preclinical pharmacology of AZD5363, an inhibitor of AKT: pharmacodynamics, antitumor activity, and correlation of monotherapy activity with genetic background.* Mol Cancer Ther, 2012. **11**(4): p. 873-87.

523. Gricks, C.S., et al., *Differential regulation of gene expression following CD40 activation of leukemic compared to healthy B cells.* Blood, 2004. **104**(13): p. 4002-9.

524. Kapoor, I., et al., *Resistance to BTK inhibition by ibrutinib can be overcome by preventing FOXO3a nuclear export and PI3K/AKT activation in B-cell lymphoid malignancies.* Cell Death Dis, 2019. **10**(12): p. 924.

525. Obrador-Hevia, A., et al., *The tumour suppressor FOXO3 is a key regulator of mantle cell lymphoma proliferation and survival.* Br J Haematol, 2012. **156**(3): p. 334-45.

526. Santamaria, C.M., et al., *High FOXO3a expression is associated with a poorer prognosis in AML with normal cytogenetics.* Leuk Res, 2009. **33**(12): p. 1706-9.

527. *Association of survival with FOXO4 expression in renal and head and neck cancers.* 2024: The Protein Atlas. Available from: https://www.proteinatlas.org/ENSG00000184481-FOXO4

528. Uhlen, M., et al., *A pathology atlas of the human cancer transcriptome.* Science, 2017. **357**(6352).

529. Lu, Y., et al., *Clinicopathological Significance of FOXO4 Expression and Correlation with Prx1 in Head and Neck Squamous Cell Carcinoma.* Anal Cell Pathol (Amst), 2021. **2021**: p. 5510753.

530. Wang, W., P.H. Zhou, and W. Hu, *Overexpression of FOXO4 induces apoptosis of clear-cell renal carcinoma cells through downregulation of Bim.* Mol Med Rep, 2016. **13**(3): p. 2229-34.

531. Jurcevic, S., Keane, S., Borgmastars, E., Lubovac-Pilay, Z., Ejeskar, K., *Bioinformatics analysis of miRNAs in the neuroblastoma 11q-deleted region reveals a role of miR-548l in both 11q-deleted and MYCN amplified tumour cells.* Scientific Reports, 2022. **12**: p. 1231.

532. Kehl, T., Kern, F., Backes, C. *et al., miRPathDB 2.0: a novel release of the miRNA Pathway Dictionary Database.* Nucleic Acids Res, 2018.

533. Coomans de Brachene, A. and J.B. Demoulin, *FOXO transcription factors in cancer development and therapy.* Cell Mol Life Sci, 2016. **73**(6): p. 1159-72.

534. Kim, D.H., et al., *FoxO6 integrates insulin signaling with gluconeogenesis in the liver.* Diabetes, 2011. **60**(11): p. 2763-74.

535. Wang, M., et al., *FoxO gene family evolution in vertebrates.* BMC Evol Biol, 2009. **9**: p. 222.

536. Zhu, X., et al., *Analysis of the major patterns of B cell gene expression changes in response to short-term stimulation with 33 single ligands.* J Immunol, 2004. **173**(12): p. 7141-9.

537. Wilhelm, K., et al., *FOXO1 couples metabolic activity and growth state in the vascular endothelium.* Nature, 2016. **529**(7585): p. 216-20.

538. Nahar, R., et al., *Pre-B cell receptor-mediated activation of BCL6 induces pre-B cell quiescence through transcriptional repression of MYC.* Blood, 2011. **118**(15): p. 4174-8.

539. Pellicano, F., et al., *FOXO transcription factor activity is partially retained in quiescent CML stem cells and induced by tyrosine kinase inhibitors in CML progenitor cells.* Blood, 2009. p. 226621.

540. Kabrani, E., et al., *Nuclear FOXO1 promotes lymphomagenesis in germinal center B cells.* Blood, 2018. **132**(25): p. 2670-2683.

541. Wang, F., et al., *Tight regulation of FOXO1 is essential for maintenance of B-cell precursor acute lymphoblastic leukemia.* Blood, 2018. **131**(26): p. 2929-2942.

542. Lin, A., et al., *FoxO transcription factors promote AKT Ser473 phosphorylation and renal tumor growth in response to pharmacologic inhibition of the PI3K-AKT pathway.* Cancer Res, 2014. **74**(6): p. 1682-93.

543. Ondrisova, L., et al, *S142: FOXO1-RICTOR AXIS INDUCES ADAPTIVE INCREASE IN AKT ACTIVITY DURING BCR INHIBITOR THERAPY IN CLL: IMPLICATIONS FOR COMBINATION THERAPY.* Hemasphere, 2023(7(Suppl)): p. e8828434.

544. Thompson, M.G., et al., *FOXO3-NF-kappaB RelA Protein Complexes Reduce Proinflammatory Cell Signaling and Function.* J Immunol, 2015. **195**(12): p. 5637-47.

545. Ryu, K.J., et al., *FOXO4 expression is related to stem cell-like properties and resistance to treatment in diffuse large B-cell lymphoma.* Oncotarget, 2017. **8**(2): p. 2466-2476.

546. Zhou, W., et al., *FoxO4 inhibits NF-kappaB and protects mice against colonic injury and inflammation.* Gastroenterology, 2009. **137**(4): p. 1403-14.

547. Chen, C.C., et al., *FoxOs inhibit mTORC1 and activate Akt by inducing the expression of Sestrin3 and Rictor.* Dev Cell, 2010. **18**(4): p. 592-604.

548. Zhou, J., et al., *FOXO3 induces FOXO1-dependent autophagy by activating the AKT1 signaling pathway.* Autophagy, 2012. **8**(12): p. 1712-23.

549. Long, J., et al., *FLT3 inhibition upregulates HDAC8 via FOXO to inactivate p53 and promote maintenance of FLT3-ITD+ acute myeloid leukemia.* Blood, 2020. **135**(17): p. 1472-1483.

550. Wagle, M., et al., *A role for FOXO1 in BCR-ABL1-independent tyrosine kinase inhibitor resistance in chronic myeloid leukemia.* Leukemia, 2016. **30**(7): p. 1493-501.

551. Seoane, J., et al., *Integration of Smad and forkhead pathways in the control of neuroepithelial and glioblastoma cell proliferation.* Cell, 2004. **117**(2): p. 211-23.

552. Brown, J.A., et al., *TGF-beta-Induced Quiescence Mediates Chemoresistance of Tumor-Propagating Cells in Squamous Cell Carcinoma.* Cell Stem Cell, 2017. **21**(5): p. 650-664 e8.

553. Holmes, K.B., et al., *Ibrutinib induces chromatin reorganisation of chronic lymphocytic leukaemia cells.* Oncogenesis, 2019. **8**(5): p. 32.

554. Kops, G.J., et al., *Forkhead transcription factor FOXO3a protects quiescent cells from oxidative stress.* Nature, 2002. **419**(6904): p. 316-21.

555. Essaghir, A., et al., *The transcription of FOXO genes is stimulated by FOXO3 and repressed by growth factors.* J Biol Chem, 2009. **284**(16): p. 10334-42.

556. Carcel-Trullols, J., A.D. Kovacs, and D.A. Pearce, *Cell biology of the NCL proteins: What they do and don't do.* Biochim Biophys Acta, 2015. **1852**(10 Pt B): p. 2242-55.

557. Lu, H. and H. Huang, *FOXO1: a potential target for human diseases.* Curr Drug Targets, 2011. **12**(9): p. 1235-44.

558. Wang, W., et al., *PDK1 regulates definitive HSCs via the FOXO pathway during murine fetal liver hematopoiesis.* Stem Cell Res, 2018. **30**: p. 192-200.

559. Coqueret, O., *New roles for p21 and p27 cell-cycle inhibitors: a function for each cell compartment?* Trends Cell Biol, 2003. **13**(2): p. 65-70.

560. Sherr, C.J., *D-type cyclins.* Trends Biochem Sci, 1995. **20**(5): p. 187-90.

561. Pacher, P. and C. Szabo, *Role of poly(ADP-ribose) polymerase 1 (PARP-1) in cardiovascular diseases: the therapeutic potential of PARP inhibitors.* Cardiovasc Drug Rev, 2007. **25**(3): p. 235-60.

562. Virag, L., et al., *Poly(ADP-ribose) signaling in cell death.* Mol Aspects Med, 2013. **34**(6): p. 1153-67.

563. Herriott, A., et al., *PARP1 expression, activity and ex vivo sensitivity to the PARP inhibitor, talazoparib (BMN 673), in chronic lymphocytic leukaemia.* Oncotarget, 2015. **6**(41): p. 43978-91.

564. Quijada-Alamo, M., et al., *CRISPR/Cas9-generated models uncover therapeutic vulnerabilities of del(11q) CLL cells to dual BCR and PARP inhibition.* Leukemia, 2020. **34**(6): p. 1599-1612.

565. Oliver, F.J., et al., *Resistance to endotoxic shock as a consequence of defective NF-kappaB activation in poly (ADP-ribose) polymerase-1 deficient mice.* EMBO J, 1999. **18**(16): p. 4446-54.

566. Weston, V.J., et al., *The PARP inhibitor olaparib induces significant killing of ATM-deficient lymphoid tumor cells in vitro and in vivo.* Blood, 2010. **116**(22): p. 4578-87.

567. Palomer, X., et al., *GADD45A: With or without you.* Med Res Rev, 2024. **44**(4): p. 1375-1403.

568. Kuo, L.J. and L.X. Yang, *Gamma-H2AX - a novel biomarker for DNA double-strand breaks.* In Vivo, 2008. **22**(3): p. 305-9.

569. Brunner, C., et al., *Bruton's tyrosine kinase is activated upon CD40 stimulation in human B lymphocytes.* Immunobiology, 2002. **206**(4): p. 432-40.

570. Kielbassa, K., et al., *Ibrutinib sensitizes CLL cells to venetoclax by interrupting TLR9-induced CD40 upregulation and protein translation.* Leukemia, 2023. **37**(6): p. 1268-1276.

571. Niiro, H. and E.A. Clark, *Regulation of B-cell fate by antigen-receptor signals.* Nat Rev Immunol, 2002. **2**(12): p. 945-56.

572. Ezell, S.A., et al., *Synergistic induction of apoptosis by combination of BTK and dual mTORC1/2 inhibitors in diffuse large B cell lymphoma.* Oncotarget, 2014. **5**(13): p. 4990-5001.

573. Grommes, C., et al., *Ibrutinib Unmasks Critical Role of Bruton Tyrosine Kinase in Primary CNS Lymphoma.* Cancer Discov, 2017. **7**(9): p. 1018-1029.

574. Calissi, G., E.W. Lam, and W. Link, *Therapeutic strategies targeting FOXO transcription factors.* Nat Rev Drug Discov, 2021. **20**(1): p. 21-38.

575. Rupp, M., et al., *FOXO3-mediated chemo-protection in high-stage neuroblastoma depends on wild-type TP53 and SESN3.* Oncogene, 2017. **36**(44): p. 6190-6203.

576. Salih, D.A. and A. Brunet, *FoxO transcription factors in the maintenance of cellular homeostasis during aging.* Curr Opin Cell Biol, 2008. **20**(2): p. 126-36.

577. Schmidt, M., et al., *Cell cycle inhibition by FoxO forkhead transcription factors involves downregulation of cyclin D.* Mol Cell Biol, 2002. **22**(22): p. 7842-52.

578. Bing, Z., et al., *FOXO3-induced oncogenic lncRNA CASC9 enhances gefitinib resistance of non-small-cell lung cancer through feedback loop.* Life Sci, 2021. **287**: p. 120012.

579. Hui, R.C., et al., *The forkhead transcription factor FOXO3a increases phosphoinositide-3 kinase/Akt activity in drug-resistant leukemic cells through induction of PIK3CA expression.* Mol Cell Biol, 2008. **28**(19): p. 5886-98.

580. Cheong, J.W., et al., *Constitutive phosphorylation of FKHR transcription factor as a prognostic variable in acute myeloid leukemia.* Leuk Res, 2003. **27**(12): p. 1159-62.

581. Zhang, B., et al., *Prognostic significance of phosphorylated FOXO1 expression in soft tissue sarcoma.* Ann Surg Oncol, 2009. **16**(7): p. 1925-37.

582. Patra, T., et al., *Akt inhibitor augments anti-proliferative efficacy of a dual mTORC1/2 inhibitor by FOXO3a activation in p53 mutated hepatocarcinoma cells.* Cell Death Dis, 2021. **12**(11): p. 1073.

583. Jimenez, L., et al., *mTORC2 Is the Major Second Layer Kinase Negatively Regulating FOXO3 Activity.* Molecules, 2022. **27**(17). p. 5414.

584. Murata, T., N.I. Obiri, and R.K. Puri, *Structure of and signal transduction through interleukin-4 and interleukin-13 receptors (review).* Int J Mol Med, 1998. **1**(3): p. 551-7.

585. Konforte, D., N. Simard, and C.J. Paige, *IL-21: an executor of B cell fate.* J Immunol, 2009. **182**(4): p. 1781-7.

586. Jin, H., et al., *Distinct activation signals determine whether IL-21 induces B cell costimulation, growth arrest, or Bim-dependent apoptosis.* J Immunol, 2004. **173**(1): p. 657-65.

587. Teoh, G., et al., *CD40 activation mediates p53-dependent cell cycle regulation in human multiple myeloma cell lines.* Blood, 2000. **95**(3): p. 1039-46.

588. Dijkers, P.F., et al., *Forkhead transcription factor FKHR-L1 modulates cytokine-dependent transcriptional regulation of p27(KIP1).* Mol Cell Biol, 2000. **20**(24): p. 9138-48.

589. Fu, G. and C. Peng, *Nodal enhances the activity of FoxO3a and its synergistic interaction with Smads to regulate cyclin G2 transcription in ovarian cancer cells.* Oncogene, 2011. **30**(37): p. 3953-66.

590. Chou, M.M. and J. Blenis, *The 70 kDa S6 kinase: regulation of a kinase with multiple roles in mitogenic signalling.* Curr Opin Cell Biol, 1995. **7**(6): p. 806-14.

591. Hashemolhosseini, S., et al., *Rapamycin inhibition of the G1 to S transition is mediated by effects on cyclin D1 mRNA and protein stability.* J Biol Chem, 1998. **273**(23): p. 14424-9.

592. Abdelnour-Berchtold, E., et al., *Rapamycin-mediated FOXO1 inactivation reduces the anticancer efficacy of rapamycin.* Anticancer Res, 2010. **30**(3): p. 799-804.

593. You, H., et al., *FOXO3a-dependent regulation of Puma in response to cytokine/growth factor withdrawal.* J Exp Med, 2006. **203**(7): p. 1657-63.

594. Bhola, P.D. and A. Letai, *Mitochondria-Judges and Executioners of Cell Death Sentences.* Mol Cell, 2016. **61**(5): p. 695-704.

595. Clybouw, C., et al., *Regulation of memory B-cell survival by the BH3-only protein Puma.* Blood, 2011. **118**(15): p. 4120-8.

596. Widden, H. and W.J. Placzek, *The multiple mechanisms of MCL1 in the regulation of cell fate.* Commun Biol, 2021. **4**(1): p. 1029.

597. Gobeil, S., et al., *Characterization of the necrotic cleavage of poly(ADP-ribose) polymerase (PARP-1): implication of lysosomal proteases.* Cell Death Differ, 2001. **8**(6): p. 588-94.

598. Castri, P., et al., *Poly(ADP-ribose) polymerase-1 and its cleavage products differentially modulate cellular protection through NF-kappaB-dependent signaling.* Biochim Biophys Acta, 2014. **1843**(3): p. 640-51.

599. O'Donnell, A., et al., *NF-kB and the CLL microenvironment.* Front Oncol, 2023. **13**: p. 1169397.

600. Maya-Mendoza, A., et al., *High speed of fork progression induces DNA replication stress and genomic instability.* Nature, 2018. **559**(7713): p. 279-284.

601. Bonner, W.M., et al., *GammaH2AX and cancer.* Nat Rev Cancer, 2008. **8**(12): p. 957-67.

602. Pinto, D.M. and A. Flaus, *Structure and function of histone H2AX.* Subcell Biochem, 2010. **50**: p. 55-78.

603. Silvera, D., et al., *mTORC1 and -2 Coordinate Transcriptional and Translational Reprogramming in Resistance to DNA Damage and Replicative Stress in Breast Cancer Cells.* Mol Cell Biol, 2017. **37**(5). p. e00577-16.

604. Chen, H., et al., *The mTOR inhibitor rapamycin suppresses DNA double-strand break repair.* Radiat Res, 2011. **175**(2): p. 214-24.

605. Huang, S., et al., *Inhibition of mTOR kinase by AZD8055 can antagonize chemotherapy-induced cell death through autophagy induction and down-regulation of p62/sequestosome 1.* J Biol Chem, 2011. **286**(46): p. 40002-12.

606. Zhou, X., et al., *Regulation of CHK1 by mTOR contributes to the evasion of DNA damage barrier of cancer cells.* Sci Rep, 2017. **7**(1): p. 1535.

607. Patel, K., M.G. Murray, and K.A. Whelan, *Roles for GADD45 in Development and Cancer.* Adv Exp Med Biol, 2022. **1360**: p. 23-39.

608. Wingert, S., et al., *DNA-damage response gene GADD45A induces differentiation in hematopoietic stem cells without inhibiting cell cycle or survival.* Stem Cells, 2016. **34**(3): p. 699-710.

609. Carrier, F., et al., *Gadd45, a p53-responsive stress protein, modifies DNA accessibility on damaged chromatin.* Mol Cell Biol, 1999. **19**(3): p. 1673-85.

610. Wang, X.W., et al., *GADD45 induction of a G2/M cell cycle checkpoint.* Proc Natl Acad Sci U S A, 1999. **96**(7): p. 3706-11.

611. Zhan, Q., et al., *Association with Cdc2 and inhibition of Cdc2/Cyclin B1 kinase activity by the p53-regulated protein Gadd45.* Oncogene, 1999. **18**(18): p. 2892-900.

612. Fragkos, M., M. Choleza, and P. Papadopoulou, *The Role of gammaH2AX in Replication Stress-induced Carcinogenesis: Possible Links and Recent Developments.* Cancer Diagn Progn, 2023. **3**(6): p. 639-648.

613. Chen, Y., et al., *The functions and roles of sestrins in regulating human diseases.* Cell Mol Biol Lett, 2022. **27**(1): p. 2.

614. Nagashima, T., et al., *Discovery of novel forkhead box O1 inhibitors for treating type 2 diabetes: improvement of fasting glycemia in diabetic db/db mice.* Mol Pharmacol, 2010. **78**(5): p. 961-70.

615. Flores, D., et al., *The FOXO1 inhibitor AS1842856 triggers apoptosis in glioblastoma multiforme and basal-like breast cancer cells.* FEBS Open Bio, 2023. **13**(2): p. 352-362.

616. Gehringer, F., et al., *FOXO1 Confers Maintenance of the Dark Zone Proliferation and Survival Program and Can Be Pharmacologically Targeted in Burkitt Lymphoma.* Cancers (Basel), 2019. **11**(10). p. 1427.

617. Kurayoshi, K., et al., *Targeting cis-regulatory elements of FOXO family is a novel therapeutic strategy for induction of leukemia cell differentiation.* Cell Death Dis, 2023. **14**(9): p. 642.

618. Bloedjes, T.A., et al., *AKT signaling restrains tumor suppressive functions of FOXO transcription factors and GSK3 kinase in multiple myeloma.* Blood Adv, 2020. **4**(17): p. 4151-4164.

619. Schmitt-Ney, M., *The FOXO's Advantages of Being a Family: Considerations on Function and Evolution.* Cells, 2020. **9**(3). p. 787.

620. Santos, B.F., et al., *FOXO family isoforms.* Cell Death Dis, 2023. **14**(10): p. 702.

621. Vajen, B., et al., *Numerical Aberrations Involving The X Chromosome As a New Recurrent Aberration In Patients With Chronic Lymphocytic Leukemia.* 2013, Blood. p. 4880.

622. Jarosova, M., et al., *Chromosome 6q deletion correlates with poor prognosis and low relative expression of FOXO3 in chronic lymphocytic leukemia patients.* Am J Hematol, 2017. **92**(10): p. E604-E607.

623. Tenbaum, S.P., et al., *beta-catenin confers resistance to PI3K and AKT inhibitors and subverts FOXO3a to promote metastasis in colon cancer.* Nat Med, 2012. **18**(6): p. 892-901.

624. Sinclair, P.B., et al., *Disruption to the FOXO-PRDM1 axis resulting from deletions of chromosome 6 in acute lymphoblastic leukaemia.* Leukemia, 2023. **37**(3): p. 636-649.

625. Petitjean, A., et al., *Impact of mutant p53 functional properties on TP53 mutation patterns and tumor phenotype: lessons from recent developments in the IARC TP53 database.* Hum Mutat, 2007. **28**(6): p. 622-9.

626. Bourgeois, B. and T. Madl, *Regulation of cellular senescence via the FOXO4-p53 axis.* FEBS Lett, 2018. **592**(12): p. 2083-2097.

627. Moskalev, A.A., et al., *Gadd45 proteins: relevance to aging, longevity and age-related pathologies.* Ageing Res Rev, 2012. **11**(1): p. 51-66.

628. Ning, N., et al., *Inhibition of acylglycerol kinase sensitizes DLBCL to venetoclax via upregulation of FOXO1-mediated BCL-2 expression.* Theranostics, 2022. **12**(12): p. 5537-5550.

629. Tang, T.T., et al., *The forkhead transcription factor AFX activates apoptosis by induction of the BCL-6 transcriptional repressor.* J Biol Chem, 2002. **277**(16): p. 14255-65.

630. Han, K., et al., *Fasting-induced FOXO4 blunts human CD4(+) T helper cell responsiveness.* Nat Metab, 2021. **3**(3): p. 318-326.

631. Ni, D., et al., *Downregulation of FOXO3a promotes tumor metastasis and is associated with metastasis-free survival of patients with clear cell renal cell carcinoma.* Clin Cancer Res, 2014. **20**(7): p. 1779-90.

632. Shiota, M., et al., *Foxo3a expression and acetylation regulate cancer cell growth and sensitivity to cisplatin.* Cancer Sci, 2010. **101**(5): p. 1177-85.

633. Li, Z., et al., *Forkhead transcription factor FOXO3a protein activates nuclear factor kappaB through B-cell lymphoma/leukemia 10 (BCL10) protein and promotes tumor cell survival in serum deprivation.* J Biol Chem, 2012. **287**(21): p. 17737-17745.

634. Su, L., et al., *The transcription factor FOXO4 is down-regulated and inhibits tumor proliferation and metastasis in gastric cancer.* BMC Cancer, 2014. **14**: p. 378.

635. Sun, Y., et al., *FOXO4 Inhibits the Migration and Metastasis of Colorectal Cancer by Regulating the APC2/beta-Catenin Axis.* Front Cell Dev Biol, 2021. **9**: p. 659731.

636. Zhong, T., et al., *Downregulation of 4-HNE and FOXO4 collaboratively promotes NSCLC cell migration and tumor growth.* Cell Death Dis, 2024. **15**(7): p. 546.

637. Xu, M.M., et al., *Low expression of the FoxO4 gene may contribute to the phenomenon of EMT in non-small cell lung cancer.* Asian Pac J Cancer Prev, 2014. **15**(9): p. 4013-8.

638. de Keizer, P.L., et al., *Activation of forkhead box O transcription factors by oncogenic BRAF promotes p21cip1-dependent senescence.* Cancer Res, 2010. **70**(21): p. 8526-36.

639. Hornsveld, M., et al., *A FOXO-dependent replication checkpoint restricts proliferation of damaged cells.* Cell Rep, 2021. **34**(4): p. 108675.

640. Tarrade, S., et al., *Histone H2AX Is Involved in FoxO3a-Mediated Transcriptional Responses to Ionizing Radiation to Maintain Genome Stability.* Int J Mol Sci, 2015. **16**(12): p. 29996-30014.

641. Kleinsimon, S., et al., *GADD45A and CDKN1A are involved in apoptosis and cell cycle modulatory effects of viscumTT with further inactivation of the STAT3 pathway.* Sci Rep, 2018. **8**(1): p. 5750.

642. Yoshiko, S. and N. Hoyoku, *Fucoxanthin, a natural carotenoid, induces G1 arrest and GADD45 gene expression in human cancer cells.* In Vivo, 2007. **21**(2): p. 305-9.

643. Lin, C.L., et al., *Norcantharidin induces mitochondrial-dependent apoptosis through Mcl-1 inhibition in human prostate cancer cells.* Biochim Biophys Acta Mol Cell Res, 2017. **1864**(10): p. 1867-1876.

644. Mandal, R., et al., *FOXO4 interacts with p53 TAD and CRD and inhibits its binding to DNA.* Protein Sci, 2022. **31**(5): p. e4287.

645. Rodier, F., et al., *DNA-SCARS: distinct nuclear structures that sustain damage-induced senescence growth arrest and inflammatory cytokine secretion.* J Cell Sci, 2011. **124**(Pt 1): p. 68-81.

646. Hurtz, C., et al., *BCL6-mediated repression of p53 is critical for leukemia stem cell survival in chronic myeloid leukemia.* J Exp Med, 2011. **208**(11): p. 2163-74.

647. Hagenbuchner, J., et al., *FOXO3-induced reactive oxygen species are regulated by BCL2L11 (Bim) and SESN3.* J Cell Sci, 2012. **125**(Pt 5): p. 1191-203.

648. Wang, J., et al., *FOXO3-mediated up-regulation of Bim contributes to rhein-induced cancer cell apoptosis.* Apoptosis, 2015. **20**(3): p. 399-409.

649. Yue, D. and X. Sun, *Idelalisib promotes Bim-dependent apoptosis through AKT/FoxO3a in hepatocellular carcinoma.* Cell Death Dis, 2018. **9**(10): p. 935.

650. Zhao, X., et al., *Threonine 32 (Thr32) of FoxO3 is critical for TGF-beta-induced apoptosis via Bim in hepatocarcinoma cells.* Protein Cell, 2015. **6**(2): p. 127-38.

651. Yun, S., et al., *4EBP1/c-MYC/PUMA and NF-kappaB/EGR1/BIM pathways underlie cytotoxicity of mTOR dual inhibitors in malignant lymphoid cells.* Blood, 2016. **127**(22): p. 2711-22.

652. Wang, Y., W. Luo, and Y. Wang, *PARP-1 and its associated nucleases in DNA damage response.* DNA Repair (Amst), 2019. **81**: p. 102651.

653. Ng, S.Y. and M.S. Davids, *Selective Bcl-2 inhibition to treat chronic lymphocytic leukemia and non-Hodgkin lymphoma.* Clin Adv Hematol Oncol, 2014. **12**(4): p. 224-9.

654. Choudhary, G.S., et al., *MCL-1 and BCL-xL-dependent resistance to the BCL-2 inhibitor ABT-199 can be overcome by preventing PI3K/AKT/mTOR activation in lymphoid malignancies.* Cell Death Dis, 2015. **6**(1): p. e1593.

655. Li, Z., S. He, and A.T. Look, *The MCL1-specific inhibitor S63845 acts synergistically with venetoclax/ABT-199 to induce apoptosis in T-cell acute lymphoblastic leukemia cells.* Leukemia, 2019. **33**(1): p. 262-266.

656. Jia, Y., et al., *Co-targeting BCL-XL and BCL-2 by PROTAC 753B eliminates leukemia cells and enhances efficacy of chemotherapy by targeting senescent cells.* Haematologica, 2023. **108**(10): p. 2626-2638.

657. Yu, C.Y., et al., *BCL-XL regulates the timing of mitotic apoptosis independently of BCL2 and MCL1 compensation.* Cell Death Dis, 2024. **15**(1): p. 2.

658. Kannike, K., et al., *Forkhead transcription factor FOXO3a levels are increased in Huntington disease because of overactivated positive autofeedback loop.* J Biol Chem, 2014. **289**(47): p. 32845-57.

659. Lutzner, N., et al., *FOXO3 is a glucocorticoid receptor target and regulates LKB1 and its own expression based on cellular AMP levels via a positive autoregulatory loop.* PLoS One, 2012. **7**(7): p. e42166.

660. Zhao, J., et al., *mTOR inhibition activates overall protein degradation by the ubiquitin proteasome system as well as by autophagy.* Proc Natl Acad Sci U S A, 2015. **112**(52): p. 15790-7.

661. Fejzo, M.S., et al., *Proteasome ubiquitin receptor PSMD4 is an amplification target in breast cancer and may predict sensitivity to PARPi.* Genes Chromosomes Cancer, 2017. **56**(8): p. 589-597.

662. Shin, S., et al., *mTOR inhibition reprograms cellular proteostasis by regulating eIF3D-mediated selective mRNA translation and promotes cell phenotype switching.* Cell Rep, 2023. **42**(8): p. 112868.

663. Kapetanou, M., et al., *FoxO1 Is a Novel Regulator of 20S Proteasome Subunits Expression and Activity.* Front Cell Dev Biol, 2021. **9**: p. 625715.

664. Vilchez, D., et al., *Increased proteasome activity in human embryonic stem cells is regulated by PSMD11.* Nature, 2012. **489**(7415): p. 304-8.

665. Nestal de Moraes, G., et al., *Insights into a Critical Role of the FOXO3a-FOXM1 Axis in DNA Damage Response and Genotoxic Drug Resistance.* Curr Drug Targets, 2016. **17**(2): p. 164-77.

666. Liu, J., et al., *Down-regulation of GADD45A enhances chemosensitivity in melanoma.* Sci Rep, 2018. **8**(1): p. 4111.

667. Hassan, N., et al., *Loss of the stress sensor GADD45A promotes stem cell activity and ferroptosis resistance in LGR4/HOXA9-dependent AML.* Blood, 2024. **144**(1): p. 84-98.

668. Stewart, G.S., et al., *RIDDLE immunodeficiency syndrome is linked to defects in 53BP1-mediated DNA damage signaling.* Proc Natl Acad Sci U S A, 2007. **104**(43): p. 16910-5.

669. Fingar, D.C., et al., *Mammalian cell size is controlled by mTOR and its downstream targets S6K1 and 4EBP1/eIF4E.* Genes Dev, 2002. **16**(12): p. 1472-87.

670. Vakana, E., et al., *Regulatory effects of sestrin 3 (SESN3) in BCR-ABL expressing cells.* PLoS One, 2013. **8**(11): p. e78780.

671. Wu, X., et al., *Beyond controlling cell size: functional analyses of S6K in tumorigenesis.* Cell Death Dis, 2022. **13**(7): p. 646.

672. Shull, A.Y., et al., *RPPA-based protein profiling reveals eIF4G overexpression and 4E-BP1 serine 65 phosphorylation as molecular events that correspond with a pro-survival phenotype in chronic lymphocytic leukemia.* Oncotarget, 2015. **6**(16): p. 14632-45.

673. Heberle, A.M., et al., *Molecular mechanisms of mTOR regulation by stress.* Mol Cell Oncol, 2015. **2**(2): p. e970489.

674. Breuleux, M., et al., *Increased AKT S473 phosphorylation after mTORC1 inhibition is rictor dependent and does not predict tumor cell response to PI3K/mTOR inhibition.* Mol Cancer Ther, 2009. **8**(4): p. 742-53.

675. Nogueira, V., et al., *Akt determines replicative senescence and oxidative or oncogenic premature senescence and sensitizes cells to oxidative apoptosis.* Cancer Cell, 2008. **14**(6): p. 458-70.

676. Nemoto, S. and T. Finkel, *Redox regulation of forkhead proteins through a p66shc-dependent signaling pathway.* Science, 2002. **295**(5564): p. 2450-2.

677. Klotz, L.O., et al., *Redox regulation of FoxO transcription factors.* Redox Biol, 2015. **6**: p. 51-72.

678. Jang, J.Y., et al., *A FOXO1-dependent transcription network is a targetable vulnerability of mantle cell lymphomas.* J Clin Invest, 2022. **132**(24).

679. Trinh, D.L., et al., *Analysis of FOXO1 mutations in diffuse large B-cell lymphoma.* Blood, 2013. **121**(18): p. 3666-74.

680. Salcher, S., et al., *A drug library screen identifies Carbenoxolone as novel FOXO inhibitor that overcomes FOXO3-mediated chemoprotection in high-stage neuroblastoma.* Oncogene, 2020. **39**(5): p. 1080-1097.

681. Baar, M.P., et al., *Targeted Apoptosis of Senescent Cells Restores Tissue Homeostasis in Response to Chemotoxicity and Aging.* Cell, 2017. **169**(1): p. 132-147 e16.

682. Langlet, F., et al., *Selective Inhibition of FOXO1 Activator/Repressor Balance Modulates Hepatic Glucose Handling.* Cell, 2017. **171**(4): p. 824-835 e18.

683. Hoogeboom, D., et al., *Interaction of FOXO with beta-catenin inhibits beta-catenin/T cell factor activity.* J Biol Chem, 2008. **283**(14): p. 9224-30.

684. Das, A., et al., *Selective inhibitors of nuclear export (SINE) in hematological malignancies.* Exp Hematol Oncol, 2015. **4**: p. 7.

685. Lapalombella, R., et al., *Selective inhibitors of nuclear export show that CRM1/XPO1 is a target in chronic lymphocytic leukemia.* Blood, 2012. **120**(23): p. 4621-34.

686. Hing, Z.A., et al., *Selinexor is effective in acquired resistance to ibrutinib and synergizes with ibrutinib in chronic lymphocytic leukemia.* Blood, 2015. **125**(20): p. 3128-32.

687. Kalakonda, N., et al., *Selinexor in patients with relapsed or refractory diffuse large B-cell lymphoma (SADAL): a single-arm, multinational, multicentre, open-label, phase 2 trial.* Lancet Haematol, 2020. **7**(7): p. e511-e522.

688. Vitale, C., et al., *Anti-tumor activity of selinexor in combination with antineoplastic agents in chronic lymphocytic leukemia.* Sci Rep, 2023. **13**(1): p. 16950.

689. Stephens, D.M., et al., *Selinexor Combined with Ibrutinib Demonstrates Tolerability and Safety in Advanced B-Cell Malignancies: A Phase I Study.* Clin Cancer Res, 2022. **28**(15): p. 3242-3247.

690. Pennington, K.L., et al., *The dynamic and stress-adaptive signaling hub of 14-3-3: emerging mechanisms of regulation and context-dependent protein-protein interactions.* Oncogene, 2018. **37**(42): p. 5587-5604.

691. Bullock, M.D., et al., *FOXO3 expression during colorectal cancer progression: biomarker potential reflects a tumour suppressor role.* Br J Cancer, 2013. **109**(2): p. 387-94.

692. Pastore, A., et al., *Integration of gene mutations in risk prognostication for patients receiving first-line immunochemotherapy for follicular lymphoma: a retrospective analysis of a prospective clinical trial and validation in a population-based registry.* Lancet Oncol, 2015. **16**(9): p. 1111-1122.

693. Kohrer, S., et al., *Pre-BCR signaling in precursor B-cell acute lymphoblastic leukemia regulates PI3K/AKT, FOXO1 and MYC, and can be targeted by SYK inhibition.* Leukemia, 2016. **30**(6): p. 1246-54.

694. Szydlowski, M., et al., *FOXO1 activation is an effector of SYK and AKT inhibition in tonic BCR signal-dependent diffuse large B-cell lymphomas.* Blood, 2016. **127**(6): p. 739-48.